# STRUCTURAL STUDIES OF BERBERINE AND BERBERRUBINE AND THEIR INTERACTION WITH DNA

**A THESIS**

*Submitted in partial fulfilment of the requirements for the award of the degree of*

DOCTOR OF PHILOSOPHY

*in*

BIOTECHNOLOGY

*by*

**LATA CHAUHAN**




DEPARTMENT OF BIOTECHNOLOGY
INDIAN INSTITUTE OF TECHNOLOGY ROORKEE
ROORKEE - 247 667 (INDIA)

JUNE, 2009

# INDIAN INSTITUTE OF TECHNOLOGY ROORKEE
# ROORKEE

## CANDIDATE'S DECLARATION

I hereby certify that the work which is being presented in the thesis entitled **STRUCTURAL STUDIES OF BERBERINE AND BERBERRUBINE AND THEIR INTERACTION WITH DNA** in partial fulfilment of the requirements for the award of the Degree of Doctor of Philosophy and submitted in the Department of Biotechnology of the Indian Institute of Technology Roorkee, Roorkee is an authentic record of my own work carried out during a period from July 2004 to June 2009 under the supervision of Prof. Ritu Barthwal, Professor & Head, Department of Biotechnology, Indian Institute of Technology Roorkee, Roorkee, India.

The matter embodied in this thesis has not been submitted by me for the award of any other degree of this or any other Institute.

Lata Chauhan
**(LATA CHAUHAN)**

This is to certify that the above statement made by the candidate is correct to the best of my knowledge.

Ritu Barthwal
(Ritu Barthwal)
Supervisor

Date: 16.06.09

The Ph.D. Viva-Voce examination of **Ms. Lata Chauhan**, Research Scholar, has been held on .....

Signature of Supervisor

Signature of External Examiner

# *ACKNOWLEDGEMENT*

*"God understands our prayers even when we can't find the words to say them."*

*This piece of work would have been never accomplished without Almighty God's blessings and His power that work within me. I thank god for everything with which I am blessed with.*

*This thesis is the end of my long journey in obtaining my degree but I have not traveled in a vacuum in this journey. There are some people who made this journey easier with their words of encouragement and contribution in assorted ways to the research and the making of this thesis. It is a pleasure to convey my gratitude to all of them in my humble acknowledgment.*

*In the first place I would like to acknowledge my appreciation to my supervisor, Prof. Ritu Barthwal, Head, Department of Biotechnology for her supervision, advice, and guidance from the very early stage of this research. Above all and the most needed, she provided me with unflinching encouragement and support in various ways which always encouraged me to work hard. Her involvement with originality has nourished my intellectual maturity and enriched my growth as a student and a researcher.*

*Token of deep regards is being rendered to Prof. A. N. Tripathi, for taking intense interest in this study as well as providing his valuable suggestions that has improved the quality of this study.*

*I am also thankful to the faculty members and staff of the Department of Biotechnology, IIT Roorkee for their support and help.*

*I would also like to gratefully acknowledge my respected seniors Dr. Monika, Dr. Manpreet, Dr. Prashansa, Dr. Durai Raj, Dr. Maya s. Nair and Dr. Sulaxana. I would like to thank my colleagues, Mr. Amit and Mrs. Kushuma for their support during my thesis. I would specially like to thank my friend and colleague Asif for always being there with me during the toughest times. I was lucky to have such a good friend. The presence of Ms. Shahdeep and Mr. Ankur provided memorable light moments during the writing of the thesis.*

*This thesis would have been a distant dream without care and support of my dearest friend Manu. He has been a pillar of support during the stressful periods, a great listener and has always been available for me. His wonderful sense of humor helped me to see the positive aspects of even the most difficult moments.*

*This thesis would not be in its present state without the support of my dearest friends Priya Kapur and Anjali Sardana. They had always encouraged me to grow and to expand my thinking. They supported me mentally during the course of this work and this had helped me to concentrate on completing my thesis. Thanks dear for always being there for me and helping me accomplish this massive task comfortably.*

*"Wherever you are its your friends who make your world", its true because of the direct and indirect support and help from my friends Mrs. Pallavi Dwivedi, Mrs. Santosh Kaushik, Mrs. Sanimer Kaur, Mrs. Sreela Dey, Mrs. Deepti Thakur, Mrs. Dhanpati Rana, Mrs. Prerana Gupta, Mrs. Shilpa Pal and Mrs. Avlokita agrawal. They provided the joyful, affectionate and healthy environment during my stay at Rooorkee for accomplishing my goal.*

*"Family is the compass that guide us", Where would I be without my family? My parents deserve special mention for their unending love, inseparable support and prayers during my Ph.D. experience. I feel deep sense of gratitude for my mummy and papa. They always encouraged me in all my endeavours and felt proud of every achievement of mine. I would like to extend my sincere thanks to my Bhaiya Bhabhi and Didi Jija ji for indirect support to make this journey so congenial and easy. I am thanking them for their memorable concern, affection and constant care.*

*How can I Forget to mention the beautiful smiles of Tiinni, Vishu, Abhi, Siya, and Harshi for always being a powerful source of freshness in life.*

*And to the rest, I extremely thankful to those people, whose names have been unknowingly left, thank you very much for your prayers. It had really helped a lot. I apologize and believe that they will be always with me as they were during the times of need.*

*Last but not the least; I would like to thank Council of Scientific & Industrial Research (CSIR) for providing financial support for my research work.*

(Lata Chauhan)

# *ABSTRACT*

Medicinal plants are the most valuable assets nowadays due to presence of small doses of active compounds which produce physiological actions in human and animal body. Some of the important bioactive compounds are alkaloids, glycosides, resins, gums and mucilages which possess anticancer, antiviral, antidiabetic and antimicrobial activity. The medicinal value of berberine, a protoberberine alkaloid found in root, rhizome and stem bark of *Berberis vulgaris* L. plant has been recognized since ancient times. Apart from its anti-cancerous property, it also displays a wide variety of biological and pharmacological activities e.g. antimicrobial, antiplasmodial, antidiarrhoeal, cardiovascular, etc. Replacement of $OCH_3$ group at position 7 (Figure 1) in berberine with OH group, resulting in a derivative called berberrubine, induces a large change in its antitumor activity. Several studies have proved that Berberine acts as an anticancerous agent by binding to DNA, but actual mode of binding is still not clear.

The molecular basis for designing DNA binding drugs with improved specificity and affinity stems from the ability to identify the structural elements of the drug and DNA which are responsible for the specificity of the binding and the stabilization of the drug–DNA complex. An analytical technique to elucidate the mode of drug-DNA interaction could be essential for the design of new drugs. Nuclear Magnetic Resonance (NMR) spectroscopy, Absorption spectroscopy, Fluorescence Spectroscopy, and restrained Molecular Dynamics (rMD) are some of the analytical techniques which have been used in this study to investigate conformation of drug, DNA and drug-DNA complexes.

The Ph.D. thesis work has been reported in the form of seven chapters.

**Chapter 1** contains introduction of the subject, a comprehensive review of the literature and scope of thesis.

**Chapter 2** deals with the materials and methods used. The detailed Nuclear Magnetic Resonance spectroscopy techniques used, that is, - 1D NMR, Double Quantum Filtered Correlation Spectroscopy (DQF-COSY), Total Correlation Spectroscopy (TOCSY), $^{1}H$ - $^{1}H$ Nuclear Overhauser Enhancement Spectroscopy (NOESY)for the proton assignment; $^{1}H$ - $^{31}P$ Heteronuclear Multiple Bond Correlation Spectroscopy (HMBC), $^{31}P$ - $^{31}P$ NOESY and Diffusion Ordered Spectroscopy (DOSY) studies are discussed. The strategies used for restrained energy minimization, restrained Molecular Dynamics (rMD) simulations and quantum mechanical calculations involving GIAO method (for chemical shift calculation) and DFT method (for optimization) are also discussed. Absorption and Fluorescence spectroscopy methods used to investigate drug-DNA interaction are discussed followed by Time-Correlated Single-Photon Counting method (TCSPC) are discussed.

**Chapter 3** deals with the structural and electronic properties of protoberberine alkaloids, berberine and berberrubine, using density functional theory (DFT) employing B3LYP exchange correlation. The geometries of these molecules have been fully optimized at B3LYP/6-311G** level. The chemical shift of $^{1}H$ and $^{13}C$ resonances phase Nuclear Magnetic Resonance (NMR) spectra of these molecules have been calculated in gaseous and solvent phase using the Gauge–invariant atomic model (GIAO) method as implemented in Gaussian 98 and 03. One- and two-dimensional HSQC ($^{1}H$-$^{13}C$), HMBC ($^{1}H$-$^{13}C$) and ROESY ($^{1}H$-$^{1}H$) spectra have been recorded at 500 MHz for berberine and berberrubine molecules in $D_2O$ solution. All proton and carbon resonances for berberine and berberrubine were unambiguously

assigned and inter proton distances have been obtained from their respective NOESY spectra. A restrained Molecular Dynamics approach was used to obtain the optimized solution structure of both drugs. Comparison of the calculated NMR chemical shifts with the experimental values revealed that DFT methods produce good results for both proton and carbon chemical shifts. The importance of the basis sets with solvent effect to the calculated NMR parameters has been discussed. It has been found that calculated structure and chemical shifts in solvent phase predicted with B3LYP/6-311G** were in good agreement with the present experimental data and measured values reported earlier.

**Chapter 4** deals with the study of berberine and berberrubine interaction with DNA using Absorption and Fluorescence spectroscopic techniques. The spectral properties of berberrubine molecules was also obtained and reported for the first time. Several DNA and oligonucleotides were used in this study to elucidate the sequence binding affinity of these drugs. Titration of these drugs with increasing amount of DNA showed that berberine binds effectively to CT DNA, Poly dA-dT, Poly dG-dC and small oligonucleotides, while berberubine does not show any binding towards alone DNA. It indicates that berberrubine binds to DNA in presence of topoisomerase. Percentage hypochromicity, binding constant, extinction coefficient of bound berberine, fluorescence-enhancement and relative fluorescence obtained from absorption and fluorescence spectroscopy were used to study the binding affinity. Maximum binding affinity of berberine was found to occur towards octamer sequence d-$(CCAATTGG)_2$, having an intrinsic promoter site as CCAAT. Sequence specificity of berberine has been proved towards AATT rich sequences. Our results also suggest minor groove mode of binding of berberine, as it needs more than two base pairs for binding. The importance of the neighbour base to the binding site has also been

discussed. It has been found that presence of guanine at +1 position to the binding site is an inhibitory factor for the interaction of berberine. TCSPC analysis of berberine-d-$(CCAATTGG)_2$ complex also substantiates effective binding.

**Chapter 5** deals with the solution structure and thermal stability studies of a promoter site containing octamer d-$(CCAATTGG)_2$ and comparison of results the with the crystal structure available in literature. The CCAAT box is one of the most common elements in eukaryotic promoters. The frequency of CCAAT box appears to be relatively higher in TATA less promoters and found to be present in several of oncogenes like MCT-1 and TLX-3. Solution structure of self complementary octamer d-$(CCAATTGG)_2$, has been investigated using NMR spectroscopy and rMD calculations. Complete resonance assignment for all the protons (except H5', 5") has been obtained following standard procedures based on DQF-COSY and 2D NOESY. $^1H$ -1D NMR has been used to study the thermal stability of the sequence d-$(CCAATTGG)_2$. Melting temperature has been found to be 308 ± 2 K by analyzing the denaturation in the base pair stacking using imino and methyl protons. Inter proton distance restraints were derived from two dimensional Nuclear Overhauser Enhancement (NOE) spectra. Constraints for torsion angles have been calculated by qualititative analysis of $^{31}P$-$^1H$ HMBC and coupling patterns in DQF COSY spectrum. Structural refinement has been carried out using rMD with B-DNA as starting structure. Final rMD model, obtained with a 0.25 RMSD value, has been compared with crystal structure and canonical B-DNA. All the helicoidal parameters showed a deviation from B-DNA, particularly at central AATT region. This was characterized by the more negative value of propeller twist indicating occurrence of deep and narrow minor groove occurrence, which can be used for designing of new minor groove binders with better activity

**Chapter 6** deals with $^{31}P$, $^{1}H$ NMR and rMD studies on binding of berberine with DNA octamer sequence d–$(CCAATTGG)_2$. The following experiments were performed on the berberine-DNA complex - $^{1}H$ and $^{31}P$ NMR titration studies at various drug (D)/DNA duplex (N) ratios up to 2.0 at 283 K, 298 K in 90% $H_2O$ and 10% $D_2O$, temperature dependence of $^{31}P$ and $^{1}H$ NMR of the berberine-DNA complex having D/N = 1.0 and 2.0 in the range of 278 - 328 K; 2D $^{31}P$ - $^{31}P$ exchange spectra of drug-DNA complex by a phase sensitive NOESY; DOSY experiments of the beberine-DNA complex and uncomplexed berberine, rMD studies on the solution structure of berberine - d-$(CCAATTGG)_2$ complex using inter-proton distance restraints obtained from 2D NOESY. Results revealed that the addition of berberine to the oligonucleotide did not induce significant chemical shift variation of the phosphate signals in the $^{31}P$ NMR spectra indicating that the phosphodiester conformation remains unaffected. The proton resonances of berberine were broad even at low values of drug/DNA (D/N = 0.5) and move upfield with respect to the free drug. An upfield shift of ~0.1-0.6 ppm was found for the drugs protons on binding with DNA up to D/N ratio = 2. Maximum upfield shift in the drug protons was found to be for H28 and H24, which are located on the concave and convex side of berberine, respectively. Thermal melting temperature calculated by change in chemical shift of methyl protons chemical shift change with temperature is found be 312 ± 2 K, which is 5 K higher than that observed for uncomplexed d-$(CCAATTGG)_2$. The presence of all sequential NOE connectivities in the NOESY spectra at D/N = 2.0, as expected in standard B–DNA geometry confirmed that the DNA duplex is intact with apparently no opening of base pairs to accommodate drug chromophore as generally observed on intercalation. 22 intermolecular peaks obtained suggested that the dug protons, H10, H14, H28 and H24 located at ring D and ring B

were giving cross peaks with the sugar protons of DNA at A3, A4, T5, T6 region, while H5, H3, H36, 37, 38, H41, 42, 43 protons gives cross peaks with the C1-G8 base pair in promoter sequence. rMD structure suggests that drug binds to the minor groove of the central part of the oligonucleotides (AATT) which clearly excludes the intercalation mode for berberine and also supports its sequential preference to AATT.

**Chapter 7** summarizes the results obtained and their implications in understanding the molecular basis of action of berberine.

# *LIST OF PUBLICATIONS*

**Published in refereed international journal**

1. Tripathi A N, **Chauhan L,** Thankanchan P P and Barthwal R. ( 2007) Quantum chemical and nuclear magnetic resonance spectral studies on molecular properties and electronic structure of berberine and berberrubine. *Magnetic Resonance in Chemistry.* **45**, 647-655.

**To be communicated:**

1. Hassan S A, **Chauhan L**, Gupta P, Dixit A, Cowsik S M, Barthwal R. A Qualitative and Quantitative assay to study anticancer drug-DNA Interactions based on the sequence Selective Inhibition of Restriction Endonucleases.
2. **Chauhan L** and Barthwal R. Interaction of anticancer drugs, Berberine and berbrrubine with DNA by spectroscopic and fluorescence techniques.
3. **Chauhan L** and Barthwal R. Structure determination of promoter site containing Octamer d-( $CCAATTGG)_2$ using Nuclear Magnetic Resonance and restrained molecular dynamics and comparison with the crystal structure.
4. **Chauhan L** and Barthwal R. Berberine binding studies with promoter site sequence d-$(CCAATTGG)_2$ using nuclear magnetic resonance and molecular modeling technique.
5. Jain A, **Chauhan L** and Barthwal R Solution structure of complex interaction of berberine with papilliomavirus E2 binding protein sequence d-$(CGTTAACG)_2$.

**Papers in International Conference:**

1. **Chauhan L**, Bisht K, Barthwal S K, and Barthwal R (2005). NMR based solution structure of antitumor drug Berberine. *XXI International Conference on Magnetic Resonance in Biological Systems, Hyderabad, Andhra Pradesh, INDIA (XXIst ICMRBS-2005)* January 16 – 21.
2. **Chauhan L**, and Barthwal R. (2009). $^{31}P$ and $^{1}H$ NMR spectroscopy studies on binding of anticancer drugs berberine and berberrubine, to DNA octamer sequence containing promoter site"6th Asian Biophysics *Association (ABA) Symposium, 27th Hong Kong Society of Neuroscience Annual Meeting, at*

*Hong Kong University of Science and Technology*, Hong Kong, January 11-15.

**Papers in National Conference:**

1. **Chauhan L,** Tripathi A N, Thankanchan P P, Barthwal S K and Barthwal R.( 2007). A density functional (DFT) approach to study the structure and molecular properties of berberine and berberrubine molecules. *XVI National Conference on Atomic and Molecular Physics, TIFR,* January 8-11-pg no. 50 Abs. no. P1/14.
2. Hassan S A, Gupta P, Cowsick S M, **Chauhan** L, Dixit A, Barthwal R (2007). DNA – Anticancer Drug Interaction Studies Using Sequence Selective Inhibition of Restriction Endonuleases. *National Symposium on Biophysics: Trends in Biomedical Research IBS 2007, Department of NMR and MRI facility AIIMS, New delhi India,* February 13-15, pg no. 181 Abs. no. pp-118.
3. **Chauhan L**, and Barthwal R (2007). Berberine –DNA Interactions by Spectroscopic and Molecular Modeling Techniques. *National symposium on Biophysics; Biophysics in Medicine and Biology, IBS 2008, Department of Biophysics Punjab University Chandigarh* November 15-17.
4. **Chauhan L**, and Barthwal R (2009). $^{31}P$ and $^{1}H$ NMR spectroscopy studies on binding of anticancer drug berberine, to DNA octamer sequence containing promoter site. *NMRS-2009, Special Symposium on Magnetic Resonance and Biomolecular Memetics, 15th National Magnetic resonance Society Meeting, IICT Hyderabad, India,* February 2-5.

# CONTENTS

# CHAPTER 1

## Introduction and Literature Review

### 1.1 General

Cancer is characterized by the uncontrolled growth of cells. Under normal conditions, cell reproduction is carefully controlled by the body. However, these controls can malfunction, resulting in abnormal cell growth and the development of a lump, mass, or tumor. Some cancers involving the blood and blood-forming organs do not form tumors but circulate through other tissues where they grow. A tumor may be benign (non-cancerous) or malignant (cancerous). Cells from cancerous tumors can spread throughout the body. This process, called metastasis, occurs when cancer cells break away from the original tumor and travel in the circulatory or lymphatic systems until they are lodged in a small capillary network in another area of the body. Common locations of metastasis are the bones, lungs, liver, and central nervous system. Although there are many new ideas and treatments being studied every day, chemotherapy and radiation are still the most widely used treatments for the majority of cancers. Chemotherapy is the treatment of cancer with drugs ("anticancer drugs") that can destroy cancer cells. In current usage, the term "chemotherapy" usually refers to *cytotoxic* drugs which affect rapidly dividing cells. Generally DNA, as carrier of genetic information is a major target for chemotherapy because of the ability to interfere with DNA transcription and replication, major steps in cell growth and division. DNA serves two central roles. First, it maintains the genetic information and is replicated to pass this information to each new cell. Second, it contains the code which is translated into RNA which is then transcribed into proteins (Figure1.1). This

has become known as the central dogma of molecular biology. By binding covalently or non covalently to DNA, drugs may inhibit replication, shield the adducts from nucleotide excision repair, and interfere with transcription by recruiting essential transcription factors from their native binding sites, thus causing the death of cancerous cells. Sequence-specificity and affinity of drugs and proteins towards particular DNA-sequences relies on sequence dependent deviations from canonical B-DNA. These sequence dependent variations can be used as finger prints by proteins and drugs, which recognize and bind selectively to specific DNA-sequences.

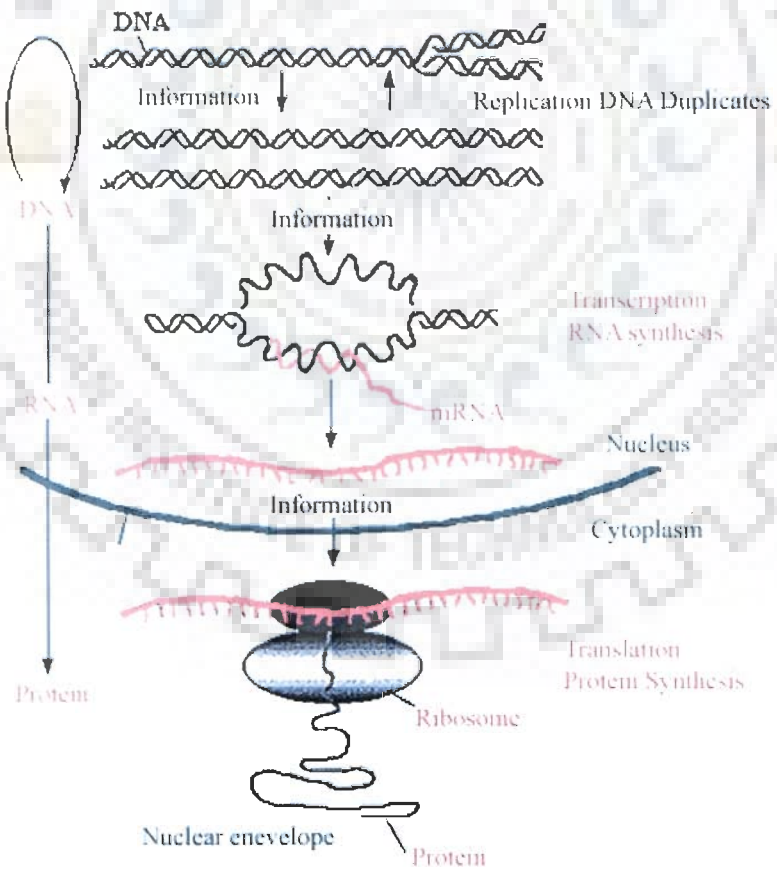


**Figure 1.1: The "Central Dogma of Molecular Biology" depicting the key cellular Processes of DNA replication and translation.**

## 1.2 Structure of Nucleic Acids

DNA can be found in three principal forms: A, B, and Z. Most common DNA conformation in vivo is B Form, which is favored at high water concentrations. The A form occurs under anhydrous conditions (<75% relative humidity), and found in most of the RNA and RNA-DNA duplex. Z Conformation is favored by high salt concentrations, some base substitutions, but requires alternating purine - pyrimidine sequence. The main features of A, B and Z DNA are listed in Table 1.1.

DNA is composed of units of purine and pyrimidine bases (Nucleotide) attached to a backbone of a 5-carbon sugar (dexoyribose) alternating with a phosphate group. The purine bases— adenine (A) and guanine (G), and pyrimidine bases— thymine (T) and cytosine (C) are paired together A to T and G to C (Figure 1.2).

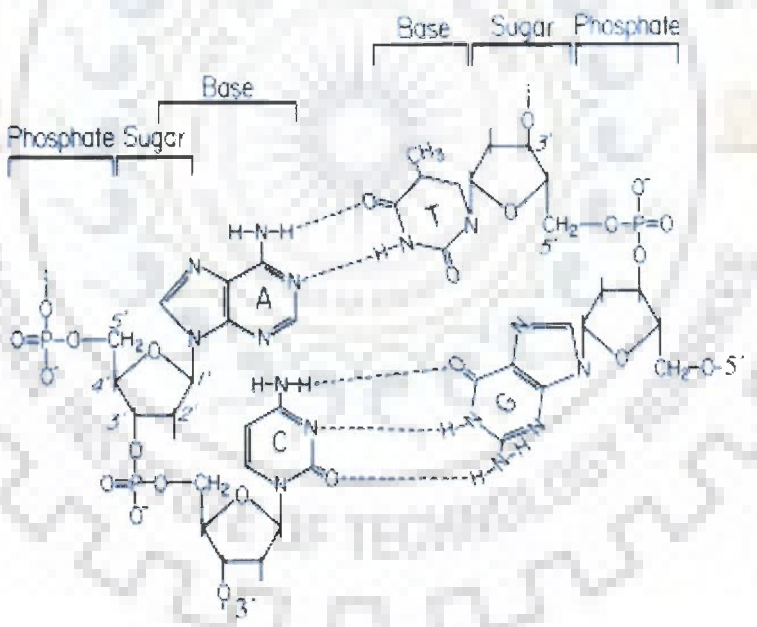


**Figure 1.2: Watson and Crick base pairing between Adenine-Thymine and Guanine-Cytosine.**

**Table 1.1: Structural characteristics of A, B and Z type of double helix nucleotides.**

| | B DNA | Z DNA | A DNA |
|---|---|---|---|
| **Helix sense** | Right-handed | Left handed | Right handed |
| **Repeating unit** | 1bp | 2 bp | 1 bp |
| **Rotation/bp** | 35.9° | 60°/2 | 33.6° |
| **Mean bp/turn** | 10.0 | 12 | 10.7 |
| **Inclination of bp to axis** | -1.2° | -9° | +19° |
| **Rise/bp along axis** | 3.32Å | 3.8 Å | 2.3 Å |
| **Pitch/turn of helix** | 33.2Å | 45.6 Å | 24.6 Å |
| **Mean propeller twist** | +16° | 0° | +18° |
| **Glycosyl angle** | anti | C: anti, G: syn | anti |
| **Sugar pucker** | C2'-endo | C: C2'-endo, G: C2'-exo | C3'-endo |
| **Diameter** | 20 Å | 18 Å | 26 Å |

### 1.2.1 Purines: Adenine and Guanine

Two different heterocyclic aromatic bases with a purine ring (composed of carbon and nitrogen) are found in DNA (Figure1.3 a). Adenine has an amino group (-$NH_2$) on the C6 position of the purine ring. Guanine has an amino group at the C2 position and a carbonyl group at the C6 position. Besides these, minor bases like inosine, 7-methyl guanosine, etc. are also found as components of nucleic acids.

### 1.2.2 Pyrimidines: Thymine, Cytosine and Uracil

Thymine contains a methyl group at the C5 position with the carbonyl group at C4 and C2 positions. Cytosine contains a hydrogen atom at the C5 position and an amino group at C4 (Figure 1.3 b). In RNA thymine is replaced by uracil.

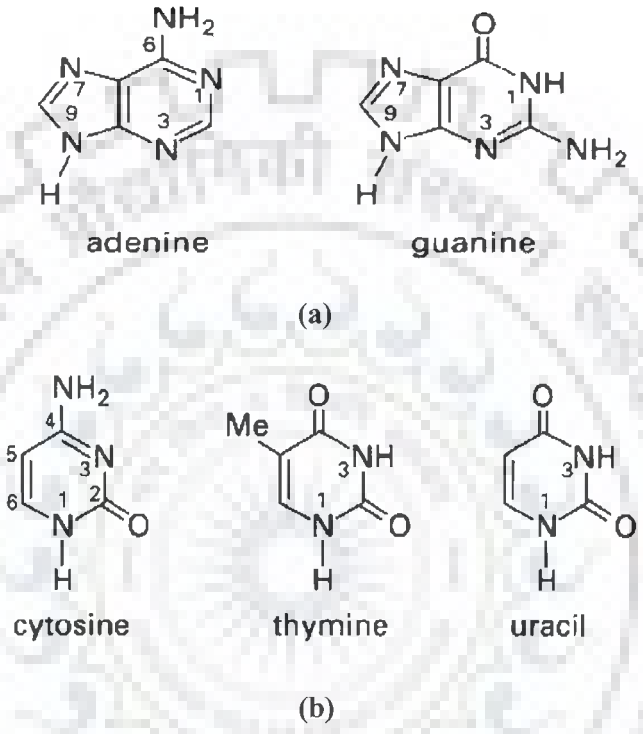


**Figure 1.3: Structural formulas of purines (a) and pyrimidines (b)**

### 1.2.3 Sugar

Ribose sugar is found in all RNA molecules while a slightly different sugar, β-D-2-deoxyribose is found in DNA. This is a derivative of β-D-ribose in which the hydroxyl (-OH) at the 2' position is replaced by hydrogen (-H) (Figure 1.4). The sugar moiety of DNA is one of the more flexible and dynamic parts of the molecule. The sugar base combination is called nucleoside unit. A nucleotide is a nucleoside phosphorylated at one of the free sugar hydroxyls.

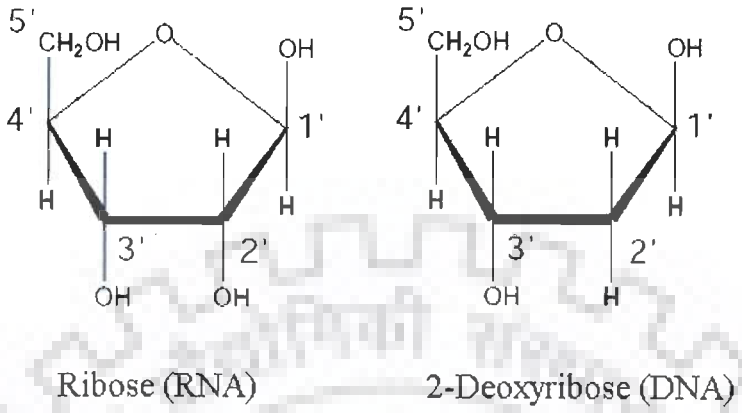


**Figure 1.4: Five membered furanose ring of deoxyribose and ribose sugar.**

### 1.2.3.1 Sugar Pucker

Usually all complexes have purine sugar at the 5' position in C3'–endo pucker. In most of them, the pyrimidine sugar at the 3' end is C2'–endo with only few cases of C3'–endo are found (Figure1.5). Upon intercalation both $\chi$ and $\beta$ increase by over 50°, $\chi$ being pushed into high anti range. Model building studies suggested that the unwinding angle is dependent on a combination of small variations in the backbone torsion angles and base–pair geometry expressed as bend and twist, and not just on sugar puckering. It is clear that a correlation exists between unwinding angle and shape of intercalator agent.

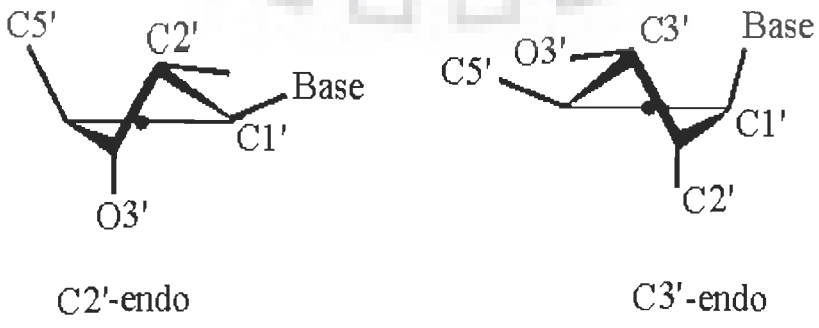


**Figure 1.5: Preferred conformations C2'–endo and C3'–endo of sugar pucker**

### 1.2.3.2 Endocyclic Torsional Angles: Furanose Sugar Ring

The sugar ring occupies a pivotal position in the nucleotide unit because it is part of both the backbone and the side chain. In order to provide a complete description of the ring conformation, it is necessary to specify the endocyclic torsion angles for the ring as well as the bond lengths and bond angles. The five endocyclic torsion angles (Figure 1.6) for the bonds O4'–C1', C1'–C2', C2'–C3', C3'–C4' and C4'–O4' are denoted by the symbols, $\upsilon_0$, $\upsilon_1$, $\upsilon_2$, $\upsilon_3$ and $\upsilon_4$ respectively.

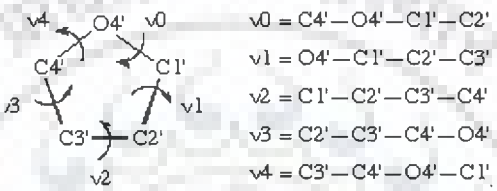


**Figure 1.6: A ribose unit showing atomic numbering and definition of torsion angles, ν0, ν1 , ν2, ν3 and ν4**

### 1.2.3.3 Sugar Ring Torsion Angles: Pseudorotation

The conformation of the ribose ring can be described by only two quantities; sugar pucker phase angle and sugar pucker amplitude. Pucker phase angle and pucker amplitude are calculated from the torsion angles about the five bonds in the ribose ring (Figure 1.6). Conformations of cyclic systems introduce some constraints due to ring closure. In sugar, there are five atoms in the ring and we need N–3 = 2 torsion angles to define its three dimensional geometry. The torsion angles in a closed ring are highly correlated. Thus, out of five torsion angles $\tau_0$-$\tau_4$ two are enough to define the geometry of the ring. C3' endo or $^3$E conformation is when C3' is on the same side of the plane described by the C5' atom (Figure 1.5). When C3' is 0.6 Å below the

plane, the conformation is called C3' exo or $_3$E. The most prominent conformations are C2'-endo in B-helices and C3'-endo in A-helices. At room temperature both conformers are in a dynamic equilibrium. Transitions occur via the O4'-endo state. Intermediates between C2'-endo and C3'-endo are found in several (time-averaged) structures obtained from NMR and X-ray crystallography. When changing the pucker phase angle from 0° to 360° we step through all possible conformations of the ribose ring. This pseudo-rotation cycle can be depicted as a conformational wheel (Figure 1.7). The values of $\tau_1$ corresponding to these conformations are ± 25.5°. The conformation of the sugar ring is described by two parameters P and $\delta$ [Altona and Sundaralingam, 1972]. The five torsion angles $\tau_0$- $\tau_4$ are related to these parameters by the equation:

$$\tau_j = \tau_m \cos [P + (j-2)\delta]$$

with

$$\tan P = \frac{(\tau_4 + \tau_1) - (\tau_3 + \tau_0)}{2(\tau_3 (\sin 36° + \sin 72°)}$$

where $\tau_m$ = 38°, $\delta$ = 144°, respectively; j = 0-4. As P goes through the complete pesudorotation cylce (0° to 360°), values of $\tau_0$-$\tau_4$ range from $-\tau_m$ to $+\tau_m$ through 0°. The conformational states that have a P value 0° ±18° and 180° ± 18° corresponds to two isomeric states, denoted by N and S to indicate that they cover the north and south parts of the conformational wheel as shown in Figure 1.7. An energy barrier of about 4.0 Kcal/mol separates these two rotational states.

### 1.2.4 The Phosphodiester Bond

In DNA and RNA the individual nucleotides are joined by a 3'-5' phosphodiester bond.

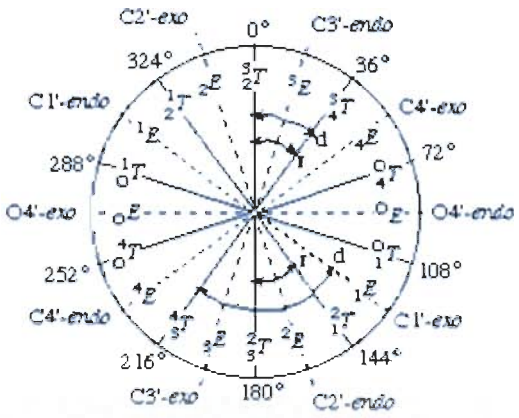


**Figure 1.7- Pseudorotation cycle of furanose ring in sugar pucker.**

The nucleotides are joined from the 3' sugar carbon of one nucleotide, through the phosphate to the 5' sugar carbon of adjacent nucleotide. This is termed as 3'-5' phosphodiester bond (Figure 1.2). The primary sequence of nucleic acids is determined by the sequence of bases along the nucleotide chain and the function of acids namely replication, transcription and translation are governed by this sequence.

### 1.2.5 Glycosyl Torsion Angle (χ)

The glycosyl torsion (χ) angle define the orientation of the purine and pyrimidine bases relative to sugar ring. For pyrimidine nucleoside, χ is defined as torsion angle O4'-C1'-N1-C2 and for purines χ is O4'-C1'-N9-C4. Relative to the sugar moiety the base can adopt two main orientations about the glycosyl C1'-N link, called *syn* and *anti* (Figure 1.8). Rotamers with *chi* values between -90° and +90° are called *syn* whereas *anti* refers to *chi* values from +90° to +270°. In Watson-Crick double helices both bases of a base pairsare in *anti* conformation. Bases in *syn* conformation indicate a distortion of the double helix due to base pair opening or mismatched base pairs.

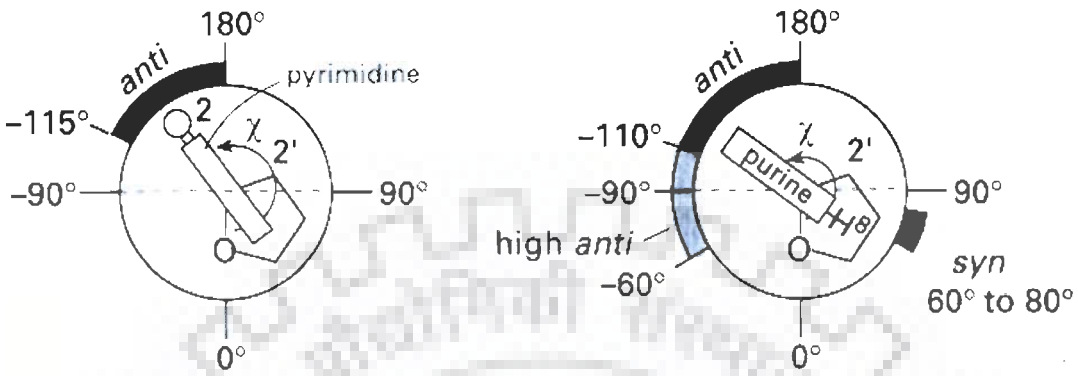


**Figure 1.8: Anti high, anti and syn orientations about the glycosidic bond in pyrimidine and purines.**

The *syn* conformation is also found with guanines in left-handed Z-DNA (zig-zag helix). In *anti*, the bulk of heterocyclic atoms i.e., the six-membered pyrimidine ring in purines and O2 in pyrimidines is pointing away from the sugar, and in *syn*, pyrimidine is over and toward the sugar. An *anti* conformation is located near $\chi = 0°$, whereas in *syn* domain is around 210°. There is also a high *anti* which denotes a torsion angle lower than *anti*.

### 1.2.6 Backbone Torsional Angles

The sugar phosphate backbone conformation is fixed by the values of six conformational angles. The sequential numbering of atoms $_{(n-1)}$P - O 5' - C5' - C4' C3' - O3' - P - O5'$_{(n+1)}$ is defined by torsion angles α, β, γ, δ, ε and ζ (Figure 1.9). Duplex DNA is a right-handed helix formed by two individual DNA strands aligned in antiparallel fashion. The bases are stacked near the center of the cylindrical helix. The hydrophobic interactions provide stability to the helix. A common feature of all the double helices is base stacking. Although the geometry of adjacent base pair

varies, in each case the distance between neighbouring base pair plane is about 3.4 Å. This is equal to van derwaal's radius of planar aromatic compound. It was shown that purines cause large upfield chemical shift due to stacking as compared to pyrimidines.

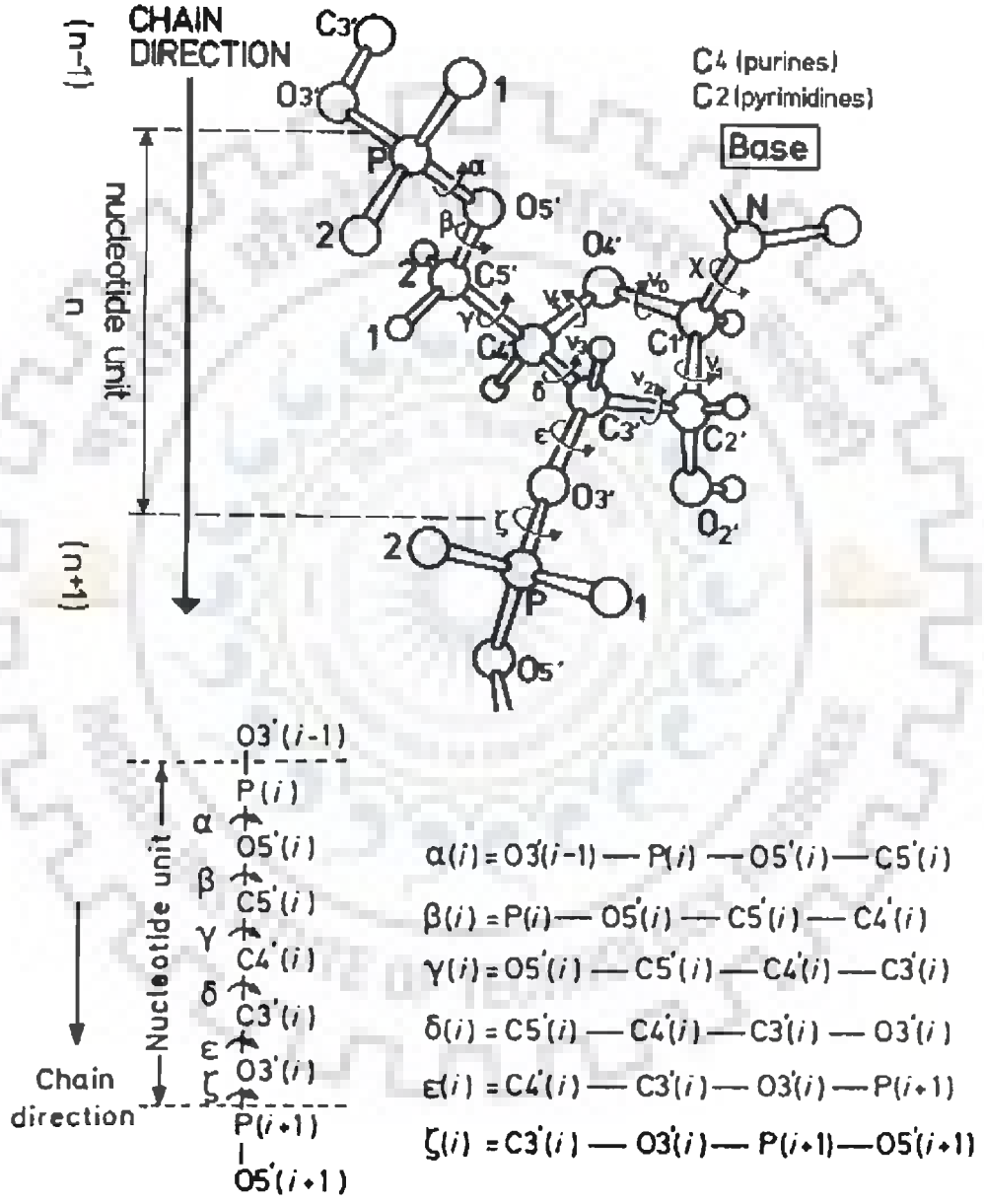


**Figure 1.9: Section of a polynucleotide backbone showing the atom numbering and the notation for torsion angles.**

## 1.3 Drug - DNA Interactions

The ability to understand the interactions of small molecules with specific DNA sequences is fundamental in any attempt to control gene expression. In designing novel chemotherapeutic agents, one of the major strategies is to develop novel DNA binding ligands that influence crucial cellular processes such as DNA topology, replication, transcription, and DNA repair [Chaires, 1998; Panousis and Phillips, 1994]. Systematic modifications of clinically effective chemotherapeutic agents have the potential for positively influencing their activity and delivery. Fundamental to this approach is the rigorous description of the interactions of known DNA binding agents with their macromolecular target. Ethidium bromide has served as a classic model for small molecule-DNA interactions for more than four decades. Anti-cancer therapies often target the DNA to inhibit the rapid replication of cancer cells. Many diseases such as diabetes, Lupus, hemophilia, Huntington's disease, and Alzheimer's disease may be traced to over- or under-production of proteins or production of mutated proteins. DNA is the genetic material that codes for proteins; therefore, drug interactions with DNA which can affect this process are potential treatments for these types of diseases. The mode of action of some drugs for the treatment of cancer, genetic disorders, and viral diseases is thought to be based on their binding to DNA and their modification of DNA activity. The activity of the drug is often linked to the binding geometry. Thus, the potential activity of a drug could be assessed by detecting the DNA binding location and fit of the drug candidate. Structural tools such as X-ray crystallography and NMR spectroscopy, coupled with molecular modeling techniques and theoretical studies have considerable impact in advancing our understanding of the structural selectivity and the molecular basis for drug-DNA interactions and may also provide a key to more rational drug design.

### 1.3.1 Binding Modes-

The three principal mode of drug-DNA binding: first, through control of transcription factors and polymerases. Here, the drugs interact with the proteins that bind to DNA. Second, through RNA binding to DNA, forming DNA-RNA hybrids, which may interfere with transcriptional activity. Third, small ligand molecules that bind to DNA double helical structures by (i) intercalating between stacked base pairs thereby distorting the DNA backbone conformation and interfering with DNA-protein interaction or (ii) the groove binders. Both work through non-covalent interactions but the latter cause little distortion of the DNA backbone. Critical to the understanding of the function of such molecules is the characterization of their binding modes, which are usually investigated through ensemble measurements.

#### 1.3.1.1 Covalent DNA Binding Drugs

DNA alkylation is a key cellular event in the mechanism of action of many carcinogens, mutagens, and clinical antitumor agents [Blackburn and Gait, 1990]. Alkylation occurs preferentially at the nitrogen and oxygens in purines (particularly the N7 of guanine, which is the most nucleophilic site [Pullman and Pullman, 1981]. There are two types of alkylating agents: mono–functional (one reactive group) which cause single–strand breaks in DNA or damage bases and bi–functional (two reactive groups) which form cross–links. A large number of first generations of anti– cancer drugs were designed to combine a simple alkylating function. Their common feature is that they form an initial physical complex with DNA before covalently bonding to it. Many of them have also shown selective anti–tumor activity, this can be attributed to DNA binding specificity or to preferential metabolic activation by tumour cells. The mechanism of action of these anticancer agents is by alkyl group transfer and

they cause alkylation of DNA at N7 or N2 position of guanine (other sites as well) and interaction may involve single strands or both strands. Anthramycin is an anti–tumor antibiotic that binds covalently to N–2 of guanine located in the minor groove of DNA. Cisplatin is a transition metal complex *cis–diamine–dichloro–platinum* and clinically used as anticancer drug. The effect of the drug is due to the ability to platinate the N–7 of guanine on the major groove site of DNA double helix. Cis-diamminedichloroplatinum(ii) a potent antitumor drug is found to be in involve in the interstrand crosslinking of DNA[Paquet et al., 1996]. Other interactions involve the reaction of these drugs with amino, hydroxyl and phosphate groups of other cellular constituents. These drugs usually form a reactive intermediate ethyleneimonium ion.

Poly functional alkylating drugs offer resistance against cancer by increased ability to repair DNA defects, decreased cellular permeability to the drug, increased glutathione synthesis, which inactivates alkylating agents through conjugation reactions. Mitomycin C is a well characterized anti–tumor antibiotic, which forms a covalent interaction with DNA after enzymatic reductive activation of its quinone to alkylate DNA. The activated antibiotic forms a cross–linking structure between guanine bases on adjacent strands of DNA thereby inhibiting single strand formation which is essential for m–RNA transcription and DNA replication.

#### 1.3.1.2 Noncovalent DNA Binding Drugs

Double-stranded (ds) DNA offers a number of potential binding sites and modes of noncovalent interactions for small molecules, namely, (a) electrostatic interactions between cationic ligands and the polyanionic backbone of DNA, (b) intercalation of a planar ring system between adjacent base pairs, and (c) hydrogen bonding interactions with the bases usually in the minor groove of DNA. There are a

number of examples of drugs that bind to DNA using combinations of these binding modes. For example, safranine T binds to DNA via intercalation and electrostatic interactions [Cao and He, 1998].

### 1.3.1.3 Intercalators

Intercalators are the most important group of compounds that interact reversibly with the DNA double helix. Intercalators typically contain a planar ring system and incorporate a positive charge. These are clinically useful anticancer antibiotics, which are primarily derived from *Streptomyces peucetius*. Some of them are valuable anticancer drugs currently used for the treatment of ovarian and breast cancers and acute leukemia, while many others are in different phases of clinical trials. Intercalating agents share common structural features such as the presence of planar polyaromatic systems, which bind by insertion between DNA base–pairs, termed as intercalation [Lerman, 1961]. Binding of peptides to polynucleotides by intercalation are also reported [Rajeswari, 1996].

Nowadays it is well accepted that the anti–tumor activity of intercalators is closely related to the ability of these compounds to stabilize the DNA–intercalator–topoisomerase II ternary complex. Majority of these drugs have shown marked preference for 5'–pyrimidine–purine–3' steps. The chromophores are linked to basic chains that might also play an important role in the affinity and selectivity shown by these compounds. Bis–intercalators have two potential intercalating ring systems connected by linkers, which can vary in length and rigidity. They also alter membrane fluidity and ion transport. One potential mechanism is based on the ability of these agents to participate in electron–transfer processes, with the subsequent generation of free radicals. The property results from the presence of two very different types of

redox–active groups, namely the quinone and hydroquinone moieties on daunomycin and adriamycin. Quinone moiety of daunomycin undergo one–electron reduction to a semiquinone radical, which in the presence of oxygen gives rise to superoxide and other reactive oxygen species. The first crystal structure with a mono–intercalator and oligonucleotide was obtained by Wang and co–workers [Wang et al., 1987] for a complex of antibiotic daunomycin and d–$(CGTACG)_2$.

### 1.3.1.4 Groove Binding Molecules

The major and minor groove differs significantly in electrostatic potential, hydrogen bonding characteristics, steric effects and hydration. Minor groove binding drugs are typically thin and crescent shaped to sterically fit into the narrow minor groove. This creates compounds, which with the appropriate twist, can fit into the helical curve of the minor groove with displacement of water from the groove and forming Van der Waalls contacts with the helical chains which define the walls of the groove. Their crescent shape is complementary to the natural curvature of the minor groove of B-DNA. They do not change the gross structure of DNA. Additional specificity in the binding comes from contacts between the bound molecule and the edges of the base pairs on the 'floor' of the groove. Thus, the aromatic rings of many groove binding molecules form close contact with AH2 protons in the minor grooves of DNA. Pullman and coworkers [Pullman and Pullman, 1981] have shown that the negative electrostatic potential is greater in the A.T minor groove than G.C rich regions, and this provides an additional important source for A.T specific minor groove binding of cations. Examples of minor groove binding drugs are berenil, netropsin and distamycin Hoechst 33258, and chromomycin [Neidle, 2001]

### 1.3.2 Other Anticancer Agents

#### 1.3.2.1 Antimetabolites - Nucleic Acid Synthesis Inhibition

Purine antagonists like mercaptopurine act by hypoxanthine–guanine phosphoribosyl transferase (HGPRT) to form 6–thioinosinic acid, which inhibits enzymes involved in purine metabolism. Thioguanine which acts as inhibitor of purine nucleotide pathway is an enzyme which decreases intracellular concentration of guanine nucleotides and inhibit glycoprotein synthesis, finally blocking DNA / RNA synthesis.

#### 1.3.2.2 Topoisomerase Targeting Drugs

Chromosomal DNA is extensively twisted and topoisomerases permit selected regions of DNA to untangle so as to allow transcription and replication. These enzymes temporarily break DNA, allowing for topological changes, and then reseal the breaks. Topoisomerase targeting drugs like etoposide stabilizes the topoisomerase II–DNA complex preventing it from making a topological change. This results in an irreversible double strand break, which is lethal to cells in S and G2 phases. Six anti–neoplastic drugs targeting topoisomerase II, i.e., doxorubicin, daunorubicin, idarubicin, mitoxantrone, etoposide and teniposide are currently approved for clinical use in the United States. Synthetic topoisomerase inhibitory analogs are also stuidied [Singh et al., 1992].

DNA topoisomerase II is a ubiquitous enzyme that is essential for the survival of all eukaryotic organisms and plays critical roles in virtually every aspect of DNA metabolism. The enzyme unknots and untangles DNA by passing an intact helix through a transient double–stranded break that it generates in a separate helix. Beyond its physiological functions, topoisomerase II is the target for some of the most active

and widely prescribed anticancer drugs currently utilized for the treatment of human cancers. DNA is an extremely important target for drug action, with a wide range of biological activities (anti-tumor, antiviral and antimicrobial) arising from the ability of compounds to bind sequence specifically to DNA and interfere with DNA topoisomerases or with transcription binding factor [Hélène et al., 1985]. These antibiotics act by intercalating between base pairs of DNA causing lengthening of the double helix and a decrease in the helical twist on unwinding, inducing mediated strand scission. These drugs act in an insidious fashion and kill cells by increasing levels of covalent topoisomerase II–cleaved DNA complexes that are normally fleeting intermediates in the catalytic cycle of the enzyme. The anti–tumor topoisomerase II inhibitors presently used in the clinic, poison the enzyme by stabilizing cleavable complexes, presumably by increasing the rate of forwards reaction i.e. more rate of DNA cleavage or by decreasing the rate of backward reaction i.e. slow rate of religation of cleaved DNA (Figure 1.10). Thus synthesis of DNA and RNA is blocked.

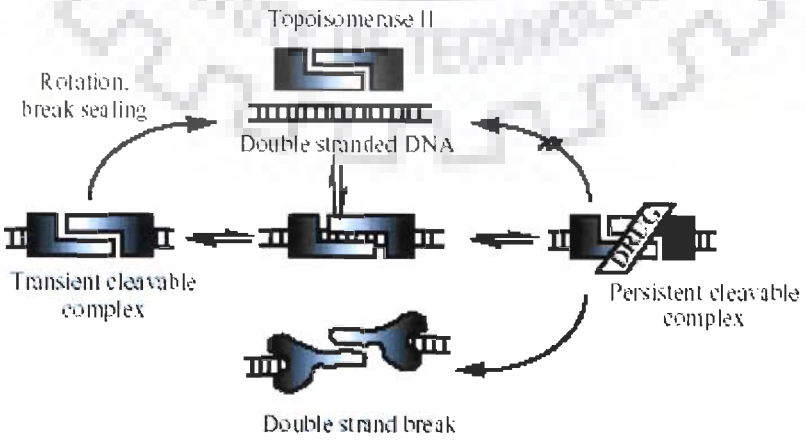


**Figure 1.10: DNA damage induced by inhibition of Topoisomerase II.**

### 1.3.2.3 Microtubule Inhibitors

Microtubules are protein polymers involved in cellular movement and morphology. Microtubules occur in equilibrium between polymerized and free tubulin dimers. Inhibitor drugs disrupt this equilibrium. Vinca alkaloids (vinblastine, vincristine) are examples of this type of drugs.

## 1.3.3 Forces Involved in Drug-DNA Interaction

### 1.3.3.1 Hydrogen Bonding

The phosphate group, sugar, bases in nucleic acids and hydrophilic groups in drug participate in hydrogen bonding with water. Since all linear hydrogen bonds have similar free energies, they make little net contribution to the favorable free energy change when drug and nucleic acid interact in solution. By contrast, formation of poorly aligned hydrogen bonds, or absence of some of them on the complex formation, carries a free energy penalty of about 4 KJ $mol^{-1}$. Thus hydrogen bonds are one of the most important means of making sequence specific interaction of nucleic acid with drug.

### 1.3.3.2 Electrostatic Forces: Salt Bridges

Salt bridges are electrostatic interactions between groups of opposite charge. They typically provide about 40 KJ $mol^{-1}$ of stabilization per salt bridge. In drug–DNA complexes, strength of salt bridges decreases with the increase in concentration of the salt. They are much stronger when there are no water molecules between the ionized groups because water has a high dielectric constant. These are relatively long–range forces.

#### 1.3.3.3 Entropic Forces: The Hydrophobic Effect

The hydrophobic effect is due to the behavior of water at an interface. Any molecule in water creates a sharply curved interface and so orders a layer of water molecules around itself. When molecules aggregate, the ordered water molecules at the interface are released and become part of the disordered bulk water, thus stabilizing the aggregate by increasing the entropy of the system.

Polar surfaces, where the enthalpy loss tends to offset the entropy gain or desolvation are less likely to aggregate than non–polar ones. Molecules of water left at the interface between the drug and the nucleic acid obviously decrease the entropy of the system. Therefore, the surface of the non–planar aromatic chromophore of drug tends to be exactly complementarily so that no unnecessary water molecules remain when the complex forms.

#### 1.3.3.4 Base Stacking: Dispersion Forces

Base stacking is caused by two kinds of interaction: the hydrophobic effect mentioned above and dispersion forces. Molecules with no net dipole moment can attract each other by a transient dipole–induced–dipole interaction. Such dispersion forces decreases with the inverse sixth power of the distance separating the two dipoles, and so are very sensitive to the thermal motion of the molecules involved. Despite their extreme distance dependence, dispersion forces are clearly important in maintaining the structure of double stranded nucleic acids because they help to cause base stacking. Besides they also allow the aromatic ring of the drug to intercalate between bases and stabilize it by base stacking.

### 1.3.4 NMR Spectroscopy, UV-visible And Fluorescence Spectroscopy Involved in Drug –DNA Interaction

Knowledge of the bound conformation of a ligand, and particularly of the key functionalities involved in binding is crucial to the rational design of more potent and specific drugs. Two-dimensional NMR methods have made it possible to assign the signals arising from the bound ligands and to use intramolecular NOEs to determine conformations of bound DNA. In addition, NOEs from the ligand to the target molecule may be used to determine the regions of the two species, which are directly involved in the intermolecular interactions. Restrained Molecular Dynamics (rMD) is a step further by NMR data obtained in the form of interproton distances and torsional angles are continually being improved. As greater accuracy is attained, greater confidence can be placed in the precision of the structures, which are solved. Obviously refinement and model building is an integral part of biomolecular NMR structure determination. Whether employed alone or in combinatorial treatment regimen, anthracycline antitumor agents such as doxorubicin (adriamycin), the prototypical agent, remain amongst the most effective drugs for certain malignancies. Unfortunately, the original anthracycline antitumor agents suffer from a number of well known and significant drawbacks including their being substrates for the p-glycoprotein (P-gp) drug efflux mechanism associated with cellular drug resistance and the unfortunate ability to produce dose-dependent cumulative cardiotoxicity. Thus, considerations of toxicity and efficacy have, over the past three decades, driven the worldwide efforts at the development of new anthracycline antitumor agents.

NMR spectroscopy has enjoyed many advances recently, and the pace of development shows no signs of slowing. These advances are allowing NMR to help solve important problems in the field of drug discovery. NMR spectroscopy is now

being used to determine protein structures, to monitor ligand-receptor binding, to study diffusion, to analyze mixtures using LC-NMR, to analyze solid-phase synthesis resins and to determine the structures of organic small molecules. It is not only limited to the solution only, its use in lyotropic crystals and Liquid crsytals is a very important for some kind of systems from ancient time [Khetrapal and Diehl, 1975; Kunwar, 1991]. Biomolecular NMR spectroscopy has expanded dramatically in recent years and is now a powerful tool for the study of structure, dynamics, and interactions of biomolecules. NMR spectroscopy is already well-established as an efficient method for ligand screening. A number of recently developed techniques show promise as aids in structure-based drug design. An advantage of the method is that all these interactions can be studied in solution-time-consuming crystallization is not necessary. Being in solution form, even structural and biochemical changes in intact cells (in vivo NMR) can be monitored. Nuclear Magnetic Resonance (NMR) spectroscopy uses radiation to induce nuclear spin state changes which are unique for different atoms and their local environment. From the 1D and 2D NMR spectrum acquired on solid or liquid samples, the structure of molecules can be deduced. NMR can observe static as well as dynamic interactions between molecules. It requires that the sample to be dissolved in a deuterated solvent. The most commonly used resonances in NMR studies are $^{1}H$, $^{13}C$, $^{31}P$ and $^{15}N$. $^{1}H$ NMR gives rise to a series of absorption lines in the region 0-15 ppm. A larger spectral dispersion of chemical shifts is observed in $^{13}C$ NMR. In $^{15}N$ NMR, chemical shifts are sensitive to primary structure as well as molecular conformation. But it has low sensitivity due to low natural abundance (0.36%) which causes difficulties in its detection hence offers limited applications of $^{15}N$ NMR. $^{31}P$ NMR has developed as a powerful probe of the structure and dynamics of DNA due to existence of spin ½, 100% natural abundance,

moderate relaxation times, wide range of chemical shifts and non-interference from solvent peaks. In $^{31}P$ NMR, chemical shifts are sensitive to molecular conformation of the phosphate group. Thus it becomes very informative in case of nucleic acid structure elucidation since backbone of DNA and RNA contains phosphorus nuclei. NMR spectroscopy can provide both qualitative and quantitative information. This information can benefit numerous disciplines in drug discovery, including natural products research, synthetic medicinal chemistry, metabolism studies, drug production, quality control, rational drug design and combinatorial chemistry. This focuses on how they might be of value in removing some of the current "bottlenecks" in structure-based drug discovery.

Fluorescence spectroscopy provides structural information on the basis of emission and excitation wavelength. The fluorophore has different emission and excitation wavelengths which gives different spectra ranging from 200-800nm. UV-Vis spectroscopy uses the wavelengths of light in the spectrum ranges of 120 to 800 nm. DNA typically absorbs in the region of 160 to 300 nm due to the electronic transitions regions of the bases. These techniques are conducted in solution and are simple to conduct, but average the results across molecules in different states. New anticancer drug can be screened, by these methods, for example specific designed peptides interaction study with different oncogenes provides sufficient knowledge about their mode of action [Aklank Jain and Rajeswari, 2003; Jain et al., 2005].

### 1.3.5 Molecular Modeling Study Involved in Drug-DNA Interactions

Molecular modeling is a broad term that encompasses ab initio quantum mechanical calculations, semi-empirical calculations, and empirical calculations (charge-dependent molecular mechanics force fields). These techniques can be used

to study the three-dimensional structure, dynamics, and properties of a molecule of interest. Molecular modeling can identify and define the possible key details of the molecular interaction and, using the graphics/computational approach, decide on optimal structural modifications likely to enhance either general binding affinity or recognition of a particular nucleotide-binding site. A number of studies have revealed the converse, with the discovery that particular patterns of chemical modification on a given drug (e.g., doxorubicin) can result in both low biological activity and low-ranking interaction energy.

The molecular modeling, particularly molecular mechanics and dynamics, are highly complementary to macromolecular NMR and X-ray crystallography. Molecular dynamics simulation can, in principle, provide a complete theoretical description of DNA structure and motions, and are thus a valuable independent means of developing models and interpreting experimental data. A combined approach is desirable and, where the parent experimental structure is available, the simulation can be partially validated by reproducing the structure, thus paving the way for 'rational drug-designing'. For "rational" drug design, choice of a target, the evaluation of a structure of that target, the pivotal questions to consider in choosing a method for drug lead discovery, and evaluation of the drug leads.

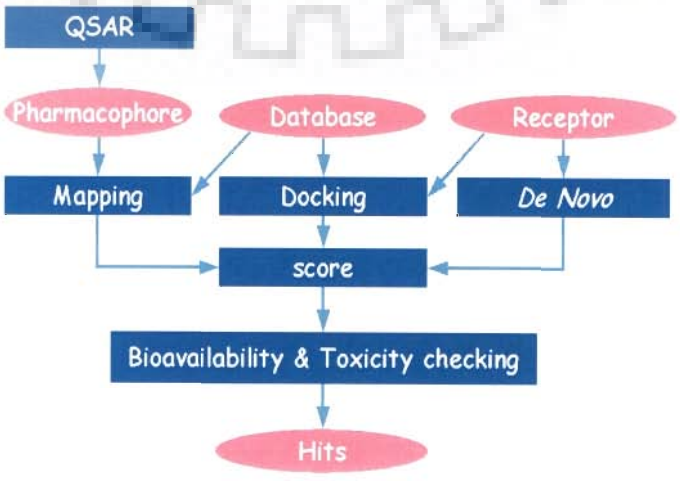

## 1.4 Literature Review

Traditional medicines, including Chinese herbal formulations, can serve as the source of potential new drugs, the development of novel plant-derived natural products and their analogs for anticancer activity details efforts to synthesize new derivatives based on bioactivity- and mechanism of action-directed isolation and characterization coupled with rational drug design - based modification. Also, the anticancer activity of certain natural products and their analogs can be enhanced by synthesizing new derivatives based on active pharmacophore models; drug resistance and solubility and metabolic limitations can be overcome by appropriate molecular modifications; and new biological properties or mechanisms of action can be added by combining other functional groups or molecules. Preclinical screening for in vitro human cell line panels and selected in vivo xenograft testing then identifies the most promising drug development targets.

The role of natural products as a source for remedies has been recognized since ancient times [Cragg et al., 1999; Farnsworth et al., 1985] Several plant-derived compounds are currently successfully employed in cancer treatment. One of the most significant examples is the vinca alkaloid family isolated from the periwinkle *Catharanthus roseus*, which is found in the rain forests of Madagascar [Noble, 1990]. Vincristine inhibits microtubule assembly, inducing tubulin self-association into coiled spiral aggregates. Another example of a highly active agent derived from a natural product is etoposide, which has produced high cure rates in testicular cancer when used in combination with bleomycin (also derived from a natural product) and cisplatin [Williams et al., 1987]. In addition, the camptothecin derivatives irinotecan and topotecan, have shown significant antitumor activity against colorectal and ovarian cancer respectively [Creemers et al., 1996]. These compounds were initially

obtained from the bark and wood of Nyssacea *Camptotheca accuminata* and act by inhibiting topoisomerase I [Liu et al., 2000]. The taxanes and the camptothecins are presently approved for human use in various countries. Flavopiridol is one of the most exciting plant-based agents currently in development, representing the first cyclindependent kinase inhibitor to enter the clinic [Kelland, 2000]. Flavopiridol is a synthetic flavone derived from the plant alkaloid rohitukine, which was isolated from the leaves and stems of *Amoora rohituka* and later from *Dysoxylum binectariferum* (Maliaceae) [Cragg and Suffness, 1988; Kelland, 2000]. However, an increasing reliance on the use of medicinal plants in the industrialized societies has been traced to the extraction and development of several drugs and chemotherapeutics from these plants Medicinal values of these plants are due to the presence of small doses of active compounds which produces physiological actions in human and animal bodies. Some of the important bioactive compounds in these plants are alkaloids, glycosides, resins, gums, & mucilage's. There are enumerating reports in the literature or the anticancer/ antiviral/ antidiabetic and anti microbial activity of these plants. One of the important medicinal plants is common Berberry. It is a well known, bushy spiny shrub, with pale–green deciduous leaves. It has different local names in different parts of India, some of them are darhaldi (Bengal), kashmoi (Garhwal), kashmal (Himachal pradesh), chitra, darhald, rasaut, kashmal (Hindi), maradarishna (kerela) chutru (Nepal), simli, sumlu,(Punjab), mullukala (Tamilnadu) suvarnavarna (Sanskrit). Almost every part of this plant has some medicinal value. This shrub wildly grows in Himalayan and Sub-Himalayan tract at high altitude. It also grows in Nilgiris and Ceylon. Many plants from which berberine alkaloid can be extracted some of them are listed in Table 1.2.

**Table 1.2: Sources of berberine.**

| Scientific name | Common name |
|---|---|
| ***Berberis vulgaris*** | (Barberry, Common) |
| ***Berberis thunbergii DC.*** | Japanese barberry |
| ***Berberis aristrata*** | (Darlahad Nepal Barberry, Ophthalmic Barberry) |
| ***Mahonia haematocarpa*** | (red barberry) |
| ***Mahonia trifoliolata*** | (algerita) |
| ***Berberis darwinii*** | (Darwin's berberis) |
| ***Berberis canadensis P. Mill.*** | (American barberry) |
| ***Mahonia bealei (Fortune) arr.*** | (Beale's barberry) |
| ***Berberis wilcoxii*** | (Wilcox's barberry) |

Alkaloids occupy an important position in chemistry and pharmacology. Alkaloids are nitrogen-containing bases produced mostly by higher plants during metabolism. Protoberberine alkaloids and related compounds represent an important class of molecules and have attracted recent attention for their various pharmacological activities. Protoberberines are the group of naturally occurring isoquinoline alkaloids having the same tetracyclic structures but different substituents. The protoberberine alkaloid berberine and berberrubine are among the most widely distributed alkaloids of the isoquinoline series and are a new class of organic cations that exhibit topoisomerase poison activity [Gatto et al., 1996; Li et al., 2000; Makhey et al., 1996].

### 1.4.1 Therapeutic Potential of Berberine

The medicinal value of protoberberine alkaloid found in root, rhizome and stem bark of *Berberis vulgaris* L. plant has been recognized since ancient times. Apart

from its anti-cancerous properties, it also displays a great variety of biological and pharmacological activity e.g. antimicrobial [Hu et al., 2000], antiplasmodial ,[Wright et al., 2000] antidiarrhoeal [Baird et al., 1997], cardiovascular [Lau et al., 2001], etc. Replacement of $OCH_3$ group at position $7^{th}$ in berberine with OH group, resulting in a derivative called berberrubine, induces a large change in the antitumor activity [Kim et al., 1998].

Over the last decade protoberberine alkaloids have attracted considerable attention as they display a wide range of biochemical and pharmacological actions The overall biological profile of protoberberines [Kettmann et al., 2004] shows a very high antineoplastic and cytotoxic activities, which have been demonstrated against numerous cancer cell lines. Some of the important biological activity has been discussed in following.

#### 1.4.1.1 Bacterial Diarrhea

Studies have been shown that berberine directly inhibits some *V. cholera* and *E. coli* enterotoxins [Sack and Froehlich, 1982], significantly reduces smooth muscle contraction and intestinal motility, and delays intestinal transit time in humans. Berberine sulfate have shown bacteriocidal activity against *V. cholera*. In the case of *E. coli*, in vitro research indicated berberine sulfate was capable of inhibiting bacterial adherence to mucosal or epithelial surfaces, the first step in the infective process. This may be a result of berberine's inhibitory effect on fimbrial structure formation on the surface of the treated bacteria.

#### 1.4.1.2 Intestinal Parasite

Berberine sulfate has been shown to posses growth inhibitory activity against *Giardia lamblia, Trichomonas vaginalis*, *Entamoeba histolytica* [Kaneda et al.,

1991]. Crude extract of *Berberis vulgaris* is more effective than the salt may be due to the cumulative effect of berberine along with other alkaloids and pharmacologically active constituents [Kaneda et al., 1990]. Berberine have shown significant effectiveness against visceral leishmaniasis.

#### 1.4.1.3 Cardiovascular Effects

Berberine upregulates the LDL receptor (LDLR) by a mechanism distinct from that of the statins, which involves stabilising the LDLR mRNA [Doggrell, 2005]]. Thus, this mechanism is unlikely to make berberine an attractive alternative to statins for lipid lowering in most circumstances. However, the other effects of berberine (antihypertensive, inotropic and class III antiarrhythmic properties) may make it a useful agent in the treatment of cardiovascular disease.

#### 1.4.1.4 Anti-Inflammatory Effects

Among berberines multi pharmacological actions is anti inflamatrory activity. In vitro a consistant and progressive inhibitory influence of beberine with increasing concentration was identified with all the mitogens [Ckless et al., 1995]. Berberine 20 mg/kg/day inhibited platelet aggregation and platelet adhesion induced by ADP, archidonic and collagen in rats [Wu and Liu, 1995]. A very recent study shows that Berberis koreana extract (BE) has a strong neuroprotective effect after ischemic stroke in gerbils, which is associated with the inhibition of the N-methyl-d-aspartate receptor. Summarizing, the potent neuroprotective effect of BE was found to be due to the inhibitions of COX-2 expression and PGE2 production and its antiinflammatory activity [Yoo et al., 2008].

### 1.4.1.5 Anti-Diabetic Activity

Berberine has been reported in the Chinese literature and several recent studies [Ko et al., 2005; Ni, 1988; Yin et al., 2002] to have beneficial effects in human type II diabetes, although its mechanism of action is not known. Lee et al demonstrated that in vivo administration of berberine has insulin sensitizing as well as lipid lowering properties in both db/db mice and high fat-fed rats. Berberine reduces fat mass primarily by decreasing the size of fat cells rather than fat cell number [Lee et al., 2006].

### 1.4.1.6 Anticancer Activity

Berberine is demonstrated to possess antitumor activity. It has been demonstrated [Hoshi et al., 1976; Ikekawa and Ikeda, 1982] that protoberberines shows significant antitumor activity on S-180, NF sarcoma, Ehrlich Carcinoma and L-120 experimental tumors by total packed cell volume method in mice. The effect of berberine is demonstrated by the flow cytometric analysis in the human hepatoma HepG2 cells. It shows that the S phase fraction is significantly reduced [Chi et al., 1994]. Dose-dependent effects of berberine are also reported on the cell cycle and apoptosis in the Balb/c 3T3 cells [Yang et al., 1996]. It is shown that berberine induces apoptosis in the promyelocytic leukemic HL-60 cells [Kuo et al., 1995]and in murine thymocytes [Miura et al., 1997]. Fukuda et al suggested that it is likely that the inhibition of COX-2 (Cyclooxygenase-2) promoter activity may be associated with antitumor and cytcistatic/cytocidal effects of berberine [Fukuda et al., 1999]. Chung et al. [Chung et al., 2000] report that berberine induces inhibition of the N-acetyltransferase activity and 2-aminofluorene-DNA adduct formation in human leukemia cell in a dose-dependent manner. The cell cycle analysis showed the

accumulation of cells in the G0/ G1 phase and a relative decrease of the S phase [Iizuka et al., 2000]. Hwang et al demonstrated that berberine exhibited significant cytotoxicity in hepatoma HepG2 cells through a mitochnondrial /caspases pathway in human hepatoma cells [Hwang et al., 2006]. In recent study effects of berberine concentration on the cell morphology, cell cycle and apoptosis/necrosis in the human promonocytic U937 as well as in the murine melanoma B16 cell lines has been proved berberine a promising anticancer agent [Letasiova et al., 2006].

### 1.4.1.7 Topoisomerase Inhibition Activity

Topoisomerase I & II are the intracellular target for a variety of active agents used in the treatment of human cancers. By stabilizing the covalent emzyme associated DNA complexes, these drugs shift the DNA cleavage/relegation equilibrium towards the cleavage state. Protoberberines are a new class of organic cations that are dual poisons of topoisomerases I and II [Gatto et al., 1996; Li et al., 2000; Makhey et al., 1996]. In the screening of the plant alkaloids for their ability to induce topoisomerase II-mediated DNA cleavage in vitro, Kim et al found that berberrubine shows a potent activity as DNA topoisomerase II poison [Kim et al., 1998]; however, despite much resemblance in chemical structure other protoberberine alkaloids such as berberine and palmatine did not act on topoisomerase II, although some are reported to target topoisomerase I [Pilch et al., 1997]. The drugs combine with enzyme-DNA complex and shift DNA cleavage-religation equilibrium towards cleavage; subsequently cause multiple DNA strand breaks leading to cell death. topoisomerase-II mediated DNA cleavage assays[Jeon et al., 2002; Kim et al., 1998]' showed that berberrubine stabilizes the topoisomerase-II-DNA cleavage complex in a site specific and concentration dependent manner. The berberine, on the other hand, is

found to be much less effective [Jeon et al., 2002; Kim et al., 1998] Further berberrubine induces unwinding of DNA suggesting intercalative binding [Kim et al., 1998]. Subsequent studies on human topoisomerase-I poisoning by protoberberine analogues have shown that substituents at 23, 25 and 26- position of ring D as well as 7-position in ring A are crucial for activity. Analogues having no subsituent or having OH group are more effective than those having $OCH_3$ group at position 7 of ring A [Li et al., 2000; Pilch et al., 1997]. Viscometric titrations and increase in $T_m$ from UV melting profiles of drug-DNA complexes show that binding of analogues having $OCH_3$ substituent at 4, 6- position is stronger than that for the analogues having $OCH_3$ at 7, 6- position. The results indicate that ring A and B intercalate between DNA base pairs in drug-DNA complex. On the other hand the drug-enzyme interactions responsible for topoisomerase-I activity involves substituent at 7-position ( OH, or $OCH_3$ or others) as well as substituents at ring D due to binding presumably to minor groove of DNA. The significance of 7-substituent in berberine analogues on drug-topoisomerase-II interaction has also been demonstrated by using 7-ethoxy carbonyl berberine, 7-N, N dimethyl carbamoyl berberine and other related complexes[Krishnan and Bastow, 2000]. Series of compounds bearing 7-O acyl, 7-O alkyl, 7-O benzoyl and 7-O esters showed strong antimicrobial activity against Gram positive bacteria and fungi as well as Ehrlich cells and S-180 tumor cells[Hong et al., 2000; Kim et al., 2002]. The relative activity of various compounds demonstrated the involvement of substituent at 7- position. Our results clearly indicate that having 7-OH group (berberrubine) is planer and hence a better binder to DNA than the compound having 7-$OCH_3$ group (berberine). Recently Qin et al has demonstrated the Topoisomerase I inhibition activity of Protoberbeines mone- and dimeric alkaoids and

suggested that the linker chain and $7^{th}$ position plays a very important role in Top I activity [Qin et al., 2007b].

### 1.4.2 Berberine Structure and Conformation-

A Few authors have attempted different experimental studies of the X-ray crystal structure and NMR of berberine [Blasko et al., 1988]. For the first time Blasko et al has reported the unambiguous assignment of the proton and carbon -13 NMR spectra of the protoberberines. Marek et al has elaborated the fact that $^{15}N$ Nuclei are sensitive indicators of structural motifs in organic and bioorganic compounds and so they did the direct measurement $^{15}N$ NMR chemical shift of several isoquinoline alkaloids using application of inverse detected NMR experiments [Mueller, 1979]. They found the chemical shift value for berbeine chloride was 194.8 in DMSO-d6 solvent [Marek et al., 1999]. $^{1}H$ and $^{13}C$ chemical shift values for berberine, palmatine and their artifacts in different solvents have been determined by Market et al to show the direct effect of internal and external environment on the chemical shifts of these compounds [Marek et al., 2003]. Further, this research on free bases of Quaternery alkaoids Dostal et al reports structural study of berberine and coptisine free bases with the help of 1D and 2D NMR spectrum and X-ray Diffraction studies [Dostál et al., 2004]. Saran et al studied the chemical shift variation of berberine and sangunarine due to interaction with CT DNA and all the proton of drug molecules were assigned using 2D COSY and 2D NOESY spectrum. It was the first reported two dimensional spectrum of berberine [Saran et al., 1995]. Jeon et al have performed 2D HMBC and 2D ROESY experiments to elucidate the structure and conformation of the berberine and berberrubine molecules. Till now It is the only study , where the authors has carried out restrained molecular dynamics simulations to get solution

structure of drug molecules using distance restraints from the ROESY spectrum. They have correlated the binding pattern of the drugs to DNA with the conformational changes at 19$^{th}$ position of berberine and berberrubine [Jeon et al., 2002]. Recently Huang et al and Danilov et al carried out an ab initio molecular orbital calculation to study the molecular properties and chemical shift of the berberine molecule [Danilov et al., 2006; Huang et al., 2005].

### 1.4.3 Physical Properties of Berberine

Spectroscopic data from absorbance, fluorescence, fluorescence lifetime, quantum efficiency, phosphorescence, phosphorescence lifetime, etc. provided a wealth of information concerning the proximity of aromatic groups, structure (identification, purity, and precise measurement of concentration), chemical behavior, and environment, long range interactions in small organic molecule–biopolymer complexes as well as biopolymer structure and dynamics [Inbaraj et al., 2001]. Berberine has a polycondensate system with partial saturation in one of the rings that renders its polycyclic system slightly buckled. The UV visible absorption spectrum of berberine is characterized by four absorption maxima centered on 230, 267, 344, and 420 nm, respectively, in aqueous buffer of pH 7.0 in the region 200–500 nm. It was observed that the absorption spectrum of berberine was not influenced by the variation of pH from 1.0 to 13.0 or temperature from 20 to 95°C indicating its high stability. In aqueous buffers, berberine has an extremely weak fluorescence that gives an emission spectrum with a λmax at 550 nm when excited at 350 nm. The fluorescence spectrum of berberine was also practically unaffected in the pH range 1.0– 13.0. Berberine was shown [Philogene et al., 1984] to be toxic to a variety of organisms in presence of light due to the production of singlet oxygen ($^1O_2$) and

subsequently Maiti and Chatterjee [Maiti and Chatterjee, 1995] had demonstrated the generation of $^1O_2$ by berberine and proposed its use as a photosensitizer for biological oxidation process.

### 1.4.4 Berberine-DNA Interaction Studies

The first suggestion of the intercalation of planar aromatic molecules between and parallel to adjacent base pairs was made on the basis of hydrodynamic and X-ray fiber diffraction studies of DNA in presence of acridine dyes. [Lerman, 1961]. Structural conformation of specific protein recognition to the oligonucleotide has also been used to elucidate the structural changes in E.coli promoter sequence [Schumacher et al., 1989]. An analytical technique to elucidate the mode of DNA/drug interaction could be important for the design of advanced drugs. X-ray crystallography, Nuclear Magnetic Resonance (NMR), absorption spectroscopy, gel electrophoresis, and Scanning Electron Microscopy (SEM) are some of the analytical techniques that have been used in attempts to investigate drug interactions with DNA and the resulting DNA conformations.

#### 1.4.4.1 UV–Visible, Fluorescence, Viscometry, Circular Dichroism, Comptetion Dialysis, Gel electrophoresis and ESI-MS studies.

Spectroscopic studies are used since ancient time to elucidate the drug DNA interaction for anticancer drugs [Shafer, 1977]. A large number of studies have been done on berberine-DNA complexation. Initial studies with calf thymes DNA shows that on binding of berberine with DNA around neutral pH, bathochromic, and hypochromic effets were observed in two long wavelength bands of the berberine, which indicated that berberine binds to DNA either by partial intercalating mode or

by completely intercalation, but causes bending of helix [Davidson et al., 1977; Maiti and Chaudhuri, 1981; Rungsitiyakorn et al., 1981]. Debnath et al studied interaction of berberine chloride with several naturally occurring DNAs (*Clostridium perfringenes*, cholera bacteriophage $\varphi$2, calf thymus, *Escherichia coli*, *Micrococcus lysodeikticus*) and synthetic DNAs ((poly(dG-dC)·poly(dG-dC), poly(dG)·poly(dC), poly(dA-dT)·poly(dA-dT), poly(dA)·poly(dT)) composition by various spectroscopic and viscometric studies, and found hypochromism, bathochromism and clear isobestic points at 355, 382, and 442nm in absorption bands, enhancement in fluorescence intensity of emission at 565 nm of berberine which actually alone does not show any fluorescence or very weak fluorescence when excited at 350nm, stabilization against thermal denaturation, perturbations in the intrinsic circular dichroic spectrum, increase in contour length of sonicated rod like DNA and induction of unwinding – re-winding process of covalently closed superhelical DNA up to 12° which can be comparable to the classical intercalator ethidium bromide unwinding angle 26°, depending on the base composition and sequences of base pairs and clearly indicates the sequence specificity for AT rich DNAs and alternate AT polymer and classical intercalation mode for binding [Debnath et al., 1989]. Nandi et al in 1990 suggested a very high affinity of berberine towards ploy A as compared to B DNA or tRNA by absorbance, fluorescence and circular dichroic studies [Nandi et al., 1990]. Debnath et al studied the extrinsic and intrinsic properties of circular dichroism spectrum of natural and synthetic DNA, complexed with berberine and found that berberine of binding causes a significant change in the 260 nm positive band of nucleic acid, while 240 nm –ve band found to be less effective. Extrinsic band occurred at 360 nm due to binding of berberine and show maximum change for AT Rich DNA rather then GC rich DNA [Debnath et al., 1991]. The salt and temperature dependence of the binding

constants were used to estimate theromodynamic parameters involved in the complex formation by Kumar et al using spectrophotometric technique. it has been concluded that the binding process is exothermic over the entire range and the values of enthalpy and entropy changes are strongly dependent on the salt concentration [Kumar et al., 1993]. Lee et al has used berberine as fluorescent probe in sensitive determination of CT DNA and RNA due to its non poisonous activity and it was found that the fluorescence intensities from the mixture of berberine and CT DNA were stable for two hours [Gong et al., 1999; Li and Lu, 1998]. Coralyne, a close relative of berberine having planer ring system shows stronger binding affinity to DNA with classical intercalation mode and GC rich base preference, while berberine with buckle ring system is partial intercalator to the AT sequences [Pal et al., 1998]. A novel, thermodynamiclay rigorous procedure, competition dialysis was used to determine berberine binding affinity towards quadruplexes, triplexes and several other natural and synthetic DNAs. Results from this study shows a very reduced binding binding of berberine to DNA's but selectivity towards poly (dA)-[poly (dT)]$_2$ was found to be larger then coralyne [Ren and Chaires, 1999]. Mazzini et al studied three oligonulceotides d(AAGAATTCTT)$_2$, d(GCGATCGC)$_2$, d(ACATCAAAAAGGT) for binding constant calculation with the help of UV spectroscopy, and found that d(AAGAATTCTT)$_2$ and d(GCGATCGC)$_2$ binding constant was found to be of same order (2.0 X $10^4$ and 1.0 X $10^4$), while d(ACATCAAAAAGGT) shows the one order less binding constant ( 1.0 X $10^3$), this suggested the binding affinity of berberine is not significantly distinguishable for AT and GC Rich DNAs but, single strand has a lower binding affinity due to lower charge density then duplex [Mazzini et al., 2003b]. Kumar et al. have compared the interaction of berberine with B-form and protonated structures of the hetero and the homo polymer of G. C. sequences. The

binding affinity of the alkaloid has been higher with the B-form structures compared to the protonated structures and varied in the order B form of poly [d(G-C)]> B form Poly (dG).poly (dC)> Protonated form of poly Poly (dG).poly (dC)> $H^L$ form of poly [d(G-C)], the observed differential binding of berberine may convey some specific meaning to its regulatory role in vitro and also potentiate its use as a probe for DNA conformations [Kumar et al., 2003]. One more study from the same group described binding of berberine to triplex and duplex DNA and RNA structures. Thermal melting, circular dichroism and thermodynamics studies with A.T, T.A x T, G.C, C.G x C, A.U, U.A x U, shows that berberine most preferentially binds to triplex helical DNA rather then their parent double helical by stabilizing the Hoogstein strand of triplex without affecting Watson and Crick [Das et al., 2003]. The interaction of berberine with DNA was interpreted to be either by an intercalation or an external stacking parallel to the base pairs, as revealed from the results of electric linear dichroic spectroscopy [Kluza et al., 2003]. Chen et al reported berberine interaction affinity with oligonucleotides in the order of $d(AAGCATGCTT)_2$ > $d(AAGGATCCTT)_2$ > $d(AAGAATTCTT)_2$ , which is in contradiction with the AT sequence preference of berberine binding to short oligonucleotides duplexes. [Chen et al., 2004] based on results from electrospray ionization -mass spectroscopy (ESI-MS) and fluorescence titration experiments. Yadav et al investigated the strong, endothermic and entropy driven binding of berberine with single stranded polyriboadenylic acid. Intensity of positive band of circular dichroism specrum of ss poly (rA) at 265 nm band with an initial molar ellipticity of around 48,000 deg $cm^2dmol^{-1}$ decreased significantly when titrated with beberine and become 10, 000 deg $cm^2dmol^{-1}$ at saturation. Scatchred plot obtained from spectrophotometric analysis showed that berberine bound strongly to ss poly (rA) in a non cooperative manner. In

contrast berberine does not show binding affinity towards double stranded poly (rA). All these findings by Yadav et al clearly support that berberine binds strongly to single stranded poly (rA) structure by a mechanism of partial intercalation leading to its use in gene regulation in eukaryotic cells [Yadav et al., 2005]. Chen et al recognized that berberine, palmatine, jatrorrhizine, coptisine, and berberrubine alkaloids bound to $d(AAGCATGCTT)_2$, $d(AAGGATCCTT)_2$ with the binding affinity comparable to hoechst 33258 (typical minor groove binder), and does not show not any remarkable sequence dependence. However all five alkaloids bound to $d(AAGAATTCTT)_2$ much weekly than Hoechst 33258 [Chen et al., 2005b]. Pang et al described the synthesis and DNA binding affinity of four new berberine derivative , having hydroethoxy, aminoethoxy, imidazolylethoxy, and N-methylpiperazinylethoxy groups at 9- position, and found that the one having primary amino group, strongly bind with calf thymes DNA, presumably by intercalation mechanism [Pang et al., 2005]. Chen et al. [Chen et al., 2005a] have synthesized several dimeric berberines linked with alkyl chains of varying lengths and compared their affinity of binding to B-DNA with respect to monomeric berberine. They reported that dimers greatly enhanced DNA binding affinities up to approximately 100-fold with two double helical oligonucleotides, $d(AAGAATTCTT)_2$ and $d(TAAGAATTCTTA)_2$ [Chen et al., 2005a]. Further, they demonstrated that these dimer's binding affinity to CT DNA increased the 100-fold as compared to the binding of monomeric berberine [Qin et al., 2006]. Furthermore, these dimers linked by different spacers showed a prominent structure–activity relationship when bound to oligodeoxyribonucleotides, $d(AAGAATTCT)_2$, $d(AAGCATGCTT)_2$ and $d(TAAGAATTCTTA)_2$ , as investigated by fluorescence titration and ethidium bromide displacement experiments. Among the dimers, a dimer linked with a propyl chain exhibited the largest binding affinity and

this suggested that a propyl chain is the most suitable spacer for bridging the two berberine units for DNA binding by intercalation. Long et al [Long et al., 2006] synthesized several jatzorrhizine homodimers and berberine–jatzorrhizine hetero dimmers and studied their binding affinities towards calf thymus DNA and three double-stranded oligodeoxyribonucleotides, $d(AAGAATTCTT)_2$, $d(TAAGAATAA)_2$ and $d(TTAAGAATTCTTAA)_2$. It was suggested that spacer length and attaching position are of great importance on modulating DNA binding affinities. Sinha et al elucidated that the binding affinity of berberine to poly (rC) .poly (rG) is very weak in comparison to methylene blue and ethidium bromide [Sinha et al., 2006]. Recently, Ovadekova et al, reported nanostructured electrochemical DNA biosensors using multi – walled carbon nano tubes (MWNT) for detection of the effect of berberine on DNA from cancer cells. The biosensor was used in testing of concentration dependent, effect on the structural stability of DNA from the U937 cancer cells. They found that berberine has an evident effect on DNA which depends on berberine concentration. DNA from keratinocytes was structurally much more stable towards the action of berberine than DNA from U937 cancer cells [Ovadekova et al., 2006].

Binding studies of berberine and palmatine with the t-RNA and their comparison with the binding affinity of ethidium to t-RNA has been performed by Islam et al and results suggested that the binding of these alkaloid molecules on the t-RNA structure appears to be mostly by partial intercalation while ethidium intercalates to the t-RNA. These results reveal the molecular aspects on the interaction of these alkaloids to t-RNA [Islam et al., 2007]. Qin et al using competitive ethedium bromide displacement experiments demonstrated that binding affinity of protoberberines enhanced remarkably by partial demethylation, it was found that berberrubine, palmatrubine and jatrorubine shows higher affinity towards CT DNA,

Poly (dA-dT).Poly (dA-dT) and Poly (dG-dC) .Poly (dG-dC) than their parent compounds [Qin et al., 2007a]. A study by Franceshin et al demonstrated berberine binding to various G-quadruplex DNA structure and its ability to inhibit telomerase. They investigated by PAGE that berberine promotes formation of inter and intra molecular G-quarduplexes [Franceschin et al., 2006]. Further Zhang et al elucidated with the help of CD, Fluorescence, PCR stop assay, competition dialysis and telomerase repeat amplification protocol (TRAP assay) that, berberine and its 9-substituted derivatives could induce and stabilize the anti parallel G-quadruplex structure formation in the presence or absence of metal cations. 9- Substituted berberine derivative showed higher inhibitory effect against telomerase activity comparing with as compared to berberine [Zhang et al., 2007]. Tian et al studied the interaction between cationic berberine and polyanioninc DNA on the glassy carbon electrode and found that interations between drug and DNA are cooperative and dominant of electrostatic nature [Tian et al., 2008]. Very recently Wang et al, demonstrate the binding affinity of 13 alkaloids with two sequences in GC rich human surviving promoter by ESI-MS which is a powerful tool for screening binders to specific DNA sequence, they found a GC preference for the alkaloids [Wang et al., 2008]. Bhadra et al studied the energetics of berberine-DNA interaction and using scatchard and isothermal titration calorimetry and found that berberine binding exhibits positive cooperativity to polypurine–polypyrimidine sequences and non-cooperativity to alternating purine–pyrimidine sequences. Isothermal titration calorimetric studies again suggest a preference of berberine to Poly(dA–dT), and the temperature dependence of binding enthalpy yields negative heat capacity, revealing that the hydrophobic interactions play a predominant role in the AT specific binding of berberine [Bhadra et al., 2008a]. Further they elucidated the interaction of

berberine, palmatine, coralyne, with mammalian herring testis DNA using a combination of isothermal titration calorimetry, differential scanning calorimetry, and optical, melting experiments to characterize the energetics of their binding. The binding in case of palmatine and coralyne was predominantly enthalpy driven with favoring smaller entropy terms, while that of berberine was favored by both negative enthalpy and positive entropy changes. Binding induced change in heat capacity for berberine, palmatine and coralyne was calculated using isothermal titration calarimetry and found -117, -135, and -157 respectively, these results clearly indicate the strong binding of coralyne than berberine and palmatine [Bhadra et al., 2008b].

### 1.4.4.2 Nuclear Magnetic Resonance Spectroscopic Studies

NMR is a powerful tool that can probe the binding site on both DNA and ligand, still very modest experiemental work has been carried out to understand the structural and conformation feature of berberine-DNA interaction. Saran et al has performed $^{1}H$ NMR to investigate interaction of berberine and sanguinarine to calf thymes DNA. All the protons of drug molecule have been assigned using 2D-COSY, NOESY and ROESY spectra. Berberine proton resonances were observed as increasing amount of Calf thymes DNA and found to be differentially downfield shifted in the range of 0.014 to 0.05 for different protons of drug. Changes in the methoxy group and the aliphatic protons were insignificant. These results suggested a partial intercalation mode of binding involving one side (C11 to C14) of drug which shows maximum shift in proton resonances that is Hi, Hj, Hk. They also suggested that the methoxy group and the aliphatic protons cause steric hindrance to interaction of the other side of molecule that is C4 to C10 [Saran et al., 1995]. $^{31}P$ and $^{1}H$ resonance experiments were performed by Mazzini et al to find a possible specificity,

mode of binding and the details of molecular structure. They have studied the interaction of berberine with the double helix oligonucleotides d(AAGAATTCTT), d(GCGATCGC), d(CGTATACG), d(CGTACG), d(ACCTTTTTTGATGT), and with single stranded d(ACATCAAAAAGGT) with one dimensional $^{31}P$ and $^{1}H$ NMR. Resonance for the protons of drug found to be braod and upfield shifted (0.30 to 0.70 for aromatic protons and 0.12 to 0.30 for aliphatic proton) due to complexation with DNA. Similar chemical shift variation was found with AT rich and GC rich sequences. Surprisingly, also with the single strand quite similar values were found. $^{31}P$ resonances of DNA did not show any significant chemical shift variation (<0.2 ppm) in presence of berberine, while $^{31}P$ shift variation was found to be in the range of 0.9 to 1.5 in case of intercalators [Gorenstein, 1994; Mazzini et al., 1998; Ragg et al., 1988]. This result was the first evidence for excluding the intercalation of beberine. Structure of berberine with $d(AAGAATTCTT)_2$ was derived from NOESY spectrum of the complex. Sequential connectivities of DNA bases with the previous base were found to be continuous throughout, hence excluding the intercalation mode unswervingly. It was found that C5, C6, C8 and methoxy group protons, all located on one side of drug shows NOE contacts with H2 of adenine, while other side of drug shows NOE contacts with H1' of neighbor cytidine. With the several interproton distances thus derived, a structural model of the complex was obtained, the berberine molecule was found to be located in the minor groove of the double helix being with the convex side on the helix grooves, and positive nitrogen atom interacting with the negative ionic surface [Mazzini et al., 2003a]. To characterize the interaction between protoberberines (berberine and berberrubine) Park et al elucidated their binding with HP14 DNA (GCCGTCGTTTACA) having topoisomerase binding site using $^{1}H$ NMR spectroscopy [Park et al., 2004a; Park et al., 2004b]. They elaborated that the

DMSO respectively. Chapter 4 deals with the berberine and berberrubine interaction with several natural and synthetic DNA's and oligonucleotides with the help of UV-visible and fluorescence spectroscopic techniques. These techniques have been used to select the sequence of oligonucleotides, with which binding is more preferred and was used for the NMR studies. Chapter 5 deals with the Resonance assignment of NMR spectrum of promoter site containing oligonucleotide d-$(CCAATTGG)_2$, its molecular structure conformation by restrained molecular dynamics and calculation of helicoidal parameters using CURVES. Chapter 6 deals with the $^{1}H$, $^{31}P$ NMR and rMD studies on binding of berberine with promoter octamer sequence d–$(CCAATTGG)_2$,. $^{1}H$ and $^{31}P$ NMR titration studies were used to study the change in chemical shifts on binding. 2D $^{31}P$ - $^{31}P$ exchange spectra of drug-DNA complex gives direct evidence for binding and conformation of the DNA backbone. 2D $^{1}H$ - $^{1}H$ NOESY studies provide detailed information on the close intermolecular contacts between the drug and DNA molecule in the complex. Restrained molecular dynamics studies using inter-proton distances obtained from 2D NOESY as restraints, provide understanding of the conformational and helical parameters of the drug-DNA complexes in solution. These studies reveal structural tools such as NMR spectroscopy, coupled with, UV-visible, Fluorescence and molecular modeling techniques have considerable impact in advancing our understanding of the structural selectivity and the molecular basis for drug-DNA interactions. Understanding the physicochemical properties of the drug as well as the mechanism by which it interacts with DNA, would ultimately lead to rational design of novel anti-cancer drugs. Chapters 7 summarize all the research work done and highlight all the concluding points.

pentanucleotide sequence are present in a wide variety of vertebrate, yeast and plant promoters and are important for transcription. All five nucleotides are almost invariably conserved. The CCAAT sequences can be found both in the direct and in the inverted orientation and it is present in both TATA containing (such as globins) and in TATA less (such as MHC class II) promoters. The frequency of CCAAT boxes appears to be relatively higher in TATA-less promoters [Mantovani, 1998]. Borghini et al [Borghini et al., 2006] pointed out the lack of conventional TATA boxes and the presence of two identical CCAAT boxes as the crucial elements involved in the transcription regulation of the human TLX3 gene which is a gene over expressed in T-cell Acute Lymphocytic leukemia. TLX3 is uniquely expressed in the developing medulla oblongata and is required for proper formation of first order relay visceral sensory neurons and of most of the (nor) adrenergic centres in the brain stem especially involved in the physiologic control of cardiovascular and respiratory systems [Qian et al., 2001], but expression of TLX3 has also been detected in leukemia samples from 20% of children's and 13% of adult affected with T-cell acute lymphocyte leukemia [Ballerini et al., 2002; Cave et al., 2004; Mauvieux et al., 2002] although this gene has never involved in normal T-cell differentiation [Ferrando et al., 2004], but based on its specific spatiotemporal expression and the correlation between upregulation and development of T-cell Acute Lymphocytic leukemia a role of this gene in either cell cycle, survival or differentiation can be postulated. These promoter sequences are rich in AT content and sequence of consecutive adenines and thymines, so called A-tracts also constitute an important class of naturally curved DNA [Boulikas, 1996; Crothers and Shakked, 1999; Marini et al., 1982]. AT rich sequences, including A-tracts, are also strongly over-represented in origins of replication in many organisms [Boulikas, 1996].

Sequence dependent local DNA structure is correlated with all biological functions and also detailed stereochemical studies have shown that the helical parameters of a DNA double helix are strongly influenced by its base sequence [Dickerson, 1992] hence it is probable that structure of control sites (eg promoters and operators) in DNA are different from the structure of genomic DNA [Nussinov, 1985]. Special structures like different cross linking, and pseudosquare knot structures are also identified by conformational studies, which shows critical importance in biological behaviuor of DNA elements [Paquet et al., 1999; Ulyanov et al., 1998]. Special structure and conformation, of packaging signal of HIV-1 RNA contains a stem-loop, which is sequence dependent, SL1, serves as the dimerization initiation site for two identical copies of the genome and is important for packaging of the RNA genome into the budding virion and for overall infectivity [Ulyanov et al., 2006]. The dependence of the local conformation on sequence may be involved in recognition by specific proteins involved in transcription and replication processes. Novel drugs, which can be oligonucleotide, peptides or small molecules, are currently being designed to target nucleic acids. In order to develop this new medicinal strategy in a rational way, there is a need for information regarding the structure, stability and dynamics of nucleic acids in the presence or in the absence of these drugs.

## 1.5 Scope of Thesis

In order to control gene expression, interactions of the small molecules with DNA have been studied for several decades for making design principles for targeting specific DNA sequences. Many small molecules that bind to DNA are clinically proven therapeutic agents although their exact modes of action are not completely defined. There is a renewed focus on the use of small molecules as therapeutic agents.

This renewed interest arises, in part, as a result of several advantages of small molecules as potential drugs, including the economics of their synthesis and their effective delivery to cells. The results of binding studies are correlated with biological (antitumor) efficiency of the compounds tested with the aim to exploit these data for design of new cytostatics with better therapeutic properties as compared to the drugs already used in the clinic. Therefore, these studies are aimed in particular at the development of new anticancer drugs whose antitumor efficacy is associated with their interactions with DNA, i.e. for which DNA is the main target inside tumor cells. Facilities available with this laboratory make it possible to acquire knowledge that is essential for designing new cytostatics and suggestions for structure requirements for pharmacological activity. Understanding the structure-function directed macromolecule-target interactions of anticancer drugs and further rational design of improved anticancer agents are the long-term research goals of our laboratory.

This thesis deals with (i) the typical procedure for studying the molecular and electronic properties of small molecules using nuclear magnetic resonance spectroscopy and quantum chemical calculations (ii) sequence specificity determination for drugs using absorbance and fluorescene spectroscopy (iii) structural studies of the berberine complexed with promoter site containing nucleotide d-$(CCAATTGG)_2$ (iii) to investigate the relationship between the structure and biological activity of the drug

The Ph.D thesis work has been reported in the form of seven chapters. Chapter 1 contains introduction as of the subject as well as review of literature. Chapter 2 deals with the materials and methods used. In chapter 3, the molecular and electronic properties of berberine and berberrubine are discussed using nuclear magnetic resonance spectroscopy and quantum chemical calculations in $D_2O$ and

structural difference of these drugs has a dramatic effect on their DNA binding behavior. In the course of titrations of HP14 with berberine and berberrubine, a line broadening effect and and upfield shift observed which is found to be in accordance with the earlier results from mazzini et al. of aliphatic resonances for berberrubine/HP14 and berberine/ HP14 complex was observed. Further in case of berberine they observed siginifaclnty broader lines as compared to berberrubine, which are indicative of difference in exchange, behavior between the two analogues. These results show that due to faster exchange kinetics and the lack of specific trend on chemical shift variation of berberine suggests a relatively low sequence specificity then bebrrubine. It suugest that the substitution of methoxy group to hydroxyl group on the $19^{th}$ position in berberine may be attributed to the enhancement in DNA binding and so on Topoisomerase poisnious activy increase the binding affinity of the drug molecule. Mazzini and Park are the only groups who have done some structural and conformational studies on berberine-DNA interaction.

### 1.4.5 Significance of the Promoter Sequence $(CCAATTGG)_2$ used in Study and Conformational Features of Oligonucleotides using NMR Spectroscopy.

Regulation of transcription is a complex set of events controlled by DNA sequences positioned in proximity to these genes (promoters) and by elements acting at a distance (enhancers). Promoters and enhancers that activate polymerase II transcribed mRNA genes are formed by a combinational puzzle of short sequences recognized by sequence specific regulators. Some such as the TATA, GC and CCAAT box are encountered at extremely high frequency [Bucher, 1990; Bucher and Trifonov, 1988]. The CCAAT box was the first element identified [Benoist et al., 1980; Efstratiadis et al., 1980]. Later studies clearly established that such

# Materials and Method

## 2.1 Materials

The deoxyribonucleic sequence d-$(CCAATTGG)_2$, d-$(CGATCG)_2$, d-$(CGTACG)_2$, d-$(TGCGCA)_2$, $(TGCGCATGCGCA)_2$, $(CGATCGCGATCG)_2$, $(CGTACGCGTACG)_2$, $(CGCGCGCGCG)_2$, $(ATATATATAT)_2$, $(CCAATTGG)_2$, Calf thymus DNA, Poly (dA-dT), poly (dG-dC), Berberine, Deuterium Oxide ($D_2O$), Dimethyl sulfoxide (DMSO) with isotopic purity 99.96% and (Trimethylsilyl) propionic-2, 2, 3, 3-$d_4$ acid sodium salt (TSP) were purchased from Sigma Chemical Co., USA. All other chemicals like sodium di hydrogen phosphate, di sodium hydrogen phoshptae, sodium chloride (NaCl), etc. used for phosphate buffer preparation were purchased from Sigma Chemical Co., USA. All HPLC grade reagents like water, triethyl amine, acetonitrile, glacial acetic acid, ammonium acetate etc. were from Qualigens, Ltd. Berberine and oligonucleotides sample were used without further purification. Berberrubine was not available in the market, so it was synthesized using standard protocol reported in literature.

## 2.2 UV-visible and Fluorescence Spectroscopy

### 2.2.1 Preparation of Buffer Solution

The stock buffer used was BPES (10mM mM; pH 7.0) prepared by mixing 1.5 mM of $Na_2HPO_4.2H_2O$ and 0.5M of $NaH_2PO_4.H_2O$ to get 10 mM Phosphate buffer (pH=7.0) at room temperature with 10 mM NaCl and 0.25 mM EDTA. This was the

working buffer solution for drugs and DNAs used in the study. The buffer was filtered through 0.2 μM pore Millex Millipore filters.

### 2.2.2 Preparation of Berberine

Berberine solution was made freshly by dissolving in to the BPES buffer (pH 6.8 ± 0.2). The concentration of berberine in buffer solution was determined spectrophotometrically using extinction coefficient of 22,500 $m^{-1}cm^{-1}$ at 344. Berberine concentration of 2-5 μM was used for all the experiments.

### 2.2.3 Preparation of Berberubine

Berberrubine was synthesized by heating 1g of berberine at 190 $^0C$ in a dry oven under vacuum (20-30 mm Hg) for 30 minutes. Than yellow color of berberine changed to dark reddish brown. Then berberrubine was separated from this brown mixture through silica gel (60-200 mesh size) Coolum chromatography using $CHCl_3$/ MeoH in 7:1 to 5:1 (v/v) solvent system. Separated dark red powder was then dissolved in BPES buffer to make a stock solution of (20.90 mM) for titration studies. Molar extinction coefficient was obtained to be 29,950 $m^{-1}cm^{-1}$ at 377 nm (in aqueous buffer) using dilution curve for different concentration. 2-5 μM concentration of berberrubine was used for all the titration studies.

### 2.2.4 Preparation of DNA Samples

The concentration of DNA samples was prepared in 10 mM BPES buffer containing 10 mM Nacl and concentration was determined using the standard values of the molar extinction coefficients tabulated in Table 2.1 by the UV–vis Spectrophotometer.

**Table 2.1 Extinction coefficient (e) of various DNA's and oligonucleotides**

| DNA | Extinction coefficient (e) ($m^{-1}cm^{-1}$ at 260 nm) |
|---|---|
| CT DNA | 6600 |
| Poly d(A-T) | 8600 |
| Poly d(G-C) | 7750 |
| d-$(CGATCG)_2$ | 57200 |
| d-$(CGTACG)_2$ | 57600 |
| d-$(TGCGCA)_2$ | 55600 |
| d-$(CGTACGCGTACG)_2$ | 97200 |
| d-$(CGATCGCGATCG)_2$ | 97200 |
| d-$(ATATATAT)_2$ | 111200 |
| d-$(CGCGCGCG)_2$ | 84800 |
| d-$(TGCGCATGCGCA)_2$ | 109900 |
| d-$(CCAATTGG)_2$ | 76300 |

Since the amount of the samples required in the absorbance and fluorescence spectroscopy is very small, it is not advisable to weigh the substance. There are great chances of losing the sample, while transferring it. So, to prepare the solutions, a small amount of the sample was dissolved in a known volume of the solvent and the absorbance was recorded on a CARY-100 Bio, UV-Visible spectrophotometer over a suitable range. The concentration of the stock solution was calculated by the formula of Beer Lambert's law-

$$O.D = \log T_0/T = \varepsilon.c.l$$



Where,

c = Concentration of solution (in moles/ liter)

ε = Molar extinction coefficient (in $M^{-1}cm^{-1}$)

l = Path length of quartz cuvette (in cm)

From the stock solution of the known concentration, the solution of desired concentration was prepared by diluting the sample suitably, in BPES buffer and

scanning the sample within the range 200-800nm for berberine and berberrubine and 200-400 nm for DNA. The absorbance at the $\lambda_{max}$ is noted from each scan and the concentration is calculated with the Lambert-Beer's equation considering the known molar extinction coefficient of berberine, berberrubine and DNA. The path length of the cuvette is fixed in each case i.e., 1 cm. The concentration of samples was taken in the range of 100-200 μM for CT DNA , poly dG-dC, and poly dA-dT , 20-50 μM for oligonuclotides and 2-5 μM for berberine and berberrubine.

### 2.2.5 Spectrophotometric Titration

Absorbance measurements were performed using Carry 100 Bio (Varian) UV-Visible Spectrophotometer equipped with the Peltier thermostat cell holder and quartz cuvette (optical path length 1 cm), with continuous stirring throughout the course of titration. Absorbance titration experiments of the berberine-DNA complex were performed keeping a fixed concentration of drug (2-4 mM) and by increasing the concentration of DNAs and recording the spectrum in the wavelength range 220-700 nm after each addition. For every experiment aliquots of nucleic acid were titrated till no further change in absorbance was noticed, i.e., presence of large excess of DNA (up to D/N =1/10) was obtained. At each step absorption maxima (A) was recorded. The absorbance maxima for 2-5 μM for drugs was denoted by $A_o$.

$$\Delta A = A_o - A$$

### 2.2.6 Fluorimetric Titration

Fluorescence spectra were measured on Fluorolog-3 spectrofluorimeter LS55 (make HORIBA Jobin Yvon Spex®). The same sample which was used for Uv – visible studies was used to record the fluorescence spectrum at each titration step.

This action reduces any error or difference in results through both the techniques due to any change of sample conditions. As both absorption and fluorescence experiments runs parallel so the results are more significant. The emission spectra were recorded in the range 400-800 nm. Titrations at 25 $^0$C were carried out and change in fluorescence intensity was recorded. At each step, the fluorescence intensity maxima (I) were recorded at ($\lambda_{max}$). The excitation wavelength was kept as 350 nm for all the experiments nm. The fluorescence intensity maxima for pure drug was denoted by $I_0$. The enhancement in each case was calculated by:

$$\Delta I = I - Io$$

### 2.2.7 Life Time Measurement using Fluorescence Spectroscopy

Model FluoroLog®-TCSPC, make HORIBA Jobin Yvon Spex® was used for the life time measurement study. This is an ultra compact fluorescence lifetime spectrometer based on time correlated single photon counting (TCSPC) and ready to perform time-domain lifetime spectroscopy building up a histogram of the sample's fluorescence decay. This instrument has sub-ns pulsed LED. For our study, we used fixed-wavelength Nano LED of 470 nm. Standard optical pulse durations are <1.5 ns for LEDs. Resolution 0.2 nm, accuracy ± 0.5 nm, speed 150 nm/s, range 0-1300 nm, TAC range given is 50 nm, excitation wavelength is 350 nm for the experiment. 2:1 complex of berberine-d-$(CCAATTGG)_2$ was used for this study.

## 2.3 Electron Spray Ionization Mass Spectrometry (ESI-MS)

Positive-ion ESI-MS spectra were obtained on Esquire 4000 (Bruker Daltonics, Germany) with the normal ESI source. Sample of drug mixture was prepared in methanol and the solution is infused directly into the mass spectrometer at

the rate of 240 µl/hr. In the cone voltage was set to 4.0 kV and the nebulizer pressure is 15 psi. Dry gas flow is 8 l/min. The capillary temperature was 100 °C. Data is collected for approximately 10 scans. The maximum accumulation time is 200 ms and scan range is 400-1700 m/z.

## 2.4 Nuclear Magnetic Resonance Studies

### 2.4.1 Sample Preparation for NMR

Stock solution of berberine (25.00 mM) was prepared by dissolving a known quantity of sample in 10 mM BPES buffer having 10 mM NaCl concentration. The final concentration was checked by absorbance measurements at wavelength of 344 nm using Cary 100 Bio Spectrophotometer. The extinction coefficient (ε) value used for berberine was ε = 22500 $M^{-1}cm^{-1}$. Solution of deoxyoligonucleotide, d-$(CCAATTGG)_2$ (2.80 mM duplex concentration) was prepared by dissolving a known quantity of sample in 100 % $D_2O$ for recording spectrum only for nonexchangeable protons. DNA sample was lyophilized and further dissolved in 90% $H_2O$ and 10% $D_2O$ BPES buffer (10 mM, of pH = 7.0 ) having 10 mM Na salt for exchangeable protons spectrum. Concentrations was determined by absorbance measurements at 260 nm using the extinction coefficient (ε) value, 76300 $M^{-1}cm^{-1}$ for d-$(CCCAATTGG)_2$. Ethylene diamine tetra acetic acid (EDTA), 0.1 mM, was added to suppress paramagnetic impurity, which may cause line broadening during NMR measurements. Typically 1µl of 0.1 M solution of TSP was added to the berberine, d-$(CCAATTGG)_2$ and complex of berberine d-$(CCAATTGG)_2$ as an internal reference.

### 2.4.1.1 Preparation of Berberine- d-$(CCAATTGG)_2$ Complex

A complex of d-$(CCAATTGG)_2$ and berberine was prepared by titration. 119 µl of 25.00 mM berberine was added in steps of 6 µl to 530 µl of 2.80 mM d-$(CCAATTGG)_2$ sample during titration in order to make 2:1 complex of berberine: d-$(CCAATTGG)_2$.

The concentration of d-$(CCAATTGG)_2$ in this solution was determined as follow

$$N_1V_1 = N_2V_2$$

$$N_1 \times 536 = 2.80 \times 530$$

$$N_1 = 2.77 \text{ mM}$$

The concentration of berberine in this solution was determined as follows:

$$N_3V_3 = N_4V_4$$

$$N_3 \times 536 = 25 \text{ mM} \times 6$$

$$N_3 = 0.28 \text{ mM}$$

The concentration of berebrine (D), d-$(CCAATTGG)_2$ (N) and drug/ nucleotide (D/N) ratio are shown in Table 2.2.

## 2.5 NMR Theory and Experiments

### 2.5.1 The Phenomenon

Subatomic particles (electrons, protons and neutrons) spin on their axis. A nucleus (of spin 1/2) when placed in a static magnetic field behaves like a small magnet. This nucleus is in the lower energy level (i.e. its magnetic moment does not oppose the applied field). In the absence of an external magnetic field, these orientations are of equal energy. Each level is given a magnetic quantum number, m, characterizing Z component of spin, I. On interaction with magnetic field, nuclei with spin I >1/2 distribute themselves among 2I + 1 energy level with the seperation by:

$$\Delta E = h \gamma B_0$$

**Table 2.2: Various concentration ratios (D/N) for the complex formed between berberine and d-$(CCAATTGG)_2$**

| Nucleotide Concentration (mM) = N | Drug Concentration (mM) = D | D/N |
|---|---|---|
| 2.80 | 0.00 | - |
| 2.77 | 0.28 | 0.1 |
| 2.73 | 0.55 | 0.2 |
| 2.70 | 0.83 | 0.3 |
| 2.67 | 1.13 | 0.4 |
| 2.47 | 1.29 | 0.5 |
| 2.45 | 1.49 | 0.6 |
| 2.43 | 1.68 | 0.7 |
| 2.41 | 1.91 | 0.8 |
| 2.39 | 2.13 | 0.9 |
| 2.36 | 2.35 | 1.0 |
| 2.34 | 2.56 | 1.1 |
| 2.32 | 2.77 | 1.2 |
| 2.30 | 2.98 | 1.3 |
| 2.28 | 3.18 | 1.4 |
| 2.26 | 3.38 | 1.5 |
| 2.24 | 3.58 | 1.6 |
| 2.22 | 3.77 | 1.7 |
| 2.20 | 3.96 | 1.8 |
| 2.18 | 4.14 | 1.9 |
| 2.16 | 4.32 | 2.0 |

The overall spin, I, is important. A nucleus with spin 1/2 will have 2 possible orientations (Figure 2.1a). These spins are capable of interacting with a beam of electromagnetic radiations. These energy levels correspond to the spins aligned along and against the applied magnetic field, $B_0$. The spin oriented to oppose $B_0$ has higher energy. These spin do not align perfectly along $B_0$ and this give rise to a permanent torque. The nucleus also has the property of angular momentum because of its spin and thus as a result the nuclei precess (Figure 2.1b), with frequency of precession given by:

$$\omega_0 = \gamma B_0$$

where, $\gamma$ is proportionately constant, $\omega_0$ is the resonant or Larmor frequency in radians/second and $B_0$ is the magnitude of the applied magnetic field. When the frequency of the beam is same as that of precessing spin then absorption of energy takes place, which causes the nuclei to flip from a lower energy state to a higher energy state by a process termed resonance (Figure 2.1c).

In an NMR sample there are many molecules, each with its spin precessing about $B_0$ at same frequency and result in a net magnetization of $M_z$ oriented along the Z-axis. On application of a rotation radio frequency field with frequency at or near $\omega_0 = \gamma B_0$, the spin resonate giving rise to net $M_{xy}$ component which is phase coherent. The following are the spectral parameters in NMR:

### 2.5.2 Chemical Shift

The magnetic field at the nucleus is not equal to the applied magnetic field, $B_0$; electrons around the nucleus shield it from the applied field. The difference between the applied magnetic field and the field at the nucleus is termed the nuclear shielding. The induced field is directly proportional to $B_0$. This is represented by the equation:

$$B_{eff} = B_0 (1-\sigma)$$

where, $\sigma$ is the shielding constant which depends on the nature of electrons around the nucleus.Chemical shift is a function of the nucleus and its environment. It is measured relative to a reference compound. For $^1H$ NMR, the reference is usually tetramethylsilane, Si $(CH_3)_4$. Chemical shift is expressed in parts per million (ppm) is given as:

$$\delta = 10^6 \text{ x } = \frac{\delta_{ref} - \delta_{obs}}{\delta_{ref}}$$

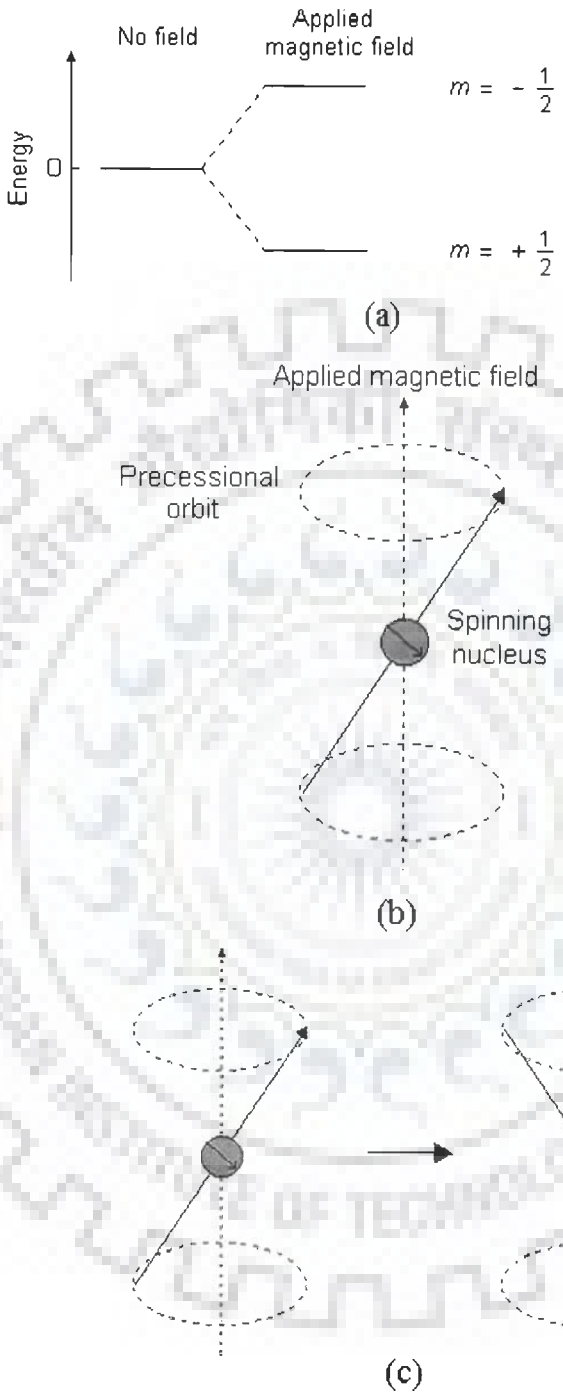


**Figure 2.1 (a) Energy levels for a nucleus with spin quantum number ½ (b) Precessional motions by nucleus spinning on its axis in presence of the external magnetic field (c) Flipping of the magnetic moment on absorption of the radiations**

where, $\delta_{ref}$ is the position observed for a reference compound and $\delta_{obs}$ is the position of the signal of interest. There are useful general conclusions that can be drawn from specific chemical shift value, or changes due to the binding of the ligand.

### 2.5.3 Spin-Spin Coupling Constant (J)

Nuclei experiencing the same chemical environment or chemical shift are called equivalent. Those nuclei experiencing different environment or having different shifts are nonequivalent. Nuclei, which are close to one another, exert an influence on each other's effective magnetic field. This effect shows up in the NMR spectrum when the nuclei are nonequivalent. If the distance between non-equivalent nuclei is less than or equal to three bond lengths, this effect is observable. This effect is called spin-spin coupling or J coupling and is expressed in Hertz. This coupling causes splitting of lines. The appearance of multiplet patterns depends on relative magnitude of $\delta$ and J for coupled nuclei. Vicinal couplings ($^3$J) display a characteristic dependence upon the involved dihedral angle (Figure 2.2a) according to the relation dihedral couplings;

$$^3J = 8.5 \cos^2\theta - 2.8$$

$$^3J = 9.5 \cos^2\theta - 2.8$$

This relationship is known as the Karplus relation. Figure 2.2a and 2.2b shows the definition of dihedral angle and relationship between J couplings and dihedrals.

### 2.5.4 Relaxation Process

The magnetization does not precess infinitely in the transverse plane but turns back to the equilibrium state. This process is called relaxation. Two different time-constants describe this behaviour. The importance of these phenomena is in the nuclear Overhauser effect (NOE), which can be used to probe internuclear distances in a

molecule. There are two major relaxation processes namely, Spin-lattice (longitudinal) relaxation ($T_1$) and spin-spin (transverse) relaxation ($T_2$). The relaxation time $T_1$ represents the "lifetime" of the first order rate process that returns the magnetization to the Boltzman equilibrium along the +Z axis.

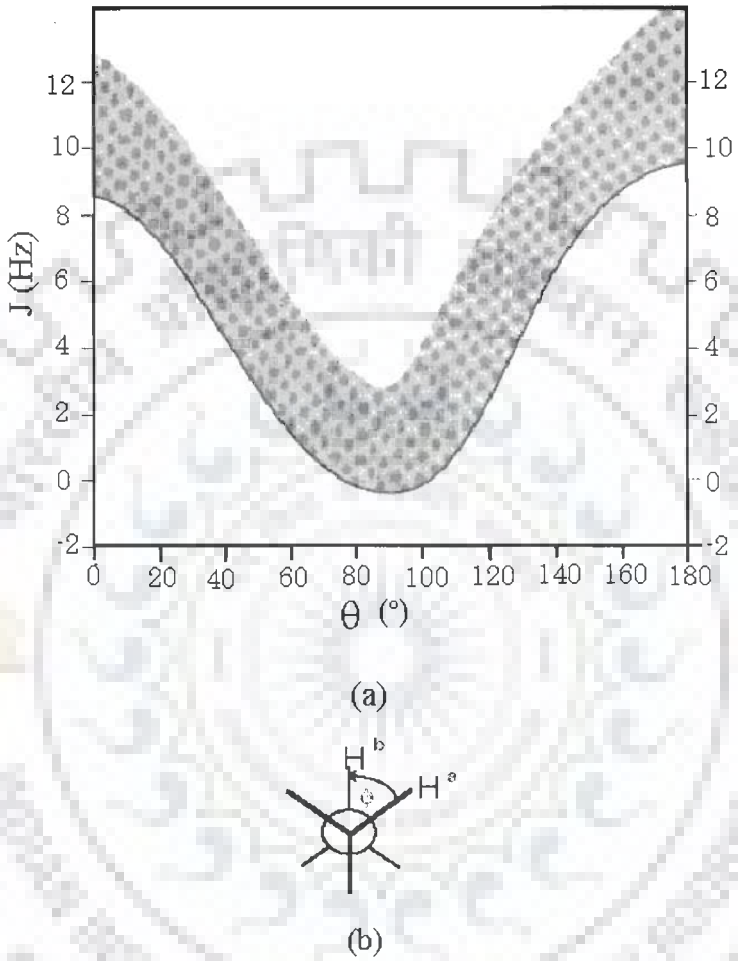


**Figure 2.2: (a) Karplus Curve showing relationship between J couplings and dihedral angle (b) definition of the dihedral angle**

The components of the lattice field can interact with nuclei in the higher energy state, and cause them to lose energy (returning to the lower state). The energy that a nucleus loses increases the amount of vibration and rotation within the lattice. The relaxation time, $T_1$ depends on the motion of the molecule. As mobility increases, the vibrational

and rotational frequencies increase, making it more likely for a component of the lattice field to be able to interact with excited nuclei. $T_1$ spin-lattice relaxation rate is then measured by plotting M as a function of $\tau$:

$$M(\tau) = Mo\ (1 - 2\exp^{-(\tau / T_1)})$$

$T_2$ represents the lifetime of the signal in the transverse plane (XY plane) and it is this relaxation time that is responsible for the line width. In Solution NMR, very often $T_2$ and $T_1$ are equal. The very fast spin-spin relaxation time provides very broad signals. The transverse relaxation constant $T_2$ is related to the linewidth of the signals. The width of the signal at half height is given by:

$$\Delta\omega)_{1/2} = 1 / \pi\, T_2$$

Fast decay leads to broad signals, slow decay to sharper lines. The transverse relaxation constant $T_2$ of spin I=1/2 nuclei is mainly governed by the homogeneity of the magnetic field and the strength of the dipolar interaction with other I=1/2 nuclei depending on the number and the distance of neighbouring nuclei the overall tumbling time of the molecule which is related to its size. Transverse relaxation ($T_2$) is faster than longitudinal relaxation. $T_2$ spin-spin relaxation rate is measured by plotting M as a function of $\tau$:

$$M(\tau) = Mo^{(-\exp(\tau/T2))}$$

**2.5.5 Two-Dimensional (2d) NMR Techniques**

In one-dimensional pulsed Fourier transform NMR the signal is recorded as a function of one time variable and then Fourier transformed to give a spectrum, which is a function of one frequency variable. In two-dimensional NMR the signal is recorded as

a function of two time variables, $t_1$ and $t_2$, and the resulting data Fourier transformed twice to yield a spectrum, which is a function of two frequency variables. The two-dimensional signal is recorded in the following way. First, $t_1$ is set to zero, the pulse sequence is executed and the resulting free induction decay recorded. Then the nuclear spins are allowed to return to equilibrium, $t_1$ is then set to $\Delta 1$, the sampling interval in $t_1$, the sequence is repeated and free induction decay is recorded and stored separately from the first. Again the spins are allowed to equilibrate, $t_1$ is set to $2\Delta 1$, the pulse sequence repeated and a free induction decay recorded and stored. The whole process is repeated again for $t_1 = 3\Delta 1$, $4\Delta 1$ and so on until sufficient data is recorded, typically 50 to 500 increments of $t_1$. Thus recording a two-dimensional data set involves repeating a pulse sequence for increasing values of $t_1$ and recording a free induction decay as a function of $t_2$ for each value of $t_1$. The general scheme for two-dimensional spectroscopy is (Figure 2.3):

***Preparation time*:** The sample is excited by one or more pulse. This consists of a delay time or a sequence of pulses separated by fixed time intervals saturation sequences. Thermal equilibrium is attained during this period.

***Evolution Period ($t_1$)*:** The resulting magnetization is allowed to evolve for the first time period, $t_1$. The evolution period is the pulse sequence element that enables frequency labelling in the indirect dimension. Further, one or several radiofrequency pulses may be applied to create coherence.

***Mixing time ($\tau_m$)*:** During this period coherence is transferred between spins. Mixing sequences utilize two mechanisms for magnetization transfer: scalar coupling or dipolar interaction (NOE). After the mixing period the signal is recorded as a function of the second time variable, $t_2$. This sequence of events is called a pulse sequence.

***Detection Period*:** The signal is recorded during the time $t_2$ at the end of the sequence, detection, often called direct evolution time; during this time the magnetization is labelled with the chemical shift of the second nucleus. The data is recorded at regularly spaced intervals in both $t_1$ and $t_2$.

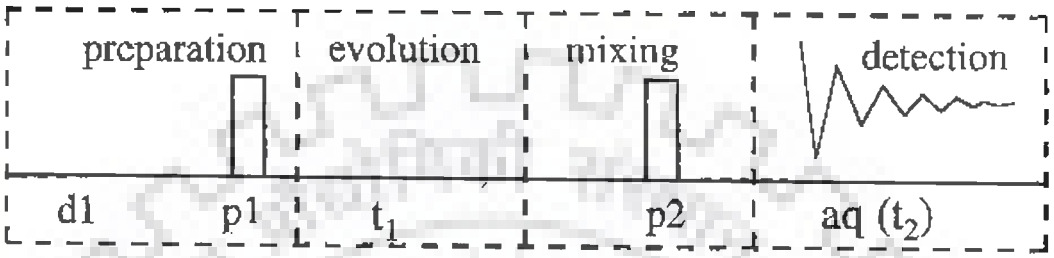


**Figure 2.3: Four different time segments of a 2D NMR experiment namely (i) preparation period (ii) evolution period ($t_1$) (iii) mixing period ($\tau_m$) (iv)detection period ($t_2$)**

### 2.5.5.1 Two – Dimensional Correlation Spectroscopy (2D-COSY)

The COSY experiment is used in determining those atoms which are connected through bonds. The basis of COSY experiment whose pulse sequence is shown in Figure 2.4 is the classical Jeener sequence [Jeener, 1971]. After the preparation period of 90° pulse constitutes brief mixing period whose effect is to mix single quantum coherence into a whole range of orders of coherence. However, only the single quantum coherence will give rise to any measurable signal during the detection period. The mixing process interchanges orders of coherence, mixes coherence among the transitions associated with a given spin and exchanges coherence between spins having a mutual scalar coupling. Thus a magnetization, initially associated with the A spin of an A-X spin system, may be transferred to spin X through the scalar coupling, $J_{ax}$. Therefore the A magnetization in the X-Y plane

will also depend upon the Larmor frequency ωx and the 2D COSY will show signals with frequency coordinates (ωA, ωX) and (ωX, ωA) as well as (ωA, ωA). The former are the characteristic cross peaks of COSY spectrum and the latter, the diagonal peaks, which corresponds to 1D spectrum.

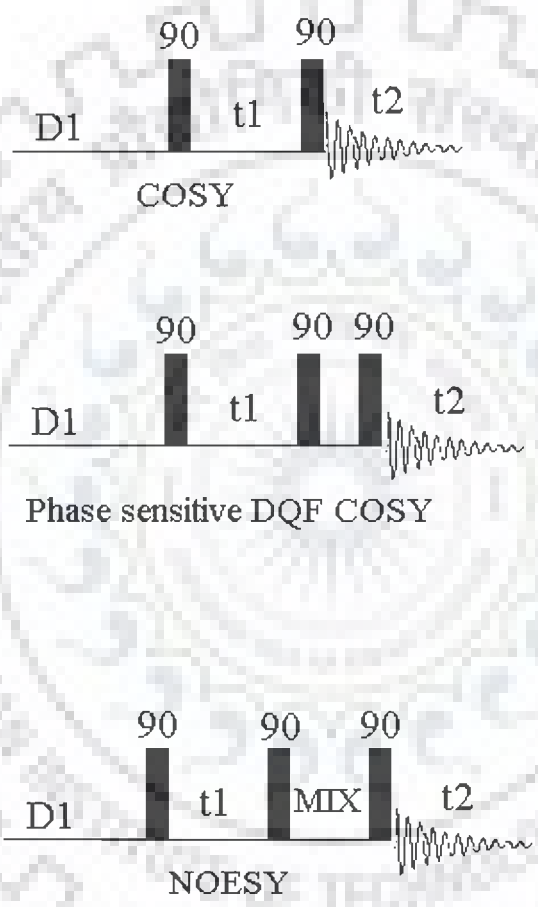


**Figure 2.4: Pulse schemes of various 2D NMR techniques**

COSY experiment can be carried out with special phase cycling and data processing to change the 2D line shape into pure 2D absorption mode, allowing the

use of phase-sensitive display. There are two different methods in use, the first requires the results of two complete COSY experiments with different phase cycling to be added [States et al., 1982] and the second known as TPPI (Time proportional phase incrementation) method uses a single experiment with phase cycling which changes with $t_1$ increment [Marion and Wüthrich, 1983]. The phase sensitive COSY spectra have cross peaks in antiphase. The antiphase multiplet structure of a cross peak only occurs in the active coupling giving rise to cross peak. Extra splitting present in multiplet but which do not give rise to cross peaks are called passive couplings and appear in phase. Thus, the advantage of phase sensitive COSY is that the phase relation between peaks can be used for accurate assignment and calculation of coupling constants.

**2.5.5.2 Phase Sensitive COSY: Double Quantum Filtered COSY (DQF-COSY)**

The experiment uses a pulse sequence $90_{\phi}$-$t_1$-$90_{\varphi}$-$90_{\zeta}$-$t_2$ where $\phi$, $\varphi$ and $\zeta$ are the appropriate phase cycles (Piantini et al, 1982). In double quantum filter COSY experiment, (Figure 2.4) the resonance from a COSY experiment is passed through a double quantum filter, thereby removing methyl and other singlets from the final spectrum. The short delays, $\Delta$, immediately before and after the final pulse, are of order of microseconds. Twice as many transients are needed in these experiments to achieve the same signal to noise ratio than in conventional COSY. Another advantage of DQF COSY is that it converts the phase of COSY diagonal signals from dispersive antiphase to absorptive antiphase. These signals then do not interfere with the cross peaks. So, the cross peaks lying close to diagonal can be observed in double quantum filtered phase-sensitive COSY. Double filter COSY can be used to determine the coupling constants [Celda et al., 1989; Gochin et al., 1990]

### 2.5.5.3 Total Correlated Spectroscopy (TOCSY)

During this pulse sequence, after the evolution period $t_1$, the magnetization is spin-locked. During this mixing time, the magnetization exchange through scalar coupling. During this spin-lock period, the magnetization behaves as a strongly coupled spin system and evolves under the influence of a "collective spin-mode". In that collective mode, coherence transfer is possible between all coupled nuclei in a spin system, (even if they are not directly coupled). This essentially gives the same information as that of COSY, except that COSY gives information only on the directly coupled spins, whereas TOCSY gives the complete spin-coupling network.

### 2.5.5.4 Nuclear Overhauser Effect Spectroscopy (NOESY)

NOESY is one of the most useful techniques as it allows correlating nuclei through space (distance smaller than 5Å). By measuring cross peak intensity, distance information can be extracted. The pulse sequence starts as usual with a 90° pulse followed by an evolution time $t_1$ (Figure 2.4). This delay is varied systematically as usual to provide chemical shift information in the F1 domain. Then 90° pulse transmits some of the magnetization to the Z-axis and during the following mixing period, the non-equilibria Z component will exchange magnetization through relaxation (dipole-dipole mechanism). This exchange of magnetization is known as Nuclear Overhauser Effect (NOE). After some time (shorter than the relaxation time T1), the transverse magnetization is restored and detected. If relaxation exchange (or chemical exchange) has taken place during the mixing time, cross peaks will be observed in the spectra. The phase cycling ensures proper detection of NOESY signal.

### 2.5.5.5 Hetero – Nuclear Multiple Bonded Correlation Spectroscopy (HMBC)

Long-range hetero-nuclear correlation can yield signals for these nuclei while suppressing one-bond correlations. The most common application of this technique is for $^{1}H$-$^{13}C$ and $^{1}H$-$^{31}P$. $\Delta_1$ is set to 1/ (2J one-bond) and $\Delta_2$ to 1/ (2J long- range). The phase is strongly dependent on the long range and hetero-nuclear proton coupling constant so each multiplet peak pattern has a different phase with an extreme first order component. The correlation experiment does not contain a diagonal. Each proton signal may be correlated with one or more carbon signals. Those signals in the 1D spectrum that do not correlate with carbons do not appear in the 2D spectrum (Figure 2.5).

| Nucleus bound to H | Ratio of 1st and 3rd gradient | J (one-bond) |
|---|---|---|
| $^{13}C$ | 3.98 | 145 Hz |
| $^{31}P$ | 12.0 | 8 Hz |

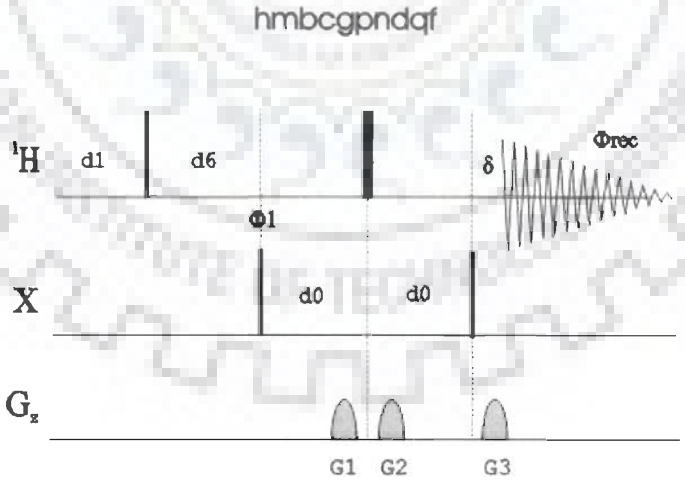


**Figure 2.5: Pulse sequence for HMBC**

### 2.5.5.6 Diffusion Ordered Spectroscopy (DOSY)

The DOSY experiment is the measure of diffusion coefficients by NMR. In DOSY spectra, chemical shift is detected along the F2 axis and diffusion coefficient is along the F1 axis. The method developed by Stejskal and Tanner which relies on two gradient pulses surrounding the 180° pulse in the spin echo was used. The first gradient dephases, the transverse magnetization in a spatially dependent manner along the z-axis and the second gradient then rephases the magnetization. The relation between translational self-diffusion and the measurable NMR parameters (Stejskal and Tanner, 1965) is:

$$A/A_0 = -\exp\left[D_t\gamma_H^2\delta^2G_z^{\,2}(\Delta - \delta/3)\right]$$

where A is the measured peak intensity (or volume), $A_0$ is the maximum peak intensity, $D_t$ is the translational diffusion constant (in $cm^2/s$), $\gamma_H$ is the gyromagnetic ratio of a proton ($2.675197 \times 10^4\ G^{-1}\ s^{-1}$), $\delta$ is the duration of the gradient, $\Delta$ is the time between gradients and $G_z$ is the strength of the gradient (in G/cm).Data can be plotted as $-\ln (A/A_0)$ versus $\gamma_H^2\delta^2G_z^2\ (\Delta-\delta/3)$. The slope of the line gives the value of $D_t$. The pulse program used is Pulsed gradient spin echo (stimulated echo sequence incorporating bipolar gradients) sequence modified with binomial water suppression (Figure 2.6). The gradient strengths were incremented as a square dependence in the range from 1 to 32 G $cm^{-1}$. It has been developed in order to facilitate the complex mixture analysis without physical separation. This experiment will monitor any modification of the solvent or of the solutes, and molecular events such as molecular interactions or associations.

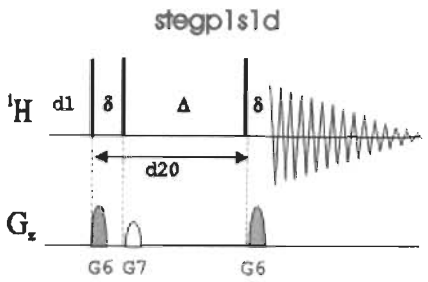


**Figure 2.6: Pulse sequence for DOSY**

### 2.5.6 Experimental Parameters

All NMR experiments were recorded on Bruker Avance 500 MHz FT-NMR spectrometer at Central NMR Facility located at Indian Institute of Technology Roorkee.

#### 2.5.6.1 Study of Drugs Berberine and Berberubine

Berberine and berberrubine have been studied in detail in $D_2O$ and DMSO respectively. *1D $^1H$ NMR* temperature dependent studies for berberine have also been carried out in $D_2O$ (278 K–353 K). $^1H$ NMR experiments were acquired with 32 / 64 K data points; number of scans = 64–128 and digital resolution = 0.25–0.5 Hz / point. $^{13}C$ 1D NMR were acquired with number of data points = 32 K / 64 K, no. of scans = 2048 and digital resolution= 0.7335 Hz / point.

***(a) Homonuclear ($^1H$–$^1H$) 2D experiments***

Acquisition parameters for the experiments are as follows

***i. DQF–COSY experiment*** 2048 data points along $t_2$ dimension; 512 induction decays in $t_1$ dimension; no. of scans = 40 and digital resolution 3.73037 Hz / point in t1 dimension and relaxation delay of 2.0 secs.

***ii. 2D ROESY experiment*** 2048 / 4096 data points along $t_2$ dimension; 512 induction decays in $t_1$ dimension; no. of scans = 40 and digital resolution 3.73037 Hz / point in t1 dimension and relaxation delay of 2.0 secs and mixing time ($\tau_m$) = 300 ms.

***iii. 2D TOCSY experiment*** 2048 data points along $t_2$ dimension; 512 induction decays in $t_1$ dimension; no. of scans = 40 digital resolution 3.73037 Hz / point in t1 dimension and relaxation delay of 2.0 secs; FnMode = TPPI and mixing time ($\tau_m$) = 70 ms.

***(b) Heteronuclear ($^{13}C - ^{1}H$) 2D experiments***

The acquisition parameters are

***i. HSQC experiment:*** 2048 data points along $t_2$ dimension; 400 induction decays in $t_1$ dimension; no. of scans = 48; digital resolution 3.09 Hz / point in t1 dimension and relaxation delay of 2.0 secs.

***ii. HMBC experiment:*** 2048 data points along $t_2$ dimension; 400 induction decays in $t_1$ dimension; no. of scans = 48 digital resolution 3.09 Hz / point in t1 dimension and relaxation delay of 2.0 secs. $\tau$ value was optimized for 8Hz coupling constants.

**2.5.6.2 Study of Berberine–DNA complex**

$^{31}P$ and $^{1}H$ NMR experiments were recorded for d-$(CCAATTGG)_2$ and its complex with berberine on successive addition of drug (Table 2.2) at 283 K in $H_2O$ + $D_2O$ ( 90:10)solvent.

The parameters were as follows:

***1D $^{1}H$, $^{31}$ NMR*** experiments were acquired with 64 K data points; number of scans = 64–128 and digital resolution = 0.15–0.3 Hz / point. Receiver gain was optimized in each instance to obtain the best signal to noise ratio.

***1D $^{31}P$ NMR*** experiments were acquired with 64 K data points, number of scan = 128 and digital resolution 0.12 Hz / point.

***$^{1}H - ^{31}P$ HMBC*** experiment were recorded with 2048 data points along $t_2$ dimension; 400 induction decays in $t_1$ dimension; no. of scans = 64 digital resolution 3.09 Hz / point in $t_1$ dimension and relaxation delay of 2.0 secs. $\tau$ value was optimized for 8 Hz coupling constants.

***$^{1}H - ^{1}H$ 2D NOESY experiment*** were recorded with variable mixing times ($\tau_m$) 100, 200 and 300 ms at 278 / 283 K. Number of data points = 2048 data points along $t_2$ dimension; 256 induction decays in $t_1$ dimension; no. of scans = 48-64 digital resolution 1.495 Hz / point in $t_1$ dimension and relaxation delay of 2.0 secs. Mixing time ($\tau_m$) = 100, 200 and 300 ms were used for D / N= 0.5, 1.0, 1.5 and 2.0 complex.

***$^{31}P - ^{31}P$ 2D NOESY*** experiments for D / N = 0.2, 0.5, 1.0, 1.5 and 2.0 at 283 and 298K K were recorded with mixing time of 150 / 200 ms; 4096 data points along $t_2$ dimension; 300 free–induction decays in $t_1$ dimension; no. of scans = 128; digital resolution 1.495 Hz / point in $t_1$ dimension and relaxation delay of 2.0 secs.

***DOSY*** experiments were recorded with diffusion time ($\Delta$) of 100 ms and the duration of the magnetic field gradients ($\delta$) 6 ms, respectively in $D_2O$. Other parameters include a sweep width of 6000 Hz, 64 K data points, 16 transients, digital resolution 0.30 Hz / point and relaxation delay of 10 s.

## 2.6 Determination of Three-Dimensional Structure

### 2.6.1 Resonance Assignments in Nucleic Acids

Resonance assignment is the first endeavour in the structural determination of DNA. From the NMR point of view, the protons can be grouped into four categories; (i) exchangeable NH and $NH_2$ protons of the bases and non-exchangeable base

protons between 7-15 ppm (ii) non-exchangeable sugar protons between 2-6.5 ppm (iii) methyl protons of thymine between 0.5-2 ppm. In order to observe NH and $NH_2$, protons, experiments have been carried out in water whereas the other protons were observed in $D_2O$ solution. The strategy for resonance assignment consists of two steps. In the first stage, the J correlated spectra are used to identify network of coupled spins. In the second stage, the spin systems so identified are assigned to particular nucleotides along the sequence of the molecule by making use of the NOESY spectrum as described below. The sugar protons H1', H2', H2", H3', H4', H5' and H5" form a complex J correlated network (Figure 2.7). The various cross peaks observed in the 2D J-correlated between these protons was used in identification of spin system within individual nucleotide units. The H1' proton shows a cross peak with H2', H2" sugar protons. The H2' and H2" protons are further coupled to H3' proton. We have used phase sensitive DQF-COSY spectra to identify the various J-coupled cross peaks. In the second phase sequential assignment is carried out using NOESY spectrum. Short internucleotide distances between adjacent nucleotide units are used as shown in Figure 2.7. In right handed DNA with sugars in C3'-endo/C2'-endo/O1'-endo pucker and glycosidic angle in anti domain, a convenient strategy for sequential assignment is

$$(H6/H8)_n \longrightarrow (H2',H2'')_{n-1}$$

$$(H6/H8)_n \longrightarrow (H1')_{n-1}$$

$$(H6/H8)_n \longrightarrow (H6/H8)_{n-1}$$

where, n stands for nth residue in 5'-3' oligonucleotide sequence. In case of Z-DNA, where the repeating unit is a dinucleotide, the internucleotide pathway is Base (2n–1) .... H5' (2n–1) .... Base (2n) .... H1' (2n) .... H2' (2n) and H2" (2n) .... Base (2n+1).

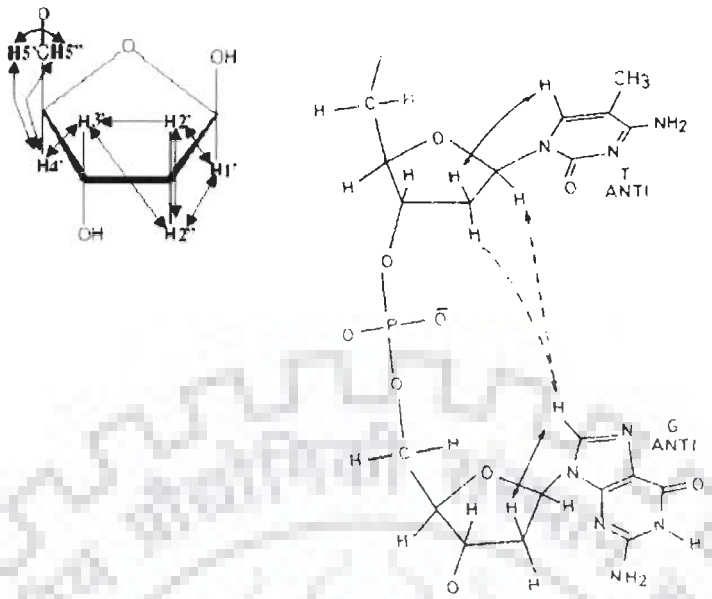


**Figure 2.7: Schematic representation of sugar J connectivities and short interproton distances between adjacent nucleotides units in right handed DNA.**

### 2.6.2 Pseudorotation

Because of the $r^{-6}$ dependence of the pre-steady state NOE, the relative magnitude of the NOEs provide a sensitive probe which can be used to obtain a qualitative view of the solution structures of short oligonucleotides. The glycosidic and sugar pucker conformations can be assessed qualitatively on the basis of the relative magnitudes of the intranucleotide sugar-base NOEs. The flexible five-membered sugar ring plays a pivotal role in nucleic acid structure and dynamic behaviour. In B-DNA family sugar responds to its surroundings (e.g. base stacking pattern) by an appropriate adaptation of its geometry. X-ray studies have now shown that P values usually occur in two distinct ranges. In a conformational wheel (Figure

1.7) one range of form occupies the "Northern" half of the circle (N-type, $P_N$ 0° ± 90°); the second range occupies the "Southern" hemisphere (S-type, $P_S$ 180 ± 90°). To a good approximation (0.4-0.7°) the torsion angles can be reproduced by a two-parameter pseudorotation equation:

$$\nu_j = \phi_m \cos [P + 0.8\pi (j-2)]$$

for j equals 0-4 and $\phi_m$ is amplitude of pucker. In crystal structures nucleotides usually a single pure N- or S-type conformer is found, but not necessarily the one that is predominant in aqueous solution. In some cases both N and S forms reside side by side in the same unit cell. Statistical analyses of X-ray data make it clear that details of sugar geometry of monomers are influenced by anisotropic crystal packing forces. The situation appears to be different in the helical oligomers, where stacking forces may play a more predominant role. NMR investigations in solution have demonstrated that N (C3'-endo) and S (C2'-endo) type conformations are in rapid equilibrium. If the interconversion rate between conformers is sufficiently rapid then observed couplings represent weighted average of couplings in individual conformers. Generally, in deoxyribose sugar, a trend to a larger proportions of C2'-endo pucker sugar is observed. A phase sensitive DQF-COSY spectrum allows J-coupling patterns to be delineated from the well-resolved cross peaks. In general, the relation between $^3J$ and φ takes the form of the semi empirical Karplus equation:

$$^3J = A \cos^2 (\varphi) + B \cos (\varphi) + C$$

The constants A, B and C have to be determined from $^3J$ values measured for compounds for which the value of φ, in solution, is known. There are five $^3J$ values in deoxyribose sugar, H1'-H2', H1'-H2", H2'-H3', H2"-H3' and H3'-H4', which are related to the relevant H-C-C-H dihedral angle, φ, according to the relation:

$$J = 10.2 \cos^2\varphi - 0.8 \cos \varphi$$

The above dihedral angles are inter-dependent and their values can be calculated in terms of the two pesudorotation parameters, P and $\varphi_m$, where $\varphi_m$ is a constant for deoxyribose and thus various geometries can be expressed in terms of P. (Figure 2.8) (Hosur et al, 1986) shows the plots of five coupling constants in a deoxyribose ring as a function of P, ($T_m$ = 38°). It is clear from the curves that the value of coupling constants $^3J$ (H1'-H2") and $^3J$ (H2'-H3') vary within a narrow range of 6-10 Hz and are comparatively insensitive to the sugar geometry. On the other hand, values of $^3J$ (H2"-H3'), $^3J$ (H3'-H4') and $^3J$ (H1'-H2') coupling constants vary in the range 0-10 Hz and can be utilized with greater advantage in fixing the domains of sugar geometry. $^2J$ (H2'-H2") is a geminal coupling which does not show significant conformational dependent variation. $^3J$ (H1'-H2'), $^3J$ (H1'-H2"), $^3J$ (H2'-H3'), $^3J$ (H2"-H3') and $^3J$ (H3'-H4') are vicinal coupling which show a strong dependence on the conformation of the deoxyribose ring. The approach used for determination of sugar geometry is based on interpretation of intra-sugar proton-proton distances.

### 2.6.3 Conformation about the Glycosidic Bond

A large body of crystallographic data for nucleotides clearly establishes that the torsional angle, $\chi_{CN}$, defining the orientation of base ring falls into two relatively narrow ranges designated as syn and anti conformation.

$$\chi \begin{cases} \text{O4'-C1'-N9-C4 (Purines)} \\ \text{O4'-C1'-N1-C2 (Pyrimidines)} \end{cases}$$

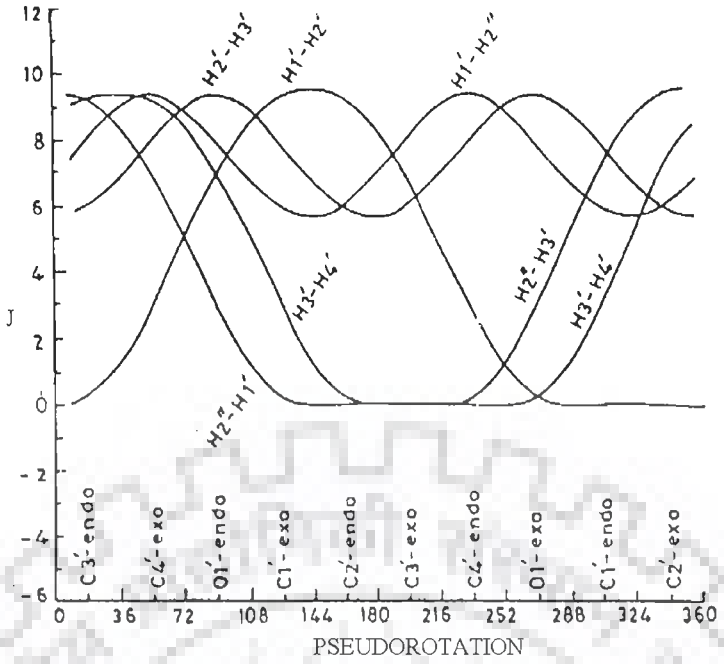


**Figure 2.8: Variation of the vicinal coupling constants in the deoxyribose ring as a function of the ring geometry.**

The relative magnitudes of the intranucleotide and internucleotide (H8/H6)-H1' and (H8/H6)-(H2', H2") cross peaks in NOESY spectra at different mixing times can be used to establish the domains of glycosidic dihedral angles of individual nucleotide unit [Roche et al., 1994]. Below the spin diffusion limit, the intensity patterns of the cross peak look similar at all mixing times although the absolute intensity may vary with the mixing time. The expected intensity patterns for the above mentioned cross peaks for different glycosidic dihedral angles are given below:

1. For the syn conformation, a strong NOE between base H8/H6 and H1' protons should be observed. At the same time, the NOEs from base to H2' and H2" protons will be relatively weak and will have different intensities.
2. In the anti conformation, the NOE from base H8/H6 to H2' is stronger than the NOE from base H8/H6 to H2". Also, for right handed structures the H2" proton shows a stronger NOE to the base proton of the next nucleotide.

3. In the high anti conformation, the (H8/H6)-H2' and (H8/H6)-H2" NOEs will have similar intensities for C2'-endo geometry.

The (H8/H6)-H1' distance depends only on $\chi$ while, other distances depend on both P and $\chi$. Iso-distance contours have been calculated by Wuthrich[Wüthrich, 1986] in (P, $\chi$) space for H8/H6-H2', H2", H3', H4' and H5' distances.

## 2.7 Estimation of Interproton Distances

If one resonance A is irradiated, an increase (positive NOE) or decrease (negative NOE) of signal intensity of other resonances such as resonance C is observed when spin C is close in space to spin A. This phenomenon is called Nuclear Overhauser Effect or NOE. The NOE effect is the method for elucidation of 3D structural features and stereochemistry using NMR together with information from scalar spin-spin couplings. The most important quantity derived from NOE cross peaks is the cross-relaxation rate between protons i and j. The cross relaxation rate $\sigma_{ij}$ between two proton spins i and j is related to the distance between protons i and j in the following way:

$$\sigma_{ij} = \langle d_{ij}^{-6} \rangle f(\tau_{ij}) \qquad (1)$$

$\langle d_{ij}^{-6} \rangle$ denotes an ensemble average of molecular structures interconverting in thermal equilibrium where $f(\tau_{ij})$ is a function of correlation time $\tau_{ij}$ for the vector connecting the two spins. This function accounts for the influence of motional averaging processes on the NOE. The cross relaxation rates can be measured from buildup rates of cross peaks in 2D NOE spectra at several mixing times. According to equation (1), the measured cross relaxation rates are a function of the ensemble average properties, which are dependent on the configurational space accessible to the molecular system at the temperature and time scale. If the interconversion between conformational

equilibria in the oligonucleotide is fast on NMR time scale, NOEs from several equilibrium conformations will be observed simultaneously. This means that the derived set of distance constraints does not necessarily represent the average structure, and there may be no single conformation that is consistent with the data set. Initially the intensity of the cross peak in equation (1) varies linearly with mixing time, and therefore this condition is referred to as "linear regime", but on higher mixing times, this condition does not exist due to multispin relaxation. Interproton distances can be estimated by measuring the intensities of cross peaks in the "linear regime". Two-spin approximation is used in NOE distance measurements in which only the rate of dipolar magnetization transfer between proximal spins i and j is monitored and all other spins are ignored. For two spin approximation, the intensity $I_{ij}$ can be written as:

when $\omega \tau_c >> 1$

$$I_{ij} = \frac{\gamma^4 \hbar^2 \tau_c \tau_m}{10 r_{ij}^{-6}}$$

where $\gamma$ is gyromagnetic ratio and $\hbar$,, is Planck's constant divided by $2\pi$. In order to determine the accurate value of $\tau_m$ for estimation of interproton distances, NOE build up curves should be obtained as a function of $\tau_m$ for several cross peaks, since spin diffusion can be different for different protons. Correlation times, $\tau_c$, can be obtained from T2 and T1 measurements, according to the equation:

$$\tau_c = \quad 2\omega^{-1}(3T_2/T_1) - ^{1/2}$$

which holds good for $\omega\tau_c >> 1$

If protons i, j, k, l have similar $\tau_c$ values and if $r_{ij}$ is a known distance, then the unknown distance $r_{kl}$ can be calculated by comparing the intensities $I_{ij}$ and $I_{kl}$ in a single spectrum. $r_{ij}$

$$\frac{I_{ij}}{I_{ij}} = \frac{r_{ij}^{6}}{r_{ij}^{6}}$$

The choice of known distance is important in the light of the mobility associated with different atoms in the nucleic acid. Gronenborn have expressed the opinion of using different yardsticks for NOEs involving different group of protons [Gronenborn and Clore, 1985]. The r(CH5-CH6) and r(H2'-H2") have different effective correlation times and can be used as reference depending on the cross peak being compared. The thymidine (H6-CH3) distance of 3.0 Å can be used as reference for all NOEs involving $CH_3$ protons, the sugar H2'-H2" protons and for the rest, cytidine H5-H6 distance of 2.45 Å can be used. Reid et al examined H2'-H2" and H5-H6 cross relaxation at 15, 30, 60, 90 and 100 ms in dodecamer DNA duplexes [Reid et al., 1989]. Results indicate that sugars and bases have the same correlation times, therefore all proton-proton distances in short DNA duplexes can be determined by scaling the initial NOE build up rate to the slope of cytosine H5-H6 cross peak, as H2'-H2" NOE cross peak are close to diagonal and are usually unresolved.

The characteristics of NMR data can be summarized as below:

1. NOEs cannot be translated into the precise distances. In practice this means that NOEs give only a number of approximate upper limits (e.g., 3 Å, 4 Å and 5 Å for strong, medium and weak NOEs). Sometimes it is not possible to make this division and only one single upper limit is used. For some proton pairs, corrections have to be applied to the upper limit value. This may arise due to stereo specific assignments (e.g., methyl group of thymine) or because

of dynamic effects such as rotation of hydrogens in a methyl group and flipping of the aromatic rings.

2. Translating NOEs into reliable lower limit constraints is difficult, and it is preferable to take the sum of van der Waals radii as a lower limit to the distance. The absence of NOEs between two assigned protons may be translated into a minimum distance of proton pair.
3. NMR data contain contributions from different molecular conformations. Not all distance constraints need to be consistent with the single conformation.
4. NOE information is limited to short distance relative to the size of the drug-DNA complex. For some part of the molecule none or only a few NOEs are observed.

## 2.8 Restrained Molecular Dynamics and Simulated Annealing

When restrained energy minimization methods are used, inevitable local energy minima are encountered which can lead to inaccurate structures. To circumvent this, restrained molecular dynamics (rMD) are usually employed. This involves including NMR restraints in one of the many molecular dynamics simulation programs. Molecular dynamics solve Newton's equation of motion,

$$F_i = m_i a_i \quad (1)$$

Where $F_i$ is the force, $m_i$ is the mass and $a_i$ is the acceleration of atom i. The force on atom i can be computed directly from the derivative of the potential energy V with respect to the coordinates $r_i$. The energy can be expressed in an explicitly differentiable form:

$$dV/dr_i = m_i d^2r_i / dt^2 \quad (2)$$

Therefore, with an adequate expression for the potential energy and the known masses, this differential equation can be solved for future positions in time $t_i$. In general, this can be solved only approximately, since V is usually a complex function of the coordinates of all (or many) of the atoms (i.e. $V = V(r_1, r_2, r_3, \ldots\ldots, r_N)$). The temperature can be calculated from the atomic velocities

$$3N/2\ k_B\ T = \sum_{i=1}^{N} 1/2\ m_i\ v_i^2 \qquad (3)$$

where, $k_B$ is Boltzmann's constant, $m_i$ and $v_i$ are the mass and velocity of atom i, and N is the number of atoms (and 3N is the number of degrees of freedom). For a simulation at constant energy, the temperature fluctuates due to the interconversion of kinetic and potential energy. If the temperature is held constant then the atomic velocities can be adjusted accordingly. If the pressure is held constant, the volume is allowed to fluctuate by rescaling the interatomic distances.

The total potential energy $V_{total}$ is usually defined as the sum of a number of terms:

$$V_{total} = V_{bond} + V_{angle} + V_{dihedr} + V_{vdw} + V_{coulomb} + V_{NMR} \qquad (4)$$

where, $V_{bond}$, $V_{angle}$ and $V_{dihedr}$ keep bond lengths, angles, and dihedral angles at their equilibrium values. The first five terms are empirical energy terms describing the physical interactions between the atoms, whereas the last term is a means of including the NMR information, but does not correspond to any real physical force. They can be summarized as follows:

$$V_{bond} = \sum_{bond} \tfrac{1}{2}\ K_b(b-b_0)^2 \qquad (5)$$

$$V_{angle} = \sum_{Angle} \tfrac{1}{2}\ K_\theta(\theta-\theta_0)^2 \qquad (6)$$

$$V_{angle} = \sum_{dihedr} K_\Phi(1+\cos(n_\Phi-\delta)) \qquad (7)$$

These are pseudo-harmonic potentials that constrain bond lengths (b), bond angles ($\theta$), and the rotamer angles ($\phi$, $\delta$) for staggered and eclipsed conformations, and K is a constant. The van der Waals and electrostatic interactions are described by $V_{vdw}$ and $V_{coulomb}$.

$$V_{vdw} = \sum_{\text{Pairs (ij)}} [C_{12}/ r_{ij}^{12} - C_6/ r_{ij}^{6}] \quad (8)$$

$$V_{coulomb} = \sum_{\text{Pairs (ij)}} qiqj / 4\pi\varepsilon_0\varepsilon_r r_{ij} \quad (9)$$

where equation (8) is the Lennard-Jones potential, containing repulsive and attractive terms (C is a constant), and equation (9) describes the coulombic interactions between two charged particles (i, j) with partial charges q that are at a distance $r_{ij}$ apart in a dielectric medium described by $\varepsilon_o\varepsilon_r$ term. The potential $V_{NMR}$ contains the NMR restraints, and has the effect of pulling the protons that show an NOE interaction closer to the measured distance $r_{ij}$. Similarly, these potentials are also pesudo-harmonic functions of similar forms to equations (5)-(7). Distance constraints which can be reasonably accurately determined may therefore be defined as follows:

$$V_{NOE} = \begin{cases} K_1(r_{ij}-r_{ij}^{0})^2 & \text{if } r_{ij} > r_{ij}^{0} \\ K_1(r_{ij}-r_{ij}^{0})^2 & \text{if } r_{ij} < r_{ij}^{0} \end{cases} \quad (10)$$

where, $r_{ij}$ and $r^{0}_{ij}$ are the calculated and experimental interproton distances, respectively, and $K_1$ and $K_2$ are force constants given by:

$$K_1 = k_B TS/ [2(\Delta^{+}_{ij})^2] \text{ and } K_2 = k_B TS/ [2(\Delta^{-}_{ij})^2] \quad (11)$$

Where $k_B$ is Boltzmann's constant, T, absolute temperature of the simulation, S a scale factor, and $\Delta^{+}_{ij}$ and $\Delta^{-}_{ij}$ are the positive and negative error estimates, respectively, of $r_{ij}$. If, however, only ranges of distances can be specified, then the distance restraints are incorporated into a pseudo-square-well potential of the form:

$$V_{NOE} = \begin{cases} K_{NOE}(r_{ij}-r_{ij}^{u})^2 & \text{if } r_{ij} > r_{ij}^{u} \\ 0 & \text{if } r_{ij} \leq r_{ij} \leq r_{ij}^{u} \\ K_{NOE}(r_{ij}-r_{ij}^{l})^2 & \text{if } r_{ij} < r_{ij}^{l} \end{cases} \quad (12)$$

where $r^{u}_{ij\ and}\ r^{l}_{ij}$ are the upper and lower limits, respectively, of the target distances obtained from the experimental, and $K_{NOE}$ is the force constant, which is typically chosen to be the order of 1000 kJ $mol^{-1}$ $nm^{-1}$.

To ensure that the experimental restraints are the dominating factor in determining the conformation of the molecule, it is very important that the force constants for the restraints are set sufficiently high that the experimental data are satisfied within the precision of the measurements. At the same time, the contribution from the empirical energy function should be such that in any individual rMD structure, the deviations from ideal geometry are small, and the non-bonded interactions are good (i.e. the Lennard-Jones potential is negative). Thus convergence on the structure is guided by the requirement to minimize NOE or other restraint violations. The number of distance restraint violations $N_{viol}$ is counted when, for example, $r_{ij} \geq r_{ij}^{0} + 1$, which would for 1 Å fluctuations. Other parameters which can be minimized in addition to $N_{viol}$ is the sum of the distances in excess of the constraints $\sum \Delta r_{viol}$ which is defined as:

$$\Sigma \Delta r_{viol} = \sum_{K=1}^{N_{viol}} ( r_{ij)k} - [ (r_{ij}^{0})_k + 1] \quad (13)$$

where the sum runs over all those interproton (or pseudoatom) distances for which $N_{viol}$ is defined. Although an arbitrary structure may be used for restrained molecular dynamics calculation, in practice a starting structure obtained from distance geometry and energy minimization is often used. The rMD approach requires a relatively large

amount of computation time compared to distance geometry methods. This problem can be overcome by using a simplified potential energy function, where all non-bonded contact interactions are described by a single van der Waals repulsion term. Also by using a cut off distance, in which non-bonded interactions for pairs of atoms that are separated by a distance greater than some reasonable value (e.g. 5-10 Å) are excluded, the number of non-bonded interactions is decreased considerably. Simulated annealing involves raising temperature of the system followed by slow cooling in order to overcome local minima and locate the global minimum region of the target function. It is computationally more efficient than rMD and yield structures of similar quality. The potentials are very similar to rMD and again Newton's laws of motion are solved as a function of time. However, in implementations found in commercial programs, the non-bonded interaction potential is modified so that there is a simple van der Waals repulsion term with a variable force constant $K_{rep}$:

$$V_{repel} = \begin{cases} 0 & \text{if } r \geq s.\ r_{min} \\ K_{rep}(s^2 r^2_{min} - r^2)^2 & \text{if } r < s.\ r_{min} \end{cases} \quad (14)$$

The values of $r_{min}$ are given by the sum of the standard values of the van der Waals radii between two atoms as represented by the Lennard-Jones potential.

## 2.9 Defining DNA Structure

The structure of DNA can be described by a number of parameters (Figure 2.9) that define the helix [Dickerson, 1983] termed as Helical Parameters. The output from helix analysis software CURVES 5.1 version of Richard Lavery [Lavery and Sklenar, 1989], includes "global helical parameters" defined relative to a global helix axis, that is, it depends on all the atoms in the structure and "local helical parameters"

defined relative to local helix axis at each base pair, that is, arises if only a subset of neighboring atoms is used to determine that quantity.

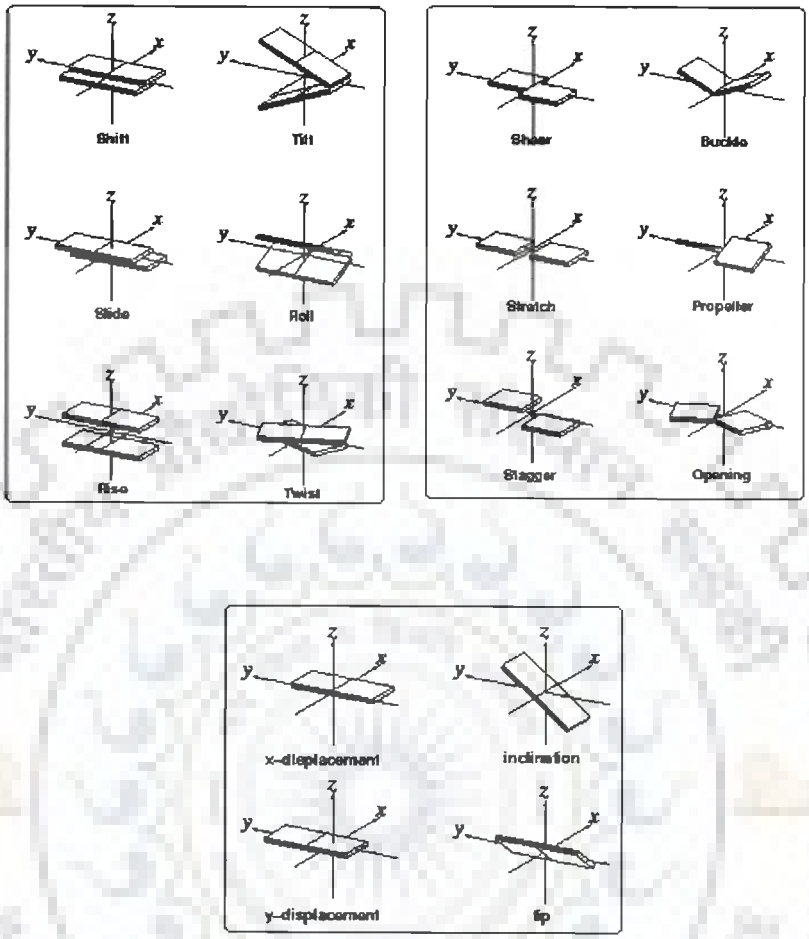


**Figure 2.9: Pictorial representation of helical parameters**

The helicoidal parameters are classified into three categories: 1.Global base pair-axis parameters 2. Intra-base pair or global base-base parameters 3. Inter-base pair or base pair-step parameters.

The global as well as the local inter-base pair parameters are related to particular base pair steps. These parameters are vector quantities, which have a defined location in 3-dimensional space and with respect to the nucleic acid sequence. In contrast, the average inter-base pair parameters are scalar values that are not related

to any part of the structure. They characterize properties of the whole structure. Intra base pair or global base-base parameters comprises of the translational components as stagger, stretch and shear, and the rotational components are propeller twist, buckle, opening. Propeller twist refers to the angle between the planes of two paired bases. A base pair is rarely a perfect flat plane with each aromatic base in the same plane. Rather, each base has a slightly different roll angle with respect to the other base. This makes two bases look like an aeroplane propeller. Twist or rotation per residue refers to the angle between two adjacent base pairs. Each step from one plate to the next can be described as a combination of a translational and a rotational movement.

The translational and the rotational displacements are three-dimensional vectors, which can be split into three orthogonal components. In inter-base pair or base pair-step parameters the three translational components are rise, shift and slide. Twist, roll and tilt are the three rotational components. Rise is the distance between adjacent planar bases in the DNA double helix i.e. it is a translation in the direction of the helical axis (z-axis), and shift is orthogonal to the helical axis and directs to the major groove side. Twist is a rotation about the helical axis (z-axis). Base pair roll refers to the angle of deflection of the base pair with respect to the helix axis along a line drawn between two adjacent base pairs relative to a line drawn perpendicular to the helix axis. A positive roll indicates that there is a cleft between two stacked base pairs, which opens towards the minor groove. A negative roll is related to an opening towards the major groove. Base pair tilt refers to the angle of the planer bases with respect to the helical axis. In the B-form DNA the bases are tilted by only –6°. In the A-form DNA the base pairs are significantly tilted at an angle of 20°. The sense of the base-pair tilt is associated with sugar puckering. In double helical polynucleotide, the normal to the base pair are not exactly parallel to the helix axis but inclined to it by up

to 20°. The sense of tilt is positive in A-type and negative in B-type of helices, and hence is correlated with sugar puckering. Base tilt angle is correlated with rise per residue. If the bases in base pairs were coplanar and the base pairs exactly perpendicular to the helix axis, the axial rise per nucleotide should correspond to the van der Waal's distance, 3.4 Å.

***Global base pair axis parameters:*** x- and y- displacement refers to the shift of bases in positive or negative x and y direction with respect to each other, besides this tip and inclination are also there

***Inter-base parameters (Base pair step parameters):*** The helical parameters are derived from the spatial location of the bases, while the sugar phosphate backbone is not taken into account. The six inter base pairs parameters (rise, twist, shift, roll, tilt, slide) describe the local conformation of a double helix at every base pair step The translational and the rotational displacements are 3-dimensional vectors, which can be split into three orthogonal components. The three translational components are rise, shift and slide. Rise is a translation component in the direction of the helical axis (z-axis) and shift is orthogonal to the helical axis and directs to the major groove side. Twist, roll and tilt are the three rotational components. Twist is a rotation about the helical axis (z-axis). A positive roll indicates that there is a cleft between two stacked base pairs which opens towards the minor groove. A negative roll is related to an opening towards the major groove. The definitions of the six inter base pair parameters are rigorous but the Cambridge convention does not define how to establish the reference coordinate system. The decomposition of the total translational and rotational movement into orthogonal components depends crucially on the reference system used. Several different algorithms and programs exist for calculating

the helical parameters. The algorithms differ mainly in the methods used to derive the reference coordinate systems.

***Intra-base pair step parameters (Base pair parameters):*** The base pairs in nucleic acid structures are not really planar. For example, the propeller twist of AT base pairs in B-DNA is usually in the range of -15° to -20°. If the base pairs are not planar, the six inter base pair parameters will give only a rough model of the helix. A more detailed picture is obtained if also the intra base pair parameters are taken into account. The Cambridge convention defines six base pair parameters which describe the deviation from planarity within a base pair. These six parameters describe the translational and rotational displacement between the two bases of a base pair. Again, the translational and rotational displacement is divided into orthogonal components. The translational components are stagger, stretch and shear, and the rotational components are propeller twist, buckle, opening Instead of determining the (intra) base pair parameters, it is also possible to calculate the inter base pair separately for each strand.

## 2.10 Quantum Mechanical Calculations

The popularity of density functional methods and their applications to a broad range of problems and biochemical interest has been growing rapidly each year (Parr et al, 1989, Labauowski et al, 1991, Kohn et al, 1996). Therefore the calculations are carried out using a Density Functional Theory (DFT). Along with it, Hartree-Fock wave function (HF) with self -consistent field (SCF) calculation is used for the comparison. The DFT method used is as follows: Hybrid B3LYP based on Becke's three parameters functional (Lee et al, 1988) and the correlation functional provided by LYP (Becke et al, 1993).

In all of these calculations, Cartesian Gaussian type orbitals (GTO's) are used as basis function for the molecular orbital. Although the capability of the basis functions to describe bonding deformations of the electronic density can be enhanced by increasing the number of basis functions for each orbital or including higher angular functions, yet as a thumb rule it should be able to yield results which are comparable with larger basis set while remaining computationally manageable, and thus at least a basis set of the split- valence type with polarization function should be employed.

All calculations presented are done using the Gaussian 98 and Gaussian 03 program package (Marek et al, 2003). Full unconstrained geometry optimizations were performed using the density function as well as Hartree-Fock wavefunction as outlined above. For each of these density functional methods several basis sets like STO-3G, 6-31G, 6-31G**, 6-311G, 6-311G** are used for optimizing the geometry. All the molecular properties and chemical shifts are computed using the optimized structure of the molecule. The chemical shifts were also calculated using the same Gaussian package with the Gauge Independent Atomic Orbital (GIAO) approach. This approach allows the computation of the absolute chemical shielding due to the electronic environment of the individual nuclei. On the ground of variational theory, the quality of wave functions has been traditionally determined by the total energy which is the average of the Hamiltonian over the wave function. The lower the energy, the better the quality and we retain this concept despite the fact that for properties other than the total energy it may not be acceptable. In view of this, the calculations for structural properties and chemical shifts only using B3LYP method are reported.

# CHAPTER 3

## Nuclear Magnetic Resonance Spectral and Quantum Chemical Studies on Molecular Properties and Electronic Structure of Berberine and Berberrubine

The discovery of anti-tumor activity exhibited by several metal complexes and molecular targets has been the subject of great attention. Among them cis-diamminedichloro-platinum II (cis-DDP) [Costa et al., 2006], organometallic compounds [Pruchnik et al., 2002] and protoberberines [Bhakuni and Jain, 1986; Preininger, 1986] are worth mentioning. Replacement of $OCH_3$ group at position 7 (Figure 3.1) in berberine with OH group, resulting in a derivative called berberrubine, induces a large change in the antitumor activity [Kim et al., 1998]. The structural and electronic properties of berberine and berberrubine have been studied extensively

In this Chapter, we present the conformational analysis properties of berberine and berberrubine. We have performed one dimensional proton NMR combined with two dimensional homonuclear ($^1H$-$^1H$) and hetronuclear ($^{13}C$-$^1H$) correlation experiments at 500 MHz to obtain the chemical shifts for berberine and berberrubine. Proton NMR studies were also carried out as a function of temperature in the range of 298-328 K. A restrained Molecular Dynamics (rMD) simulation was carried out to obtain most preferred conformations of the molecules.

In addition to experimental investigations, we report quantum chemical calculations based on density functional theory (DFT) and its variant to compute several molecular parameters and chemical shift for both berberine and berberrubine molecules.

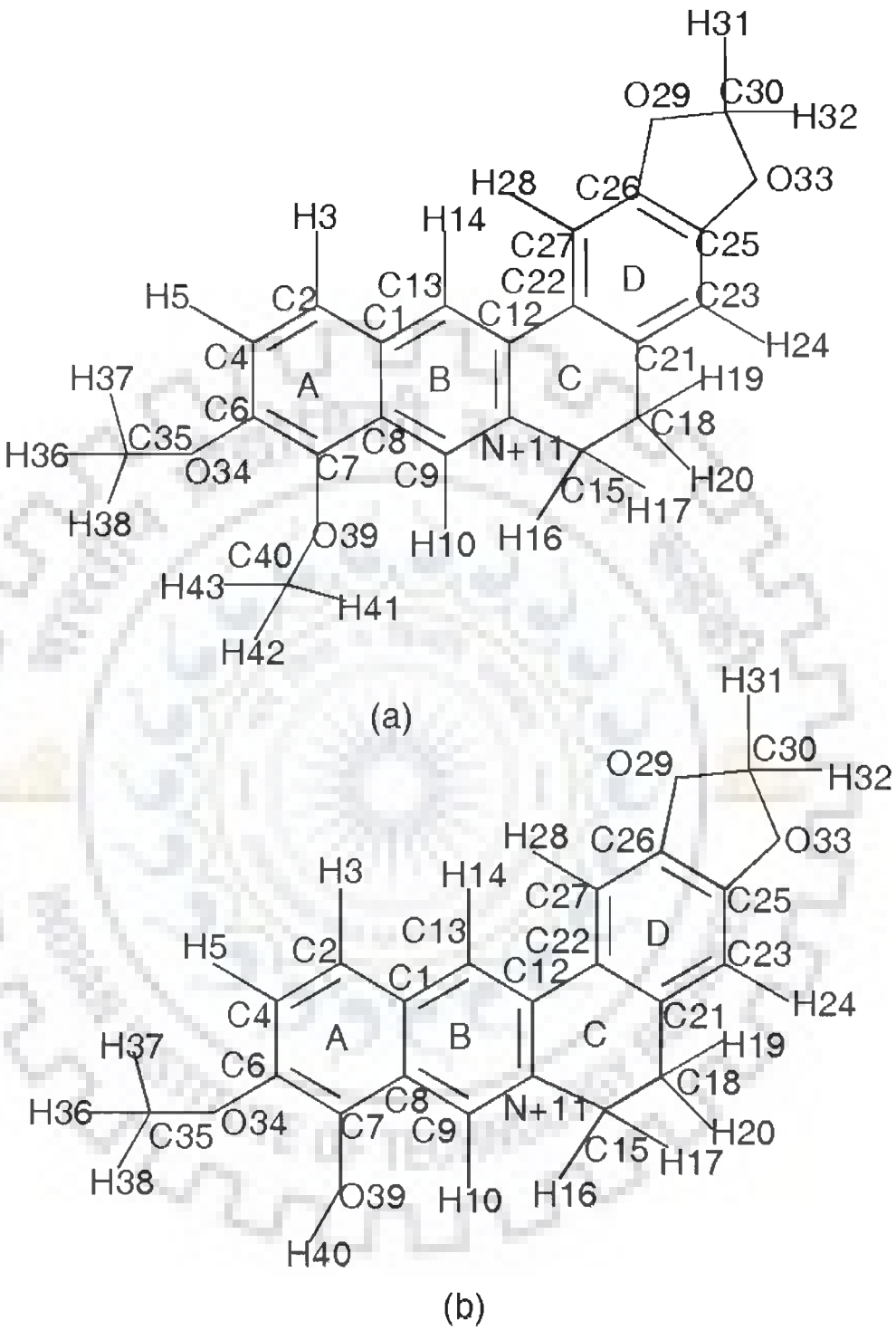


**Figure 3.1: Structure of (a) berberine and (b) berberrubine.**

In recent years the NMR chemical shift has become an important tool in the spectral assignment and rationalizing the experimental chemical shift data. The chemical shift is widely calculated using Gauge Invariant Atomic Orbital (GIAO) method as implemented in Gaussian 98 and Gaussian 03 package [Frisch et al., 1998]. We have followed the same approach to obtain these chemical shift positions along with other structural parameters. Several authors [Abraham et al., 2004; Casanovas et al., 2001; Colombo et al., 2002; Kupka et al., 2000; Lampert et al., 1997; Pulay and Hinton, 1995] have used this method successfully for calculating the chemical shifts of heavy atoms, organic compounds and complexes used in pharmaceutical systems. The popularity of density functional methods and their applications to a broad range of problems of biochemical interest has been growing rapidly each year [Kohn and Sham, 1965; Labanowski and Andzelm, 1991; Parr and Yang, 1989]. The most important contributing factor is simply the reliability and cost effectiveness of the calculations. The results of our rMD simulations in combination with DFT calculations provide a better insight of the observed features of the measured NMR spectra.

## 3.1 Results and Discussion

### 3.1.1 Nuclear Magnetic Resonance Studies of berberine and berberrubine

The $^{1}H$ NMR spectra of berberine in $D_2O$ (concentration 26.95 mM) is shown in Figure 3.2. Typical parameters for one–dimensional NMR experiments were: pulse width ~ 7.7 μs, no. of data points = 32 to 64 K, spectral width 5000 Hz, number of scans = 32–64, relaxation delay 1.0 s and digital resolution 0.08 Hz/point.

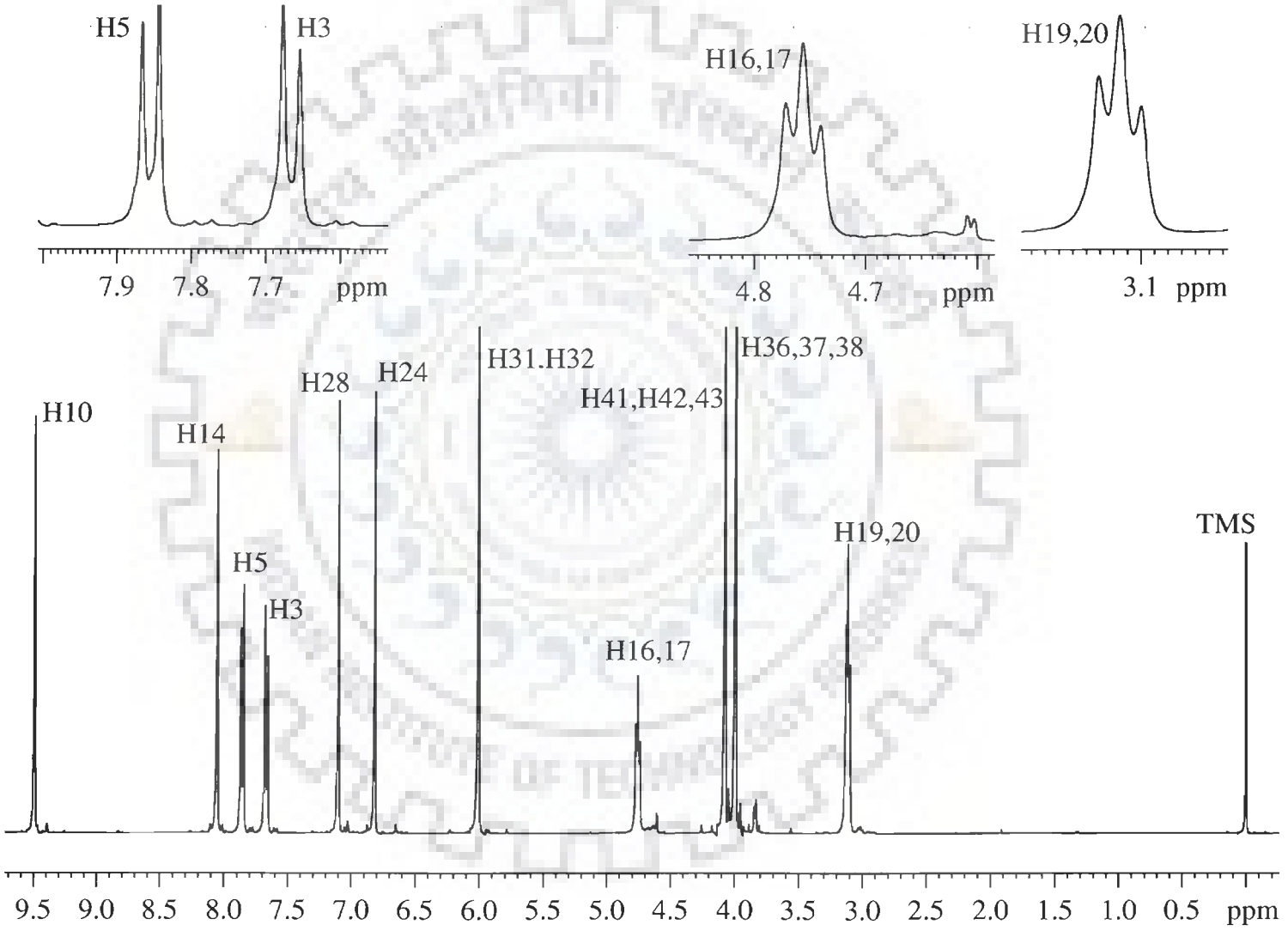


**Figure 3.2: 1D-$^{1}$H Spectra of Berberine in $D_2O$.**

The typical parameters for the 2D Rotating frame nuclear Overhauser Enhancement Spectroscopy (ROESY), Hetero-nuclear Single Quantum Correlation (HSQC), and Hetero-nuclear Multiple Bond Correlation (HMBC) experiments were: 1024-2048 data points along t2 dimension, 512 free induction decays in t1 dimension, pulse width ~7.7 μs, spectral width 6000 Hz ($^{1}H$) / 24000 Hz ($^{13}C$), number of scans 64, digital resolution 3.0 Hz/point and relaxation delay 1.0 s. A mixing time of 300 ms was used for ROESY experiments. A constant temperature of 298 K was maintained all through by using temperature controller.

### 3.1.1.1 Resonance Assignment of Berberine

The $^{1}H$ NMR spectra of berberine in $D_2O$ has been analyzed to do assignment for all the protons (Figure 3.2). The area under peaks shows that the resonances at 4.04 and 4.10 ppm correspond to three ($-CH_3$) protons, while those at 3.18, 4.90 and 6.11 ppm correspond to two protons ($-CH_2$) and all other resonances correspond to one proton (-CH). Since $OCH_3$ protons attached to C40 atom are closer to an electronegative atom N11, they are expected to be shifted downfield with respect to those attached to C5 atom. Accordingly the H41, 42, 43 and H36, 37, 38 are assigned to peaks at 4.10 and 4.04 ppm, respectively. In the same way, the methylene protons at 4.90 and 3.18 ppm are triplets having a spin – spin coupling of 6.0 Hz and are assigned to $CH_2$ protons attached to C15 and C18, designated as H16, 17 and H19, 20 atoms, respectively. The H31, 32 appear at 6.11 ppm, being shifted downfield considerably due to neighboring O29 and O30 atoms. Of the 6-CH protons appearing in the range 6.8-9.5 ppm, the two doublets are assigned to H3 and H5 having $^{3}J$ = 9.1 Hz; H5 is shifted downfield with respect to H3 due to

proximity to O34 atom. Among the ring B protons (H10, H14), H10 is expected to be more downfield being closer to N11 atom. Accordingly assignments have been made to H10, H14, H28 and H24 protons and are listed in Table 3.1. The $^{1}H$-$^{13}C$ Hetero-nuclear Single Quantum Coherence (HSQC) spectra (Figure 3.3) shows the coupling of 11 carbon atoms to protons which they are directly bonded through a single bond. The other 9 carbon atoms are easily assigned with the help of Hetero-nuclear Multiple Bond Correlation (HMBC) spectra (Figure 3.4). The observed carbon chemical shifts and carbon-proton bond correlations are listed in Tables 3.2 and 3.3, respectively. It may be noted that the proton chemical shifts are close to that observed by several groups [Huang et al., 2005; Jeon et al., 2002; Saran et al., 1995]. The difference in resonance positions in $C_6D_6$, $CD_2Cl_2$ and DMSO solvents [Blasko et al., 1988; Marek et al., 2003], are attributed to the effect of solvent on conformation of the molecules. The carbon chemical shifts are comparable to those cited in literature [Blasko et al., 1988; Huang et al., 2005; Jeon et al., 2002; Marek et al., 2003].

Figure 3.5 shows the ROESY spectra of berberine in $D_2O$ solution. We observe nine cross peaks and calculated the corresponding interproton distances from integrals using distance H3-H5 = 2.44 Å as reference (Table 3.4.)

### 3.1.1.2 Temperature Dependence Study of Berberine

We have also monitored the temperature dependence of berberine (26.95 mM) protons, by the change in chemical shift with increasing temperature (Figure 3.6) No significant variation was observed for any of the proton chemical shift.

**Table 3.1: Comparison of observed Proton chemical shifts (ppm) from spectra of berberine in different solvents with the experimental results reported in literature and with present calculated chemical shifts (ppm) with different wave functions and in different solvents by GIAO method using B3LYP method.**

| | Experimental | | | | | | Theoretical | | | | | | |
|---|---|---|---|---|---|---|---|---|---|---|---|---|---|
| **Proton** | Present work ($D_2O$) | Saran & Srivastava[15] ($D_2O$) | Jeon *et al*[12] ($D_2O$) | Marek *et al*[13] ($CD_2Cl_2$) | Marek *et al*[13] ($C_6D_6$) | Huang *et al*[13] ($D_2O$) | STO-3G | 3-21G | 6-31G | 6-31G** | 6-311G** | 6-311+ G(2d,p) | 6-311G** DMSO |
| **H3** | 7.93 | 7.83 | 7.9 | 6.90 | 6.87 | 7.30 | 7.97 | 7.42 | 7.65 | 7.75 | 7.82 | 7.88 | 8.47 |
| **H5** | 8.03 | 7.97 | 8.0 | 6.94 | 6.73 | 7.56 | 7.79 | 7.27 | 7.65 | 7.87 | 7.86 | 8.15 | 8.19 |
| **H10** | 9.64 | 9.62 | 9.5 | 6.18 | 6.36 | 9.29 | 9.44 | 9.23 | 9.31 | 9.09 | 9.17 | 9.30 | 9.55 |
| **H14** | 8.46 | 8.29 | 8.7 | 6.08 | 6.11 | 7.59 | 8.58 | 7.84 | 8.04 | 8.01 | 8.16 | 8.28 | 8.80 |
| **H16, 17#** | 4.90 | 4.87 | 4.9 | 3.57 | 3.57 | 4.53 | 4.65 | 4.70 | 4.65 | 4.60 | 4.46 | 4.61 | 4.84 |
| **H19, 20#** | 3.18 | 3.28 | 3.3 | 2.87 | 2.40 | 2.88 | 3.31 | 3.28 | 3.30 | 3.11 | 3.13 | 3.16 | 3.45 |
| **H24** | 6.96 | 6.93 | 6.9 | 6.62 | 6.36 | 6.55 | 7.09 | 6.55 | 6.95 | 6.82 | 6.91 | 6.94 | 7.32 |
| **H28** | 7.47 | 7.30 | 7.5 | 7.15 | 7.23 | 6.63 | 7.36 | 6.93 | 7.31 | 7.22 | 7.32 | 7.39 | 7.89 |
| **H31, 32#** | 6.11 | 6.10 | 6.1 | 5.94 | 5.34 | 5.78 | 5.75 | 6.94 | 6.81 | 6.56 | 6.48 | 6.56 | 6.52 |
| **H36, 37, 38#** | 4.04 | 4.14 | 4.0 | 3.85 | 3.44 | 3.75 | 3.79 | 4.50 | 4.40 | 4.20 | 4.12 | 4.18 | 4.19 |
| **H41, 42, 43#** | 4.10 | 4.08 | 4.1 | 3.91 | 3.98 | 3.88 | 4.64 | 5.17 | 5.09 | 4.70 | 4.55 | 4.48 | 4.35 |
| | | | | | | | | | | | | | |

# Pseudoatoms

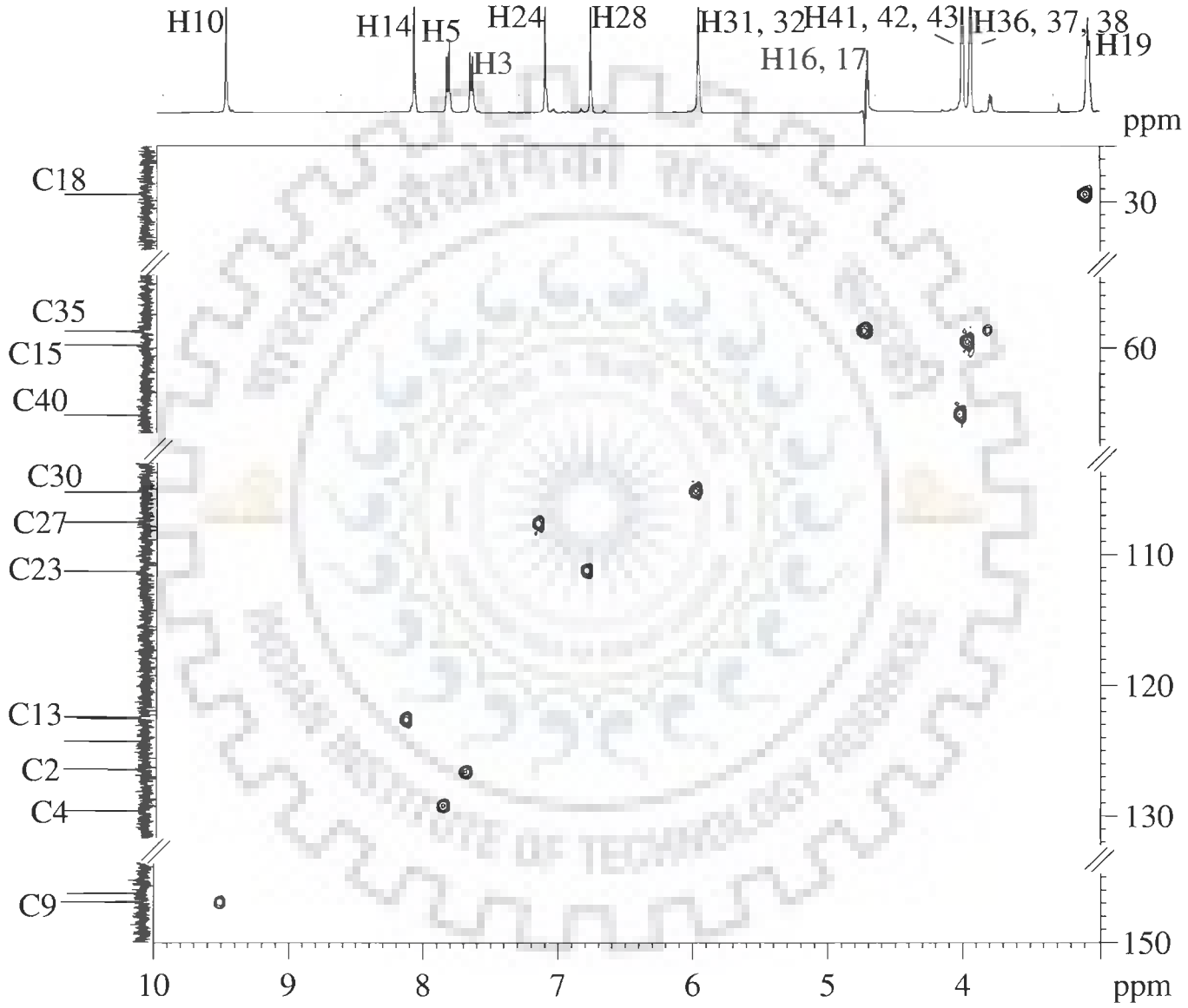


**Figure 3.3: HSQC spectra of berberine in $D_2O$ showing $^{1}H$-$^{13}C$ single bond correlations.**

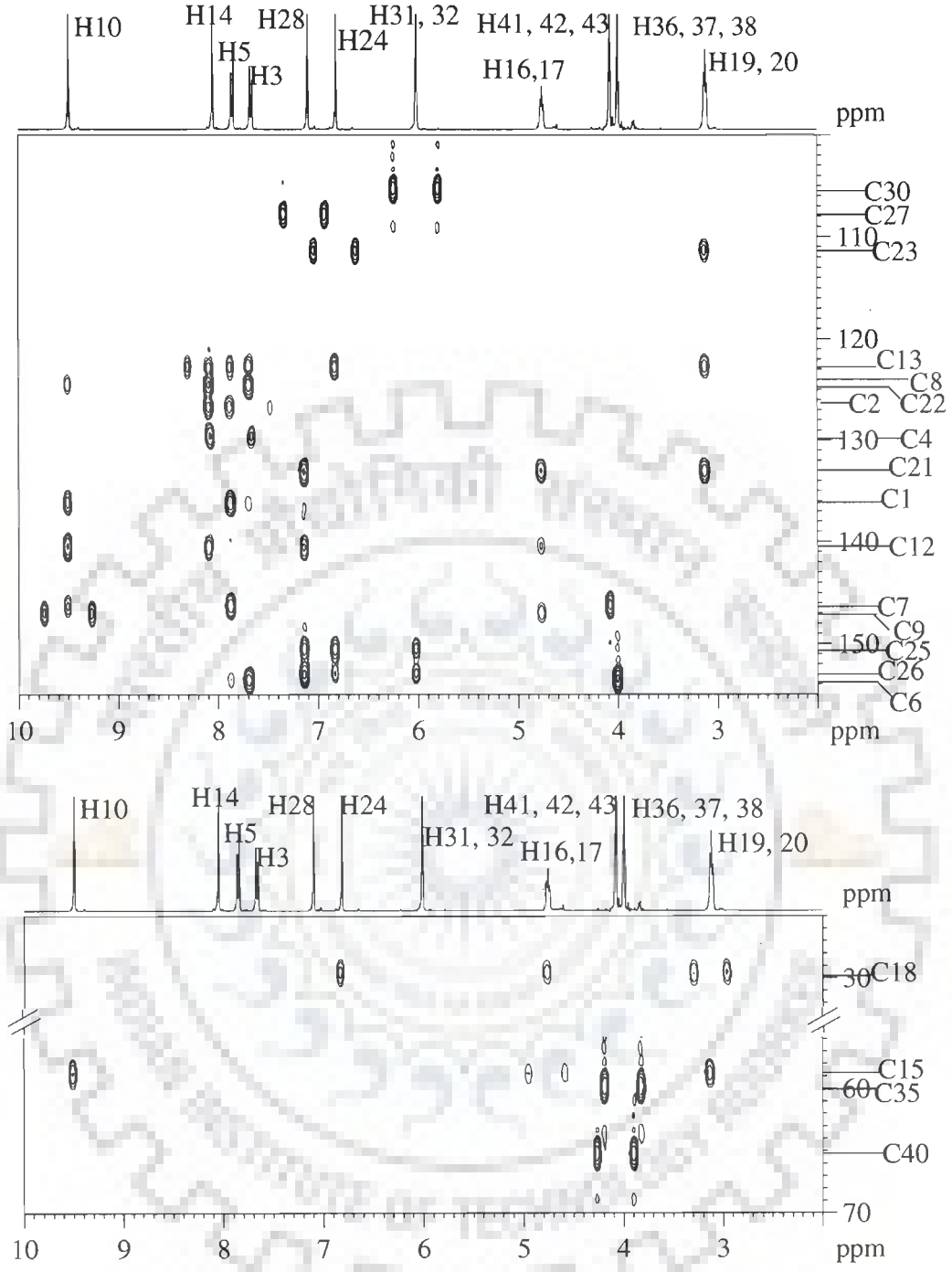


**Figure 3.4: Expansions of specific regions of HMBC spectra of berberine in $D_2O$ showing $^{1}H$ -$^{13}C$ multiple bond correlations.**

**Table 3.2: Comparison of observed Carbon chemical shifts (ppm) from spectra of berberine in different solvents with the experimental results reported in literature and with present calculated chemical shifts (ppm) with different wave functions by GIAO method using B3LYP method.**

| | Experimental | | | | | | Theoretical | | | | | | |
|---|---|---|---|---|---|---|---|---|---|---|---|---|---|
| **Carbon** | Present work ($D_2O$) | Huang *et al*[11] ($D_2O$) | Blasko *et al*[14] (DMSO) | Jeon *et al*[12] ($D_2O$) | Marek *et al*[13] ($CD_2Cl_2$) | Marek *et al*[13] ($C_6D_6$) | STO-3G | 3-21G | 6-31G | 6-31G** | 6-311G** | 6-311+G(2d,p) | 6-311G** (DMSO) |
| **C1** | 136.20 | 132.8 | 132.94 | * | 127.68 | 127.03 | 116.18 | 118.18 | 130.30 | 125.33 | 138.40 | 137.51 | 139.01 |
| **C2** | 126.50 | 123.5 | 123.53 | 130 | 119.72 | 119.82 | 109.47 | 107.73 | 117.97 | 120.70 | 125.70 | 125.59 | 130.48 |
| **C4** | 129.59 | 126.4 | 126.67 | 134 | 114.58 | 114.34 | 113.66 | 114.65 | 124.74 | 124.64 | 131.69 | 131.14 | 130.91 |
| **C6** | 154.00 | 150.6 | 150.36 | * | 150.33 | 150.20 | 134.95 | 137.11 | 148.30 | 150.49 | 156.17 | 156.54 | 159.33 |
| **C7** | 146.00 | 143.2 | 143.61 | * | 146.17 | 145.46 | 132.95 | 134.53 | 144.60 | 147.85 | 152.99 | 152.63 | 152.62 |
| **C8** | 124.00 | 121.2 | 121.37 | * | 123.46 | 122.70 | 109.87 | 108.79 | 119.43 | 114.70 | 125.32 | 125.81 | 127.24 |
| **C9** | 147.06 | 144.3 | 145.42 | 145 | 79.50 | 79.39 | 127.73 | 129.89 | 142.02 | 140.89 | 148.49 | 147.17 | 149.81 |
| **C12** | 140.50 | 137.2 | 137.41 | * | 136.72 | 139.29 | 125.36 | 126.46 | 137.71 | 135.71 | 145.85 | 145.34 | 145.58 |
| **C13** | 122.57 | 119.2 | 120.18 | 125 | 95.34 | 95.06 | 110.50 | 109.32 | 118.65 | 119.31 | 125.25 | 125.29 | 127.43 |
| **C15** | 58.81 | 56.0 | 55.19 | 62 | 46.66 | 46.96 | 61.92 | 56.61 | 59.43 | 57.72 | 61.44 | 61.17 | 61.39 |
| **C18** | 29.42 | 26.7 | 26.35 | 36 | 30.48 | 30.80 | 35.29 | 30.29 | 31.18 | 29.79 | 32.44 | 31.88 | 32.11 |
| **C21** | 133.00 | 129.9 | 130.64 | * | 129.73 | 129.85 | 113.33 | 117.25 | 128.63 | 128.84 | 136.01 | 136.28 | 138.73 |
| **C22** | 124.10 | 119.4 | 120.42 | * | 126.21 | 125.78 | 108.81 | 109.28 | 119.40 | 118.85 | 124.97 | 124.47 | 127.34 |
| **C23** | 111.49 | 108.6 | 108.43 | 116 | 108.16 | 108.21 | 102.64 | 99.79 | 108.86 | 108.83 | 113.23 | 112.03 | 113.42 |
| **C25** | 150.50 | 150.1 | 149.76 | * | 147.82 | 147.93 | 135.74 | 197.76 | 151.74 | 146.01 | 160.51 | 160.98 | 158.10 |
| **C26** | 153.00 | 147.7 | 120.42 | 114 | 147.29 | 147.24 | 132.77 | 138.18 | 149.05 | 143.11 | 157.40 | 157.47 | 155.55 |
| **C27** | 107.65 | 104.3 | 105.43 | * | 104.96 | 104.60 | 100.33 | 96.34 | 104.77 | 105.36 | 108.90 | 107.38 | 110.46 |
| **C30** | 105.06 | 102.7 | 102.07 | 109 | 100.99 | 101.68 | 103.40 | 106.62 | 111.49 | 55.98 | 111.80 | 111.26 | 111.18 |
| **C35** | 59.83 | 56.7 | 57.06 | 63 | 56.07 | 56.56 | 56.81 | 55.06 | 57.63 | 54.52 | 57.76 | 57.80 | 57.74 |
| **C40** | 65.15 | 62.4 | 61.95 | 70 | 61.01 | 61.44 | 59.36 | 63.56 | 66.77 | 61.29 | 65.94 | 65.97 | 63.31 |

**Table 3.3: Observed correlation of carbon atoms with specific protons in HSQC and HMBC spectra of berberine.**

| Carbon | HSQC | HMBC | | |
|---|---|---|---|---|
| | | ss* | m* | w* |
| **C1** | - | H5 | H10 | - |
| **C2** | H3 | H14 | - | - |
| **C4** | H5 | - | - | - |
| **C6** | - | H3, H36, 37, 38 | - | H5 |
| **C7** | - | H5,H41, 42, 43 | H10 | - |
| **C8** | - | H3 | - | H10 |
| **C9** | H10 | - | H16 | - |
| **C12** | - | H10, H28 | H14 | H16, 17 |
| **C13** | H14 | H24, H19, 20 | H3 | - |
| **C15** | H16, 17 | H10 | - | - |
| **C18** | H19, 20 | - | H24 | H16, 17 |
| **C21** | - | H28, H19, 20, H16, 17 | - | - |
| **C22** | - | H14 | - | - |
| **C23** | H24 | - | H19, 20 | - |
| **C25** | - | H24 | H31, 32, H28 | - |
| **C26** | - | H28 | H31, 32, H24 | - |
| **C27** | H28 | - | - | - |
| **C30** | H31, 32 | - | - | - |
| **C35** | H36, 37, 38 | - | - | - |
| **C40** | H41, 42, 43 | - | - | - |

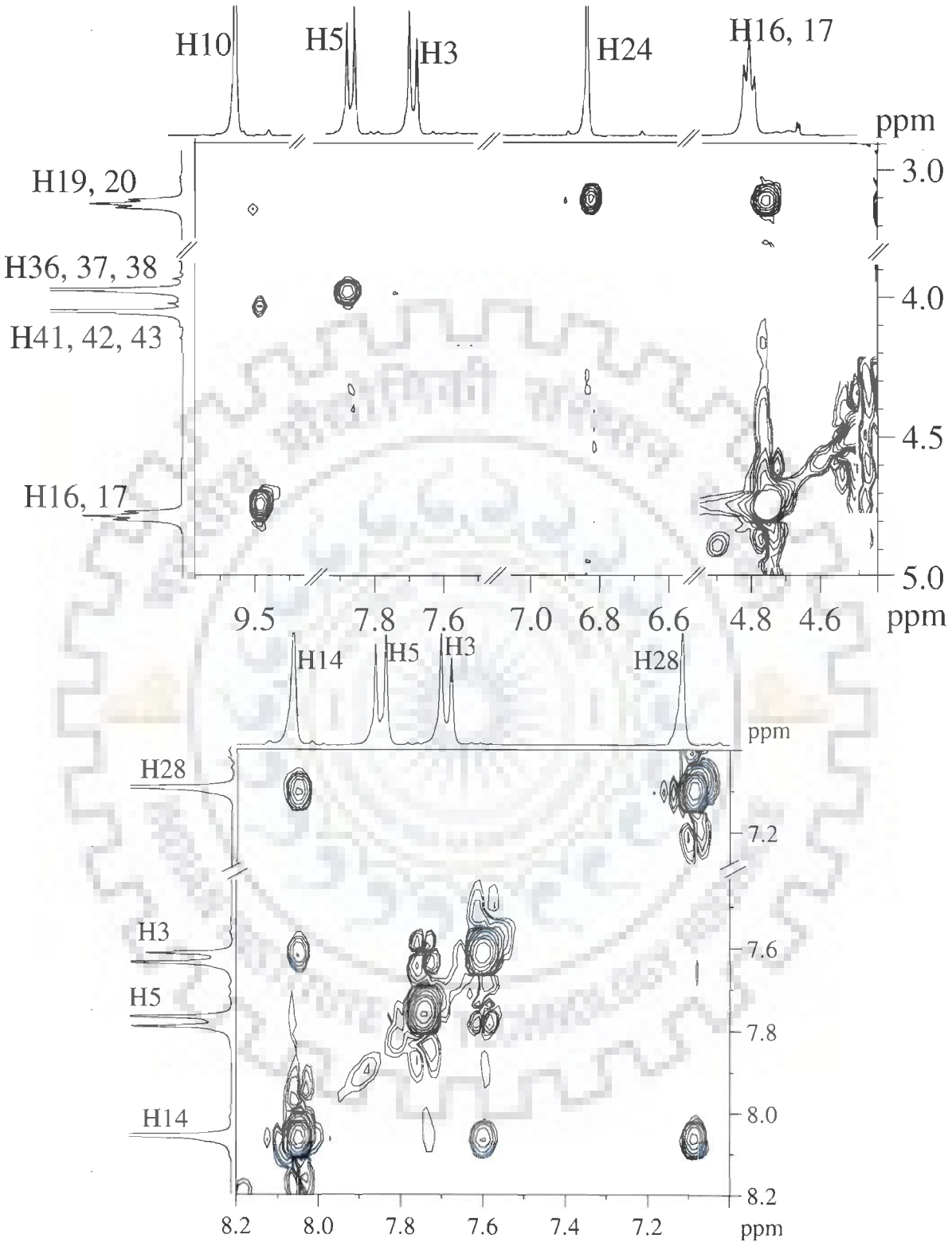


**Figure 3.5: Expansions of specific regions of ROESY spectra of Berberine in $D_2O$ showing interproton contacts.**

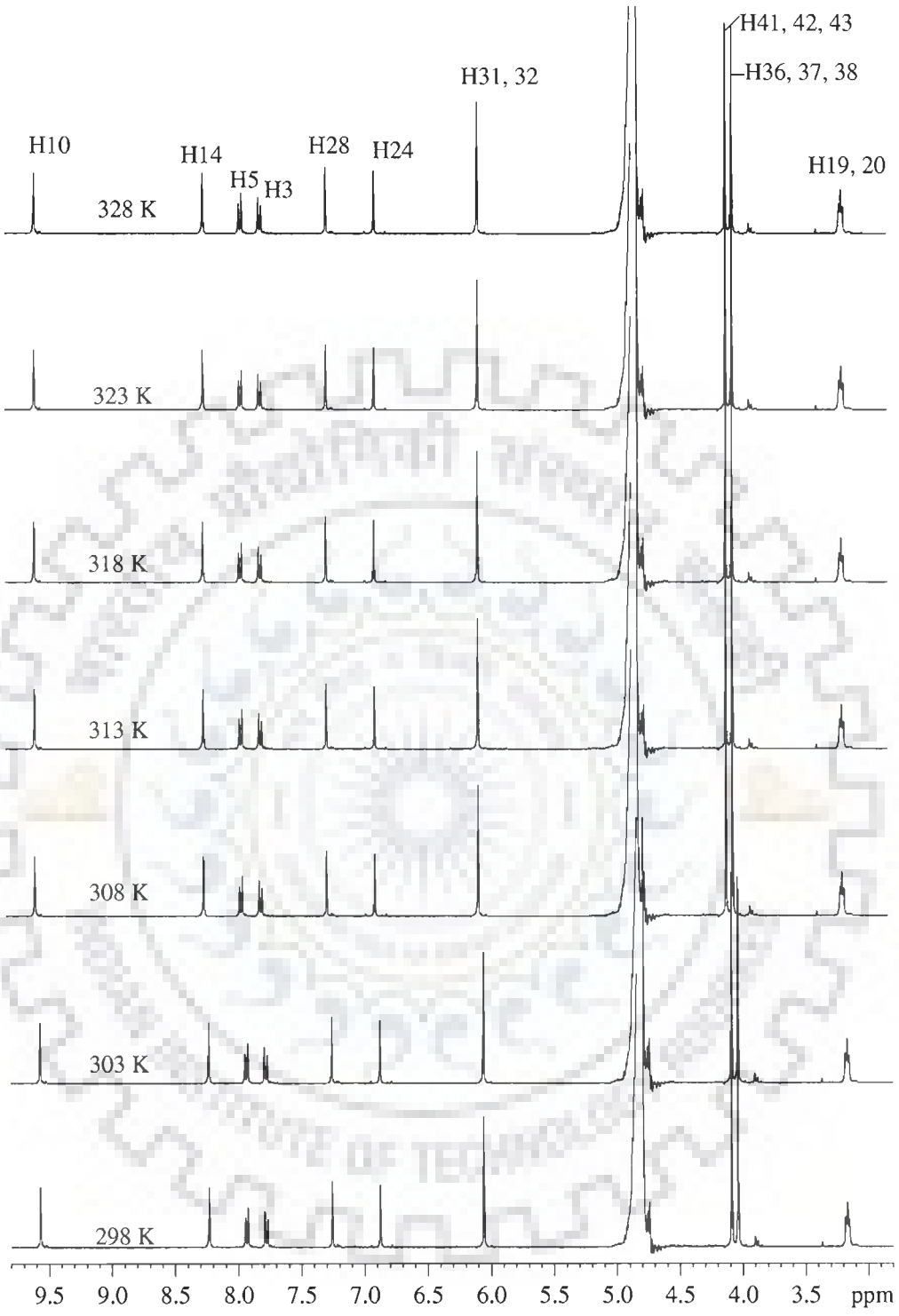


**Figure 3.6: $^{1}$H Proton spectrum of berberine with varying temperature in the range 298-328 K.**

**Table 3.4: Connectivities and interproton distances (Å) from ROESY spectra of berberine and berberrubine. The corresponding distances obtained from optimized rMD structure are also shown.**

| | Berberine | | | | | Berberrubine | | | | |
|---|---|---|---|---|---|---|---|---|---|---|
| **S.N.** | **Connectivities** | **Inter-proton distance (Å)** | **Distance in rMD structure (Å)** | **Inter- proton distance (Å) [Jeon et al., 2002]** | **Distance in rMD structure (Å)** | **Connectivities (Jeon *et al*)[12]** | **Inter-proton distance (Å)** | **Distance in rMD structure (Å)** | **Inter-proton distance (Å) [Jeon et al., 2002]** | **Distance in rMD structure (Å)** |
| **1** | **H24-H19, 20#** | 2.20 | 2.43 | 1.8-2.7 | 2.64 | **H24-H19, 20#** | 3.03 | 2.72 | 1.8-2.7 | 2.51 |
| **2** | **H16, 17#- H19, 20#** | 3.95 | 3.65 | 1.8-2.7 | 2.60 | **H16, 17#- H19, 20#** | 2.28 | 2.34 | 1.8-2.7 | 3.02 |
| **3** | **H5-H36, 37, 38#** | 3.13 | 2.78 | 1.8-3.3 | 3.89 | **H5-H36, 37, 38#** | 2.37 | 2.69 | 1.8-3.3 | 3.33 |
| **4** | **H10-H41, 42, 43#** | 2.57 | 2.76 | 1.8-3.3 | 3.51 | **H10-H16, 17#** | 2.86 | 2.50 | 1.8-3.3 | 2.87 |
| **5** | **H10-H16, 17#** | 2.35 | 2.23 | 1.8-3.3 | 3.00 | **H14-H28** | 2.30 | 2.26 | 1.8-3.3 | 2.24 |
| **6** | **H14-H28** | 2.25 | 2.24 | 1.8-3.3 | 2.31 | **H14-H3** | 2.23 | 2.03 | 1.8-3.3 | 2.49 |
| **7** | **H14-H3** | 2.48 | 2.47 | 1.8-3.3 | 2.48 | **H5-H3** | 2.44 | 2.43 | 1.8-3.3 | 2.46 |
| **8** | **H5-H3** | 2.44 | 2.43 | 1.8-3.3 | 2.46 | **H10-H19, 20#** | - | - | 1.8-5.0 | 4.52 |
| **9** | **H10-H19, 20#** | 5.15 | 4.76 | 1.8-5.0 | 4.63 | **H3-H36, 37, 38#** | - | - | 1.8-5.0 | 5.20 |
| **10** | **H36, 37, 38#-H41, 42, 43#** | o | o | 1.8-3.3 | 3.45 | **H16, 17#-H24** | - | - | 1.8-5.0 | 4.56 |

# - Pseudoatom
o- Overlap

It may be attributed to the presence of monomeric berberine at all the temperature as there is no change in the chemical environment of any of the protons and berberine remains in the same conformational and configurationally state even at high concentration of 26.95 mM

### 3.1.1.3 Preparation of 7$^{th}$ position analogue of berberine ( berberrubine)

Berberrubine was synthesized by using standard protocol [Iwasa et al., 1996]. Berberine (1 g) was heated at 190$^0$C in a dry oven under vacuum (20-30 mm Hg) for 30 minutes. Yellow colored berberine was changed to dark reddish brown. Later this mixture was dissolved in MeOH/$CHCl_3$ in 1:9 ratio (v/v) and subjected to silical gel (60-200 mesh size) CC with $CHCl_3$/ MeOH in 7:1 to 5:1 (v/v) to obtain the demethylated derivative of berberine i.e. berberrubine. Conversion of berberine to berberrubine is shown in Figure 3.7 and its characterization by ESI-MS mass spectrometry is picturized in Figure 3.8.

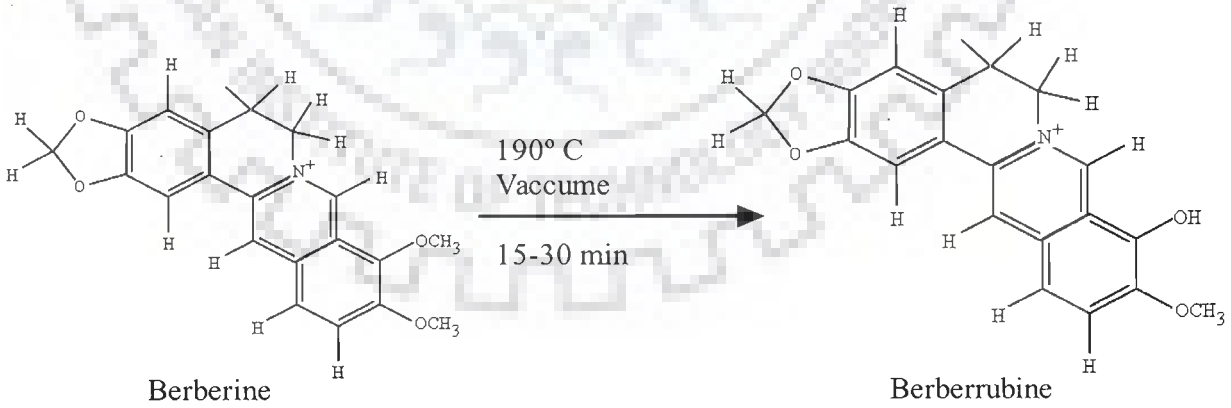


**Figure 3.7: Synthesis of berberrubine.**

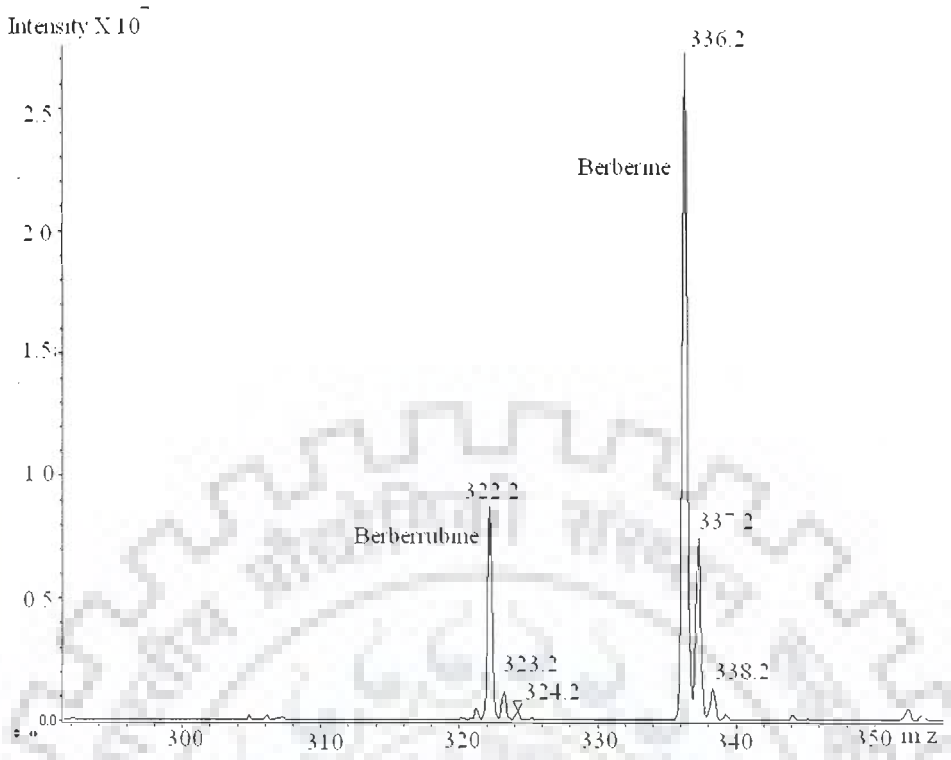


**Figure 3.8: ESI-MS spectra of berberine and berberrubine.**

Berberine has molecular weight of 336 dalton and is only single charged due to N+ at 11$^{th}$ position. When intact it gives peak at the equaling 336 dalton mass only but when heated up to 190$^0$C in vacuum it undergoes demethylation at 7$^{th}$ position and replacement with hydroxyl group occurs. This results in the reduction of 14 amu in its molecular weight generating berberrubine with molecular weight of 322 amu (Figure 3.8).

### 3.1.1.4 Resonance Assignment of Berberrubine

Berberrubine was insoluble in $D_2O$ and therefore the spectras were recorded in DMSO. The $^1$H NMR spectra of berberrubine in DMSO is shown in Figure 3.9. Berberrubine has almost similar spectra to berberine but it showed an upfield shift for all

the protons. It was observed that the only peak present in spectra, having area under peak corresponds to three ($-CH_3$) protons which resonate at 3.76 ppm and were assigned as H36, 37, 38, while those at 3.06, 4.50 and 6.11 ppm correspond to two protons ($-CH_2$) and all other resonances correspond to one proton (-CH). The methylene protons at 4.50 and 3.06 ppm are triplets having a spin – spin coupling of 6.0 Hz and are assigned to $CH_2$ protons attached to C15 and C18, designated as H16, 17 and H19, 20 atoms respectively. The H31, 32 appear at 6.11 ppm, being shifted downfield considerably due to neighboring O29 and O30 atoms. Of the 6-CH protons appearing in the range 6.8-9.5 ppm, the two doublets are assigned to H3 and H5 having $^3J$ = 9.0 Hz; H5 is shifted downfield with respect to H3 due to proximity to O34 atom and assigned at 7.24 and 6.40 respectively. Among the ring B protons (H10, H14), H10 is expected to be more downfield being closer to N11 atom. Accordingly assignments have been made to H10, H14, H28 and H24 protons and are listed in Table 3.5. All of berberrubine protons shows downfield shift with reference to the berberine except H24, H28 which shows a minor downfield shift of 0.03 and 0.16 respectively, it may be attributed to the far most position from the group displacement ($OCH_3$ to OH), due to the same reason H31, H32 do not shows any chemical shift change. H5 and H3 of berberrubine was found to be most upfield shift of value 0.79 and 1.5 ppm respectively, while H10, H14, H36,37,38, H16, 17 and H19,20 also shows significant upfield shift of 0.55, 0.45, 0.28, 0.40 and 0.12 ppm respectively. It clearly tells that the group displacement at $7^{th}$ position in ring A of berberine induces maximum effect on ring A and it decreases gradually by moving from ring A to D. Chemical shift position of all the protons of berberrubine is tabulated in Table 3.5

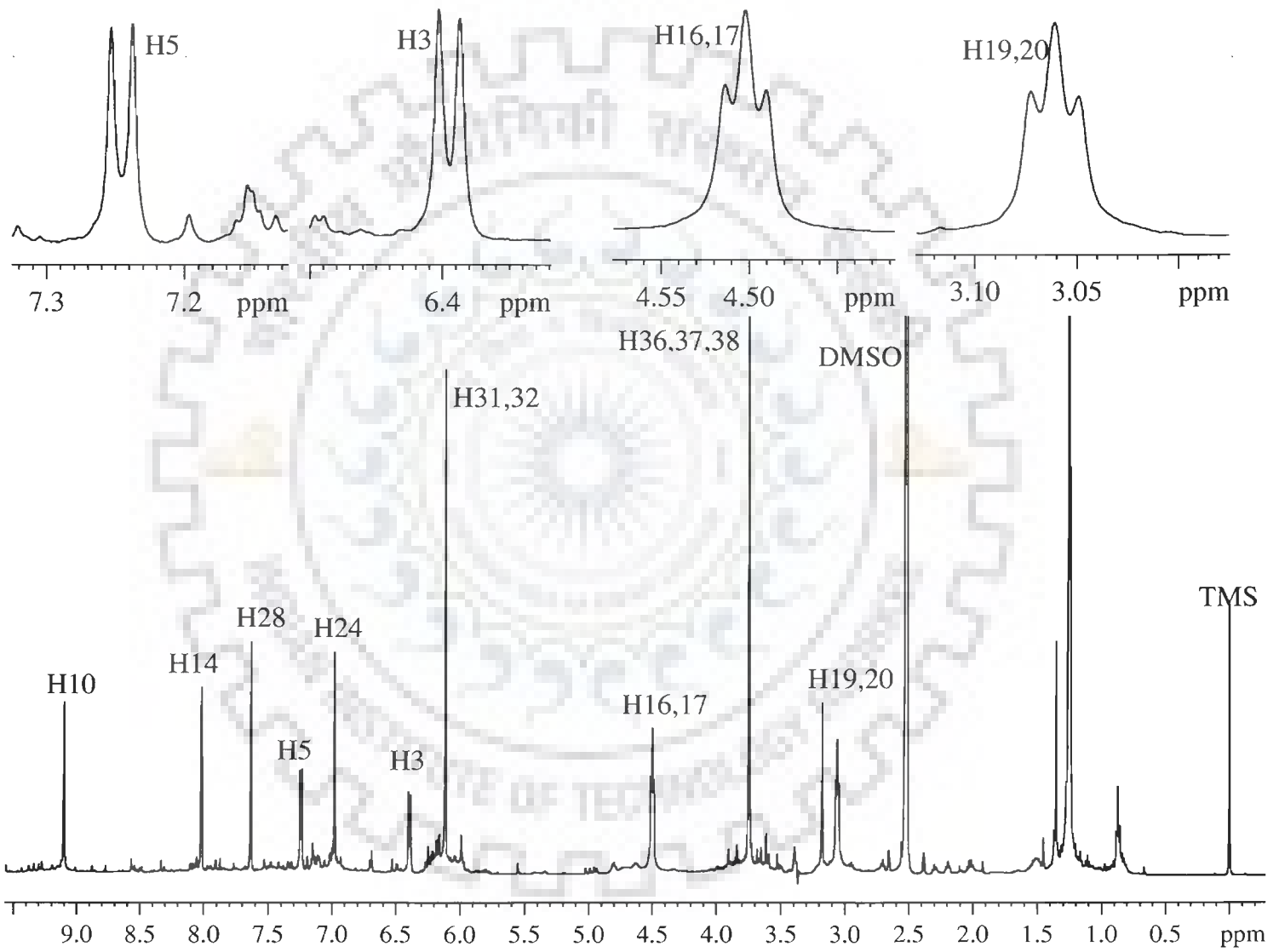


**Figure 3.9: 1D-$^{1}$H spectra of berberrubine in DMSO.**

The $^{1}H$-$^{13}C$ Hetero-nuclear Single Quantum Coherence (HSQC) spectra (Figure 3.10) shows the coupling of 10 carbon atoms to protons which are directly bonded through a single bond. The observed carbon chemical shifts are listed in Tables 3.6. It may be noted that the proton and carbon chemical shifts are in accordance with the literature [Jeon et al., 2002] A little difference may be due to the experimental conditions. Figure 3.11 shows the ROESY spectra of berberubine in DMSO solution. We observe seven cross peaks and calculated the corresponding interproton distances from integrals using distance H3-H5 = 2.44 Å as reference (Table 3.4).

### 3.1.2 Restrained Molecular Dynamics and solution structure of berberine and berberrubine

For restrained Molecular Dynamics (rMD) simulations, initial structures of berberine and berberrubine have been built using builder module in MOE (Molecular Operating Environment, Chemical Computing Group, Canada) software. For berberine and berberrubine inter proton distance restraints were taken from experimental and also from literature[Jeon et al., 2002]. We observe nine cross peaks for berberine and calculated the corresponding interproton distances from integrals using distance H3-H5 = 2.44 Å as reference (Table 3.4). For berberrubine, we observed seven cross peaks in the ROESY spectra, and distances were calculated. Distances were also extracted from data available in literature [Jeon et al., 2002]. These distances were used as restrains in restrained Molecular Dynamics to get the solution structure for both the drugs. Restrained Molecular Dynamics simulations were carried out to search for optimum conformation. A dielectric constant of 1 was used for restrained Molecular Dynamics simulations in vacuum.

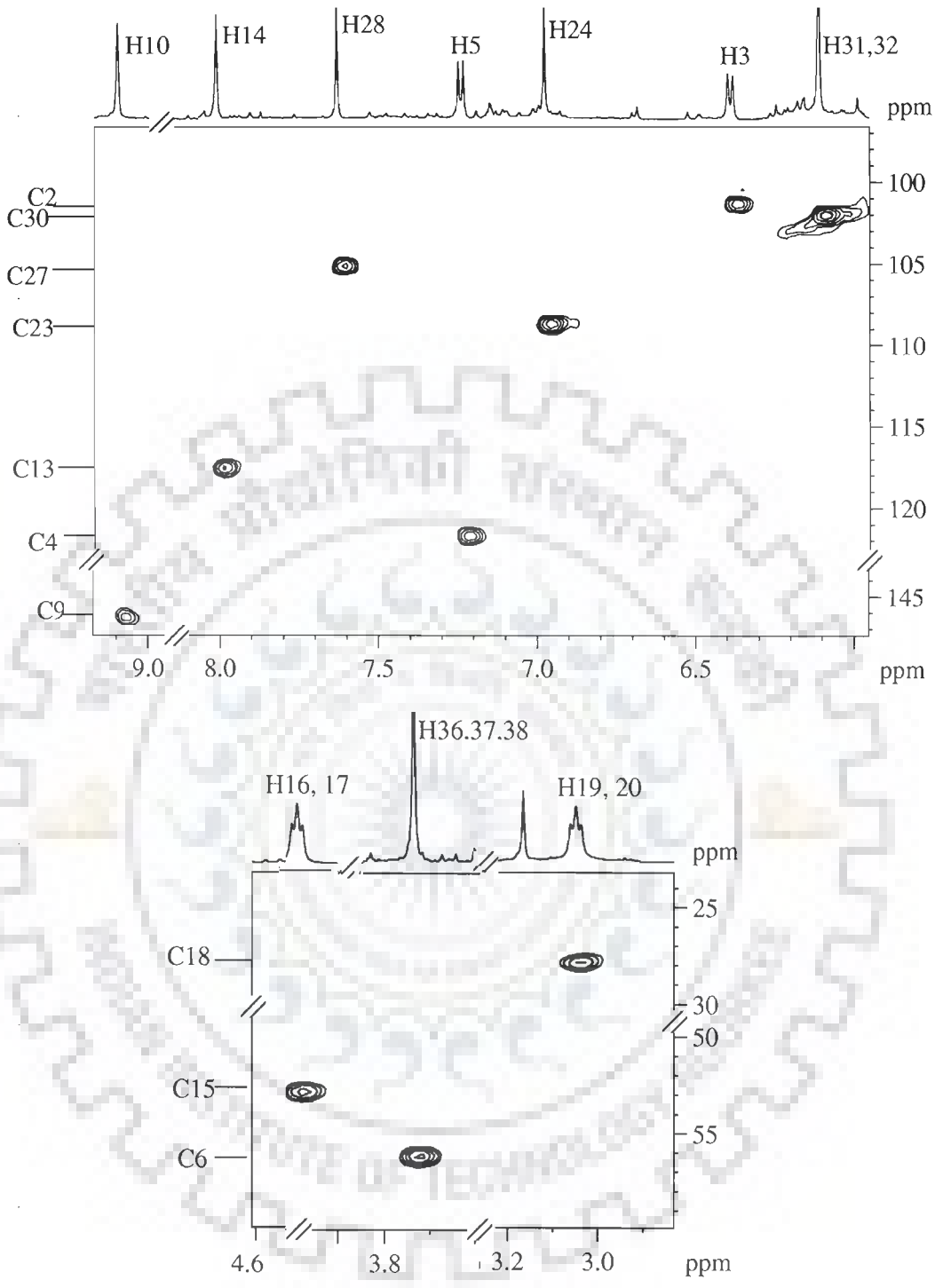


**Figure 3.10: Expansions of specific regions of HSQC spectra of berberrubine in DMSO showing $^{1}H$ -$^{13}C$ single bond correlations.**

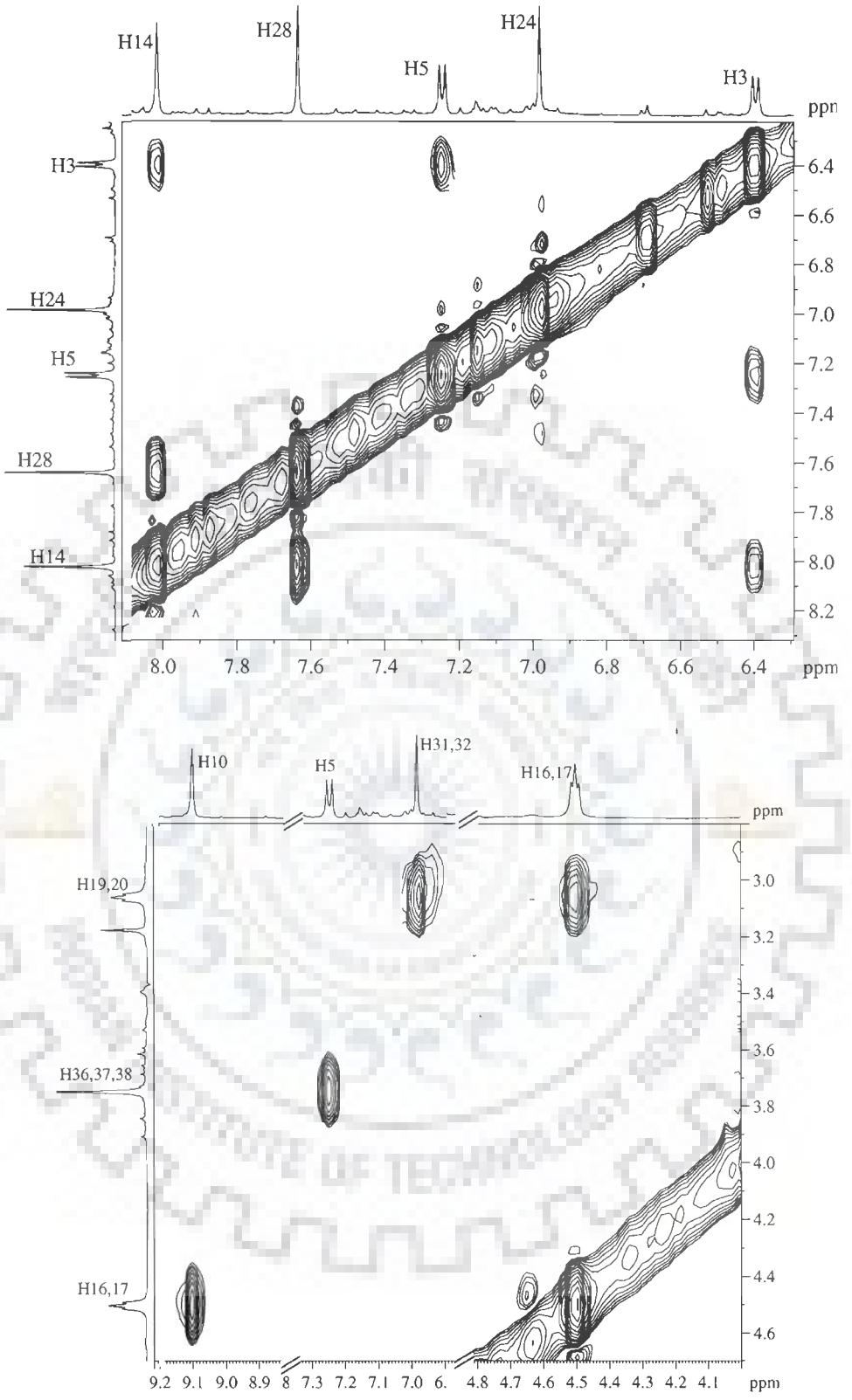


**Figure 3.11: Expansions of specific regions of ROESY spectra of berberrubine in DMSO showing interproton contacts.**

**Table 3.5: Comparison of observed Proton chemical shifts (ppm) from spectra of berberrubine in DMSO with the experimental results reported in literature and with present calculated chemical shifts (ppm) with different wave functions and in different solvents by GIAO method using B3LYP method.**

| | Experimental | | Theoretical | | | | | |
|---|---|---|---|---|---|---|---|---|
| Proton | Present work (DMSO) | Jeon *et al*[12] (DMSO) | STO-3G | 3-21G | 6-31G | 6-31G** | 6-311G** | 6-311G** (DMSO) |
| **H3** | 6.40 | 6.8 | 8.12 | 7.52 | 7.33 | 7.71 | 7.80 | 8.09 |
| **H5** | 7.24 | 7.5 | 7.94 | 7.30 | 7.11 | 7.84 | 7.84 | 8.12 |
| **H10** | 9.09 | 9.5 | 8.10 | 9.30 | 9.11 | 9.17 | 9.24 | 9.91 |
| **H14** | 8.01 | 8.0 | 8.65 | 7.93 | 7.74 | 8.04 | 8.20 | 8.99 |
| **H16, 17#** | 4.50 | 3.1 | 4.55 | 4.77 | 4.58 | 4.50 | 4.50 | 4.63 |
| **H19, 20#** | 3.06 | 4.5 | 3.28 | 3.31 | 3.12 | 3.13 | 3.16 | 3.78 |
| **H24** | 6.99 | 7.0 | 7.07 | 6.58 | 6.39 | 6.84 | 6.93 | 8.22 |
| **H28** | 7.63 | 7.8 | 7.34 | 6.95 | 6.76 | 7.22 | 7.31 | 7.88 |
| **H31, 32#** | 6.11 | 6.5 | 5.76 | 6.96 | 6.77 | 6.57 | 6.50 | 6.77 |
| **H36, 37, 38#** | 3.76 | 3.9 | 3.92 | 4.62 | 4.55 | 4.30 | 4.30 | 4.28 |
| **H40** | * | * | 6.82 | 7.56 | 7.37 | 6.67 | 6.57 | 7.92 |

**Table 3.6: Comparison of observed Carbon chemical shifts (ppm) from spectra of berberrubine in different solvents with the experimental result reported in literature and with present calculated chemical shifts (ppm) with different wave functions and in different solvents by GIAO method using B3LYP method.**

| | Experimental | | Theoretical | | | | | |
|---|---|---|---|---|---|---|---|---|
| Carbon | Present work (DMSO) | Jeon *et al*[12] (DMSO) | STO-3G | 3-21G | 6-31G | 6-31G** | 6-311G** | 6-311G** (DMSO) |
| **C1** | * | * | 115.37 | 117.39 | 129.56 | 128.08 | 137.56 | 138.05 |
| **C2** | **102** | 125 | 110.60 | 107.69 | 118.14 | 115.28 | 124.11 | 125.17 |
| **C4** | **128** | * | 113.56 | 111.86 | 122.17 | 120.43 | 128.78 | 128.85 |
| **C6** | **158** | * | 133.86 | 134.85 | 145.59 | 141.18 | 151.91 | 151.88 |
| **C7** | * | * | 131.92 | 134.37 | 142.98 | 140.69 | 151.42 | 151.32 |
| **C8** | * | 110 | 106.70 | 104.84 | 115.47 | 112.78 | 119.88 | 121.05 |
| **C9** | **145** | * | 123.67 | 129.29 | 141.40 | 138.61 | 147.81 | 150.41 |
| **C12** | * | * | 124.42 | 126.63 | 137.94 | 169.53 | 145.91 | 144.85 |
| **C13** | **121** | 122 | 111.74 | 109.72 | 119.11 | 135.94 | 125.63 | 126.92 |
| **C15** | **53** | 58 | 62.64 | 56.86 | 59.6771 | 117.18 | 61.52 | 61.20 |
| **C18** | **29** | 30 | 35.26 | 30.31 | 31.18 | 57.93 | 32.43 | 32.26 |
| **C21** | * | * | 112.96 | 117.40 | 128.76 | 30.17 | 136.16 | 138.65 |
| **C22** | * | * | 108.55 | 109.25 | 119.34 | 126.31 | 124.93 | 127.46 |
| **C23** | 111 | 118 | 102.60 | 99.85 | 108.92 | 116.57 | 113.28 | 113.46 |
| **C25** | * | * | 135.84 | 140.99 | 152.01 | 105.11 | 160.66 | 157.97 |
| **C26** | * | * | 132.86 | 138.31 | 149.20 | 149.08 | 157.51 | 155.55 |
| **C27** | 107 | 115 | 100.19 | 96.38 | 104.79 | 146.10 | 108.93 | 110.29 |
| **C30** | 104 | 112 | 103.51 | 106.73 | 111.64 | 100.99 | 111.86 | 111.24 |
| **C35** | * | * | 57.74 | 55.99 | 58.66 | 104.41 | 58.99 | 58.44 |

These molecules were subjected to 100 steps of Steepest Descent and 100 steps of Conjugate Gradient and 200 steps of Truncated Newton methods of minimization to remove any short contacts in starting structures using Molecular Mechanics Force Field (MMF94) [Levitt et al., 1995]. A typical rMD run consisted of 250 ps simulations at 300 K during which total 100 structures were saved. During the final equilibrium stage, there was no significant change in either the potential energy or restraint deviation energy. The various structures at these time intervals differed only marginally from each other and hence indicate that the structure obtained is a minimum energy conformer. Ten such minimized structures obtained by random selection superimposed over each other are shown in Figure 3.12. The minimum energy conformer is shown in Figure 3.13.

### 3.1.3 Quantum Chemical calculations

The present calculations were carried out using a density functional theory (DFT). Three different DFT methods used are as follows:

(a) SVWN (local spin density approximation) which uses the Slater exchange function VWN from uniform electron gas.

(b) BLYP using the gradient-correlated Becke exchange functional [Becke, 1988] and the LYP correlation functional [Lee et al., 1988]

(c) Hybrid B3LYP based on Becke's three parameters functional [Becke, 1993] and the correlation functional provided by LYP [Lee et al., 1988].

In all of these calculations, Cartesian Gaussian type orbitals (GTO's) were used as basis function for the molecular orbitals. Although the capability of the basis functions to describe bonding deformations of the electronic density can be enhanced by increasing the number of basis functions for each orbital or including higher angular functions.

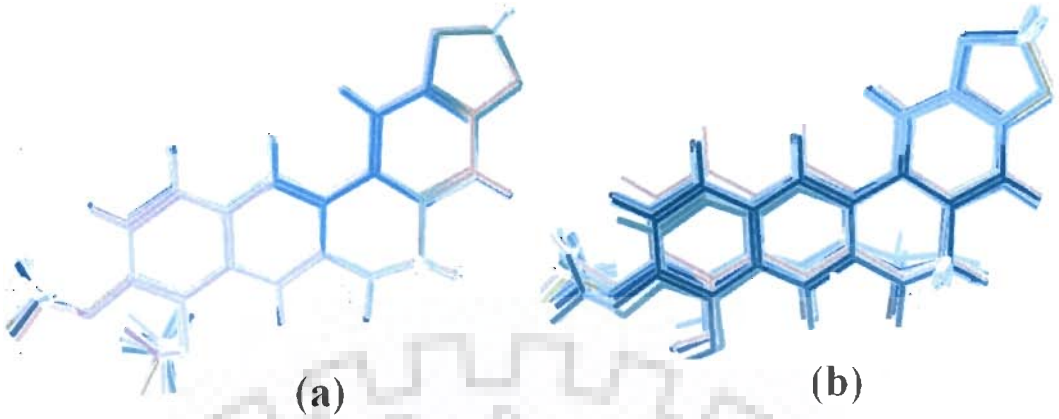


**Figure 3.12: Ten superimosed structures of (a) berberine and (b) berberrubine obtained after rMD simulations.**

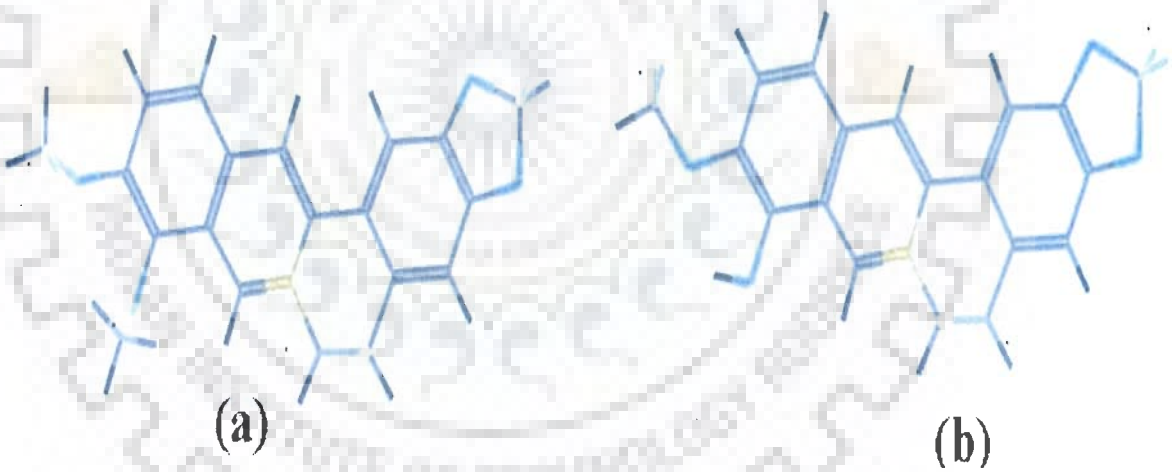


**Figure 3.13: Energy minimized solution structure of (a) berberine and (b) berberrubine.**

Yet as a thumb rule it should be able to yield results which are comparable with larger basis set while remaining computationally manageable, and thus at least a basis set of the split-valence type with polarization function should be employed.

All calculations presented here were done using the Gaussian 98 and Gaussian 03 program package[Frisch et al., 1998]. Full unconstrained geometry optimizations were performed using three different density functional methods as outlined above. For each of these density functional methods, several basis sets like STO-3G, 3-21G, 6-31G, 6-31G**, 6-311G** were used for optimizing the geometry . All the molecular properties and chemical shifts were computed using the optimized structure of the molecule. The chemical shifts were also calculated using the same Gaussian package with the gauge independent atomic orbital (GIAO) approach. This approach allows the computation of the absolute chemical shielding due to the electronic environment of the individual nuclei. Here we report our calculations for structural properties and chemical shifts by using B3LYP method only.

### 3.1.3.1 Structural Parameters

We have calculated values for bond length, bond angle and dihedral angles for five basis sets ranging from minimal basis set to 6-311G** using DFT method with Becke's three parameter hybrid exchange functional (B3LYP). The results for berberine and berberrubine molecules are shown in Tables 3.7 and 3.8, respectively. We have also obtained these structural parameters from the solution structure based on rMD simulations (Figure 3.13)

**Table 3.7: Comparison of structural parameters in experimental solution structure, X-ray structure and calculated optimized structure with different wave functions and different solvents for berberine using B3LYP method.**

| Bond Length (Å) | STO-3G | 3-21G | 6-31G | 6-31G** | 6-311G** | 6-311G** DMSO | Present solution structure | Solution structure Jeon *et al*[12] | Xray Berberine thiocynate[10] | Xray Berberine azide[10] |
|---|---|---|---|---|---|---|---|---|---|---|
| C22-C21 | 1.429 | 1.411 | 1.416 | 1.410 | 1.407 | 1.407 | 1.422 | 1.422 | 1.402 | 1.400 |
| C21-C18 | 1.539 | 1.518 | 1.513 | 1.510 | 1.509 | 1.508 | 1.514 | 1.50 | 1.506 | 1.504 |
| C15-N11 | 1.527 | 1.508 | 1.499 | 1.488 | 1.488 | 1.489 | 1.482 | 1.484 | 1.484 | 1.492 |
| N11-C12 | 1.440 | 1.403 | 1.405 | 1.396 | 1.395 | 1.392 | 1.374 | 1.366 | 1.390 | 1.391 |
| C12-C22 | 1.492 | 1.470 | 1.470 | 1.469 | 1.468 | 1.471 | 1.488 | 1.489 | 1.469 | 1.464 |
| C9-C8 | 1.414 | 1.394 | 1.398 | 1.397 | 1.395 | 1.399 | 1.398 | 1.408 | 1.400 | 1.398 |
| C1-C13 | 1.434 | 1.415 | 1.415 | 1.411 | 1.409 | 1.409 | 1.405 | 1.400 | 1.406 | 1.404 |
| C26-O33 | 1.419 | 1.393 | 1.395 | 1.363 | 1.361 | 1.369 | 1.371 | 1.372 | 1.366 | 1.380 |
| 033-C30 | 1.496 | 1.483 | 1.472 | 1.437 | 1.438 | 1.439 | 1.443 | 1.443 | 1.433 | 1.433 |
| O29-C25 | 1.410 | 1.385 | 1.388 | 1.356 | 1.353 | 1.362 | 1.375 | 1.377 | 1.366 | 1.379 |
| C7-O39 | 1.401 | 1.362 | 1.369 | 1.350 | 1.347 | 1.359 | 1.395 | 1.399 | 1.364 | 1.376 |
| O39-C40 | 1.490 | 1.484 | 1.477 | 1.445 | 1.447 | 1.447 | 1.432 | 1.437 | 1.427 | 1.443 |
| C6-O34 | 1.415 | 1.377 | 1.380 | 1.353 | 1.352 | 1.353 | 1.392 | 1.385 | 1.350 | 1.358 |
| O34-C35 | 1.480 | 1.469 | 1.462 | 1.431 | 1.433 | 1.433 | 1.438 | 1.434 | 1.436 | 1.431 |
| N11-C9 | 1.380 | 1.341 | 1.346 | 1.338 | 1.335 | 1.333 | 1.356 | 1.363 | 1.332 | 1.334 |
| C8-C1 | 1.457 | 1.438 | 1.440 | 1.436 | 1.434 | 1.431 | 1.411 | 1.410 | 1.410 | 1.423 |
| **Bond Angle** | | | | | | | | | | |
| 9-11-15 | 119.23 | 119.57 | 119.15 | 119.16 | 119.11 | 118.87 | 117.30 | 117.54 | 118.62 | 117.5 |
| 9-11-12 | 121.69 | 122.07 | 122.27 | 122.37 | 122.33 | 122.56 | 120.99 | 120.93 | 122.47 | 122.3 |
| 12-11-15 | 119.04 | 118.34 | 118.54 | 118.44 | 118.51 | 118.53 | 121.74 | 121.57 | 118.94 | 118.8 |
| 8-7-39 | 112.59 | 114.03 | 114.00 | 115.26 | 115.19 | 117.31 | 118.69 | 118.88 | 119.79 | 113.3 |
| 7-39-40 | 115.23 | 123.96 | 124.71 | 121.68 | 122.14 | 118.13 | 110.22 | 110.51 | 115.08 | 121.2 |
| 6-7-39 | 129.54 | 127.97 | 127.52 | 126.30 | 126.46 | 123.73 | 120.54 | 121.04 | 121.19 | 116.7 |
| 7-6-34 | 117.16 | 117.09 | 117.25 | 117.20 | 117.28 | 116.34 | 116.67 | 122.16 | 116.72 | 118.0 |
| 6-34-35 | 114.61 | 119.44 | 120.13 | 119.63 | 119.86 | 119.46 | 115.65 | 110.08 | 117.54 | 123.6 |
| 4-6-34 | 123.91 | 123.52 | 123.07 | 123.48 | 123.42 | 123.76 | 124.22 | 117.60 | 124.37 | |
| **Dihedral Angle** | | | | | | | | | | |
| 8-7-39-40 | -159.80 | 179.94 | -166.35 | -147.92 | -149.46 | -126.7791 | -98.44 | -107.10 | -97.17 | 96.8 |
| 6-7-39-40 | 24.56 | 0.046 | 15.28 | 35.29 | 33.64 | 56.2279 | 85.02 | 75.92 | 84.11 | -86.3 |
| 7-6-34-35 | -174.78 | -179.60 | 179.75 | -179.79 | -179.91 | -178.24 | 158.14 | 81.61 | 167.15 | -179.0 |
| 4-6-34-35 | 7.14 | -0.49 | 0.43 | 1.44 | 1.32 | 2.97 | 23.81 | -70.12 | -12.15 | 0.9 |
| **Total Energy** | -1114.209 | -1122.19 | -1128.07 | -1128.42 | -1128.66 | -1128.72 | - | - | - | - |
| **μ (D)** | 3.88 | 4.48 | 4.48 | 3.54 | 3.53 | 3.62 | - | - | - | - |

**Table 3.8: Comparison of structural parameter in experimental solution structure and calculated optimized structure with different wave functions and different solvents for berberrrubine using B3LYP method.**

| Bond Length (Å) | STO-3G | 3-21G | 6-31G | 6-31G** | 6-311G** | 6-311G** DMSO | Present solution structure | Solution structure Jeon *et al*[12] |
|---|---|---|---|---|---|---|---|---|
| C22-C21 | 1.428 | 1.411 | 1.416 | 1.410 | 1.407 | 1.407 | 1.407 | 1.420 |
| C21-C19 | 1.539 | 1.518 | 1.513 | 1.510 | 1.509 | 1.510 | 1.512 | 1.500 |
| C19-C15 | 1.552 | 1.531 | 1.526 | 1.522 | 1.520 | 1.521 | 1.523 | 1.520 |
| C15-N11 | 1.528 | 1.509 | 1.499 | 1.488 | 1.488 | 1.488 | 1.487 | 1.490 |
| N11-C12 | 1.438 | 1.404 | 1.406 | 1.398 | 1.397 | 1.395 | 1.397 | 1.370 |
| C12-C22 | 1.491 | 1.469 | 1.469 | 1.468 | 1.407 | 1.471 | 1.472 | 1.482 |
| C9-C8 | 1.417 | 1.394 | 1.397 | 1.396 | 1.394 | 1.397 | 1.396 | 1.393 |
| C1-C13 | 1.432 | 1.415 | 1.415 | 1.412 | 1.410 | 1.411 | 1.411 | 1.405 |
| C26-O33 | 1.418 | 1.392 | 1.394 | 1.364 | 1.361 | 1.369 | 1.369 | 1.371 |
| 033-C30 | 1.496 | 1.4832 | 1.477 | 1.445 | 1.438 | 1.439 | 1.438 | 1.455 |
| C30-O29 | 1.501 | 1.489 | 1.481 | 1.441 | 1.442 | 1.443 | 1.445 | 1.452 |
| O29-C25 | 1.410 | 1.384 | 1.387 | 1.356 | 1.353 | 1.362 | 1.363 | 1.373 |
| C7-O39 | 1.403 | 1.363 | 1.369 | 1.347 | 1.346 | 1.345 | 1.345 | 1.382 |
| O39-C40 | 1.026 | 1.000 | 0.981 | 0.972 | 0.969 | 0.979 | 0.979 | 0.988 |
| C6-O34 | 1.405 | 1.378 | 1.380 | 1.358 | 1.356 | 1.358 | 1.359 | 1.395 |
| O34-C35 | 1.482 | 1.470 | 1.463 | 1.433 | 1.435 | 1.433 | 1.435 | 1.435 |
| N11-C9 | 1.379 | 1.340 | 1.344 | 1.337 | 1.334 | 1.332 | 1.334 | 1.364 |
| C8-C1 | 1.469 | 1.441 | 1.442 | 1.409 | 1.436 | 1.434 | 1.435 | 1.401 |
| **Bond Angle (deg.)** | | | | | | | | |
| 9-11-15 | 119.15 | 119.62 | 119.18 | 119.20 | 119.16 | 118.93 | 118.91 | 117.42 |
| 9-11-12 | 121.94 | 122.02 | 122.24 | 122.28 | 122.25 | 122.38 | 121.21 | 121.02 |
| 12-11-15 | 118.86 | 118.35 | 118.54 | 118.49 | 118.56 | 118.66 | 117.21 | 121.58 |
| 8-7-39 | 125.98 | 119.46 | 118.63 | 118.97 | 118.98 | 118.04 | 121.10 | 119.55 |
| 7-39-40 | 105.163 | 107.87 | 110.43 | 108.14 | 108.34 | 111.60 | 107.24 | 104.94 |
| 6-7-39 | 114.68 | 121.16 | 121.51 | 121.61 | 121.63 | 122.91 | 114.23 | 118.67 |
| 7-6-34 | 113.29 | 112.60 | 113.44 | 113.81 | 113.88 | 114.69 | 114.12 | 114.61 |
| 6-34-35 | 113.47 | 119.49 | 120.22 | 119.44 | 119.72 | 119.13 | 121.20 | 106.43 |
| 4-6-34 | 127.09 | 127.22 | 126.27 | 126.19 | 126.176 | 125.29 | 117.12 | 126.45 |

It may be noted that as we move towards a better basis set, the difference between the calculated and experimental results narrows down due to the fact that polarization functions are found to be more effective than the corresponding diffused ones. Further the influence of solvent on the geometrical parameters is found very negligible as can be seen from the tabulated values in Table 3.7 and 3.8. For the berberine molecule, we found that all the calculated bond lengths are very close to the present solution structure based on NMR experimental data and also compare reasonably well with the two X-ray measurements reported in literature; the difference lies within a few hundredth of an angstrom. A similar trend is also seen for the bond angles. The maximum variation in the calculated and measured values is less than 3° except that for angles which are related to $OCH_3$ group position. For example, the angles 7-39-40, 6-7-39 and 6-34-35 have a difference of 12°, 6° and 4°, respectively. From the analysis of bond lengths and bond angles, we notice that such differences between calculated and measured values arise due to the fact that the molecule is in dynamic state in solution phase (i.e. Ring C and $OCH_3$ group's position) as compared to that in gas phase. These changes in the optimized structures can be seen more clearly through the difference in the magnitude of the dihedral angles at $OCH_3$ group than that at the ring C position. The difference between their dihedral angles (8-7-39-40, 6-7-39-40, 7-6-34-35, 4-6-34-35) are of the order of 20° to 50°, implying that the molecule in the solution phase has more freedom at the $OCH_3$ group.

The berberrubine molecule is very similar to berberine except that the $OCH_3$ group at position 7 is replaced by OH group. From the calculated optimized structure of this molecule, we saw that the pattern of variation of the bond lengths and bond angles in

general are very similar to that of berberine molecule. Further, we also notice that for berberrubine, the calculated dihedral angles at position 6 (7-6-34-35, 4-6-34-35) are quite different from the experimental values; it being >40° whereas at position 7 (8-7-39-40, 6-7-39-40) the difference is negligibly small, it being <1°. But the values of dihedral angles at position 7 in berberrubine (8-7-39-40, 6-7-39-40) have changed significantly, being >80° with respect to that in berberine. This large variation in the calculated values of the dihedral angles at position 7 of berberine and berberrubine reflects the difference in structure on replacing -$OCH_3$ with OH group. The atoms at position 7 in berberrubine that is, C6, C7, O39, H40 and C8 lie in the same plane (Figure 3.14).

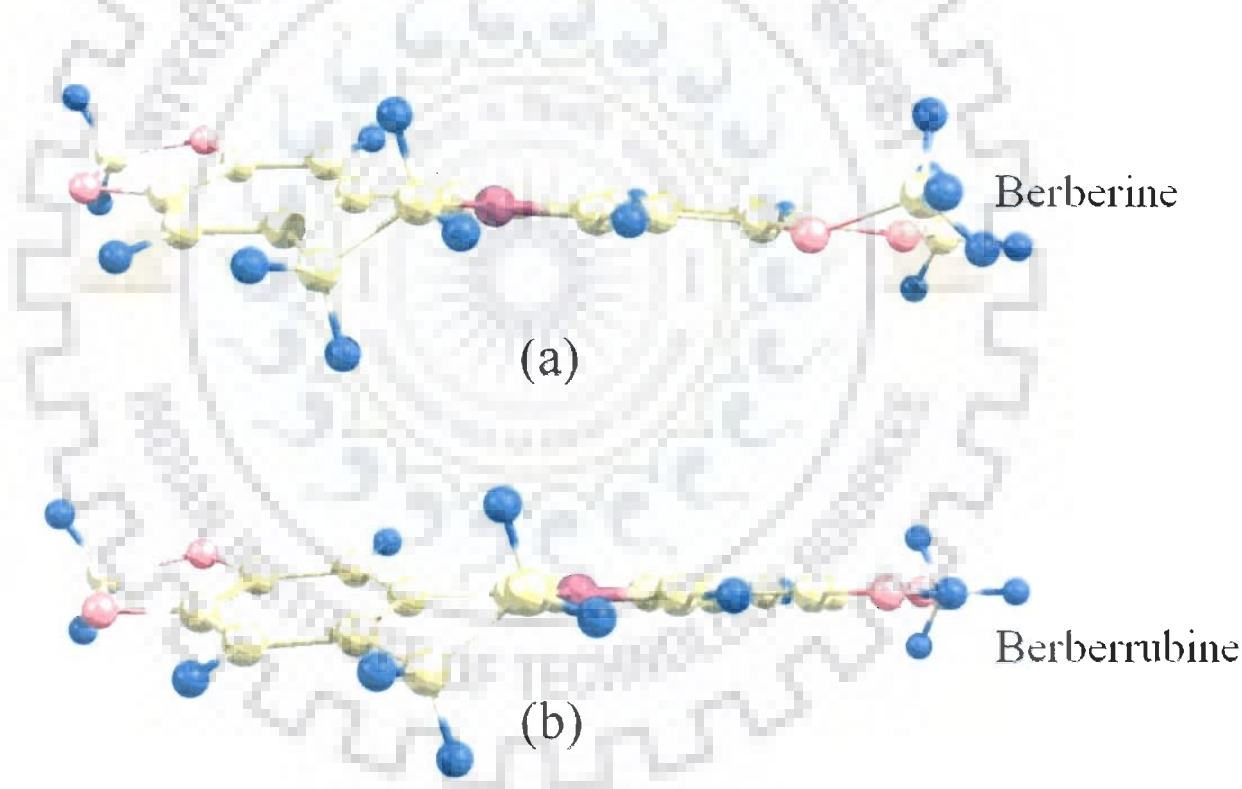


**Figure 3.14: Gaussian optimized structure of (a) berberine and (b)berberrubine with the help of 6-311G** wave function by using B3LYP method.**

This feature makes the berberrubine molecule a good binder with DNA than berberine. These findings are expected to have profound effect on role of drug in topoisomerase-I / II poisoning and hence anticancer action.

Eukaryotic DNA topoisomerase-I / II are the target for a variety of drugs used for the treatment of human cancers. The drugs combine with enzyme-DNA complex and shift DNA cleavage-religation equilibrium towards cleavage; subsequently cause multiple DNA strand breaks leading to cell death. topoisomerase-II mediated DNA cleavage assays [Jeon et al., 2002; Kim et al., 1998] showed that berberrubine stabilizes the topoisomerase-II-DNA cleavage complex in a site specific and concentration dependent manner. The berberine, on the other hand, is found to be much less effective [Jeon et al., 2002; Kim et al., 1998]. Further berberrubine induces unwinding of DNA suggesting intercalative binding [Kim et al., 1998]. Subsequent studies on human topoisomerase-I poisoning by protoberberine analogues have shown that substituents at 23, 25 and 26-position of ring D as well as 7-position in ring A are crucial for activity. Analogues having no subsituent or having OH group are more effective than those having $OCH_3$ group at position 7 of ring A [Li et al., 2000; Pilch et al., 1997] viscometric titrations and increase in $T_m$ from UV melting profiles of drug-DNA complexes show that binding of analogues having $OCH_3$ substituent at 4, 6- position is stronger than that for the analogues having $OCH_3$ at 7, 6- position. The results indicate that ring A and B intercalate between DNA base pairs in drug-DNA complex. On the other hand the drug-enzyme interactions responsible for topoisomerase-I activity involves substituent at 7-position ( OH, or $OCH_3$ or others) as well as substituents at ring D due to binding presumably to minor groove of DNA. The significance of 7-substituent in berberine analogues on drug-topoisomerase-II

interaction has also been demonstrated by using 7-ethoxy carbonyl berberine, 7-N, N dimethyl carbamoyl berberine and other related complexes [Krishnan and Bastow, 2000]. Series of compounds bearing 7-O acyl, 7-O alkyl, 7-O benzoyl and 7-O esters showed strong antimicrobial activity against Gram positive bacteria and fungi[Hong et al., 2000; Kim et al., 2002] as well as Ehrlich cells and S-180 tumor cells [Hoshi et al., 1976; Ikekawa and Ikeda, 1982]. The relative activity of various compounds demonstrated the involvement of substituent at 7- position. Our results clearly indicate that having 7-OH group (berberrubine) is planar and hence a better binder to DNA than the compound having 7-$OCH_3$ group (berberine).

### 3.1.3.2 Chemical Shift

All the $^{1}H$ and $^{13}C$ chemical shifts were referenced to those of Tetra Methyl Silane (TMS). The absolute $^{1}H$ and $^{13}C$ shielding of TMS based on the B3LYP were calculated at the level basis set which was same as that used in the calculation to which they refer. These values are listed in Table 3.9.

**Table 3.9: Calculated isotropic shielding of carbon and proton for Tetra Methyl Silane (TMS) with different wave functions by GIAO method using B3LYP method.**

| Basis sets | Carbon chemical shielding | Proton chemical shielding |
|---|---|---|
| **STO-3G** | 233.16 | 32.92 |
| **3-21G** | 204.30 | 33.12 |
| **6-31G** | 195.86 | 32.93 |
| **6-31G**** | 192.17 | 31.81 |
| **6-311G**** | 184.51 | 32.01 |
| **6-311+G(2d,p)** | 183.38 | 31.94 |

In this way we compute chemical shifts to values in ppm, by subtracting the absolute shielding of each atom ($^{1}H$ and $^{13}C$) from the reference value for TMS.

The calculated chemical shift from STO-3G to 6-311G** with GIAO method for berberine and berberrubine along with the present experimental results are listed in Tables 1, 2 and 8. A quick look at the tables tells us that calculated chemical shifts for $^{1}H$ are more sensitive to the variation of basis sets as compared to that of $^{13}C$. This can be rationalized by the fact that $^{1}H$ atoms are the smallest of all atoms and are mostly localized on periphery of the molecules. Therefore their chemical shifts would be more susceptible to intermolecular interactions in the aqueous solutions as compared to that for other heavier atoms.

The tabulated values show that the percentage variation of the difference between measured data and calculated results for berberine, is largest for proton than that for the carbon; it being 12 % and 7 % for proton and carbon, respectively. While for berberrubine the values for proton and carbon was found to be 17 % and 12% for proton and carbon respectively.

Considering the fact that NMR chemical shifts are affected by the chemical environment i.e., molecular conformation and interaction with the solvent molecules, it is seen that the overall agreement between the calculated and measured values both for $^{1}H$ and $^{13}C$ chemical shifts is satisfactory. It is of interest, however to see, how good is the correlation between experimental and calculated results? We therefore plot our experimental NMR results versus theoretical calculations obtained with different basis sets (Tables 3.1, 3.2, 3.5 and 3.6) for the berberine and berberrubine. A linear correlation between theoretical and experimental results for carbon and proton chemical shifts in gas

and solvent phase for berberine and berberrubine can be clearly seen in Figure 3.15 and 3.16 respectively. A correlation coefficient r for berberine proton and carbon in gas phase are 0.984 and 0.995 and their corresponding value in solvent (DMSO) phase is 0.992 and 0.997, respectively i.e. very close to 1. A similar correlation plot was also obtained for berberrubine. Here the correlation coefficient r found to be 0.941 and 0.966 in gas phase and in solvent (DMSO) 0.979 and 0.964 for proton and carbon respectively. In case of berberrubine calculated coefficient is rather poor but its value is reasonably good and approaches to 1. The poor correlation may be attributed to the fact that we were able to extract only a few values of chemical shifts from the measured spectra of HSQC and from literature [Jeon et al., 2002].

It can be seen from the correlation analysis that solvent shows a significant effect on the calculated values of the berberrubine protons rather than berberine, because a better correlation was found between experimental and calculated values in solvent phase. It can be attributed to the the fact that OH group at $7^{th}$ position of berberine make it a more sensitive to any change in the chemistry of environment. On the other hand berberine does not show significant effect of solvent on chemical shift calculation; this is in accordance with the experimental results available in literature whish shows independence of solvent on the chemical shift. On the whole good correlation demonstrates that in general 6-311G** basis set predicts the best NMR parameters. Further we also see that largest difference between the calculated carbon chemical shift of berberine and berberrubine are at the position of C8, C6 and C4.

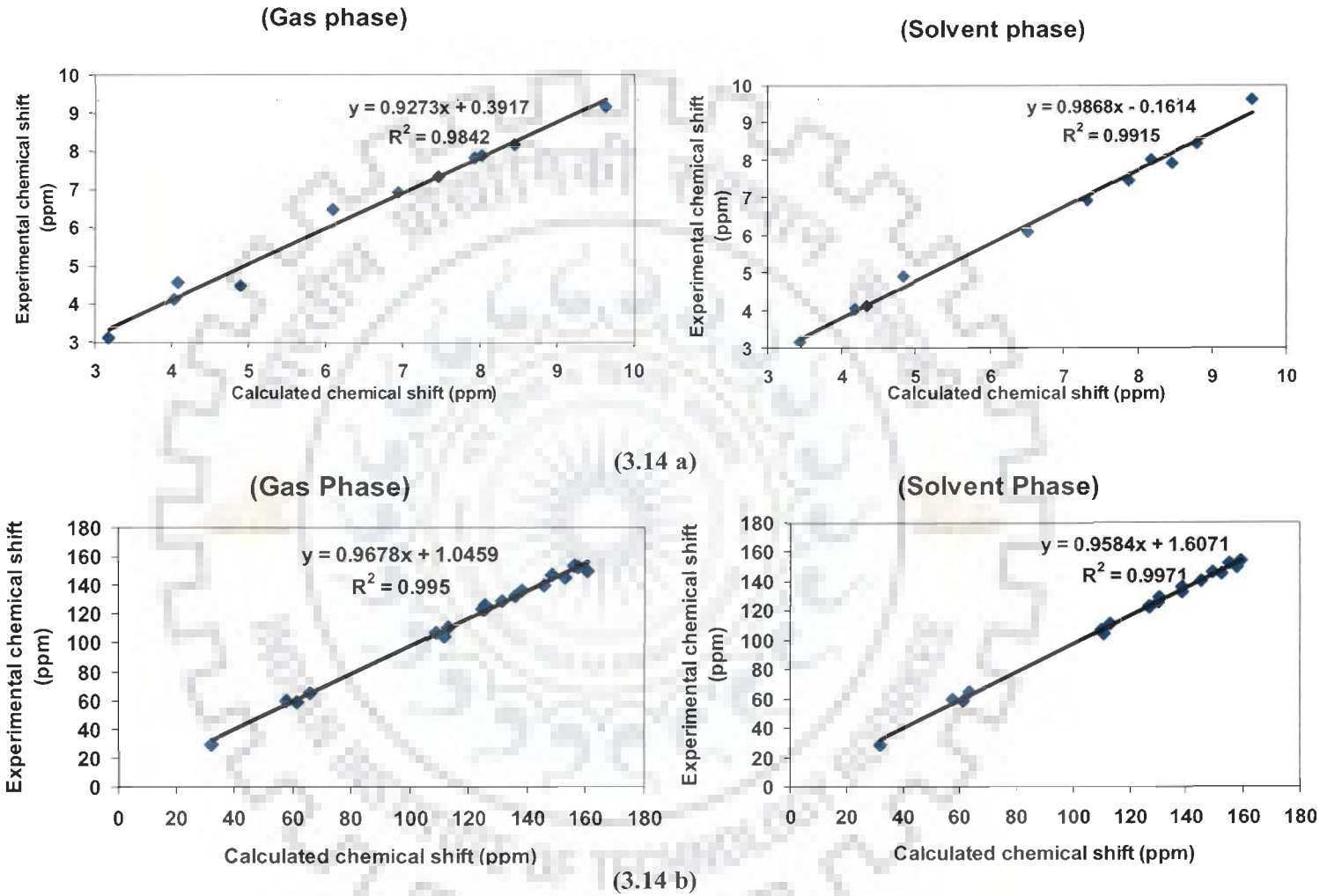


**Figure 3.15: Correlation of experimental and calculated (a) proton and (b) carbon NMR chemical shifts of berberine with B3LYP/6-311G**/GIAO method in gas and solvent (DMSO) phase.**

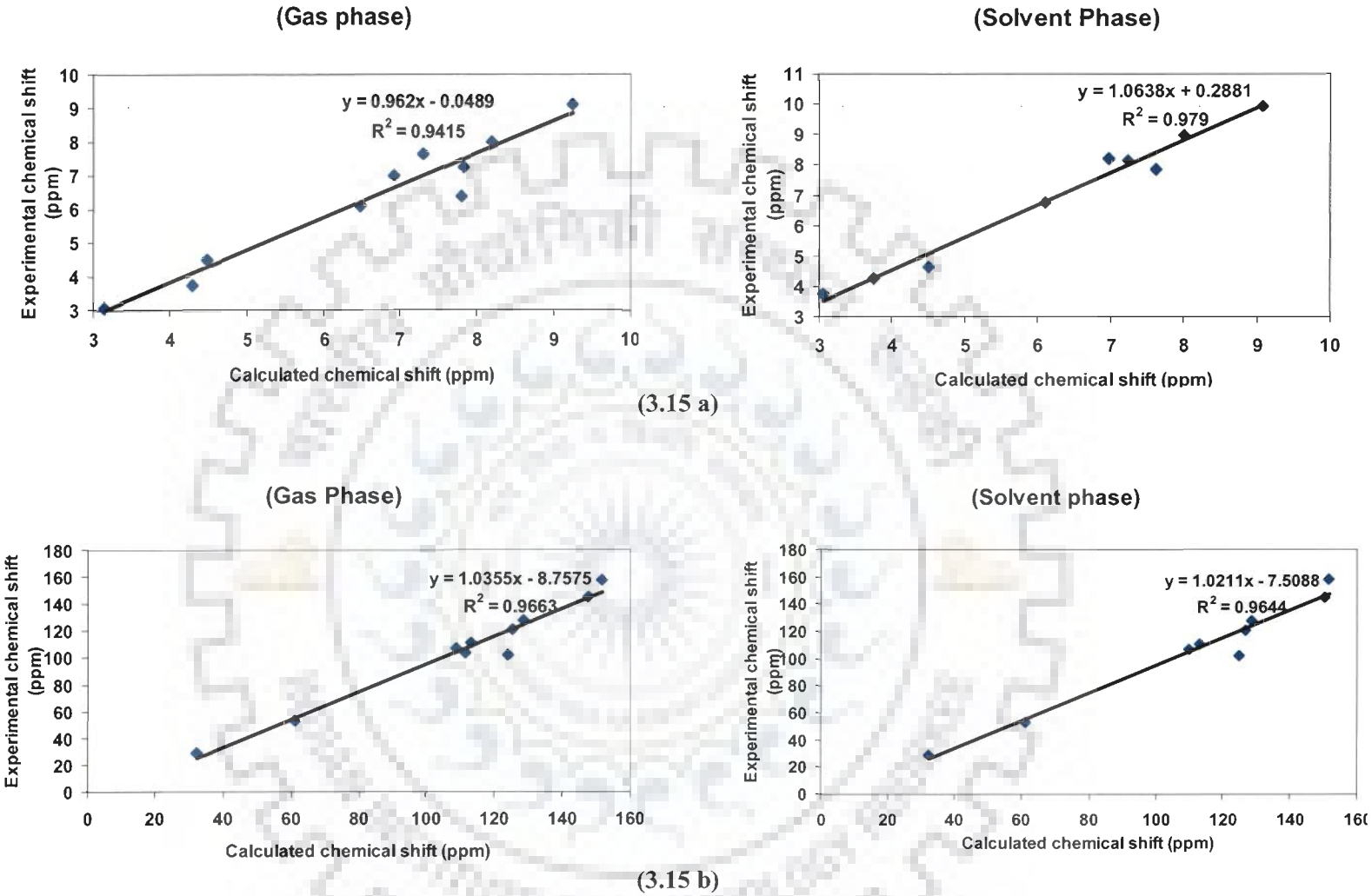


**Figure 3.16: Correlation of experimental and calculated (a) proton and (b) carbon NMR chemical shifts of berberrubine with B3LYP/6-311G**/GIAO method in gas and solvent (DMSO) phase.**

The magnitude of difference in ppm for carbon is 5.44, 4.25 and 2.91 respectively while for the proton the difference lies at the position of H36, 37, 38 and H10 with magnitude of 0.18 and 0.07, respectively. These large changes in the chemical shift in the neighborhood of the group replaced (That is, $OCH_3$ by OH at O39 position) of the two molecules are a clear signature of the difference in the conformation of the two molecules (Figure 3.14a-b.)

## 3.2 Summary and Conclusion

The structural and electronic properties of berberine and berberrubine have been studied extensively using density functional theory (DFT) employing B3LYP exchange correlation. The geometries of these molecules have been fully optimized at B3LYP/6-311G** level. The chemical shift of $^{1}H$ and $^{13}C$ resonances in Nuclear Magnetic Resonance (NMR) spectra of these molecules have been calculated using the Gauge–invariant atomic model (GIAO) method as implemented in Gaussian 98. One- and two-dimensional HSQC ($^{1}H$-$^{13}C$), HMBC ($^{1}H$-$^{13}C$) and ROESY ($^{1}H$-$^{1}H$) spectra have been recorded at 500 MHz for berberine molecule in $D_2O$ solution. All proton and carbon resonances are unambiguously assigned and inter proton distances have been obtained from ten observed NOE contacts. An optimized solution structure has been determined by restrained Molecular Dynamics simulations using distance restraints from the 2D NMR data. A restrained Molecular Dynamics (rMD) approach was used to get the optimized solution structure of berberine. The structure of berberine and berberrubine molecules was also obtained using the ROESY data available in literature. Comparison of the calculated NMR chemical shifts with the experimental values revealed that DFT methods produce very good results for both proton and carbon chemical shifts. The

importance of the basis sets to the calculated NMR parameters has been discussed. It has been found that calculated structure and chemical shifts in gas phase predicted with B3LYP/6-311G** are in very good agreement with the present experimental data and measured values reported earlier. The experimental findings were compared with theoretical investigations using density functional theory (DFT) and its variant namely VSWN, BLYP and B3LYP methods for berberine together with berberrubine drug molecule in gaseous phase and solvent DMSO. All the geometries for the molecules studied were fully optimized without using constraints with all the three different functionals. Among all the methods, B3LYP functional shows best results for geometries, energies, and all other NMR parameters and the same are reported here. A variety of basis sets (STO-3G, 3-21G. 6-31G, 6-31G**, 6-311G** and 6-311+G (2d, p)) were used. The effect of increasing size of the basis set slows down the calculations but tends towards accurate results. 6-311G** and 6-311+G (2d, p) give more or less comparable results. Further, the geometrical parameters are relatively less influenced by the solvent effect but a noticeable change is seen in the values of chemical shift due to inclusion of solvent. An overall analysis shows that B3LYP/6-311G**level of theory predicts results which are quantitatively good and compare well with the experiment. Based on the analysis of theoretical estimates of the chemical shift and the positions of the atoms in the $OCH_3$ and OH groups of these two molecules, a clear signature in the conformation of the berberrubine is observed. This suggests that binding of berberrubine with DNA or DNA-topoisomerase complex is more favorable, which is in accordance with the earlier observations.

# Berberine and Berberrubine – DNA Interaction studies by Absorption and Fluorescence Spectroscopic Techniques

The medicinal value of protoberberine alkaloids found in root, rhizome and stem bark of *Berberis vulgaris* L. plant has been recognized since ancient times. Berberine and berberrubine (Figure 3.1) belong to this important class of alkaloids having anticancer properties for their ability to inhibit topoisomerase and many other cellular processes. Their anticancer property is also correlated to their strong binding to DNA, which further inhibits the biosynthesis of DNA and RNA [Kim et al., 1998]. There have been considerable interests from ancient times in elucidating the factors that govern the affinity and specificity of binding of drugs to DNA [Bhakuni and Jain, 1986; Davidson et al., 1977; Hahn and Ciak, 1975]. Berberine's non covalent interactions have been studied extensively using various physicochemical tools and have provided detailed account on its mode of action as anticancerous drug [Davidson et al., 1977; Debnath et al., 1989; Maiti and Chaudhuri, 1981]. The binding of the alkaloid berberine chloride to natural and synthetic DNA has been studied by several methods like UV-visible spectroscopy, fluorescence spectroscopy, circular dichroism, mass spectrometry, viscometry, and NMR spectroscopy. Findings suggest that the mode of interaction of berberine with several genomic and synthetic polynucleotides can be intercalative [Debnath et al., 1989; Qin et al., 2007]. NMR studies of complexes with several AT containing oligonucleotides and molecular dynamics simulations provide siginificant facts about the minor groove binding nature of berberine [Mazzini et al., 2003]. The fundamental mechanistic studies on such

interactions continue to be of interest and significant. In most of the berberine-DNA studies the ultimate aim was to develop understanding about designing improved derivatives for better sequence recognition and site specific binding in DNA because of its potential application in medicine.

In the present study, in order to find the sequence specificity and mode of binding of berberine and berberrubine and their interaction with different DNA has been investigated by UV-visible and fluorescence spectroscopic techniques. Calf thymus DNA, Poly dA-dT, Poly dG-dC and several oligonucleotides with different sequences and length were used to elucidate the binding affinity of berberine and berberrubine. Oligonucleotides having different sequences were designed with different number of repeated sequences and length variation. It is well-known that these drugs bind to DNA rich in AT sequences [Debnath et al., 1991; Debnath et al., 1989; Maiti and Kumar, 2007] but since the mode of binding is still indistinguishable, oligonucleotides with different number of AT sites and different length of oligonucleotides ( 6 to 12 bases) were studied.

## 4.1 Results and Discussion

### 4.1.1 UV-visible spectroscopy

#### 4.1.1.1 Spectral characteristics of berberine

The berberine has three wavelength maxima in the UV visible region i.e. 260, 344 and 420 nm (Figure 4.1). Absorption band observed at 344 nm is more distinct from other bands and the extinction coefficient value was 22500 $m^{-1}cm^{-1}$ reported in literature [Maiti and Kumar, 2007]. It is noted that the successive addition of DNA to berberine can be easily monitored by calculating the absorbance at 344 nm. The band at 420 nm is less intense and band at 260 nm can not be used as it coincides with the

DNA absorption maxima. In the present study for berberine-DNA interaction, the change in the absorption intensity of 344 nm band was observed.

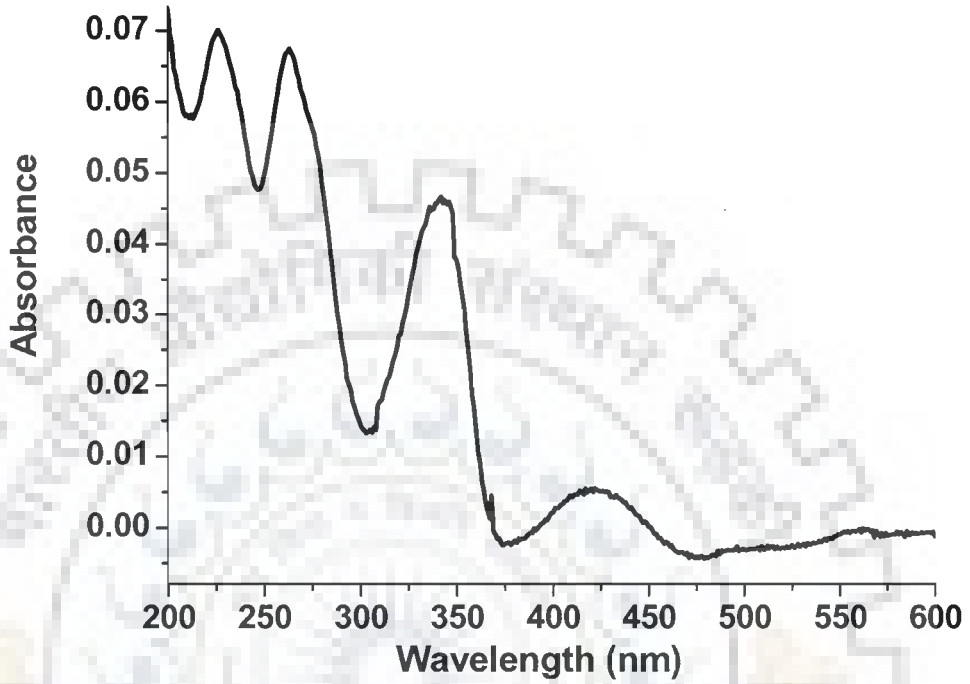


**Figure 4.1: UV-visible absorption spectrum for berberine.**

#### 4.1.1.2 Spectral characteristics of berberrubine

Although berberrubine is almost similar to berberine in the basic structure, some variation in their spectral characteristics do occur. It is characterized by four sharp peaks i.e. 260, 330, 377 and 460 nm (Figure 4.2). Replacement of OH group at $7^{th}$ position in berberine can be reflected as splitting of 344 nm band into 330 and 377 nm bands for berberrubine. No information is available in the literature regarding the absorption characteristic of berberrubine. Using dilution curve, the extinction coefficient for the intense and well separated band at 377 nm was calculated as 29950

$m^{-1}cm^{-1}$. Some physicochemical properties of berberine and berberrubine are presented in Table 4.1

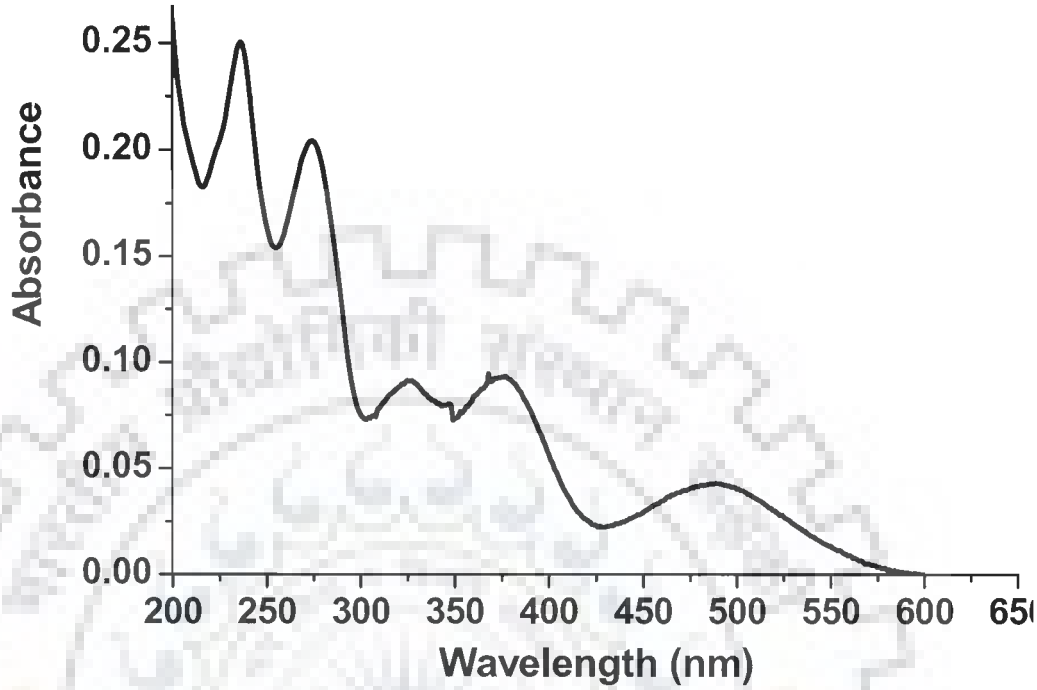


**Figure 4.2: UV-visible spectrum of berberrubine**

**4.1.1.3 Berberine-DNA Interaction**

All experiments involving DNA interactions were carried out in BPES buffer (pH 7.0). The DNA concentration per nucleotide was determined by absorption spectroscopy using their respective molar extinction coefficient listed in Table 4.2. Absorption titration of berberine was carried out as described earlier [Barve et al., 2005].The intrinsic binding constant 'Kb' was determined according to the equation

$$[DNA] / (\varepsilon_a-\varepsilon_f) = [DNA]/ (\varepsilon_b-\varepsilon_f) + 1/Kb\ (\varepsilon_b-\varepsilon_f) \quad \text{----------(1)}$$

Where [DNA] is the total concentration of DNA at each step of titration. $\varepsilon_a$, $\varepsilon_f$ and $\varepsilon_b$ are the extinction coefficients of berberine-DNA complex at each step, free berberine and berberine-DNA complex at saturation respectively. In plots of [DNA] / ($\varepsilon_a$-$\varepsilon_f$) versus [DNA], $K_b$ is given by the ratio of slope to the intercept.

**Table-4.1: Physical properties of berberine and berberrubine.**

| Property | Berberine [Maiti and Kumar, 2007] | Berberrubine (Present Work) |
|---|---|---|
| **Empirical Formula** | $C_{20}H_{18}O_4N^+$ | $C_{19}H_{16}O_4N^+$ |
| **Chemical name** | 7, 8, 13, 13 a – tetrahydro, 9, 10- dimethoxy, 2, 3 methylene dioxy berberinium | 7, 8, 13, 13 a – tetrahydro, 9, hydroxyl, 10- methoxy, 2, 3 methylene dioxy berberinium |
| **Crystal color** | Yellow | Red |
| **Solubility** | Water | Water (sparingly) Methanol, DMSO |
| **Molecular weight** | 336 | 322 |
| **Melting point** | 210 (chloride salt) | Not available |
| **Peak position of absorption spectrum** | 230, 267, 344 and 420 (in aqueous buffer) | 220, 262, 330, 377, 460 (in aqueous buffer) |
| **Molar Extinction Coefficient** | 22,500 $m^{-1}cm^{-1}$at 344 nm (in aqueous buffer) | 29,950 $m^{-1}cm^{-1}$ at 377 nm (in aqueous buffer) |
| **LD value (in mice)** | 27.5 mg/kg | 30 mg/kg [Ikekawa and Ikeda, 1982] |

**Table 4.2: Absorption spectral characteristics of berberine interaction with various DNA's and oligonucleotides.**

| DNA | $\varepsilon_{free}$ DNA $m^{-1}cm^{-1}$ | $\varepsilon_{bound}$ Drug $m^{-1}cm^{-1}$ | $\Delta\varepsilon$ (drug) (#$\varepsilon_{free}$-$\varepsilon_{bound}$) $m^{-1}cm^{-1}$ | $\lambda$ Final | $\Delta\lambda$* | Isobestic points | Hypochromicity | Binding constant |
|---|---|---|---|---|---|---|---|---|
| **CT DNA** | 6600 | 14500 | 8000 | 348 | 5 | 310, 357, 420 | 52% | $3.3 \times 10^5$ |
| **Poly d(A-T)** | 8600 | 11752 | 10748 | 349 | 6 | 305, 362, 382 | 65% | $3.0 \times 10^6$ |
| **Poly d(G-C)** | 7750 | 19613 | 2887 | 346 | 3 | 318, 358, 385, 448 | 44% | $8.0 \times 10^4$ |
| **$(CGATCG)_2$** | 57200 | 21500 | 1000 | 344 | 1 | 303, 357, | 37% | - |
| **$(CGTACG)_2$** | 57600 | 22122 | 378 | 344 | 1 | 305, 448 | 28% | - |
| **$(TGCGCA)_2$** | 55600 | 15000 | 7500 | 344 | 1 | 310, 377, 448 | 62% | - |
| **$(CGTACGCGTACG)_2$** | 97200 | 11793 | 10707 | 346 | 3 | 310, 377, 460 | 89% | - |
| **$(CGATCGCGATCG)_2$** | 97200 | 18333 | 4167 | | | 303, 360, 462 | 69% | $2.7 \times 10^6$ |
| **$(ATATATAT)_2$** | 111200 | 14908 | 7592 | 345 | 2 | 305, 360, 463 | 95% | $5.0 \times 10^5$ |
| **$(CGCGCGCG)_2$** | 84800 | 11041 | 11459 | 343 | 0 | 305, 355, 380, 455 | 61% | $2.5 \times 10^4$ |
| **$(TGCGCATGCGCA)_2$** | 109900 | 13473 | 9027 | 350 | 7 | 303, 350, 380, 450 | 90% | $8.0 \times 10^5$ |
| **$(CCAATTGG)_2$** | 76300 | 7913 | 14587 | 350 | 7 | 300, 360, 460 | 98% | $6.0 \times 10^6$ |

*($\Delta\lambda = \lambda_{initial=343nm} - \lambda_{Final}$), # ($\varepsilon_{free}$ (drug) = 22500)

The determination of change in the UV spectra of DNA bound with ligand is a major and convenient assay for DNA-binding agents [Kluza et al., 2003; Yadav et al., 2005]. Although berberine does not exhibit any pH dependence, [Sinha et al., 2006] a pH 7.0 was maintained throughout the experiments. The effect of progressive increase in the concentration of DNA to a fixed concentration of berberine (2-5 μM was used for all the titration studies) is presented in Figure 4.3a-l. The addition of calf thymus DNA (Figure 4.3a), polynucleotide (Figure 4.3b-c), and designed deoxyoligonucleotides d-$(CGATCG)_2$, d-$(TGCGCA)_2$, d-$(CGTACG)_2$, d-$(CGTACGCGTACG)_2$, d-$(CGATCGCGATCG)_2$, d-$(ATATATATAT)_2$, d-$(CGCGCGCGCG)_2$, d-$(TGCGCATGCGCA)_2$, d-$(CCAATTGG)_2$ (Figure 4.3d-l) to the solution having fixed concentration of berberine induces different redshifts and hypochromicities, which are tabulated in Table 4.2. Magnitude of the absorption spectra alternations may provide evidence for the intercalative binding because it was established that π system of berberine are in intimate contact with those of DNA bases [Suh and Chaires, 1995; Sundquist and Lippard, 1990; Wall et al., 2001]. The characteristics of binding like hypochromism, bathochromism and presence of sharp isobestic points clearly indicate the equilibrium in the binding phenomenon for all the observations. Intrinsic binding constant for some of the DNA studied were determined using Eq. (1) which is in accordance to those obtained for protoberberine-oligonucleotide complexes in literature [Bhadra et al., 2007; Chen et al., 2005; Giri et al., 2006a; Giri et al., 2006b; Long et al., 2006; Mazzini et al., 2003]. [DNA] / $(\varepsilon_a - \varepsilon_f)$ versus [DNA] plot for d-$(CCAATTGG)_2$ is shown in Figure 4.4.

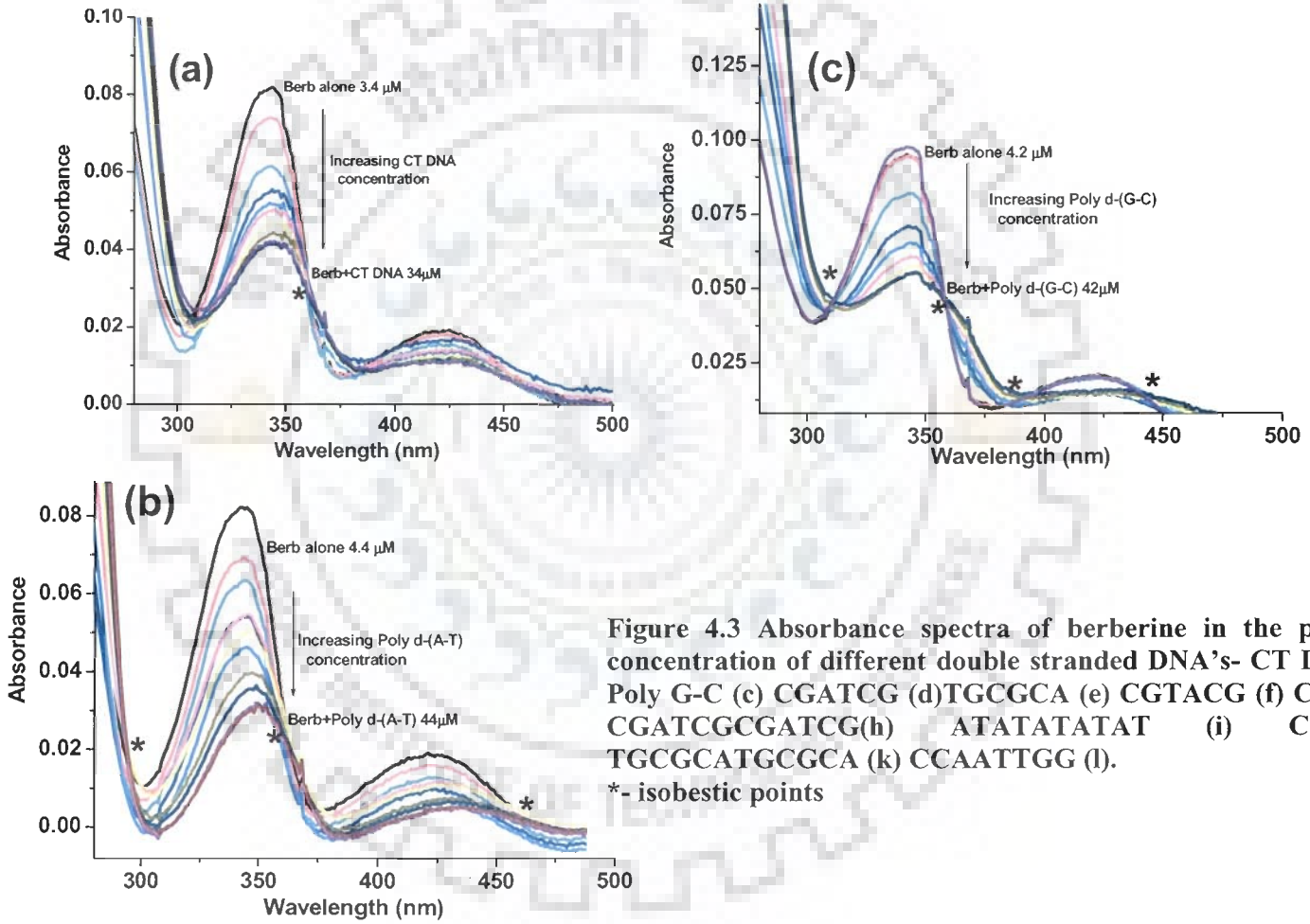


**Figure 4.3 Absorbance spectra of berberine in the presence of increasing concentration of different double stranded DNA's- CT DNA (a), Poly A-T (b), Poly G-C (c) CGATCG (d)TGCGCA (e) CGTACG (f) CGTACGCGTACG (g) CGATCGCGATCG(h) ATATATATAT (i) CGCGCGCGCG (j) TGCGCATGCGCA (k) CCAATTGG (l).**
***- isobestic points**

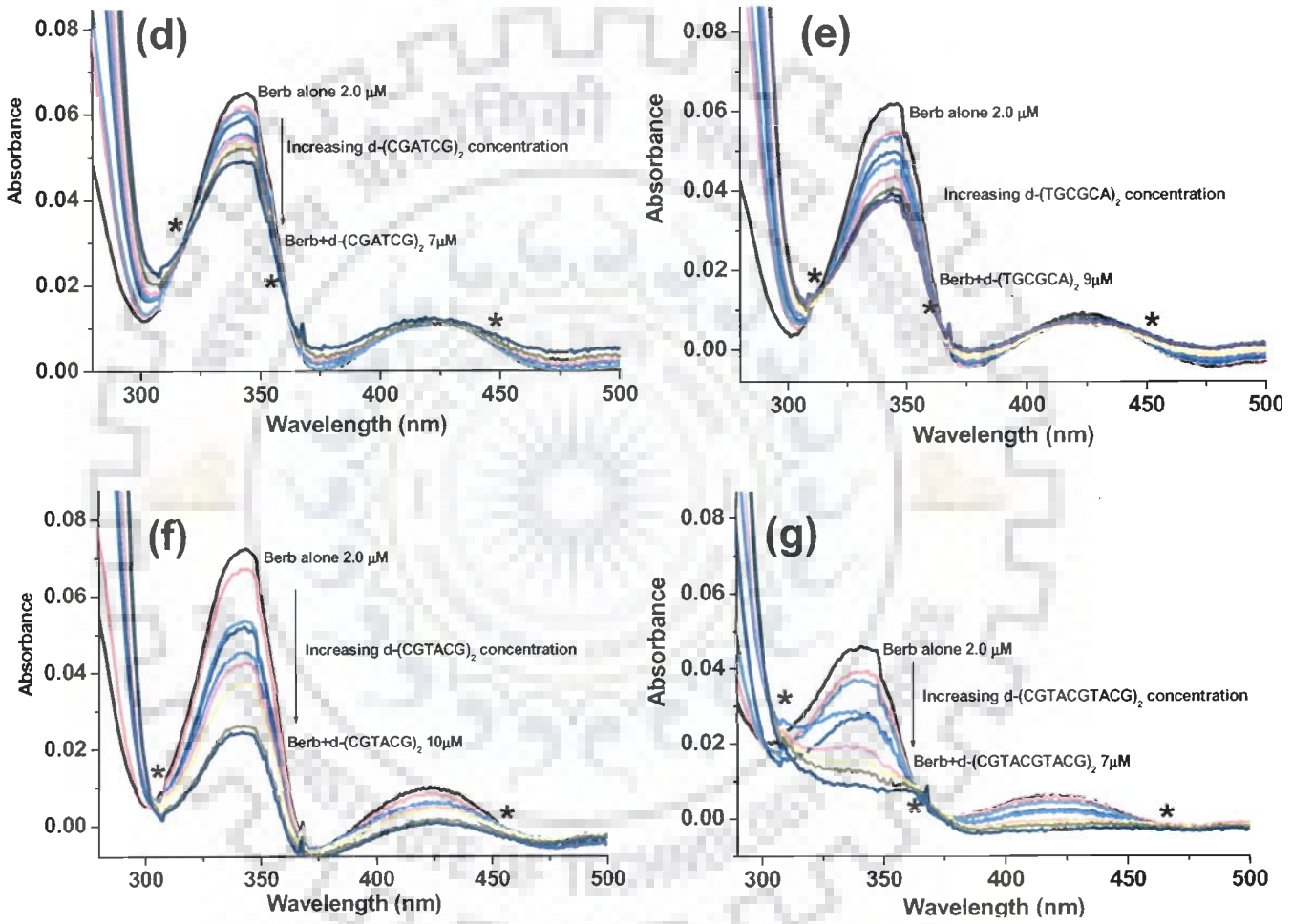
(d)
Berb alone 2.0 μM
Increasing d-(CGATCG)2 concentration
Berb+d-(CGATCG)2 7μM
(e)
Berb alone 2.0 μM
Increasing d-(TGCGCA)2 concentration
Berb+d-(TGCGCA)2 9μM
(f)
Berb alone 2.0 μM
Increasing d-(CGTACG)2 concentration
Berb+d-(CGTACG)2 10μM
(g)
Berb alone 2.0 μM
Increasing d-(CGTACGTACG)2 concentration
Berb+d-(CGTACGTACG)2 7μM
Absorbance
Wavelength (nm)

(Fig. 4.3)

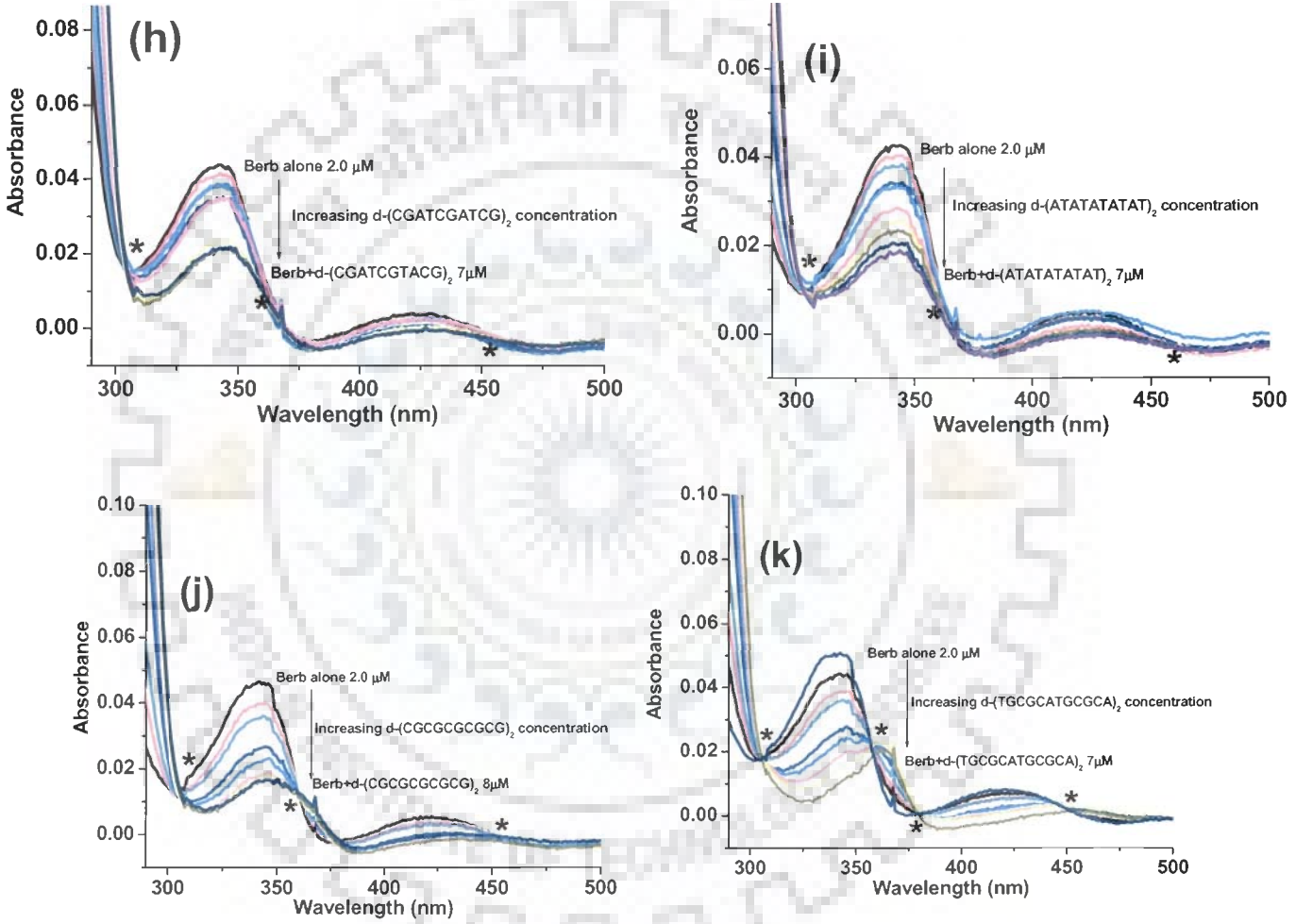
(h)
Absorbance
Wavelength (nm)
Berb alone 2.0 μM
Increasing d-(CGATCGATCG)2 concentration
Berb+d-(CGATCGTACG)2 7μM
(i)
Absorbance
Wavelength (nm)
Berb alone 2.0 μM
Increasing d-(ATATATATAT)2 concentration
Berb+d-(ATATATATAT)2 7μM
(j)
Absorbance
Wavelength (nm)
Berb alone 2.0 μM
Increasing d-(CGCGCGCGCG)2 concentration
Berb+d-(CGCGCGCGCG)2 8μM
(k)
Absorbance
Wavelength (nm)
Berb alone 2.0 μM
Increasing d-(TGCGCATGCGCA)2 concentration
Berb+d-(TGCGCATGCGCA)2 7μM

(Fig. 4.3)

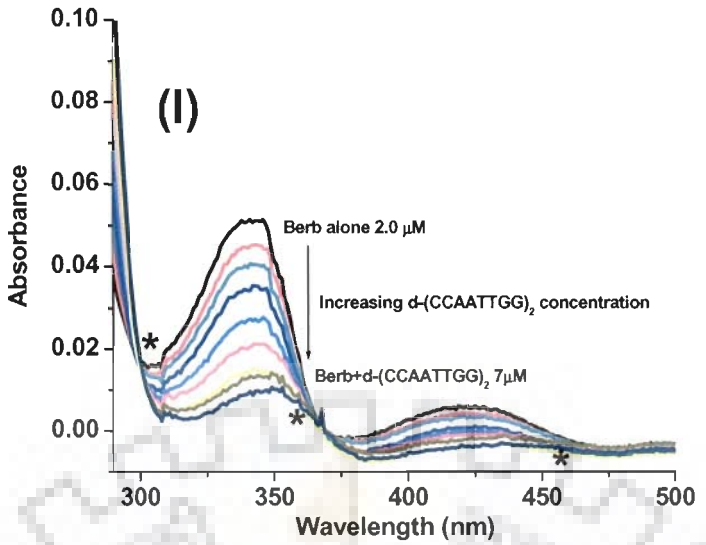


(Fig. 4.3)

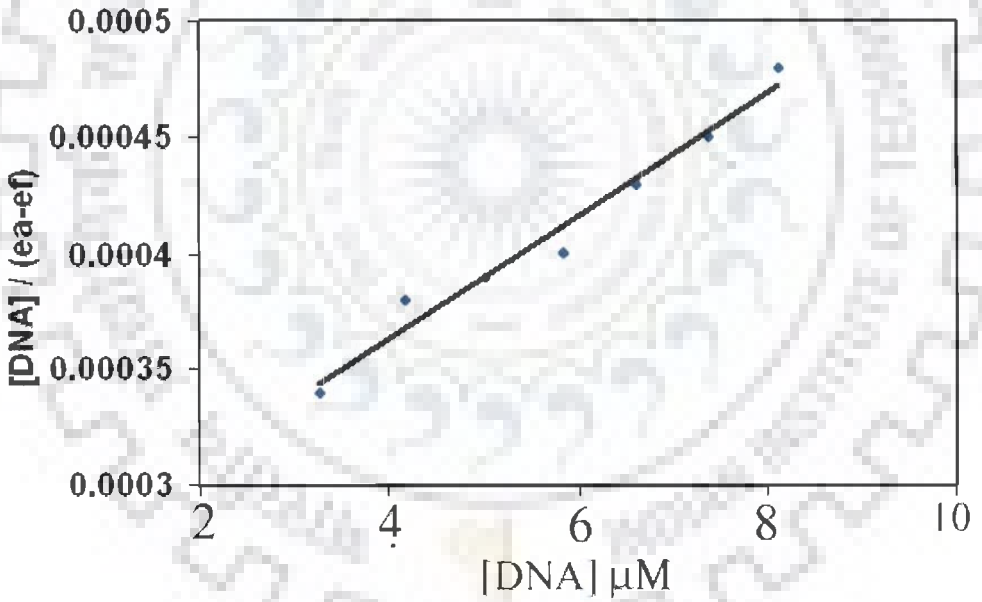


**Figure 4.4: Plot of binding of d-(CCAATTGG)$_2$ with berberine from absorption titration, linear equation gives the binding constant value.**

Addition of DNA induced reasonable hypochromic change and bathochromic effects in the 344 nm and 420 nm peaks of the berberine with three isobestic points at ~360nm, ~452nm, and ~374nm (Figure 4.3 a-l), which indicates interaction of berberine and DNA. These spectral variations observed during successive addition of DNA are considered as the characteristic feature of $\pi$ - $\pi^*$ interactions between aromatic chromophore of berberine and bases of nucleic acid [Yadav et al., 2005].

Percentage of hypochromicity, epsilon for bound drug ($\varepsilon_b$) and binding constant were calculated from the data recorded with UV-vis spectroscopy and is tabulated in Table 4.2. Hypochromicity % observed for all the DNA sequences is shown in Figure 4.5. It was observed that in case of Poly dA-dT, percentage of hypochromicity and value of change in epsilon were higher; 65 % and 10748 $m^{-1}cm^{-1}$ as compared to 44 % and 2887 $m^{-1}cm^{-1}$ with Poly dG-dC. These results suggest that berberine has preferable binding affinities with AT rich DNA, the phenomenon reported earlier by several authors [Debnath et al., 1989; Maiti and Chaudhuri, 1981; Maiti and Kumar, 2007]. Further, the small oligonuclotides having variable number and position for AT sites in base sequence, were selected to investigate the sequence specificity of berberine [Maiti and Kumar, 2007]. Hypochromicity and epsilon bound value obtained on binding with berberine were analyzed for these sequences. It can be noted from Table 4.2 that hypochromicity and change in epsilon bound value is 62 % and 7500 $m^{-1}cm^{-1}$ for d-$(CGTACG)_2$, 37 % and 1000 $m^{-1}cm^{-1}$ for d-$(CGATCG)_2$ and 28 % hypochromicity and 378 $m^{-1}cm^{-1}$ for d-$(TGCGCA)_2$. These results clearly show that binding affinity of berberine is in the order of d-$(CGTACG)_2$ >d-$(CGATCG)_2$ > d-$(TGCGCA)_2$ for hexamer sequences. Minimum binding affinity observed with d-$(TGCGCA)_2$ confirms that berberine prefer A-T base pair to G-C base pair for binding

while maximum binding affinity with d-$(CGTACG)_2$ suggests berberine base pair preference towards TpA than ApT.

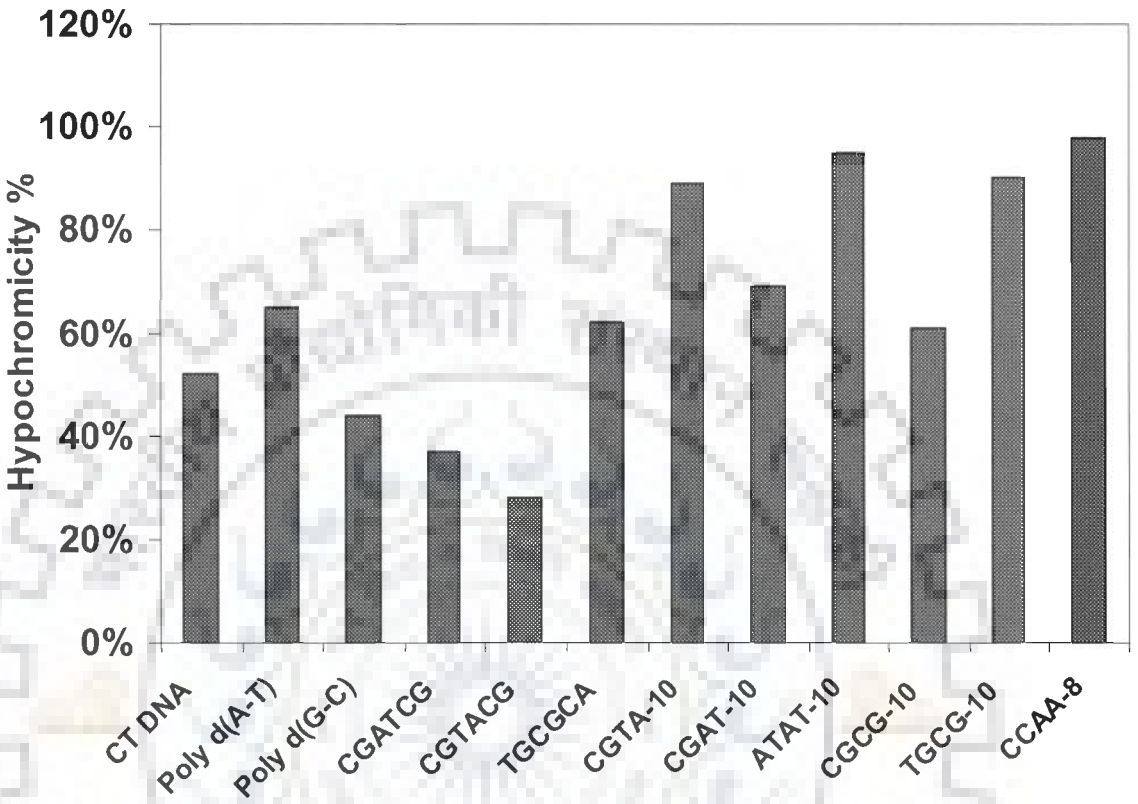


**Figure 4.5: Observed hypochromicty of berberine DNA complexes.**

Additionally to see the effect of binding affinity due to variation in length and number of sites present in oligonucleotides which contains 8-12 bases for e.g. d-$(TGCGCATGCGCA)_2$, d-$(CGATCGCGATCG)_2$, d-$(CGTACGCGTACG)_2$, d-$(CGCGCGCGCG)_2$, d-$(ATATATATAT)_2$ and d-$(CCAATTGG)_2$ were used. It was observed that binding affinity observed for decanucleotides, used in this study was found to be in the order of d-$(ATATATATAT)_2$> d-$(CGTACGCGTACG)_2$> d-$(CGATCGCGATCG)_2$> d-$(CGCGCGCGCG)_2$, which supports the AT preference for

berberine. While in case of dodecanucleotide and octanucleotide d-$(CCAATTGG)_2$ shows more effective binding to berberine than d-$(TGCGCATGCGCA)_2$. These results suggest that increasing length of DNA does not effectively increase the binding but incorporation of AATT enhanced binding of berberine. The maximum binding affinity of berberine observed with d-$(CCAATTGG)_2$, can also be correlated to minimum requirement of 8 bases for binding and a greater affinity towards the consecutive AATT site which supports the minor groove binding of berberine to AATT region of dodecamer sequences d-$(AAGAATTCTT)_2$ already reported in literature using nuclear magnetic resonance spectroscopy. [Mazzini et al., 2003]. It is also observed that in the oligonucleotides when AT site is preceded by guanine residue like in d-$(CGTACGCGTACG)_2$ and d-$(CGATCGCGATCG)_2$, it shows less binding as compared to AT or AATT site preceded by cytosine like in d-$(TGCGCATGCGCA)_2$ and d-$(CCAATTGG)_2$. These results are in accordance with the study of Chen et al, in which berberine interaction using different oligonucleotides showed a sequence preference in the order of d-$(AAGCATGCTT)_2$> d-$(AAGCATGCTT)_2$> d-$(AAGAATTCTT)_2$ [Chen et al., 2004]. It was also reported by Chen et al that berberine bound the former two DNA sequences with binding affinities comparable to that of Hoechst 33258 which is a typical minor groove binder. Therefore, our results and literature clearly explains that berberine binds to oligonucleotides preferably by minor groove binding mode and its affinity for binding gets reduced due to the presence of guanine residue at +1 position of the binding site.

#### 4.1.1.4 Berberrubine-DNA Interaction

It was found that berberrubine shows very less hypochromicity and not worth mentioning shift in $\lambda_{max}$ even with high amount (150 μM) of CT DNA added (Figure

4.6). A very less hypochromicity with genomic DNA itself suggests a very weak binding of berberrubine with DNA alone. Also, the absorbance and fluorescence of berberrubine with other DNA's were studied but no significant changes were observed in the spectra during addition of DNA. It can be attributed to the recognized fact that berberrubine is more potent topoisomerase posion and it binds to DNA-topoisomerase complex rather than DNA alone [Park et al., 2004]

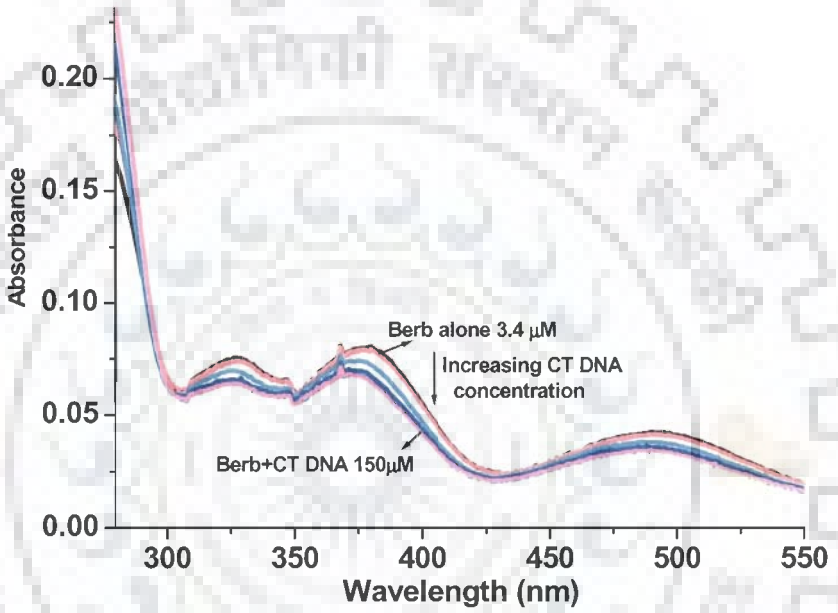


**Figure 4.6: Absorbance spectra of berberrubine in the presence of increasing concentration of CT DNA.**

### 4.1.2 Fluorescence Spectroscopy

#### 4.1.2.1 Steady state Fluorescence studies of berberine DNA interaction

Various techniques have been developed which help to determine binding and provide information for understanding the nature of complexes between small molecules and biomacromolecules. Fluorescence spectrometry is one such technique. It has been widely used in the investigation of non covalent complexes of small

organic molecules with DNA [Chaires and Waring, 2001; Fox, 1997] and the complex formation occurrence is reflected in terms of the change observed in the fluorescence intensities (either enhancement or quenching).

In an aqueous buffer, berberine alone exhibits extremely weak fluorescence that has an emission spectrum with a $\lambda_{max}$ centered around 545 nm when excited at 355 nm. When bound to DNA; this weak intrinsic fluorescence is remarkably enhanced. About two fold enhancement in the fluorescence intensity was observed at 532 nm during successive addition of DNAs to a fixed amount of beberine. Poly d-(dA-dT) shows higher degree of enhancement than Poly d-(dG-dC) when binding to DNA (Figure 4.7a-c, Table 4.3). Addition of d-$(CGTACG)_2$ , d-$(CGATCG)_2$ and d-$(TGCGCA)_2$ sequences to berberine did not increase the fluorescence but the sequences with at least 8 bp length showed significant enhancement in the fluorescence intensity. The order observed was d-$(CCAATTGG)_2$> d-$(CGTACGCGTACG)_2$> d-$(CGCGCGCGCG)_2$ > d-$(ATATATATAT)_2$> d-$(TGCGCATGCGCA)_2$ > d-$CGATCGCGATCG)_2$ (Figure 4.7d-i). Relative fluorescence intensity of berberine DNA complex with CT DNA, Poly dA-dT, Poly dG-dC and oligonucleotides has been shown in Figure 4.8. Results obtained shows that relative fluorescence enhancement was found maximum in case of Poly dA-dT and $(CCAATTGG)_2$ in long polymers and small oligonucleotides respectively. Its clear from Figure 4.8 and Table 4.3 that at saturation level, the steady state fluorescence of berberine enhanced by more than 90 % by Poly dA-dT and CT DNA and by more than 75 % by $(CCAATTGG)_2$ indicating a strong association of berberine chromophore with AT rich DNAs'. This study clearly underscores the remarkably specific and higher affinity of binding of berberine to AT rich DNA's and AATT containing sequence.

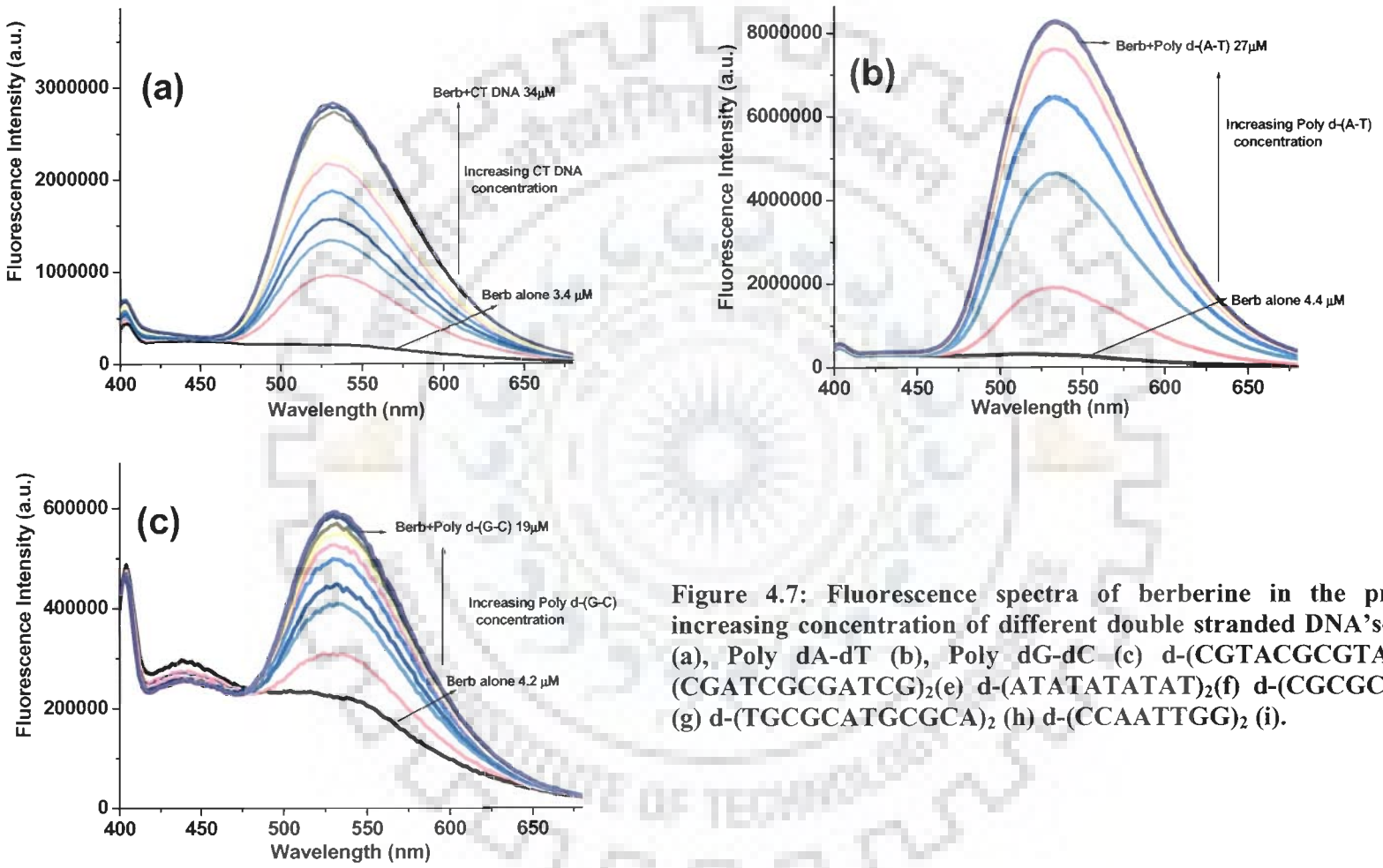


**Figure 4.7: Fluorescence spectra of berberine in the presence of increasing concentration of different double stranded DNA's- CT DNA (a), Poly dA-dT (b), Poly dG-dC (c) d-$(CGTACGCGTACG)_2$(d)d-$(CGATCGCGATCG)_2$(e) d-$(ATATATATAT)_2$(f) d-$(CGCGCGCGCG)_2$ (g) d-$(TGCGCATGCGCA)_2$ (h) d-$(CCAATTGG)_2$ (i).**

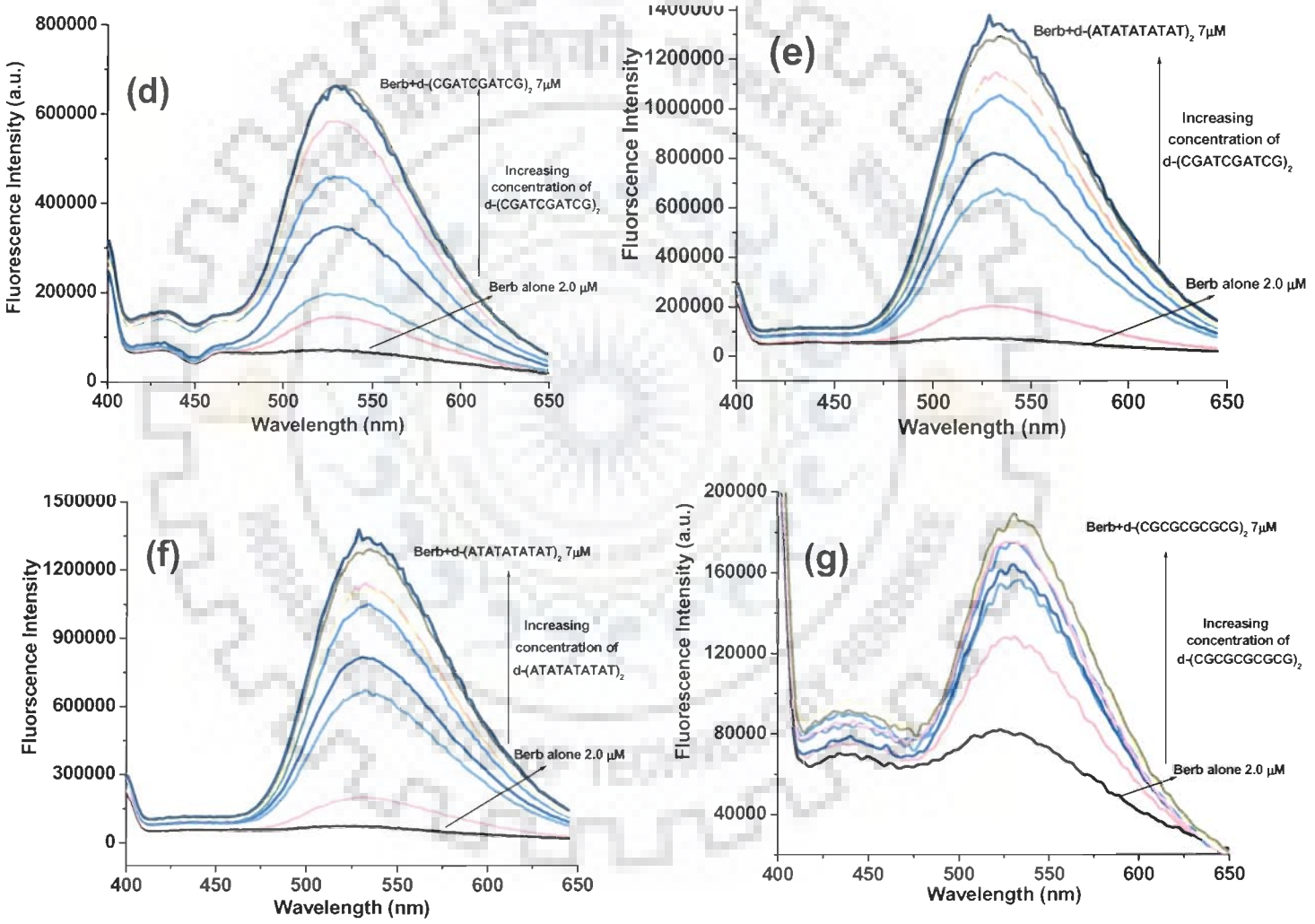
(d)
Berb+d-(CGATCGATCG)2 7μM
Increasing concentration of d-(CGATCGATCG)2
Berb alone 2.0 μM
Fluorescence Intensity (a.u.)
Wavelength (nm)
(e)
Berb+d-(ATATATATAT)2 7μM
Increasing concentration of d-(CGATCGATCG)2
Berb alone 2.0 μM
Fluorscence Intensity
Wavelength (nm)
(f)
Berb+d-(ATATATATAT)2 7μM
Increasing concentration of d-(ATATATATAT)2
Berb alone 2.0 μM
Fluorscence Intensity
Wavelength (nm)
(g)
Berb+d-(CGCGCGCGCG)2 7μM
Increasing concentration of d-(CGCGCGCGCG)2
Berb alone 2.0 μM
Fluorescence Intensity (a.u.)
Wavelength (nm)

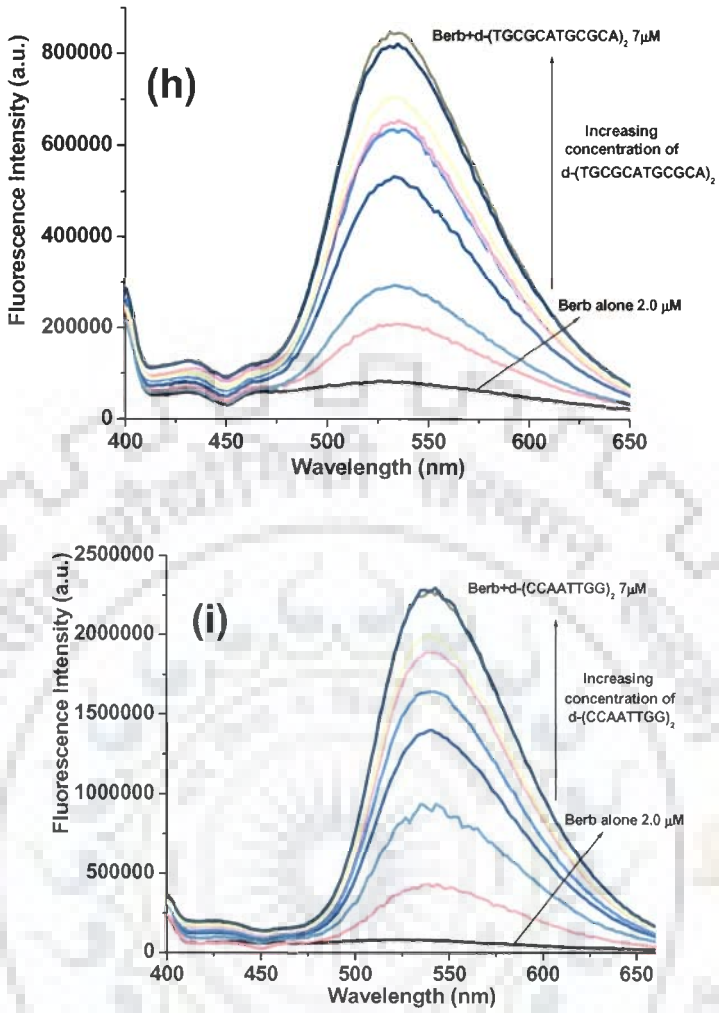


(Fig. 4.7)

**Table 4.3: Enhancement in the fluorescence intensity of drug by adding different DNA.**

| DNA | Increase in Fluorescence |
|---|---|
| CT DNA | 93% |
| Poly dA-dT) | 94% |
| Poly dG-dC | 64% |
| d-(5′-CGTACGCGTACG-3′)$_2$ | 63% |
| d-(5′-CGATCGCGATCG-3′)$_2$ | 52% |
| d-(5′-ATATATAT-3′)$_2$ | 60% |
| d-(5′-CGCGCGCG-3′)$_2$ | 63% |
| d-(5′-TGCGCATGCGCA-3′)$_2$ | 59% |
| d-(5′-CCAATTGG-3′)$_2$ | 77% |

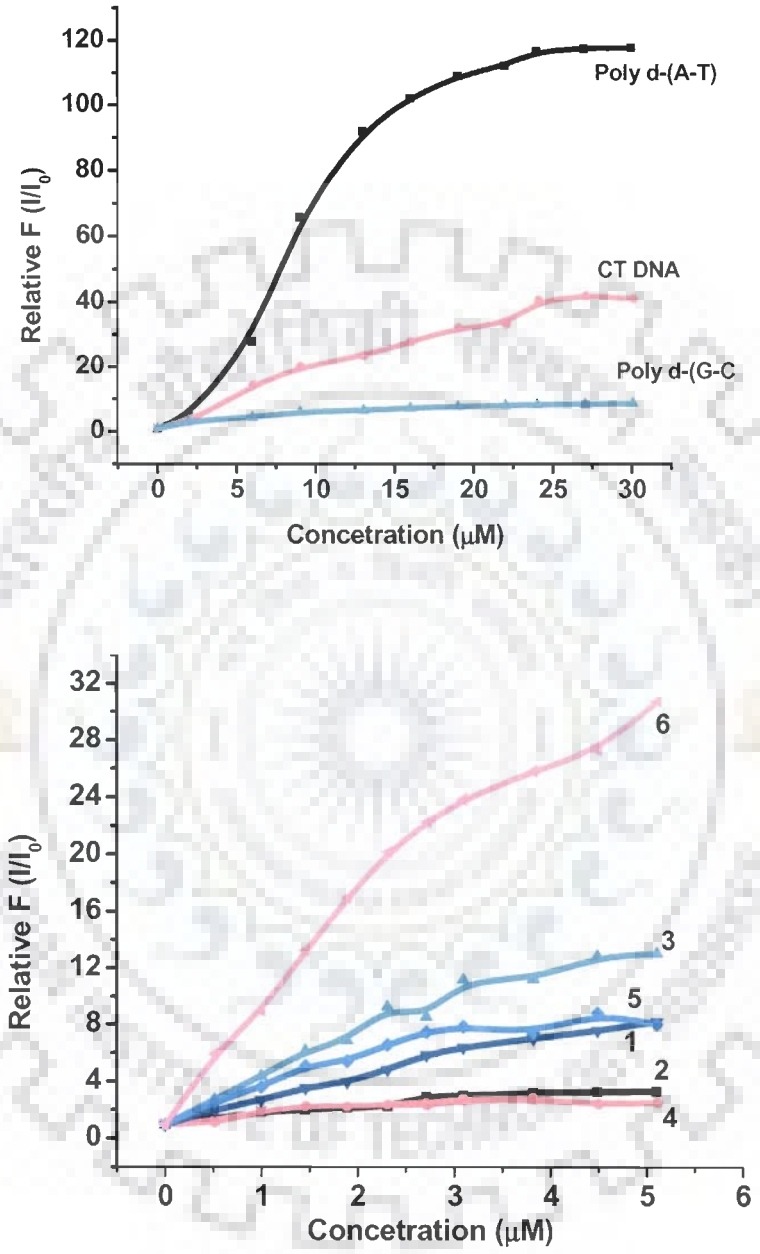


**Figure 4.8:Relative fluorescence intensity of berberine DNA complex with (a) CT DNA, Poly d-(A-T) and Poly d(G-C) and (b) oligonucleotides; (1): d-$(CGTACGCGTACG)_2$, (2): d-$(CGATCGCGATCG)_2$, (3): d-$(ATATATATAT)_2$, (4): d-$(CGCGCGCGCG)_2$, (5): d-$(TGCGCATGCGCA)_2$, and (6): d-$(CCAATTGG)_2$.**

### 4.1.2.2 TCSPC Analysis: Time-Resolved Fluorescence Measurements of Berberine d-$(CCAATTGG)_2$ Complex

Fluorescence excited state lifetimes are very sensitive to the structure and dynamics of a fluorescent molecule. Time resolved fluorescence decays were obtained by the Time-Correlated Single-Photon Counting method on the Spectrofluorimeter (model FluoroLog-TCSPC, make HORIBA Jobin Yvon Spex), used for the life time measurement study of berberine and its complex with $(CCAATTGG)_2$. The excitation source, $\lambda_{ex}$ = 344 nm was a fixed-wavelength NanoLED. The emission was detected at the emission wavelength, $\lambda_{em}$ = 534 nm. The fluorescence emission of the berberine and its complex with d- $(CCAATTGG)_2$ was counted by a micro channel plate photo multiplier tube, after passing through the monochromator and processed through constant fraction discriminator (CFD), time-to-amplitude converter (TAC) and multi channel analyzer (MCA). All measurements were performed at 298 K in 10 mM BPES buffer. The fluorescence decay was obtained and all the parameters were systematically analysed and processed by the software program DAS provided by FluoroLog-TCSPC instrument.

Global analysis was performed on each set of fluorescence decays and found that complexity of the model is well calculated with a tri exponential decay function which fits with an excellent statistical quality having global $\chi^2$ value of 1.37 and 1.10 for berberine and its complex with -d- $(CCAATTGG)_2$ respectively (Table 4.4). The low global values for $\chi^2$ indicate that the tri exponential decay function is an excellent statistical description of both the systems [Byrne and de Mello, 1998]. The exponential function with three lifetimes ($\tau$1, $\tau$2 and $\tau$3) and three amplitudes (B1, B2 and B3) indicate the presence of three conformation of berberine correspondingly. This is because berberine is a heterocyclic compound containing one saturated ring,

two methoxy group and one methylne dioxy group having rotational and can have more than one conformer in solution [Ojha et al., 2009]. For free berberine, the values τ1, τ2 and τ3 are 4.4 ns, 2.4 ns and 97 ns respectively. The relative contributions from these components were 40 %, 24 % and 36 % respectively. Most dyes of high quantum efficiency, such as laser dyes and fluorescence markers for biological samples have natural fluorescence decay times of the order of 1 to 10 ns due to their aromatic chromophore while less fluorescence chromphores have lesser lifetimes of 100 ns to 200 ns. Therefore τ1 and τ2 can be correlated to the planer structure of berberine and τ3 can be correlated to non planer moiety of the berberine. It can be noted from Table 4.4 that the numerical values of τ1, τ2 and τ3 and their relative distribution have varied in the presence of d-$(CCAATTGG)_2$. The values of τ1, τ2 and τ3 were decreased to 0.14, 0.39 and 2.6 respectively, showing that there is shortening of the decay time of berberine due to binding (Table 4.3, Figure 4.8). However, the relative contributions of τ1 increased to 70 % and the contribution from τ2 and τ3 has decreased to 18 % and 12 % (Table 4.4) which clearly elucidate the involvement of the planer moiety of berberine in interaction with the d-$(CCAATTGG)_2$.

The analysis of fluorescence decay time of berberine and berberine d-$(CCAATTGG)_2$ complex clearly elucidate the binding of berberine. Also the increase in the relative contribution of t1 and decrease in the relative contribution of t2 and t3 indicates that berberine mostly interact with the planer conformation in complex [Ojha et al., 2009]. The significant change in the values of both the decay components and their relative contributions of berberine upon binding with d-$(CCAATTGG)_2$ indicate the change in the microenvironment of berberine in the presence of d-$(CCAATTGG)_2$.

**Table 4.4: Lifetimes parameters of beberine fluorescence and its 2:1 complex with d-$(CCAATTGG)_2$ in BPES buffer at 298 K.**

| samples | Lifetime decay (ns) | | | Amplitude % | | | |
|---|---|---|---|---|---|---|---|
| | τ1 | τ2 | τ3 | B1 | B2 | B3 | $\chi^2$ |
| **Berberine** | 4.4 | 0.24 | 97 | 40 | 24 | 36 | 1.36 |
| **Berberine d-$(CCAATTGG)_2$ 2:1 complex** | 0.14 | 0.39 | 2.6 | 70 | 18 | 12 | 1.10 |

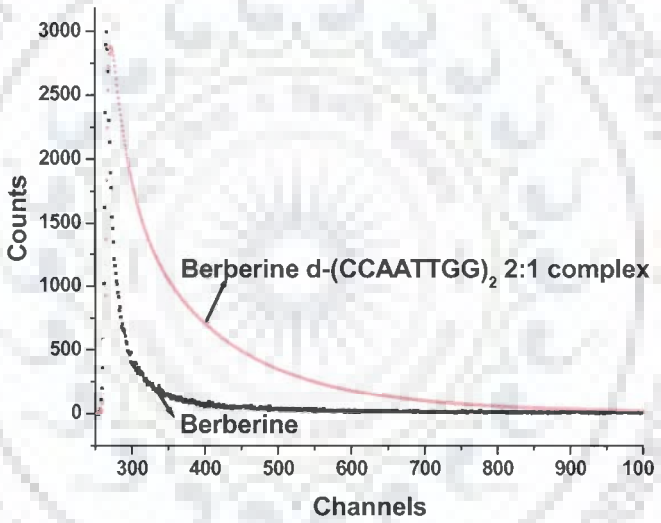


**Figure 4.9: Fluorescence lifetime decay measurement profile of beberine and 2:1 beberine-d-$(CCAATTGG)_2$ complex**

## 4.2 Summary and conclusions

The interaction of berberine, an antitumor alkaloid with natural and synthetic double stranded DNA was investigated using spectrophotometric and spectrofluorometric techniques. The absorption spectrum of berberine showed

hypochromic and bathochromic effects on binding to DNA. The fluorescence of berberine was enhanced by its interaction with the double stranded and single stranded DNA. Interaction study with different polynucleotides showed that berberine binds specifically to AT rich DNA sequences. A monomodified berberine analogue berberrubine having OH group replacement at $7^{th}$ position has been reported as better topoisomerase poison than berberine. Binding affinity of berberrubine was not found by absorbance and fluorescence techniques used. It may be attributed to the fact that berberrubine is a more potent topoisomerase inhibitor [Kim et al., 1998] which might bind to the complex of topoisomerase rather than DNA alone. This study also shows that binding is not only depending on length of the oligonucleotide, but shows a preference for AATT in octanucleotide rather than dodecanucleotide which have a single AT site. Neighbor base sequences also have impact on its binding affinity. Negative potential at AT minor groove enhanced the binding affinity of berberine while guanine at +1 position weakens the interaction. The strong interaction of berberine with promoter containing sequence d-$(CCAATTGG)_2$ was evident from the observation of higher order and magnitude of hypochromicity, fluorescence enhancement, epsilon bound value, and binding constant calculated from the spectrophotometric data. For further structural studies d-$(CCAATTGG)_2$ sequence was used.

# *Structure Determination of Promoter site containing octamer d-(CCAATTGG)$_2$ using Nuclear Magnetic Resonance and restrained Molecular Dynamics and comparison with the crystal structure*

Abundant evidences are available in literature that the sequence dependent local DNA structure is correlated with all biological functions. Also, the detailed stereochemical studies have shown that the helical parameters of a DNA double helix are strongly influenced by its base sequence [Dornberger et al., 1998; Mujeeb et al., 1993]. Hence, it is probable that structure of control sites (e.g. promoters and operators) in DNA is different from the structure of genomic DNA. The dependence of the local conformation on sequence may be involved in recognition by specific proteins involved in replication and transcription processes. Novel drugs, which can be oligonucleotides, peptides or small molecules are currently being designed to target nucleic acids. In order to develop this new medicinal strategy in a rational way there is a need to generate information regarding the structure, stability and dynamics of nucleic acids in the presence or absence of these drugs. It is believed that the three dimensional structure of individual molecules play a dominant role in the nature and specificity of interactions between nucleic acids and ligands. Two dimensional nuclear magnetic resonance spectroscopy has become a reliable tool for elucidating the solution structure of DNA oligomer. Restrained energy minimization and molecular dynamics calculation which search conformational space to find structures consistent with the experimental data have contributed significantly to the

improvements in structure determination [Celda et al., 1989; Dornberger et al., 1998; Radha et al., 1995; Tonelli et al., 1998; Ulyanov et al., 2006].

In the present study, all the structural and conformation parameters of octanucleotide d-$(CCAATTGG)_2$ having promoter site CCAAT as intrinsic part of the sequence have been elucidated. Terminal TGG at 3' position was added to provide stability to DNA duplex and to make it a complementary sequence. This sequence was used because of two reasons: First, due to its biological significance as a promoter site in various oncogenes and second, due to it's AT rich regions which gives a unique conformational pattern in DNA. One dimensional (1D) and two dimensional (2D) $^{1}H$ and $^{31}P$ techniques combined with restrained Molecular Dynamics. (rMD) were used to elucidate the solution structure of octanucleotide d-$(CCAATTGG)_2$. A detailed analysis of the helical parameters of the NMR derived solution structure and comparison with the crystal structure of this DNA octamer has been presented. Residues of the complementary octamer duplex were labeled and numbered according to the Figure below:

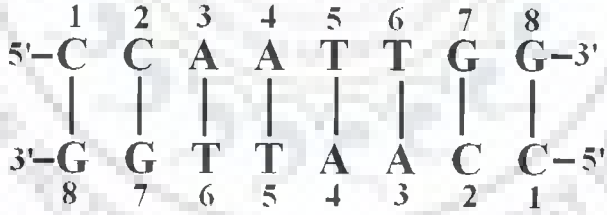


## 5.1 Results and Discussion

The assignment of various resonances of protons in d-$(CCAATTGG)_2$ was done by combining the analysis of 1D and 2D NMR experiments recorded in $H_2O$. Change in chemical shifts of nucleotide protons as a function of temperature (278 to 328 K) was investigated to obtain the thermal melting behaviour of d-(CCAATTGG).

Later, the conformational analysis of deoxyribose sugar and glycosidic bond rotation ($\chi$) of the various nucleotide residue based on analysis of 2D phase sensitive DQF-COSY and NOESY spectra recorded at 100, 200 and 300 ms at 283 K was done. Solution structure of DNA duplex was also elucidated with the help of restrained Molecular Dynamics (rMD) and all the helical parameters were calculated with CURVES. Stacking interaction between the base pairs was studied using X-3DNA.

### 5.1.1 Proton Resonance Assignment of d-(CCAATTGG)$_2$

The NMR resonances of the two strands of DNA octamer coincide owing to the two fold symmetry of the duplex. As a result only one set of resonance was observed. Figure 5.1a-g shows the full and expanded one dimensional NMR spectra of the octamer in water at 283 K. All non-labile and labile protons can be observed in the spectra recorded in $H_2O$. The region between 7.2 to 8.4 ppm shows the resonances due to the aromatic protons i.e., that is the AH8, AH2, GH8, CH6 and TH6. The region between 5.2 to 6.4 ppm shows resonances due to eight deoxyribose sugar H1' protons and two CH5 protons. The resonances in the range 1.7 to 3.0 ppm are due to H2' and H2" protons. Sugar H3' protons resonate in the range 4.6 to 5.2 ppm. Sugar H4'protons are observed in the range 4.0 to 4.5 ppm and the sugar H5', H5" protons were observed in the range 3.6 to 4.3 ppm. The methyl of thymine resonates between 1.3 to 1.6 ppm. It also shows all the expected amino and imino protons resonances. The imino protons of the non-terminal guanine and thymine bases in the DNA octamer were observed in the low field region of 12 to 14.5 ppm. The low field chemical shifts are characteristic of hydrogen bonded imino protons in Watson-Crick base pair [Wüthrich, 1986] and are direct evidence for the formation of double helical structure.

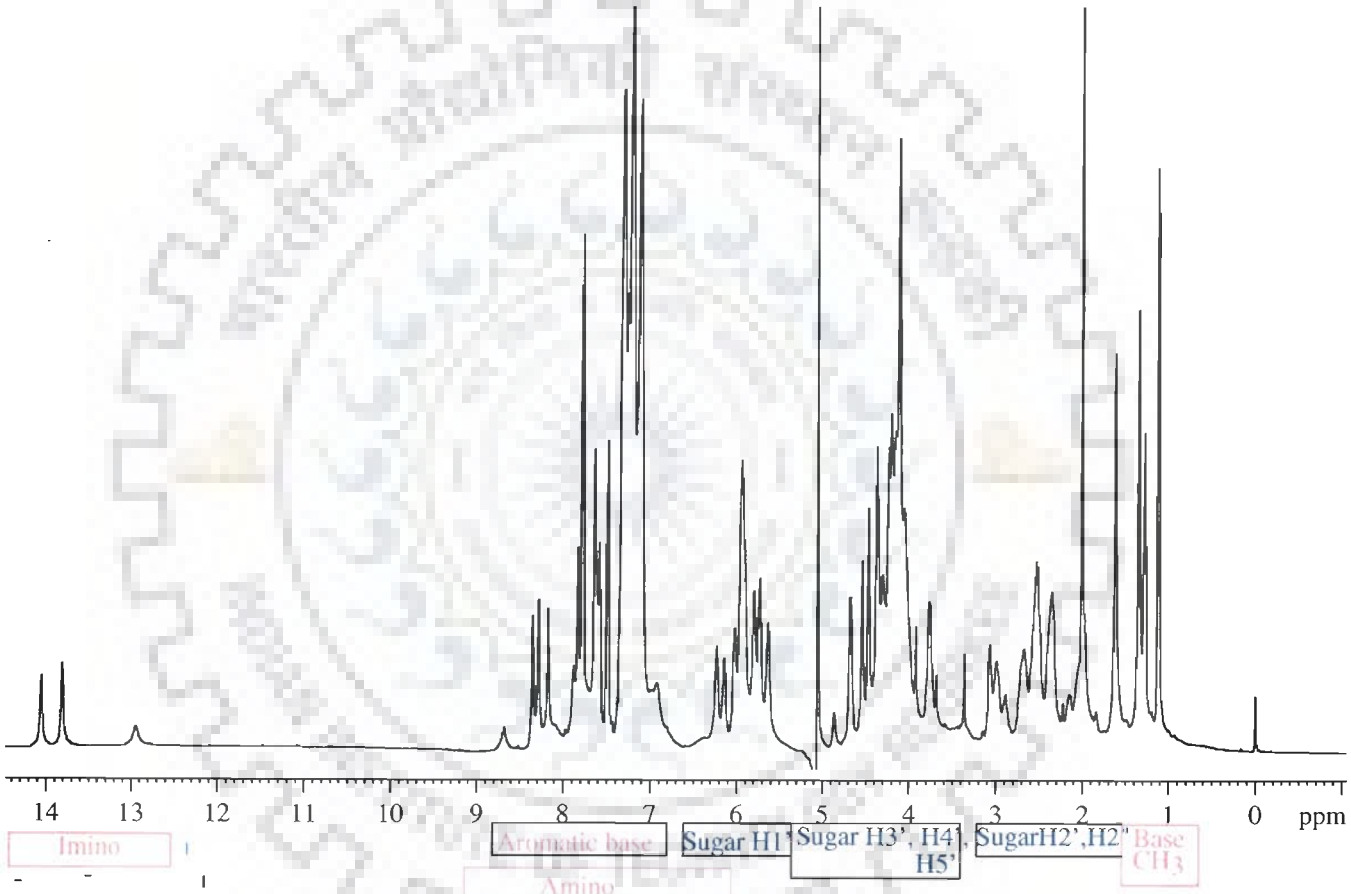


(Fig. 5.1a)

**Figure 5.1a-g: 1D $^1$H spectra of d-(CCAATTGG)$_2$ in H2O showing (a) full spectrum (b) Base Protons H8/H6 and amino protons (c) H1' and amino Protons (d) H2' and H2" (e) H3' and H4' (f) Methyl Protons (g) Imino protons.**

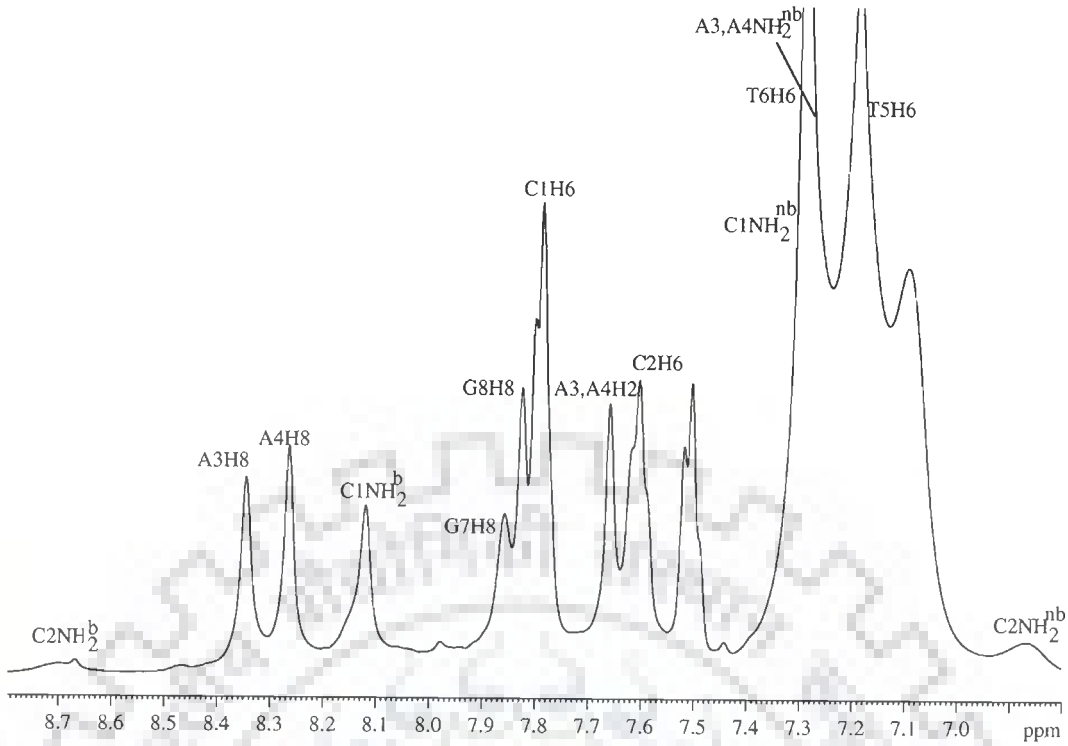


**(Fig. 5.1b)**

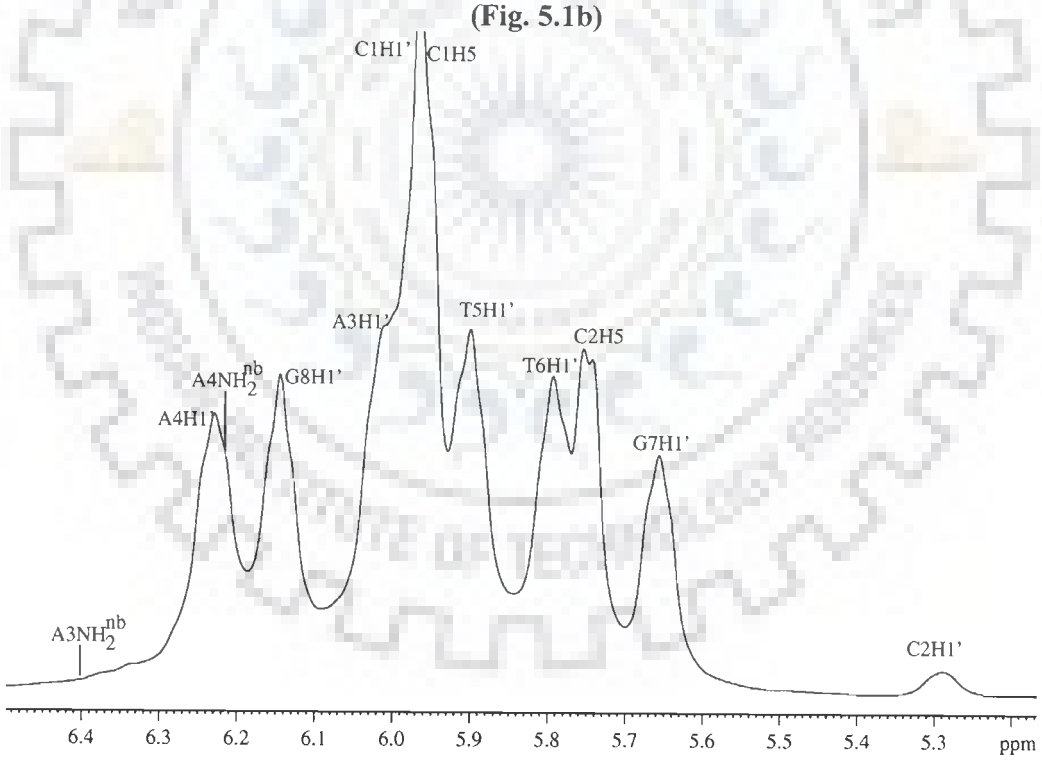


**(Fig. 5.1c)**

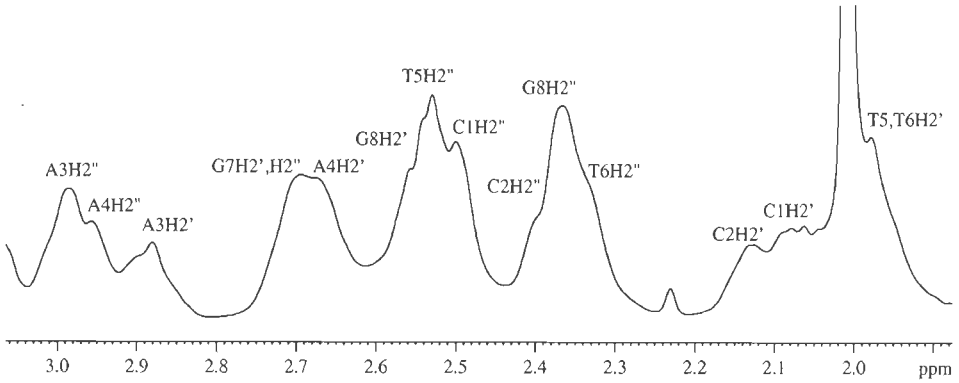


**(Fig. 5.1d)**

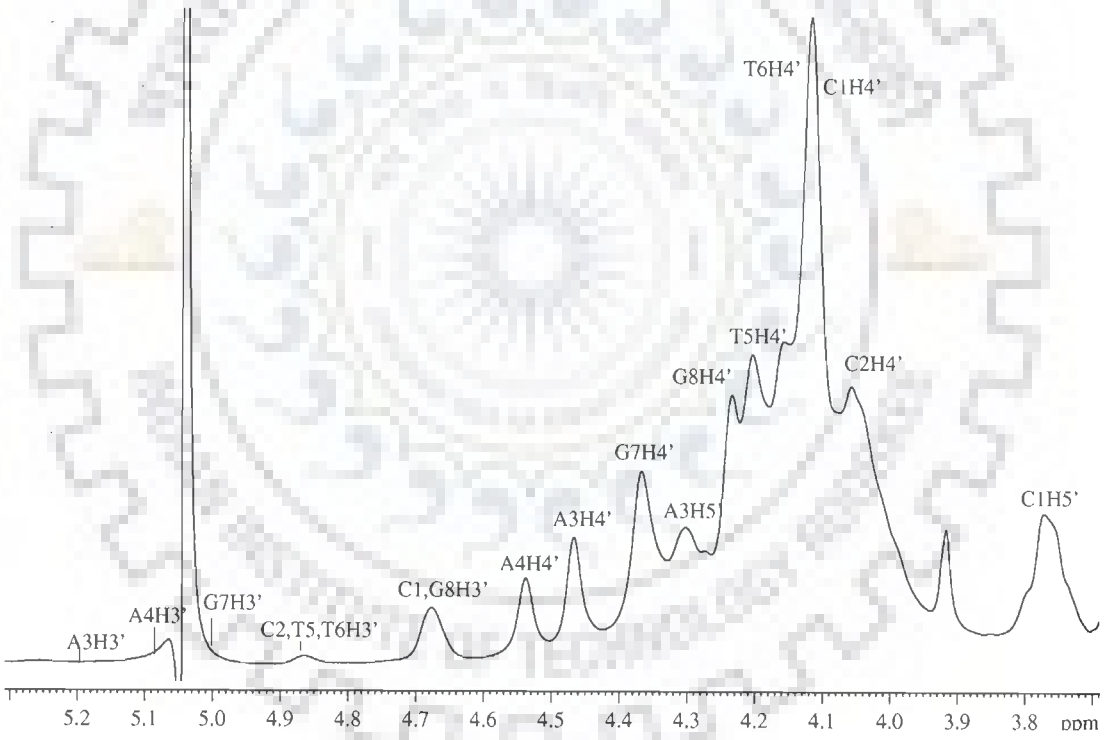


**(Fig. 5.1e)**

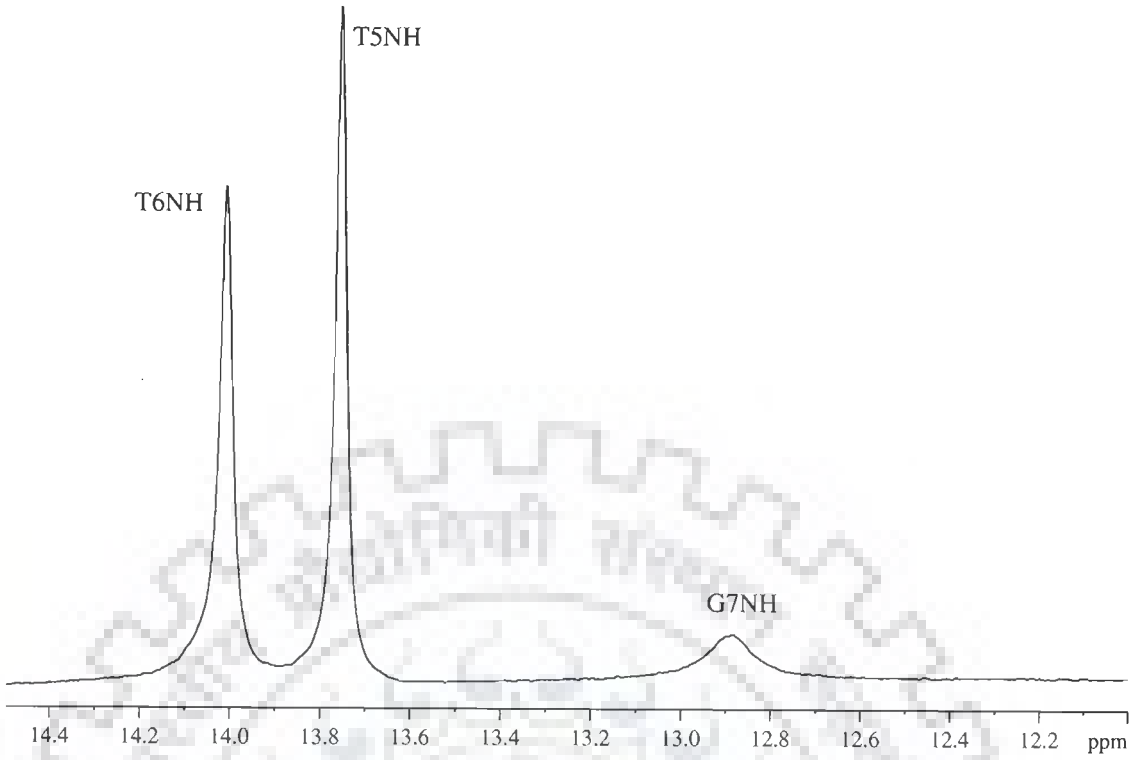


**(Fig. 5.1f)**

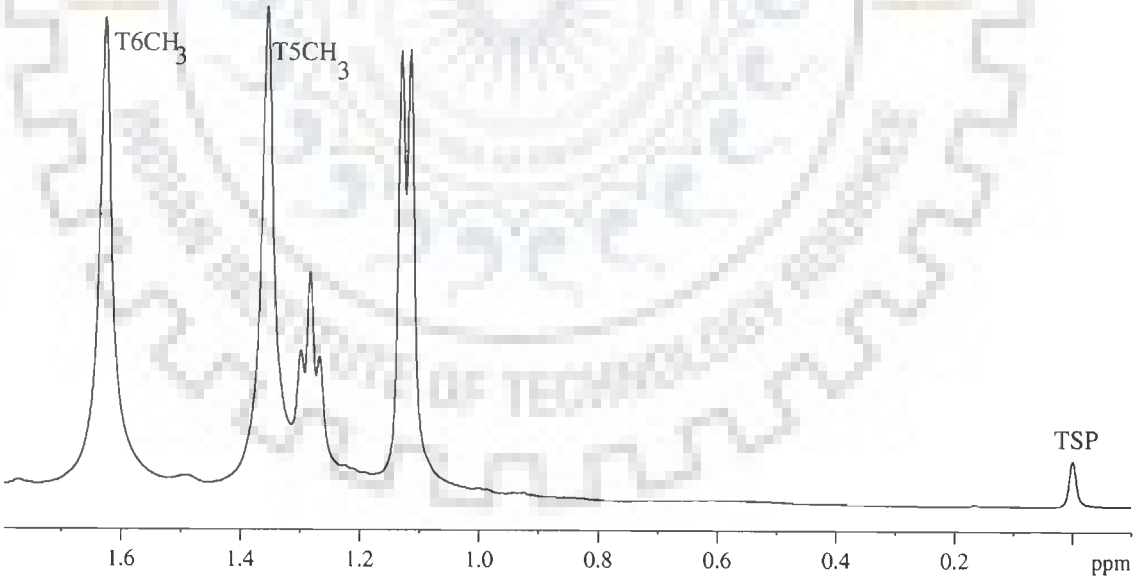


**(Fig. 5.1g)**

Amino protons of adenine and cytosine were also found in the range 6.2 to 9.0.ppm. Each amino proton gives two peaks corresponding to non-bonded and bonded protons. Bonded amino protons are involved in hydrogen bonding in the Watson-Crick base pairing and always found to be downfield shifted with respect to non-bonded (not involved in Watson-Crick base pairing) amino signal.

All the non-exchangeable protons were assigned by standard methods using NOESY, TOCSY and DQF COSY spectra at 278 and 283 K in $D_2O$. The chemical shifts δ (in ppm) for various protons at 283 K are listed in Table 5.1. The phase sensitive 2D DQF COSY and NOESY spectra recorded at 200 ms are shown in Figure 5.2a-e and 5.3a-e respectively along with expansions of certain regions to highlight specific connectivities. In DQF-COSY (Figure 5.2a-e) the sets of sugar proton resonances were easily recognizable and are listed in Table 5.2. Seven intense cross peaks of pair H2'-H2" can be seen in Figure 5.2a for the sugar residues however one pair of H2'-H2" connectivity is not distinct. Each of the H2' and H2" pair of coupled protons showed intense cross peak with H1' protons of its respective base in the range 5.2 to 6.4 ppm and H3' in range of 4.6-5.2 ppm (Figure 5.2b). Figure 5.2c shows that every H3' gives cross peak with the H4' of their respective basis. Thus, each set of sugar protons of a residue is assigned, the position of which matches with the corresponding position in 1D spectrum. The cytosine's and thymine's H6 protons are distinguishable in Figure 5.2d and 5.2e since they are coupled to their corresponding H5 and $CH_3$ protons. Further, assignment of the sugar protons to a specific nucleotide residue was made using the strategies available in literature [Assa-Munt and Kearns, 1984; Gronenborn and Clore, 1985; Hosur et al., 1988; Lown et al., 1984] for sequential assignment in right handed B-DNA with sugar in C2'-endo/ C3'-endo / O1- endo conformations and glycosidic angle in anti domain.

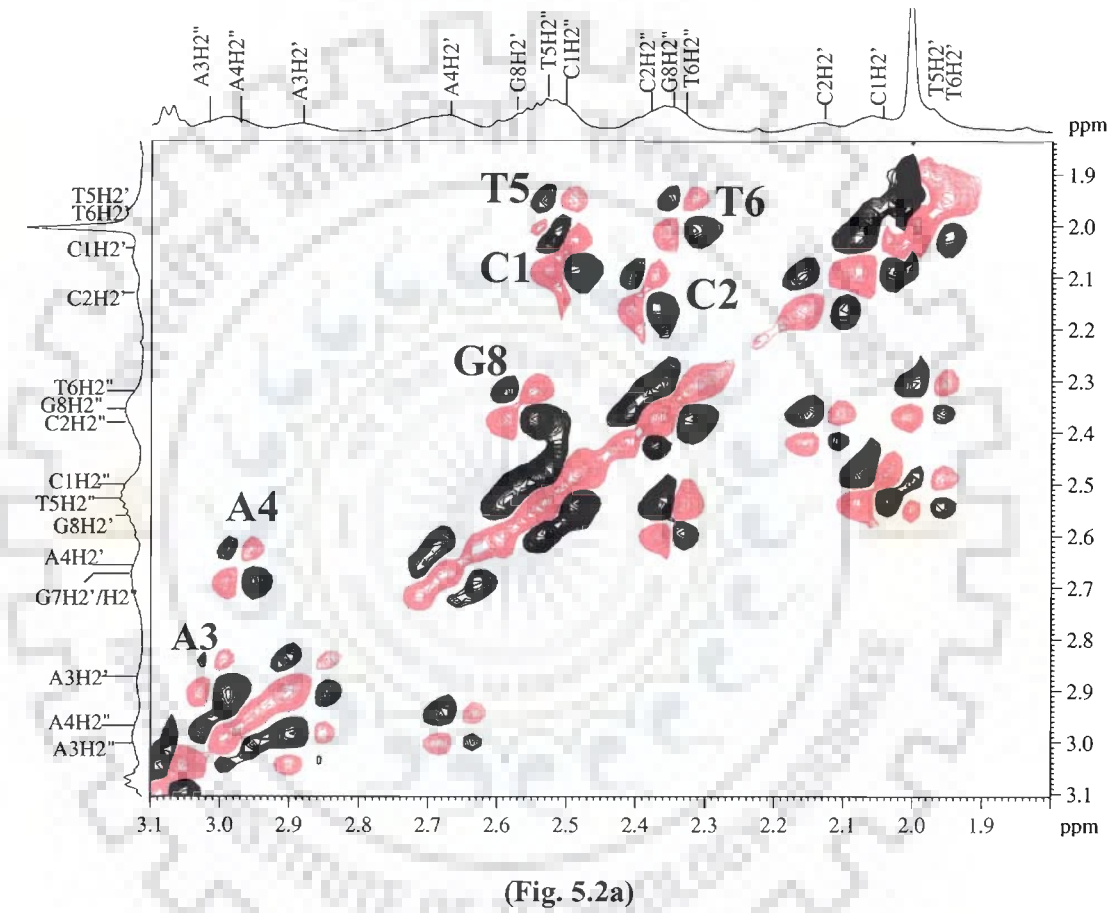


**(Fig. 5.2a)**

**Figure 5.2: Expansions of selected regions of 500 MHz DQF-COSY spectrum of d-$(CCAATTGG)_2$ in $D_2O$showing specific J- coupling Correlations (a) H2',H2" with H1', H3' (b) H2' with H2" (c) H3' with H4' (d) H5 with H6 (e) H5 with $CH_3$.**

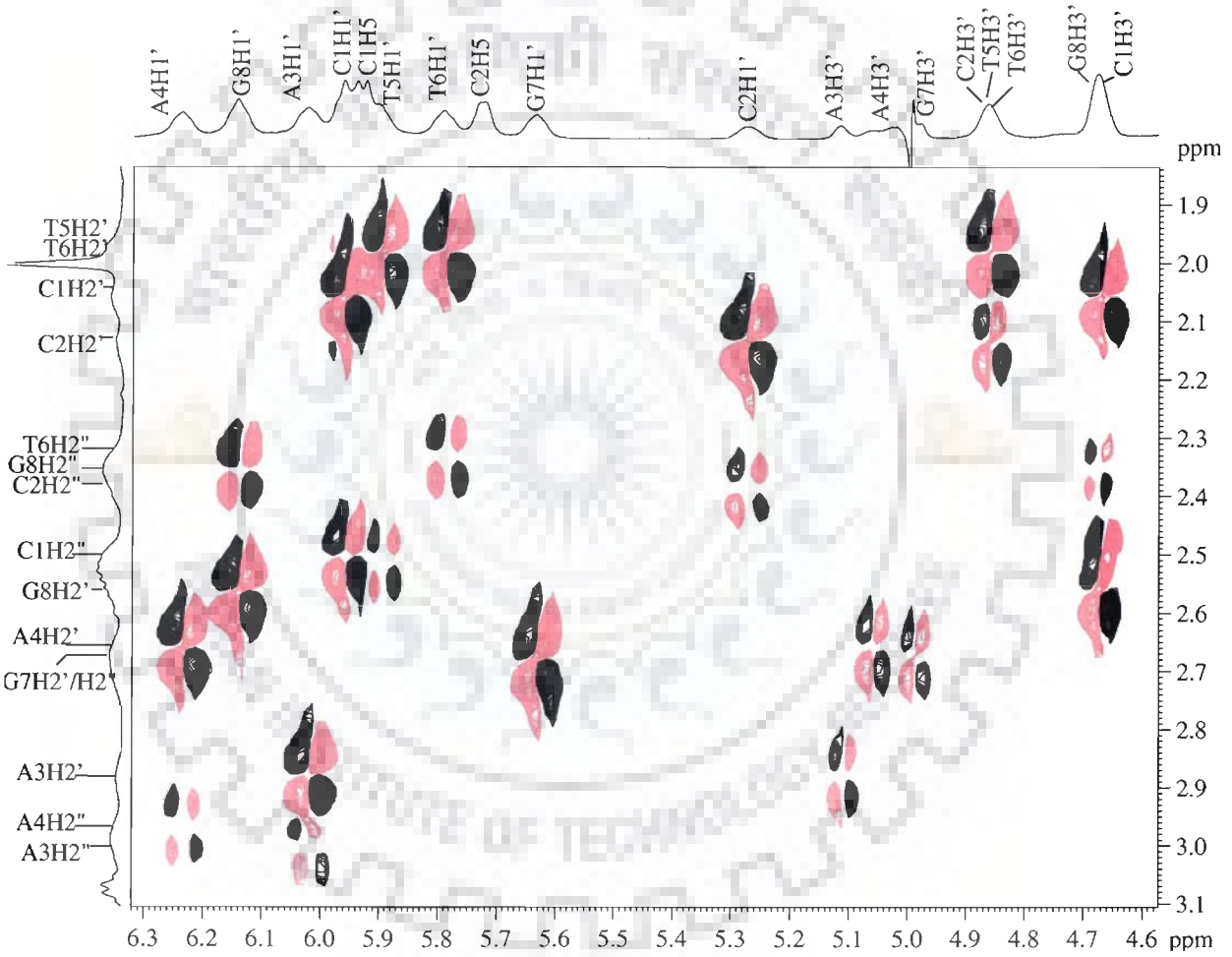
A4H1'
G8H1'
A3H1'
C1H1'
C1H5
T5H1'
T6H1'
C2H5
G7H1'
C2H1'
A3H3'
A4H3'
G7H3'
C2H3'
T5H3'
T6H3'
G8H3'
C1H3'
ppm
T5H2'
T6H2'
C1H2'
C2H2'
T6H2"
G8H2"
C2H2"
C1H2"
G8H2'
A4H2'
G7H2'/H2'
A3H2'
A4H2"
A3H2"
1.9
2.0
2.1
2.2
2.3
2.4
2.5
2.6
2.7
2.8
2.9
3.0
3.1
6.3 6.2 6.1 6.0 5.9 5.8 5.7 5.6 5.5 5.4 5.3 5.2 5.1 5.0 4.9 4.8 4.7 4.6 ppm

**(Fig. 5.2b)**

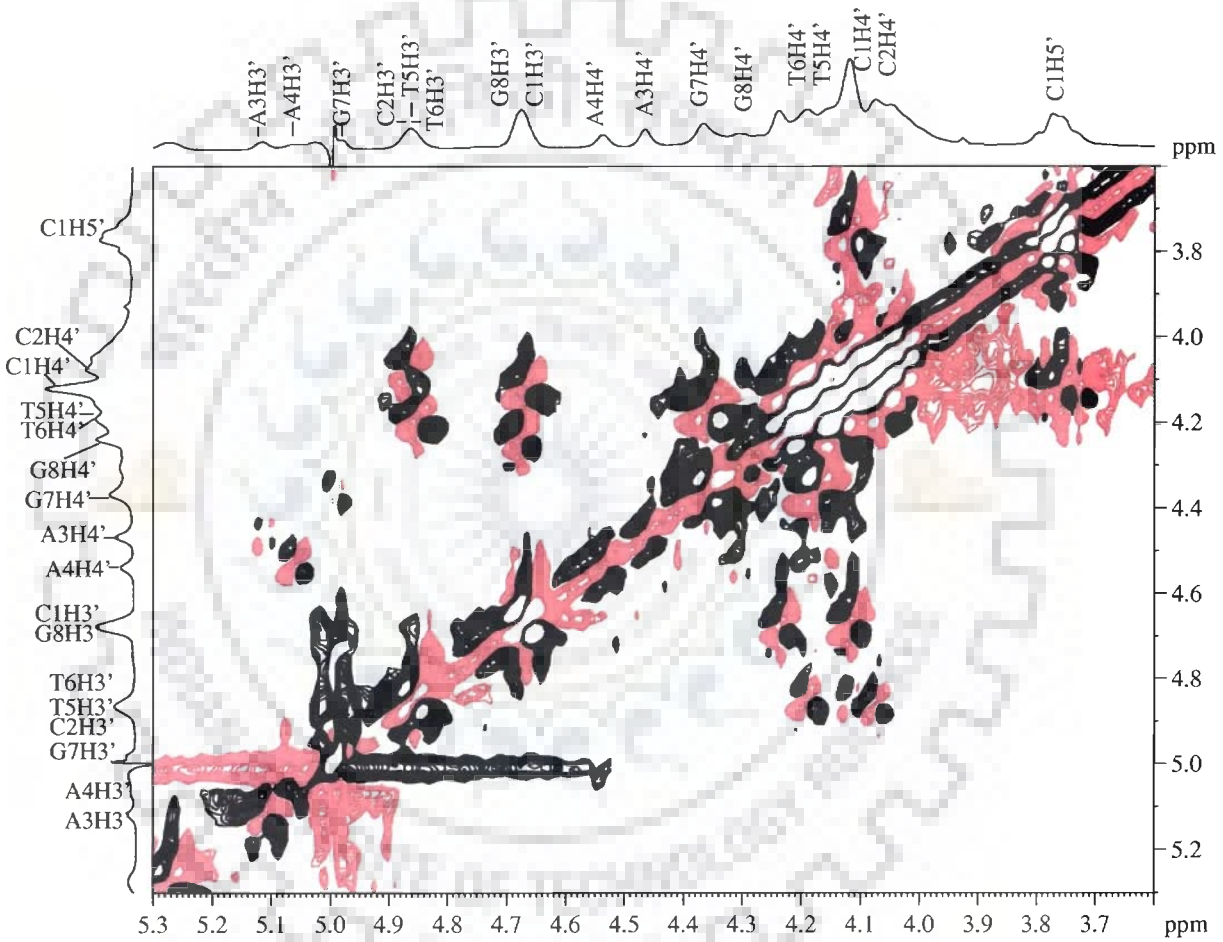
A3H3'
A4H3'
G7H3'
C2H3'
T5H3'
T6H3'
G8H3'
C1H3'
A4H4'
A3H4'
G7H4'
G8H4'
T6H4'
T5H4'
C1H4'
C2H4'
C1H5'
ppm
C1H5'
C2H4'
C1H4'
T5H4'
T6H4'
G8H4'
G7H4'
A3H4'
A4H4'
C1H3'
G8H3
T6H3'
T5H3'
C2H3'
G7H3'
A4H3'
A3H3
3.8
4.0
4.2
4.4
4.6
4.8
5.0
5.2
5.3 5.2 5.1 5.0 4.9 4.8 4.7 4.6 4.5 4.4 4.3 4.2 4.1 4.0 3.9 3.8 3.7
ppm

**(Fig. 5.2c)**

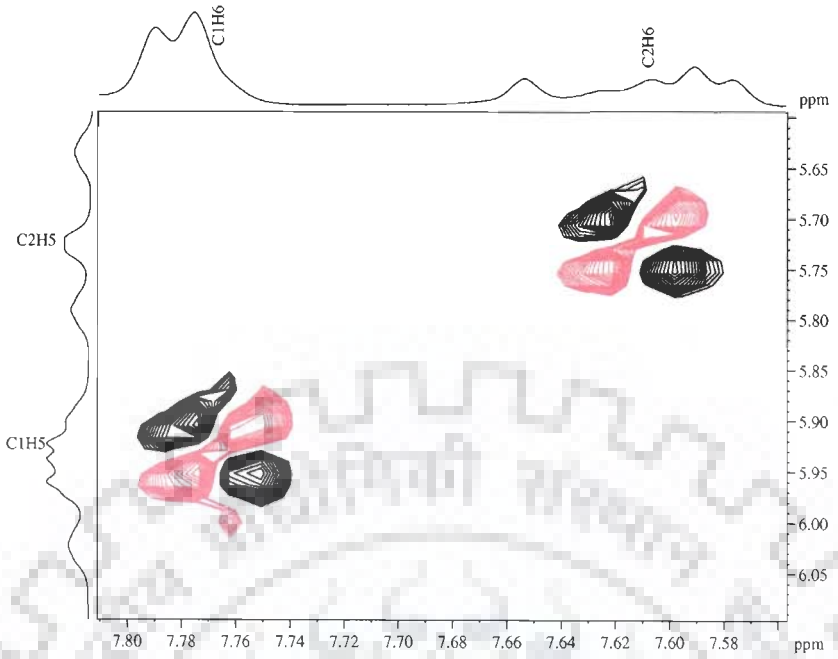


**(Fig. 5.2d)**

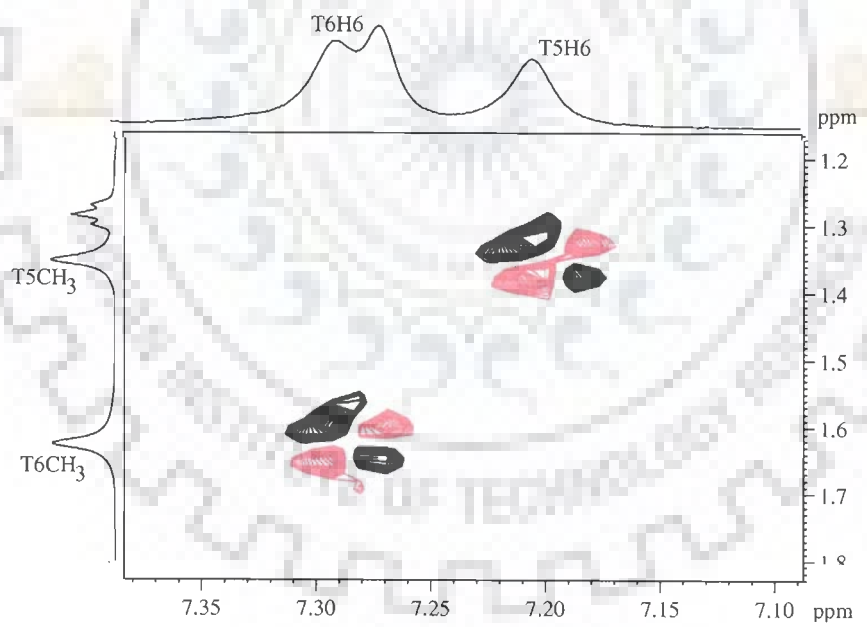


**(Fig. 5.2e)**

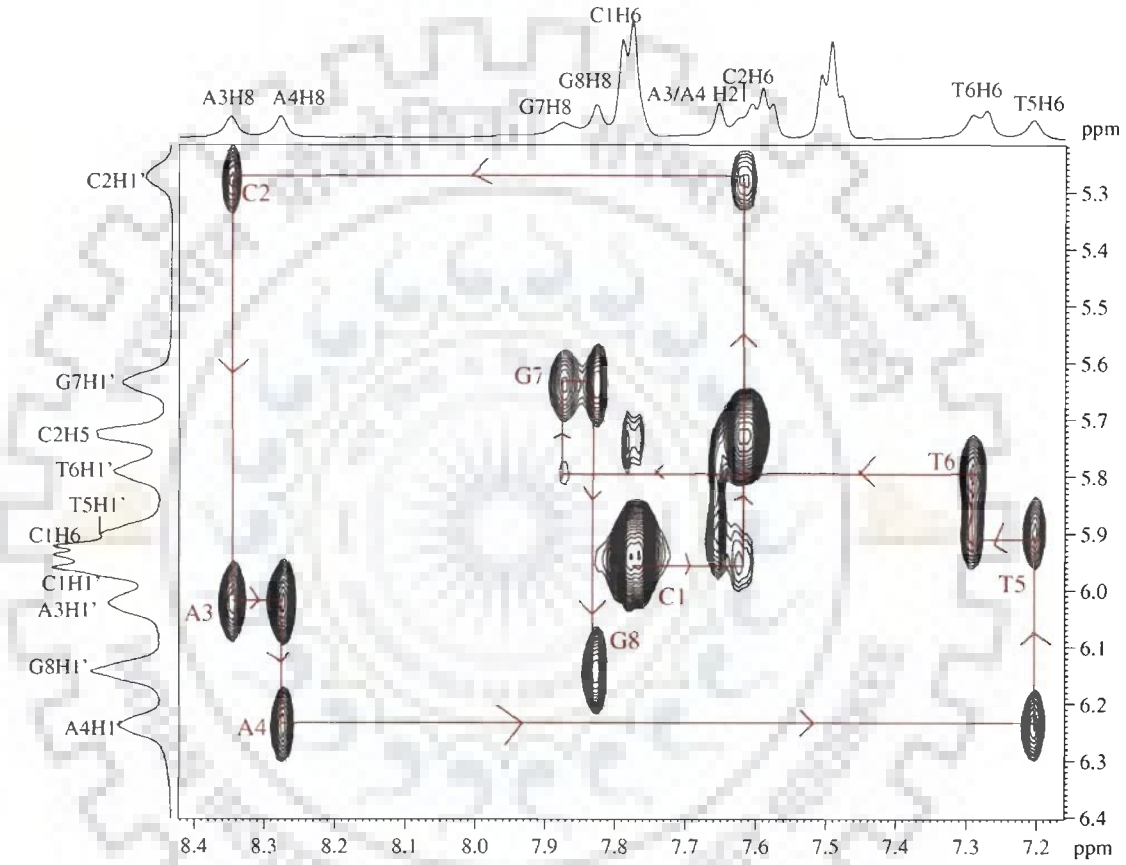


**(Fig. 5.3a)**

**Figure 5.3:Expansions of selected regions of 500 MHz NOESY spectrum of d-(CCAATTGG)$_2$ in $D_2O$ showing specific Dipolar couplings(a) base with H1'(b) base with H2' and H2" (c) base with H3' and H4' (d) H2' with H2" (e) H1' with H2', H2".**

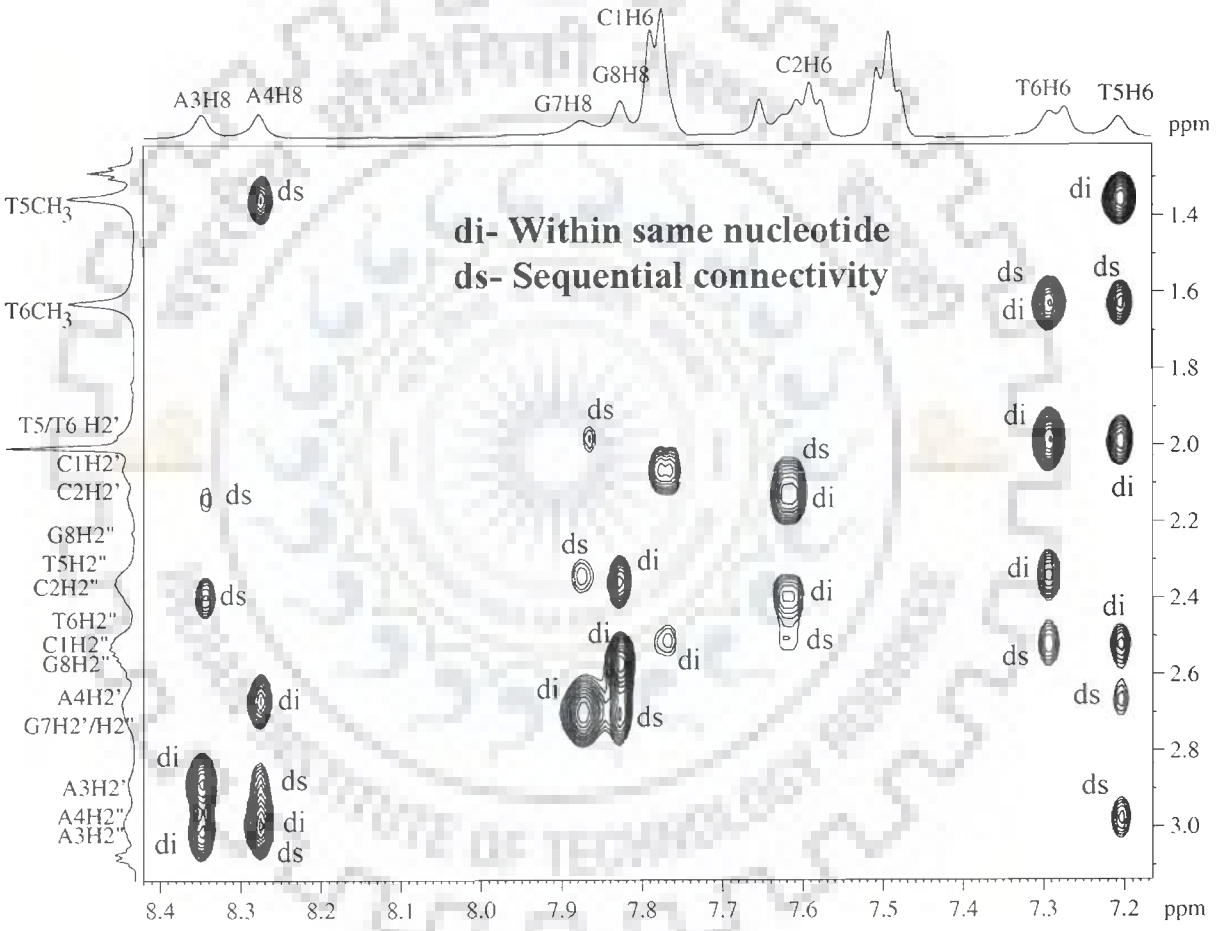
C1H6
G8H8
C2H6
A3H8
A4H8
G7H8
T6H6
T5H6
ppm
T5CH3
T6CH3
T5/T6 H2'
C1H2'
C2H2'
G8H2"
T5H2"
C2H2"
T6H2"
C1H2"
G8H2"
A4H2'
G7H2'/H2"
A3H2'
A4H2"
A3H2"
di- Within same nucleotide
ds- Sequential connectivity
8.4
8.3
8.2
8.1
8.0
7.9
7.8
7.7
7.6
7.5
7.4
7.3
7.2
ppm
1.4
1.6
1.8
2.0
2.2
2.4
2.6
2.8
3.0

**(Fig. 5.3b)**

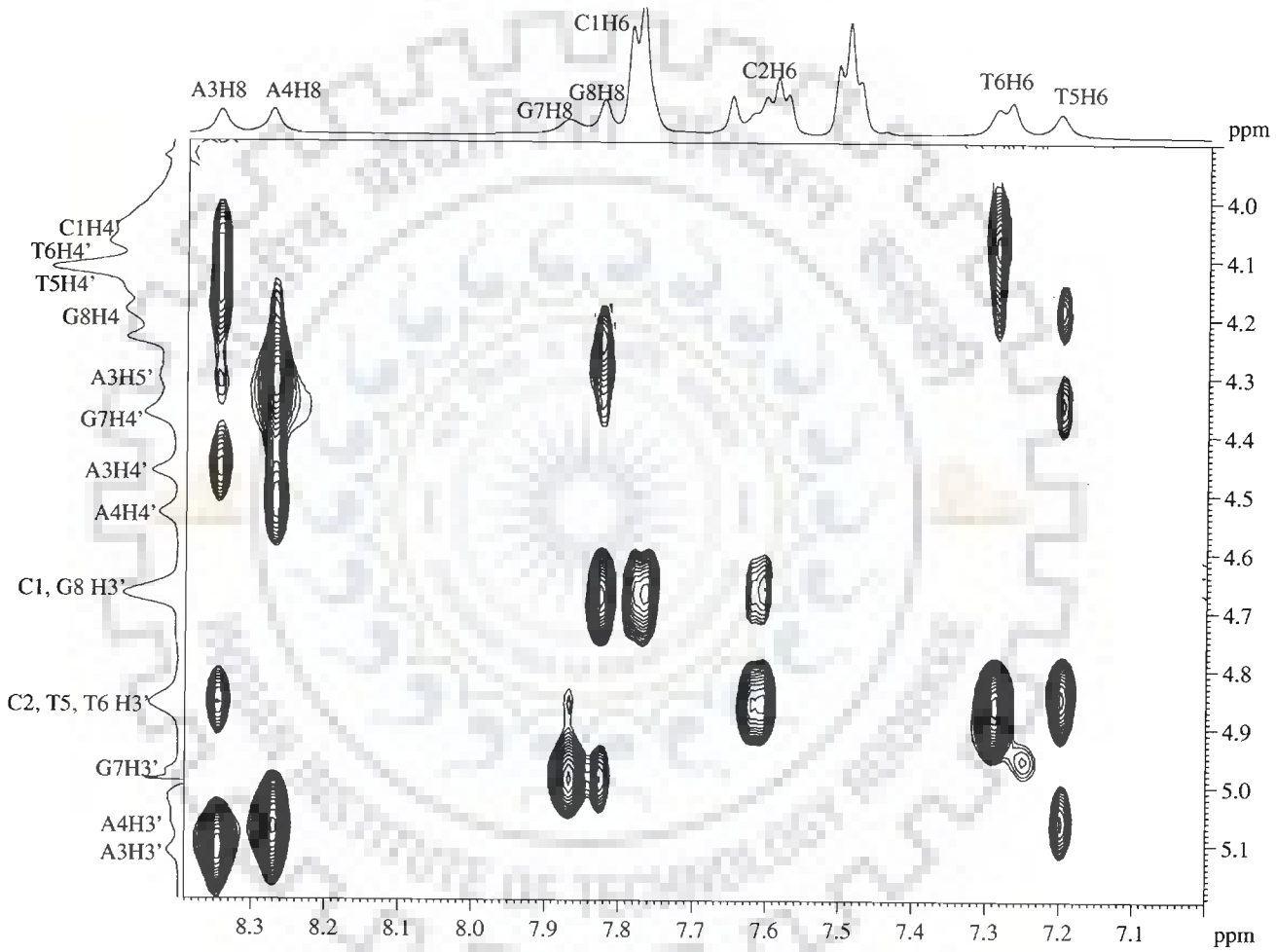
C1H6
A3H8
A4H8
G8H8
G7H8
C2H6
T6H6
T5H6
ppm
C1H4'
T6H4'
T5H4'
G8H4
A3H5'
G7H4'
A3H4'
A4H4'
C1, G8 H3'
C2, T5, T6 H3'
G7H3'
A4H3'
A3H3'
4.0
4.1
4.2
4.3
4.4
4.5
4.6
4.7
4.8
4.9
5.0
5.1
8.3
8.2
8.1
8.0
7.9
7.8
7.7
7.6
7.5
7.4
7.3
7.2
7.1
ppm

**(Fig. 5.3c)**

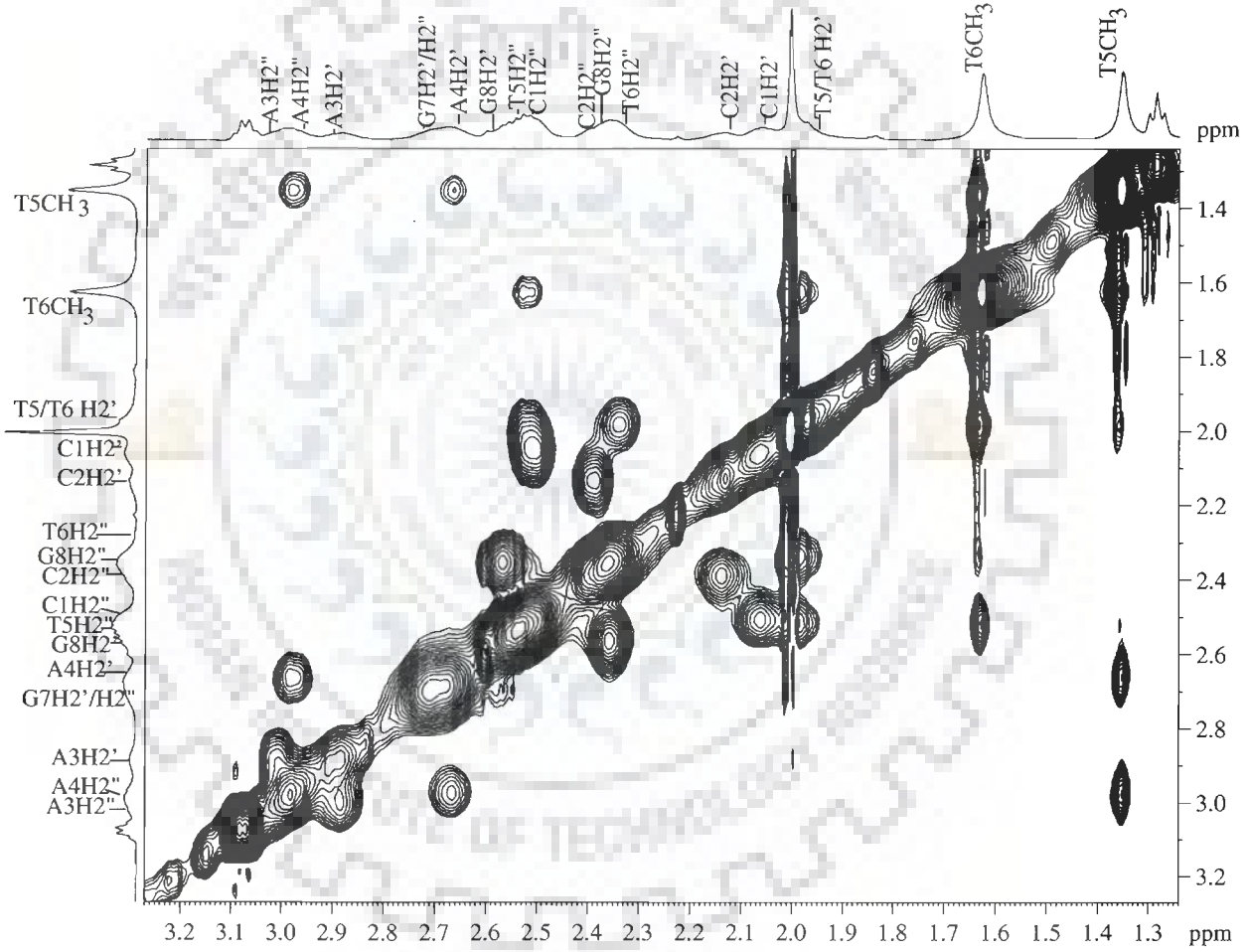
A3H2"
A4H2"
A3H2'
G7H2'/H2"
A4H2'
G8H2'
T5H2"
C1H2"
C2H2"
G8H2"
T6H2"
C2H2'
C1H2'
T5/T6 H2'
T6CH3
T5CH3
ppm
T5CH3
T6CH3
T5/T6 H2'
C1H2'
C2H2'
T6H2"
G8H2"
C2H2"
C1H2"
T5H2"
G8H2'
A4H2'
G7H2'/H2"
A3H2'
A4H2"
A3H2"
1.4
1.6
1.8
2.0
2.2
2.4
2.6
2.8
3.0
3.2
3.2 3.1 3.0 2.9 2.8 2.7 2.6 2.5 2.4 2.3 2.2 2.1 2.0 1.9 1.8 1.7 1.6 1.5 1.4 1.3
ppm

**(Fig. 5.3d)**

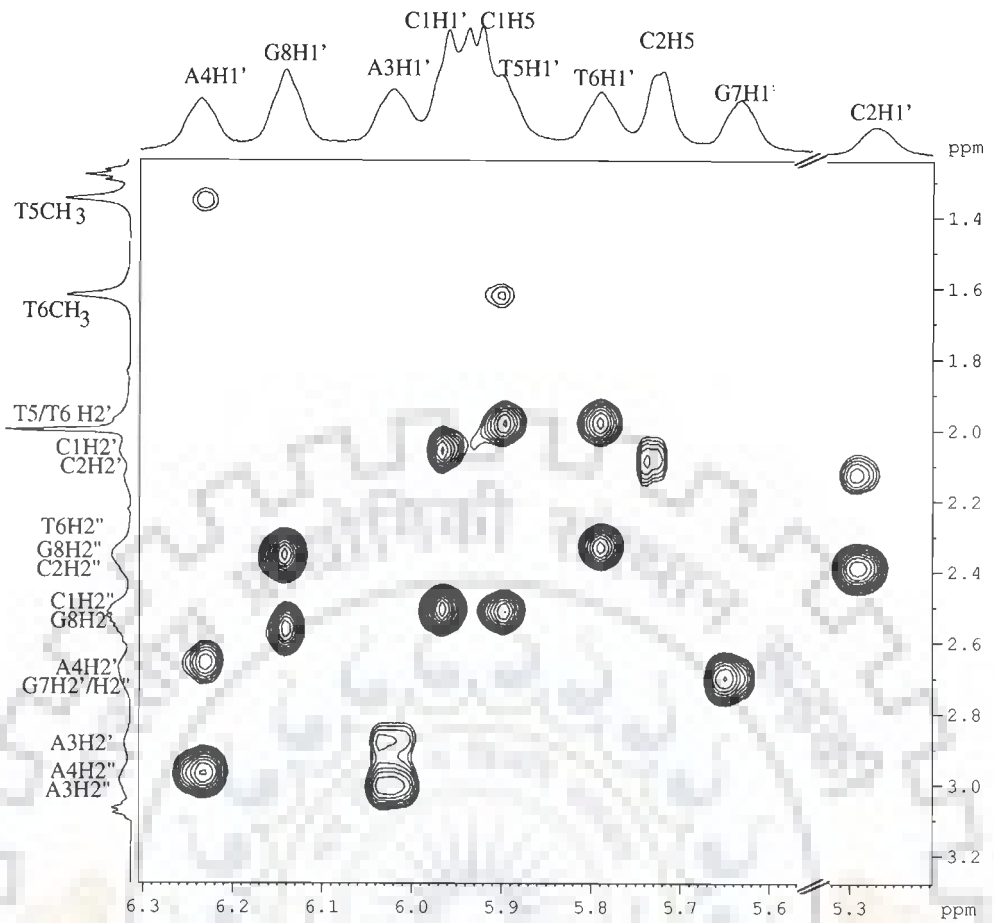


**(Fig. 5.3e)**

**Table 5.1: Chemical shift (ppm) of d-(CCAATTGG)$_2$ as observed in $D_2O$.**

| BASE | H1' | H2' | H2" | H3' | H4' | H2/H5/CH3 | H6/H8 | $NH_2^b$ | $NH_2^{nb}$ | NH |
|---|---|---|---|---|---|---|---|---|---|---|
| C1 | 5.97 | 2.06 | 2.50 | 4.53 | 4.11 | 5.95 | 7.82 | 8.16 | 7.33 | - |
| C2 | 5.29 | 2.13 | 2.39 | 4.67 | 4.06 | 5.73 | 7.60 | 8.69 | 6.98 | - |
| A3 | 6.01 | 2.86 | 2.99 | 5.11 | 4.46 | 7.66 | 8.35 | 7.28 | 6.40 | - |
| A4 | 6.23 | 2.67 | 2.97 | 5.06 | 4.52 | 7.66 | 8.28 | 7.32 | 6.24 | - |
| T5 | 5.90 | 1.97 | 2.53 | 4.67 | 4.19 | 1.35 | 7.19 | - | - | 13.80 |
| T6 | 5.79 | 1.98 | 2.35 | 4.67 | 4.11 | 1.63 | 7.29 | - | - | 14.04 |
| G7 | 5.65 | 2.66 | 2.68 | 4.87 | 4.36 | | 7.86 | - | - | 12.94 |
| G8 | 6.14 | 2.35 | 2.56 | 4.53 | 4.20 | | 7.83 | - | - | - |

**Table 5.2: Presence (+) and absence (-) of intra residue cross-peak patterns involving deoxyribose sugar protons in d-(CCAATTGG)$_2$ from DQF COSY spectra in D2O at 283 K**

| | H1'-H2' | H1'-H2" | H2'-H2" | H2'-H3' | H2"-H3' | H3'-H4' | H4'-H5' |
|---|---|---|---|---|---|---|---|
| C1 | + | + | + | + | - | + | + |
| C2 | + | + | + | + | - | + | - |
| A3 | + | + | + | + | - | + | - |
| A4 | + | + | + | + | - | + | - |
| T5 | + | + | + | + (o) | - | + | - |
| T6 | + | + | + | +(o) | - | + | - |
| G7 | + (o) | +(o) | - | + | - | + | + |
| G8 | + | + | + | + | + | + | - |

Connectivities in the finger print region (Base-H1') were contiguous through out the whole molecule and each of the base protons gave cross peaks with two H1' namely the sugar belonging to the base itself and the sugar of the base preceding it in the sequence 5'-3' direction (Figure 5.3a). One of the H1' gave only one cross peak with its own base proton and that was assigned to as the terminal H1' at 3'-end as G8H1' and corresponding base assigned to as G8H8. As expected, each of the base proton also gave NOE cross peak with two pair of H2'-H2", one with the sugar of base itself and other with sugar of the base preceding (Figure 5.3b). It was noted that seven of H8/H6 protons gave NOE cross peak with two (H2', H2") pair of proton. One of the CH6 gives only 2 NOE cross peaks and therefore assigned as the terminal one at 5'-end. Thus, all the protons were ambiguously assigned and all the expected cross peaks between base with H3' and H4', H2' with H2", H1' with H2' and H2", H5 with H6, H5-$CH_3$ can be seen in Figure 5.3c-g. The whole base–base, base-sugar and sugar–sugar intra residue and peaks which were used for conformational analysis through restrained Molecular Dynamics (rMD) are tabulated in Table 5.3 and 5.4 respectively.

**Table 5.3: Interproton distance (Å) obtained from intra nucleotide NOE connectivities (di) of base to sugar protons , sugar –sugar protons, and base to base protons of d-(CCAATTGG)$_2$ estimated from NOESY spectra at 200 ms(Figure 5.3) using C2H6-C2H5 = 2.44Å as a standard reference. Overlap of peaks is indicated as o. (all distances taken from 200ms).**

| Base-Sugar | H8/H6- H1' | | | H8/H6-H2' | | | H8/H6-H2" | | | H8/H6-H3' | | |
|---|---|---|---|---|---|---|---|---|---|---|---|---|
| | BDNA | Distance | rMD | BDNA | Distance | rMD | BDNA | Distance | rMD | BDNA | Distance | rMD |
| C1 | 3.66/ 3.88 | 2.08 | 3.17 | 2.2 | 2.18 | 2.61 | 3.4 | 3.73 | 3.81 | 4.2 | 3.53 | 3.98 |
| C2 | | 2.99 | 3.62 | | 2.46 | 2.14 | | 2.55 | 3.99 | | 3.06 | 4.13 |
| A3 | | 3.26 | 3.60 | | 2.44 | 3.82 | | m(o) | 2.51 | | 3.10 | 3.62 |
| A4 | | 3.20 | 3.49 | | 2.71 | 3.28 | | 2.48 | 2.57 | | 2.96 | 3.79 |
| T5 | | 3.34 | 3.70 | | 2.59 | 2.26 | | 3.08 | 3.53 | | 3.09 | 4.26 |
| T6 | | 2.55 | 3.44 | | 2.30 | 3.19 | | 2.81 | 1.94 | | 2.87 | 3.62 |
| G7 | | 3.40 | 3.80 | | s(o) | 3.57 | | s(o) | 1.98 | | 3.62 | 4.01 |
| G8 | | 2.94 | 3.70 | | 2.54 | 3.11 | | 3.20 | 1.99 | | 3.03 | 4.02 |
| Sugar-Sugar | H1'- H2' | | | H1'- H2" | | | H1'- H3' | | | H1'- H4' | | |
| | BDNA | Distance | rMD | BDNA | Distance | rMD | BDNA | Distance | rMD | BDNA | Distance | rMD |
| C1 | 2.8 | 3.08 | 3.06 | 2.2 | 2.65 | 2.32 | 3.6 | 3.41 | 3.70 | 2.8 | 2.89 | 3.09 |
| C2 | | 2.61 | 3.02 | | 2.39 | 2.54 | | 3.34 | 3.59 | | 2.67 | 2.91 |
| A3 | | 2.98 | 3.00 | | 2.78 | 2.36 | | 2.69 | 3.62 | | 2.94 | 2.59 |
| A4 | | 2.80 | 3.06 | | 2.43 | 2.19 | | 3.24 | 3.70 | | 2.95 | 3.10 |
| T5 | | 3.08 | 3.07 | | 2.86 | 2.47 | | 3.66 | 3.85 | | 2.97 | 3.04 |
| T6 | | 2.69 | 3.03 | | 2.49 | 2.42 | | 3.36 | 3.70 | | 3.01 | 2.79 |
| G7 | | 2.35 | 3.01 | | - | 2.69 | | 3.34 | 3.75 | | 3.57 | 3.48 |
| G8 | | 2.75 | 3.03 | | 2.48 | 2.32 | | 3.30 | 3.71 | | 3.38 | 3.15 |

**Table 5.4: Interproton distance (Å) obtained from Sequential NOE connectivities (ds) of nucleotide protons of the drug-DNA complex at D/N = 1.0 at 278 K estimated from NOESY spectra at 200 ms (Fig. 4.8) using C5H6-C5H5 = 2.40Å as a standard reference. Overlap of peaks is indicated as o.**

| Base-Sugar | C1pC2 | | | C2pA3 | | | A3pA4 | | | A4pT5 | | |
|---|---|---|---|---|---|---|---|---|---|---|---|---|
| | BDNA | Distance | rMD | BDNA | Distance | rMD | BDNA | Distance | rMD | BDNA | Distance | rMD |
| **H1'-H6/H8** | 3.50 | m(o) | 4.52 | 3.60 | 3.42 | 3.22 | 3.60 | 2.97 | 3.36 | 3.50 | 3.14 | 3.43 |
| **H1'-H5/CH3** | 4.30 | m(o) | 4.24 | | - | - | | - | | - | 4.32 | 3.76 |
| **H2'-H6/H8** | 4.00 | m(o) | 3.28 | 3.80 | 3.61 | 3.57 | 3.80 | m(o) | 3.70 | 4.00 | 3.59 | 3.77 |
| **H2"-H6/H8** | 2.70 | m(o) | 4.52 | 2.10 | 2.12 | 2.27 | 2.10 | 2.15 | 1.97 | 2.20 | 2.57 | 2.36 |
| **H2'-H5/CH3** | 3.60 | 2.69 | 3.32 | | - | - | | - | | 3.40 | 3.41 | 2.14 |
| **H2"-H5/CH3** | 2.70 | - | 2.63 | | - | - | | - | | 2.90 | 3.01 | 2.06 |
| **H3'-H6/H8/** | 4.60 | 3.50 | 5.80 | 4.60 | 3.56 | 4.43 | 4.60 | (o) | 5.20 | 4.60 | 3.48 | 4.90 |
| **H3'-H5/CH3** | - | 3.67 | 5.31 | | - | | | | | | | |
| **H6-H5** | 3.90 | 3.66 | 3.28 | | | | | | | | | |
| **H6-H8** | | | | 4.80 | 3.25 | 3.80 | | | | | | |
| **H2-H2** | | | | | | | 3.6 | 3.72 | 3.19 | | | |
| | **T5pT6** | | | **T6pG7** | | | **G7pG8** | | | | | |
| | BDNA | Distance | rMD | BDNA | Distance | rMD | BDNA | Distance | rMD | BDNA | Distance | rMD |
| **H1'-H6/H8** | 3.50 | 1.97 | 3.67 | 3.60 | 4.00 | 3.92 | 3.60 | 3.4 | 2.94 | | | |
| **H1'-H5/CH3** | 4.30 | 4.20 | 4.35 | | - | - | | - | - | | | |
| **H2'-H6/H8** | 4.00 | 2.3 | 2.83 | 3.80 | 4.70 | 4.15 | 3.80 | 3.25 | 3.90 | | | |
| **H2"-H6/H8** | 2.20 | 2.66 | 3.91 | 2.10 | 3.11 | 2.52 | 2.10 | (o) | 2.55 | | | |
| **H2'-H5/CH3** | 3.40 | (o) | 2.81 | | - | - | | - | - | | | |
| **H2"-H5/CH3** | 2.90 | 3.19 | 2.83 | | - | - | | - | - | | | |
| **H3'-H6/H8/** | 4.6 | (o) | 4.79 | 4.6 | 5.12 | 4.90 | 4.6 | 3.81 | -4.70 | | | |
| **CH3- CH3** | - | 3.52 | 3.93 | | | | | | | | | |
| | | | | | | | | | | | | |

In general, both the amino and imino resonances of DNA were exchanged too fast to be observed in $D_2O$ and therefore $H_2O$ solution was used [Kearns et al., 1971]. Assignment of exchangeable protons was done with the help of NOESY spectra recorded in 90% $H_2O$ and 10% $D_2O$ (Figure 5.4a-c). As we know that the amino and imino protons are important indicators of the hydrogen bonding of bases and also provide some of the few cross strands connectivities therefore, they are essential for structural determination [Feigon et al., 1992]. Assignment of the amino, imino and adenine H2 resonances were obtained using the strategy available in literature [Boelens et al., 1985; Hore, 1989; Rajagopal et al., 1988; Sklenar and Feigon, 1990]. Imino protons were assigned by sequential imino-imino connectivities between adjacent base pairs. Amino protons and AH2 were assigned using their cross peak with the corresponding base pair iminos. In the range 12.0 to 14.5 ppm we found three resonances which were attributed to NH protons for T6, T5, and G7 (Figure 5.1e). As expected, G8NH was not found due to the fraying end effect. Imino protons of GC base pair always resonated between 12.00 to 13.50 ppm, while those of AT base pairs were found between 13.00 to 15.00 ppm [Boelens et al., 1985]. Hence, the proton resonating at 12.94 ppm was assigned as G7NH. G7NH gave a cross peak with its preceding base imino proton, thus proton resonating at 14.04 ppm was assigned to T6NH. Further, T6NH gave a cross peak with T5NH at 13.80 ppm (Figure 5.4a). All the NH protons available in the palindromic sequence were assigned except G8NH, which was not available due to fast exchange with water. Figure 5.4b shows that on the frequency of each imino proton a number of cross peaks were found in NOESY spectra. These cross peaks can be of direct use in the assignment of amino protons and adenine H2 protons since these protons were close enough to the imino proton within each base pair.

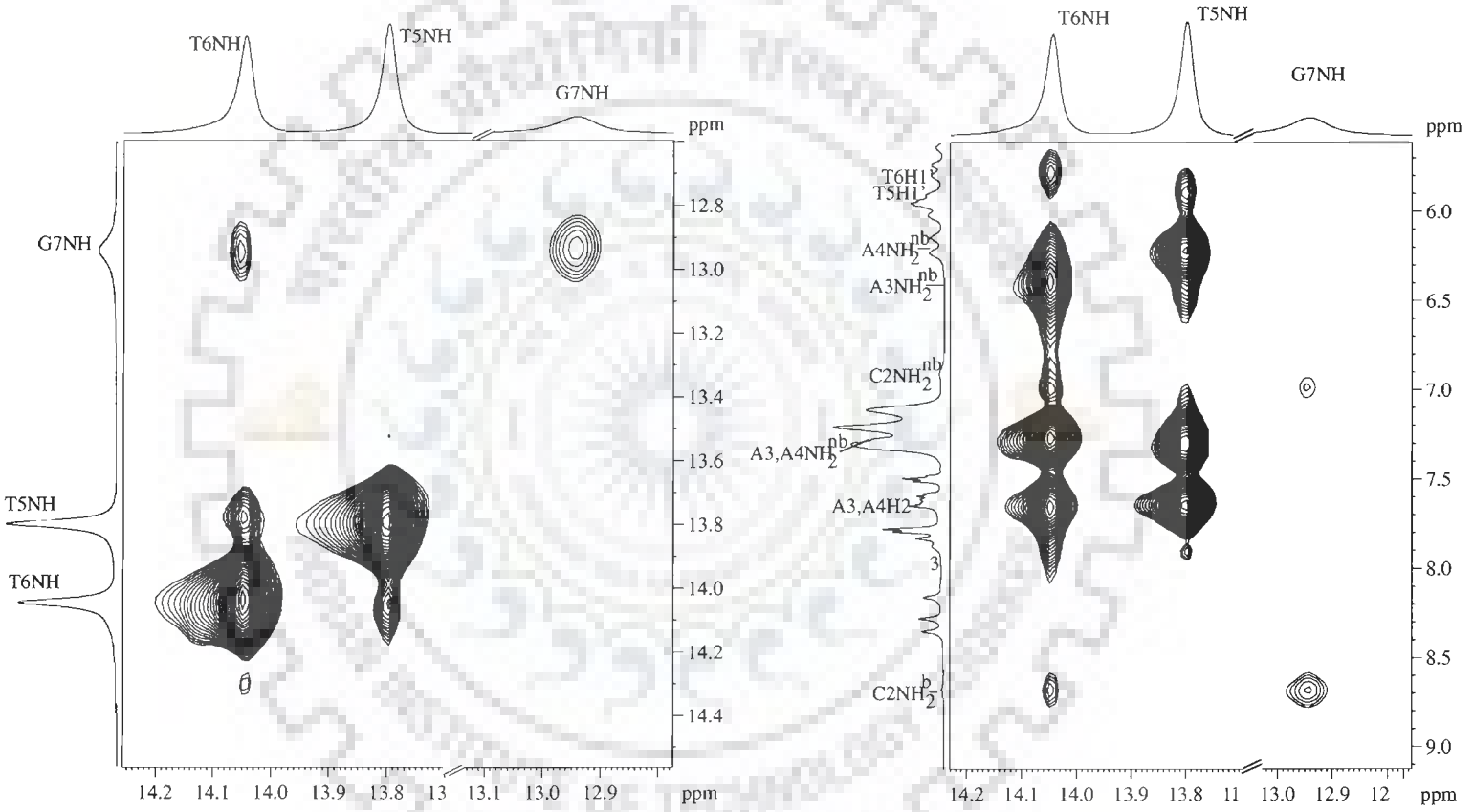


(5.4a) (Fig. 5.4 b)

**Figure 5.4- Expansions of selected regions of 500 MHz NOESY spectrum of d-CCAATTGG in H2O showing specific Dipolar couplings(a) imino-imino'(b) imino-amino (c) amino-amino/base (d) imino-methyl**

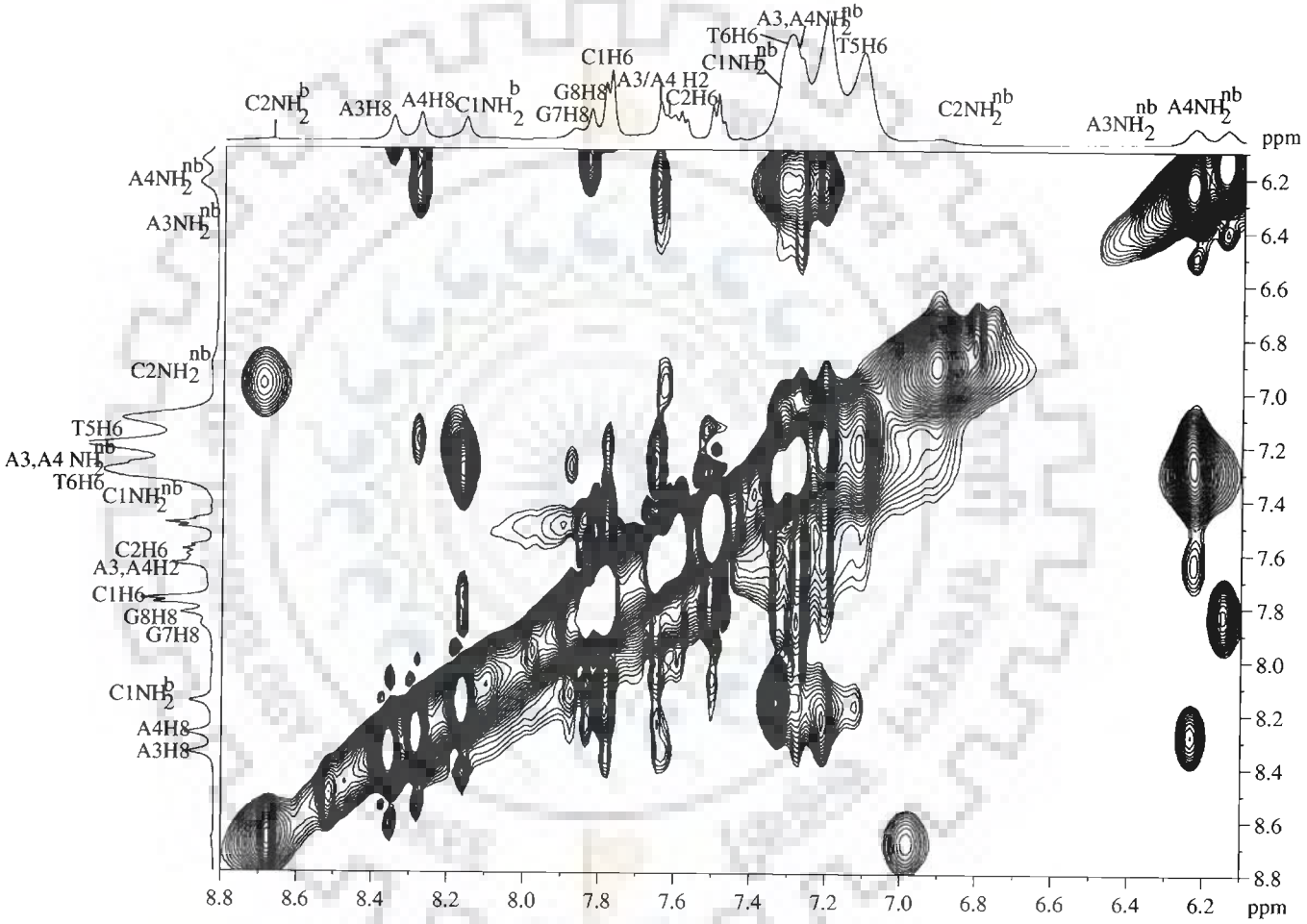
C2NH2b
A3H8
A4H8
C1NH2b
G8H8
G7H8
C1H6
A3/A4 H2
C2H6
T6H6
A3,A4NH2nb
C1NH2nb
T5H6
C2NH2nb
A3NH2nb
A4NH2nb
ppm
A4NH2nb
A3NH2nb
C2NH2nb
T5H6
A3,A4 NH2nb
T6H6
C1NH2nb
C2H6
A3,A4H2
C1H6
G8H8
G7H8
C1NH2b
A4H8
A3H8
8.8 8.6 8.4 8.2 8.0 7.8 7.6 7.4 7.2 7.0 6.8 6.6 6.4 6.2 ppm

**(Fig. 5.4c)**

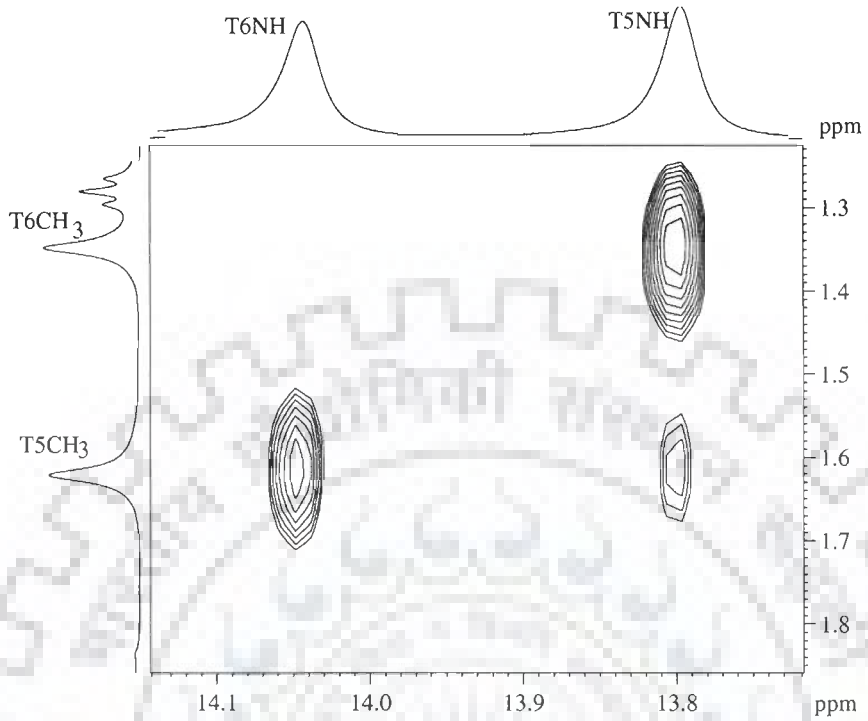


**(Fig. 5.4d)**

On each AT imino-amino proton frequency spectrum of Figure 5.4b, three very intense cross peaks were observed and they were recognized as the $NH_2^{b}$, $NH_2^{nb}$, and H2 proton of corresponding base pair. The most upfield cross peaks of both the base pairs were assigned as $A3NH_2^{nb}$ and $A4NH_2^{nb}$ at 6.40 and 6.24 ppm respectively. The proton resonating the most downfield were assigned as A3H2 and A4H2 corresponding to the same position at 7.66 ppm. Consequently the third cross peak corresponds to the $A3NH_2^{b}$ and $A4NH_2^{b}$ at 7.28 and 7.31 ppm respectively. Cytosine amino protons gave intense cross peak between $NH^{b}$ and $NH^{nb}$ protons. (Figure 5.4c), which were further identified using NH-$NH_2$ cross peaks. It can be seen from Figure 5.4b that G7NH is giving cross peak at 6.98 and 8.69 ppm which were

assigned as $C2NH_2^{nb}$ and $C2NH_2^{b}$ respectively, because low field cytosine amino proton gives stronger cross peak with the guanine imino protons due to the involvement in the Watson crick hydrogen bond. The other cytosine amino protons were assigned to $C1NH_2^{nb}$ and $C1NH_2^{b}$ at 7.33 and 8.16 ppm respectively. In most cases the cytosine are the easiest to find out since they exchange slowly on the NMR scale and give rise to sharp cross peaks. The adenine aminos can be found intermediate to slow and therefore they can also be assigned. The guanine aminos are generally exchanged more rapidly and give rise to very broad resonances therefore it was difficult to assign them. Intra base contacts were observed in cystosine amino and H5 protons for both the cytosines bases (Figure 5.4c) and AT imino and thymine 5-methyl protons (Figure 5.4d).

### 5.1.2 Duplex to Single Strand Transition

In order to monitor the duplex to single strand transition, one dimensional NMR spectra were recorded in the temperature range 278-328 K. A typical temperature profile is given in Figure 5.5a-j. The values for chemical shift with temperature for protons are tabulated in Table 5.5. Its known that thermal denaturation of DNA can be studied either by following the change of chemical shift of the non-exchngaeable protons [Braunlin and Bloomfield, 1991; Pardi et al., 1981; Petersheim and Turner, 1983] or the disappearance of signals of the imino protons [Braunlin and Bloomfield, 1988]. Conformational changes associated with denaturation modify the local environment of the protons, leading to a change in their chemical shifts. Plots for chemical shift variation with temperature are shown in Figure 5.6. The melting temperature can be extracted from this data.

### 5.1.2.1 Thymine Methyl Protons

The signals corresponding to the thymine methyl groups are the easiest to study because of their well separation in the $^1H$ NMR spectrum (1.3 to 1.8 ppm). The promoter octamer d-$(CCAATTGG)_2$ contains two thymines which are situated in the central part of the DNA. The variation with temperature in the thymine methyl signal is presented in Figure 5.5j. It's reported in the literature that in most of the cases, protons for double stranded and single stranded DNA are found to be in fast exchange, therefore methyl protons of thymine residues are also expected to show fast exchange on NMR time scale [Feigon et al., 1983; Pardi et al., 1981; Patel et al., 1982; Petersheim and Turner, 1983; Tran-Dinh et al., 1982]. When the methyl protons are in fast exchange, a melting temperature can be obtained from a plot of the observed chemical shift as a function of temperature. These chemical shifts are the weighted average of the chemical shifts in the single stranded and double stranded form of the oligonucleotide. Some authors commented on the fact that they observed intermediate exchange for methyl protons and estimated that in these cases the error on $T_m$ extraction was in the order of 4-6 K [Feigon et al., 1983; Pardi et al., 1981]. In our study it was observed that $T5CH_3$ and $T6CH_3$ protons were in fast exchange and resonate at same frequency for double and single stranded signals (Figure 5.5j). $T_m$ value is the temperature where half of the DNA is denatured, and can be extracted directly from methyl protons chemical shift change with temperature. Therefore $T_m$ for d-$(CCAATTGG)_2$ was calculated as 310 ± 2 K using the plot of chemical shift versus temperature for $T5CH_3$ and $T6CH_3$ (Figure 5.6c).

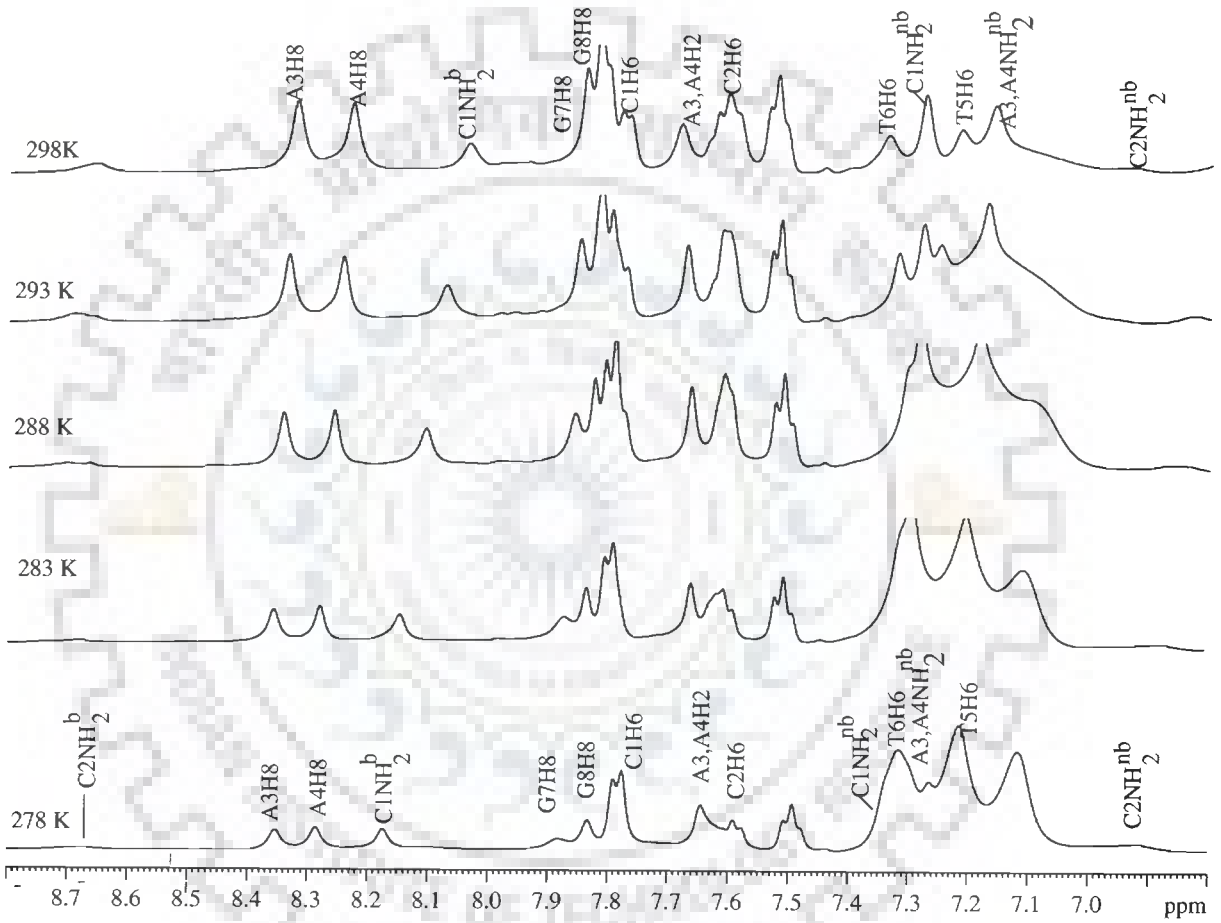


**(5.5a)**

**Figure 5.5a-i: Proton NMR spectrum of -d $(CCAATTGG)_2$ as a function of temperature (278 - 328 K).**

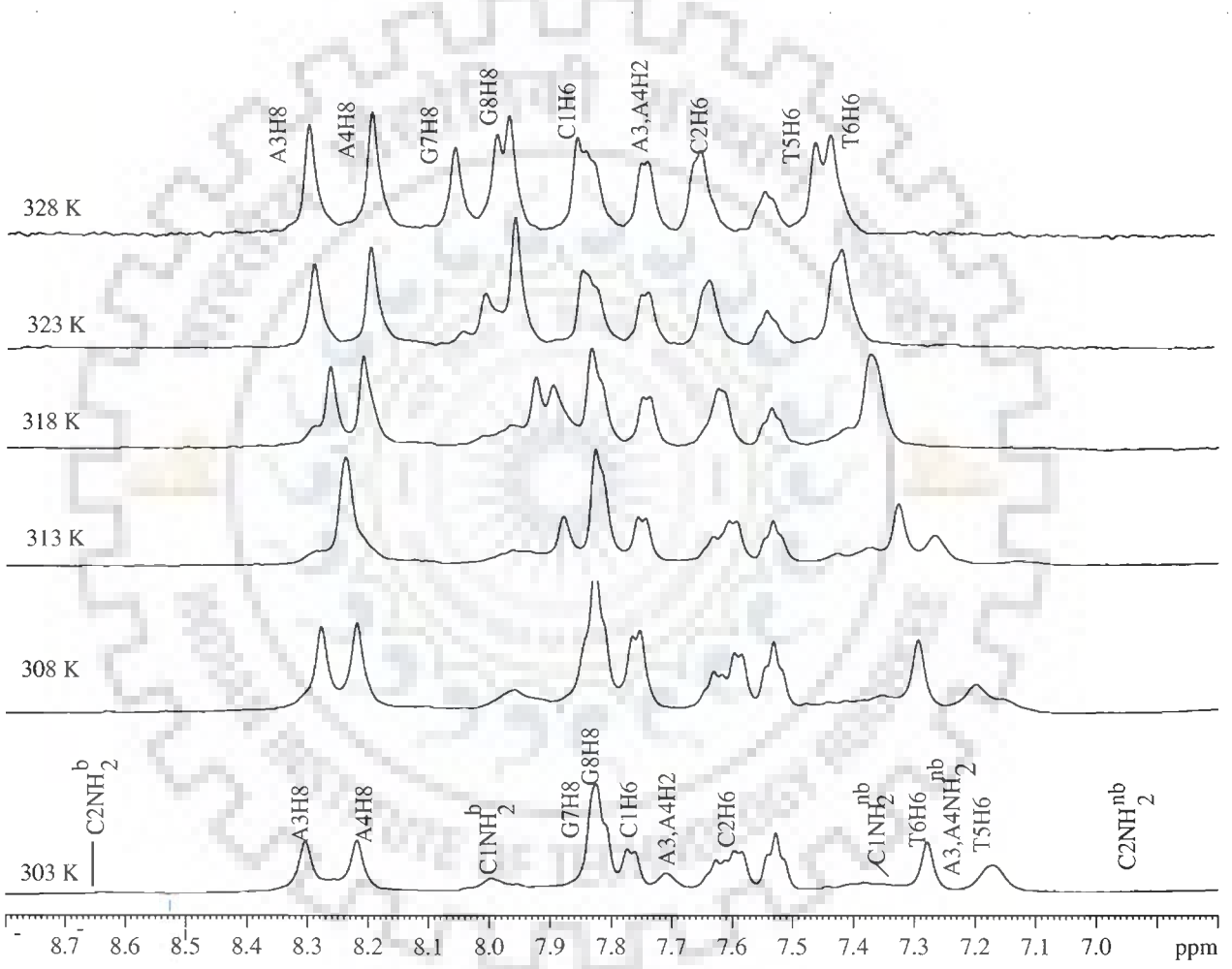
A3H8
A4H8
G7H8
G8H8
C1H6
A3,A4H2
C2H6
T5H6
T6H6
328 K
323 K
318 K
313 K
308 K
303 K
C2NH2b
A3H8
A4H8
C1NH2b
G7H8
G8H8
C1H6
A3,A4H2
C2H6
C1NH2nb
T6H6
A3,A4NH2nb
T5H6
C2NH2nb
8.7 8.6 8.5 8.4 8.3 8.2 8.1 8.0 7.9 7.8 7.7 7.6 7.5 7.4 7.3 7.2 7.1 7.0
ppm

**(Fig. 5.5b)**

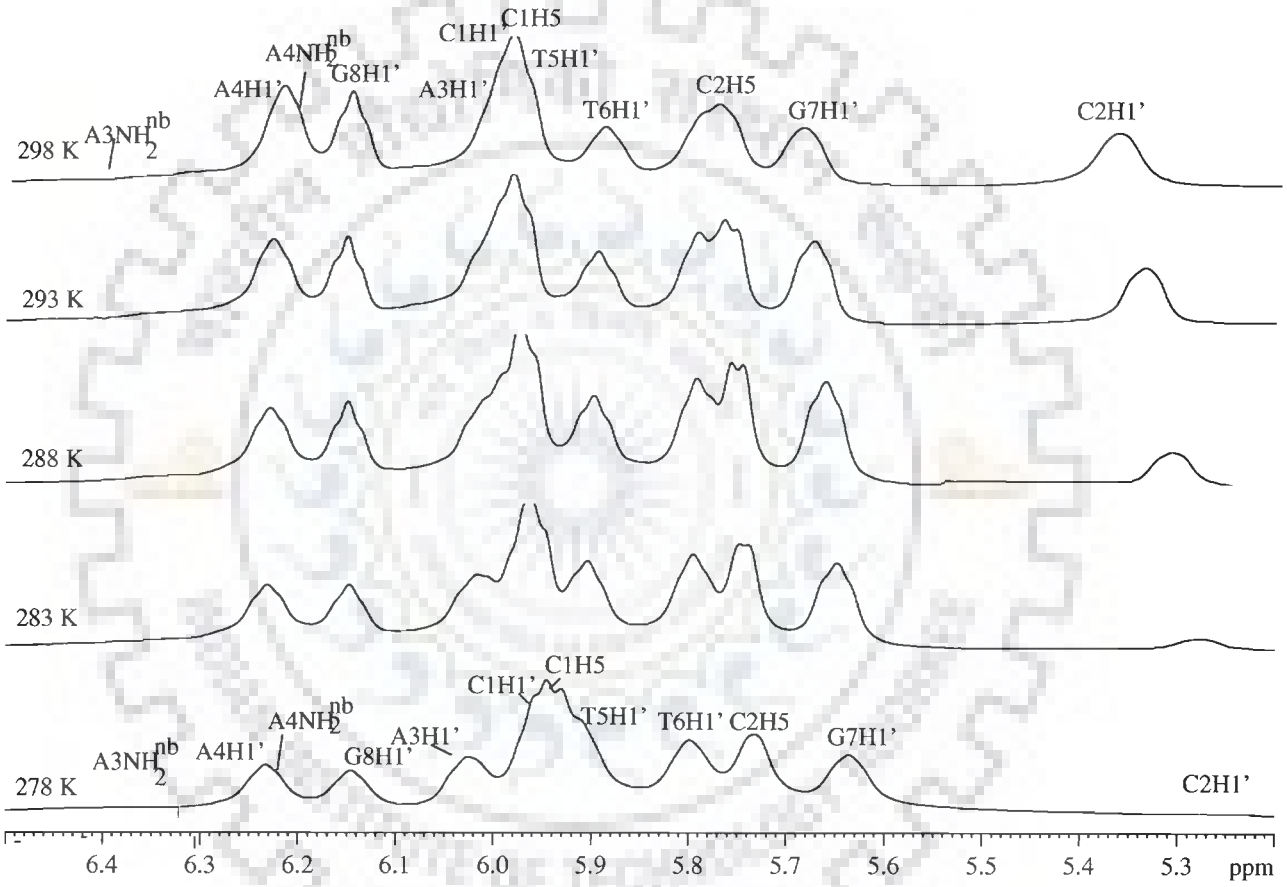
298 K
293 K
288 K
283 K
278 K
A3NH2nb
A4NH2nb
A4H1'
G8H1'
C1H1'
C1H5
A3H1'
T5H1'
T6H1'
C2H5
G7H1'
C2H1'
6.4
6.3
6.2
6.1
6.0
5.9
5.8
5.7
5.6
5.5
5.4
5.3
ppm

**(Fig. 5.5c)**

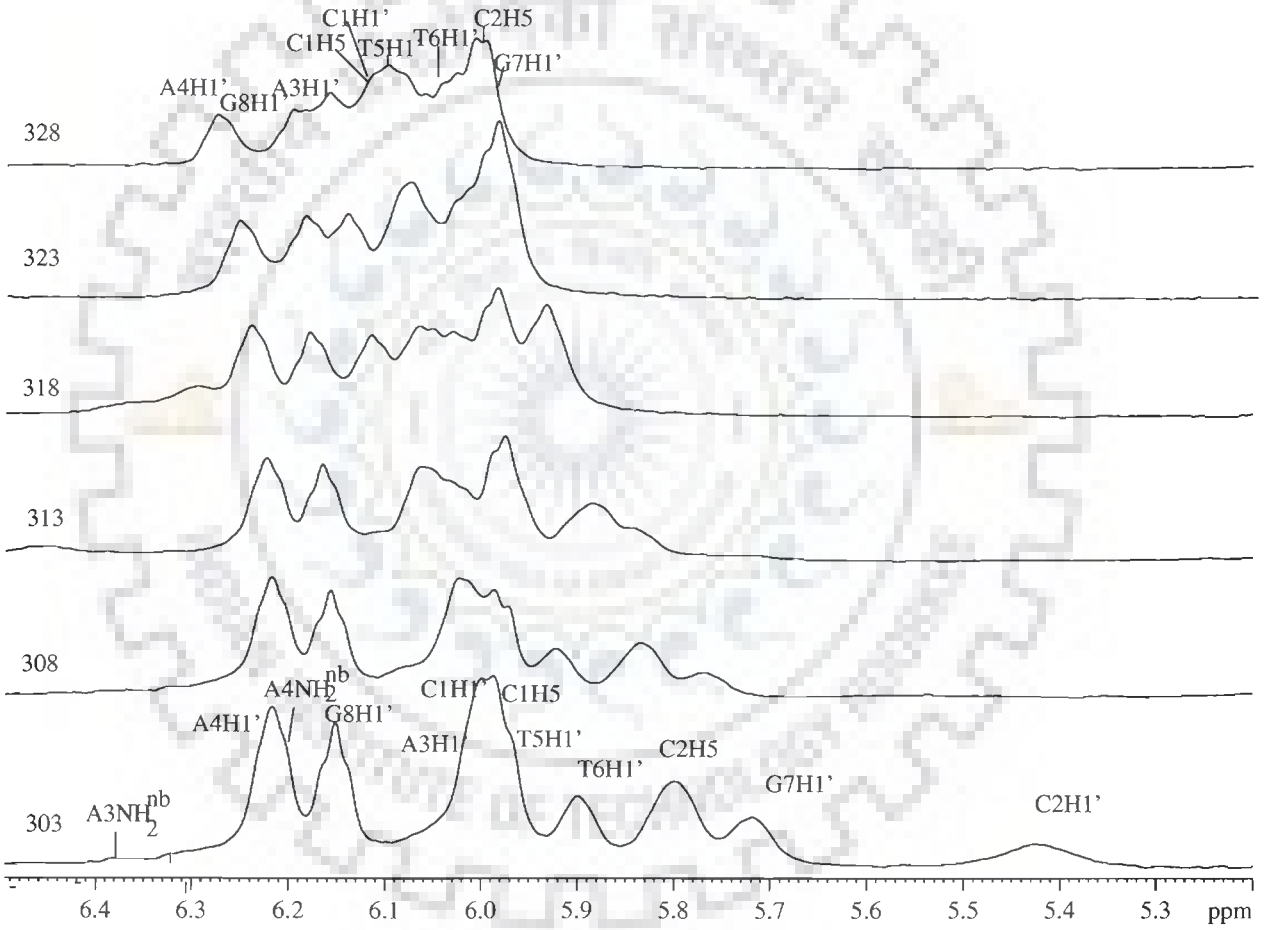
C1H1'
C2H5
C1H5
T5H1'
T6H1'
G7H1'
A4H1'
A3H1'
G8H1'
328
323
318
313
308
303
A4NH2nb
G8H1'
C1H1'
C1H5
A4H1'
A3H1'
T5H1'
T6H1'
C2H5
G7H1'
C2H1'
A3NH2nb
6.4
6.3
6.2
6.1
6.0
5.9
5.8
5.7
5.6
5.5
5.4
5.3
ppm

**(Fig. 5.5d)**

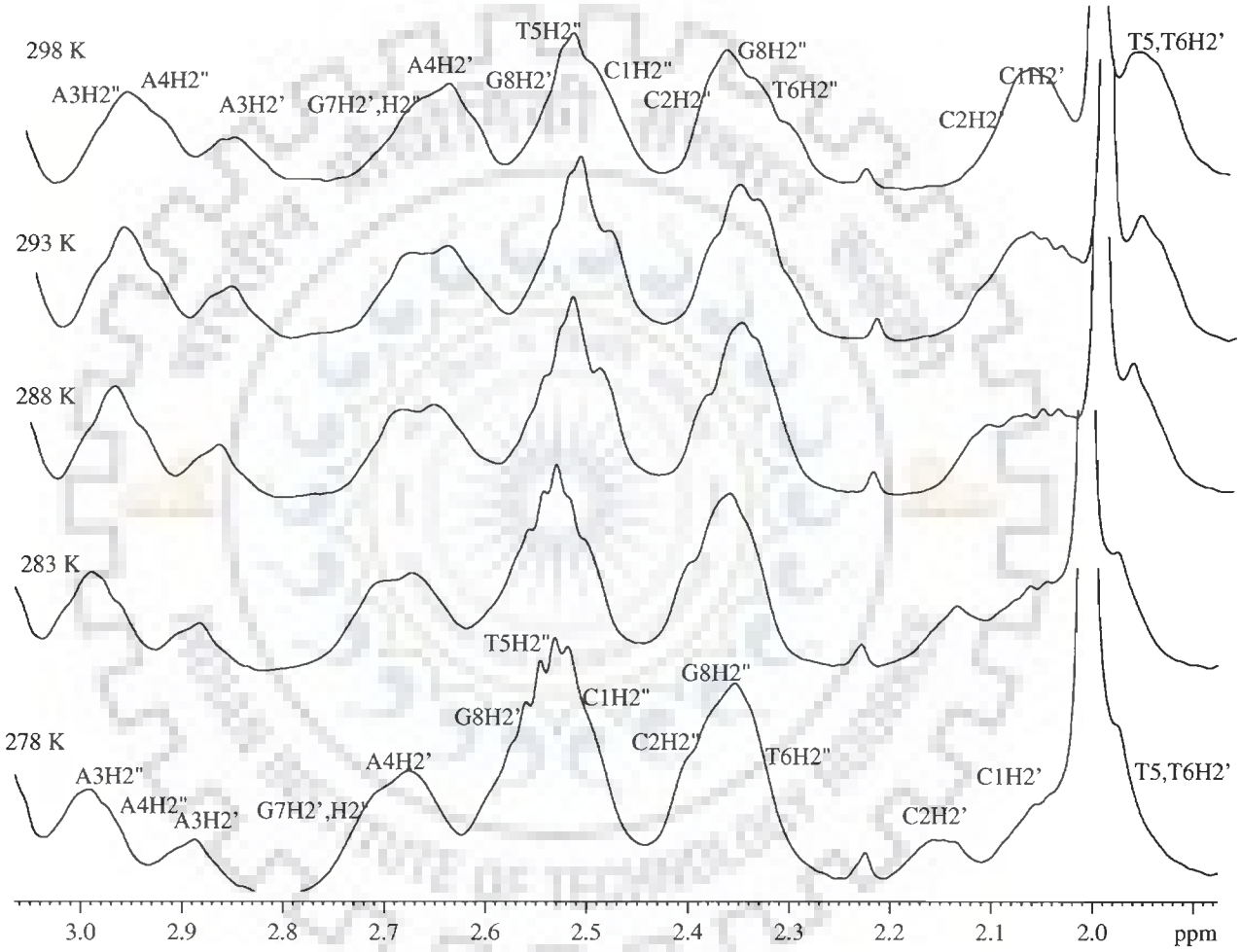
298 K
A3H2"
A4H2"
A3H2'
G7H2',H2"
A4H2'
T5H2"
G8H2'
C1H2"
C2H2"
G8H2"
T6H2"
C2H2'
C1H2'
T5,T6H2'
293 K
288 K
283 K
278 K
A3H2"
A4H2"
A3H2'
G7H2',H2"
A4H2'
T5H2"
G8H2'
C1H2"
C2H2"
G8H2"
T6H2"
C2H2'
C1H2'
T5,T6H2'
3.0
2.9
2.8
2.7
2.6
2.5
2.4
2.3
2.2
2.1
2.0
ppm

**(Fig. 5.5e)**

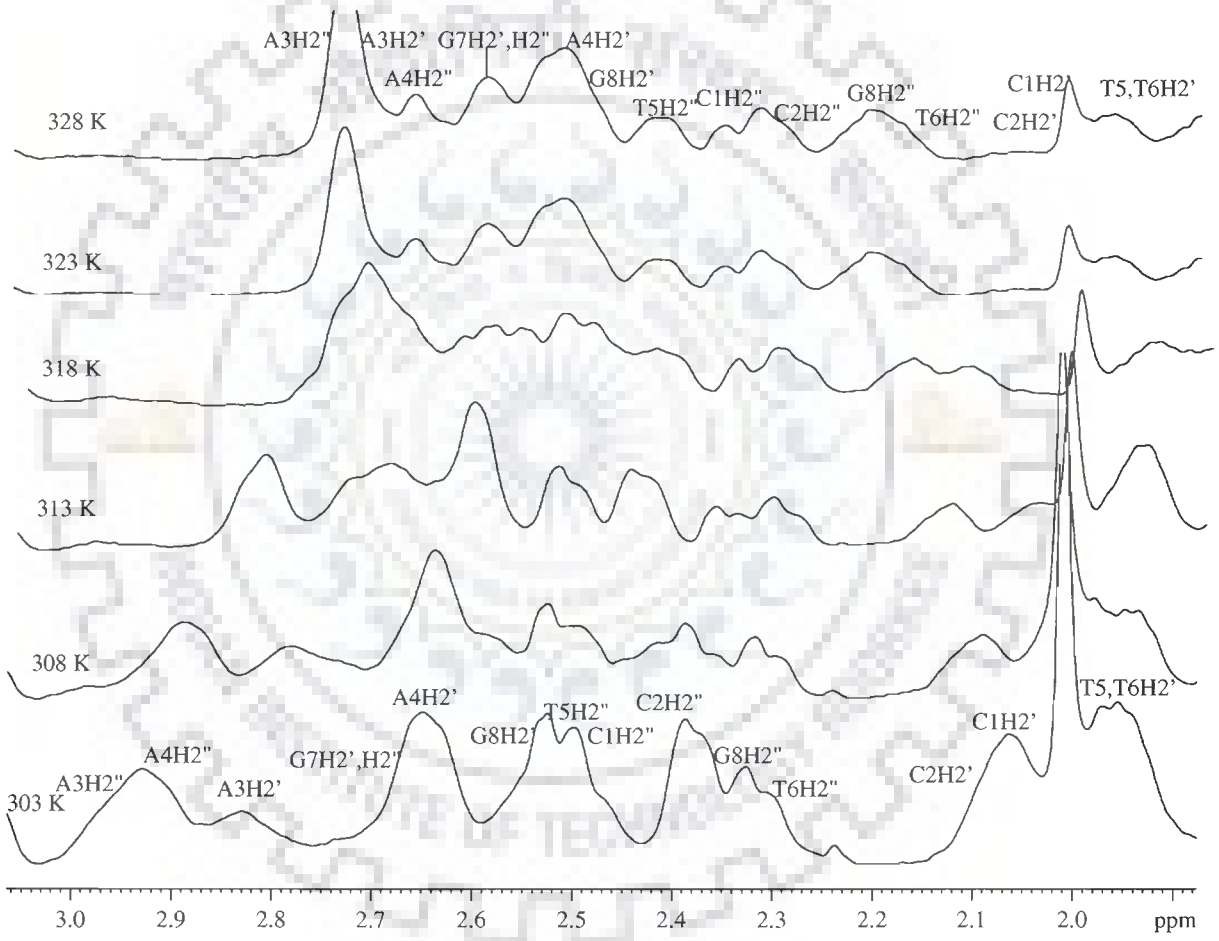
328 K
323 K
318 K
313 K
308 K
303 K
A3H2"
A3H2'
G7H2',H2"
A4H2'
A4H2"
G8H2'
T5H2"
C1H2"
C2H2"
G8H2"
T6H2"
C1H2'
C2H2'
T5,T6H2'
3.0
2.9
2.8
2.7
2.6
2.5
2.4
2.3
2.2
2.1
2.0
ppm

**(Fig. 5.5f)**

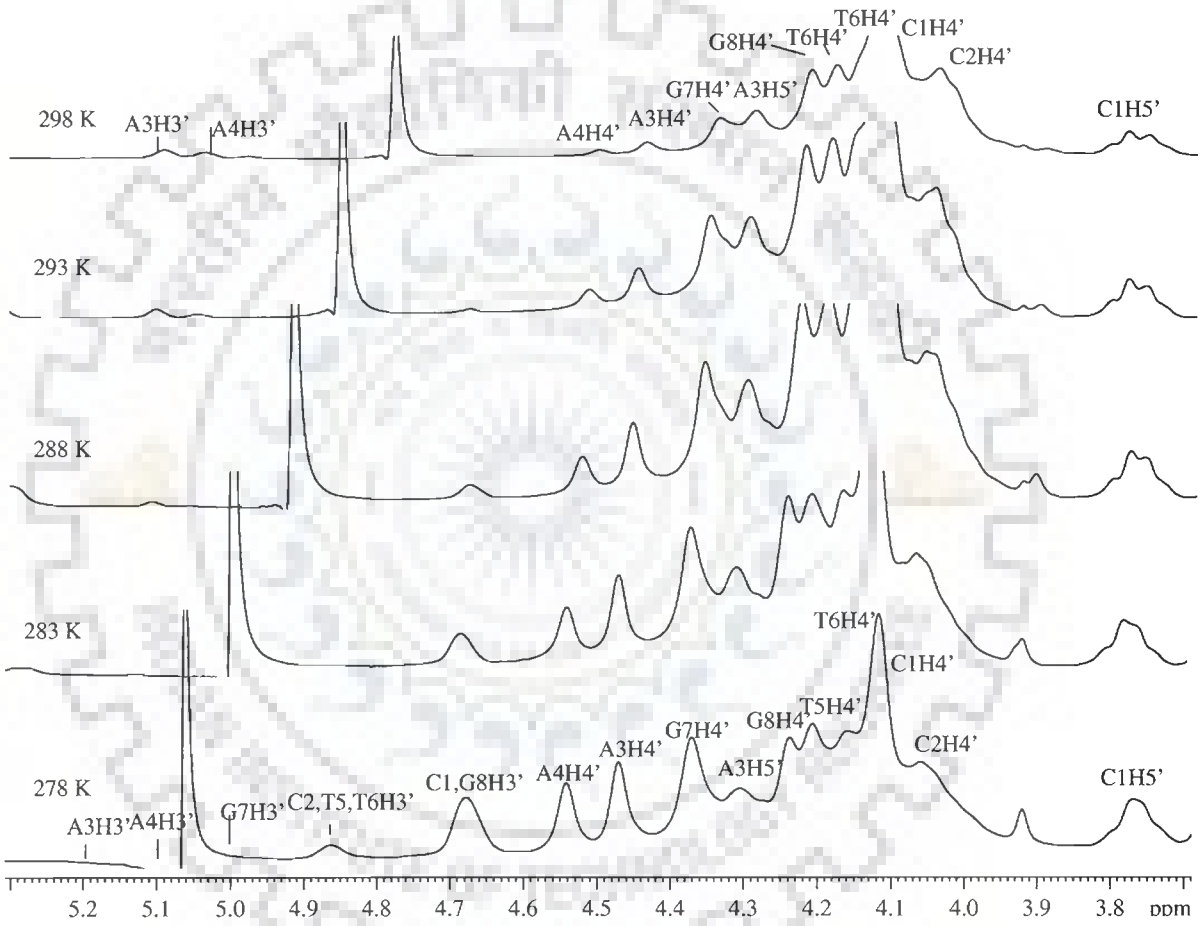
298 K
293 K
288 K
283 K
278 K
A3H3'
A4H3'
A4H4'
A3H4'
G7H4'
A3H5'
G8H4'
T6H4'
T6H4'
C1H4'
C2H4'
C1H5'
A3H3'
A4H3'
G7H3'
C2,T5,T6H3'
C1,G8H3'
A4H4'
A3H4'
G7H4'
A3H5'
G8H4'
T5H4'
T6H4'
C1H4'
C2H4'
C1H5'
5.2
5.1
5.0
4.9
4.8
4.7
4.6
4.5
4.4
4.3
4.2
4.1
4.0
3.9
3.8
ppm

**(Fig. 5.5g)**

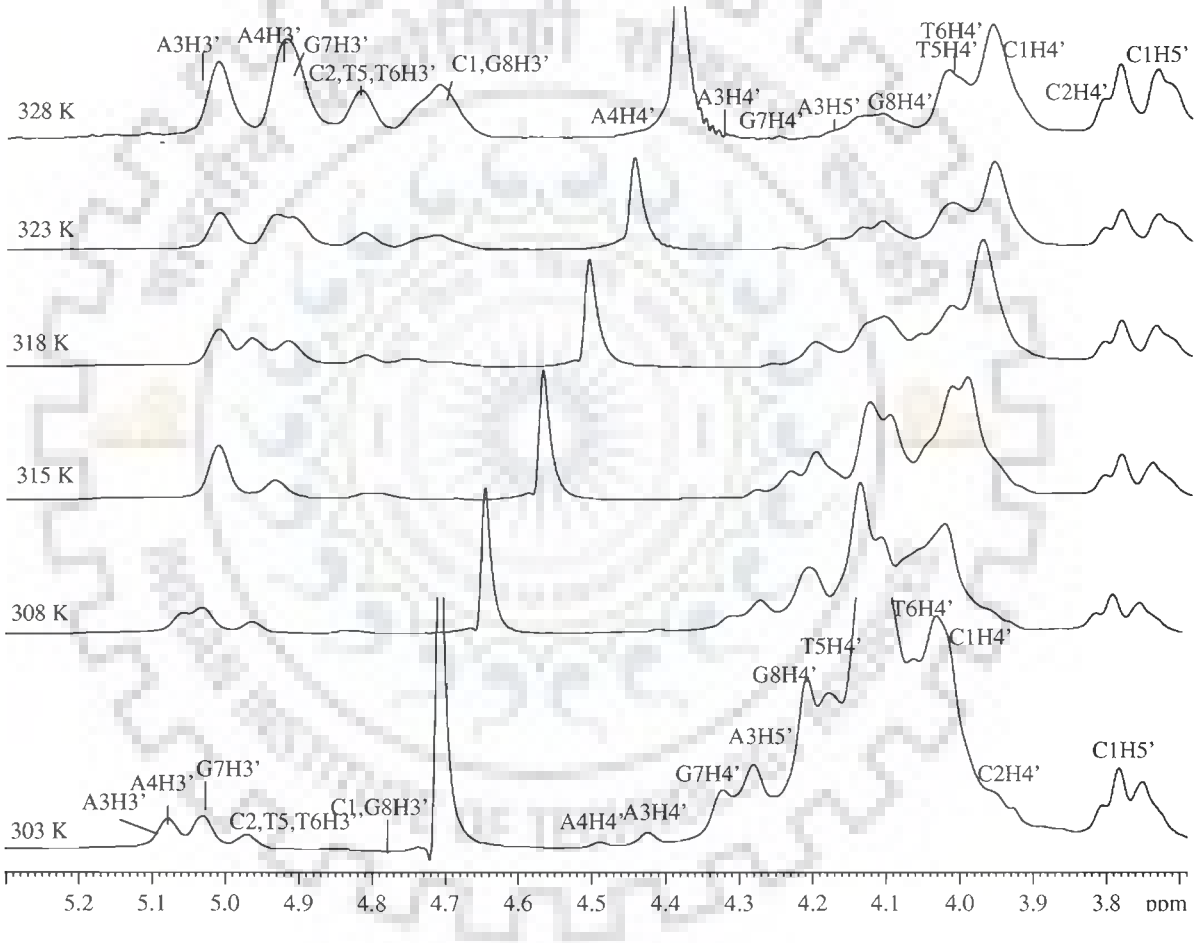
328 K
323 K
318 K
315 K
308 K
303 K
A3H3'
A4H3'
G7H3'
C2,T5,T6H3'
C1,G8H3'
A4H4'
A3H4'
G7H4'
A3H5'
G8H4'
T6H4'
T5H4'
C1H4'
C2H4'
C1H5'
5.2
5.1
5.0
4.9
4.8
4.7
4.6
4.5
4.4
4.3
4.2
4.1
4.0
3.9
3.8
ppm

**(Fig. 5.5h)**

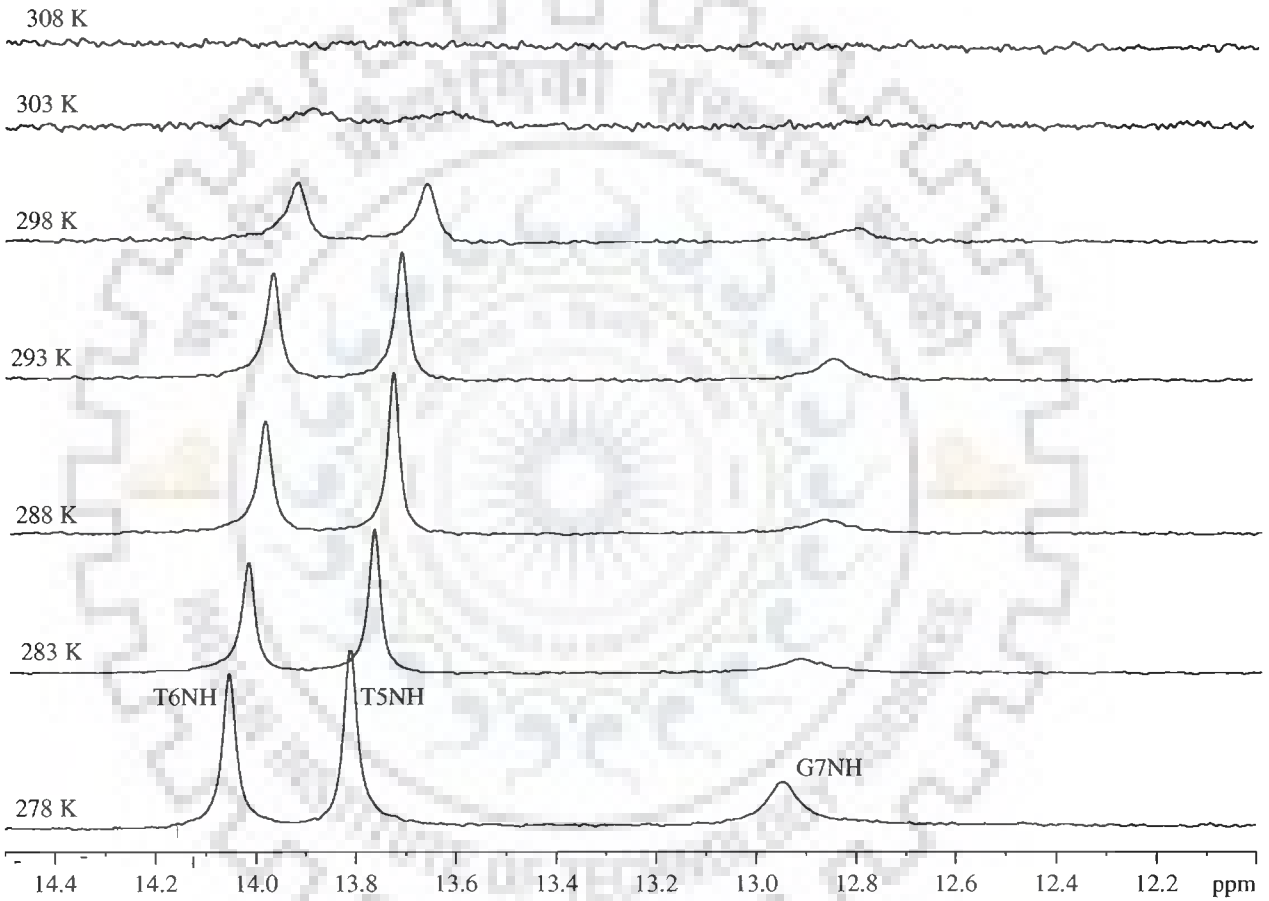
308 K
303 K
298 K
293 K
288 K
283 K
278 K
T6NH
T5NH
G7NH
14.4
14.2
14.0
13.8
13.6
13.4
13.2
13.0
12.8
12.6
12.4
12.2
ppm

**(Fig. 5.5i)**

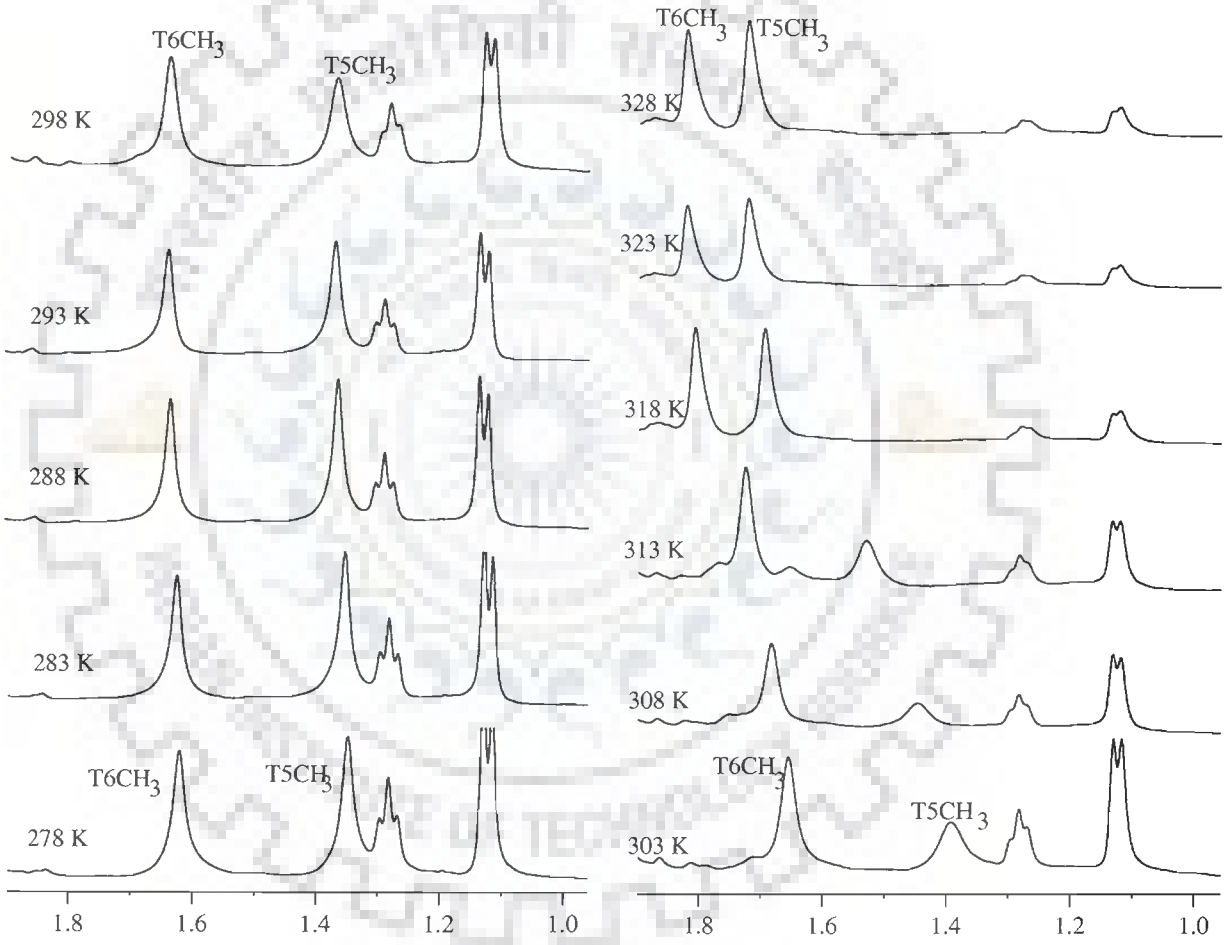
T6CH3
T5CH3
298 K
293 K
288 K
283 K
278 K
328 K
323 K
318 K
313 K
308 K
303 K
1.8
1.6
1.4
1.2
1.0

**(Fig. 5.5j)**

**Table 5.5 Chemical shift (ppm) of d-(CCAATTGG)$_2$ as a function of temperature. Also shown here is the net change in chemical shift with temperature, that is, $\Delta\delta = \delta$ (328 K) - $\delta$ (278 K) -ve $\Delta\delta$ indicates upfield shift and +ve $\Delta\delta$ indicates downfield shift.**

| Temp. (K) | C1H1' | C2H1' | A3H1' | A4H1' | T5H1' | T6H1' | G7H1' | G8H1' | T5CH3 | T6CH3 | C1H5 | C2H5 | C2NH2[b] | C2NH2[nb] |
|---|---|---|---|---|---|---|---|---|---|---|---|---|---|---|
| **278** | 5.96 | 5.27 | 6.02 | 6.15 | 5.90 | 5.80 | 5.64 | 6.24 | 1.35 | 1.62 | 5.94 | 5.73 | 8.68 | 6.91 |
| **283** | 5.96 | 5.27 | 6.02 | 6.15 | 5.90 | 5.80 | 5.65 | 6.24 | 1.35 | 1.62 | 5.95 | 5.74 | 8.68 | 6.88 |
| **288** | 5.98 | 5.31 | 6.02 | 6.15 | 5.90 | 5.80 | 5.65 | 6.24 | 1.36 | 1.62 | 5.96 | 5.75 | 8.68 | 6.82 |
| **293** | 5.98 | 5.34 | 6.03 | 6.15 | 5.90 | 5.80 | 5.66 | 6.24 | 1.36 | 1.62 | 5.97 | 5.76 | 8.66 | 6.78 |
| **298** | 5.99 | 5.37 | 6.04 | 6.16 | 5.90 | 5.80 | 5.67 | 6.24 | 1.37 | 1.64 | 5.98 | 5.77 | 8.64 | 6.73 |
| **303** | 5.99 | 5.39 | 6.05 | 6.18 | 5.92 | 5.85 | 5.69 | 6.24 | 1.40 | 1.66 | 6.01 | 5.80 | - | - |
| **308** | 6.04 | 5.41 | 6.07 | 6.20 | 5.94 | 5.90 | 5.72 | 6.24 | 1.45 | 1.69 | 6.03 | 5.84 | - | - |
| **313** | 6.06 | 5.42 | 6.10 | 6.24 | 5.96 | 9.1 | 5.77 | 6.24 | 1.53 | 1.72 | 6.05 | 5.88 | - | - |
| **318** | 6.08 | 5.43 | 6.13 | 6.26 | 5.98 | 5.92 | 5.83 | 6.25 | 1.63 | 1.78 | 6.08 | 5.93 | - | - |
| **323** | 6.10 | 5.43 | 6.16 | 6.27 | 6.10 | 5.96 | 5.93 | 6.26 | 1.70 | 1.82 | 6.10 | 6.00 | - | - |
| **328** | 6.10 | 5.43 | 6.16 | 6.27 | 6.10 | 6.03 | 5.98 | 6.27 | 1.72 | 1.82 | 6.10 | 6.00 | - | - |
| **$\Delta\delta$** | 0.14 | 0.16 | 0.14 | 0.12 | 0.20 | 0.23 | 0.34 | 0.03 | 0.37 | 0.20 | 0.16 | 0.27 | -0.04 | -0.18 |
| **Temp. (K)** | **C1H6** | **C2H6** | **A3H8** | **A4H8** | **T5H6** | **T6H6** | **G7H8** | **G8H8** | **T5NH** | **T6NH** | **G7NH** | **C1NH2[b]** | **A3/4 NH2[b]** | |
| **278** | 7.79 | 7.59 | 8.36 | 8.29 | 7.21 | 7.32 | 7.89 | 7.83 | 13.81 | 14.06 | 12.95 | 8.18 | 6.91 | |
| **283** | 7.79 | 7.60 | 8.35 | 8.27 | 7.19 | 7.28 | 7.87 | 7.83 | 13.77 | 14.03 | 12.93 | 8.14 | 6.88 | |
| **288** | 7.80 | 7.61 | 8.34 | 8.26 | 7.19 | 7.28 | 7.86 | 7.83 | 13.74 | 13.99 | 12.87 | 8.10 | 6.86 | |
| **293** | 7.80 | 7.61 | 8.33 | 8.24 | 7.19 | 7.27 | 7.85 | 7.81 | 13.70 | 13.95 | 12.83 | 8.07 | 6.82 | |
| **298** | 7.80 | 7.61 | 8.31 | 8.24 | 7.16 | 7.27 | 7.85 | 7.82 | 13.67 | 13.98 | 12.81 | 8.04 | 8.78 | |
| **303** | 7.80 | 7.61 | 8.29 | 8.22 | 7.17 | 7.28 | 7.85 | 7.83 | - | - | - | 8.00 | 6.73 | |
| **308** | 7.80 | 7.61 | 8.29 | 8.22 | 7.21 | 7.30 | 7.85 | 7.83 | - | - | - | 7.96 | - | |
| **313** | 7.81 | 7.62 | 8.29 | 8.21 | 7.27 | 7.33 | 7.86 | 7.83 | - | - | - | - | - | |
| **318** | 7.82 | 7.63 | 8.29 | 8.21 | 7.36 | 7.37 | 7.92 | 7.89 | - | - | - | - | - | |
| **323** | 7.83 | 7.64 | 8.29 | 8.21 | 7.43 | 7.43 | 8.01 | 7.96 | - | - | - | - | - | |
| **328** | 7.84 | 7.65 | 8.29 | 8.21 | 7.43 | 7.45 | 8.05 | 7.97 | - | - | - | - | - | |
| **$\Delta\delta$** | 0.05 | 0.06 | -0.07 | -0.08 | 0.22 | 0.13 | 0.16 | 0.14 | -0.14 | -0.08 | -0.14 | -0.22 | -0.19 | |

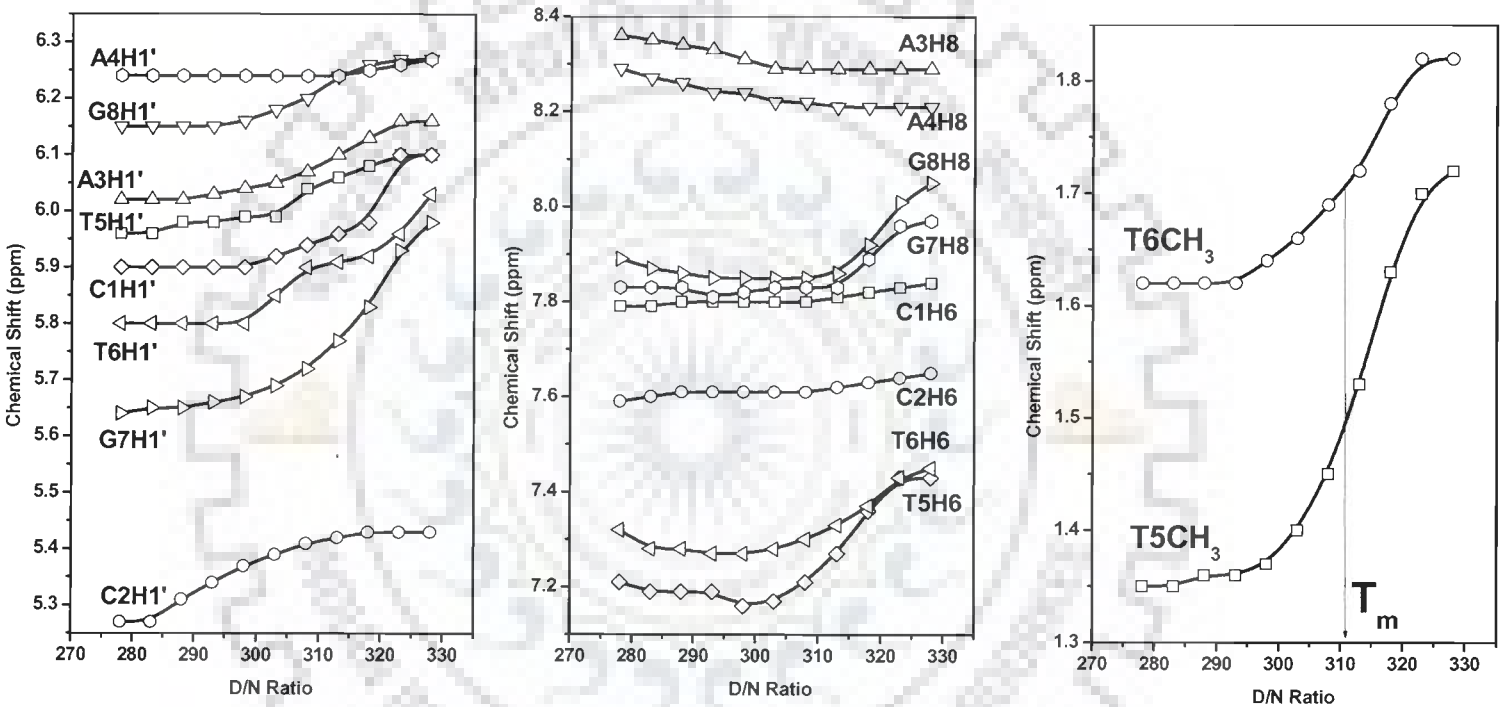


**Figure 5.6a-c Chemical Shift of various protons of d–$(CCAATTGG)_2$ as a function of temperature (278 - 328 K).**

### 5.1.2.2 Imino Protons

Regarding the imino protons, they are involved in the inter-strand hydrogen bonds and when the base is accessible to water, they can exchange. This leads to broadening and disappearance of the imino signals. The disappearance temperature for imino protons, under certain conditions can be related to the melting temperature and can be extracted from NMR data. The spectrum of imino protons for increasing temperature is shown in Figure 5.5i. Assignment of the signals were done and is indicated in Figure 5.4a. As the temperature increases, the signals of the imino protons disappeared due to their fast exchange on the NMR time scale with the solvent protons. This occurs following denaturation or following the small scale opening of an individual or a few base pairs [Braunlin and Bloomfield, 1988]. The disappearance of the imino protons therefore depends on the rate of strand dissociation ($k_d$) and association ($k_a.C_0$, where $C_0$ = [strand 1] = [strand 2] ), on the rate of single base pair opening ($k_{op}$) and closing ($k_{cl}$), and also on the rate of proton exchange from a single open base ($k^I_{tr}$) and from a base in an unpaired strand ($k^I_{Itr}$). If an assumption is made, that the proton exchange with solvent for unpaired strand is much faster than the rate of strand association ($k^{II} >> ka.\ C_0$), the rate of proton exchange can be given by following equation [Braunlin and Bloomfield, 1988]

$$K_{ex} = k_d + k_{op}\, k^I_{tr} / (k_{cl} + k^I_{tr})$$

This expression shows that the imino proton exchange cannot, in all cases, be directly related to denaturation. In the octamer oligonucleotide studied here, the first signals to disappear were those corresponding to terminal guanine (G8-C1), as they were not observed at 278 K, which clearly indicate that the fraying of the two last base pairs

occurred. The signals of the guanines next to the terminal one (G7-C2) broadened at 283 K and disappeared at 303 K. While the signals for the central imino protons (T5-A4, T6-A3), broadened towards 293 K and disappeared at 308 K. Hence 308 ± 2 K is the expected $T_m$ of oligonulceotide. This observation suggests that same value is obtained for the calculated $T_m$ from the thymine chemical shift variation and observed imino protons disappearance. Our results also support the fact that disappearance temperature of imino protons are usually less than or equal to the melting temperature measured by $^1$H NMR of non-exchangeable protons [Feigon et al., 1983; Pardi et al., 1981; Patel et al., 1982]. These results also suggest that all imino protons disappeared due to fast exchange with water even though 50 % of the time at thermal melting temperature ($T_m$) the oligonucleotide was in the double strand form. This is what was observed for the d-$(CCAATTGG)_2$ at a very less salt concentration i.e., 10 mM. The melting temperature for the oligonucleotide was 310 K and the disappearance for the oligonucleotide lie between 306 and 310 K.

### 5.1.3 Phosphorous-31 NMR Studies of d-$(CCAATTGG)_2$

Even though $^1$H NMR can provide detailed information on the overall conformation of the sugar rings and bases of oligonucleotides, it is incapable to provide information regarding the conformation of the phosphate ester backbone. Of the six torsional angles, C3'-O3'-P-O5' ($\zeta$) was found as the most variable one in the B-form of the DNA double helix and O3'-P-O5'-C5' ($\alpha$ ) was the most variable in the A form of the RNA or DNA duplex. Hence, it can be noted that P-O bonds can provide major information regarding DNA structures. Therefore, phosphorus-31 NMR was developed as a probe for studying conformational flexibility of nucleic acid backbone.

### 5.1.3.1 Assignment of Phosphate Resonances of d–$(CCAATTGG)_2$

The positions of the bases in d-$(CCAATTGG)_2$ were designated as d–$(C1pC2pA3pA4pT5pT6pG7pG8)_2$. Two dimenisnoal $^{31}P$-$^{1}H$ heteronuclear correlation NMR spectra was used for the assignment of oligonucleotide [Gorenstein et al., 1984; Pardi et al., 1983]. The Heteronuclear Multiple Bond Correlation (HMBC) spectra of the self complementry 8 base pair oligonucleotides d-$(CCAATTGG)_2$ is shown in Figure 5.7. The cross peaks represent the scalar coupling between $^{31}P$ nuclei of the backbone and H3', H4'and H5' deoxyribose protons. The chemical shift of these protons has been already determined from $^{1}H$-$^{1}H$ NOESY using the sequential assignment methodology (refer to previous discussion). Assignment of $^{31}P$ signal of the $i^{th}$ phosphate was achieved through connectivities with both the H3' (n) and H4' (n+1) deoxyribose protons [Gorenstein, 1992]. The H5' (n+1) and H5" (n+1) also expected to give cross peaks with $i^{th}$ residue $^{31}P$ signal but due to its overlap with the H4' protons, the intensities for the $^{31}P$-H5' and $^{31}P$-H5" cross peaks appeared to be much weaker than the $^{31}P$-H4'cross peaks [Gorenstein, 1992]. Figure 5.7 illustrates that total 6 separate phosphorus signals were found for the octamer studied. The area under peaks shows that the resonance at -1.76 ppm corresponds to two signals while rest of others corresponds to single phosphorous.

The assignment of $^{31}P$ nucleotide resonances were quite straightforward and can be seen in figure 5.7 which clearly illustrate the three bond scalar coupling of $^{31}P$ with $(H3')_n$ ( **a, b, c, d, e, f, g**) and $^{4}J$ couplings of the phosphorous to the $(H4')_n$, (**a', b', c', d', e', f' g'**) and $(H4')_{n+1}$ (**a", b", c", d" e", f", g"**) protons of the deoxyribose sugar residues for all the phosphorus signals present in the oligonucleotide.

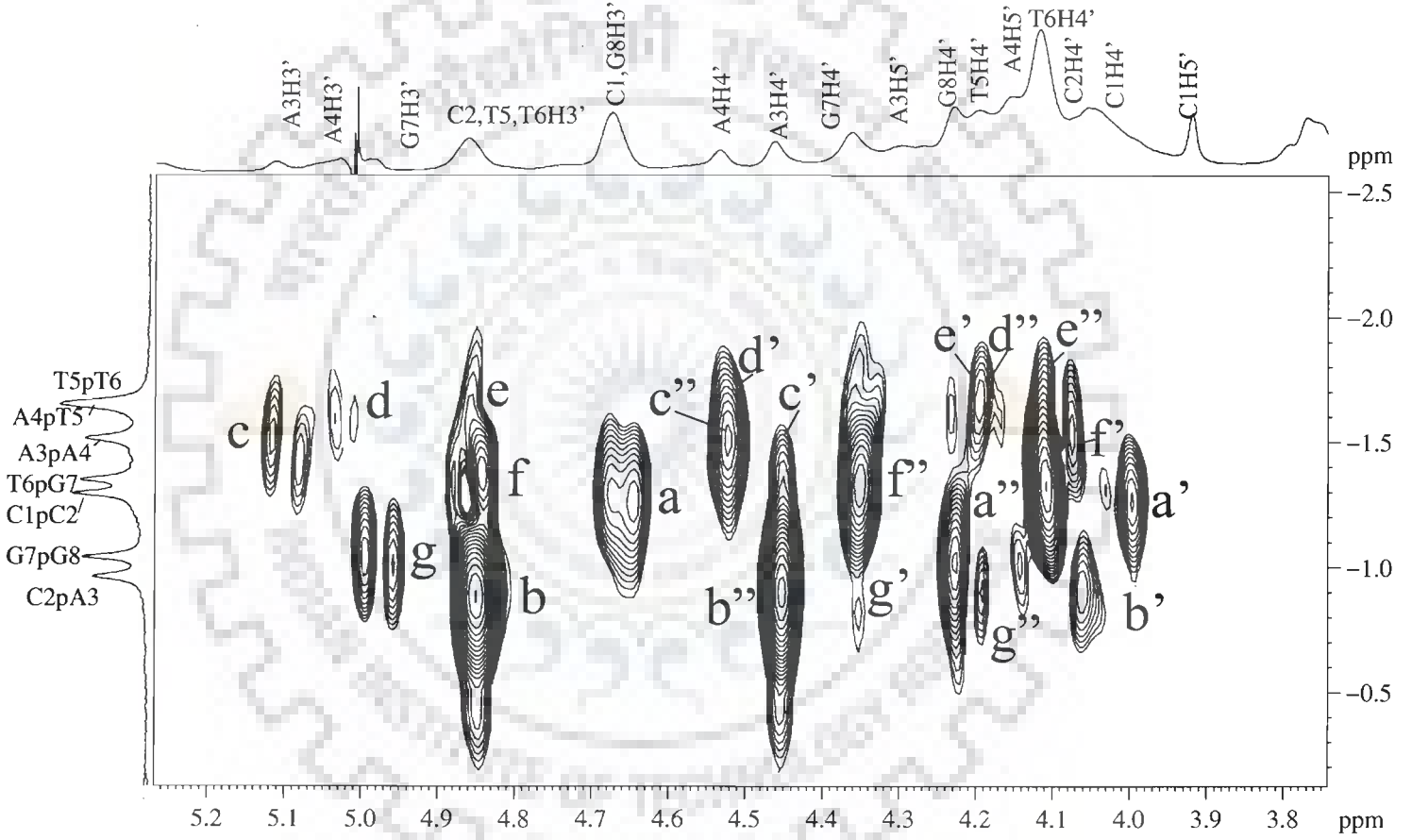


**Figure 5.7: Two Dimensional $^{31}P$ –$^{1}H$ Heteronuclear Multiple Bond Correlation (HMBC) spectra of d–$(CCAATTGG)_2$ at 283 K.**

Therefore, with the help of HMBC spectra of d-$(CCAATTGG)_2$, all the phosphate resonances were assigned to their respective ppm positions. The phosphate resonances at -1.03 ppm, -1.13 ppm, -1.40 ppm, -1.47 ppm and -1.66 ppm were assigned as C2pA3, G7pG8, C1pC2, T6pG7 and A3pA4 respectively at 283 K and the A4pT5 and T5pT6 were assigned the same position at -1.76 ppm.

### 5.1.4 Structure of d-$(CCAATTGG)_2$ By Restrained Molecular Dynamics

#### 5.1.4.1 Distance and Torsional Angle Restrains

Cross peaks in the NOESY spectra were integrated and intensities at mixing times of 200 ms were translated into inter proton distances using C2H5-C2H6 cross peaks of cytosine as reference (2.44 Å). Figure 5.3 shows the NOESY spectra of d-$(CCAATTGG)_2$ at $\tau_m$ = 200 ms. Table 5.4 and 5.5 lists interproton distances within sugar, base protons with deoxyribose sugar and sequential distances d-$(CCAATTGG)_2$. Using these interproton distances and torsional angles as restraints the restrained Molecular Dynamics of d-$(CCAATTGG)_2$ was carried out. Distances were calculated using SPARKY software. A range of ±0.2 Å was provided to distance to account for any errors in integration and force constant of 25.0 Kcal $mol^{-1}Å^{-2}$ was used. Total of 20 hydrogen bond restraints were given. The force constant for hydrogen bonds was fixed as 40 Kcal $mol^{-1}Å^{-2}$ throughout the simulations for all the base pairs except terminal C1-G8 pair due to fraying effects. A visual analysis of DQF COSY cross peaks pattern for rigid deoxyribose conformations for various spin system was made. Absence of H2"-H3' cross peak in all the residues except G8 (Figure 5.2 b) indicate that active coupling is < 2.3 Hz and therefore the pseudorotation phase angle lies in the range 90° to 225° [Celda et al., 1989; Majumdar and Hosur, 1992]. The glycosidic torsional angle $\chi$ was set between -150°

and -90° based on the examination of the H8/H6-H1'/H2'/H3' distances obtained from the NOESY spectra. A set of backbone torsional angle was derived from the qualititative evaluation of $^{31}$P-$^{1}$H heteronuclear correlation spectrum and the 2D NOE spectra. We observed seven $^{3}$J H3'-$^{31}$P and seven $^{4}$J H4'-$^{31}$P cross peaks in the $^{1}$H-$^{31}$-P correlation spectrum (Figure 5.7). The ability to detect long range four bond $^{4}$J H4'-$^{31}$P coupling indicates that the four consecutive bonds in the H4'-C4'-C5'-O5'-P backbone linkage lie in the same plane forming a W shaped conformation. This is the case in B DNA where the β and γ torsional angles are in trans and gauche+ domain respectively [Altona, 1982]. Based on these observations a β torsional angle from 150° to 210° was employed for all residues and torsional angle γ was restricted to the gauche + conformation i.e. 30° to 90°. Presence of eight $^{3}$J H3'-P cross peaks and absence of detectable $^{4}$J H2'-P in HMBC spectra, enabled us to conclude that ε torsional angle was predominantly in trans conformation. This was further supported by the information from NOESY spectra, that all sugars are predominantly C2'endo and suggests value for ε torsional angle in the range of -150° to 210° [Blommers et al., 1991].

**5.1.4.2 Strategy Followed**

The model of d-(CCAATTGG)$_2$ was made using BIOPOLYMER module. Pseudoatom corrections were used for methyl and other equivalent protons. An initial model of double helical B-DNA structure was generated using INSIGHT II version 97.0, (Molecular Simulations Inc. MSI, San Diego) using Silicon Graphics O2 workstation R5000. The energy of the molecule was minimized using 1000 steps each for Steepest Descent and Conjugate Gradient methods to remove any internal strain due to short contacts in starting structure using CFF91 force fields [Maple et al., 1988;

Maple et al., 1990] in DISCOVER version 97.0 (MSI). Dielectric constant was fixed as 1 for calculation of electrostatic interactions. Conformational search was performed by the following simulated annealing restrained Molecular Dynamics protocol. The molecule was heated to a temperature of 800 K in steps of 100 K. Molecular Dynamics was carried out for 25 ps (1000 iterations steps of 1 fs each) at 800 K during which 25 structures were saved at regular intervals. Each of them was then slowly cooled to 300 K in steps of 50 K. At each step of cooling the molecule was equilibrated for 25 ps (2500 iterations steps of 1 fs each). At the end of simulated annealing, 1000 steps of Steepest Descent minimized all the structures until a predefined convergence limit of root mean square derivative of energy with respect to atomic coordinates of < 0.01 Kcal $mol^{-1}$ $Å^{-1}$ was reached. The results obtained by NMR indicated the existence of a structure within B-family of DNA structures.

### 5.1.4.3 Restrained Molecular Dynamics (rMD) Studies

Restrained Molecular Dynamics permits the system to undergo conformational and momentum change so that different parts of the phase space accessible to the molecule can be explored and stable conformations are identified by energy minimization. Simulated annealing was carried out upto 800 K but it was found that convergence to a final structure could be readily achieved even at 300 K. The stereo view of various rMD structures is shown in Figure 5.8. Several structures obtained after equilibration at different time intervals during the dynamics run at 800 K and 300 K were examined. It was observed that they differ only marginally from each other in their structure on the whole feature. Further, no significant drift in either potential energy or restraint deviations was observed during the final equilibration. It can therefore be concluded that the system reached a minimum energy conformation.

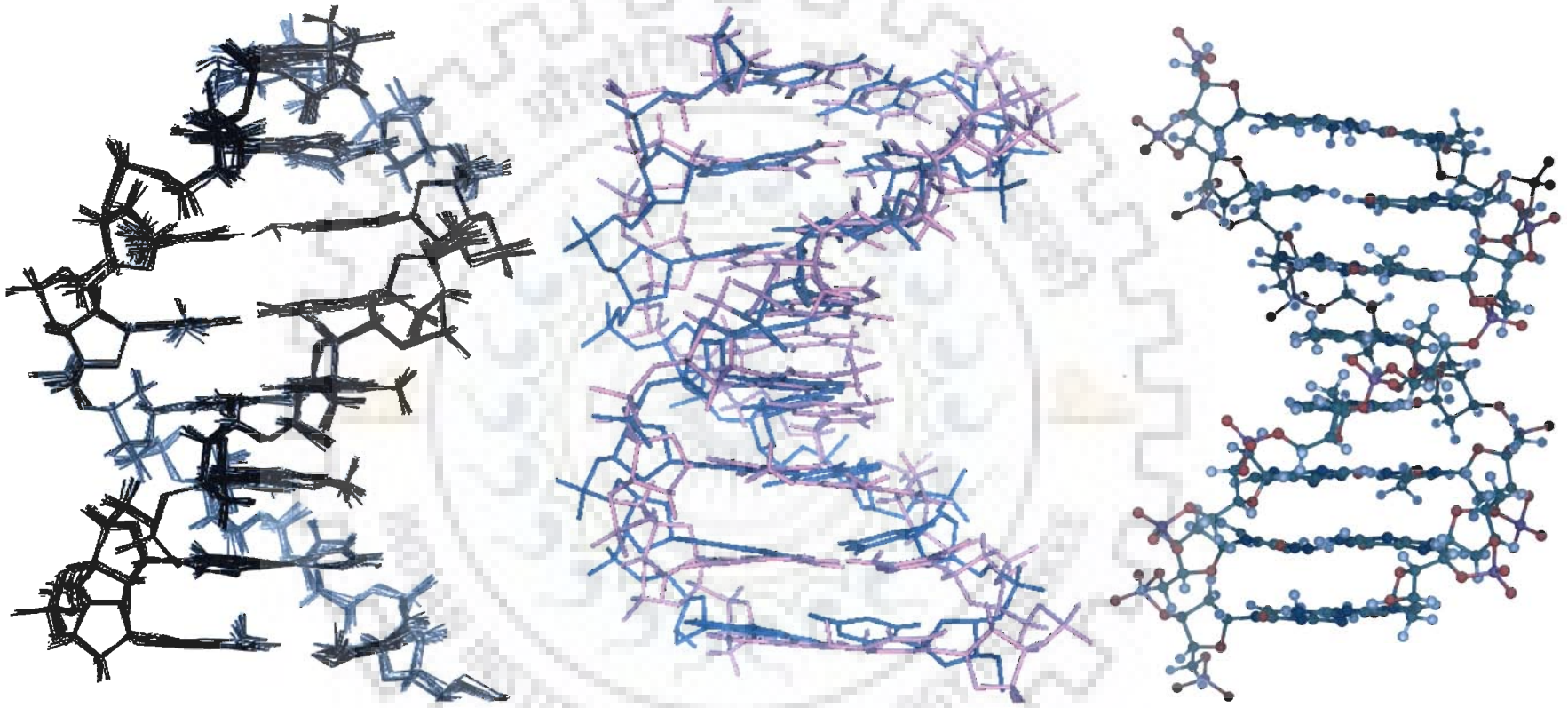


**Figure 5.8: Sequential stereo view of the (a) superimposed various rMD structures and (b) rMD- structure of d-$(CCAATTGG)_2$ superimposed with standard crystal structure (c) Optimized rMD structure.**

Table 5.6 indicates an assessment of refined structures after equilibration (at the end of 25/100 picoseconds) in terms of energetics including restraint violations energies and root mean square derivative of energy with respect to atomic coordinates. The total potential energy and other energy terms for rMD structure generated by restrained Molecular Dynamics (rMD) are shown in Table 5.7. Resulting rMD structure was thoroughly analyzed with CURVES software, version 5.1 [Lavery and Sklenar, 1996]. The structural characteristics of various rMD structures are discussed in the following sections:

**Table 5.6 Summary of experimental restraints and statistical analysis of final structure generated by restrained molecular dynamics (rMD).**

| Parameters | No. of distance restraints |
|---|---|
| **Intra residue** | 126 |
| **Inter residue** | 80 |
| **Total NOE violations** | 46 |
| **Average RMSD** | Initial = 0.0<br>Final = 0.25 |
| **Average residue wise RMSD** | C1 = 0.32, C2 = 0.0.41, A3 = 0.11, A4 = 0.16, T5 = 0.09, T6 = 0.08, G7=0.21, G8= 0.19 |
| **Minor groove** | Width = 6.31 Å; Depth = 4.29 Å |
| **Major groove** | Width = 13.69 Å; Depth = 1.97 Å |

### 5.1.5 Helicoidal Parameters

Plot of various helix axis parameters (global, unless specified otherwise) of d-$(CCAATTGG)_2$ in rMD structure as a function of residue position in duplex, two classical structures of A-DNA, B-DNA and the reported crystal structure of d-$(CCAATTGG)_2$ [Vlieghe et al., 1999] are shown in Figure 5.9a-c. Base sequence dependent variations in helicoidal parameters were evident. The results of rMD and crystal structure were closer to that of B-DNA as compared to that of A-DNA.

**Table 5.7 Energy terms (Kcal $mol^{-1}$) for starting models and rMD structure of d-$(CCAATTGG)_2$.**

| Energy | BDNA starting structure | rMD structure |
|---|---|---|
| **Total** | 3101.35 | 2674 |
| **Bond** | 243 | 94.71 |
| **Angle** | 908 | 776.65 |
| **Repulsion** | 1636.37 | 1536.35 |
| **Dispersive** | -1579 | -1503.69 |
| **Electrostatic** | 1855.05 | 1785.84 |
| **Restraint** | 467.96 | 417.09 |

The helicoidal parameters are classified into three categories: global base pair-axis parameters, intra-base pair or global base-base parameters and the inter-base pair or base pair- step parameters. Among the base pairs-axis parameters, the x-displacement for rMD and crystal structures (dx) was ~ –1.0 Å for all residues which is very close to a value of –0.7 Å as seen in canonical B-DNA structure. The y-axis displacement (dy) varied from +0.15 to –0.15 Å along the sequence. The base pairs were inclined ($\eta$) at an angle of $-5^{\circ}$ to $-7^{\circ}$ with significant variation in base sequence having a more negative value for the central AATT region (Figure 5.9a). The tip angle ($\theta$) fluctuated from $-8^{\circ}$ (at 5' end) to $+10^{\circ}$ (at 3' end) in rMD structure and -10 (at 5' end) to + 4 (at 3'end) in crystal structure. Such variations have been reported in literature [Mujeeb et al., 1993]. Among the intra base parameters, the shear (Sx) and

stretch (Sy) values varied from their ideal values for both the calculated structures and again the more negative value for stretch was found to be for central AATT region. The stagger (Sz) values lied within the range 0.1 to -0.6 Å but had comparative positive values for the four middle base pairs. The buckle varied in a large range from -5 to +5 Å and -20 to +20 Å for rMD and crystal structure respectively. The variation in buckle was observed more for the terminal end residues and was therefore attributed to the fraying effects of the terminal residues. Central region of AATT showed lesser variation in buckle.

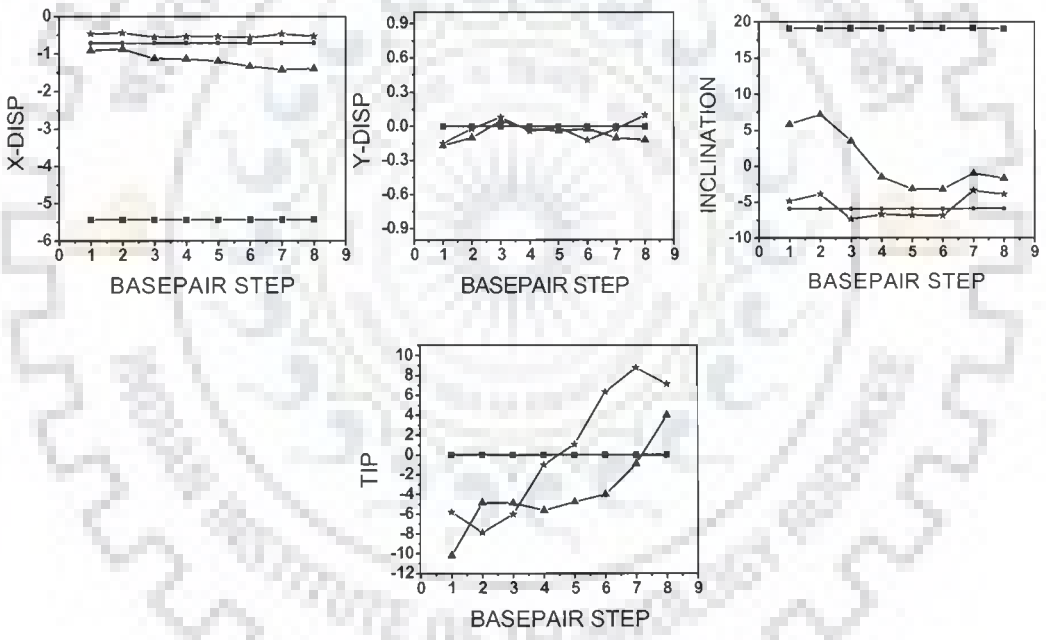


**(Fig. 5.9a)**

**Figure 5.9: Helical (a) base pair axis (b) intra base pair (c) global base base parameters for d-(CCAATTGG)$_2$ calculated for canonical A-DNA, (■), B-DNA (●), crystal structure (▲) and structure obtained by restrained molecular dynamics simulations rMD (*).**

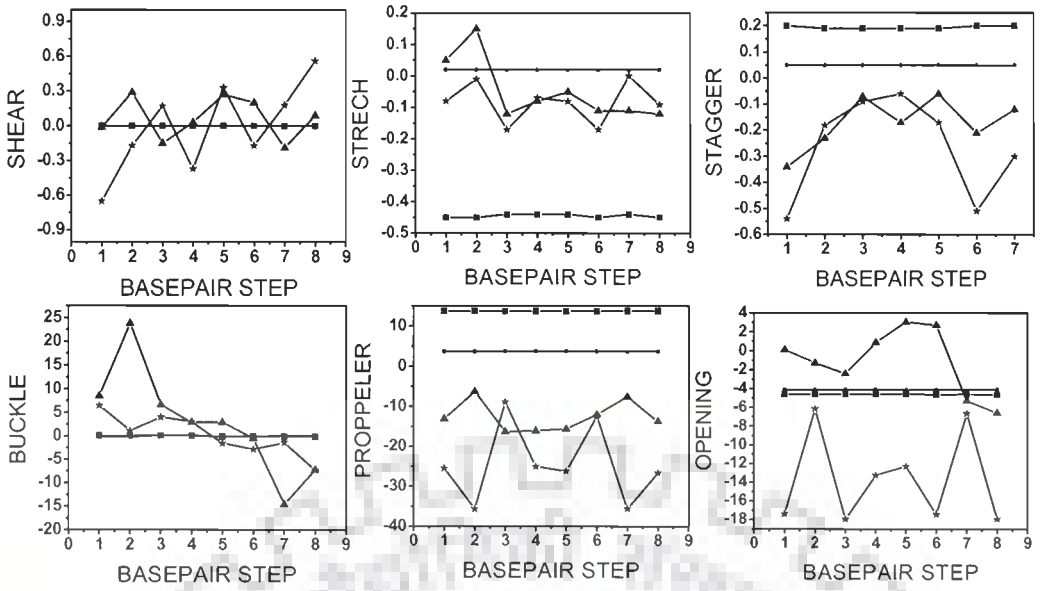


**(Fig. 5.9b)**

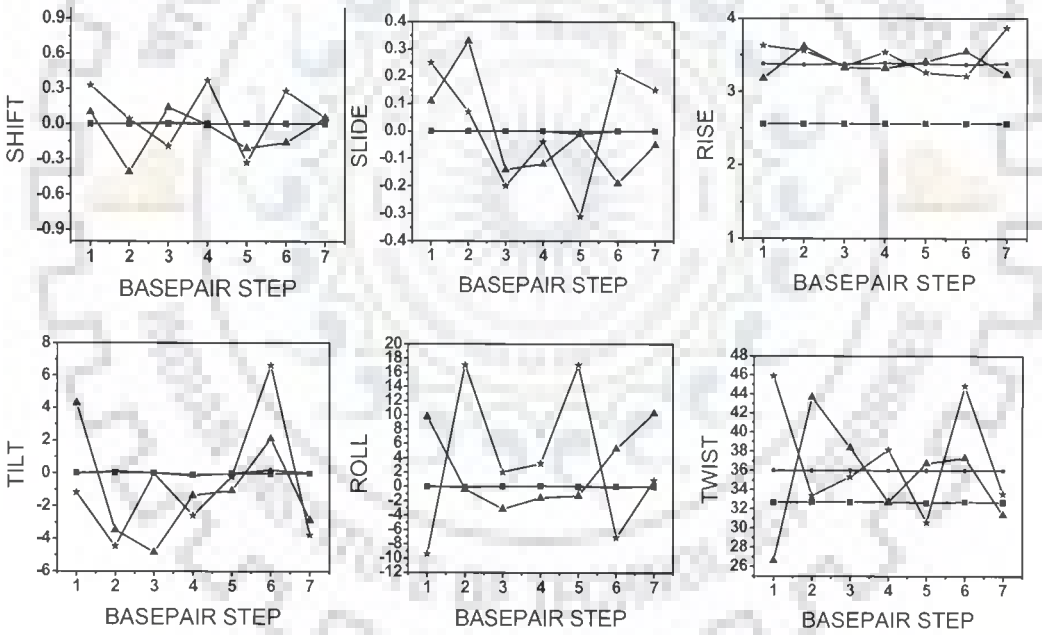


**(Fig. 5.9c)**

The variations in the propeller twist were significantly large for all the residues except A3-T6. For the two base pairs in the middle i.e. A4-T5, large negative values in the range $13^{o}$-$35^{o}$ were observed. Large negative values of propeller twist in AT and TA

base pairs have been reported in literature [Dornberger et al., 1998; Mujeeb et al., 1993] and may possibly occur to avoid steric clashes between the $CH_3$ group of thymine and 5' neighboring sugar in AX/XT base pairs step [Hunter, 1993]. The base pair opening lies between $-8^o$ to $-18^o$ for all base pairs and was larger in magnitude for terminal base pairs, while surprisingly the opening value for crystal structure was found to be positive. In regular A-DNA and B-DNA geometries, global values of the inter base pair parameters shift (Dx), slide (Dy), roll (rho) and tilt (tau) are essentially zero. For different rMD and crystal structures, the shift showed variation in the values but was within ± 4 Å and did not appear to be sequence dependent. The roll angle on the other hand, showed large positive value of ~ $8^o$ to $12^o$ at either end of the helix, – $2^o$ to – $4^o$ at the central AATT base pair step in case of crystal structure and for rMD structure all the values were found to be positive. A less positive roll opens the angle between base pairs towards the minor groove, as a result of which narrower minor groove and bending towards major groove causing a curvature in helix axis occurred. The large positive roll at C2pA3 (~ $18^o$) step indicates reduced base stacking and hence demonstrated flexibility at pyrimidine 3'-5' purine step [Dornberger et al., 1998]. The twist angle for all base pairs in different structures were in the range $34^o$-$36^o$ except for the terminal and T6pG7 base pair in which it was ~ $45^o$. The local helical parameters showed trends in roll and twist angle similar to that observed in global parameters.

### 5.1.6 Torsional Angles

The variation of torsional angles with base sequence (Figure 5.10) showed equivalence of the strands of duplex. Although the angles $\alpha$ through $\xi$ showed variations with base sequence, they had values closer to B-DNA for most residues

rather than to the corresponding A-DNA structure. The angle $\alpha$ varied in a narrow range of $-60^{o}$ to $-85^{o}$ and was largest in negative magnitude for G7 base in rMD structures. The $\beta$ angle was found either in $-150^{o}$ or $+150^{o}$ value appreciably with base sequence and adopted a trans-conformation. The variation of $\gamma$ was in the range $50^{o}$-$70^{o}$ except at 5' end where it was unusually large for crystal structure and adopted trans conformation. The angle $\delta$ reflects the deoxyribose puckering and adopted conformation between that of A–DNA and B–DNA.

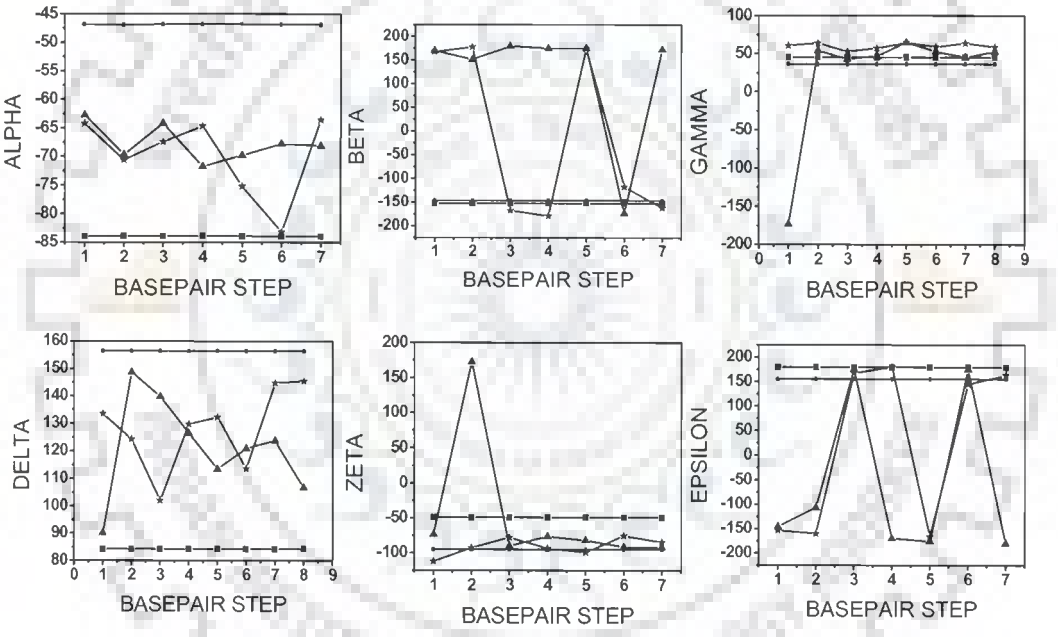


**(Fig. 5.10a)**

**Figure 5.10 Backbone torsional angles (a) and Phase angle (b) calculated for canonical A-DNA, (■), B-DNA (•), crystal structure (▲) and structure obtained by restrained molecular dynamics simulations rMD (*).**

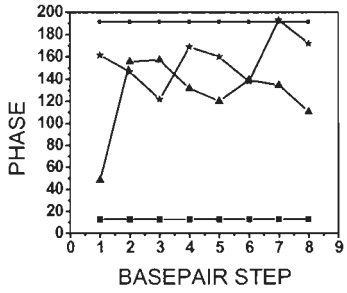


**(Fig. 5.10b)**

In rMD structure δ was mostly found towards B-DNA, except the A3 residue, while in case of crystal structure C1 was more close to A DNA. The angle ε was in trans conformation for two alternating residues while ξ was closer to the corresponding value in B-DNA in both the structures. The value of P angle in structure resulting from our rMD was essentially consistent with the results of the NMR data explained above and shows that it lies in the range 138°-178°. C1 residue in case of crystal structure had minimum P value (~40°).

The observed stacking patterns observed by X3-DNA software between base pairs at seven individual base pair steps viewed along the global helix axis for rMD structure are shown in Figure 5.11a-b. It is noted that overlap of bases at C1pC2 step was particularly low. The relatively less magnitude positive roll at A3pA4, A4pT5, and T5pT6 step indicate increased base stacking interactions which are clearly shown in Figure 5.10a-b. The central AATT quartet of the NMR structure forms a tight stack.

All these helicoidal and torsional angle analysis suggests that the maximum variation from B-DNA was found at C2pA3 and T6pG7 step in both crystal and rMD structure. Calculated NMR conformer and crystal structure showed considerable differences for all the helicoidal parameters. The largest deviations were observed for roll and twist angle for C1pC2 step and T6pG7.

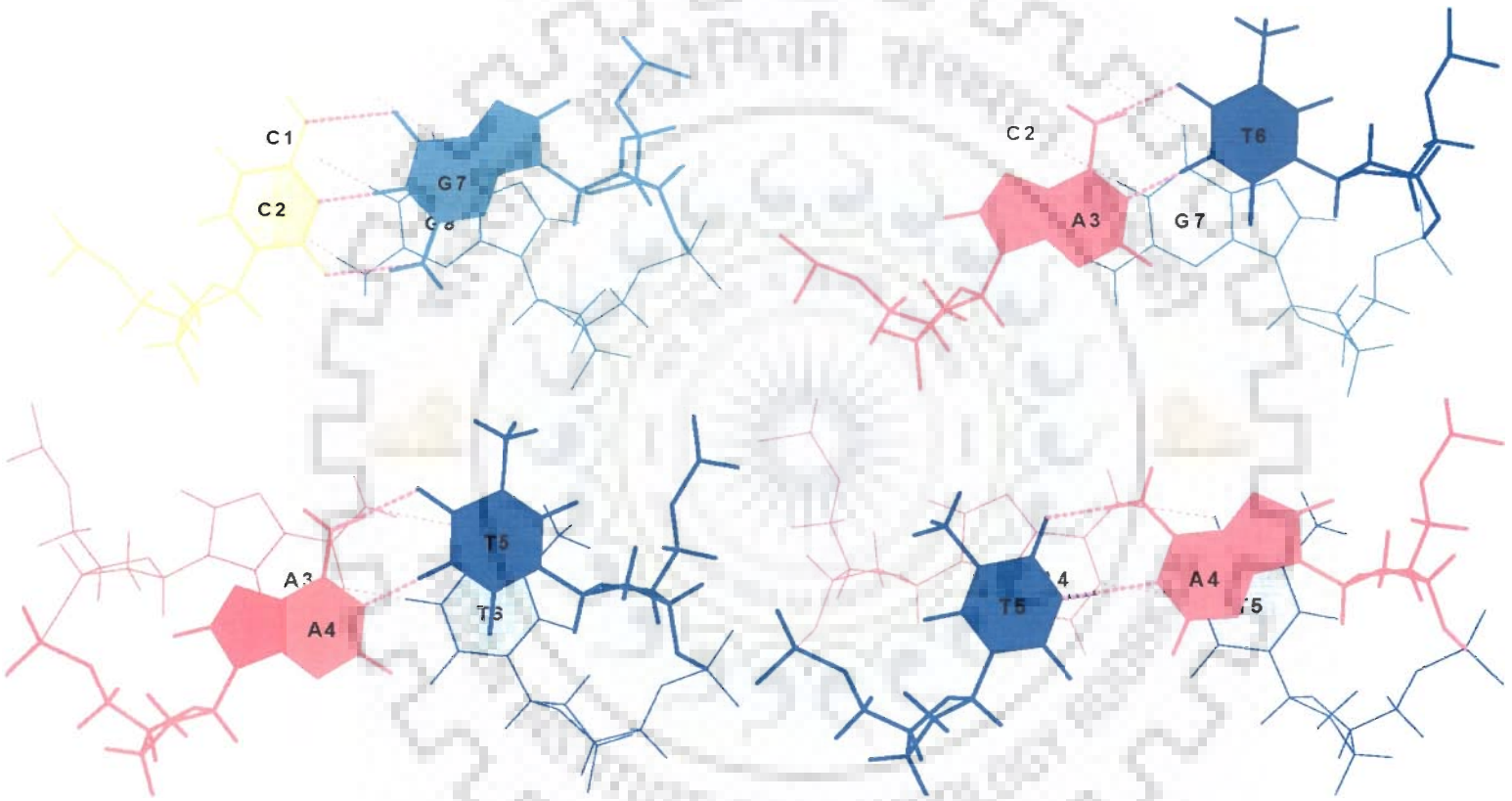


(Fig. 5.11a)

**Figure 5.11a-b: Stereo view of seven individual base pair steps viewed down the global helix axis showing stacking between adjacent base pairs in d–$(CCAATTGG)_2$**

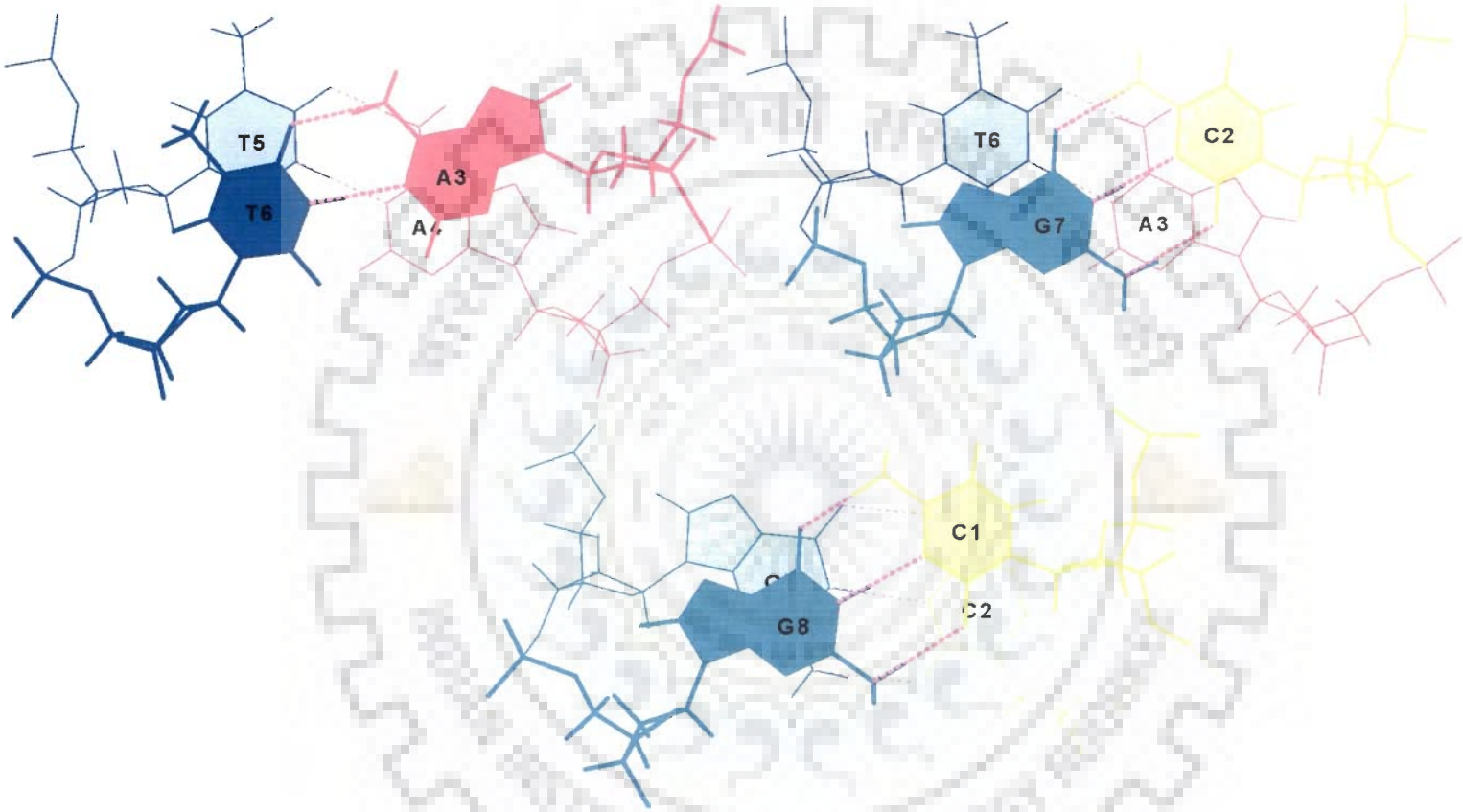


(Fig. 5.11b)

A high magnitude deviation for twist angle value from B-DNA ($36^{o}$) was found in rMD structure (~$46^{o}$) at C1pC2 and T6pG7 and comparatively low value change was obtained for crystal structure ($26^{o}$) at C1pC2 step. Such large twist angles were observed for TG/CA base pair for several crystal structures [Grzeskowiak, 1996]. Structural flexibility of DNA at TpG/CpA base pair step has also been reported by NMR [Cheung et al., 1984; Donlan and Lu, 1992; Dornberger et al., 1998], X–ray crystallographic [Gorin et al., 1995; Grzeskowiak, 1996] and other techniques [Beutel and Gold, 1992; Lyubchenko et al., 1993]. The central part of the d-$(CCAATTGG)_2$ gave a narrow minor groove with B1 conformation. This was confirmed by the quantitative analysis of sequential connectivies between H1'-H8/H6, H2'-H8/H6, H2"-H8/H6 which were found more closer to 3.95, 3.41, 2.48 Å respectively and intranucleotide distance for H3'-H6/H8 was found closer to 3.78 Å [Teletchea et al., 2004].

## 5.2 Summary and Conclusion

An extensive solution structure study of the biologically significant oligonucleotide d-$(CCAATTGG)_2$ having promoter site CCAAT was performed. Solution structure of octmaer has been elucidated using one and two dimensional $^{1}H$ and $^{31}P$ NMR spectra in $D_2O$ and in $H_2O$: $D_2O$ (90:10) solution. All proton and phosphorus resonances have been assigned. Thermal melting studies have been performed with $^{1}H$ NMR versus temperature and melting profile of d-$(CCAATTGG)_2$ sequence was achieved. An optimized solution structure has been determined by restrained Molecular Dynamics simulations using restraints from the 2D DQF COSY, $^{1}H$-$^{1}H$ NOESY, and $^{31}P$-$^{1}H$ coupling spectra. All restraints were obtained quantitatively and qualitatively from these recorded spectras. Detailed analysis for

the features of rMD and crystal structure [Vlieghe et al., 1999] has been done using CURVES software and later compared with the standard B-DNA and A-DNA. Although the crystal and rMD structures were found closer to canonical form of BDNA, both structures deviate from B-DNA in a number of observable characteristics. Particularly, both structures displayed specific patterns of stacking interaction for the central AATT base quartet. Observed changes in the minor groove width has also been correlated to DNA bending [Chuprina et al., 1991] and other helicoidal parameters [Dornberger et al., 1998] and is believed to play an important role in the process of recognition by proteins and minor groove binding ligands such as drugs. An understanding of the structural heterogeneity of DNA leads to design of new drugs, targeted to interact with DNA sequence of interest. This analysis also supports the structural insight and hydration patterns elucidated by vlieghe et al which showed that d-$(CCAATTGG)_2$ have narrow minor-groove width and BI conformation and can be used to design new minor-groove binders [Vlieghe et al., 1999]. Anti-tumor minor-groove binders have a crescent shape which allows the molecules to bind at the contour surface of the B-DNA minor groove displacing the well known hydration spine [Wang and Teng, 1990]. In future, it should be taken into account for designing new generations of minor-groove binders which not only interact with the DNA bases but also with the phosphates.

# *Studies on Complex of Berberine with promoter site containing octamer d-(CCAATTGG)$_2$ by using Phosphorous-31 and Proton Nuclear Magnetic Resonance Spectroscopy and Restrained Molecular Dynamics Approach*

The molecular basis for designing DNA binding drugs with improved specificity and affinity stems from the ability to identify the structural elements of the drug and DNA which are responsible for the specificity of the binding and the stabilization of the drug-DNA complex. In this chapter, we highlight the specific intermolecular contacts between drug and DNA molecules and provide information on the conformational changes occurring in DNA and drug during complex formation. The following set of studies were done with berberine-d-(CCAATTGG)$_2$ complex:

- 1D $^1$H and $^{31}$P NMR titration studies of berberine-d-(CCAATTGG)$_2$ complex at drug (D)/ DNA duplex (N) ratios of 0.1, 0.2, 0.3, 0.5, 0.6, 0.7, 0.8, 0.9, 1.0, 1.1, 1.2, 1.3, 1.4, 1.5, 1.6, 1.7, 1.8,1.9, 2.0 at 283 K and 298 K in 90% $H_2O$ and 10% $D_2O$.
- The temperature dependence of $^{31}$P and $^1$H chemical shift of 2.77 mM d-(CCAATTGG)$_2$ duplex in the range of 278 - 328 K.
- Temperature dependence of $^{31}$P and $^1$H NMR of the berberine-d-(CCAATTGG)$_2$ complex having D/N = 1.0 and 2.0 in the range of 278 - 328 K.
- 2D $^{31}$P - $^{31}$P exchange spectra of berberine-DNA complex by a phase-sensitive NOESY using mixing time of 150 and 200 ms at 283 K for D/N = 0.5, 1.0, 1.5 and 2.0.

- 2D NOESY $^{1}H$ - $^{1}H$ at D/N = 1.0, 1.5, 2.0 using mixing time $\tau_m$ = 100, 200, 300 ms at 283 K in 90 % $H_2O$ and 10 % $D_2O$.
- Diffusion Ordered Spectroscopy (DOSY) experiments on complex of berberine-d-$(CCAATTGG)_2$ and uncomplexed berberine and d-$(CCAATTGG)_2$.
- Restrained molecular dynamics (rMD) studies on the solution structure of berberine- d-$(CCAATTGG)_2$ complex using inter-proton distances obtained from 2D NOESY as restraints.
- Analysis of the converged structures in terms of time average for the various conformational and helical parameters.

## 6.1 Results And Discussion

### 6.1.1 Phosphorous-31 NMR Studies of Berberine-d-$(CCAATTGG)_2$ Complex

For the purpose of this discussion, the position of the bases in the octamer were designated as follows: d-$(C1pC2pA3pA4pT5pT6pG7pG8)_2$. The assignment of $^{31}P$ nucleotide resonances were quite straightforward using the three bond scalar coupling of $^{31}P$ with $(H3')_n$ of the sugar residue. In addition $^{4}J$ couplings of phosphorous to $(H4')_{n+1}$ protons of the sugar residues are also clearly evident. The positions for phosphate resonances for uncomplexed DNA were assigned as C2pA3, G7pG8, C1pC2, T6pG7 and A3pA4 at -1.03, -1.13, -1.40, -1.47 and -1.66 ppm respectively at 283 K, while -1.76 ppm has been assigned for the combined position of A4pT5 and T5pT6 (Figure 5.7, Chapter 5).

#### 6.1.1.1 Chemical Shift

Successive addition of berberine to d-$(CCAATTGG)_2$ was investigated by titrating a known concentration of berberine (25 mM) to a fixed concentration of 2.80 mM d-

$(CCAATTGG)_2$ . To arrive at Drug to Nucleotide (D/N) stoichiometric ratios from 0 to 2.0 at 283 and 298 K a slow increment in D/N ratio of 0.1 was done. It was observed that only a slight difference in the chemical shift was achieved even at high concentration of berberine and the obtained results were similar at 283 and 298 K. Figure 6.1 shows the change in $^{31}P$ chemical shift due to binding as a function of increased concentration of berberine at 283 K. Only seven resonances were observed on the formation of berberine-DNA complex. These resonances showed a modest shift as compared to the resonances from free octamer but with increase in D/N ratio they broaden severely due to fast chemical exchange on the NMR time scale. Chemical shift values for all the phosphorus signals at different D/N ratio are tabulated in Table 6.1. It shows that very less downfield shift was observed for C1pC2, C2pA3, A3pA4 and G7pG8 all the phosphorus signals. C1pC2, resonance shift ($\Delta\delta = \delta^b - \delta^f$) downfield by 0.09, which was maximum among all phosphorus signal observed, can be attributed to the opening of C1-G8 base pair due to binding of berberine. G7pG8, C2pA3 and A3pA4 showed equivalent downfield shift of 0.02 ppm. A4pT5 and T5pT6 showed a upfield shift of 0.04 ppm and T6pG7 showed an upfield shift of 0.01 ppm only. Upfield shifts observed with A4pT5 and T5pT6 resonances shows that berberine might be interacting with d-$(CCAATTGG)_2$ at A4pT5 and T5pT6 site through electrostatic interaction [Patel, 1979; Wilson and Jones, 1982]. Figure 6.2 shows the plot of chemical shift versus D/N ratio. Little or no variation was observed in the chemical shift of T6pG7 with increasing berberine concentration. It is known that $^{31}P$ chemical shifts vary in response to local, sequence specific and induced environmental distortions in the duplex geometry [Calladine, 1982; Dickerson, 1983; Ott and Eckstein, 1985; Schroeder et al., 1989].

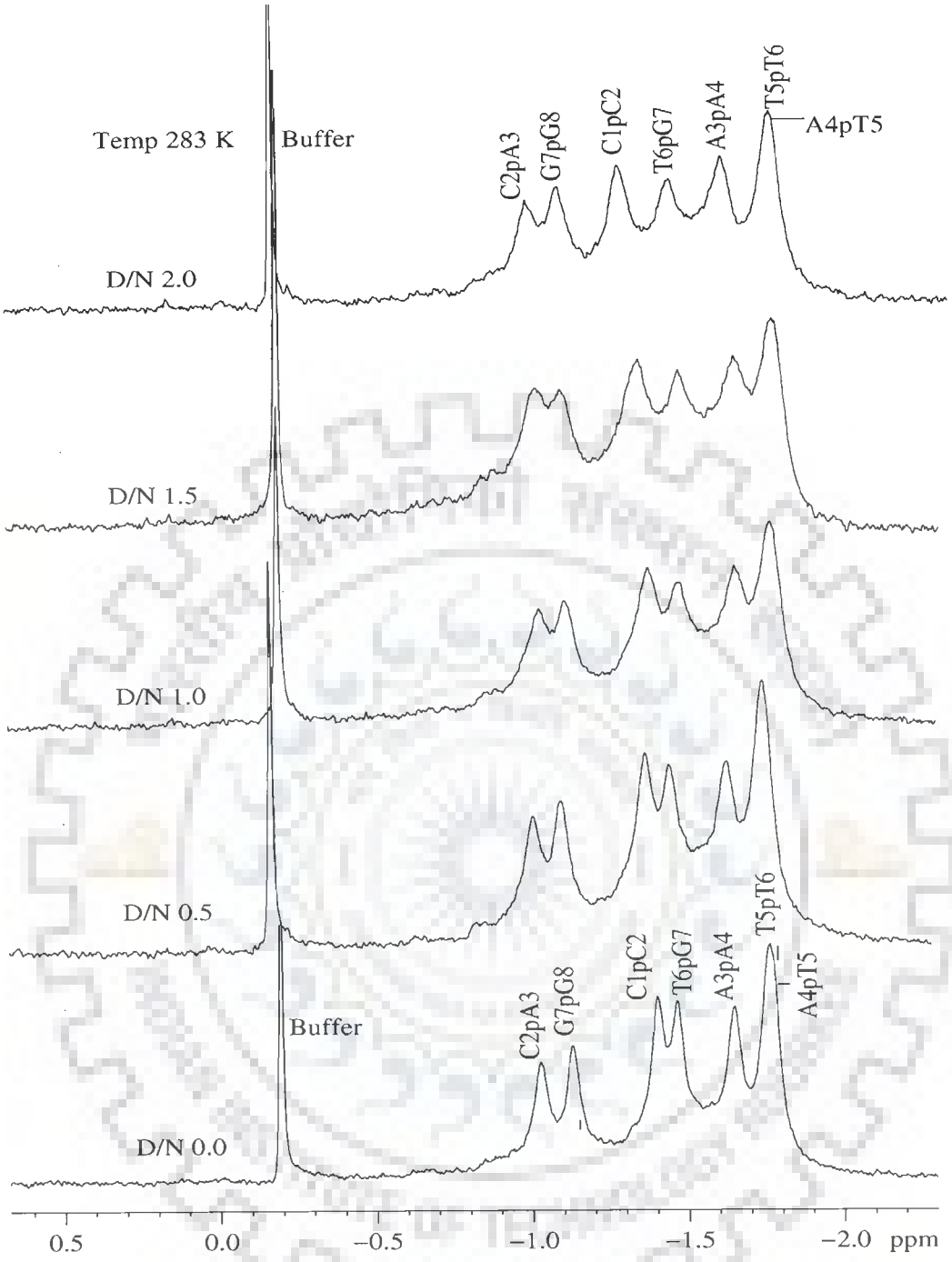


**Figure 6.1: Proton decoupled $^{31}P$ NMR spectra of 2.76 mM d-$(CCAATTGG)_2$ in uncomplexed state and complexed with berberine with increasing drug (D) to nucleic acid duplex (N) ratio, D/N, at 283 K.**

**Table 6.1: Chemical shift of $^{31}P$ resonances of the phosphate groups of DNA Octamer, in complex of berberine with d-(CCAATTGG)$_2$ at 283 K with different drug (D) to nucleic acid duplex (N) ratios (D / N). $\Delta\delta = (\delta_{D/N=2.0} - \delta_{D/N=0})$.**

| D/N | C1pC2 | C2pA3 | A3pA4 | A4pT5 | T5pT6 | T6pG7 | G7pG8 |
|---|---|---|---|---|---|---|---|
| **0.0** | -1.40 | -1.03 | -1.66 | -1.76 | -1.76 | -1.47 | -1.13 |
| **0.5** | -1.40 | -1.03 | -1.65 | -1.77 | -1.77 | -1.48 | -1.12 |
| **1.0** | -1.38 | -1.03 | -1.65 | -1.78 | -1.78 | -1.48 | -1.11 |
| **1.5** | -1.35 | -1.01 | -1.65 | -1.79 | -1.79 | -1.48 | -1.11 |
| **2.0** | -1.31 | -1.01 | -1.64 | -1.80 | -1.80 | -1.48 | -1.11 |
| **$\Delta\delta$** | +0.09 | +0.02 | +0.02 | -0.04 | -0.04 | -0.01 | +0.02 |

+ve $\Delta\delta$ indicates downfield shift
-ve $\Delta\delta$ indicates upfield shift

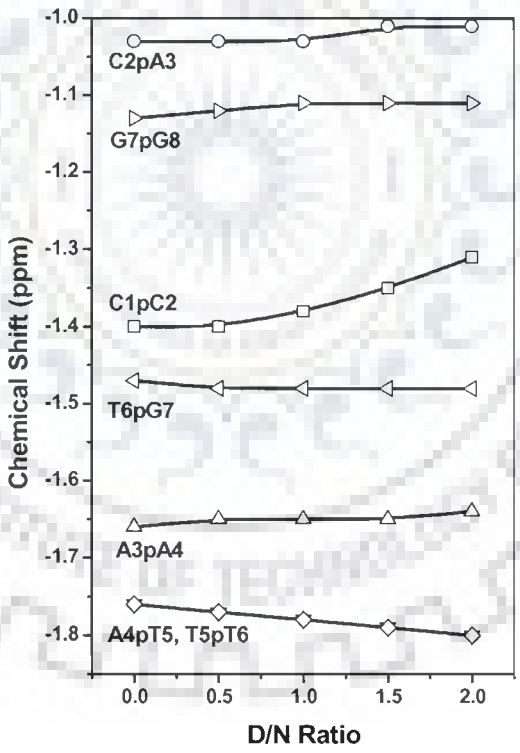


**Figure 6.2: $^{31}P$ Chemical shift variation of d-(CCAATTGG)$_2$ in complex with berberine, as a function D/N ratio at 283 K.**

Theoretical studies have shown that variation in the conformation of two (α: O3'-P-O5'-C5' and ζ: C3'-O3'-P-O5') out of six torsional angles can cause perturbations in $^{31}P$ shifts. Switching from energetically more favorable $B_I$ conformation ($\zeta = g^-$, $\alpha = g^-$) to the more flexible $B_{II}$ conformation ($\zeta = t$, $\alpha = g^-$) having 1 Kcal/mol higher energy than $B_I$, introduces a downfield shift of about 1.5 ppm [Gorenstein et al., 1977], which is the condition when intercalating drugs binds to BDNA. The dispersion in $^{31}P$ chemical shifts of oligonucleotides has also been attributed to different populations of $B_I$ and $B_{II}$ states [Gorenstein, 1992]. $^{31}P$ chemical shift has also been correlated with degree of duplex DNA unwinding resulting from increase in the length of sugar phosphate backbone to accommodate intercalation of drug chromophore. Besides, the ester O-P-O bond angle distortions in drug-duplex DNA complexes also affect the chemical shift. Widening of ester O-P-O angle is expected to produce an upfield shift [Gorenstein and Kar, 1975; Gorenstein et al., 1984] while narrowing of this bond angle causes a downfield shift. Purely electrostatic associations between drug and nucleic acid on the other hand produce only small and generally upfield $^{31}P$ chemical shifts [Patel, 1979; Wilson and Jones, 1982].

The change in the chemical shifts obtained for $^{31}P$ resonances of berberine-d-$(CCAATTGG)_2$ complex were compared with corresponding $\Delta\delta$ values reported in literature (Table 6.2 and Table 6.3) for binding berberine with d-$(AAGAATTCTT)_2$ [Mazzini et al., 2003], binding of mitoxantrone with d-$(CGCG)_2$ [Lown and Hanstock, 1985]. d-$(CGATCG)_2$ [Kotovych et al., 1986], 2-pyrido[1, 2-e]purine-4-yl)amino-ethanol with d-$(CGATCG)_2$ [Favier et al., 2001], nogalamycin with d-$(GCATGC)_2$ [Searle et al., 1988], adriamycin and methoxy-morpholinodoxorubicin with d-$(CGATCG)_2$ and d-$(CGTACG)_2$ [Mazzini et al., 1998].

**Table 6.2: Chemical shift of free ($\delta^f$ bound ($\delta^b$), and change in chemical shift due to binding, $\Delta\delta = \delta^b - \delta^f$ in phosphate groups of some of the drug-DNA complexes taken from literature.**

| Phosphate Group | [Mazzini et al., 1998], d-$(CGATCG)_2$ + Adriamycin | | | [Mazzini et al., 1998]., d-$(CGTACG)_2$ + Adriamycin | | | [Searle et al., 1988] d -$(GCATGC)_2$ + Nogalamycin | | |
|---|---|---|---|---|---|---|---|---|---|
| | $\delta^f$ | $\delta^b$ | $\Delta\delta$ | $\delta^f$ | $\delta^b$ | $\Delta\delta$ | $\delta^f$ | $\delta^b$* | $\Delta\delta$ |
| **C1pG2/ G1pC2** | -0.91 | -0.48 | +0.43 | -1.03 | -0.58 | +0.45 | -3.30 | -2.90 | +0.20 |
| **G2pA3/ C2pA3** | -0.86 | 0.67 | +1.53 | -1.40 | -0.56 | +0.84 | -3.00 | -2.50 | +0.50 |
| **A3pT4/ T3pA4** | -1.26 | -1.28 | ≤0.2 | -1.12 | -1.26 | -0.14 | -3.40 | -3.20 | +0.20 |
| **T4pC5/T4pG6** | -1.06 | -1.12 | -0.06 | -1.20 | -1.34 | -0.14 | -3.10 | -1.60 | +1.50 |
| **C5pG6/G5pC6** | -0.73 | 0.84 | +1.57 | -0.90 | +0.63 | +1.53 | -3.00 | -3.00 | +0.00 |
| | **[Mazzini et al., 1998] d-$(CGATCG)_2$+ Morpholinodoxorubicin** | | | **[Mazzini et al., 1998] d-$(CGTACG)_2$+ Morpholinodoxorubicin** | | | **[Ragg et al., 1988] d-$(CGTACG)_2$+ Daunorubicin** | | |
| | | | | | | | | | |
| **C1pG2** | -0.91 | -0.32 | +0.59 | -1.03 | -0.56 | +0.47 | -1.02 | -1.45 | -0.43 |
| **G2pA3 / G2pT3** | -0.86 | 0.19 | +1.05 | -1.40 | -0.50 | +0.90 | -1.42 | -1.95 | -0.53 |
| **A3pT4/T3pA4** | -1.26 | -1.36 | -0.10 | -1.12 | -1.45 | -0.33 | -1.08 | -1.28 | -0.20 |
| **T4pC5/A4pC5** | -1.06 | -1.11 | -0.05 | -1.20 | -1.46 | -0.26 | -1.28 | -1.48 | -0.20 |
| **C5pG6** | -0.73 | 0.52 | +1.25 | -0.90 | +0.22 | +1.12 | -0.88 | +0.44 | +1.32 |

+ve $\Delta\delta$ indicates downfield shift.
-ve $\Delta\delta$ indicates upfield shift.
* Tentative assignment

**Table 6.3: Chemical shift of free ($\delta^f$), bound ($\delta^b$), and the change in chemical shift due to binding, $\Delta\delta = \delta^b - \delta^f$ in phosphate resonances of some of the drug-DNA complexes taken from literature.**

| Phosphate Group | [Lown and Hanstock, et d-( CGCG)$_2$ + mitoxantrone | | | [Kotovych et al., 1986] d-( CGATCG)$_2$ + mitoxantrone | | | | [Favier et al., 2001] d-(CGATCG)$_2$ + pyridopurine | | | | [Mazzini et al., 2003] d-(AAGAATTCTT)$_2$ + berberine | | | |
|---|---|---|---|---|---|---|---|---|---|---|---|---|---|---|---|
| | $\delta^f$ | $\delta^b$ | $\Delta\delta$ | | $\delta^f$ | $\delta^b$ | $\Delta\delta$ | | $\delta^f$ | $\delta^b$ | $\Delta\delta$ | | $\delta^f$ | $\delta^b$ | $\Delta\delta$ |
| **C1pG2** | -3.46 | -3.31 | +0.15 | **C1pG2** | -1.71 | -1.70 | + 0.01 | **C1pG2** | 1.2 | 1.1 | -0.1 | **A1pA2** | -1.31 | -1.19 | +0.12 |
| **G2pA3** | -3.30 | -3.40 | -0.10 | **G2pA3** | -1.71 | -1.70 | + 0.01 | **G2pA3** | 1.1 | 1.1 | 0.0 | **A2pG3** | -1.00 | -0.98 | +0.02 |
| **C3pG4** | -3.46 | -3.31 | +0.15 | **A3pT4** | -2.19 | -2.21 | -0.02 | **A3pT4** | 0.7 | 0.8 | -0.1 | **G3pA4** | -1.14 | -1.12 | +0.02 |
| | | | | **T4pC5** | -1.95 | -1.97 | -0.02 | **T4pC5** | 0.4 | 0.5 | -0.1 | **A4pA5** | -1.40 | -1.23 | +0.17 |
| | | | | **C5pG6** | -1.59 | -1..25 | +0.34 | **C5pG6** | 1.2 | 1.2 | 0.0 | **A5pT6** | -1.37 | -1.40 | +0.03 |
| **[Mazzini et al., 2004] Topotecan+d(CGTACG)$_2$** | | | | **[Mazzini et al., 2004] Camptothecin+d(CGTACG)$_2$** | | | | **[Mazzini et al., 2004] Camptothecin+d(CGTATACG)$_2$** | | | | **T6pT7** | -1.18 | -1.10 | +0.08 |
| **C1pG2** | -1.00 | -1.00 | 0.00 | **C1pG2** | -0.88 | -0.95 | +0.07 | **C1pG2** | -0.94 | -0.96 | +0.02 | **T7pC8** | -1.11 | -1.07 | +0.04 |
| **G2pT3** | -1.29 | -1.35 | -0.06 | **G2pT3** | -1.32 | -1.33 | +0.01 | **G2pT3** | -1.33 | -1.33 | +0.00 | **C8pT9** | -1.14 | -1.10 | +0.04 |
| **T3pA4** | -1.08 | -1.10 | -0.02 | **T3pA4** | -1.14 | -1.17 | -0.03 | **T3pA4** | -1.03 | -1.03 | +0.00 | **T9pT10** | -1.04 | -1.07 | +0.03 |
| **A4pC5** | -1.12 | -1.20 | -0.08 | **A4pC5** | -1.14 | -1.17 | -0.03 | **A4pC5** | -1.33 | -1.33 | +0.00 | | | | |
| **C5pG6** | -0.90 | -1.00 | -0.10 | **C5pG6** | -0.78 | -0.85 | +0.07 | **T5pA6** | -1.10 | -1.13 | -0.03 | | | | |
| | | | | | | | | **A6pC7** | -1.09 | -1.11 | +0.02 | | | | |
| | | | | | | | | **C7pG8** | -0.82 | -0.84 | -0.02 | | | | |

+ve $\Delta\delta$ indicates downfield shift
-ve $\Delta\delta$ indicates upfield shift

Drugs like adriamycin, morpholinoldoxorubicin, daunorubicin and nogalamycin [Mazzini et al., 1998; Ragg et al., 1988; Searle et al., 1988] which intercalate between two base pairs of DNA oligomer, lead to downfield shifts up to 1.57 ppm of phosphorus resonances at the intercalation site or at site adjacent to it. Earlier, shifts of ~2.6 ppm has been reported on intercalation of aromatic chromophores in DNA [Gorenstein, 1992; Patel, 1974; Patel and Canuel, 1976; Patel et al., 1982]. In case of external binding drugs like pyridopurine, [Favier et al., 2001] and mitoxantrone downfield shift up to 0.15-0.34 ppm were observed [Kotovych et al., 1986; Lown and Hanstock, 1985]. Only Mazzini et al has reported $^{31}P$ NMR studies of berberine with several oligonucleotides. They have reported downfield shift in the range 0-0.17 ppm, which is an indicative of the external binding of berberine to oligonucleotides studied [Mazzini et al., 2003].

$^{31}P$ chemical shift variations in nucleotides reflect the conformation of the phosphodiester groups at the level of the P-O5' and O3'-P bonds i.e. the values of torsion angles $\alpha$ = O3'-P--O5'-C5'and $\zeta$ = C3'-O3'-P-O5'. B-DNA conformation have phosphate groups normally in gauche$^-$, gauche$^-$ (g$^-$, g$^-$) conformation with $\alpha$ and $\zeta$ angles of -60° and -90° respectively. When intercalating drugs bind to B-DNA, the backbone $\alpha$ and $\zeta$ angles change to g$^-$, t whereas the gauche$^-$, trans (g$^-$, t) conformation ($\alpha$ = -60°, $\zeta$ = 180°) is generally associated with deshielding of 1.5 ppm. Such transition from g$^-$, g$^-$ to g$^-$, t on intercalation of drug chromophore by opening of adjacent base pairs at intercalation site from a distance of 3.4 to 6.8 Å have been reported in X-ray crystallographic structure of adriamycin and daunomycin binding to d-CGATCG, d-TGATCA, d-CGTACG sequences [Frederick et al., 1990] as well in similar NMR structures [Mazzini et al., 1998]. The pyridopurine [Favier et al., 2001]

and berberine [Mazzini et al., 2003], which does not show such large shifts in the phosphorus resonances on binding to DNA, have been shown to bind externally in the restrained molecular dynamics structures obtained by using inter molecular inter proton distances from NOESY spectra.The pyridopurine [Favier et al., 2001] and berberine [Mazzini et al., 2003], which does not show such large shifts in the phosphorus resonances on binding to DNA, have been shown to bind externally in the restrained molecular dynamics structures obtained by using experimental intermolecular inter proton distances from NOESY spectra. Thus, it may be inferred that binding of berberine to d-$(CCAATTGG)_2$ does not lead to opening of base pairs, which is generally associated with large down field shifts of $^{31}P$ resonance of the order of 1.6-2.6 ppm [Gorenstein, 1992; Patel, 1974; Patel and Canuel, 1976; Patel et al., 1982]. Since, we also found that change in the chemical shifts was very less (< 0.10) as compared to other DNA binding drug, intercalative mode can be excluded and the external mode of binding of berberine can be suggested. But still predicting the binding site of berberine on the basis of alone $^{31}P$ chemical shift variation can be more imaginary.

### 6.1.1.2 2D $^{31}P$ - $^{31}P$ Exchange Spectra

Figure 6.3a-b shows 2D $^{31}P$ NMR exchange spectrum of the complex of berberine with d-$(CCAATTGG)_2$ at drug to DNA (D/N) ratio of 1.0 and 2.0 at 283K. The one dimensional $^{31}P$ spectra are shown along both axes. In 2D $^{31}P$ NMR exchange spectrum each of the 7 phosphorus signals seen in uncomplexed DNA is expected to give cross peak due to chemical exchange with its respective bound resonance. On binding of berberine to d-$(CCAATTGG)_2$, only considerable

broadening was observed with no additional cross peaks due to exchange between the bound and free phosphate resonances.

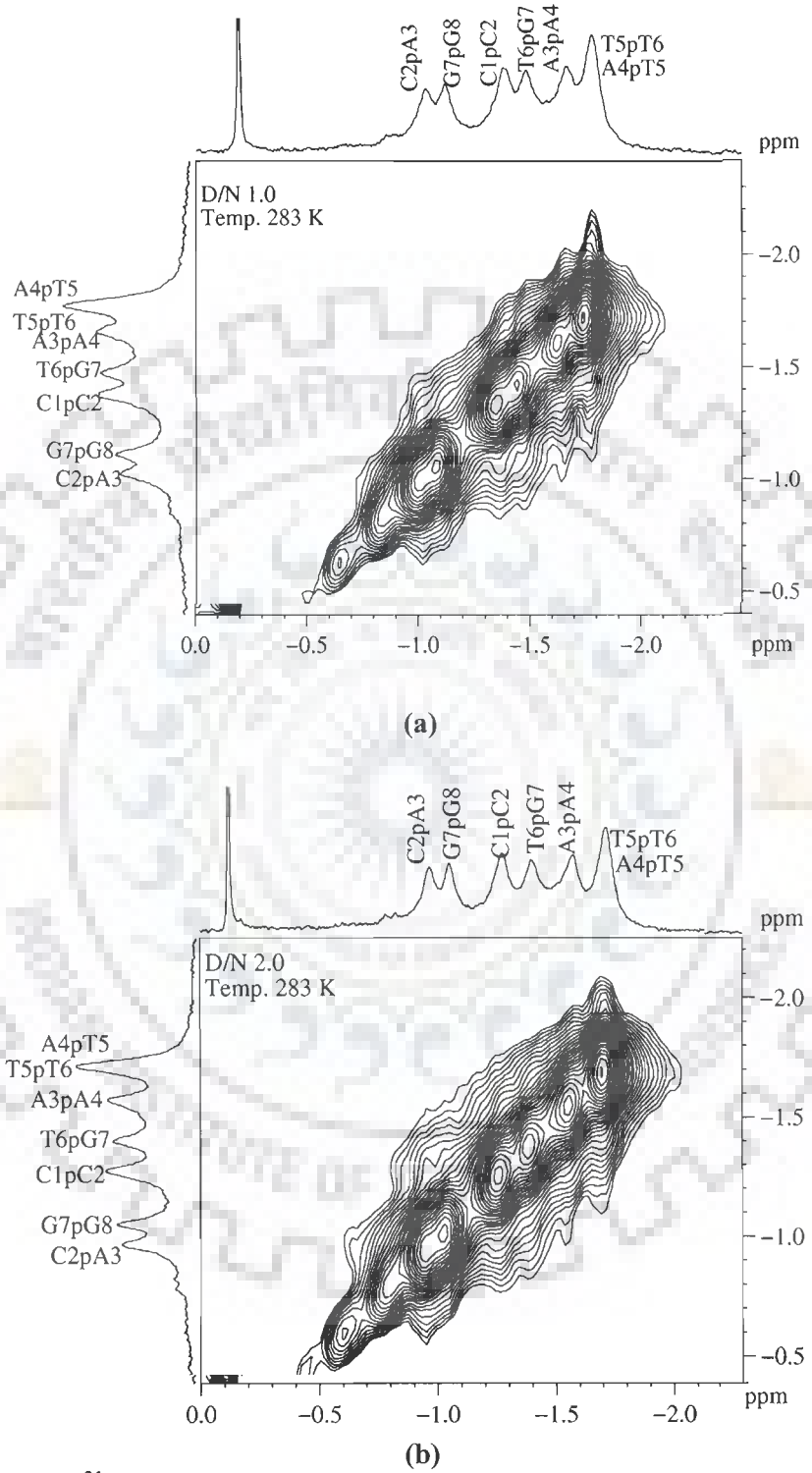


**Figure 6.3: $^{31}$P NMR exchange spectrum of the complex of berberine with d-(CCAATTGG)$_2$ at drug (D) to nucleic acid duplex (N) ratio, D/N of (a) 1.0 at 283 K (b) 2.0 at 283 K.**

Since, only one set of resonances were observed for the complexes at different D/N ratios for free octamer and octamer bound to berberine, it is expected that $^{31}P$ signals from the bound DNA were in fast exchange with the corresponding signals from free DNA to be followed individually at 283 K on NMR time scale. Even P-P NOESY recorded at 278 K shows no separate signals for free and bound species due to fast exchange on NMR time scale (data not shown).

### 6.1.1.3 Temperature Dependence Studies

The variation of $^{31}P$ NMR spectrum of d-$(CCAATTGG)_2$ and its complex with berberine at D/N ratios of 0.0, 1.0, and 2.0 in the range 278 K to 328 K was examined (Figure 6.4a-c). Table 6.4 shows the variation of chemical shift as a function of temperature. The signals were found to be shifted with temperature, which may be due to shift in the following equilibrium:

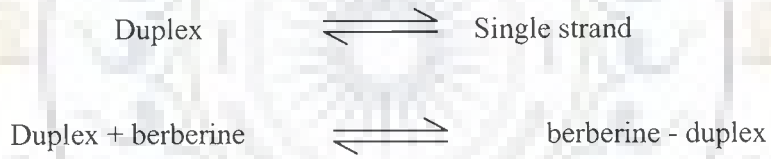


These reactions correspond to single strand transition and drug-DNA complexation respectively. It was observed that shift in $^{31}P$ resonances in uncomplexed and complexed d-$(CCAATTGG)_2$ in the range 278-328 K were very gradual and not abrupt (Figure 6.5). The observation was consistent with the earlier studies reported in literature on change in chemical shift with temperature due to helix to coil transition [Patel, 1977]. Table 6.4 shows the shift in $^{31}P$ resonances with temperature in the bound complexes, which was found to be gradual and the total change i.e. $\Delta\delta = \delta_{328\ K} - \delta_{278\ K}$, was different for complexes having different D/N ratios. At D/N 2.0 chemical shift change due to temperature was much less than the alone DNA.

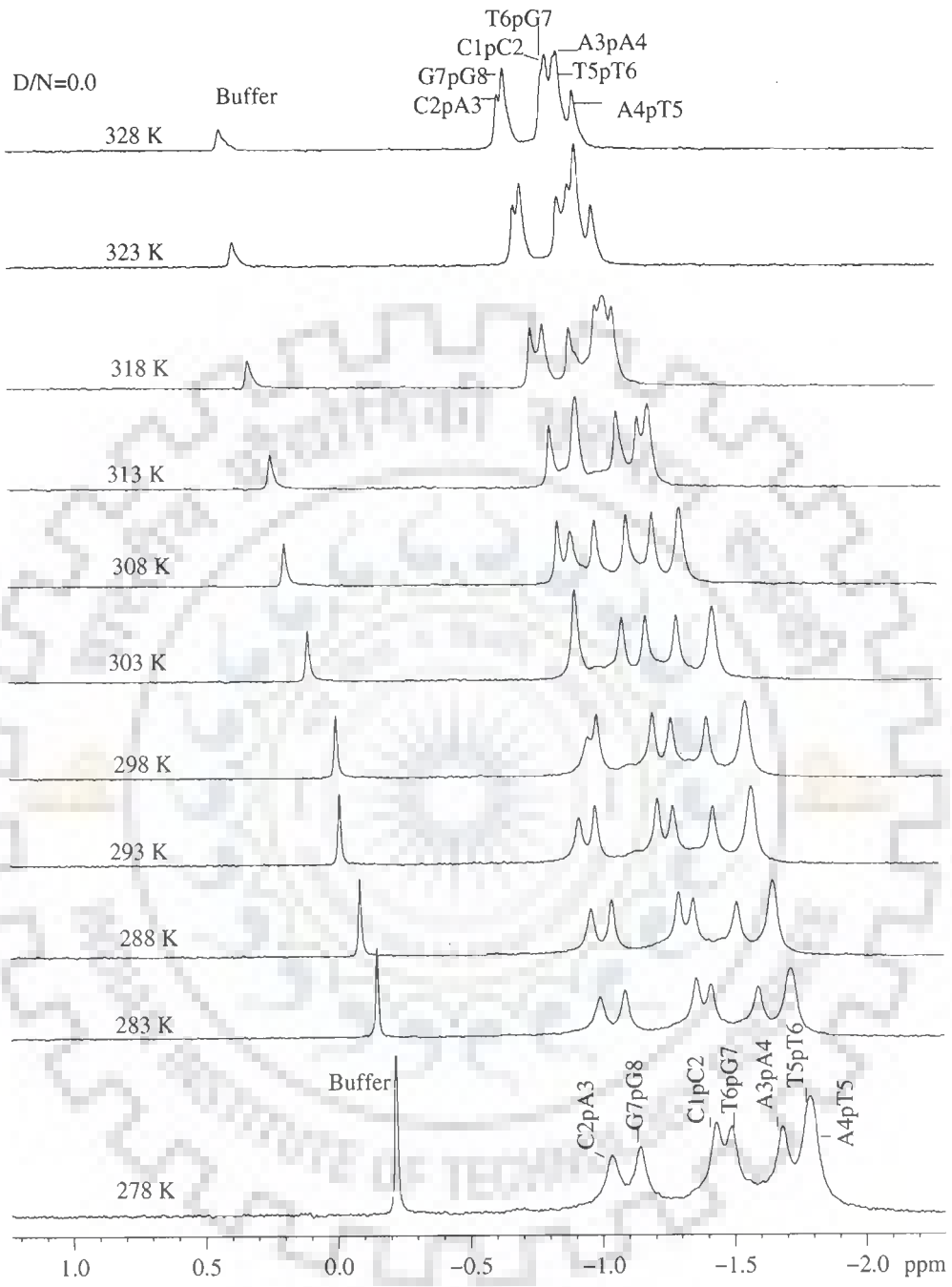


**(Fig. 6.4a)**

**Figure 6.4: Proton decoupled $^{31}P$ NMR spectra of d-$(CCAATTGG)_2$ as a function of temperature (a) at D/N 0.0 (b) at D/N 1.0 (c) D/N 2.0.**

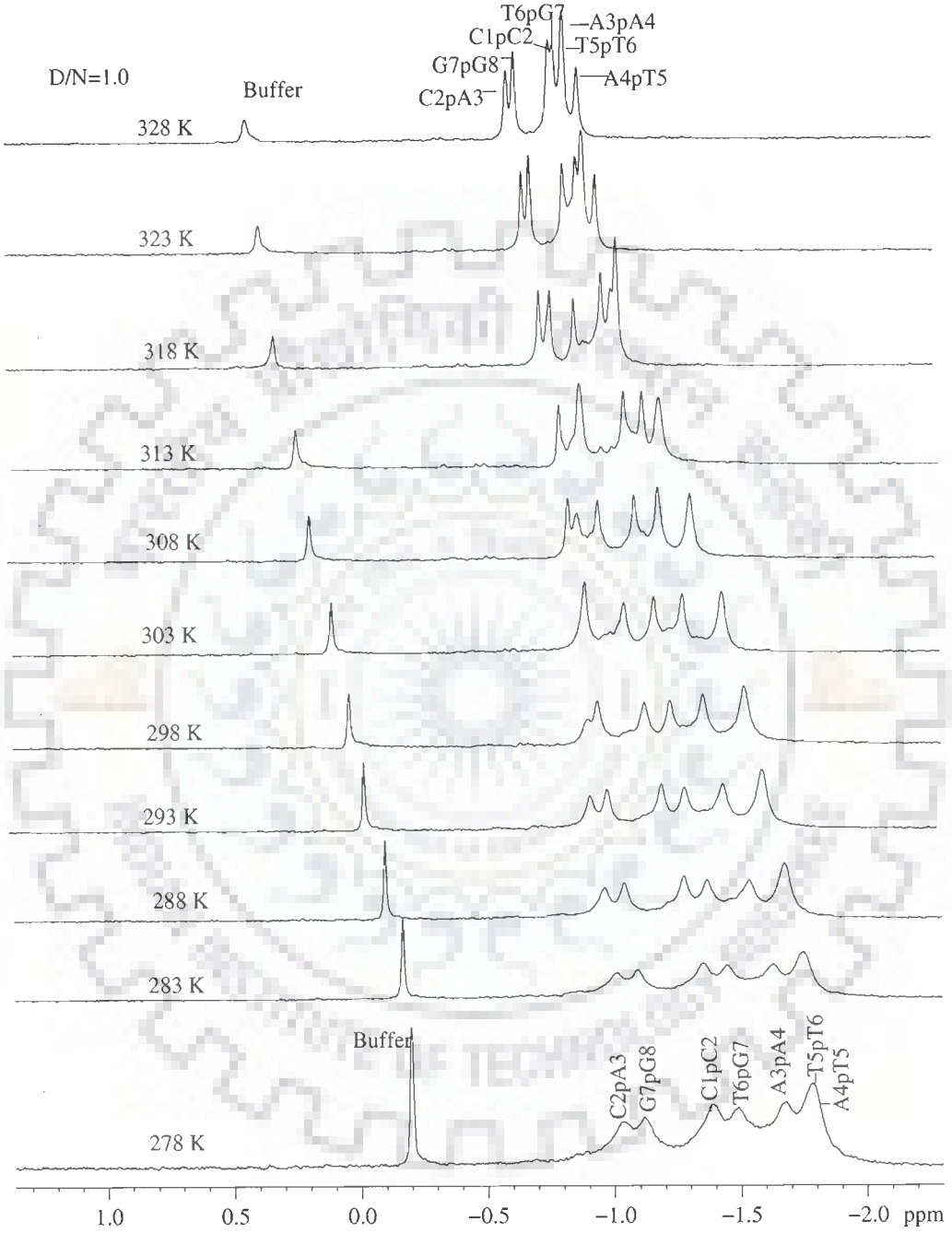
D/N=1.0
Buffer
T6pG7
A3pA4
C1pC2
T5pT6
G7pG8
A4pT5
C2pA3
328 K
323 K
318 K
313 K
308 K
303 K
298 K
293 K
288 K
283 K
278 K
Buffer
C2pA3
G7pG8
C1pC2
T6pG7
A3pA4
T5pT6
A4pT5
1.0
0.5
0.0
−0.5
−1.0
−1.5
−2.0 ppm

**(Fig. 6.4b)**

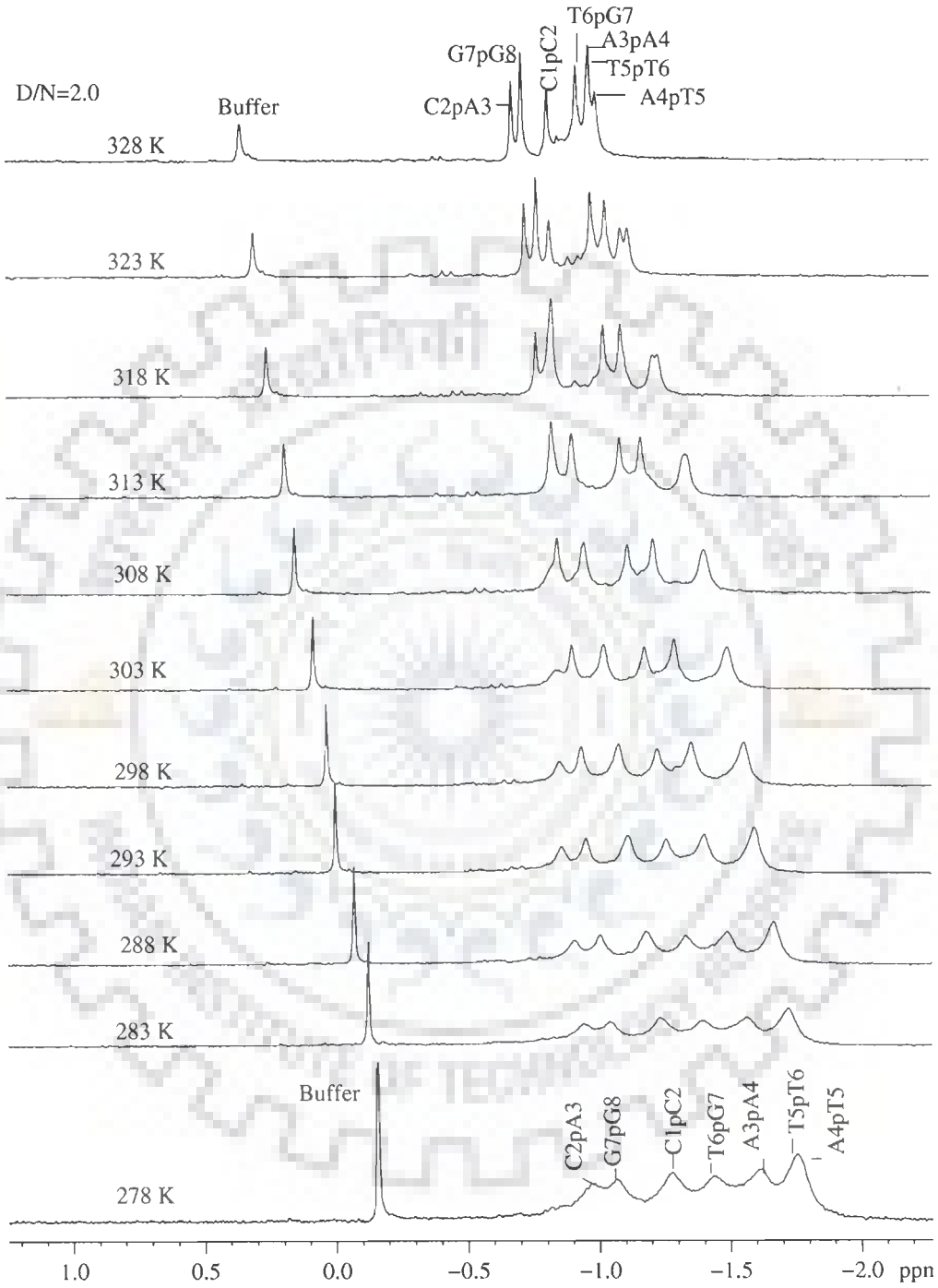
D/N=2.0
328 K
323 K
318 K
313 K
308 K
303 K
298 K
293 K
288 K
283 K
278 K
Buffer
C2pA3
G7pG8
C1pC2
T6pG7
A3pA4
T5pT6
A4pT5
1.0
0.5
0.0
−0.5
−1.0
−1.5
−2.0
ppn

**(Fig. 6.4c)**

**Table 6.4: $^{31}$P chemical shift d-(CCAATTGG)$_2$-berberine complex (D/N = 0, 1.0, 2.0) as a function of temperature in the range 278-328 K where $\Delta\delta = \delta_{328K} - \delta_{278K}$.**

| Temp. | D/N 0.0 | | | | | | | D/N 1.0 | | | | | | |
|---|---|---|---|---|---|---|---|---|---|---|---|---|---|---|
| | C1pC2 | C2pA3 | A3pA4 | A4pT5 | T5pT6 | T6pG7 | G7pG8 | C1pC2 | C2pA3 | A3pA4 | A4pT5 | T5pT6 | T6pG7 | G7pG8 |
| **278** | -1.43 | -1.04 | -1.69 | -1.79 | -1.79 | -1.49 | -1.14 | -1.38 | -1.04 | -1.67 | -1.79 | -1.79 | -1.49 | -1.12 |
| **283** | -1.36 | -0.99 | -1.59 | -1.72 | -1.72 | -1.42 | -1.08 | -1.35 | -1.01 | -1.64 | -1.75 | -1.75 | -1.45 | -1.09 |
| **288** | -1.29 | -0.96 | -1.51 | -1.65 | -1.65 | -1.35 | -1.04 | -1.28 | -0.96 | -1.53 | -1.68 | -1.68 | -1.37 | -1.04 |
| **293** | -1.23 | -0.93 | -1.44 | -1.59 | -1.59 | -1.29 | -0.99 | -1.21 | -0.93 | -1.45 | -1.61 | -1.61 | -1.30 | -0.99 |
| **298** | -1.19 | -0.95 | -1.40 | -1.55 | -1.55 | -1.27 | -0.98 | -1.13 | -0.90 | -1.36 | -1.52 | -1.52 | -1.22 | -0.94 |
| **303** | -1.09 | -0.91 | -1.29 | -1.43 | -1.43 | -1.17 | -0.91 | -1.05 | -0.85 | -1.28 | -1.44 | -1.44 | -1.17 | -0.90 |
| **308** | -1.00 | -0.86 | -1.22 | -1.32 | -1.32 | -1.12 | -0.86 | -0.96 | -0.80 | -1.20 | -1.33 | -1.33 | -1.11 | -0.88 |
| **313** | -0.91 | -0.81 | -1.14 | -1.19 | -1.19 | -1.06 | -0.82 | -0.88 | -0.74 | -1.13 | -1.20 | -1.20 | -1.05 | -0.86 |
| **318** | -0.88 | -0.76 | -1.03 | -1.07 | -1.04 | -1.01 | -0.78 | -0.87 | -0.67 | -1.02 | -1.05 | -1.05 | -0.99 | -0.77 |
| **323** | -0.86 | -0.70 | -0.93 | -0.99 | -0.93 | -0.91 | -0.73 | -0.84 | -0.64 | -0.92 | -0.96 | -0.91 | -0.88 | -0.71 |
| **328** | -0.81 | -0.64 | -0.85 | -0.93 | -0.88 | -0.82 | -0.66 | -0.79 | -0.62 | -0.84 | -0.90 | -0.84 | -0.80 | -0.64 |
| **δΔ** | +0.62 | +0.40 | +0.84 | +0.86 | +0.91 | +0.67 | +0.48 | +0.59 | +0.42 | +0.83 | +0.89 | +0.95 | +0.69 | +0.48 |
| **Temp.** | **D/N 2.0** | | | | | | | | | | | | | |
| | C1pC2 | C2pA3 | A3pA4 | A4pT5 | T5pT6 | T6pG7 | G7pG8 | | | | | | | |
| **278** | -1.28 | -0.97 | -1.61 | -1.75 | -1.75 | -1.43 | -1.07 | | | | | | | |
| **283** | -1.24 | -0.93 | -1.55 | -1.71 | -1.71 | -1.39 | -1.04 | | | | | | | |
| **288** | -1.18 | -0.91 | -1.48 | -1.67 | -1.67 | -1.33 | -1.00 | | | | | | | |
| **293** | -1.13 | -0.87 | -1.42 | -1.61 | -1.61 | -1.27 | -0.96 | | | | | | | |
| **298** | -1.07 | -0.85 | -1.35 | -1.55 | -1.55 | -1.22 | -0.93 | | | | | | | |
| **303** | -1.02 | -0.84 | -1.29 | -1.49 | -1.49 | -1.17 | -0.89 | | | | | | | |
| **308** | -0.96 | -0.82 | -1.22 | -1.42 | -1.42 | -1.13 | -0.90 | | | | | | | |
| **313** | -0.90 | -0.78 | -1.16 | -1.34 | -1.34 | -1.09 | -0.90 | | | | | | | |
| **318** | -0.85 | -0.76 | -1.11 | -1.25 | -1.22 | -1.03 | -0.84 | | | | | | | |
| **323** | -0.79 | -0.74 | -1.05 | -1.14 | -1.11 | -0.99 | -0.76 | | | | | | | |
| **328** | -0.73 | -0.69 | -0.99 | -1.00 | -0.98 | -0.94 | -0.72 | | | | | | | |
| **δΔ** | +0.55 | +0.28 | +0.62 | +0.75 | +0.77 | +0.49 | +0.35 | | | | | | | |

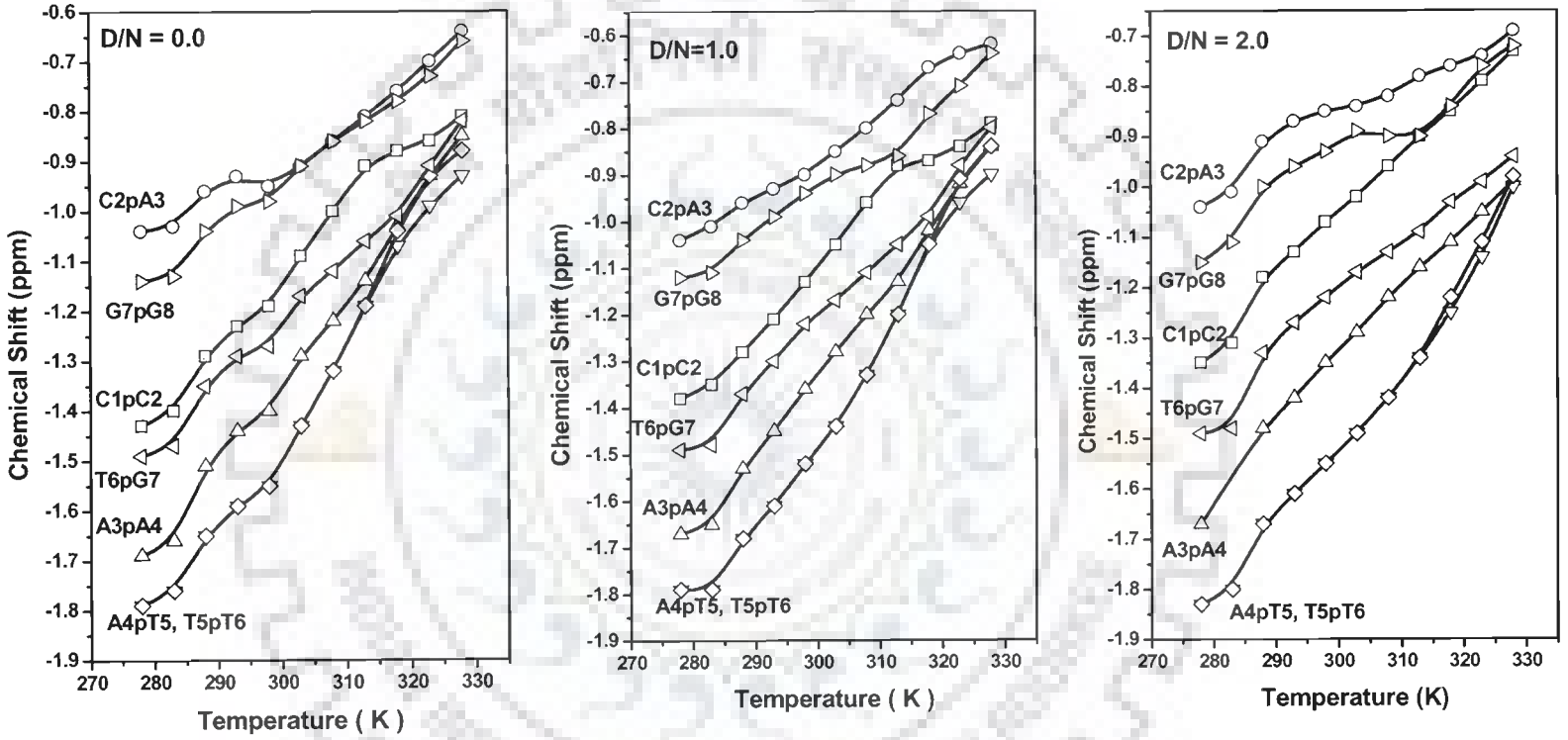


**Figure 6.5: $^{31}$P Chemical shift variation of d-(CCAATTGG)$_2$ in complex with berberine, as a function temperature at different D/N ratio.**

It was observed that double to single strand transition was not much affected by adding low concentration of berberine; while at D/N ratio 2.0 it was affected to a much larger extent (Figure 6.6). This means that when berberine is in higher amount its binding to DNA is tighter and it resists its helix to coil transition. It can be noted from the Figure 6.6 that the maximum effect on chemical shift change due to temperature at D/N 2.0 on berberine binding was found at A3pA4 (Table 6.4). It suggests that berberine binds to A3pA4 site and DNA becomes more resistant to temperature perturbation. It has been already discussed that chemical shift change due to addition of berberine at 283 K was negligible, which excludes directly the intercalation mode of the berberine binding. It has been reported earlier by Mazzini et al that berberine binds to d-$(AAGAATTCTT)_2$ at the minor groove [Mazzini et al., 2003]. Most of the minor groove binding drugs binds to $A_nT_n$ regions and require 4-5 base pair length for good binding [Neidle, 2001].

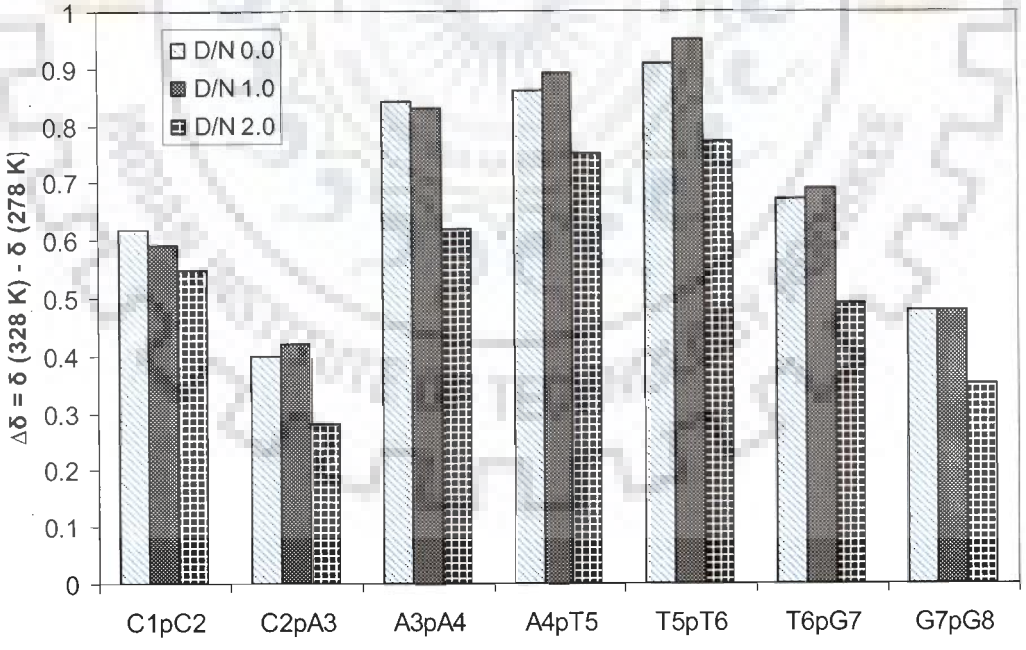


**Figure 6.6: The change in $^{31}P$ chemical shift, $\Delta\delta = \delta_{328K} - \delta_{278K}$, due to temperature in d-$(CCAATTGG)_2$ and in complex with berberine at drug (D) to nucleic acid duplex (N) ratio, D/N = 0, 1.0 and 2.0.**

Our results shows that berberine affects other phosphorus signals temperature dependence in the order of A3pA4> T5pT6> T6pG7> C2pA3> A4pT5> G7pG8> C1pC2 (Figure 6.6) which supports the finding that berberine binds at A3pT4 site of d-$(CCAATTGG)_2$ and significantly effect the neighboring residues. Although $^{31}P$ NMR studies provide information on the conformation of the phosphate ester backbone and the mode of binding of berberine but it is unable to provide detailed information on the overall conformation of the sugar rings and bases of oligonucleotides. Direct inter-proton distances (NOE) which are available through $^{1}H$ NMR studies will be discussed further in this chapter.

### 6.1.2 Proton NMR Studies of Berberine-d-$(CCAATTGG)_2$ Complex

The titration of the octanucleotide d-$(CCAATTGG)_2$ with berberine was carried out at 283 and 298 K with addition of drug at D/N ratio 0.1 to 2.0 with an increment of 0.1. Upon the addition of berberine, a set of new signals corresponding to NMR resonances of berberine proton and slow shift in d-$(CCAATTGG)_2$ protons signals were observed. The 2D NMR experiments of berberine-DNA complex were carried out at 283 K because the imino protons were sharpened and intensified and the DNA was expected to be in duplex state. Figure 6.7a-k show expansions of specific regions of 2D NOESY spectra of berberine complexed to d-$(CCAATTGG)_2$.

The assignment of nucleotide protons was carried out by following the strategies adopted for standard B-DNA structures i.e. sequential NOEs (base $H8/H6)_n$-sugar $(H1')_{n-1}$ (Figure 6.7a), (base $H8/H6)_n$-sugar$(H2'')_{n-1}$ (Figure 6.7b),, (base $H8/H6)_n$-sugar$(H2')_{n-1}$ (Figure 6.7b); expected NOEs due to several short intra nucleotide distances (Figure 6.7c-f) [Wüthrich, 1986] and the NMR data of uncomplexed d-$(CCAATTGG)_2$ (Chapter 5).

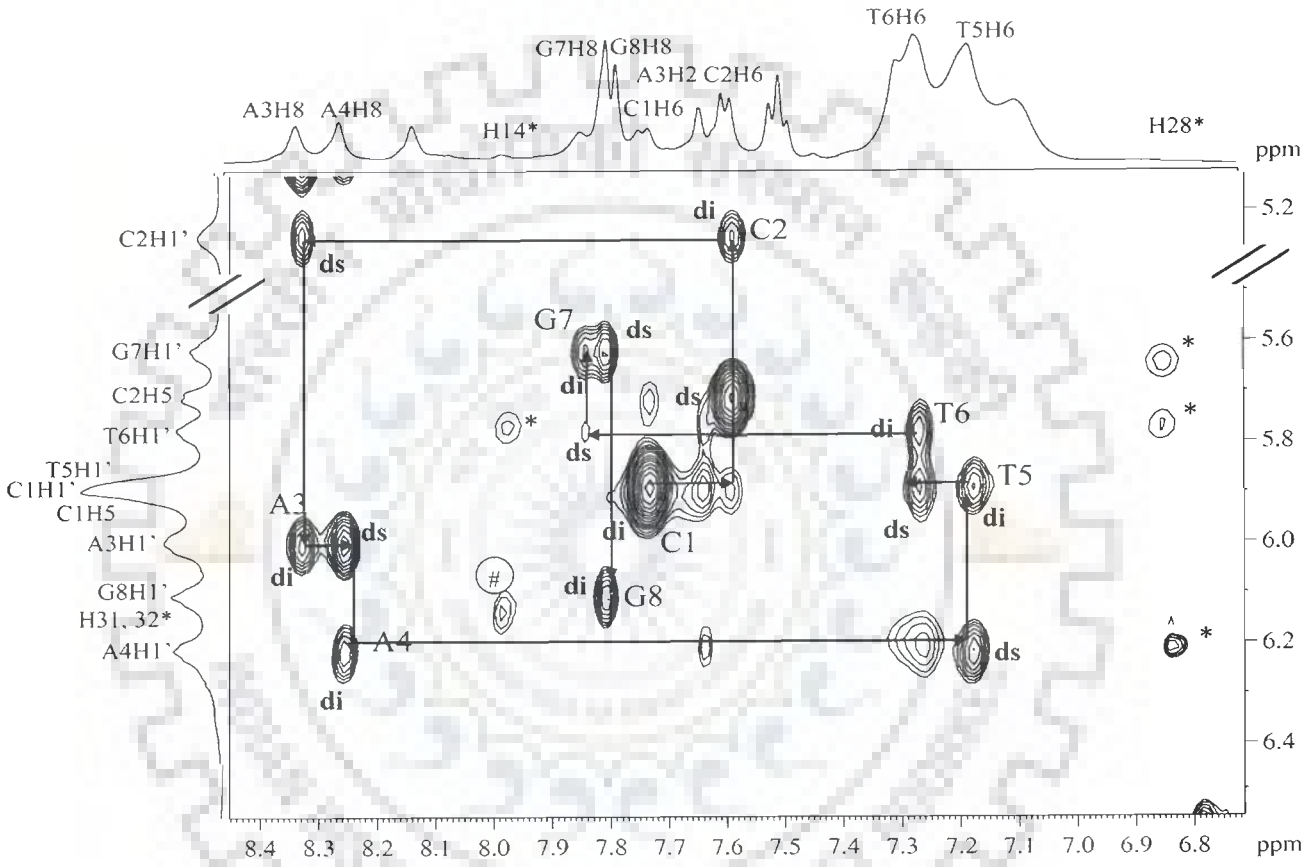


(Fig. 6.7a)

**Figure 6.7 (a-i): Expansions of the specific regions of NOESY spectra of berberine complexed with d-(CCAATTGG)$_2$ to highlight specific connectivities (intramolcular peaks of berberine: "#"present in uncomplxed berberine; "(#)" absent in uncomplexed berberine, "*" Intermolecular peaks in berberine-d-(CCAATTGG)$_2$ complex).**

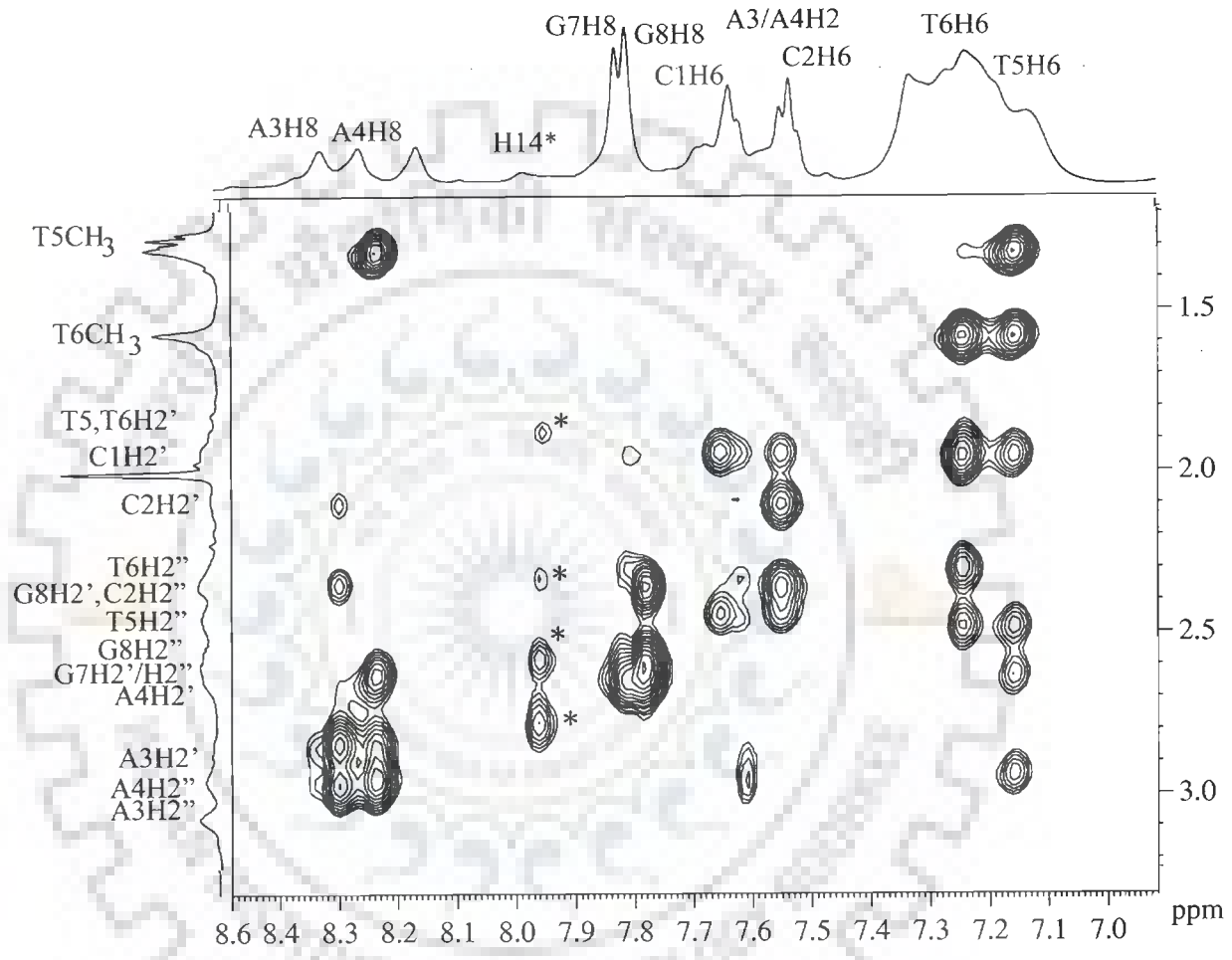
G7H8
G8H8
A3/A4H2
C2H6
T6H6
T5H6
C1H6
A3H8
A4H8
H14*
T5CH3
T6CH3
T5,T6H2'
C1H2'
C2H2'
T6H2"
G8H2',C2H2"
T5H2"
G8H2"
G7H2'/H2"
A4H2'
A3H2'
A4H2"
A3H2"
1.5
2.0
2.5
3.0
ppm
8.6 8.4 8.3 8.2 8.1 8.0 7.9 7.8 7.7 7.6 7.5 7.4 7.3 7.2 7.1 7.0

**(Fig. 6.7b)**

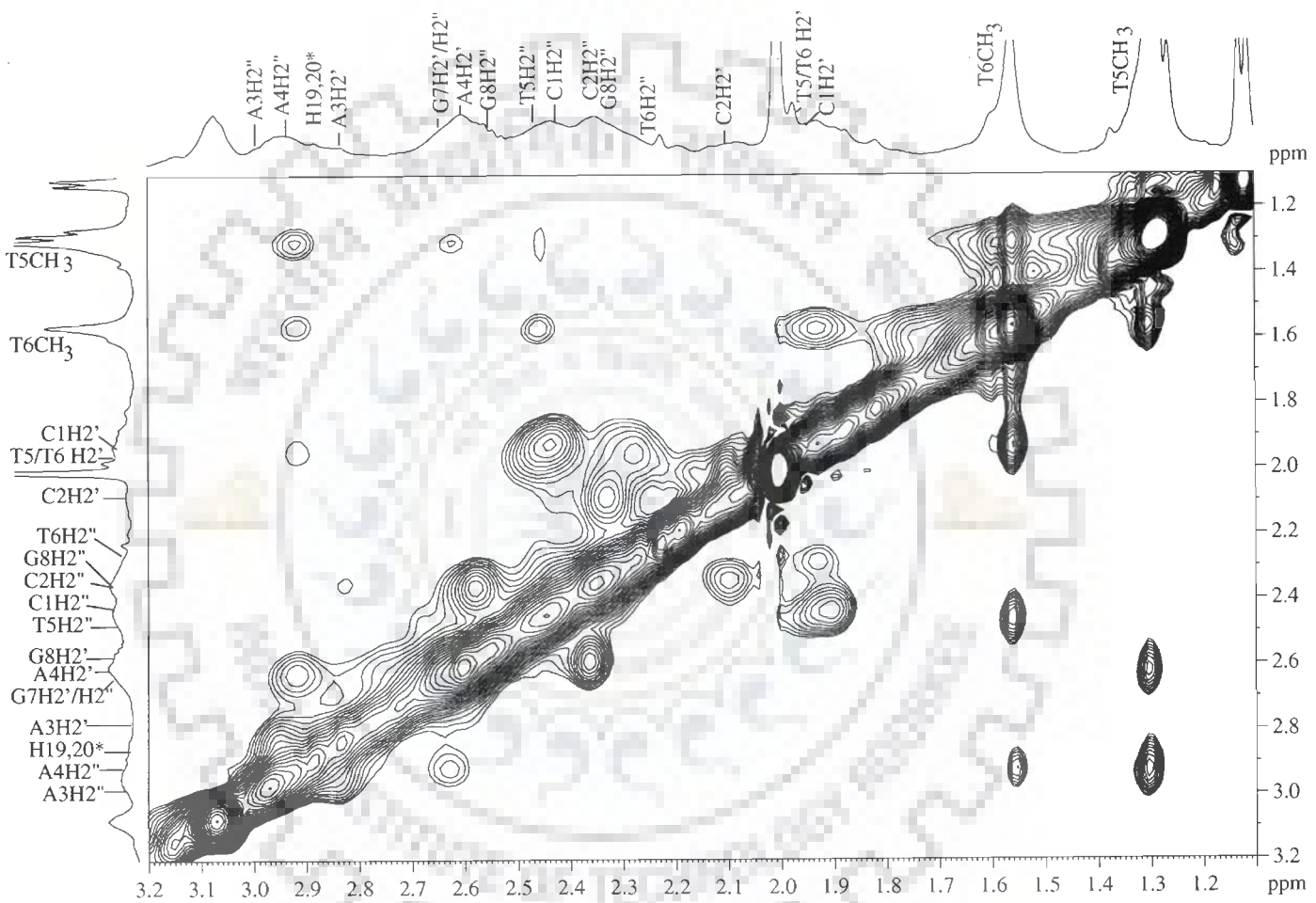
A3H2"
A4H2"
H19,20*
A3H2'
G7H2'/H2"
A4H2'
G8H2"
T5H2"
C1H2"
C2H2"
G8H2"
T6H2"
C2H2'
T5/T6 H2'
C1H2'
T6CH3
T5CH3
ppm
T5CH3
T6CH3
C1H2'
T5/T6 H2'
C2H2'
T6H2"
G8H2"
C2H2"
C1H2"
T5H2"
G8H2'
A4H2'
G7H2'/H2"
A3H2'
H19,20*
A4H2"
A3H2"
1.2
1.4
1.6
1.8
2.0
2.2
2.4
2.6
2.8
3.0
3.2
3.2 3.1 3.0 2.9 2.8 2.7 2.6 2.5 2.4 2.3 2.2 2.1 2.0 1.9 1.8 1.7 1.6 1.5 1.4 1.3 1.2
ppm

**(Fig. 6.7c)**

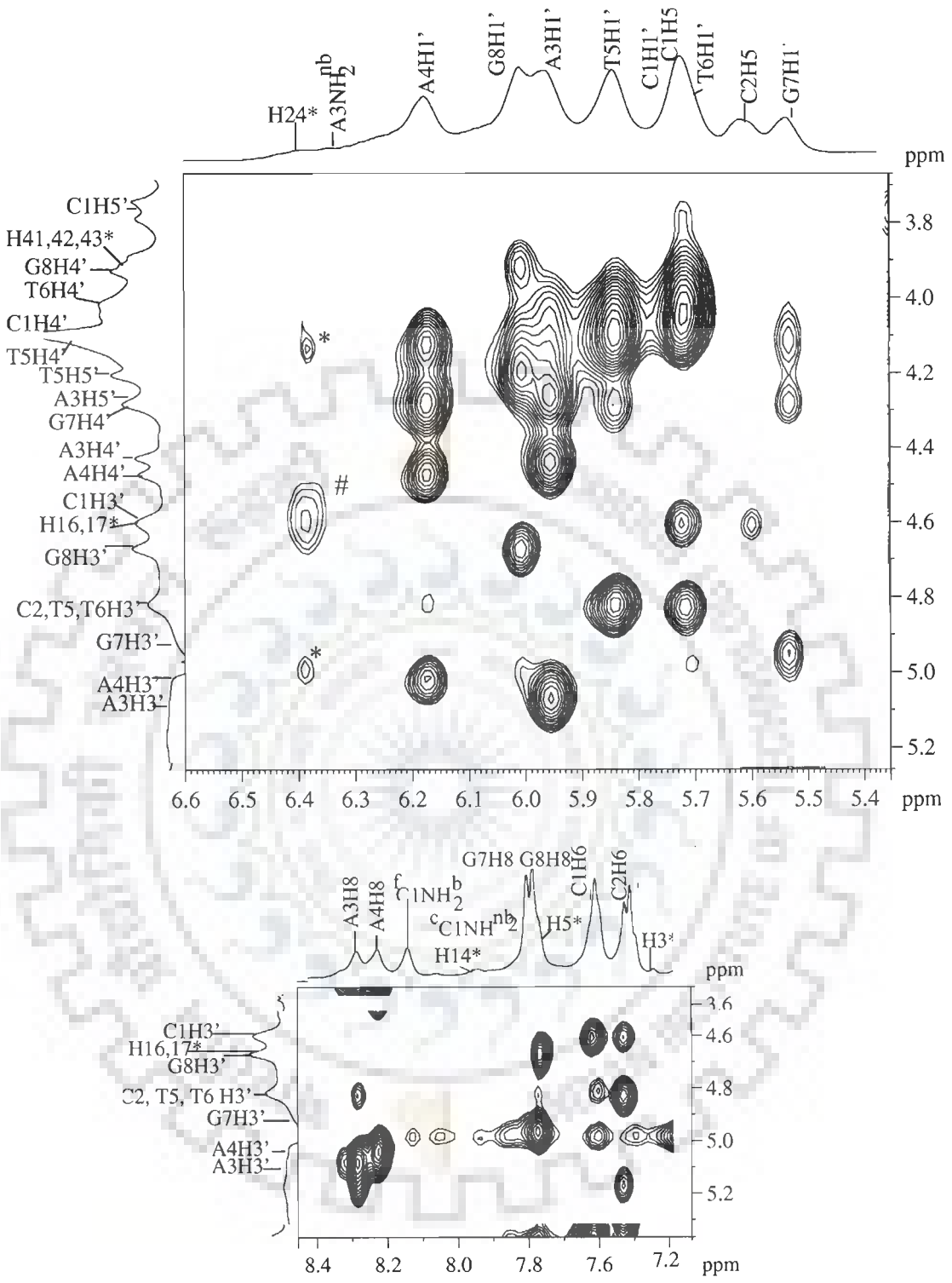
H24*
A3NH2nb
A4H1'
G8H1'
A3H1'
T5H1'
C1H1'
C1H5
T6H1'
C2H5
G7H1'
ppm
C1H5'
H41,42,43*
G8H4'
T6H4'
C1H4'
T5H4'
T5H5'
A3H5'
G7H4'
A3H4'
A4H4'
C1H3'
H16,17*
G8H3'
C2,T5,T6H3'
G7H3'
A4H3'
A3H3'
*
#
6.6 6.5 6.4 6.3 6.2 6.1 6.0 5.9 5.8 5.7 5.6 5.5 5.4 ppm
3.8 4.0 4.2 4.4 4.6 4.8 5.0 5.2
A3H8
A4H8
f C1NH2b
c C1NHnb2
H14*
G7H8 G8H8
C1H6
C2H6
H5*
H3'
ppm
C1H3'
H16,17*
G8H3'
C2, T5, T6 H3'
G7H3'
A4H3'
A3H3'
8.4 8.2 8.0 7.8 7.6 7.2 ppm
3.6 4.6 4.8 5.0 5.2

**(Fig. 6.7d)**

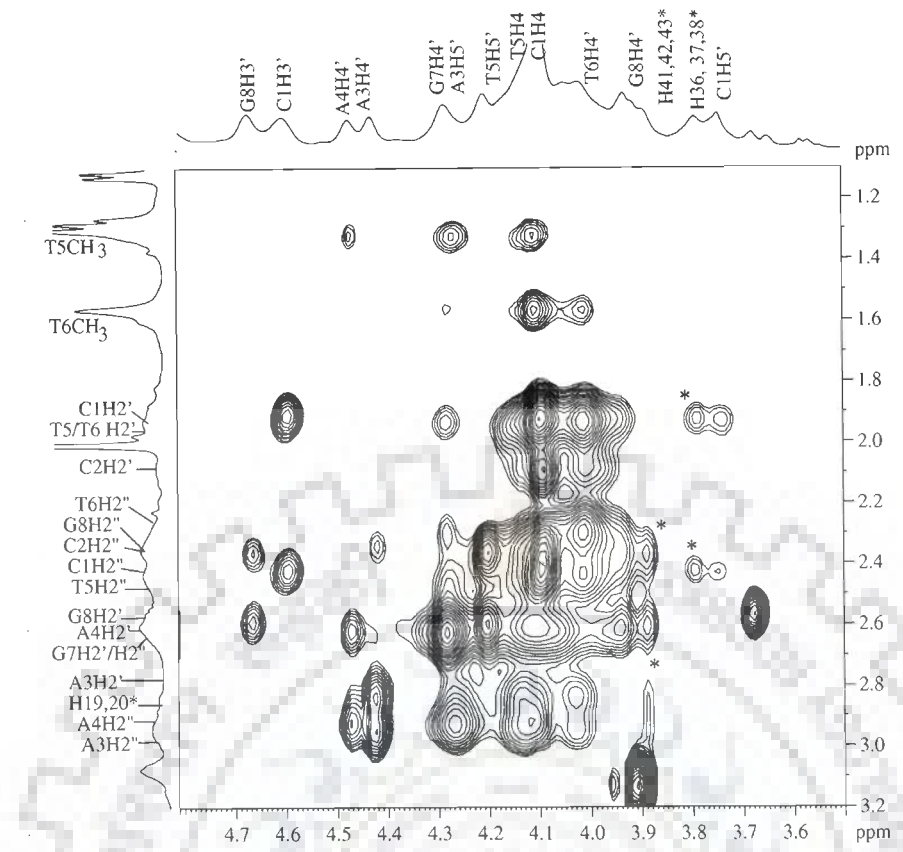


**(Fig. 6.7e)**

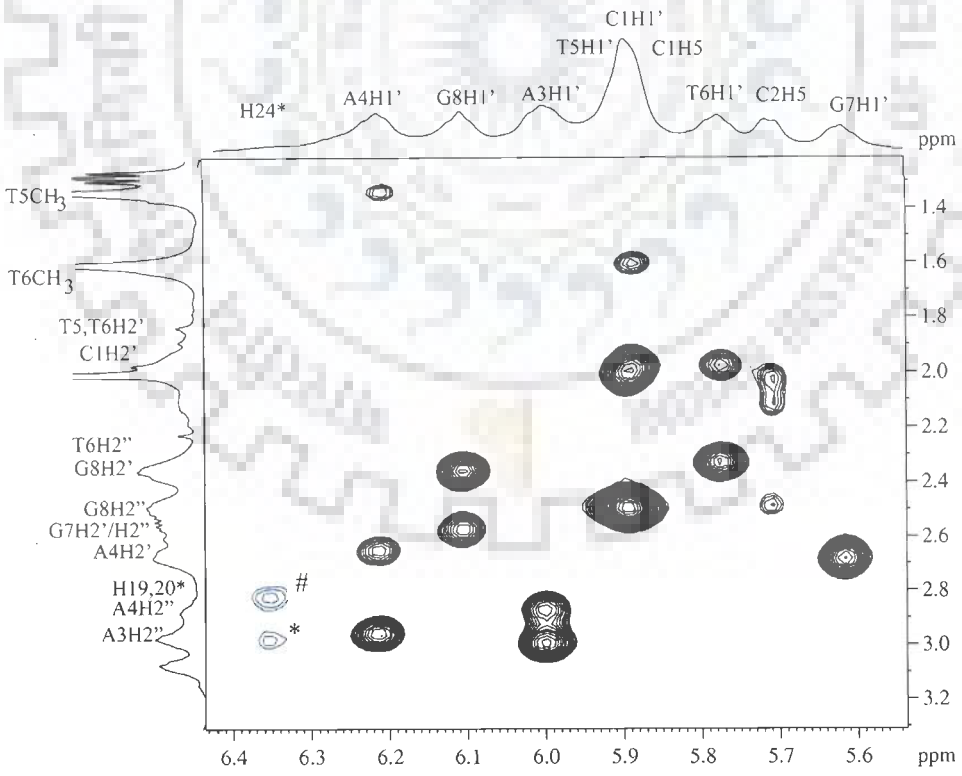


**(Fig. 6.7f)**

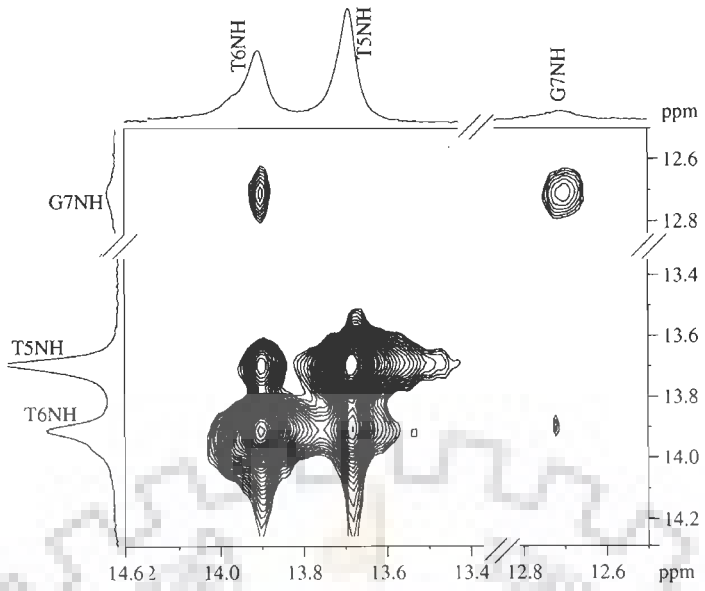


**(Fig 6.7g)**

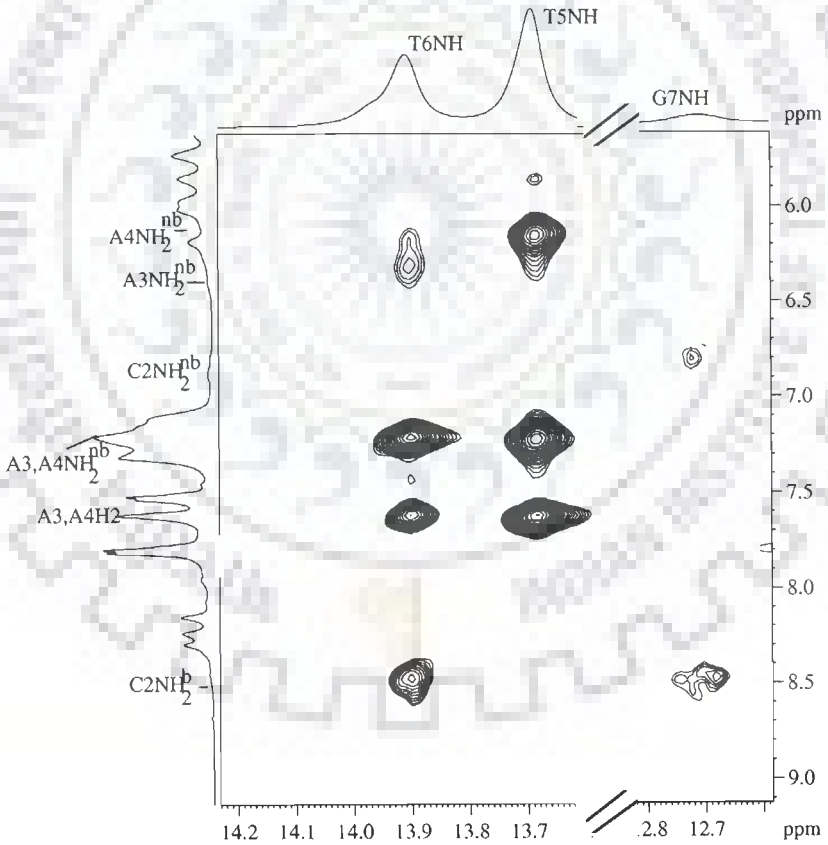


**(Fig. 6.7h)**

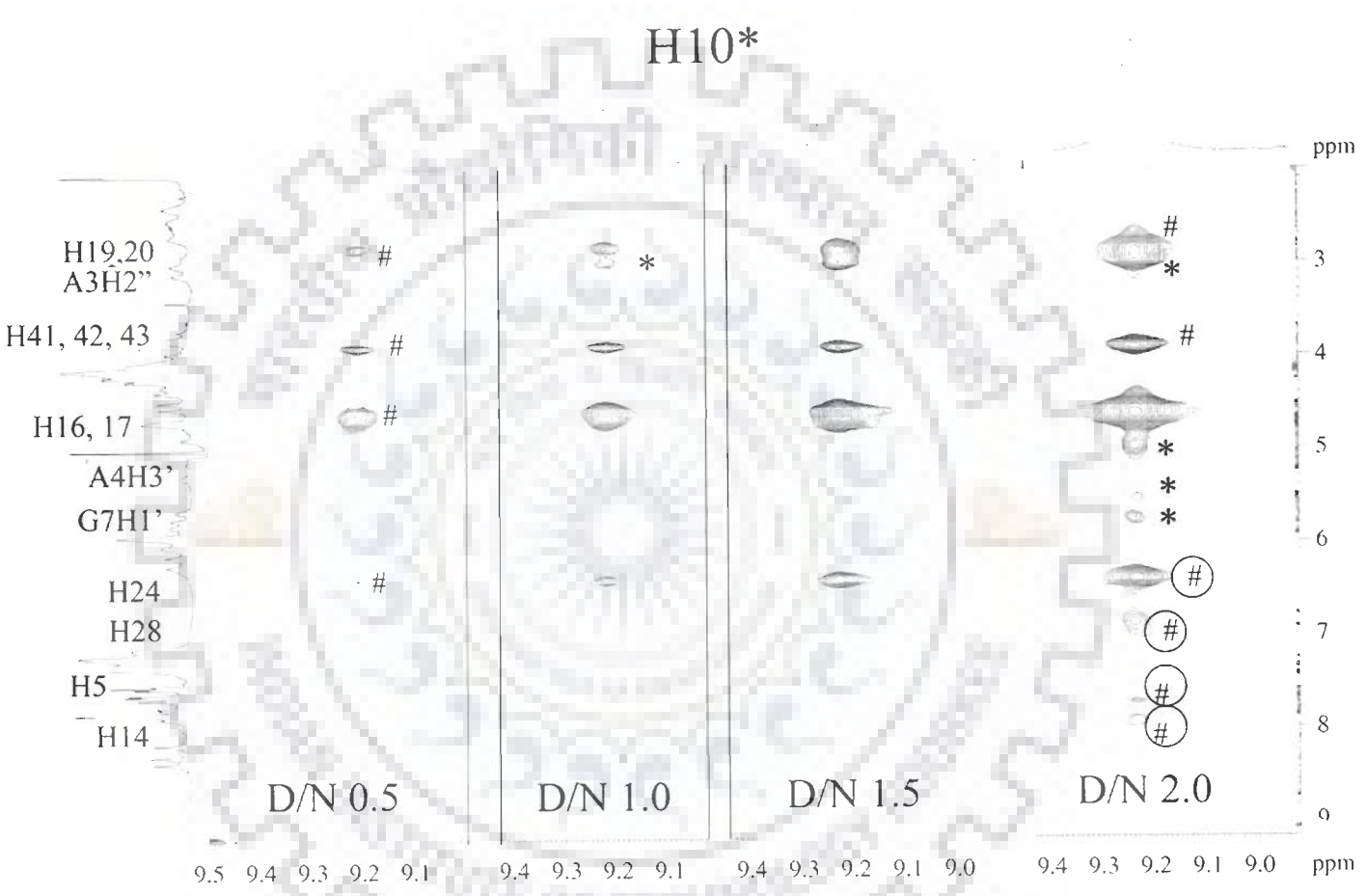
H10*
H19,20
A3H2"
H41, 42, 43
H16, 17
A4H3'
G7H1'
H24
H28
H5
H14
D/N 0.5
D/N 1.0
D/N 1.5
D/N 2.0
ppm
9.5 9.4 9.3 9.2 9.1
9.4 9.3 9.2 9.1
9.4 9.3 9.2 9.1 9.0
9.4 9.3 9.2 9.1 9.0
ppm

**(Fig. 6.7i)**

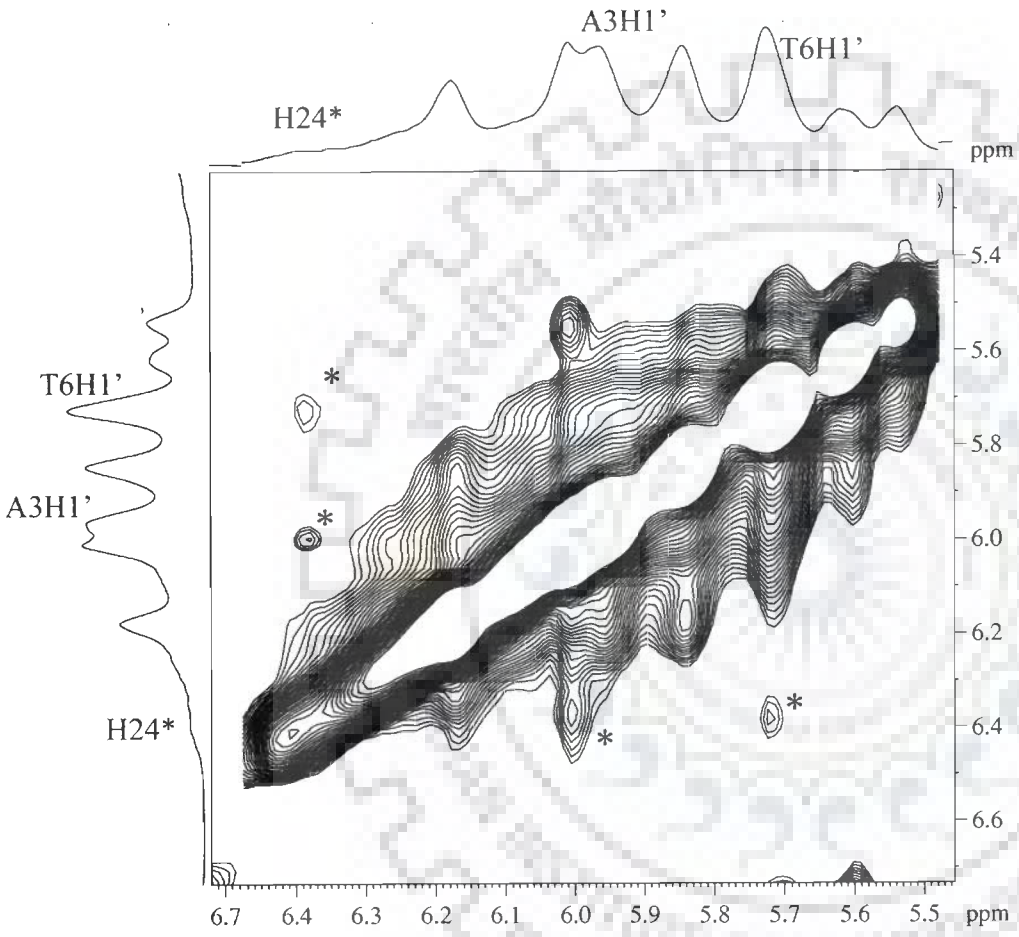


(Fig. 6.7j)

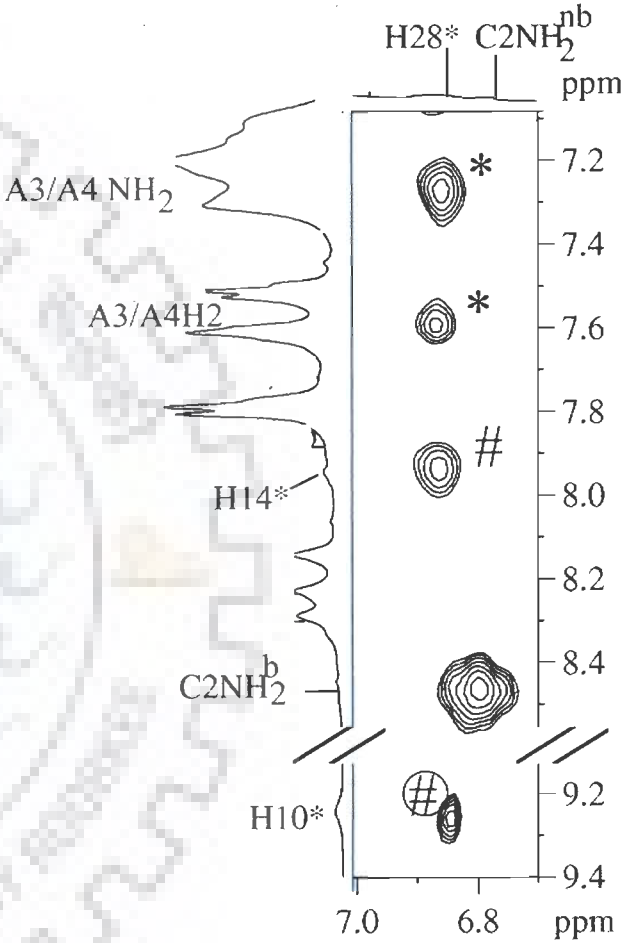


(Fig. 6.7k)

The imino proton was assigned based on the intense cross peak with adenine H2 and NOEs with adenine amino protons of the corresponding base pair (Figure 6.7g-h). The position of each and every resonance was thus ascertained and unambiguous assignment was done. The chemical shift positions of uncomplexed berberine and DNA, berberine-DNA complex (D/N = 2.0) and the change in chemical shift due to binding are given in Tables 6.5 and 6.6. The observed intranucleotide (di), sequential and interstrand sequential peaks for DNA are listed in Table 6.7, 6.8 and 6.9. The assignment of spectral lines to specific protons of berberine was made by following the strategies used for assignment in NMR spectra of uncomplexed berberine (Chapter 3) and the intramolecular peaks observed at different D/N ratios shown by "# and "ⓗ" in all the NOESY spectras (Figure 6.7a-k). All the berberine intramolecular cross peaks are listed in Table 6.10.

### 6.1.2.1 Effects of Titrimetric Addition of Berberine

The titration of octamer d-$(CCAATTGG)_2$ with berberine was carried out at 283 and 298 K. Almost same pattern of change was observed for the all the protons of d-$(CCAATTGG)_2$ upon adding berberine at both the temperatures. It was also noted that chemical shift for d-$(CCAATTGG)_2$ did not change significantly by adding a low amount of berberine. Therefore, data recorded at D/N 0.1 interval and at 298 K has not been shown here. $^1$H 1D NMR spectra of d-$(CCAATTGG)_2$ and change in spectra on successive addition of berberine to DNA at D/N 0.0, 0.5, 1.0, 2.0 at 283 K is shown in Figure 6.8a-e. On addition of berberine to DNA, new resonance peaks pertaining to berberine protons appeared with increase in intensity proportional to D/N ratio.

**Table 6.5: Chemical shift (ppm) of d-(CCAATTGG)$_2$ protons in uncomplexed state ($\delta^f$) and that bound to berberine ($\delta^b$) at drug (D) to nucleic acid duplex (N) ratio D/N=2.0 at 283 K. Also shown here is the change in chemical shift on binding, that is. $\Delta\delta = \delta^b_{(D/N=2.0)} - \delta^f_{(D/N=0.0)}$.**

| Protons | C1 | | | C2 | | | A3 | | | A4 | | |
|---|---|---|---|---|---|---|---|---|---|---|---|---|
| | $\delta_b$ | $\delta_f$ | $\Delta\delta$ | $\delta_b$ | $\delta_f$ | $\Delta\delta$ | $\delta_b$ | $\delta_f$ | $\Delta\delta$ | $\delta_b$ | $\delta_f$ | $\Delta\delta$ |
| H8/H6 | 7.62 | 7.80 | - | 7.53 | 7.61 | -0.08 | 8.29 | 8.35 | -0.06 | 8.23 | 8.27 | -0.04 |
| H1' | 5.71 | 5.97 | - | 5.17 | 5.29 | -0.12 | 5.96 | 6.01 | -0.05 | 6.18 | 6.23 | -0.05 |
| H2' | 1.91 | 2.06 | - | 2.10 | 2.13 | -0.03 | 2.85 | 2.88 | -0.03 | 2.63 | 2.67 | -0.04 |
| H2" | 2.43 | 2.50 | - | 2.10 | 2.39 | 0.29 | 2.96 | 2.99 | -0.03 | 2.93 | 2.97 | -0.04 |
| H3' | 4.60 | 4.53 | 0.07 | 4.83 | 4.67 | 0.16 | 5.07 | 5.11 | -0.04 | 5.02 | 5.06 | -0.04 |
| H4' | - | - | - | 4.14 | 4.06 | +0.08 | 4.45 | 4.46 | -0.01 | 4.43 | 4.52 | -0.09 |
| H5/H2/$CH_3$ | 5.71 | 5.95 | - | 5.61 | 5.74 | 0.13 | 7.61 | 7.66 | -0.05 | 7.61 | 7.66 | -0.05 |
| $NH_2{}^b$ | 7.92 | 8.16 | - | 8.47 | 8.69 | -0.22 | 7.21 | 7.32 | -0.11 | 7.21 | 7.32 | -0.11 |
| $NH_2{}^{nb}$ | 7.33 | 6.97 | - | 8.47 | 8.69 | -0.22 | 6.31 | 6.40 | -0.07 | 6.15 | 6.23 | -0.08 |
| | T5 | | | T6 | | | G7 | | | G8 | | |
| | $\delta_b$ | $\delta_f$ | $\Delta\delta$ | $\delta_b$ | $\delta_f$ | $\Delta\delta$ | $\delta_b$ | $\delta_f$ | $\Delta\delta$ | $\delta_b$ | $\delta_f$ | $\Delta\delta$ |
| H8/H6 | 7.15 | 7.19 | - | 7.23 | 7.29 | -0.06 | 7.84 | 7.86 | -0.02 | 7.77 | 7.83 | -0.06 |
| H1' | 5.85 | 5.90 | - | 5.70 | 5.79 | -0.07 | 5.54 | 5.65 | -0.11 | 6.01 | 6.14 | -0.13 |
| H2' | 1.94 | 1.98 | - | 1.94 | 1.98 | -0.04 | 2.64 | 2.68 | -0.04 | 2.59 | 2.55 | +0.04 |
| H2" | 2.45 | 2.53 | - | 2.28 | 2.35 | -0.07 | 2.64 | 2.68 | -0.04 | 2.37 | 2.35 | +0.02 |
| H3' | 4.83 | 4.67 | 0.16 | 4.83 | 4.67 | 0.16 | 4.98 | 4.87 | +0.11 | 4.68 | 4.53 | +0.15 |
| H4' | 4.06 | 4.19 | - | 4.14 | 4.11 | +0.03 | - | - | - | 4.19 | 4.20 | -0.01 |
| H5/H2/$CH_3$ | 1.31 | 1.36 | - | 1.57 | 1.63 | 0.06 | - | - | - | - | - | - |
| NH | 13.69 | 13.80 | - | 13.93 | 14.05 | -0.12 | 12.71 | 12.94 | -0.23 | - | - | - |

+ve $\Delta\delta$ indicates downfield shift
-ve $\Delta\delta$ indicates upfield shift

**Table 6.6: Chemical shift (ppm) of berberine protons as a function of drug (D) to nucleic acid duplex (N) ratio, D/N, at 283 K. Also shown here is the maximum change in chemical shift due to binding, with respect to berberine in free form.** $\Delta\delta = \delta^{b}_{(D/N=2.0)} - \delta^{f}_{(D/N=0.0)}$.

| Berberine Proton | $\delta_f$ D/N 0.0 | $\delta_b$ D/N 0.5 | $\delta_b$ D/N 1.0 | $\delta_b$ D/N 1.5 | $\delta_b$ D/N 2.0 | $\Delta\delta$ (Present work) | $\Delta\delta^*$ (T5GA) | $\Delta\delta^*$ (A5) | $\Delta\delta^*$ (A2T2) | $\Delta\delta^*$ (GATC) | $\Delta\delta^*$ (TATA) | $\Delta\delta^*$ (TA) | $\Delta\delta^{\#}$ (HP14) |
|---|---|---|---|---|---|---|---|---|---|---|---|---|---|
| **H10** | 9.64 | 9.22 | 9.22 | 9.23 | 9.24 | -0.40 | -0.44 | 0.50 | 0.29 | 0.35 | 0.35 | 0.34 | 0.06 |
| **H14** | 8.46 | 7.95 | 7.95 | 7.95 | 7.98 | -0.48 | -0.67 | 0.69 | 0.55 | 0.62 | 0.49 | 0.49 | 0.11 |
| **H5** | 8.03 | 7.70 | 7.70 | 7.71 | 7.71 | -0.32 | -0.65 | 0.51 | 0.38 | 0.41 | 0.40 | 0.38 | 0.05 |
| **H3** | 7.93 | 7.47 | 7.47 | 7.48 | 7.49 | -0.44 | -0.28 | - | 0.20 | 0.18 | 0.23 | 0.22 | 0.07 |
| **H28** | 7.47 | 6.88 | 6.88 | 6.89 | 6.89 | -0.58 | -0.20 | 0.89 | 0.54 | 0.62 | 0.49 | 0.50 | 0.03 |
| **H24** | 6.96 | 6.38 | 6.38 | 6.38 | 6.38 | -0.58 | -0.27 | 0.57 | 0.38 | 0.52 | 0.38 | 0.38 | 0.06 |
| **H31,32** | 6.10 | 6.14 | 6.14 | 6.14 | 6.15 | +0.05 | - | - | 0.13 | 0.14 | - | 0.12 | 0.02 |
| **H16, 17** | 4.90 | 4.56 | 4.60 | 4.60 | 4.60 | -0.30 | -0.24 | - | 0.17 | 0.22 | - | 0.13 | - |
| **H41,42,43** | 4.12 | 3.91 | 3.93 | 3.93 | 3.93 | -0.20 | -0.26 | 0.30 | 0.13 | 0.13 | 0.13 | 0.19 | - |
| **H36,37,38** | 4.05 | 3.79 | 3.79 | 3.79 | 3.80 | -0.26 | -0.33 | 0.30 | 0.15 | 0.15 | 0.20 | 0.24 | - |
| **H19,20** | 3.17 | 2.83 | 2.83 | 2.83 | 2.84 | -0.24 | -0.39 | 0.40 | 0.24 | 0.26 | 0.24 | - | 0.04 |

*-[Mazzini et al., 2003]
#- [Jeon et al., 2002]
+ve $\Delta\delta$ indicates downfield shift
-ve $\Delta\delta$ indicates upfield shift

**Table 6.7: Interproton distance (Å) obtained from intra nucleotide NOE connectivities (di) of base to sugar protons , sugar -sugar protons, and base to base protons of d-$(CCAATTGG)_2$ in berberine- d-$(CCAATTGG)_2$ complex estimated from NOESY spectra. The strong intense (ss), strong (s), medium (m), weak (w), very weakly (vw) intense cross peaks correspond to distances in the range ss 1.8 - 2.5 Å, s 2.5 - 3.0 Å, m 3.0 - 3.5 Å, w 3.5 - 4.0 Å, vw 4.0 - 5.0 Å, respectively.**

| | H8/H6- H1' | | | H8/H6-H2' | | | H8/H6-H2" | | | H8/H6-H3' | | |
|---|---|---|---|---|---|---|---|---|---|---|---|---|
| | Intensity | Strand I | Strand II | Intensity | Strand I | Strand II | Intensity | Strand I | Strand II | Intensity | Strand I | Strand II |
| C1 | m (o) | 2.77 | 3.83 | s | 3.40 | 2.65 | s | 4.36 | 2.23 | s | 4.22 | 4.47 |
| C2 | m | 3.65 | 3.79 | s | 2.25 | 2.39 | s(o) | 3.03 | 2.25 | s | 4.66 | 4.52 |
| A3 | s | 3.50 | 3.92 | s (o) | 4.85 | 4.70 | s(o) | 4.18 | 4.28 | s(o) | 5.55 | 4.38 |
| A4 | s | 3.76 | 3.81 | s | 3.76 | 5.26 | s(o) | 4.79 | 5.43 | s(o) | 4.49 | 4.45 |
| T5 | s | 3.42 | 3.49 | m | 3.13 | 4.73 | s | 4.34 | 3.84 | s | 4.58 | 5.48 |
| T6 | s | 3.77 | 3.95 | s | 3.30 | 3.56 | s | 2.01 | 4.71 | s(o) | 4.21 | 3.40 |
| G7 | s | 3.89 | 3.87 | s (o) | 3.72 | 3.46 | s(o) | 2.36 | 2.29 | s | 4.44 | 4.63 |
| G8 | s | 3.92 | 3.81 | s (o) | 3.90 | 3.61 | s(o) | 2.52 | 2.13 | s | 4.57 | 4.02 |
| | H8/H6-H4' | | | H1'- H2' | | | H1'- H2" | | | H1'- H3' | | |
| | Intensity | Strand I | Strand II | Intensity | Strand I | Strand II | Intensity | Strand I | Strand II | Intensity | Strand I | Strand II |
| C1 | m | 5.68 | 4.68 | m | 2.67 | 2.37 | s | 3.10 | 3.06 | s | 3.82 | 3.81 |
| C2 | s | 5.55 | 4.84 | - | 2.34 | 2.50 | - | 3.06 | 3.09 | - | 3.85 | 3.70 |
| A3 | m | 4.55 | 4.14 | s | 2.65 | 2.12 | s | 2.91 | 3.06 | ss | 3.58 | 4.22 |
| A4 | m | 5.09 | 4.96 | m | 2.26 | 2.35 | s | 2.98 | 2.64 | s | 3.53 | 3.86 |
| T5 | m | 4.50 | 4.54 | m | 2.88 | 2.71 | s | 3.13 | 3.22 | ss | 3.70 | 4.00 |
| T6 | m | 4.95 | 4.89 | m | 1.75 | 2.41 | s | 3.09 | 3.02 | s | 3.95 | 3.94 |
| G7 | m | 4.85 | 5.17 | s | 2.50 | 2.43 | | 3.08 | 3.07 | m | 3.92 | 3.78 |
| G8 | m | 4.85 | 4.63 | s | 2.41 | 2.37 | s | 3.08 | 3.07 | s | 3.89 | 4.06 |
| Base-Base | H1'- H4' | | | H2'-H4' | | | H2"-H4' | | | $CH_3$-H6/ H5-H6 | | |
| | Intensity | Strand I | Strand II | Intensity | Strand I | Strand II | Intensity | Strand I | Strand II | Intensity | Strand I | Strand II |
| C1 | s | 4.02 | 3.54 | s | 3.36 | 4.20 | s | 4.30 | 3.78 | s(o) | 2.06 | 2.40 |
| C2 | - | 3.41 | 3.11 | m | 3.85 | 4.14 | m | 4.11 | 3.74 | s | 2.40 | 2.40 |
| A3 | ss | 2.02 | 3.75 | m | 3.91 | 3.75 | m | 3.55 | 4.88 | | | |
| A4 | s | 1.85 | 3.76 | m | 2.72 | 2.90 | m | 3.62 | 4.19 | | | |
| T5 | - | 1.89 | 2.82 | ss | 3.74 | 3.97 | ss | 3.84 | 3.81 | ss | 2.83 | 3.61 |
| T6 | - | 3.41 | 2.71 | ss | 4.10 | 2.69 | ss | 3.76 | 3.71 | ss | 2.35 | 2.46 |
| G7 | m | 3.88 | 3.22 | - | 4.14 | 4.13 | | 3.79 | 3.82 | | | |
| G8 | m | 3.44 | 3.75 | m | 4.15 | 4.14 | m | 3.88 | 3.96 | | | |

**Table 6.8: Interproton distance (Å) obtained from Sequential NOE connectivities (ds) of d-(CCAATTGG)$_2$ protons of the berberine - d-(CCAATTGG)$_2$ complex at D/N = 2.0 at 283 K estimated from NOESY spectra recorded with 200ms mixing time (Fig. 4.8) The strong intense (ss), strong (s), medium (m), weak (w), very weakly (ww) intense cross peaks correspond to distances in the range ss 1.8 - 2.5 Å, s 2.5 - 3.0 Å, m 3.0 - 3.5 Å, w 3.5 - 4.0 Å, vw 4.0 - 5.0 Å, respectively.**

| Base-Sugar | C1pC2 | | | C2pA3 | | | A3pA4 | | | A4pT5 | | |
|---|---|---|---|---|---|---|---|---|---|---|---|---|
| | Intensity | Strand I | Strand II | Intensity | Strand I | Strand II | Intensity | Strand I | Strand II | Intensity | Strand I | Strand II |
| H1'-H6/H8 | S (o) | 4.80 | 3.27 | M (o) | 4.25 | 2.56 | s | 4.68 | 5.08 | m | 5.78 | 2.90 |
| H1'-H5/CH3 | - | 4.85 | 4.12 | | | | | | | m | 5.74 | 4.19 |
| H2'-H6/H8 | m | 2.70 | 2.39 | w | 3.14 | 3.38 | M (o) | 3.56 | 3.49 | m | 3.36 | 2.06 |
| H2"-H6/H8 | S (o) | 3.55 | 2.84 | m | 2.29 | 2.20 | M (o) | 2.13 | 3.13 | s | 4.76 | 3.78 |
| H2'-H5/CH3 | m | 2.70 | 3.27 | | | | | | | w | 4.24 | 2.35 |
| H2"-H5/CH3 | w | 4.30 | 3.61 | | | | | | | m | 5.77 | 3.48 |
| H3'-H6/H8/ | m | 4.02 | 5.08 | w | 4.46 | 4.52 | W (o) | 3.65 | 2.05 | W (o) | 5.23 | 4.30 |
| H3'-H5/CH3 | w | 4.67 | 5.79 | | | | | | | | 5.47 | 4.89 |
| H2"-H2' | | 3.33 | 3.87 | | 4.52 | 6.35 | (o) | 4.31 | 4.42 | | 4.60 | 5.51 |
| H6-H5 | | 5.57 | 3.75 | | | | | | | | | |
| H6-H8 | | | | w | 4.64 | 4.83 | | | | | | |
| H2-H2 | | | | | | | | 3.78 | 3.78 | | | |
| H8-H8 | | | | | | | | 4.38 | 6.14 | | | |
| H8-CH3 | | | | | | | | | | s | 2.73 | |
| | T5pT6 | | | T6pG7 | | | G7pG8 | | | | | |
| | Intensity | Strand I | Strand II | Intensity | Strand I | Strand II | Intensity | Strand I | Strand II | Intensity | Strand I | Strand II |
| H1'-H6/H8 | m | 5.06 | 2.90 | w | 3.14 | 5.11 | o | 3.12 | 3.91 | | | |
| H1'-H5/CH3 | m | 4.35 | 4.19 | | | | | | | | | |
| H2'-H6/H8 | m | 2.47 | 2.06 | (0) | 1.96 | 2.30 | S (o) | 1.97 | 2.36 | | | |
| H2"-H6/H8 | s | 3.12 | 3.78 | (0) | 3.54 | 3.56 | S (o) | 3.51 | 4.03 | | | |
| H2'-H5/CH3 | S (o) | 2.41 | 2.35 | | | | | | | | | |
| H2"-H5/CH3 | m | 3.50 | 3.07 | | | | | | | | | |
| H3'-H6/H8/ | M (o) | 4.74 | 4.30 | w | 4.56 | 4.11 | S (o) | 4.62 | 4.60 | | | |
| H3'-H5/CH3 | | 4.54 | 4.89 | | | | | | | | | |
| H6-H8 | | | | vw | 4.51 | 5.02 | | | | | | |
| H2"-H2' | | 3.68 | 5.51 | | 3.84 | 3.81 | | 3.95 | 4.18 | | | |
| Me-Me | s | 3.91 | 2.71 | | | | | | | | | |

**Table 6.9: NOE connnectivities observed in NOESY spectra for exchangeable protons of the berberine - $(CCAATTGG)_2$ complex at Drug/DNA ratio (D/N) = 2.0 at 283 K. The strong intense (ss), strong (s), medium (m), weak (w), very weakly (ww) intense cross peaks correspond to distances in the range ss 1.8 - 2.5 Å, s 2.5 - 3.0 Å, m 3.0 - 3.5 Å, w 3.5 - 4.0 Å, vw 4.0 - 5.0 Å, respectively.**

| Cross peak | NOE Intensity | Cross peak | NOE Intensity |
|---|---|---|---|
| G7NH - $C2NH_2^{b}$ | m | T6NH - $C2NH_2^{nb}$ | m |
| G7NH - $C2NH_2^{nb}$ | m | T6NH - $C2NH_2^{b}$ | m |
| $A4NH_2^{b}$ - T5NH | s | $A3NH_2^{b}$ - G2NH | vw |
| $A4NH_2^{nb}$ - T5NH | s | G7NH-T6NH | m |
| T5NH-A4H2 | s | T6NH-T5NH | m |
| $A3NH_2^{b}$ - T6NH | s | | |
| $A3NH_2^{nb}$ - T6NH | s | | |
| T6NH-A3H2 | s | | |

**Table 6.10: Relative intensities of intramolecular NOE cross peaks within the berberine molecule in the berberine-d-$(CCAATTGG)_2$ complex at D/N = 2.0, at 283. The strong intense (ss), strong (s), medium (m), weak (w), very weakly (ww) intense cross peaks correspond to distances in the range ss 1.8 - 2.5 Å, s 2.5 - 3.0 Å, m 3.0 - 3.5 Å, w 3.5 - 4.0 Å, vw 4.0 - 5.0 Å, respectively in the NOESY spectra.**

| S. No. | Cross peak | Intensity | distances (Å) from rMD |
|---|---|---|---|
| 1. | H10-H19,20 | s | 2.59 |
| 2. | H10-H41,42,43 | m | 3.45 |
| 3. | H10-H24 | s | 2.80 |
| 4. | H10-H28 | m | 4.81 |
| 5. | H14-H31,32 | m | 4.90 |
| 6. | H14-H28 | s | 2.49 |
| 7. | H24-H16,17 | m | 4.66 |
| 8. | H31,32-H14 | m | 4.83 |
| 9. | H16,17-H10 | s | 2.55 |
| 10. | H10-H14 | m | 3.84 |
| 11. | H10-H5 | w | 5.21 |
| 12. | H24-H19, 20 | s | 2.34 |

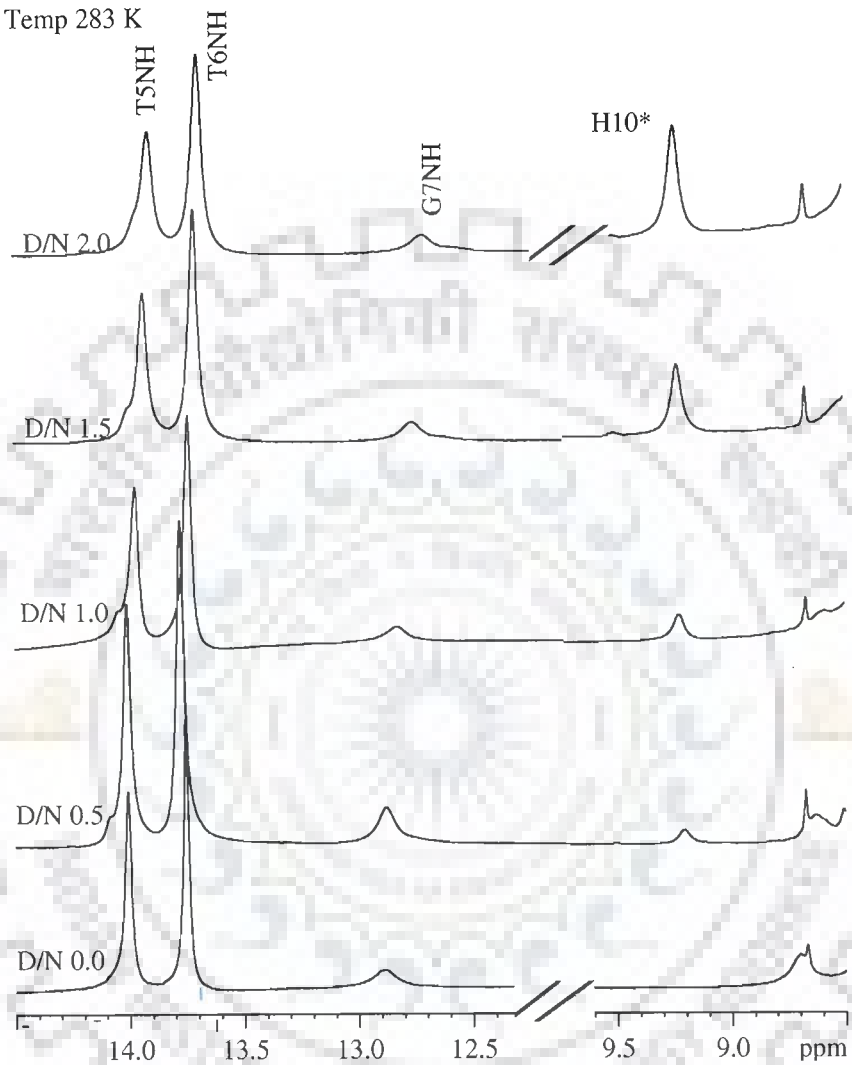


**(Fig. 6.7 a)**

**Figure 6.8 a-e: Proton NMR spectra of complex of berberine with d-(CCAATTGG)$_2$ as a function of D/N ratio at 278 K ( * berbrine proton in berberine -d-(CCAATTGG)$_2$ complex).**

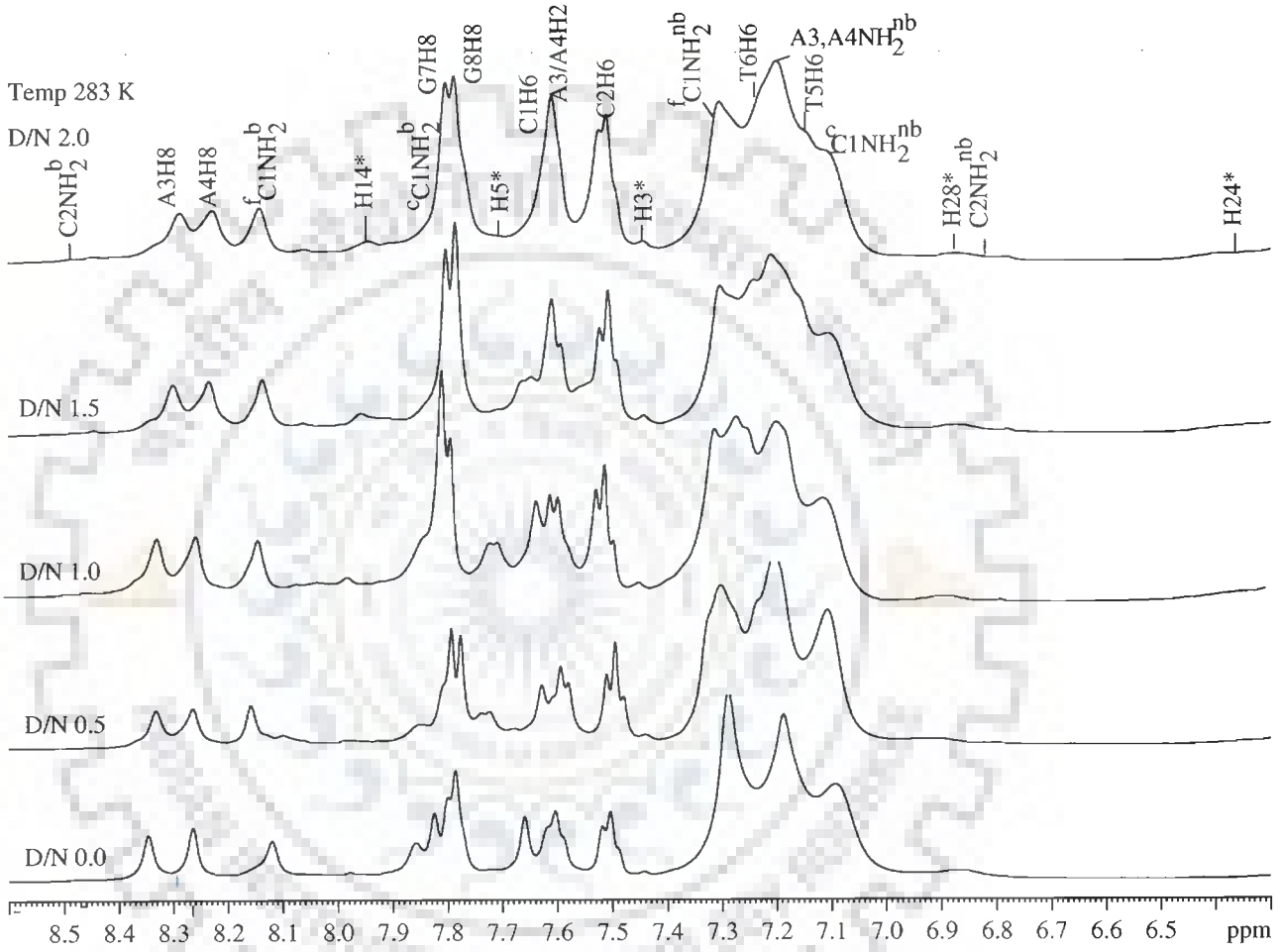
Temp 283 K
D/N 2.0
D/N 1.5
D/N 1.0
D/N 0.5
D/N 0.0
C2NH2b
A3H8
A4H8
fC1NH2b
H14*
cC1NH2b
G7H8
G8H8
H5*
C1H6
A3/A4H2
C2H6
H3*
fC1NH2nb
T6H6
T5H6
A3,A4NH2nb
cC1NH2nb
H28*
C2NH2nb
H24*
8.5 8.4 8.3 8.2 8.1 8.0 7.9 7.8 7.7 7.6 7.5 7.4 7.3 7.2 7.1 7.0 6.9 6.8 6.7 6.6 6.5 ppm

**(Fig. 6.8b)**

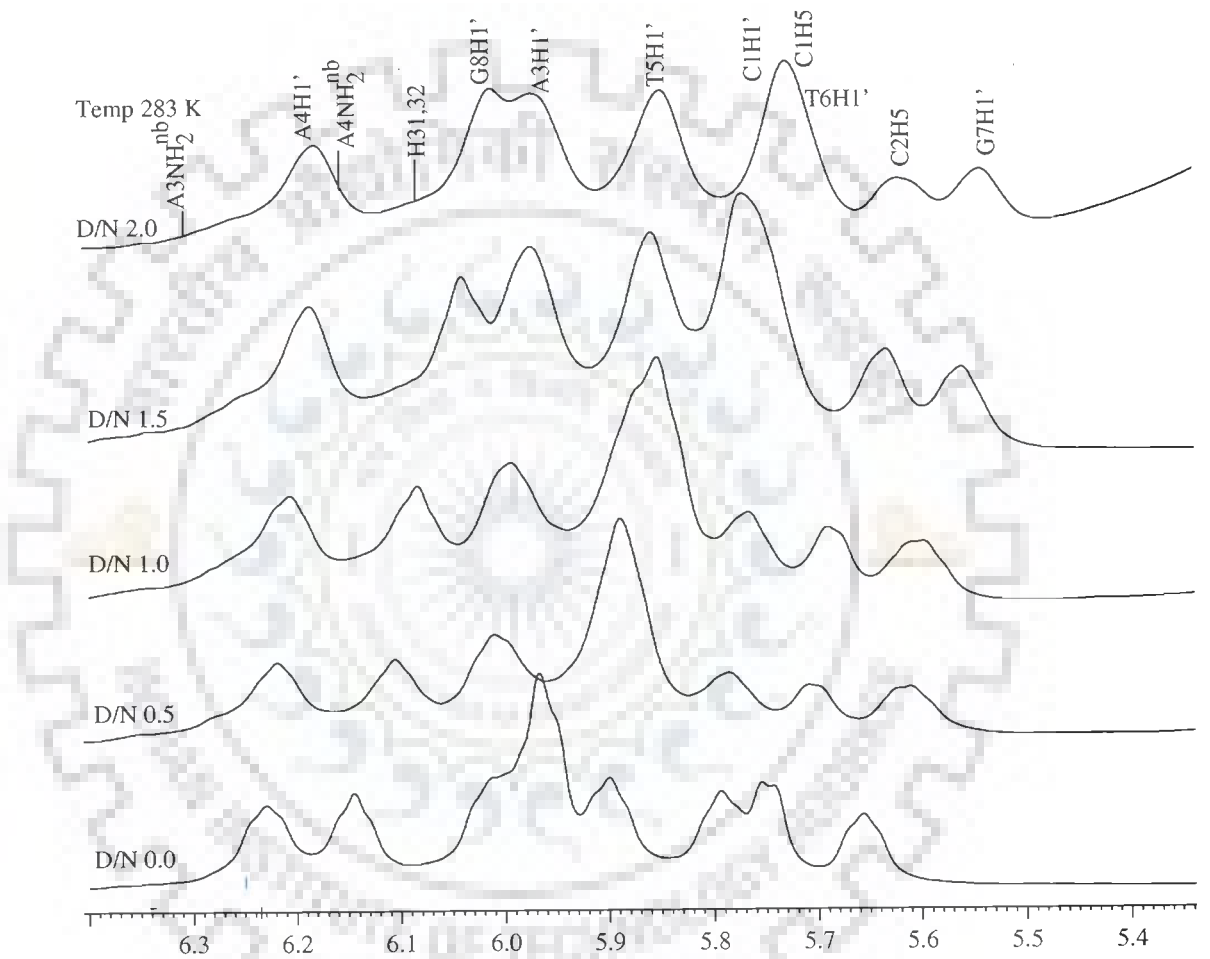
Temp 283 K
A3NH2nb
A4H1'
A4NH2nb
H31,32
G8H1'
A3H1'
T5H1'
C1H1'
C1H5
T6H1'
C2H5
G7H1'
D/N 2.0
D/N 1.5
D/N 1.0
D/N 0.5
D/N 0.0
6.3
6.2
6.1
6.0
5.9
5.8
5.7
5.6
5.5
5.4

**(Fig. 6.8c)**

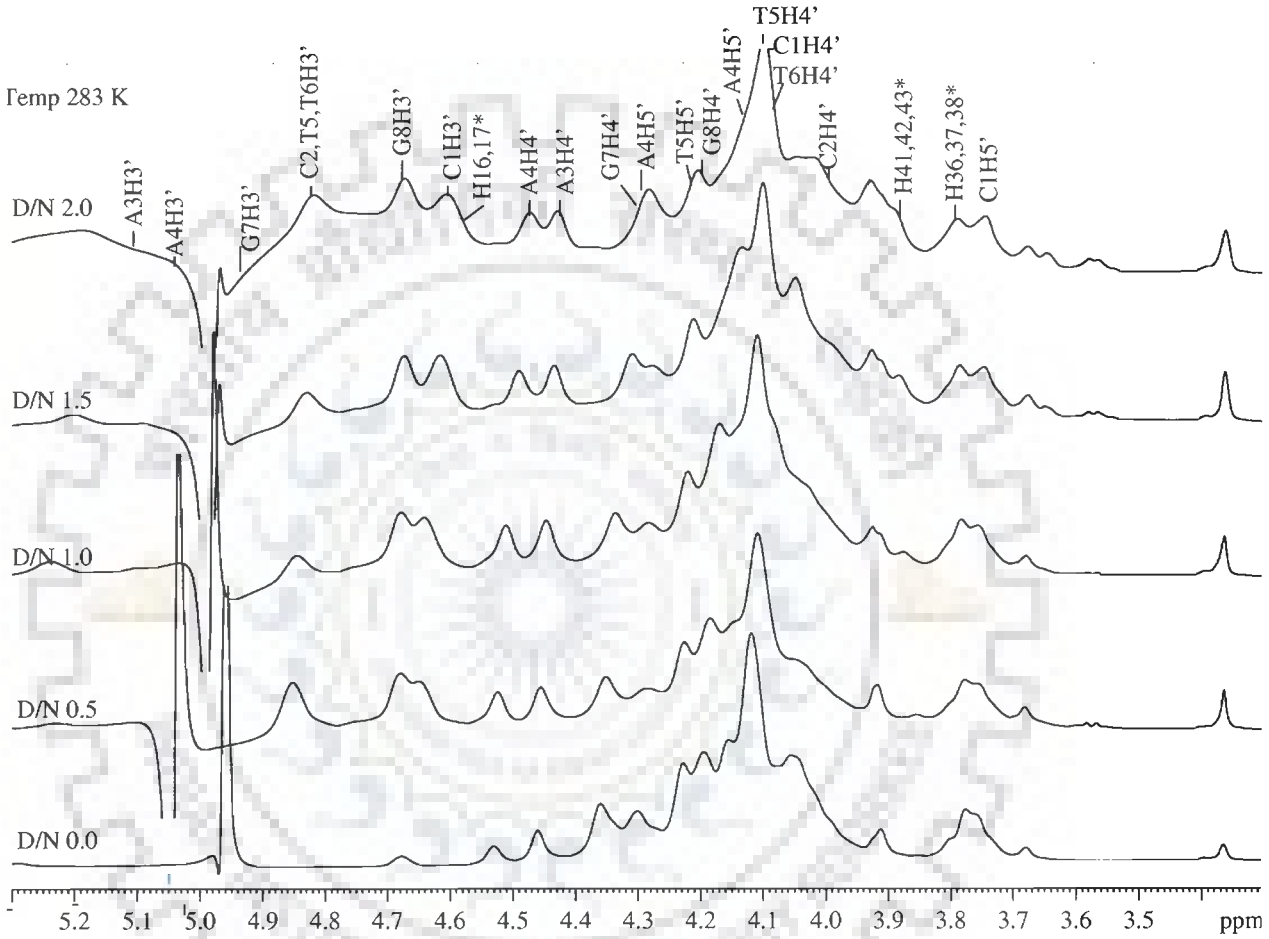
Temp 283 K
D/N 2.0
D/N 1.5
D/N 1.0
D/N 0.5
D/N 0.0
A3H3'
A4H3'
G7H3'
C2,T5,T6H3'
G8H3'
C1H3'
H16,17*
A4H4'
A3H4'
G7H4'
A4H5'
T5H5'
G8H4'
A4H5'
T5H4'
C1H4'
T6H4'
C2H4'
H41,42,43*
H36,37,38*
C1H5'
5.2
5.1
5.0
4.9
4.8
4.7
4.6
4.5
4.4
4.3
4.2
4.1
4.0
3.9
3.8
3.7
3.6
3.5
ppm

**(Fig. 6.8d)**

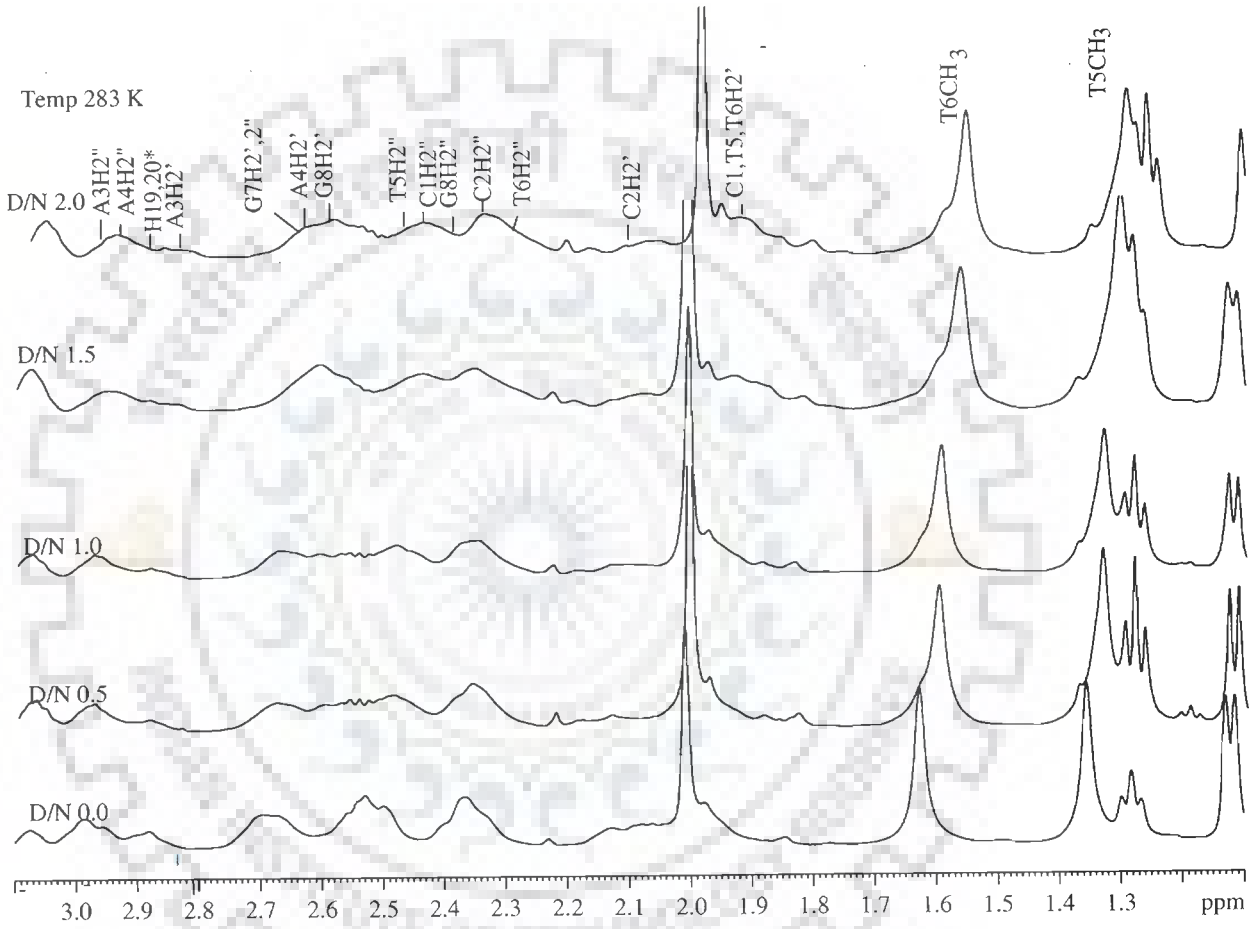
Temp 283 K
D/N 2.0
D/N 1.5
D/N 1.0
D/N 0.5
D/N 0.0
A3H2"
A4H2"
H19,20*
A3H2'
G7H2',2"
A4H2'
G8H2'
T5H2"
C1H2"
G8H2"
C2H2"
T6H2"
C2H2'
C1,T5,T6H2'
T6CH3
T5CH3
3.0 2.9 2.8 2.7 2.6 2.5 2.4 2.3 2.2 2.1 2.0 1.9 1.8 1.7 1.6 1.5 1.4 1.3 ppm

**(Fig. 6.8e)**

There were only one set of DNA resonances and one set of bound berberine resonances observed through out the titration. Titration of the duplex with berberine produced gradual changes in the chemical shift with increasing concentration of berberine which is typical of fast exchange on the chemical shift time scale. The spectral lines broadened uniformly at higher ratios indicating the binding of berberine to d-$(CCAATTGG)_2$. Figure 6.9 shows the change in proton chemical shift for berberine as a function of D/N ratio. It shows that the chemical shift change for bound berberine protons from values for free berberine was maximum at low D/N ratio and remain constant through out titration, which indicates that maximum amount of berberine added to duplex was in bound form. The resonances of berberine were considerably broad and showed upfield shift w.r.t to free berberine which was up to 0.58 ppm (Table 6.6). Maximum upfield shift in berberine protons was found to be 0.58 ppm for H24 and H28 protons, which are located on the D ring of berberine (Figure 3.1). Berberine protons H10, H16, 17, and H19, 20 located on the concave side of berberine molecule showed upfield shift of 0.41, 0.30 and 0.24 ppm respectively while the protons located on convex side i.e. H14, H5 and H3, showed 0.48, 0.32 and 0.44 ppm shift respectively. Side group protons of berberine, H41, 42, 43, and H36, 37, 38 showed an upfield shift of 0.20 and 0.26 ppm respectively. It can be noted that very little downfield shift (0.5 ppm) was observed for H31, 32 which suggests that the whole central part of the berberine was participating in the interaction with DNA, while H31, 32 which is located towards one end of berberine (ring D; Figure 3.1) was least interacting. Our results are in accordance with earlier structural studies done by a few authors using NMR spectroscopy [Mazzini et al., 2003; Park et al., 2004a; Park et al., 2004b].

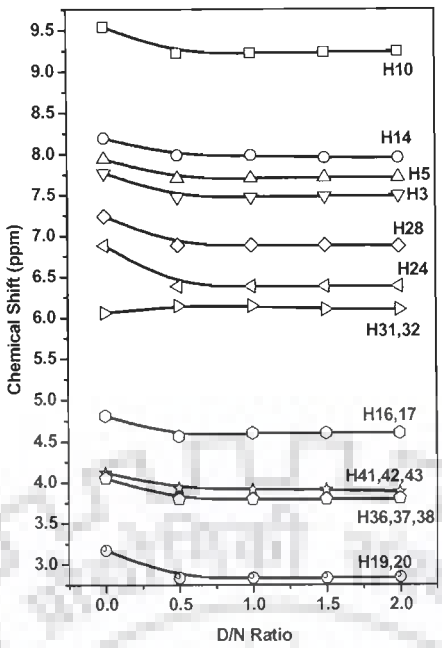


**Figure 6.9: Change in $^1$H chemical shift of berberine protons complexed with d-(CCAATTGG)$_2$ at various D/N ratio, 283 K.**

Mazzini et al has studied 1D spectra for berberine interaction with several oligonucleotides i.e., d-(AAGAATTCTT)$_2$ (A2T2), d-(GCGATCGC)$_2$ (GATC), d-(CGTACG)$_2$ (TA), d(CGTATACG)$_2$ (TATA), d-(ACATCAAAAAGGT) (ss-A5) and d-(ACCTTTTTGATGT)$_2$ (T5GA) (listed in Table 6.6) [Mazzini et al., 2003].They have reported that H10, H14, H28 and H24 protons of berberine shows maximum shift with binding to different oligonucleotides (Table 6.6). Park et al has also reported the chemical shift values for berberine on binding to oligonucleotide d-(GCCGTCGTTTTACA)$_2$ (HP14) which contains topoisomerase cleavage site. Overall very little shielding for berberine protons with a maximum value of 0.11 for H14 was observed on berberine binding with HP14 [Park et al., 2004a]. Less shielding observed by Park et al can be attributed to high GC content and absence of AT site (which has been proved as preferred binding site for berberine in literature) in HP14 oligonucleotide. Therefore, our results support the fact that there are more

upfield shifts for centrally located aromatic protons on berberine chromphore and low magnitude shifts for aliphatic protons located towards the end sides. Anticancer drugs like camptothecin and topotecon which are proved as external binder of DNA by stacking at the terminal end of oligonucleoiteds also shows a chemical shift variation of < 0.50 for several oligonucleotides [Mazzini et al., 2004]. Jenkins et al has studied interactions of minor groove binder berenil with several oligonucleotides having different length for central AAT region and reported that binding induced effect in chemical shift of 0.10 to 0.30 ppm in berenil increased with increased length. It is now well established from the obtained results and literature that a uniform shielding effect for berberine molecule was found due to binding effect, which is closer to shielding observed for minor groove binder i.e. Berenil and the external binding drug through end stacking i.e. Camptothecin [Jenkins et al., 1993; Mazzini et al., 2004]. It is also worth mentioning that the shielding effect was more or less spread over the whole berberine molecule, but the values were found to be more significant for aromatic protons. Hence, these results suggest that aromatic chromophore (ring B and D, Figure 3.1) of berberine might be stacked with base pairs of DNA. Conformational features of berberine has already been mentioned in Chapter 3 suggesting that saturation at C15 and C18 at ring C gives a crescent shape to the molecule. It is already proved in literature that crescent shape is complementary [Neidle, 2001] to the shape of minor groove of BDNA and facilitates binding by promoting wall interactions [Slickers et al., 1998].

The change in chemical shift ($\Delta\delta$) of d-$(CCAATTGG)_2$ protons with increasing D/N ratio was gradual and small in magnitude (Figure 6.8a-f). The $\Delta\delta$ increased with D/N ratio as more and more octamer binds to berberine. The results are tabulated in Table 6.11.

**Table 6.11: Chemical shift (ppm) of d-(CCAATTGG)$_2$ protons in berberine -d-(CCAATTGG)$_2$ complex as a function of drug (D) to nucleic acid duplex (N) ratio, D/N, at 283 K. Also shown here is the change in chemical shift on binding, that is, $\Delta\delta = \delta$(D/ N=2.0) - $\delta$(D/ N= 0.0) equivalent to $\delta$Total $= \delta^b$ (D/ N=2.0)- $\delta^f$.**

| D/N | C1H1' | C2H1' | A3H1' | A4H1' | T5H1' | T6H1' | G7H1' | G8H1' | T5CH3 | T6CH3 | C1H5 | C2H5 | C2NH2$^b$ | C2NH2$^{nb}$ | A3/4NH2$^b$ |
|---|---|---|---|---|---|---|---|---|---|---|---|---|---|---|---|
| 0.0 | 5.97 | 5.29 | 6.01 | 6.23 | 5.90 | 5.79 | 5.65 | 6.14 | 1.36 | 1.63 | 5.95 | 5.74 | 8.69 | 6.94 | 7.32 |
| 0.5 | 5.90 | 5.25 | 6.00 | 6.21 | 5.89 | 5.78 | 5.63 | 6.11 | 1.34 | 1.61 | 5.90 | 5.71 | 8.64 | 6.93 | 7.28 |
| 1.0 | 5.86 | 5.24 | 6.00 | 6.20 | 5.78 | 5.76 | 5.60 | 6.08 | 1.37 | 1.80 | 5.84 | 5.69 | 8.60 | 6.90 | 7.26 |
| 1.5 | 5.78 | 5.56 | 5.97 | 6.19 | 5.86 | 5.75 | 5.56 | 6.04 | 1.32 | 1.58 | 5.76 | 5.56 | 8.53 | 6.84 | 7.22 |
| 2.0 | 5.71 | 5.17 | 5.96 | 6.18 | 5.85 | 5.72 | 5.54 | 6.01 | 1.31 | 1.57 | 5.71 | 5.61 | 8.48 | 6.81 | 7.21 |
| $\Delta\delta$ | -0.26 | -0.12 | -0.05 | -0.05 | -0.05 | -0.07 | -0.11 | -0.13 | -0.05 | -0.06 | -0.24 | -0.13 | -0.21 | -0.17 | -0.11 |
| D/N | C1H6 | C2H6 | A3H8 | A4H8 | T5H6 | T6H6 | G7H8 | G8H8 | T5NH | T6NH | G7NH | $^f$C1NH2$^b$ | $^f$C1NH2$^{nb}$ | A3NH2$^{nb}$ | A4NH2$^{nb}$ |
| 0.0 | 7.80 | 7.61 | 8.35 | 8.27 | 7.19 | 7.29 | 7.86 | 7.83 | 13.80 | 14.05 | 12.94 | 8.17 | 7.32 | 6.40 | 6.23 |
| 0.5 | 7.74 | 7.60 | 8.33 | 8.25 | 7.18 | 7.27 | 7.84 | 7.81 | 13.75 | 13.98 | 12.86 | 8.17 | 7.32 | 6.38 | 6.20 |
| 1.0 | 7.70 | 7.58 | 8.32 | 8.25 | 7.17 | 7.26 | 7.83 | 7.80 | 13.73 | 13.97 | 12.83 | 8.17 | 7.32 | 6.35 | 6.18 |
| 1.5 | 7.65 | 7.55 | 8.30 | 8.23 | 7.15 | 7.24 | 7.80 | 7.78 | 13.71 | 13.93 | 12.75 | 8.17 | 7.31 | 6.32 | 6.17 |
| 2.0 | 7.62 | 7.53 | 8.29 | 8.23 | 7.15 | 7.23 | 7.84 | 7.77 | 13.68 | 13.90 | 12.71 | 8.14 | 7.31 | 6.31 | 6.15 |
| $\Delta\delta$ | -0.18 | -0.08 | -0.06 | -0.04 | -0.04 | -0.06 | -0.02 | -0.06 | -0.12 | -0.15 | -0.23 | -0.03 | -0.01 | -0.09 | -0.08 |
| D/N | $^c$C1NH2$^b$ | $^c$C1NH2$^{nb}$ | A3H2 | A4H2 | C1H2' | C2H2' | A3H2' | A4H2' | T5H2' | T6H2' | G7H2' | G8H2' | C1H2" | C2H2" | A3H2" |
| 0.0 | 8.17 | 7.32 | 7.66 | 7.66 | 2.06 | 2.13 | 2.88 | 2.67 | 1.98 | 1.98 | 2.68 | 2.35 | 2.50 | 2.39 | 2.99 |
| 0.5 | 8.09 | 7.14 | 7.64 | 7.64 | 2.02 | 2.12 | 2.86 | 2.65 | 1.97 | 1.97 | 2.68 | 2.58 | 2.49 | 2.35 | 2.99 |
| 1.0 | 8.03 | 7.10 | 7.62 | 7.62 | 1.99 | 2.12 | 2.86 | 2.64 | 1.97 | 1.97 | 2.66 | 2.56 | 2.45 | 2.37 | 2.99 |
| 1.5 | 7.93 | 7.03 | 7.61 | 7.61 | 1.95 | 2.10 | 2.84 | 2.63 | 1.95 | 1.95 | 2.65 | 2.61 | 2.45 | 2.35 | 2.97 |
| 2.0 | 7.87 | 6.97 | 7.61 | 7.61 | 1.91 | 2.10 | 2.84 | 2.63 | 1.94 | 1.94 | 2.64 | 2.59 | 2.43 | 2.10 | 2.96 |
| $\Delta\delta$ | -0.30 | -0.35 | -0.05 | -0.05 | -0.15 | -0.03 | -0.03 | -0.04 | -0.04 | -0.04 | -0.04 | -0.24 | -0.07 | -0.29 | -0.03 |

Contd....**Table-6.11**

| D/N | A4H2" | T5H2" | T6H2" | G7H2" | G8H2" | C1H3' | C2H3' | A3H3' | A4H3' | T5H3' | T6H3' | A3H4' | A4H4' | T5H4' | T6H4' |
|---|---|---|---|---|---|---|---|---|---|---|---|---|---|---|---|
| **0.0** | 2.97 | 2.53 | 2.35 | 2.68 | 2.55 | 4.53 | 4.67 | 5.11 | 5.06 | 4.67 | 4.67 | 4.46 | 4.52 | 4.19 | 4.11 |
| **0.5** | 2.97 | 2.51 | 2.32 | 2.68 | 2.35 | 4.55 | 4.78 | 5.09 | 5.04 | 4.78 | 4.78 | 4.46 | 4.52 | 4.14 | 4.09 |
| **1.0** | 2.95 | 2.50 | 2.32 | 2.66 | 2.35 | 4.58 | 4.80 | 5.085 | 5.041 | 4.854 | 4.854 | 4.45 | 4.511 | 4.17 | 4.14 |
| **1.5** | 2.94 | 2.48 | 2.30 | 2.65 | 2.36 | 4.60 | 4.84 | 5.08 | 5.031 | 4.84 | 4.84 | 4.44 | 4.50 | 4.06 | 4.14 |
| **2.0** | 2.93 | 2.45 | 2.28 | 2.64 | 2.36 | 4.60 | 4.84 | 5.07 | 5.02 | 4.83 | 4.83 | 4.45 | 4.43 | 4.06 | 4.14 |
| **Δ δ** | -0.04 | -0.08 | -0.07 | -0.04 | -0.18 | -0.07 | -0.16 | -0.04 | -0.04 | -0.16 | -0.16 | -0.01 | -0.09 | -0.13 | +0.03 |

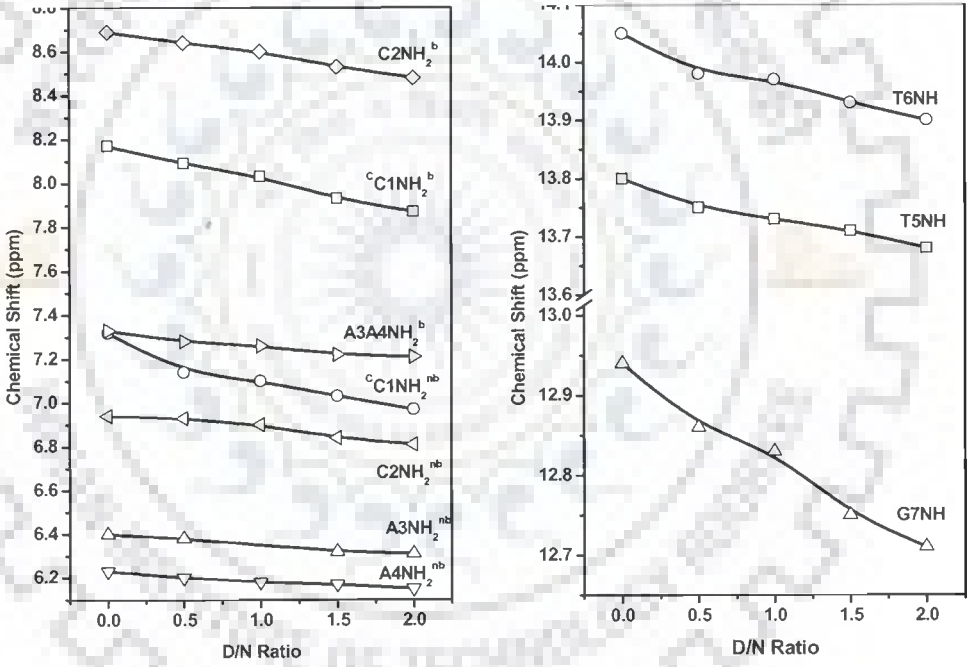


**(Fig. 6.10 a)**

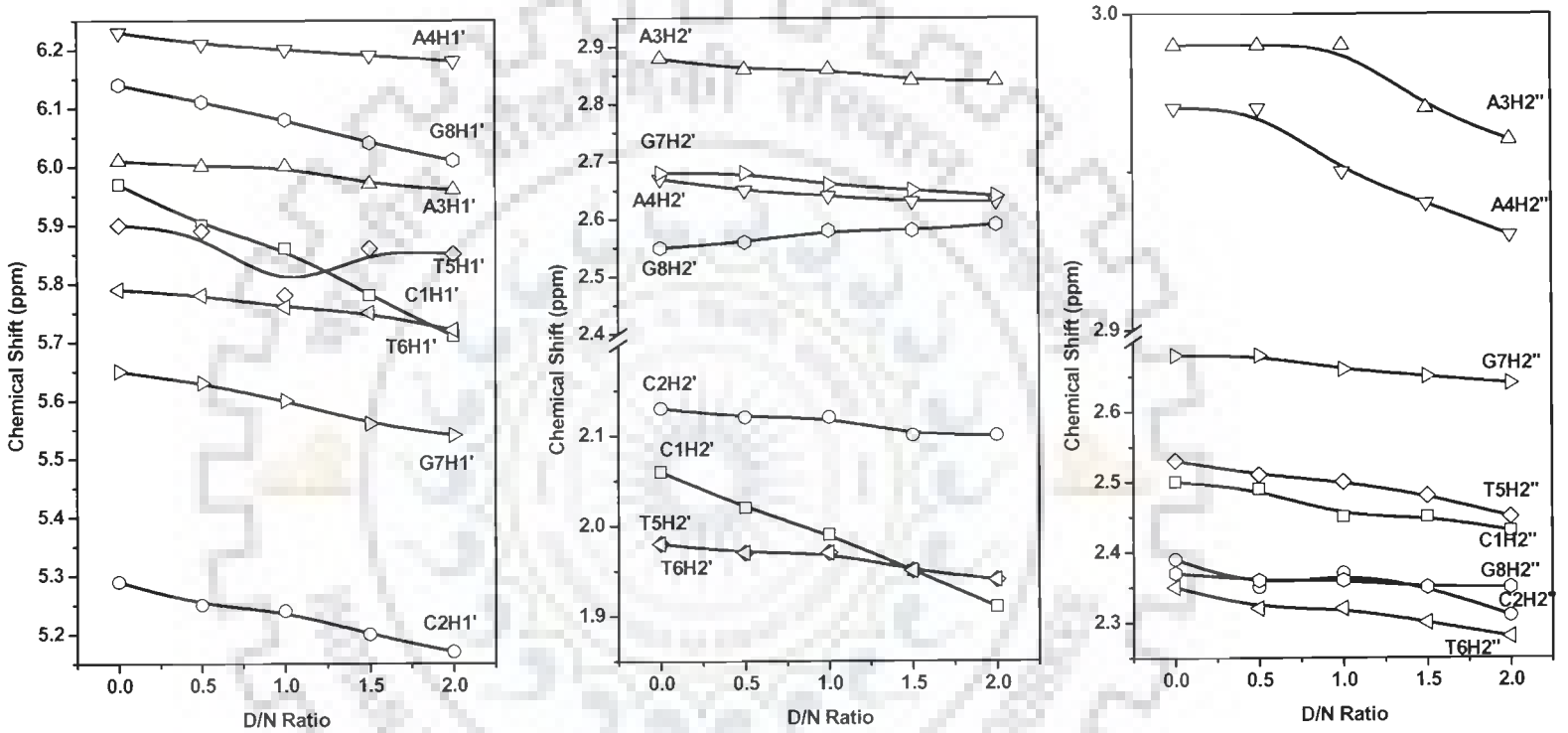


(Fig. 6.10 b)

**Figure 6.10 (a-c): Change in chemical shift of d-(CCAATTGG)$_2$ protons complexed with berberine as a function of drug to DNA (D/N) ratio, 283 K.**

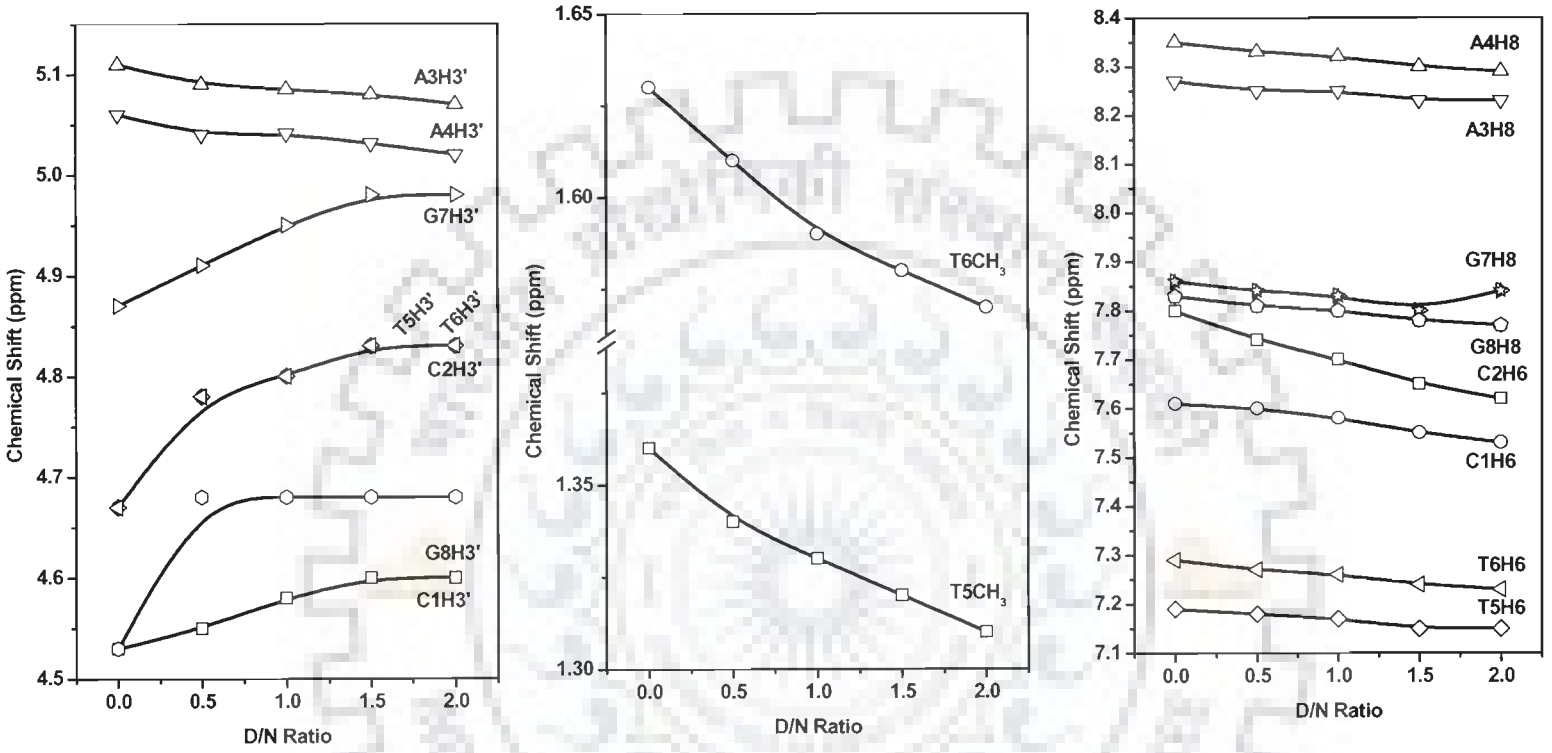
Chemical Shift (ppm)
D/N Ratio
A3H3'
A4H3'
G7H3'
T5H3'
T6H3'
C2H3'
G8H3'
C1H3'
T6CH3
T5CH3
A4H8
A3H8
G7H8
G8H8
C2H6
C1H6
T6H6
T5H6

(Fig. 6.10c)

DNA proton chemical shift change ($\Delta\delta$) versus D/N ratio is shown in Figure 6.10a-c. All the spectral lines for DNA were somewhat uniformly broadened on binding because the internal motions were affected and the protons were getting immobilized. The resonances of d-$(CCAATTGG)_2$ did not show any significant change during addition of increased amount of berberine except the imino, methyl and some of the sugar protons (Figure 6.10a-c). In uncomplexed d-$(CCAATTGG)_2$, G7NH, T6NH and T5NH resonances appeared at 12.94, 14.05 and 13.80 ppm, respectively. G8NH resonance was not observed presumably due to exchange with water solvent. All the three imino protons broadened considerably with increasing ratio of berberine, the broadening was found to be more significant at D/N ratio of 2.0. G7NH, T6NH and T5NH protons showed considerable shift of 0.23, 0.15 and 0.12 ppm respectively on increasing the D/N up to 2.0. G7NH proton's more shielding (Figure 6.10a) due to binding was in accordance with the results from literature [Park et al., 2004a], which showed that the guanines imino protons were more effected due to binding with berberine and berberrubine. Park et al demonstrated that imino protons of HP14 showed line broadening effect and a gradual chemical shift change up to ~0.16 ppm when molar ratio of berberine to HP14 was increased. However, the up-field shift of imino protons in berberrubine - HP14 complex was most evident at molar ratio 1:1 but became less pronounced as the ratio of the bound to free berberrubine decreased during titration with the berberine [Park et al., 2004a]. In the base and H1', H2', H2", H3' and H4' proton, resonances became broader but the chemical shifts remained unchanged or showed a very moderate shift. For the base region of d-$(CCAATTGG)_2$ a shielding of 0.02 to 0.18 ppm was observed. Terminal cytosine C1H6 showed the maximum effect of 0.18 ppm. Maximum shielding was observed for T5H3' and T6H3' protons among protons in H3' region (Figure 6.10 c).

A3H2" and A4H2" also showed significant upfield shift during titration. Significant upfield shift for both the methyl protons was observed when berberine was added successively to the octamer. Overall the resonances of oligomer showed insignificant chemical shift change ($\Delta\delta = 0.02 - 0.35$) during the titration. The change in chemical shift is not the sufficient indicator of the interaction; instead the observed intermolecular short contacts are the direct proof of the structure of a specific drug-DNA complex.

### 6.1.2.2 Temperature Dependence Studies

Binding of berberine to d-$(CCAATTGG)_2$ gradually became weak with increase in temperature. Therefore, to spot the changes in resonances of drug and DNA protons due to dissociation of bound berberine from d-$(CCAATTGG)_2$, 1D-$^1$H versus temperature studies were performed at D/N, 0.0 (Figure 5.5 a-i), 1.0 and 2.0. $^1$H NMR spectra of the berberine -d-$(CCAATTGG)_2$ complex at D/N=1.0 and 2.0, was observed for the temperature range of 278 to 328 K (Figure 6.11a-e and Figure 6.12a-e). The observation of the shifts as a function of temperature further helped to resolve the overlapping resonance peaks.

Berberine resonances, which were broad and tough to identify in 1D $^1$H spectrum of complex were identified at higher temperature due to signal sharpening with increased temperature. It can be clearly seen from Figure 6.11 and 6.12 that berberine resonances H10, H14, H28, H24 of berberine-d-$(CCAATTGG)_2$ complex were broad at low temperature, whereas at high temperature the berberine binding with d-$(CCAATTGG)_2$ weakened and resonances became sharp.

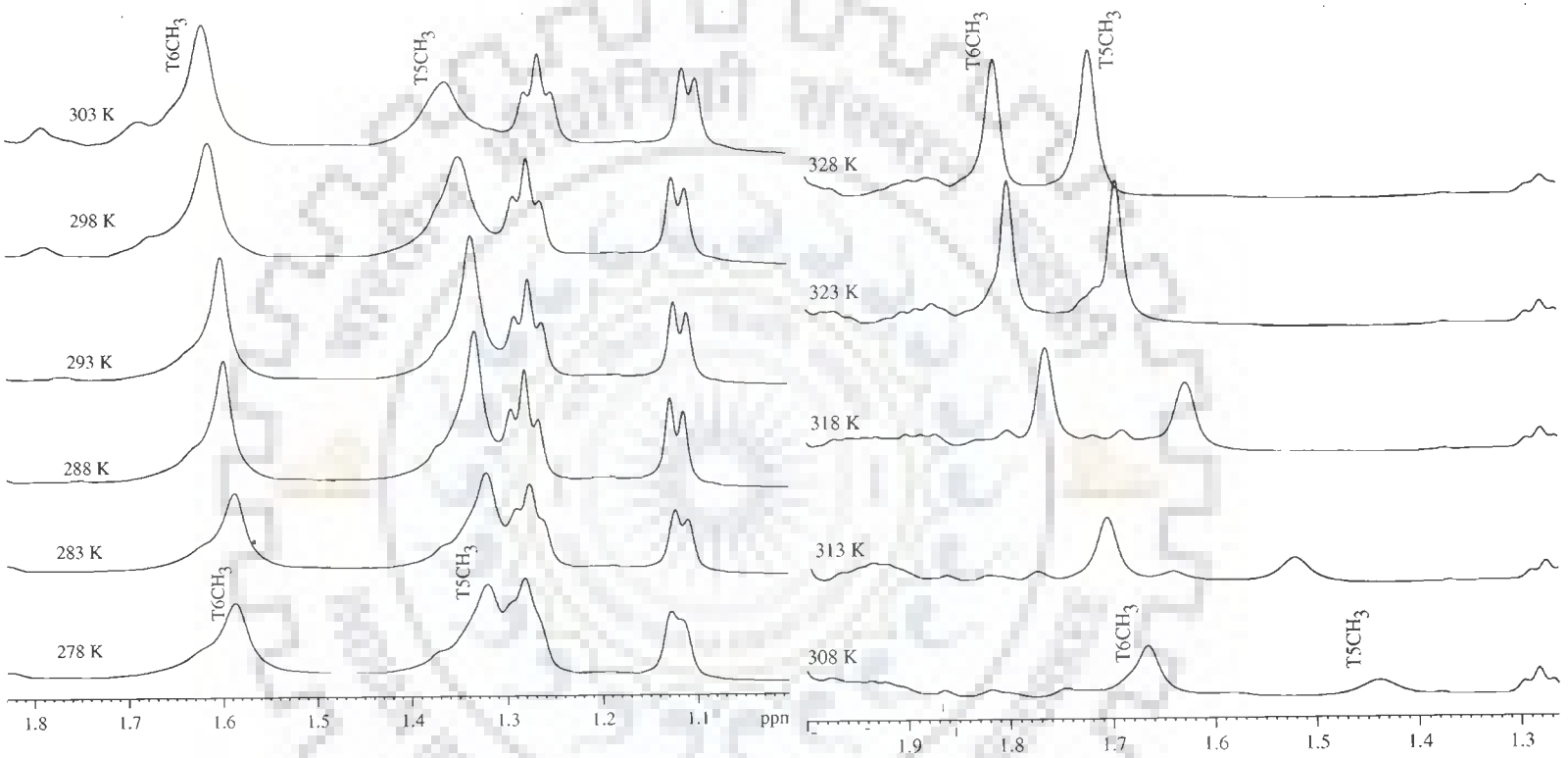


**(Fig. 6.11a)**

**Figure 6.11a-e: Proton NMR spectra of complex of beberine with d-$(CCAATTGG)_2$ as a function of temperature at D/N = 1.0 (* berbrine proton in berberine -d-$(CCAATTGG)_2$ complex).**

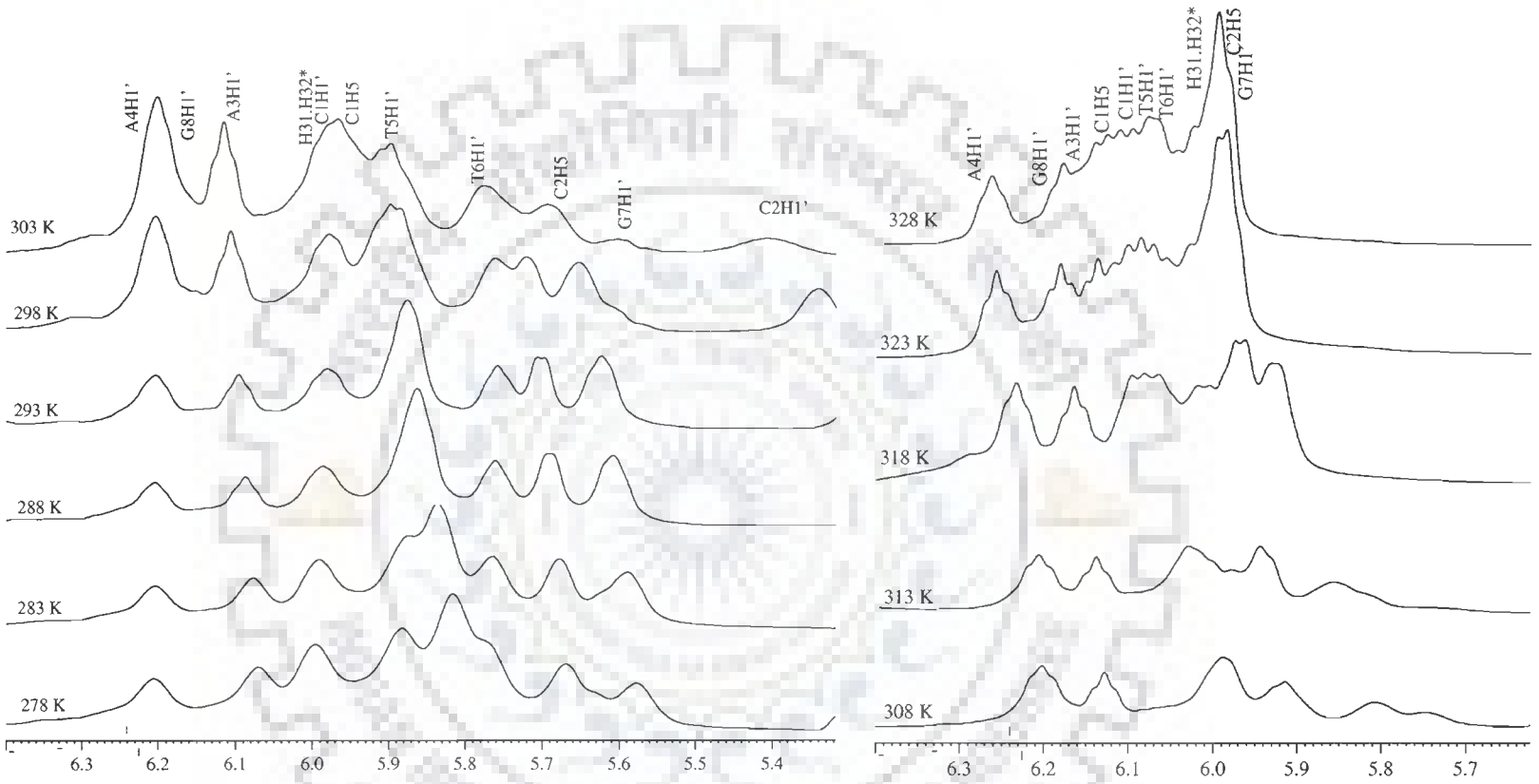
A4H1'
G8H1'
A3H1'
H31.H32*
C1H1'
C1H5
T5H1'
T6H1'
C2H5
G7H1'
C2H1'
303 K
298 K
293 K
288 K
283 K
278 K
6.3
6.2
6.1
6.0
5.9
5.8
5.7
5.6
5.5
5.4
A4H1'
G8H1'
A3H1'
C1H5
C1H1'
T5H1'
T6H1'
H31.H32*
G7H1'
C2H5
328 K
323 K
318 K
313 K
308 K
6.3
6.2
6.1
6.0
5.9
5.8
5.7

**(Fig. 6.11 b)**

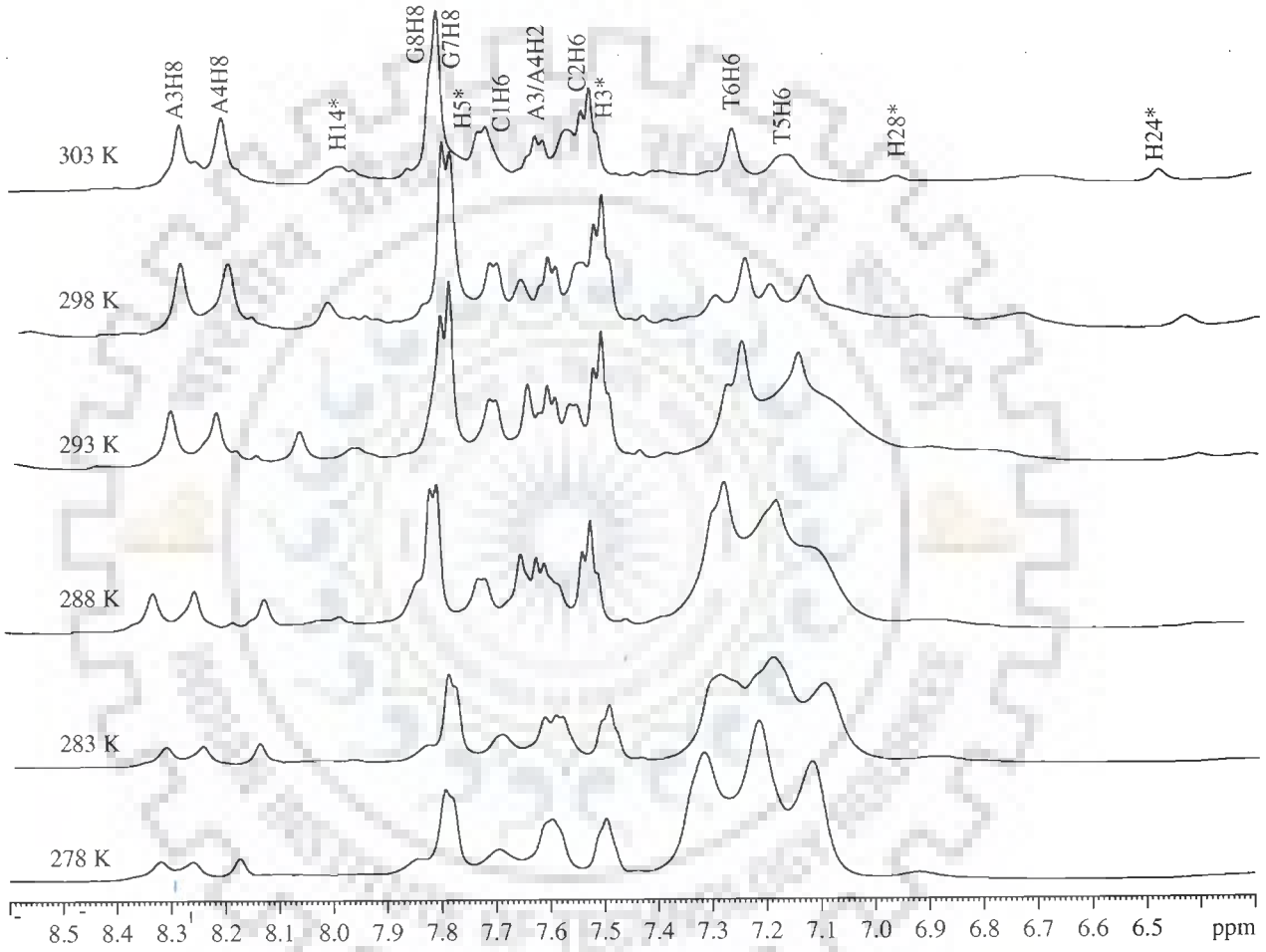
A3H8
A4H8
H14*
G8H8
G7H8
H5*
C1H6
A3/A4H2
C2H6
H3*
T6H6
T5H6
H28*
H24*
303 K
298 K
293 K
288 K
283 K
278 K
8.5 8.4 8.3 8.2 8.1 8.0 7.9 7.8 7.7 7.6 7.5 7.4 7.3 7.2 7.1 7.0 6.9 6.8 6.7 6.6 6.5 ppm

**(Fig. 6.11c)**

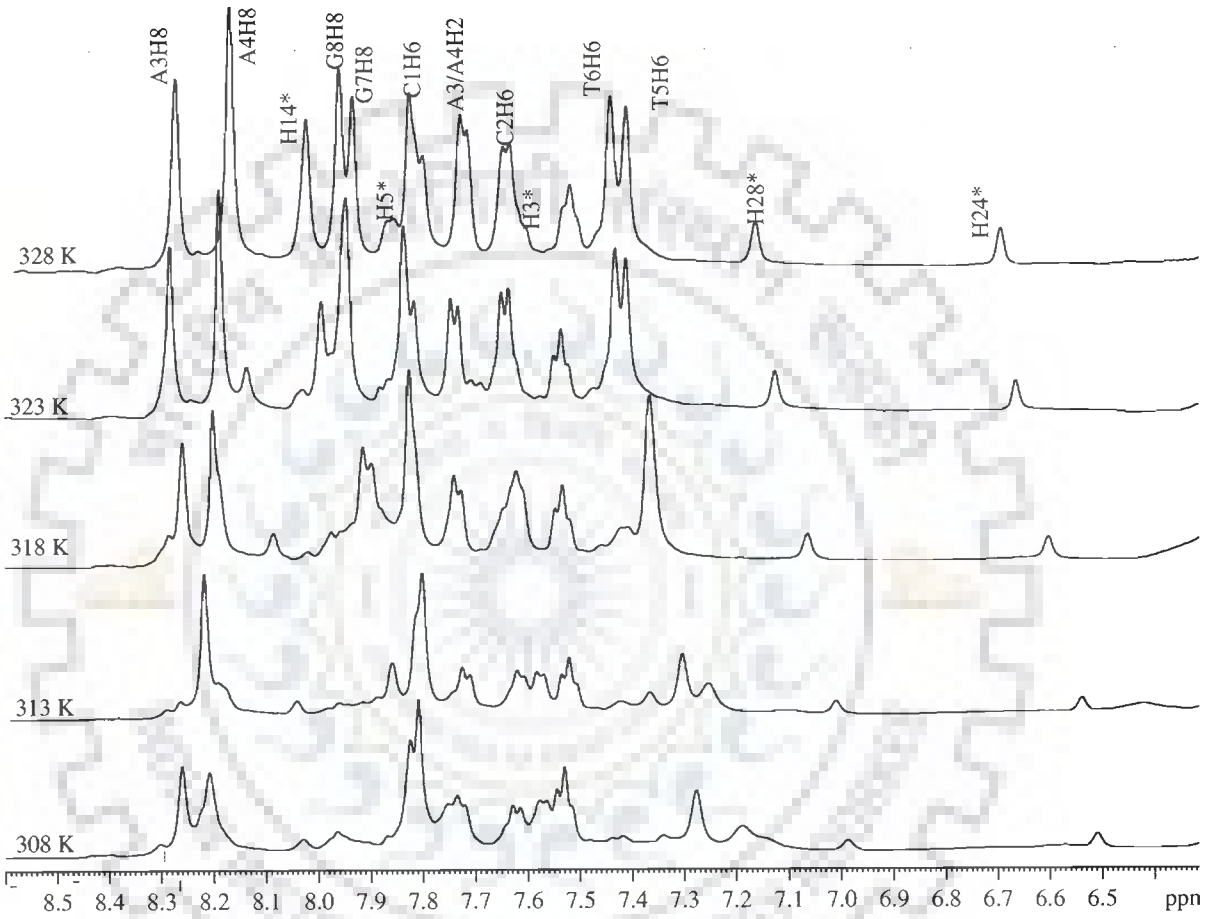
A3H8
A4H8
H14*
G8H8
G7H8
H5*
C1H6
A3/A4H2
C2H6
H3*
T6H6
T5H6
H128*
H24*
328 K
323 K
318 K
313 K
308 K
8.5 8.4 8.3 8.2 8.1 8.0 7.9 7.8 7.7 7.6 7.5 7.4 7.3 7.2 7.1 7.0 6.9 6.8 6.7 6.6 6.5
ppm

**(Fig. 6.11 d)**

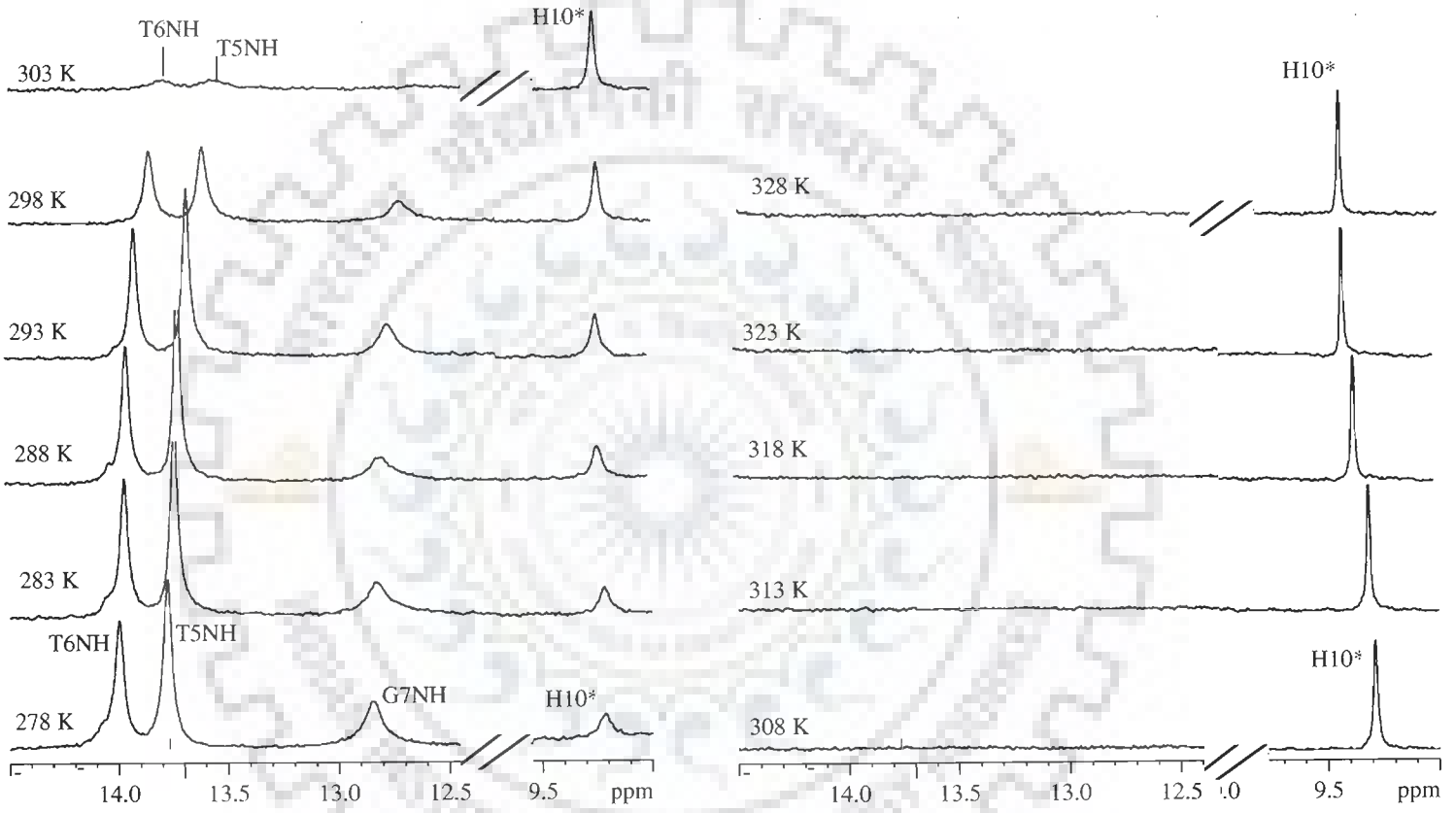
T6NH
T5NH
H10*
303 K
298 K
293 K
288 K
283 K
278 K
328 K
323 K
318 K
313 K
308 K
G7NH
14.0
13.5
13.0
12.5
9.5
ppm

**(Fig. 611e)**

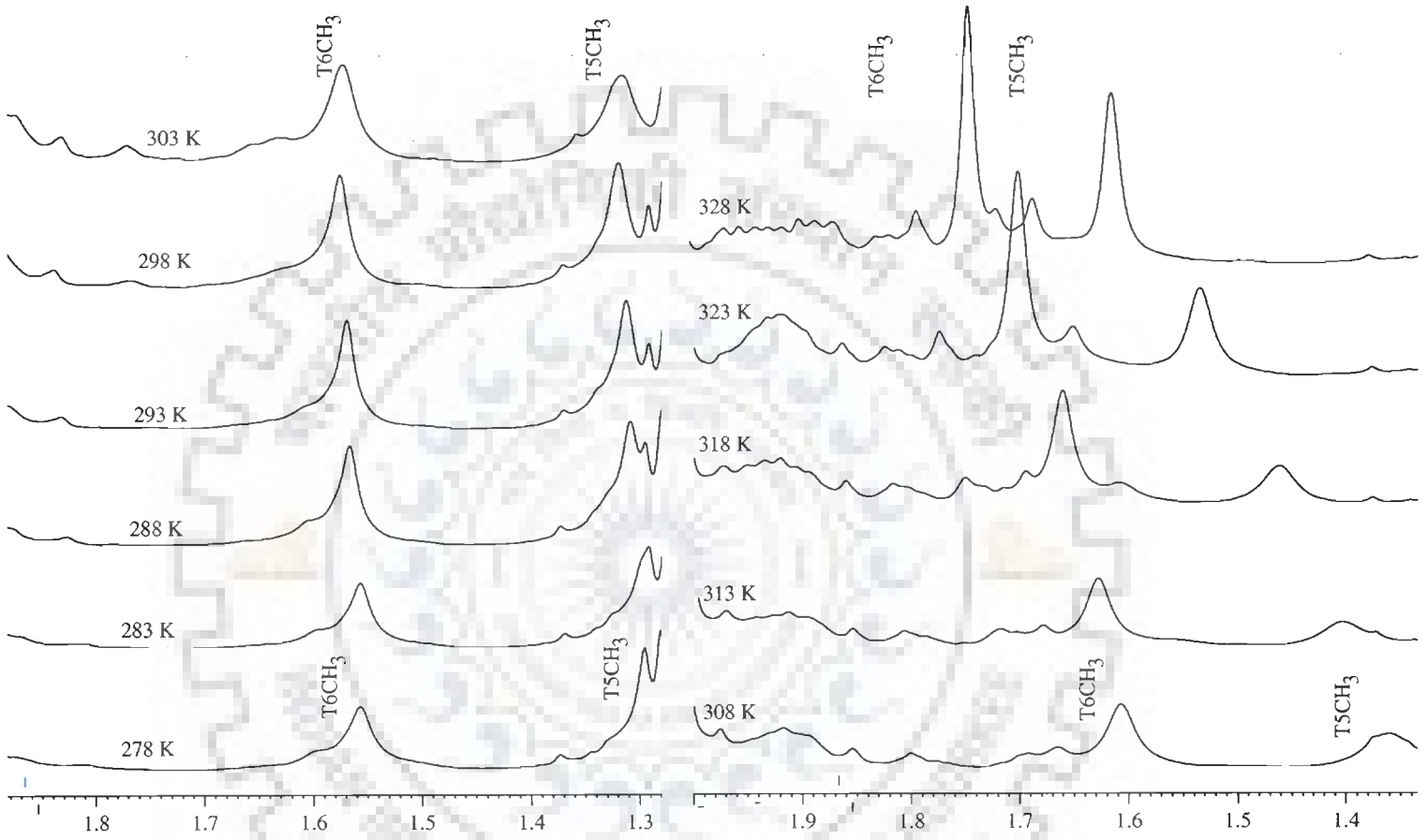


(Fig. 6.12a)

**Figure 6.12a-e: Proton NMR spectra of complex of beberine with d-$(CCAATTGG)_2$ as a function of temperature at D/N = 2.0 (* berbrine proton in berberine -d-$(CCAATTGG)_2$ complex).**

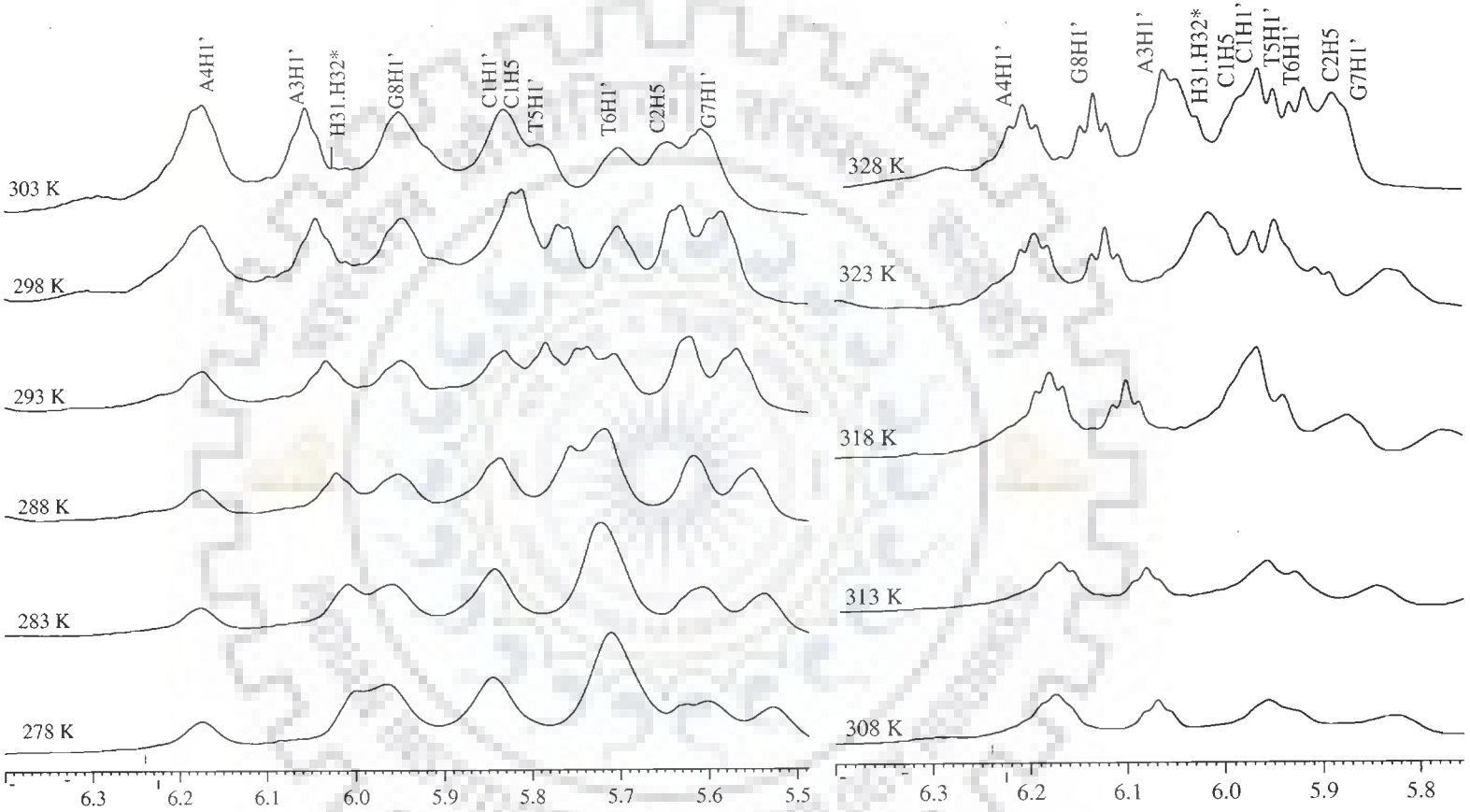
A4H1'
A3H1'
H31.H32*
G8H1'
C1H1'
C1H5
T5H1'
T6H1'
C2H5
G7H1'
303 K
298 K
293 K
288 K
283 K
278 K
328 K
323 K
318 K
313 K
308 K
6.3
6.2
6.1
6.0
5.9
5.8
5.7
5.6
5.5

**(Fig. 6.12b)**

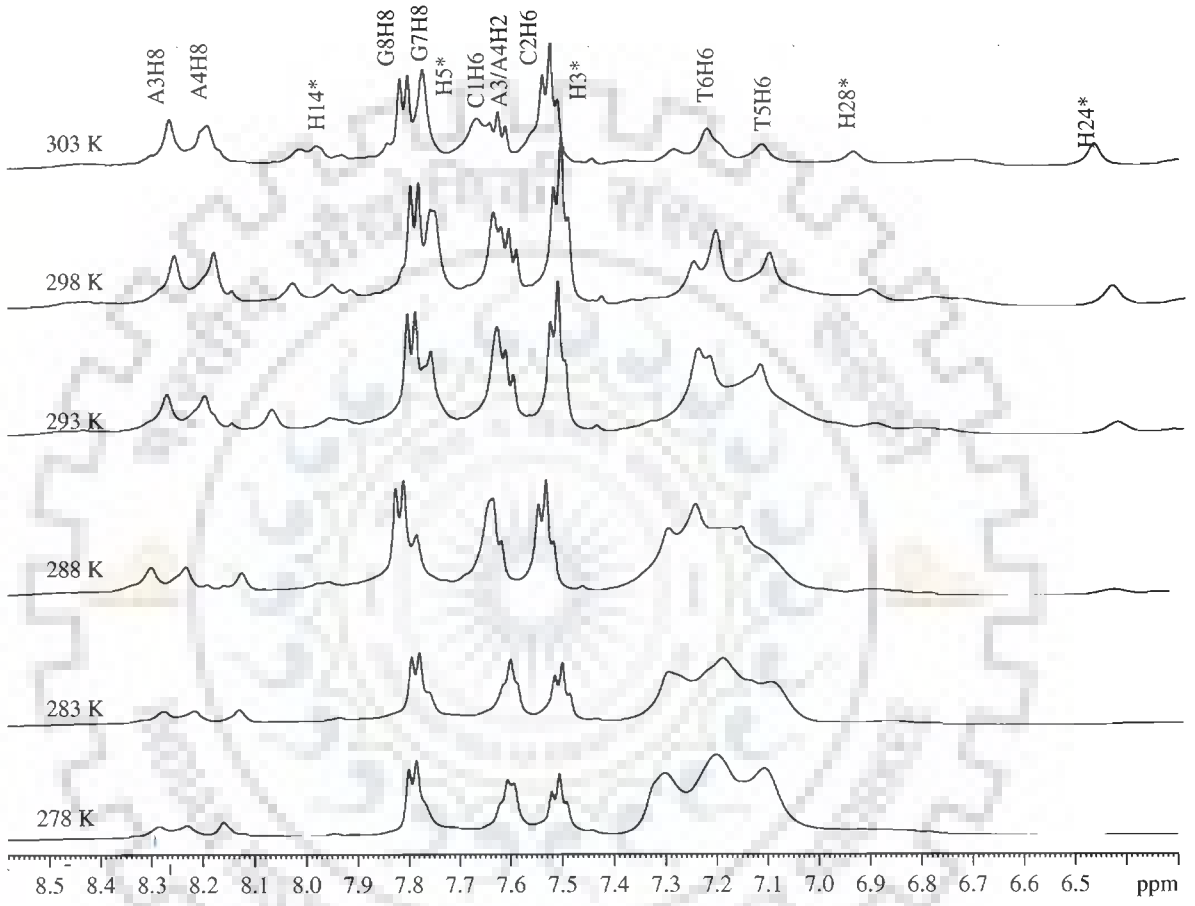
A3H8
A4H8
H14*
G8H8
G7H8
H5*
C1H6
A3/A4H2
C2H6
H3*
T6H6
T5H6
H28*
H24*
303 K
298 K
293 K
288 K
283 K
278 K
8.5 8.4 8.3 8.2 8.1 8.0 7.9 7.8 7.7 7.6 7.5 7.4 7.3 7.2 7.1 7.0 6.9 6.8 6.7 6.6 6.5
ppm

**(Fig. 6.12c)**

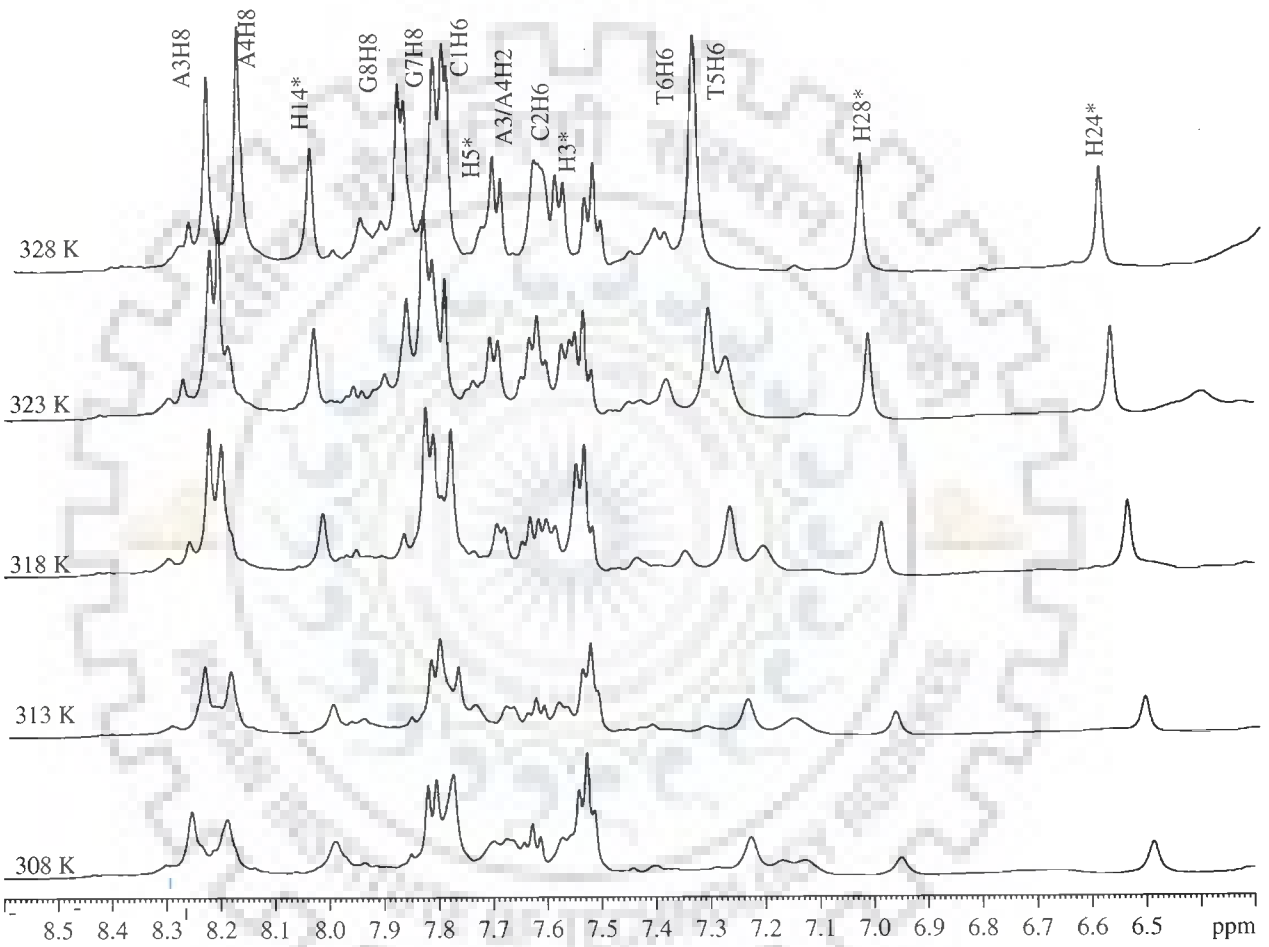
A3H8
A4H8
H14*
G8H8
G7H8
C1H6
H5*
A3/A4H2
C2H6
H3*
T6H6
T5H6
H28*
H24*
328 K
323 K
318 K
313 K
308 K
8.5 8.4 8.3 8.2 8.1 8.0 7.9 7.8 7.7 7.6 7.5 7.4 7.3 7.2 7.1 7.0 6.9 6.8 6.7 6.6 6.5 ppm

**(Fig. 6.12d)**

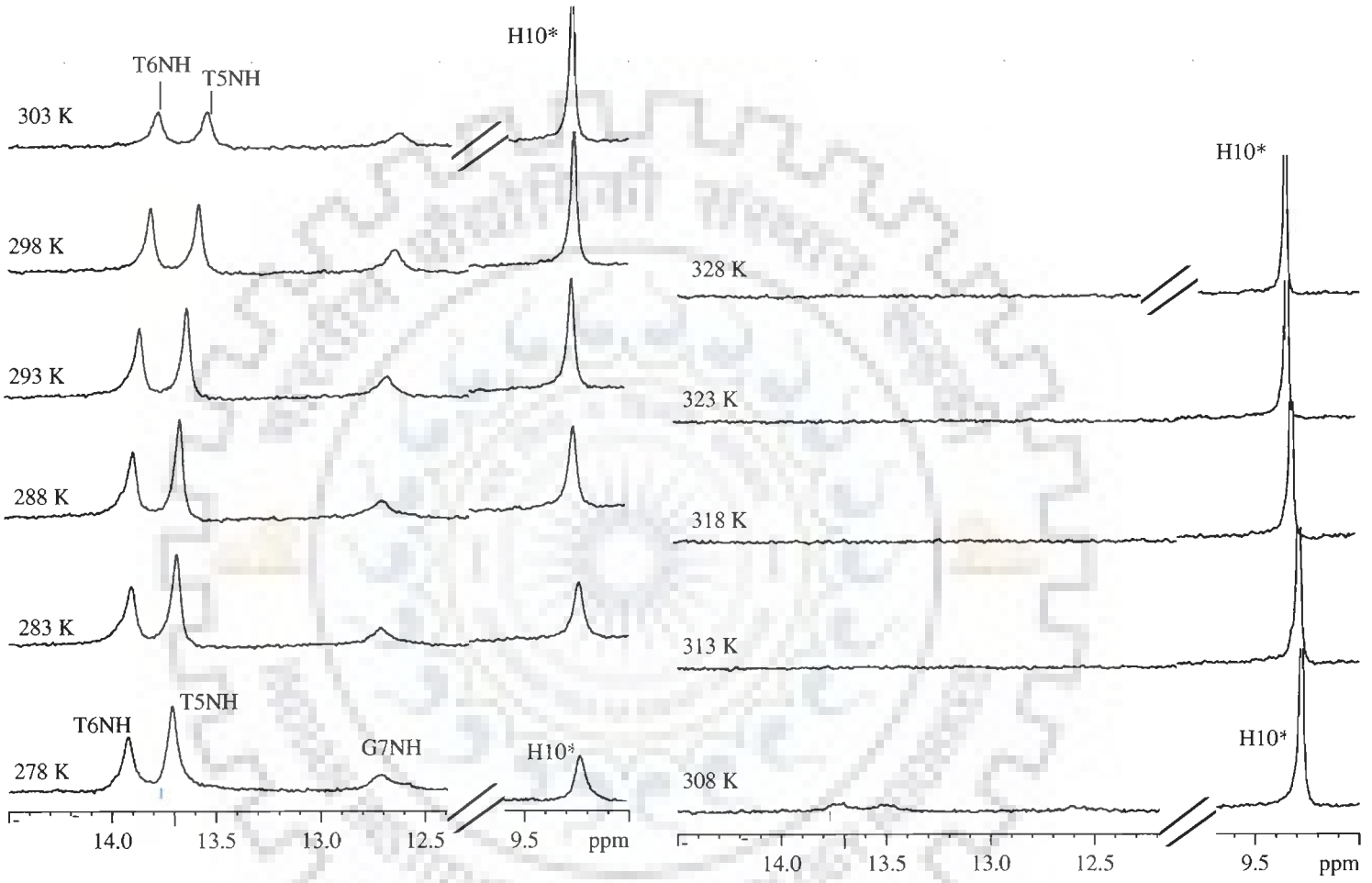
H10*
T6NH
T5NH
303 K
298 K
293 K
288 K
283 K
T6NH
T5NH
G7NH
H10*
278 K
14.0
13.5
13.0
12.5
9.5
ppm
H10*
328 K
323 K
318 K
313 K
H10*
308 K
14.0
13.5
13.0
12.5
9.5
ppm

**(Fig. 6.12e)**

Resonances of berberine protons in berberine-d-$(CCAATTGG)_2$ complex shift downfield with high temperature which is in contrast to free berberine where no chemical shift change was observed with enhanced temperature (Figure 3.6).This clearly indicates that these berberine protons were involved in binding with the d-$(CCAATTGG)_2$. Chemical shift value for these berberine protons at different temperatures at D/N 1.0 and 2.0 are tabulated in Table 6.12. Figure 6.13 shows the difference in chemical shift $\Delta\delta = \delta$ (328 K) - $\delta$ (278 K) at D/N 1.0 and 2.0. It was found that $\Delta\delta$ values for H10, H14, H28, H24 at D/N 2.0 were comparatively lesser than at D/N 1.0. It may be credited to the tight binding of berberine to d-$(CCAATTGG)_2$ at 2.0 rather than 1.0. Consequently, as we found that even on 328 K chemical shift value for H10, H28 and H24 protons of berberine in berberine-d-$(CCAATTGG)_2$ was found to be downfield shift then their position in berberine alone. These results clearly indicate that berberine binds to d-$(CCAATTGG)_2$ at higher concentration and amount of berberine is in bound form even at higher temperature (328 K).

**Table 6.12: Chemical shift (ppm) of some of the berberine protons as a function of temperature. Also shown here is the net change in chemical shift with temperature, that is, $\Delta\delta = \delta$ (328 K) - $\delta$ (278 K) -ve $\Delta\delta$ indicates upfield shift and +ve $\Delta\delta$ indicates downfield shift.**

| | D/N = 1.0 | | | | D/N = 2.0 | | | |
|---|---|---|---|---|---|---|---|---|
| **Temperature** | **H10** | **H14** | **H28** | **H24** | **H10** | **H14** | **H28** | **H24** |
| **278** | 9.20 | 7.97 | 6.88 | 6.38 | 9.24 | 7.95 | 6.86 | 6.38 |
| **283** | 9.21 | 7.97 | 6.88 | 6.38 | 9.24 | 7.95 | 6.88 | 6.40 |
| **288** | 9.22 | 7.97 | 6.88 | 6.38 | 9.25 | 7.95 | 6.88 | 6.41 |
| **293** | 9.23 | 7.97 | 6.90 | 6.41 | 9.25 | 7.97 | 6.91 | 6.43 |
| **298** | 9.26 | 7.97 | 6.93 | 6.45 | 9.27 | 7.99 | 6.93 | 6.45 |
| **303** | 9.27 | 7.99 | 6.96 | 6.48 | 9.28 | 8.00 | 6.96 | 6.47 |
| **308** | 9.29 | 8.03 | 6.98 | 6.51 | 9.28 | 8.00 | 6.97 | 6.49 |
| **313** | 9.32 | 8.06 | 7.02 | 6.55 | 9.30 | 8.02 | 6.99 | 6.52 |
| **318** | 9.36 | 8.09 | 7.07 | 6.61 | 9.31 | 8.03 | 7.02 | 6.54 |
| **323** | 9.41 | 8.14 | 7.13 | 6.66 | 9.34 | 8.05 | 7.04 | 6.57 |
| **328** | 9.45 | 8.19 | 7.16 | 6.71 | 9.37 | 8.07 | 7.06 | 6.61 |
| **$\Delta\delta$** | +0.25 | +0.22 | +0.28 | +0.33 | +0.13 | +0.12 | +0.20 | +0.23 |

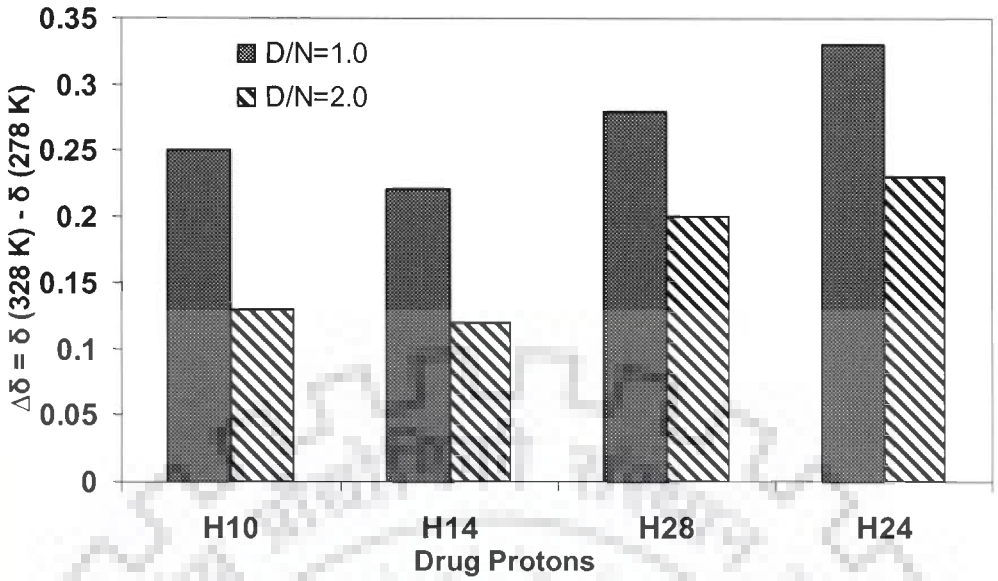


**Figure 6.13: The change in $^1$Hchemical shift of berberine protons, $\Delta\delta = \delta_{328K} - \delta_{278K}$, due to temperature in berberine -d-(CCAATTGG)$_2$ complex at drug (D) to nucleic acid duplex (N) ratio, D/N = 1.0 and 2.0.**

The chemical shift for d-(CCAATTGG)$_2$ protons showed a linear dependence on temperature in the range of 278- 328 K (Figure 6.11a-e and Figure 6.12a-e).It was observed that chemical shift of octamer varied with temperature. Downfield shift was observed for all the DNA protons except A3H8, A4H8 and imino protons which showed an upfield shift. All the DNA protons chemical shift values at different temperatures for D/N ratio 1.0 and 2.0 are listed in Table 6.13 and 6.14 respectively. Values obtained for chemical shifts indicate that structurally only one complex was formed and the chemical shift at any one temperature was an average of bound and unbound d-(CCAATTGG)$_2$ the equilibrium of which was likely to shift with temperature. The resonances for imino protons of thymine and guanines were in fast exchange with water at higher than the melting temperature and hence imino protons

disappeared at $T_m$. The spectras for imino protons vs increasing temperature are shown in Figure 6.11e and 6.12e for D/N 1.0 and 2.0 respectively. It can be clearly seen from the Figure 6.11e that imino signals completely disappeared at 308 K, which was same as found for d-(CCAATTGG)$_2$ alone (Figure 5.5i ). At D/N 2.0 imino signals were broad but observed at 308 K (Figure 6.12 e). This suggests that the melting temperature of d-(CCAATTGG)$_2$ at D/N 1.0 lied between 303- 308 K whereas at D/N 2.0 it should be between 308-313 K.

**Table 6.13: Chemical shift (ppm) of d-(CCAATTGG)$_2$ as a function of temperature at D/N 1.0. Also shown here is the net change in chemical shift with temperature, that is, $\Delta\delta = \delta$ (328 K) - $\delta$ (278 K.**

| Temp. (K) | C1H1' | C2H1' | A3H1' | A4H1' | T5H1' | T6H1' | G7H1' | G8H1' | T5CH3 | T6CH3 | C1H5 | C2H5 |
|---|---|---|---|---|---|---|---|---|---|---|---|---|
| 278 | 5.89 | 5.29 | 5.98 | 6.21 | 5.78 | 5.75 | 5.57 | 6.07 | 1.33 | 1.59 | 5.81 | 5.69 |
| 283 | 5.89 | 5.27 | 5.98 | 6.21 | 5.79 | 5.76 | 5.60 | 6.08 | 1.33 | 1.59 | 5.84 | 5.69 |
| 288 | 5.91 | 5.30 | 5.99 | 6.23 | 5.83 | 5.76 | 5.61 | 6.09 | 1.34 | 1.60 | 5.87 | 5.70 |
| 293 | 5.93 | 5.35 | 6.02 | 6.24 | 5.85 | 5.78 | 5.63 | 6.10 | 1.36 | 1.62 | 5.88 | 5.71 |
| 298 | 5.94 | 5.42 | 6.04 | 6.24 | 5.88 | 5.81 | 5.65 | 6.11 | 1.39 | 1.63 | 5.90 | 5.73 |
| 303 | 5.96 | 5.61 | 6.05 | 6.25 | 5.90 | 5.83 | 5.69 | 6.12 | 1.45 | 1.64 | 5.98 | 5.78 |
| 308 | 5.97 | 5.68 | 6.06 | 6.26 | 5.92 | 5.86 | 5.74 | 6.13 | 1.53 | 1.67 | 6.00 | 5.82 |
| 313 | 5.99 | 5.69 | 6.09 | 6.27 | 5.94 | 5.89 | 5.82 | 6.14 | 1.66 | 1.72 | 6.04 | 5.87 |
| 318 | 6.03 | 5.70 | 6.13 | 6.28 | 5.96 | 5.90 | 5.93 | 6.17 | 1.70 | 1.77 | 6.09 | 5.97 |
| 323 | 6.08 | 5.72 | 6.16 | 6.29 | 5.98 | 5.95 | 5.96 | 6.18 | 1.71 | 1.81 | 6.10 | 5.99 |
| 328 | 6.10 | 5.75 | 6.18 | 6.29 | 6.05 | 6.02 | 5.98 | 6.19 | 1.72 | 1.82 | 6.10 | 6.01 |
| $\Delta\delta$ | +0.22 | +0.46 | +0.20 | +0.08 | +0.27 | +0.27 | +0.41 | +0.12 | +0.39 | +0.23 | +0.29 | +0.32 |
| Temp. (K) | C1H6 | C2H6 | A3H8 | A4H8 | T5H6 | T6H6 | G7H8 | G8H8 | T5NH | T6NH | G7NH | C1NH2[b] |
| 278 | 7.69 | 7.60 | 8.32 | 8.26 | 7.21 | 7.31 | 7.85 | 7.79 | 13.77 | 14.00 | 12.85 | 8.18 |
| 283 | 7.71 | 7.60 | 8.32 | 8.25 | 7.21 | 7.31 | 7.85 | 7.79 | 13.78 | 13.98 | 12.83 | 8.14 |
| 288 | 7.71 | 7.60 | 8.33 | 8.24 | 7.21 | 7.31 | 7.85 | 7.81 | 13.75 | 13.97 | 12.77 | 8.11 |
| 293 | 7.73 | 7.61 | 8.31 | 8.23 | 7.21 | 7.33 | 7.86 | 7.81 | 13.71 | 13.95 | 12.76 | 8.07 |
| 298 | 7.73 | 7.62 | 8.30 | 8.22 | 7.24 | 7.35 | 7.86 | 7.87 | 13.67 | 13.91 | 12.73 | 8.03 |
| 303 | 7.73 | 7.63 | 8.28 | 8.21 | 7.25 | 7.36 | 7.87 | 7.91 | 13.61 | 13.87 | - | |
| 308 | 7.73 | 7.63 | 8.26 | 8.20 | 7.26 | 7.39 | 7.92 | 7.95 | | | | |
| 313 | 7.73 | 7.63 | 8.23 | 8.21 | 7.27 | 7.41 | 7.99 | 7.98 | | | | |
| 318 | 7.73 | 7.64 | 8.26 | 8.21 | 7.37 | 7.42 | 7.99 | 7.98 | | | | |
| 323 | 7.73 | 7.65 | 8.28 | 8.19 | 7.41 | 7.43 | 8.04 | 7.98 | | | | |
| 328 | 7.73 | 7.66 | 8.29 | 8.18 | 7.43 | 7.46 | 8.04 | 7.98 | | | | |
| $\Delta\delta$ | +0.04 | +0.06 | -0.03 | -0.08 | +0.22 | +0.15 | +0.19 | +0.19 | -0.16 | -0.13 | -0.12 | -0.15 |

-ve $\Delta\delta$ indicates upfield shift
+ve $\Delta\delta$ indicates downfield shift.

**Table 6.14: Chemical shift (ppm) of d-(CCAATTGG)$_2$ as a function of temperature at D/N 2 .0. Also shown here is the net change in chemical shift with temperature, that is, $\Delta\delta = \delta$ (328 K) - $\delta$ (278 K) -ve $\Delta\delta$ indicates upfield shift and +ve $\Delta\delta$ indicates downfield shift**

| Temp. (K) | C1H1' | C2H1' | A3H1' | A4H1' | T5H1' | T6H1' | G7H1' | G8H1' | T5CH3 | T6CH3 | C2H5 |
|---|---|---|---|---|---|---|---|---|---|---|---|
| 278 | 5.71 | 5.17 | 5.96 | 6.18 | 5.85 | 5.72 | 5.54 | 6.01 | 1.30 | 1.56 | 5.61 |
| 283 | 5.71 | 5.19 | 5.96 | 6.18 | 5.87 | 5.74 | 5.55 | 6.01 | 1.30 | 1.57 | 5.61 |
| 288 | 5.75 | 5.24 | 5.96 | 6.18 | 5.90 | 5.76 | 5.56 | 6.03 | 1.31 | 1.57 | 5.62 |
| 293 | 5.76 | 5.27 | 5.99 | 6.18 | 5.91 | 5.80 | 5.57 | 6.04 | 1.32 | 1.57 | 5.63 |
| 298 | 5.77 | 5.32 | 6.02 | 6.19 | 5.93 | 5.82 | 5.59 | 6.05 | 1.33 | 1.58 | 5.65 |
| 303 | 5.79 | 5.38 | 6.04 | 6.20 | 5.95 | 5.84 | 5.61 | 6.06 | 1.34 | 1.59 | 5.72 |
| 308 | 5.83 | 5.60 | 6.06 | 6.20 | 5.96 | 5.88 | 5.64 | 6.07 | 1.37 | 1.61 | 5.74 |
| 313 | 5.87 | 5.68 | 6.08 | 6.20 | 5.97 | 5.90 | 5.69 | 6.09 | 1.41 | 1.63 | 5.86 |
| 318 | 5.94 | 5.73 | 6.08 | 6.20 | 5.98 | 5.91 | 5.77 | 6.10 | 1.47 | 1.66 | 5.89 |
| 323 | 5.98 | 5.80 | 6.09 | 6.20 | 5.99 | 5.93 | 5.84 | 6.12 | 1.53 | 1.70 | 5.90 |
| 328 | 6.08 | 5.88 | 6.10 | 6.22 | 6.00 | 5.95 | 5.89 | 6.15 | 1.61 | 1.75 | 5.92 |
| $\Delta\delta$ | +0.37 | +0.71 | +0.14 | +0.04 | +0.15 | +0.23 | +0.35 | +0.14 | +0.31 | +0.19 | +0.31 |
| Temp. (K) | C1H6 | C2H6 | A3H8 | A4H8 | T5H6 | T6H6 | G7H8 | G8H8 | T5NH | T6NH | G7NH |
| 278 | 7.63 | 7.52 | 8.29 | 8.23 | 7.15 | 7.23 | 7.80 | 7.79 | 13.71 | 13.93 | 12.73 |
| 283 | 7.63 | 7.52 | 8.29 | 8.22 | 7.15 | 7.23 | 7.80 | 7.79 | 13.69 | 13.91 | 12.71 |
| 288 | 7.63 | 7.52 | 8.28 | 8.22 | 7.15 | 7.23 | 7.81 | 7.79 | 13.66 | 13.89 | 12.69 |
| 293 | 7.65 | 7.55 | 8.28 | 8.21 | 7.16 | 7.24 | 7.81 | 7.80 | 13.61 | 13.85 | 12.67 |
| 298 | 7.65 | 7.60 | 8.28 | 8.20 | 7.18 | 7.25 | 7.82 | 7.80 | 13.58 | 13.82 | 12.63 |
| 303 | 7.66 | 7.62 | 8.27 | 8.19 | 7.18 | 7.26 | 7.83 | 7.81 | 13.55 | 13.77 | 12.61 |
| 308 | 7.70 | 7.65 | 8.26 | 8.19 | 7.18 | 7.27 | 7.83 | 7.81 | 13.51 | 13.75 | - |
| 313 | 7.75 | 7.66 | 8.24 | 8.19 | 7.19 | 7.28 | 7.84 | 7.82 | - | - | - |
| 318 | 7.78 | 7.69 | 8.22 | 8.19 | 7.20 | 7.28 | 7.84 | 7.82 | - | - | - |
| 323 | 7.80 | 7.70 | 8.22 | 8.19 | 7.28 | 7.31 | 7.86 | 7.83 | - | - | - |
| 328 | 7.81 | 7.71 | 8.22 | 8.19 | 7.35 | 7.35 | 7.88 | 7.83 | - | - | - |
| $\Delta\delta$ | +0.18 | +0.19 | -0.07 | -0.04 | +0.20 | +0.12 | +0.08 | +0.04 | -0.20 | -0.18 | -0.12 |

Methyl chemical shifts are the weighted average of the chemical shifts in the single and the double strand form of oligonucleotide. A plot of chemical shift for methyl protons at D/N 1.0 and 2.0 vs temperature was plotted and is shown in Figure 6.14. $T_m$ value obtained in this way was found to be 312 ± 2 K at D/N 1.0 and 318 ± 2 K at D/N 2.0. The difference between $T_m$ calculated from methyl protons and disappearance temperature for imino protons was increased due to binding of berberine to d-(CCAATTGG)$_2$. These changes in chemical shift due to titrimetric and

temperature dependent studies showed that berberine binds to d-$(CCAATTGG)_2$ more firmly at D/N ratio 2.0.

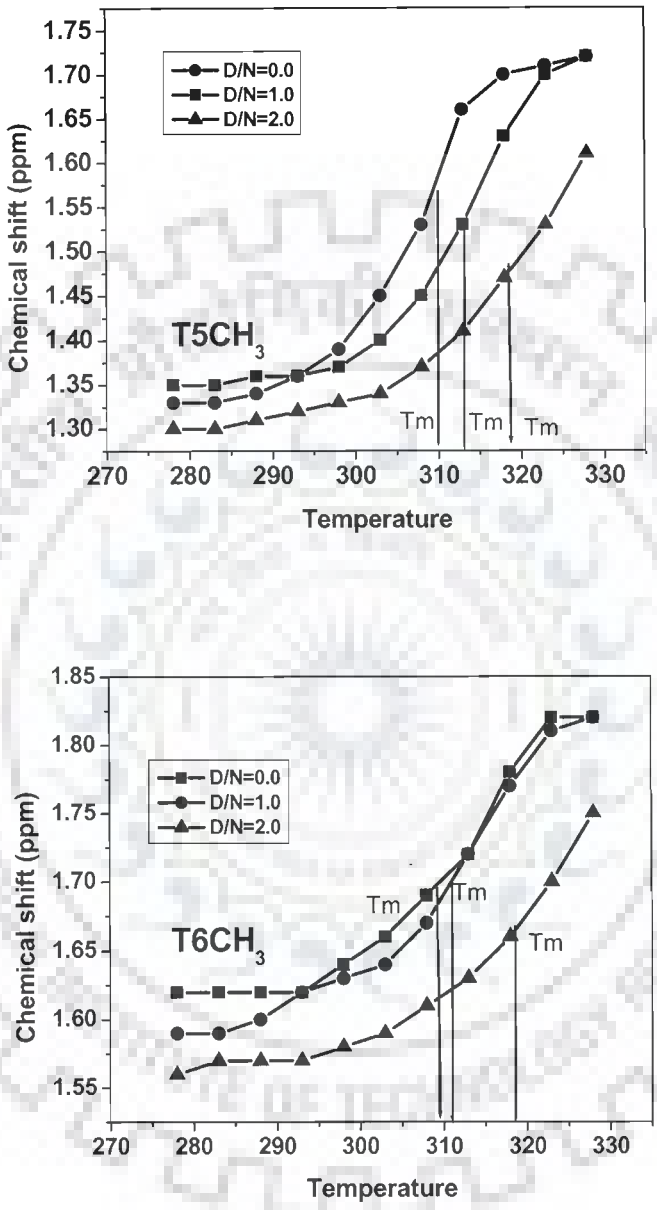


**Figure 6.14: Chemical Shift of methyl protons of d–$(CCAATTGG)_2$ as a function of temperature (278 - 328 K) at D/N 1.0 and 2.0.**

We know that the changes in chemical shift of DNA might result due to structural alterations on binding and not directly related to a specific structural parameter therefore one needs to look at the structure of the specific complex by alternate ways such as inter-proton contacts, which will be discussed further in this chapter. To confirm the binding of berberine to d-$(CCAATTGG)_2$, DOSY studies were done.

### 6.1.2.3 Diffusion Ordered Spectroscopy (DOSY) studies on berberine-d-$(CCAATTGG)_2$ complex

Complexed and noncomplexed forms in a mixture can be distinguished using Diffusion Ordered Spectroscopy (DOSY) due to differences in their relative diffusion coefficient values. Diffusion observed for any interacting molecule in complexed state forms is an average of the populations of the diffusion of the molecule in free and complexed forms in equilibrium. A change in the chemical shift does not provide sufficient indication about the strength of interaction between the components which could be due to other effects influencing the chemical shift but DOSY plots can provide a better insight about the strength of such interactions which are clearly manifested in the diffusion dimension.

The NMR diffusion measurements for berberine (5 mM) and berberine-d-$(CCAATTGG)_2$- complex of D/N ratio 2.0 were done at 298K in $D_2O$ according to the following conditions: 16 spectra were acquired using stimulated echo sequence incorporating bipolar gradients. The gradient strengths were incremented as a square dependence in the range of 1 to 32 G $cm^{-1}$. The diffusion time ($\Delta$) and the length of diffusion gradient ($\delta$) used were 100ms and 6ms respectively. The data were processed by fitting the diffusion decays using the SimFit algorithm provided with

Bruker processing software- Topspin (version 1.3) and verified by plotting -ln(I/Io) versus $\gamma_H^2\delta^2G_z^2(\Delta-\delta/3)$. The slope of the line provides the Diffusion coefficient according to the equation:

$$I / Io = -\exp[D\gamma_H^2\delta^2G_z^2(\Delta-\delta/3]$$

DOSY spectra of berberine and berberine-d-$(CCAATTGG)_2$ complex of 2:1 D/N ratio is shown in Figure 6.15. We found that berberine alone has a diffusion coefficient (D) of ~ 4.0 x $10^{-10}$ $m^2/s$. However, in the presence of d-$(CCAATTGG)_2$, berberine diffused with D = ~1.0 x $10^{-10}$ $m^2/s$, indicating a strong interaction. Accurate measurement of the diffusion was not possible for each proton except for H10, H14, H28, H24 in the complex because the signals broadened on berberine binding with d-$(CCAATTGG)_2$ and merged with other proton signals of DNA. Diffusion constant for H10, H14, H28, H24 resonances corresponding to free and complexed berberine with d-$(CCAATTGG)_2$ is present in Table 6.15. It can be noted from Table 6.15 that protons H24, H10 located on one side (convex) while H14 and H28 located on other side (concave) showed almost equal magnitude change in their respective diffusion constant of free berberine on complexation, which indicate that both sides of berberine were equally involved in the interaction with d-$(CCAATTGG)_2$, which is in accordance to our chemical shift analysis. Since, H10 was found well separated from other proton resonances and values for all the 16 gradients used were calculated, diffusion plot for H10 in free berberine and H10* in complex with d-$(CCAATTGG)_2$ was made. The results are shown in Figure 6.16. Figure clearly shows that on complex formation, the value of diffusion coefficient of the berberine resonances decreased in the complex compared to that in the berberine alone.

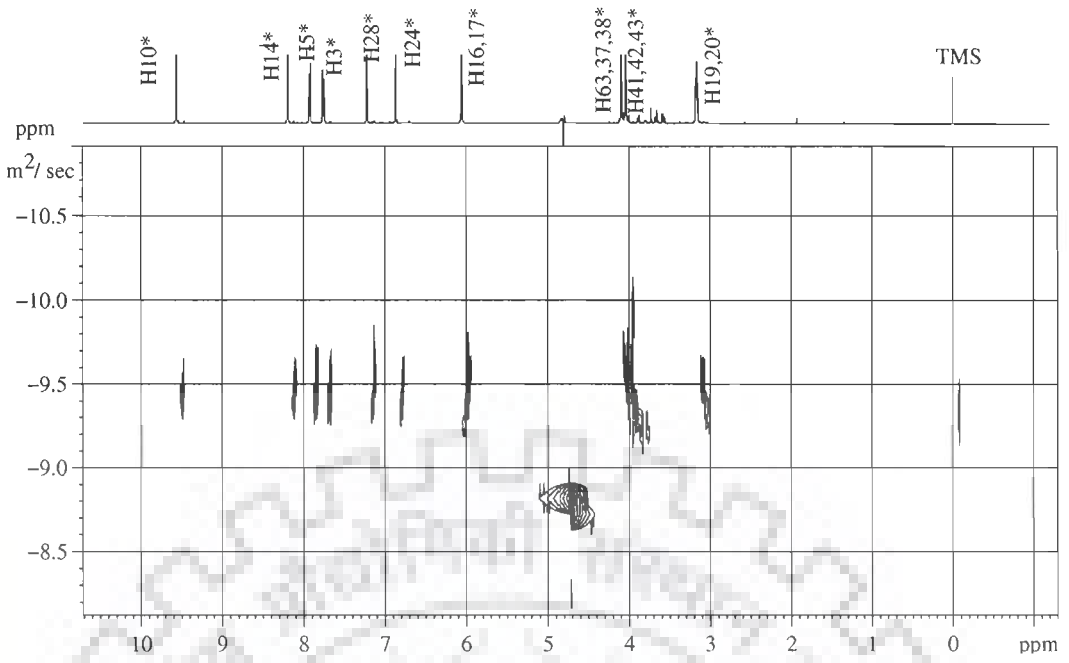


(a)

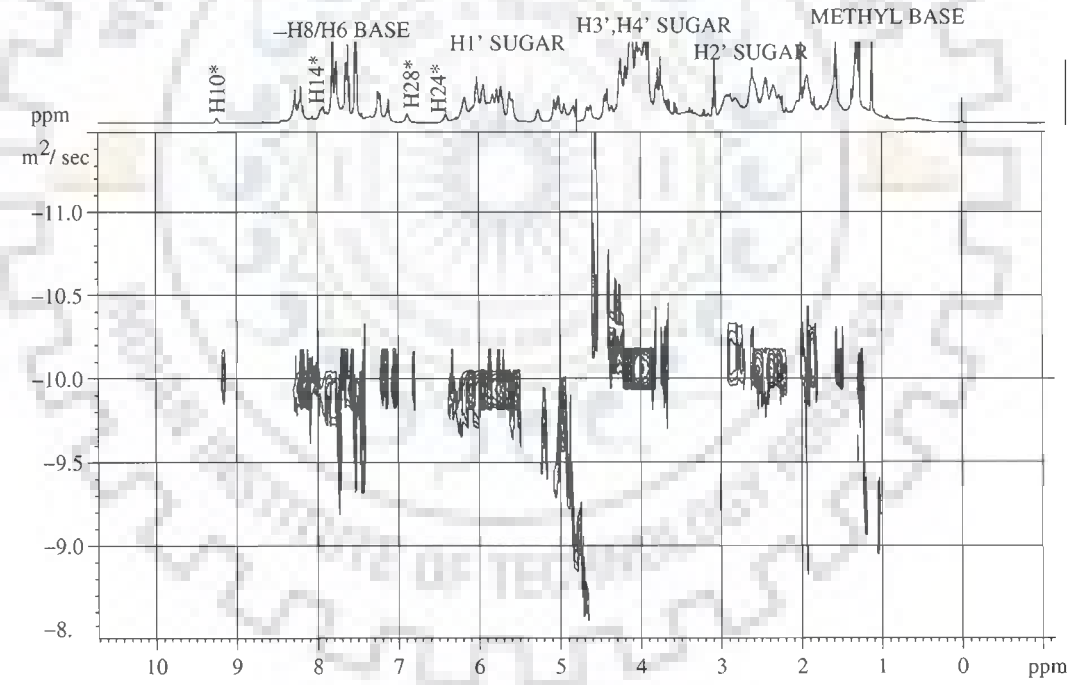


(b)

**Figure 6.15: DOSY of berberine (a) and berberine- d-(CCAATTGG)$_2$ complex (b) in $D_2O$ at 298 K. (* berbrine proton in berberine -d-(CCAATTGG)$_2$ complex).**

**Table 6.15: Diffusion coefficients ($10^{-10}$ $m^2/s$) of berberine protons alone and in complex with d-$(CCAATTGG)_2$ at 298 K.**

| Proton | Berberine 5mM 298 K | Berb- $(CCAATTGG)_2$ (D/N =2.0) 298 K |
|---|---|---|
| H10 | 4.070 | 0.959 |
| H14 | 3.993 | 1.570 |
| H28 | 3.967 | 0.942 |
| H24 | 4.092 | 0.997 |

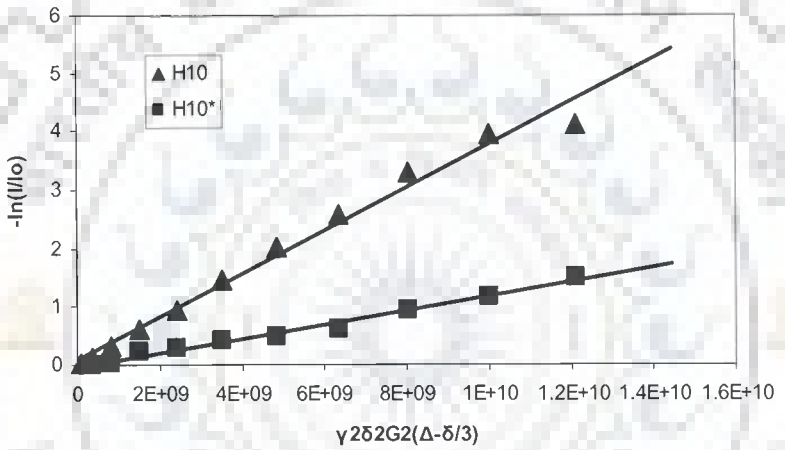


**Figure 6.16: NMR diffusion measurements at 298 K for berberine protons alone (▲) and in complex with d-$(CCAATTGG)_2$ (■). The diffusion coefficient is the slope of the plot -ln(I/Io) versus $\gamma_H^2\delta^2G_z^2(\Delta-\delta/3)$ in $D_2O$ (* berbrine proton in berberine -d-$(CCAATTGG)_2$ complex)**

This is because of the interaction of the berberine with d-$(CCAATTGG)_2$ which slows down the rate of diffusion. However, only one set of peaks was present, which is due to averaging of the diffusion coefficients for complexed and non-complexed resonances of berberine. The diffusion measurements indicated that the majority of

the ligand was associated with DNA even though it was present in 2-fold molar excess.

### 6.1.2.4 Structure of the Complex

The 2D NOESY spectra of berberine-d-$(CCAATTGG)_2$ complex at D/N=2.0 was investigated extensively at mixing time ($\tau_m$) of 300, 200, 150 and 100ms. The intensities of cross peaks were estimated qualitatively as strong intense (ss), strong (s) medium (m) weakly (w) and very weakly (vw) for distances of about 1.8 - 2.5, 2.5 - 3.0, 3.0 - 3.5, 3.5 - 4.0, and 4.0 - 5.0 Å respectively from the spectra recorded at $\tau_m$ = 200 ms (Figure 6.7) The observed NOEs for intranucleotide connectivities, sequential connectivities, and connectivities involving amino and imino protons of base pairs are given in Table 6.7, 6.8 and 6.9 respectively.

**(a) Base pairing**

G8NH was not observed at D/N 2.0 due to fraying effect at the end of d-$(CCAATTGG)_2$. The observation of NOEs G7NH$^b$ with C2N$H_2^b$, C2N$H_2^{nb}$, T6NH with A3N$H_2^b$, A3N$H_2^{nb}$, A3H2, and T5NH with A4N$H_2^b$, A4N$H_2^{nb}$, A4H2 established Watson-Crick base pairing between C2.....G7 and T6....A3 and T5 ....A4 base pairs in the duplex d-$(CCAATTGG)_2$ (Figure 6.7h).

**(b) Sequential connectivities of d-$(CCAATTGG)_2$**

The sequential connectivities base $(H6/H8)_n$ to $(H1')_{n-1}$, $(H2')_{n-1}$, $(H2'')_{n-1}$, base $(H6/H8)_{n-1}$ connectivities were observed at all base pair steps (Figure 6.7a-b, Table 6.8). The sequential connectivity between G7NH-T6NH, T6NH-T5NH imino protons were observed (Table 6.9 and Figure 6.7g) and confirmed the B-DNA geometry for d-(CCAATTGG) in complex with berberine, which was further supported by intrastrand sequential connectivity T5NH- A4N$H_2^{nb}$, interstrand

sequential connectivities T6NH- $C2NH_2^b$ and $C2NH_2^{nb}$ observed in the complex. This clearly demonstrates that DNA duplex was intact all through the sequence d-$(CCAATTGG)_2$ even after the addition of high concentration of berberine (D/N = 2.0). This clearly demonstrates that DNA duplex was intact and predominantly adopts a B-DNA structure apparently with no opening between base pairs to accommodate drug chromophore as expected on binding by a typical intercalator.

**(c) Conformational feature of d-$(CCAATTGG)_2$**

Sugar conformation can be determined from the intensities of cross peaks in NOESY spectra (Table 6.7) at 283 K. The deoxyribose conformation can be estimated from intra-sugar distances of a nucleotide residue. Intra residue inter-proton distances H1'-H2', H1'-H2", H2'-H3', H2"-H3', H2'-H4' and H3'-H4' varied with $P_S$ and $\chi_S$ in a narrow range while the H1'-H4' and H2"-H4' distances varied significantly with PS and $\chi$S, respectively [Wüthrich, 1986] and can be used for conformational analysis. The base H6/H8-H1' connectivity (Table 6.8) suggests the residues to be more close to anti conformation. The deoxyribose conformations were estimated from intrasugar distances of a nucleotide residue [Wüthrich, 1986] . Strong intense cross peaks were observed for H1'-H2", H1'-H2', H1'-H3'. The presence of more intense intraresidue H6/H8-H2' than interresidue H6/H8-H2' (Figure 6.7b) shows the predominance of S-conformation for the deoxyribose ring. The observed intense cross peaks corresponding to H2"-H3' (Figure 6.7e) and H3'-H4' showed that N-conformer might be present. The presence of moderately intense intranucleotide base H6/H8-H3' connectivities (Figure 6.7d) also confirms the presence of minor N-conformer [Barthwal et al., 2004]. The NOE connectivity corresponding to H1'- H4' for G7 and G8 residue was weakly intense as compared to A3 and A4 residues (Figure 6.7d and Table 6.7) indicating that pseudo rotation phase angle for G7 and G8

residue was ~162-180° while that for A3 and A4 might be ≤162°. Among purines, the intensity of H8-H1' cross peak in Figure 6.7a decreased in order A4~A3>G8~G7> so that χ value for G8 and G7 was close to that of B DNA ~ -105° while that for A4 and A3 residues deviated from -105°. Among pyrimidines, H6-H1' cross peak intensity decreased T5~T6> C2~C1 (Figure 6.7a) so that corresponding χ of C2 and C1 was close to ~ -105° whereas, T5, T4 deviated from this value.

**(d) Conformation of berberine**

The intramolecular NOE connectivities within the berberine molecule in berberine-d-$(CCAATTGG)_2$ complex gave information about the conformation of berberine (Table 6.10). The intensities of berberine protons were increased with D/N ratio (Figure 6.7i), but were lesser than its expected intensity i.e. equal to the d-$(CCAATTGG)_2$ at 1:1 and double at 2:1. This is due to the broadening of peaks at higher ratios. Table 6.10 shows the intramolecular NOE connectivities observed within the berberine molecule in the berberine-d-$(CCAATTGG)_2$ complex at D/N= 2.0. It was observed that some new intermolecular cross peaks appeared in the NOESY spectrum of berberine-d-$(CCAATTGG)_2$ complex (Figure 6.7) , while those were absent in berberine alone (Figure 3.5 and Table 3.4). These new cross peaks which were observed on complex formation are shown as"Ⓗ" in Figure 6.7 and are tabulated in Table 6.10. H10 proton of berberine gave cross peaks with distantly placed protons H24, H28, H14 and H5 protons which can be attributed to rotation at ring C of berberine due to its complexation with d-$(CCAATTGG)_2$ and consequently ring D protons came closer to ring A and suggests that the relative orientation of rings w.r.t each other was affected and the conformation of berberine was changed due to binding.

**(e) Intermolecular Interactions**

Specific interactions between protons of berberine and protons of d-$(CCAATTGG)_2$ were observed from proton 2D NOESY spectra recorded at D/N 0.0, 0.5, 1.0, 1.5 and 2.0. The results are shown in Figure 6.7. It was observed that berberine interacts with d-$(CCAATTGG)_2$ even at low concentration and signals were sharp at lower D/N ratio. It is clear from Figure 6.7i that maximum intermolecular interaction was observed at D/N 2.0 but they were broad and merged as compared to separated signals in D/N 0.5 and 1.0. All the intermolecular NOE's observed with their respective intensity are tabulated in Table 6.16. NOE data was used to determine and recognize the interaction site and to define the exact binding mode of berberine to d-$(CCAATTGG)_2$. In the complex, NOEs were observed between the berberine aromatic protons with retention of symmetry for d-$(CCAATTGG)_2$. NOE peaks between aromatic protons of berberine and adenine H2, and sugar protons of DNA were observed. H14 present at concave side of berberine gave cross peaks with T6H2', T6H2", A3H2' and A4H2" in an order of increasing intensity (Figure 6.7b), and H28 cross peaks with G7H1', T6H1' and A4H1' suggest that berberine was not particularly interacting with single specific base pair and suppose to be fit along the length of DNA. Intermolecular peaks between the sugar protons of DNA at A3, A4, T5, T6 region with H10, H14, H28, H14 suggested that the ring D and ring B are supposed to fit in the minor groove of the DNA. H3, H5, H36, 37, 38, H41, 42, 43 protons located on one end of berberine gave NOEs cross peaks with C1-G8 base pair of octamer d-$(CCAATTGG)_2$. H31, 32 on the other hand were found closer to A3, A4 bases giving cross peaks with A3H2' and A4H2'. Cross peaks between H28 of berberine and A3/A4$NH_2$ and A3/A4H2suggests its binding in to the minor groove of d-$(CCAATTGG)_2$.

**Table 6.16 Relative intensities of intermolecular NOE connectivity's between d-(CCAATTGG)$_2$ and the berberine molecule in the berberine-d-(CCAATTGG)$_2$complex at drug to DNA ratio D / N =2.0 from NOESY spectra at 283 K.**

| S.No | Sequence connectivity | Intensity | DISTANCE from minimized model (Å) |
|---|---|---|---|
| 1. | H14-T6H1' | w | 4.67 |
| 2. | H14-T6H2' | w | 4.34 |
| 3. | H14-T6H2" | w | 4.25 |
| 4. | H14-A4H2' | m | 3.45 |
| 5. | H14-A3H2' | m | 3.83 |
| 6. | H28-G7H1' | w | 5.37 |
| 7. | H28-T6H1' | w | 3.68 |
| 8. | H28-A4H1' | m | 2.98 |
| 9. | H28-A3/A4NH$_2$[nb] | s | 1.80 |
| 10. | H28-A3/A4H2 | s | 2.34 |
| 11. | H24-A3H2" | m | 3.54 |
| 12. | H24-T6H1' | w | 5.02 |
| 13. | H24-A3H1' | m | 3.76 |
| 14. | H24-T5H4' | w | 5.73 |
| 15. | H24-A4H3' | w | 4.41 |
| 16. | H10-A3H2" | m | 3.28 |
| 17. | H10-A4H3' | m | 3.70 |
| 18. | H10-G7H1' | vw | 5.69 |
| 19. | H10-T6H1' | w | 4.74 |
| 20. | H41, 42, 43-G8H2' | m | 3.99 |
| 21. | H41, 42, 43-G8H2" | m | 3.48 |
| 22. | H36, 37, 38-C1H2' | m | 3.55 |
| 23. | H36, 37, 38-C1H2" | m | 3.34 |

A schematic representation model based on observed intermolecular peaks with DNA is shown in Figure 6.17. These results propose a binding of berberine that involve ring D and C for interaction with central AATT region, while ring A is supposed to interact with C1-G8. Free rotation at ring C actually gave the whole molecule a specific conformation and makes it crescent in shape. It is reported in literature very exhaustively that most of the DNA minor groove binder are crescent shaped, [Neidle, 2001] which is complementary to minor groove of DNA. Mazzini et al studied the structure of berberine with d-(AAGAATTCTT)$_2$ and found that H10,

H16, 17, H19, 20, H41, 42, 43, H36, H37, 38, H28 and H31, 32 gave cross peak with A4-T7 and A5-T6 base pair while H3, H5 and H24 were observed to give cross peak with C8 base pair. This suggests that central chromphore is interacting with AATT. It was previously discussed by chemical shift analysis, intact sequential connectivity in octamer d-$(CCAATTGG)_2$ and supported by literature [Mazzini et al., 2003] that berberine dose not intercalate into DNA and could possibly be a minor groove binder. Therefore, we proposed a model of berberine binding to the minor groove of central AATT region of d-$(CCAATTGG)_2$ shown in Figure 6.17. Due to the palindromic symmetry of octmaer d-$(CCAATTGG)_2$ and the symmetry observed for the complex in chemical shift resonances, it is clear that d-$(CCAATTGG)_2$ has two equaling sites for berberine binding. Because sites were equal in conformation so we used one site model for berberine-d-$(CCAATTGG)_2$ interaction for rMD studies on the basis of relative intensities of observed cross peaks.

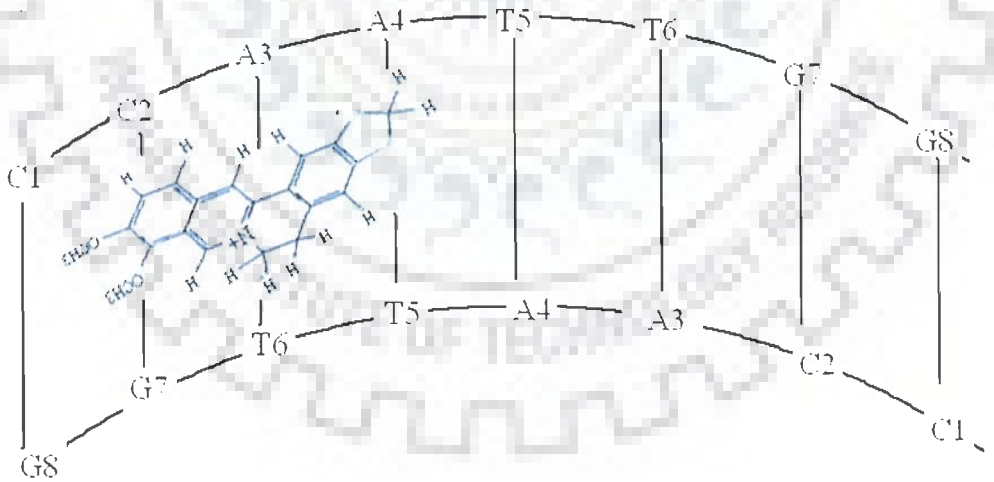


**Figure 6.17: Schematic Representation of Berberine - d-$(CCAATTGG)_2$ Complex.**

### 6.1.3 Restrained Molecular Dynamics Studies

Restrained Molecular Dynamics (rMD) permits the system to undergo conformational and momentum change so that different parts of the phase space accessible to the molecule can be explored and stable conformations identified by energy minimization. Based on the observed intermolecular and intramolecular NOE data an initial model with berberine located in the minor groove of d-$(CCAATTGG)_2$ was considered. The schematic representation of the initial model used in rMD, is shown in Figure 6.17. For rMD, only one molecule of berberine at one site was used for further studies due to the presence of equal sites in d-$(CCAATTGG)_2$. The relative strengths of the cross peaks were used only in qualitative manner. Distances used were about 1.8 - 2.5, 2.5 - 3.0, 3.0 - 3.5, 3.5 - 4.0, and 4.0 - 5.0 Å for strong intense (ss), strong (s) medium (m) and weakly (w) and very weakly (vw) intense peaks, respectively. Distance restraints between atoms involved in the Watson-Crick hydrogen bonding pairs were imposed in the structure calculations based on the experimental evidence from NOESY spectra. All other restrains for the intramolecular and intermolecular connectivities were also given. The final structure obtained after rMD is shown in Figure 6.18. Table 6.17 indicates an assessment of refined structures after equilibration (at the end of 25 ps) in terms of energetics including restraint violations energies and root mean square derivative of energy w.r.t atomic coordinates. The total potential energy of the final structure was 3819 kcal $mol^{-1}$, which was lower than the corresponding energy of initial model structure (4165 kcal $mol^{-1}$). The forcing potential, which indicates contribution to potential energy due to violations of both experimental distances data, exhibited a decrease from 1339 to 1168 kcal $mol^{-1}$ after restrained energy minimization and restrained molecular dynamics simulations.

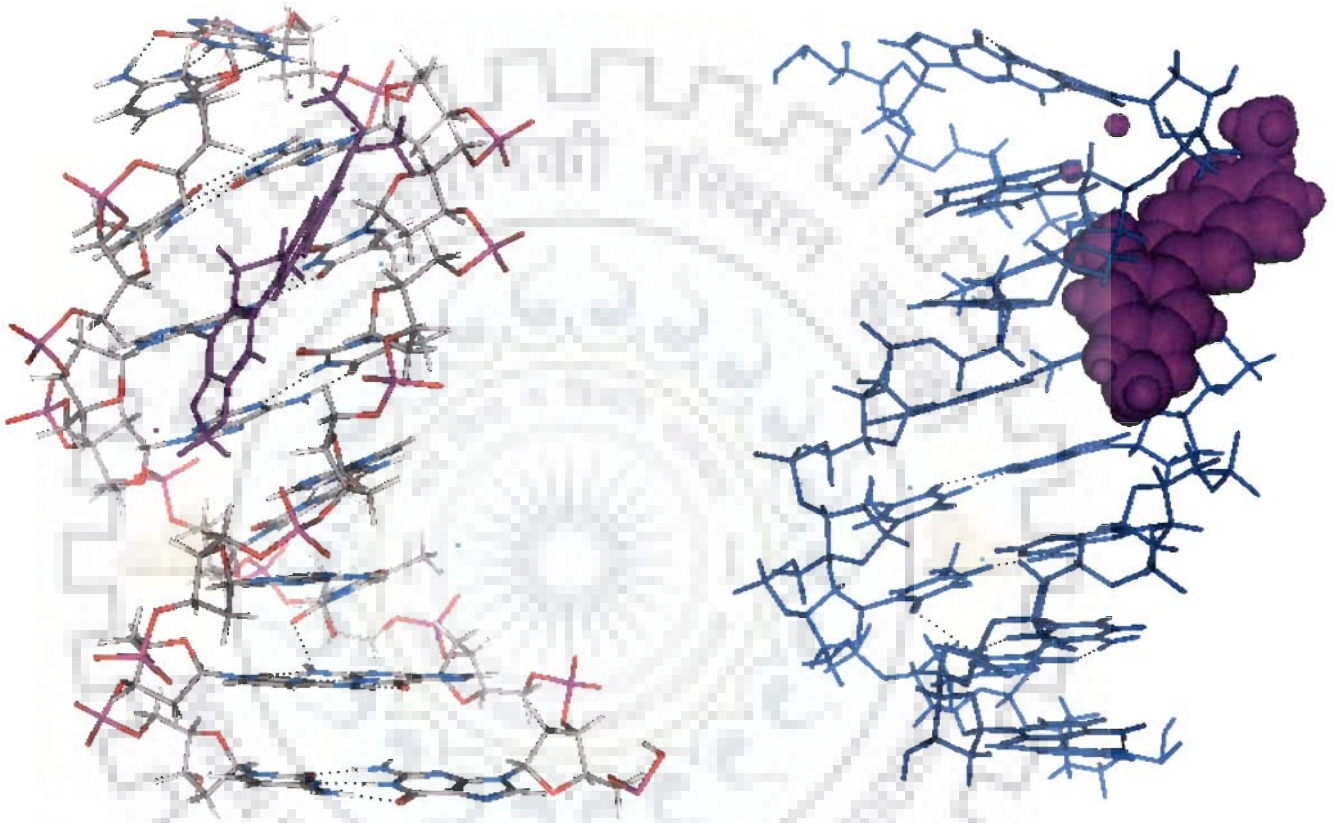

**Figure 6.18: Front view and Side view of the final structure of berberine-d-$(CCATTGG)_2$ complex obtained by restrained molecular dynamics simulations.**

**Table 6.17a: Energy terms (Kcal $mol^{-1}$) for starting structure and final rMD structure.**

| Structure | Total | Bond | Angle | Dihedral |
|---|---|---|---|---|
| Initial | 4165 | 519 | 1228 | 432 |
| Final | 3819 | 340 | 1119 | 398 |
| | **Vdw** | **Electrostatic** | **Restraint** | **Out of plane** |
| Initial | 409 | -181 | 1339 | 86 |
| Final | 406 | -152 | 1168 | 72 |

**Table 6.17b: Summary of experimental restraints and statistical analysis of final structure generated by restrained molecular dynamics (rMD)**

| Parameter | |
|---|---|
| | **No. of Distance Restraints** |
| **Intra residue** | 256 |
| **Inter residue** | 92 |
| **Inter molecular** | 23 |
| **Average pairwise RMSD** | Initial = 0<br>Final = 0.88 |
| **Minor groove width** | Initial = 6.27<br>Final = 7.26 |
| **Minor groove depth** | Initial = 4.29<br>Final = 5.89 |
| **Average residuewise RMSD** | C1=0.93, C2=0.82, A3=1.22<br>A4=1.10, T5=1.18, T6=0.99<br>G7= 0.95, G8= 0.89<br>Berberine=1.12 |

The best-fit refined structure showing all atoms of the front and side view of the complex is shown in Figure 6.18. The berberine -d-$(CCAATTGG)_2$ complex was stabilized via close contacts which involved specific vander Waal's and electrostatic interactions and which is clearly shown in Figure 6.19.

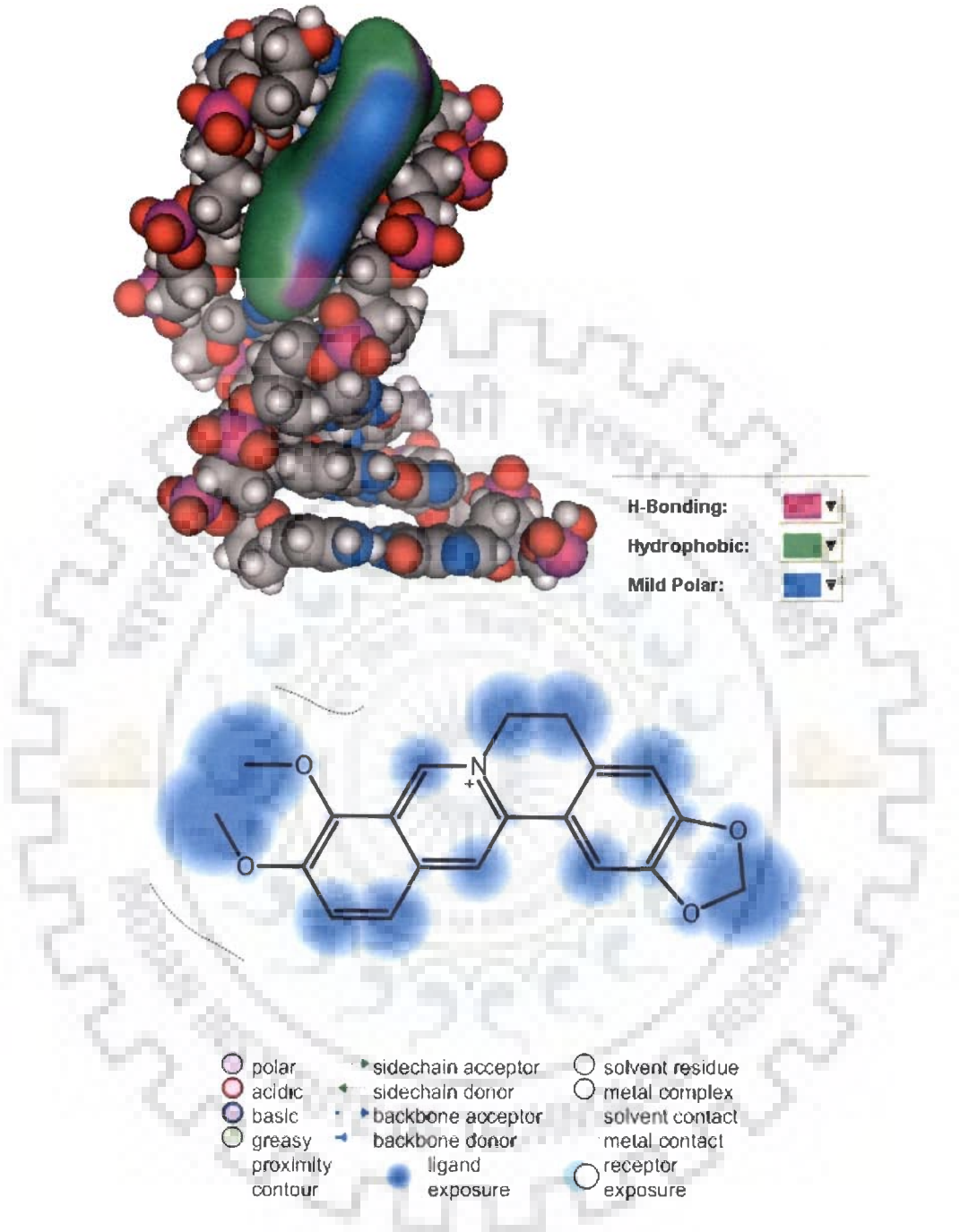


**Figure 6.19: Various Interactions present in 2:1 berberine d-$(CCAATTGG)_2$ complex.**

Several authors have reported the necessity of hydrogen bond formation between ligand and the adenine H2 at the minor groove floor to establish minor groove binding

[Jenkins and Lane, 1997; Jenkins et al., 1993; Lane et al., 1991; Yang et al., 1996]. But in the present study we did not find any hydrogen bond between berberine and d-$(CCAATTGG)_2$ in the final rMD model. Absence of hydrogen bond in berberine binding to the minor groove of d-$(CCAATTGG)_2$ can be explained by extensive study done by Tabernero et al. They studied extensively the role of ligand -DNA hydrogen bond for 22 minor groove ligand-oligonucleotide crystal structure and found that the ligand cationinc group did not show a preference to hydrogen bonding suggesting that presence of hydrogen bond has less importance [Tabernero et al., 1996]. It is in support with several studies done with empirical force field, which concluded the absence of any hydrogen bond formation and found that vander Waals terms are the dominant factor in minor groove binding [Chang and Cheng, 1996; Sauers, 1995]. This view has been supported by Czarny et al by a combined solution binding and structural study on a series of bis-benzimidazole -DNA complexes, which showed that increasing the number of charged group did not significantly affect binding affinity whereas, increasing the number of contacts with the minor groove walls increased the ability to bind [Czarny et al., 1995]. Our results were also in accordance with the study reported in literature on two fold symmetry and sequence specificity of minor groove binders bisquaternary heterocycles SN-6999 and bis-benzimidazole drug Hoechst 33258, which formed a 2:1 complex such that both AT tracts are drug binding sites and the complex has overall pseudo-twofold symmetry [Gavathiotis et al., 2000; Rydzewski et al., 1996]. Therefore it is established with the help of rMD that berberine binds to d-$(CCAATTGG)_2$ in a minor groove binding mode. Model obtained through rMD supports the results from the $^{31}P$ NMR, proton chemical shift analysis, DOSY and intramolecular and intermolecular interaction obtained from 2D NOESY spectrum.

All helical parameters, backbone torsional angles, and sugar conformations of the resulting rMD structures were thoroughly analyzed with the CURVES software, version 5.1 [Lavery and Sklenar, 1989; Lavery et al., 1986]. Plot of the helicoidal parameters as a function of residue position in the duplex is shown in Figure 6.20a-b, along with that for structures of A-DNA and B-DNA and conformation of alone d-$(CCAATTGG)_2$ studied previously in Chapter 5. The overlap geometry at different base pair steps along the sequence in berberine- d-$(CCAATTGG)_2$ is shown in Figure 6.21. Base sequence dependent variations in helicoidal parameters were evident. The octamer in the complexed state with berberine adopts generally B-type conformation with little disruption in some of the parameters. Among the base pairs-axis parameters, the X-displacement (dx) ~ 1 Å for all residues which is close to a value of -0.7 Å was observed in canonical B-DNA and uncomplexed structure of d-$(CCAATTGG)_2$ sequence. But it was also apparent that a little deviation at A3, A4, T5, T6 steps from alone d-$(CCAATTGG)_2$. The y-axis displacement (dy) varies from +0.8 Å to -0.2 Å with no significant variation with base sequence. Large displacements were generally observed in the intercalated complexes [Langlois d'Estaintot et al., 1992; Leonard et al., 1992; Nunn et al., 1991]. The base pairs were inclined (η) at an angle of -15° to +15° and for C1 and C2 residue values were close to A-DNA, which being close to B-DNA when moving towards 3' end. Among the intra-base parameters, the stretch, stagger, and buckle fluctuate along the base sequence. It was observed that berberine induced perturbations, manifest more negative value for propeller at C2, A3, A4 residues, while opening per base also shows a higher value of ~30° for the central AATT residues. These results suggest that the binding of berberine is at A3-T6 and A4-T5 base pair which disturb the DNA helix.

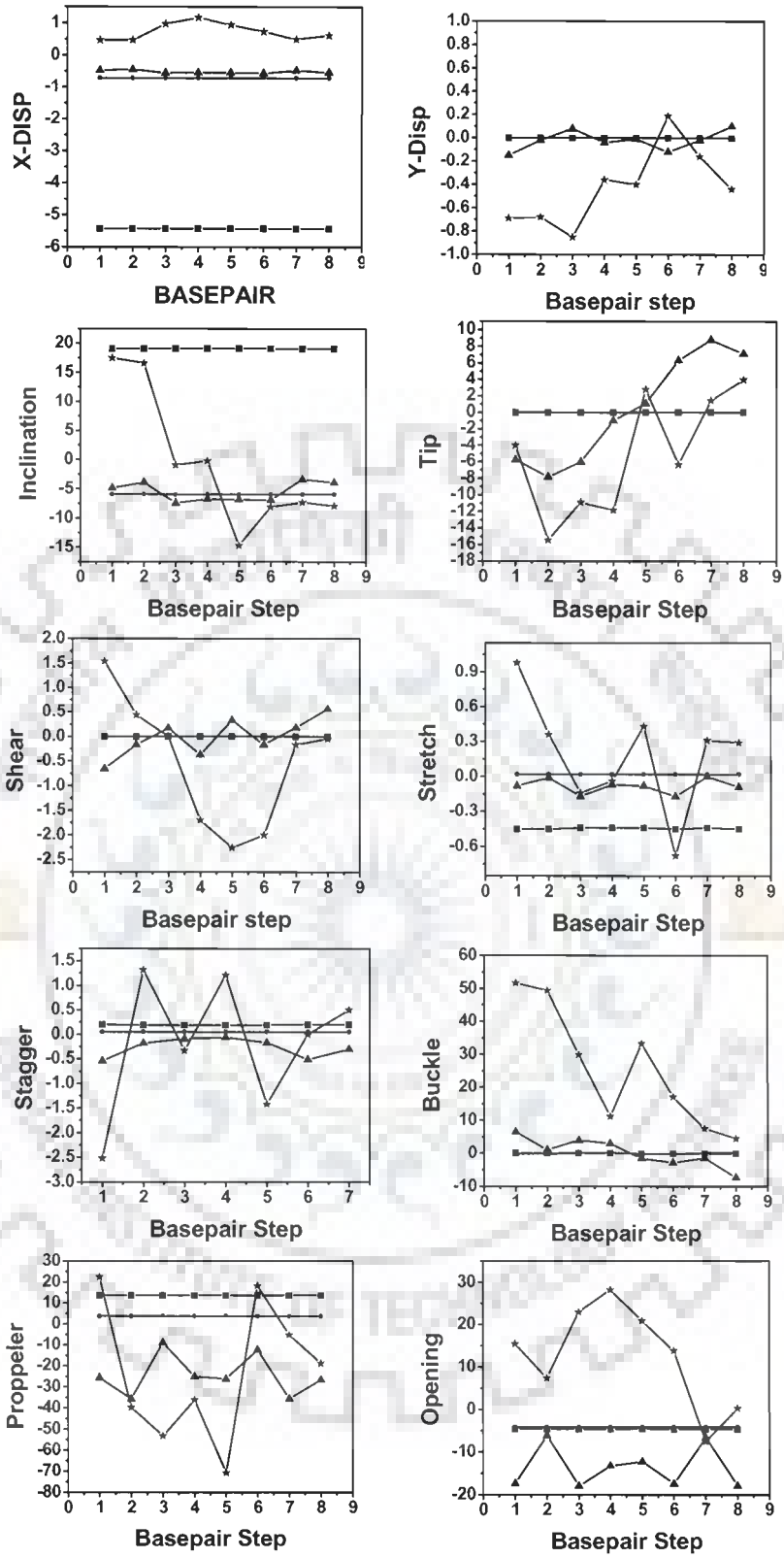
X-DISP
BASEPAIR
Y-Disp
Basepair step
Inclination
Basepair Step
Tip
Basepair Step
Shear
Basepair step
Stretch
Basepair Step
Stagger
Basepair Step
Buckle
Basepair Step
Proppeler
Basepair Step
Opening
Basepair Step

**(Fig. 6.20a)**

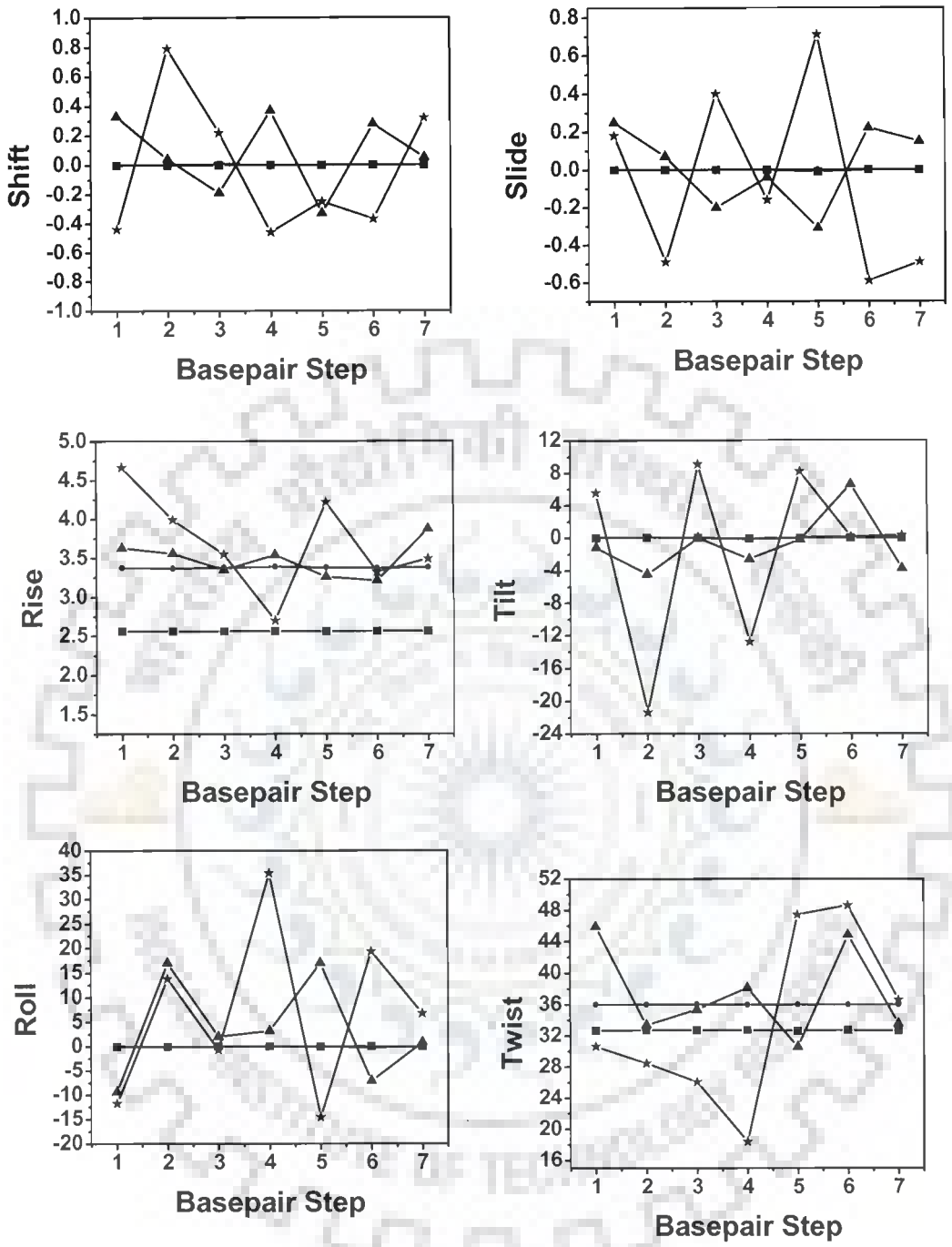


(Fig. 6.20b)

**Figure 6.20a-b: Helical parameters for d-(CCAATTGG)$_2$ complexed with berberine calculated for structure obtained by restrained molecular dynamics simulation d-(CCAATTGG)$_2$ alone- ▲; d-(CCAATTGG)$_2$ + berberine- (★) and that for canonical A-DNA (■) and B-DNA (●).**

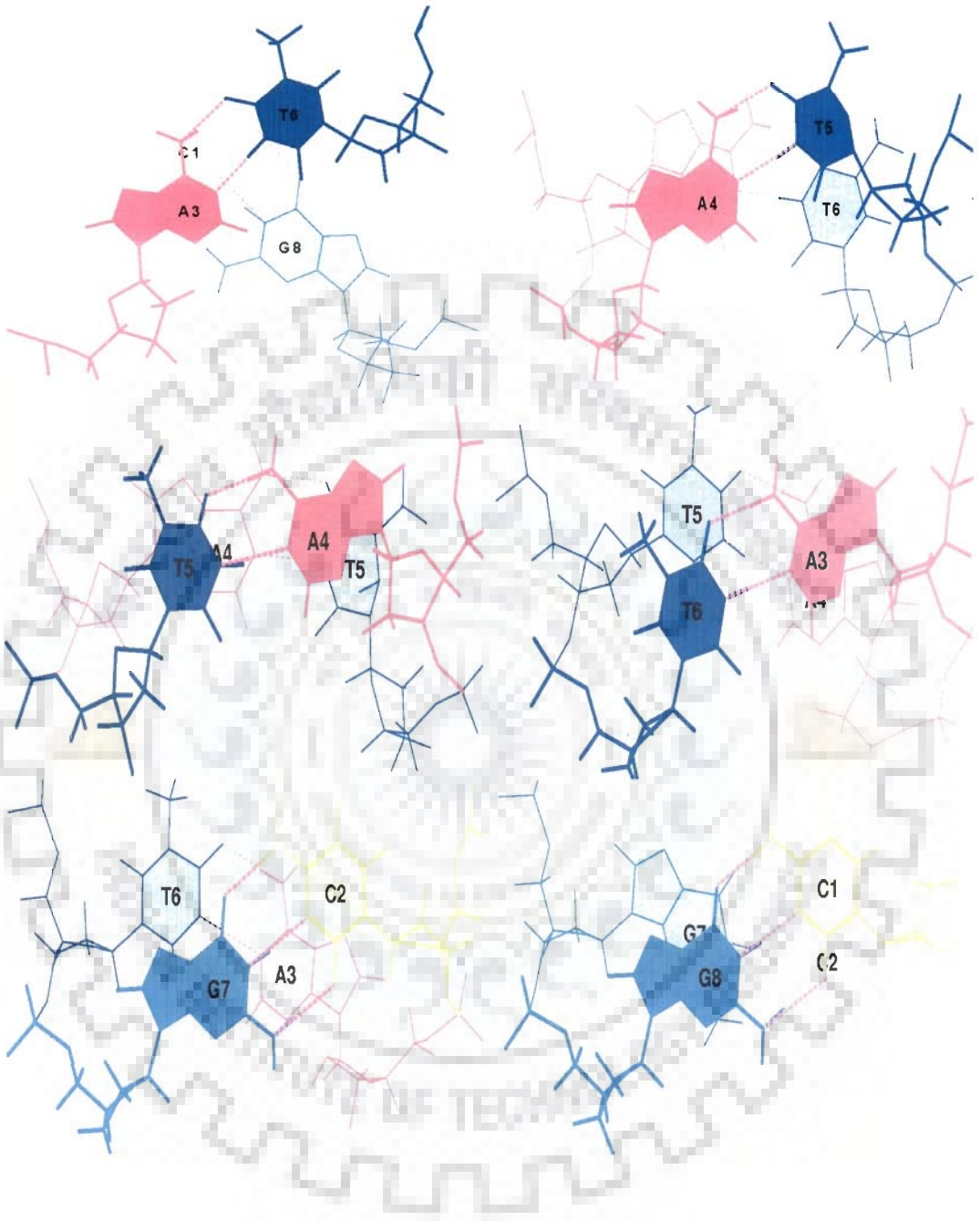


**Figure 6.21: Overlap geometry of base pairs in d-(CCAATTGG)$_2$ at different steps along the sequence in berberine- d-(CCAATTGG)$_2$ complex.**

This indicates that binding of berberine altered significantly the conformation of d-$(CCAATTGG)_2$ at A3-T6 and A4-T5 base while distortions were very less towards the 3' end of the DNA.

The values of torsional angles obtained for the final rMD structure using CURVES software, along with the values for canonical B-DNA are given in Table 6.18.

**Table 6.18: Backbone torsional angles, pseudoratation phase angle and glycosidic bond rotation of the final structure.**

| d-$(CCAATTGG)_2$ | | α | | β | | γ | | δ | |
|---|---|---|---|---|---|---|---|---|---|
| Strand I | Strand II | Strand I | Strand II | Strand I | Strand II | Strand I | Strand II | Strand I | Strand II |
| C1 | G16 | -127.83 | 65.68 | 172.82 | 127.88 | -98.73 | -42.55 | 105.78 | 156.25 |
| C2 | G15 | -65.32 | -65.73 | 89.17 | 175.3 | 54.42 | 63.82 | 148.11 | 148.78 |
| A3 | T14 | -59.63 | -60.08 | 126.93 | 113.61 | 163.07 | 41.52 | 79.28 | 66.57 |
| A4 | T13 | -64.03 | -60.68 | 144.09 | 168.06 | 86.72 | 49.27 | 51.42 | 131.13 |
| T5 | A12 | -88.96 | -80.64 | 177.5 | 110.09 | 120.39 | 85.46 | 75.37 | 107.19 |
| T6 | A11 | -63.79 | 152.32 | -171.89 | 168.66 | 70.73 | 155.05 | 133.09 | 152.99 |
| G7 | C10 | -61.62 | -82.34 | -160.39 | 172.92 | 52.65 | 61.77 | 138.74 | 146.02 |
| G8 | C9 | | | | | 53.37 | -71.61 | 149.54 | 162.1 |
| B-DNA | | -63 | | 136 | | 54.0 | | 123 | |

| d-$(CCAATTGG)_2$ | | ε | | ζ | | χ | | P | |
|---|---|---|---|---|---|---|---|---|---|
| Strand I | Strand II | Strand I | Strand II | Strand I | Strand II | Strand I | Strand II | Strand I | Strand II |
| C1 | G16 | 55.54 | -158.57 | 64.91 | -164.42 | -80.61 | -88.84 | 298.64 | 216.03 |
| C2 | G15 | -113.59 | -170.66 | -115.97 | -77.16 | -43.55 | -109.51 | 185.5 | 169.94 |
| A3 | T14 | -103.65 | -95.2 | -58.46 | 159.37 | -161.11 | -144.95 | 102.97 | 52.7 |
| A4 | T13 | -144.96 | -95.72 | -60.98 | -65.79 | -125.42 | -87.73 | 70.3 | 130.47 |
| T5 | A12 | -163.89 | -107.48 | -86.92 | -103.2 | -141.04 | -164.83 | 97.83 | 310.25 |
| T6 | A11 | -174.3 | -172.95 | -103.53 | -127.74 | -94.4 | -178.63 | 182.56 | 240.68 |
| G7 | C10 | 171.63 | -164.61 | -93.86 | -106.26 | -102.63 | -107.32 | 176.09 | 163.09 |
| G8 | C9 | | | | | -97.32 | -94.83 | 184.16 | 194.24 |
| B-DNA | | -169 | | -108 | | -105 | | 162 | |

There was difference in absolute values of torsional angles of the two strand of DNA, but the general features and trends with base sequence were identical. The backbone torsional angles were not defined by the restraints obtained from NOESY spectra. We

used a low force constant to permit a smooth search, which was conformationally compatible with other structural features. The torsional angle β, adopts a *trans* conformation similar to that of B-DNA for all residues except for the C2 for at the binding strand (strand I) of d-$(CCAATTGG)_2$. The torsional angle α did not fluctuate from the B-DNA except at the C1pC2 base pair, may be attributed to the fraying effect. Torsional angle γ mostly adopts gauche+ and *trans* conformation respectively for various residues. Notable exception for γ is for A3 and T5 at strand I and for T6 at strand II. A3,-T5 base pair and T6 and strand II of DNA molecules suggesting the deviation of γ from BDNA at base pair due to binding of berberine. Torsional angle analysis support the fact demonstrated by $^{31}P$ NMR, that there is no significant change in the phosphate backbone due to binding.

## 6.2. Summary and Conclusions

Even at higher berberine concentration the variation of chemical shift with D/N ratio is small and did not show any saturation behavior as would be expected if chromophore of berberine was to intercalate between base pairs. There was absence of a large downfield shift ~1.5 ppm in $^{31}P$ chemical shifts, as observed with intercalators. These observations rule out intercalation and suggest the external binding mode of berberine with d-$(CCAATTGG)_2$. $^{31}P$-$^{31}P$ exchange spectrum of the d-$(CCAATTGG)_2$ - berberine complex at various D/N ratios did not show any exchange peaks for free and bound resonances. Shift in $^{31}P$ resonances versus temperature in the bound complexes were gradual and the total change, $\Delta\delta = \delta_{328\ K} - \delta_{278\ K}$, was higher for D/N 2.0 as compared to D/N 1.0. Maximum effect of temperature was found to be for A3pA4. These results suggest berberine's external binding involving, A3pA4, A4pT5 and T5pT6 bases. Proton chemical shift was also

observed through titration and we found that only one resonance signal was observed for both DNA and berberine protons, with gradual change in chemical shift with increasing concentration of berberine. It is suggested that the signals were in fast exchange regime and the observed resonance was considered to be an average of free and bound proton. It was proved by titrimataric analysis of $^{1}H$ chemical shift and temperature dependence studies at D/N 1.0 and 2.0 that the central aromatic chromophore of the berberine was involved in the interaction with d-$(CCAATTGG)_2$. Thermal melting temperature calculated by methyl protons chemical shift change with temperature also proved the binding of berberine. Binding was also proved by DOSY which showed majority of the berberine binding to DNA even at D/N ratio 2.0, which was further supported by NOESY data analysis. Presence of all internucleotide sequential connectivities suggests that the DNA did not open up to accommodate the berberine chromophore as observed with intercalators. All the duplex pair peaks, sequential intra and inter-strand peaks exist. Consecutive base pairs did not open and therefore we concluded that berberine binds externally to the d-$(CCAATTGG)_2$ duplex. Intermolecular peaks obtained from NOESY spectra recorded at D/N 2.0 suggested that the drug protons, H10, H14, H28 and H24 located at ring D and ring B were giving cross peaks with sugar protons of DNA at A3, A4, T5, T6 region. This supports significantly that berberine binds to DNA through minor groove binding mode, which is in accordance with the literature [Mazzini et al., 2003]. Hence $^{31}P$ and $^{1}H$ NMR studies also support the external mode of binding. Major participation of vander Waals interaction in the complex formation was also observed in the final rMD model. Conformational analysis showed that DNA octamer in the complexed state adopted conformation close to that of canonical B-DNA structure.

# Summary and Conclusions

Cancer is a class of diseases in which a group of cells begin to grow out of control. Normal body cells grow, divide, and die in an orderly fashion but cancer cells continue to grow and divide and Instead of dying, they outlive normal cells and continue to form new abnormal cells. Chemotherapy is the most widely used treatment for most of the cancer types, which actually involves taking one or more of a type of drug that interferes with the DNA (genes) of fast-growing cells. These drugs are further subdivided into specific classes such as alkylating agents, antimetabolites, anthracyclines, and topoisomerase inhibitors. Currently there is considerable interest among oncologists to find anticancer drugs in chinese herbal medicine. Clinical data from several studies in past showed that some constituents from herbs are having well-known medicinal values including anticancer properties. Berberine is an important alkaloid among the range of herbal medicines which can be obtained from several plants of *Berberidaceae* and *Ranunculaceae* i.e. *Berberis vulgaris*. Experiments showed that berberine acts as anticancer agent by inducing apoptosis and topoisomerase inhibition. Enhancement in the topoisomerase inhibition activity was observed for berberrubine which is an analogue of berberine having OH group replacement at $7^{th}$ position. Several biophysical and structural studies were performed to obtain data on the conformational and structural features of berberine and berberrubine and their interaction with DNA which help us to understand their mode of action.

We have obtained the structural and conformational features of berberine and berberrubine using nuclear magnetic resonance, restrained Molecular Dynamics

(rMD) and quantum chemical calculations. For both the drugs all proton and carbon were assigned using 1D-$^{1}$H and 2D-$^{1}$H NOESY, and 2D-$^{1}$H-$^{13}$C ; HSQC, HMBC experiments. rMD for both the drugs was performed using distance restraints from their respective ROESY spectrum. rMD structure and optimized structure using quantum chemical calculations with B3LYP method showed significant variation in the conformation of both drugs at 7$^{th}$ position. This was also supported by chemical shift calculations using Gauge Invariant Atomic Orbital (GIAO) method with density functional method and basis sets from STO-3G to 6-311G**. The effect of increasing size of basis set for STO-3G, 3-21G. 6-31G, 6-31G**, 6-311G** and 6-311+G (2d, p) showed that the bigger basis set slowed down the calculations but gave more accurate results. B3LYP method with 6-311G** basis set was found to be the best for calculations. Solvent effect was also observed during quantum chemical calculations and revealed that the geometrical parameters were relatively less influenced by solvent then the chemical shift. Proton chemical shift were more sensitive to solvent then carbon due to their position on the periphery of the berberine and berberrubine. All these theoretical and experimental observations (chemical shift and structural parameters) for both drugs showed a variation in the positions of the atoms in the $OCH_3$ and OH groups and provide a clear signature in the conformation of the berberrubine. This suggests that berberrubine has more planer group at 7$^{th}$ position as compared to berberine which can be directly attributed to its better binding with DNA or DNA-topoisomerase complex and further correlated to its enhanced topoisomerase poison activity.

An attempt was also made to elucidate the binding affinity of berberine and berberrubine with DNA. To identify their preferred binding site, UV-visible and fluorescence spectroscopy was used. CT DNA, Poly dA-dT, Poly dG-dC and

oligonucleotides: d-$(CGATCG)_2$, d-$(TGCGCA)_2$, d-$(CGTACG)_2$, d-$(CGTACGCGTACG)_2$, d-$(CGATCGCGATCG)_2$, d-$(ATATATATAT)_2$, d-$(CGCGCGCGCG)_2$, d-$(TGCGCATGCGCA)_2$, d-$(CCAATTGG)_2$ having 6-12 base pairs were used in this study. Berberine-DNA interaction was investigated by observing the change in absorption intensity of 344 nm band of UV spectrum and 545 nm emission band of fluorescence spectrum when excited at 350 nm. Hypochromicity and sharp isobestic points in UV spectrum and enhancement in the fluorescence intensities were observed on successive addition of DNA to a fixed concentration of berberine. Interaction studies of berberine with different polynucleotides showed that berberine preferred AT rich DNA sequences. A preferential binding of berberine towards d-$(CCAATTGG)_2$ over d-$(TGCGCATGCGCA)_2$ showed that binding not only depend on the length of oligonucleotide but also shows specificity to the nucleotide sequence. Berberine preference for AATT site then single AT site was observe. The effect of neighbour base to the binding site was also elucidated. Results showed that negative potential at minor groove was reduced due to the presence of guanine at +1 position of AT site. The strong interaction of berberine with promoter containing sequence d-$(CCAATTGG)_2$ was observed and this sequence was further used for structural studies to reveal its exact mode of binding. Berberrubine spectral characteristics were demonstrated for the first time. It was observed that berberrubine did not show any significant variation in Uv-visible spectrum ($\lambda_{max}$= 377 nm) even after addition of high amount of DNA, which was further supported by fluorescence studies. Although it was reported in literature [Kim et al., 1998; Kim et al., 2002] and also supported by our conformational studies [Tripathi et al., 2007] that berberrubine has a planar group at $7^{th}$ position which is supposed to enhance its binding affinity but very weak binding was observed for berberrubine using UV-visible and fluorescence

studies. It can be attributed to the fact that berberrubine is a more potent topoisomerase inhibitor [Kim et al., 1998] which might bind to the complex of topoisomerase rather than DNA alone.

The CCAAT box was the first element identified among enhancers and promoters, which helps in transcription process of genes. This sequence is widely present in TATA less promoters and several of oncogenes such as TLX3 gene which is over expressed in T-cell acute lymphocytic leukemia. It is proved by uncountable studies that local DNA structure is correlated with all biological functions. Therefore, all the structural and conformational studies of d-$(CCAATTGG)_2$ sequence which contains the CCAAT box as an intrinsic part was done using nuclear magnetic resonance, restrained molecular dynamics and helix analysis. Temperature dependence studies were also done to elucidate the thermal melting behaviour of d-$(CCAATTGG)_2$ using imino and methyl protons in particular. Thermal melting temperature for d-$(CCAATTGG)_2$ was calculated to be 308 ±2 K. The results for conformational analysis of d-$(CCAATTGG)_2$ were compared with the standard A and B-DNA along with crystal structure available in the literature. It was found that solution structure obtained in this study was almost similar to crystal structure. Both the crystal and rMD structures were comparatively closer to canonical form of B-DNA then A-DNA but still both structures deviate from B-DNA in a few numbers of observable characteristics. Some of the helicoidal parameters, such as propeller twist, roll angle and minor groove width showed deviation from B-DNA particularly at central AATT region. This analysis also supports the structural insight and hydration patterns elucidated by vlieghe et al which showed that d-$(CCAATTGG)_2$ has narrow minor-groove width and BI conformation [Vlieghe et al., 1999] and can be used to design new minor-groove binders.

It is well established that berberine inhibits the biosynthesis of DNA and RNA by interacting with DNA and hence shows anti cancer activity. In order to achieve exact mode for binding of berberine to DNA; $^{31}P$ and $^{1}H$ Nuclear Magnetic Resonance spectroscopy followed by restrained Molecular Dynamics simulations were used to study conformation of berberine-d-$(CCAATTGG)_2$ complex. It was inferred from $^{31}P$ NMR that a little change (< 0.10) in the chemical shift of phosphorus signals does not lead to opening of base pairs, which is generally found in case of intercalators associated with large down field shifts of 1.6-2.6 ppm [Gorenstein, 1992; Patel, 1974; Patel and Canuel, 1976; Patel et al., 1982]. $^{31}P$-$^{31}P$ NOESY exchange studies of complex showed single bound and free $^{31}P$ signals due to fast exchange on NMR time scale. Temperature dependence studies of 1D-$^{31}P$ NMR showed that berberine not only binds to A3pA4 site but also interacts with the neighboring residues. $^{1}H$ NMR titrimatric analysis, temperature dependence studies, and DOSY studies reveal that berberine binds to d-$(CCAATTGG)_2$ at higher concentration i.e. drug to nucleotide ratio (D/N) 2. This was further supported by NOESY data analysis. The presence of intra base pair, sequential inter base pair and all sequential intramolecular NOE connectivities expected in standard B–DNA geometry confirmed that DNA duplex is intact in all three complexes with apparently no opening of base pairs to accommodate drug chromophore as generally observed with drug intercalation. Conformational analysis of the final rMD structure showed DNA octmaer d-$(CCAATTGG)_2$ in complex state adopted a conformation close to that of canonical B–DNA structure. Several intermolecular contacts observed between berberine and d-$(CCAATTGG)_2$ protons confirmed the proximity of aromatic chromophore to central AATT base pair. Berberine protons H10, H14, H28 and H24 located at ring D and ring B were found simultaneously close to sugar protons of A3-

T6 and A4-T5 base pairs. While H41, 42, 43 and H36, 37, 38 protons of berberine were in proximity to the C1-G8 base pair. Such NOE connectivities were possible only if berberine aromatic chromophore binds to the minor groove of the d-$(CCAATTGG)_2$. Minor groove binding of berberine is confirmed by the rMD studies which showed that vander Waals interaction were the preferred interactions in the complex formation.

Present investigations explored the structure–activity basis for direct anticancer and topoisomerase inhibition activities of berberine.

# References


1. Abraham RJ, Mobli M and Smith RJ (2004). $^{1}$H chemical shifts in NMR. Part 20—Anisotropic and steric effects in halogen substituent chemical shifts (SCS), a modelling and ab initio investigation. *Magn Reson Chem* **42**: 436-444.
2. Akalank J and Rajeswari MR (2003). Binding studies on peptide–oligonucleotide complex: intercalation of tryptophan in GC-rich region of c-myc gene. *Biochim Biophys Acta - General Subjects* **1622**, 2: 73-81.
3. Altona C (1982). Conformational analysis of nucleic acids. Determination of backbone geometry of single-helical RNA and DNA in aqueous solution. *Recl Trav Chim Pays-Bas* **101**: 413-433.
4. Altona C and Sundaralingam M (1972). Conformational analysis of the sugar ring in nucleosides and nucleotides. New description using the concept of pseudorotation. *J Am Chem Soc* **94**, 23: 8205-8212.
5. Assa-Munt N and Kearns DR (1984). Poly (dA-dT) has a right-handed B conformation in solution: a two-dimensional NMR study. *Biochemistry* **23**, 5: 791-796.
6. Baird AW, Taylor CT and Brayden DJ (1997). Non-antibiotic anti-diarrhoeal drugs: factors affecting oral bioavailability of berberine and loperamide in intestinal tissue. *Adv Drug Deliv Rev* **23**, 1-3: 111-120.
7. Ballerini P, Blaise A, Busson-Le Coniat M, Su XY, Zucman-Rossi J, Adam M, van den Akker J, Perot C, Pellegrino B and Landman-Parker J (2002). HOX11L2 expression defines a clinical subtype of pediatric T-ALL associated with poor prognosis. *Blood* **100**, 3: 991-997.
8. Barthwal R, Awasthi P, Kaur M, Sharma U, Srivastava N, Barthwal SK and Govil G (2004). Structure of DNA sequence d-TGATCA by two-dimensional nuclear magnetic resonance spectroscopy and restrained molecular dynamics. *J Struct Biol* **148**, 1: 34-50.

9. Barve AC, Ghosh S, Kumbhar AA, Kumbhar AS and Puranik VG (2005). DNA-binding studies of mixed ligand cobalt (III) complexes. *Transition Metal Chemistry* **30**, 3: 312-316.

10. Becke AD (1988). Density-functional exchange-energy approximation with correct asymptotic behavior. *Phys Rev A* **38**, 6: 3098-3100.

11. Becke AD (1993). Density-functional thermochemistry. III. The role of exact exchange. *J Chem Phys* **98**: 5648-5652.

12. Benoist C, O'Hare K, Breathnach R and Chambon P (1980). The ovalbumin gene-sequence of putative control regions. *Nucleic Acids Res* **8**, 1: 127-142.

13. Beutel BA and Gold L (1992). In vitro evolution of intrinsically bent DNA. *J Mol Biol* **228**, 3: 803-812.

14. Bhadra K, Maiti M and Kumar GS (2007). Molecular recognition of DNA by small molecules: AT base pair specific intercalative binding of cytotoxic plant alkaloid palmatine. *Biochim Biophys Acta -General Subjects* **1770**, 7: 1071-1080.

15. Bhadra K, Maiti M and Kumar GS (2008a). Berberine-DNA complexation: new insights into the cooperative binding and energetic aspects. *Biochim Biophys Acta* **1780**, 9: 1054-1061.

16. Bhadra K, Maiti M and Kumar GS (2008b). DNA-binding cytotoxic alkaloids: comparative study of the energetics of binding of berberine, palmatine, and coralyne. *DNA Cell Biol* **27**, 12: 675-685.

17. Bhakuni D and Jain S (1986). Protoberberine alkaloids. *The Alkaloids: Chemistry and Pharmacology* **28**: 95-181.

18. Blackburn GM and Gait MJ 1990 Nucleic acids in Chemistry and Biology. *Oxford.*

19. Blasko G, Cordell GA, Bhamarapravati S and Beecher CWW (1988). Carbon-13 NMR assignments of berberine and sanguinarine. *Heterocycles (Sendai)* **27**, 4: 911-916.

20. Blommers MJJ, Ven FJM, Marel GA, Boom JH and Hilbers CW (1991). Two-dimensional NMR studies and structural analysis of d (ATCCTATTTATAGGAT). *Eur J Biochem* **201**, 1: 33-51.

21. Boelens R, Scheek RM, Dijkstra K and Kaptein R (1985). Sequential assignment of imino- and amino-proton resonances in $^{1}H$ NMR spectra of oligonucleotides by two-dimensional NMR spectroscopy: application to a lac operator fragment. J. *Magn. Reson.* **62**, 3: 378-386.

22. Borghini S, Vargiolu M, Di Duca M, Ravazzolo R and Ceccherini I (2006). Nuclear Factor Y Drives Basal Transcription of the Human TLX3, a Gene Overexpressed in T-Cell Acute Lymphocytic Leukemia. *Molecular Cancer Research* **4**, 9: 635.

23. Boulikas T (1996). Common structural features of replication origins in all life forms. *J. Cell. Biochem.* **60**, 3: 297-316.

24. Braunlin WH and Bloomfield VA (1988). $^{1}H$ NMR study of the base-pairing reactions of $d(GGAATTCC)_2$: salt and polyamine effects on the imino proton exchange. *Biochemistry* **27**, 4: 1184-1191.

25. Braunlin WH and Bloomfield VA (1991). 1H NMR study of the base-pairing reactions of d(GGAATTCC): salt effects on the equilibria and kinetics of strand association. *Biochemistry* **30**, 3: 754-758.

26. Bucher P (1990). Weight matrix descriptions of four eukaryotic RNA polymerase II promoter elements derived from 502 unrelated promoter sequences. *J. Mol. Biol* **212**, 4: 563.

27. Bucher P and Trifonov EN (1988). CCAAT box revisited: bidirectionality, location and context. *Journal of biomolecular structure & dynamics* **5**, 6: 1231.

28. Byrne CD and de Mello AJ (1998). Photophysics of ethidium bromide complexed to ct-DNA: a maximum entropy study. *Biophysical chemistry* **70**, 3: 173-184.

29. Calladine CR (1982). Mechanics of sequence-dependent stacking of bases in B-DNA. *J Mol Biol* **161**, 2: 343-352.

30. Cao Y and He XW (1998). Studies of interaction between safranine T and double helix DNA by spectral methods. *Spectrochim Acta A Mol Biomol Spectrosc* **54A**, 6: 883-892.

31. Casanovas J, Am Namba S, Leo N, Glb A, Da Silva G and Alema C (2001). Calculated and experimental NMR chemical shifts of p-menthane-3-9-dioles. A

combination of molecular dynamics and quantum mechnaics to detrmine the structure and the solvent effect. *J Org Chem* **66**: 3775-3782.

32. Cave H, Suciu S, Preudhomme C, Poppe B, Robert A, Uyttebroeck A, Malet M, Boutard P, Benoit Y and Mauvieux L (2004). Clinical significance of HOX11L2 expression linked to t (5; 14)(q35; q32), of HOX11 expression, and of SIL-TAL fusion in childhood T-cell malignancies: results of EORTC studies 58881 and 58951. *Blood* **103**, 2: 442-450.

33. Celda B, Widmer H, Leupin W, Chazin WJ, Denny WA and Wuthrich K (1989). Conformational studies of d-$(AAAAATTTTT)_2$ using constraints from nuclear overhauser effects and from quantitative analysis of the cross-peak fine structures in two-dimensional $^1H$ nuclear magnetic resonance spectra. *Biochemistry* **28**, 4: 1462-1471.

34. Chaires JB (1998). Drug--DNA interactions. *Curr Opin Struct Biol* **8**, 3: 314-320.

35. Chaires JB and Waring MJ 2001 Drug-nucleic acid interactions. *Academic Press*.

36. Chang DK and Cheng SF (1996). On the importance of van der Waals interaction in the groove binding of DNA with ligands: restrained molecular dynamics study. *Int J Biol Macromol* **19**, 4: 279-285.

37. Chen WH, Chan CL, Cai Z, Luo GA and Jiang ZH (2004). Study on noncovalent complexes of cytotoxic protoberberine alkaloids with double-stranded DNA by using electrospray ionization mass spectrometry. *Bioorg Med Chem Lett* **14**, 19: 4955-4959.

38. Chen WH, Pang JY, Qin Y, Peng Q, Cai Z and Jiang ZH (2005a). Synthesis of linked berberine dimers and their remarkably enhanced DNA-binding affinities. *Bioorg Med Chem Lett* **15**, 10: 2689-2692.

39. Chen WH, Qin Y, Cai Z, Chan CL, Luo GA and Jiang ZH (2005b). Spectrometric studies of cytotoxic protoberberine alkaloids binding to double-stranded DNA. *Bioorg Med Chem* **13**, 5: 1859-1866.

40. Cheung S, Arndt K and Lu P (1984). Correlation of lac operator DNA imino proton exchange kinetics with its function. *Proc Nat Acad Sci U.S.A.* **81**, 12: 3665-3669.

41. Chi CW, Chang YF, Chao TW, Chiang SH, P'Eng F K, Lui WY and Liu TY (1994). Flowcytometric analysis of the effect of berberine on the expression of glucocorticoid receptors in human hepatoma HepG2 cells. *Life Sci* **54**, 26: 2099-2107.

42. Chung JG, Chen GW, Hung CF, Lee JH, Ho CC, Ho HC, Chang HL, Lin WC and Lin JG (2000). Effects of berberine on arylamine N-acetyltransferase activity and 2-aminofluorene-DNA adduct formation in human leukemia cells. *Am J Chin Med* **28**, 2: 227-238.

43. Chuprina VP, Lipanov AA, Fedoroff OY, Kim S, Kintanar A and Reid BR (1991). Sequence effects on local DNA topology. *Proc Nat Acad Sci USA* **88**, 20: 9087-9091.

44. Ckless K, Schlottfeldt JL, Pasqual M, Moyna P, Henriques JA and Wajner M (1995). Inhibition of in-vitro lymphocyte transformation by the isoquinoline alkaloid berberine. *J Pharm Pharmacol* **47**, 12A: 1029-1031.

45. Colombo D, Ferraboschi P, Ronchetti F and Toma L (2002). Stereochemical analysis of the 3 greek small letter alpha-and 3ß-hydroxymetabolites of tibolone through NMR and quantum-chemical investigations. An experimental test of GIAO calculations. *Magn Reson Chem* **40**: 581–588.

46. Costa LAS, Hambley TW, Rocha WR, De Almeida WB and Dos Santos HF (2006). Kinetics and structural aspects of the cisplatin interactions with guanine: A quantum mechanical description. *Int J Quantum Chem* **106**, 9: 2129-2144.

47. Cragg G and Suffness M (1988). Metabolism of plant-derived anticancer agents. *Pharmacol Ther* **37**, 3: 425-461.

48. Cragg GM, Newman DJ and Snader KM (1999). Drug discovery and development from natural plant.11th NAPRECA Symposium Book of Proceedings, Antananarivo, Madagascar. 56-69.

49. Creemers GJ, Bolis G, Gore M, Scarfone G, Lacave AJ, Guastalla JP, Despax R, Favalli G, Kreinberg R, Van Belle S, Hudson I, Verweij J and Ten Bokkel Huinink WW (1996). Topotecan, an active drug in the second-line treatment of epithelial ovarian cancer: results of a large European phase II study. *J Clin Oncol* **14**, 12: 3056-3061.

50. Crothers DM and Shakked Z (1999). Oxford Handbook of Nucleic Acid Structure.

51. Czarny A, Boykin DW, Wood AA, Nunn CM, Neidle S, Zhao M and Wilson WD (1995). Analysis of van der Waals and electrostatic contributions in the interactions of minor groove binding benzimidazoles with DNA. *J Am Chem Soc* **117**, 16: 4716-4717.

52. Danilov VI, Dailidonis VV, Hovorun DM, Kurita N, Murayama Y, Natsume T, Potopalsky AI and Zaika LA (2006). Berberine alkaloid: Quantum chemical study of different forms by the DFT and MP2 methods. *Chem Phys Lett* **430**, 4-6: 409-413.

53. Das S, Kumar GS, Ray A and Maiti M (2003). Spectroscopic and thermodynamic studies on the binding of sanguinarine and berberine to triple and double helical DNA and RNA structures. *J Biomol Struct Dyn* **20**, 5: 703-714.

54. Davidson MW, Lopp I, Alexander S and Wilson WD (1977). The interaction of plant alkaloids with DNA. II. Berberinium chloride. *Nucleic Acids Res* **4**, 8: 2697-2712.

55. Debnath D, Kumar GS and Maiti M (1991). Circular dichroism studies of the structure of DNA complex with berberine. *J Biomol Struct Dyn* **9**, 1: 61-79.

56. Debnath D, Kumar GS, Nandi R and Maiti M (1989). Interaction of berberine chloride with deoxyribonucleic acids: evidence for base and sequence specificity. *Indian J Biochem Biophys* **26**, 4: 201-208.

57. Dickerson RE (1983). Base sequence and helix structure variation in B and A DNA. *J Mol Biol* **166**, 3: 419.

58. Dickerson RE (1992). DNA structure from A to Z. *Methods Enzymol* **211**: 67-111.

59. Doggrell SA (2005). Berberine--a novel approach to cholesterol lowering. *Expert Opin Investig Drugs* **14**, 5: 683-685.

60. Donlan ME and Lu P (1992). Transcriptional enhancer related DNA sequences: anomalous $^{1}$H NMR NOE crosspeaks. *Nucleic Acids Res* **20**, 3: 525.

61. Dornberger U, Flemming J and Fritzsche H (1998). Structure determination and analysis of helix parameters in the DNA decamer d $(CATGGCCATG)_2$

comparison of results from NMR and crystallography. *J Mol Biol* **284**, 5: 1453-1463.

62. Dostál J, Man S, Seckárová P, Hulová D, Necas M, Potácek M, Toušek J, Dommisse R, Van Dongen W and Marek R (2004). Berberine and coptisine free bases. *J Mol Struct* **87**, 1-3: 135-142.

63. Efstratiadis A, Posakony JW, Maniatis T, Lawn RM, O'Connell C, Spritz RA, DeRiel JK, Forget BG, Weissman SM and Slightom JL (1980). The structure and evolution of the human B-globin gene family. *Cell* **21**: 653-668.

64. Farnsworth NR, Akerele O, Bingel AS, Soejarto DD and Guo Z (1985). Medicinal plants in therapy. *Bulletin of the World Health Organization* **63**, 6: 965-981.

65. Favier A, Blackledge M, Simorre JP, Crouzy S, Dabouis V, Gueiffier A, Marion D and Debouzy JC (2001). Solution Structure of 2-(Pyrido [1, 2-e] purin-4-yl) amino-ethanol Intercalated in the DNA Duplex d $(CGATCG)_2$. *Biochemistry* **40**, 30: 8717-8726.

66. Feigon J, Denny WA, Leupin W and Kearns DR (1983). Proton nuclear magnetic resonance investigation of the conformation and dynamics in the synthetic deoxyribonucleic acid decamers $d(ATATCGATAT)_2$ and $d(ATATGCATAT)_2$. *Biochemistry* **22**, 25: 5930-5942.

67. Feigon J, Sklenar V, Wang E, Gilbert DE, Macaya RF and Schultze P (1992). $^1H$ NMR spectroscopy of DNA. *Methods Enzymol* **211**: 235-253.

68. Ferrando AA, Herblot S, Palomero T, Hansen M, Hoang T, Fox EA and Look AT (2004) Biallelic transcriptional activation of oncogenic transcription factors in T-cell acute lymphoblastic leukemia. *Am Soc Hematology* **103** 1909-1911.

69. Fox KR (1997) Drug-DNA interaction protocols. *Humana Press.*

70. Franceschin M, Rossetti L, D'Ambrosio A, Schirripa S, Bianco A, Ortaggi G, Savino M, Schultes C and Neidle S (2006). Natural and synthetic G-quadruplex interactive berberine derivatives. *Bioorg Med Chem Lett* **16**, 6: 1707-1711.

71. Frederick CA, Williams LD, Ughetto G, Van der Marel GA, Van Boom JH, Rich A and Wang AHJ (1990). Structural comparison of anticancer drug-DNA complexes: adriamycin and daunomycin. *Biochemistry* **29**, 10: 2538-2549.

72. Frisch MJ, Trucks GW, Schlegel HB, Scuseria GE, Robb MA, Cheeseman JR, Zakrzewski VG, Montgomery Jr JA, Stratmann RE and Burant JC (1998). Gaussian 98, Revision A. 7, Gaussian. *Inc., Pittsburgh, PA*.

73. Fukuda K, Hibiya Y, Mutoh M, Koshiji M, Akao S and Fujiwara H (1999). Inhibition by berberine of cyclooxygenase-2 transcriptional activity in human colon cancer cells. *J Ethnopharmacol* **66**, 2: 227-233.

74. Gatto B, Sanders MM, Yu C, Wu HY, Makhey D, LaVoie EJ and Liu LF (1996). Identification of topoisomerase I as the cytotoxic target of the protoberberine alkaloid coralyne. *Cancer Res* **56**, 12: 2795-2800.

75. Gavathiotis E, Sharman GJ and Searle MS (2000). Sequence-dependent variation in DNA minor groove width dictates orientational preference of Hoechst 33258 in A-tract recognition: solution NMR structure of the 2:1 complex with $d(CTTTTGCAAAAG)_2$. *Nucleic Acids Res* **28**, 3: 728-735.

76. Giri P, Hossain M and Kumar GS (2006a). Molecular aspects on the specific interaction of cytotoxic plant alkaloid palmatine to poly (A). *Int J Biol Macromol* **39**, 4-5: 210-221.

77. Giri P, Hossain M and Kumar GS (2006b). RNA specific molecules: Cytotoxic plant alkaloid palmatine binds strongly to poly (A). *Bioorg Med Chem Lett* **16**, 9: 2364-2368.

78. Gochin M, Zon G and James TL (1990). Two-dimensional COSY and two-dimensional NOE spectroscopy of d (AC) 4. cntdot. d (GT) 4-extraction of structural constraints. *Biochemistry* **29**, 51: 11161-11171.

79. Gong G, Zong Z and Song Y (1999). Spectrofluorometric determination of DNA and RNA with berberine. *Spectrochimica Acta Part A* **55**, 9:1903-1907.

80. Gorenstein DG (1992). $^{31}P$ NMR of DNA. *Methods in enzymology* **211**: 254-286.

81. Gorenstein DG (1994). Conformation and dynamics of DNA and protein-DNA complexes by $^{31}P$ NMR. *Chem Rev* **94**, 5: 1315-1338.

82. Gorenstein DG and Kar D (1975). $^{31}P$ chemical shifts in phosphate diester monoanions. Bond angle and torsional angle effects. *Biochem Biophys Res Commun* **65**, 3: 1073-1080.

83. Gorenstein DG, Lai K and Shah DO (1984). $^{31}P$ and two-dimensional $^{31}P/^{1}H$ correlated NMR spectra of Duplex d (Ap [17O] Gp [18O] Cp [16O] T) and assignment of $^{31}P$ signals in d $(ApGpCpT)_2$-actinomycin D complex. *Biochemistry* **23**, 26: 6717-6723.

84. Gorenstein DG, Luxon BA and Findlay JB (1977). The torsional potential for phosphate diesters. The effect of geometry optimization in CNDO and ab initio molecular orbital calculations. *Biochimica et biophysica acta* **475**, 1: 184.

85. Gorin AA, Zhurkin VB and Wilma K (1995). B-DNA twisting correlates with base-pair morphology. *Journal of molecular biology* **247**, 1: 34-48.

86. Gronenborn AM and Clore GM (1985). Investigation of the solution structures of short nucleic acid fragments by means of nuclear Overhauser enhancement measurements. *Prog. Nucl. Magn. Reson. Spectrosc.* **17**: 1-32.

87. Grzeskowiak K (1996). Sequence-dependent structural variation in B-DNA. *Chem Biol* **3**, 10: 785-790.

88. Hahn FE and Ciak J 1975 In JW Corcoran and F. E. Hahn (ed.), Antibiotics. *Springer-Verlag,* Berlin.

89. Hélène C, Montenay-Garestier T, Saison T, Takasugi M, Toulmé JJ, Asseline U, Lancelot G, Maurizot JC, Toulmé F and Thuong NT (1985). Oligodeoxynucleotides covalently linked to intercalating agents: a new class of gene regulatory substances. *Biochimie* **67**, 7-8: 777-783.

90. Hong SW, Kim SH, Jeun JA, Lee SJ, Kim SU and Kim JH (2000). Antimicrobial activity of 9-O-acyl-and 9-O-benzoyl-substituted berberrubines. *Planta medica* **66**, 4: 361-363.

91. Hore PJ (1989). Nuclear magnetic resonance. Solvent suppression. *Methods Enzymol* **176**: 64-77.

92. Hoshi A, Ikekawa T, Ikeda Y, Shirakawa S and Iigo M (1976). Antitumor activity of berberrubine derivatives. *Gann* **67**, 2: 321-325.

93. Hosur RV, Govil G and Miles HT (1988). Application of two-dimensional NMR spectroscopy in the determination of solution conformation of nucleic acids. *Magnetic Resonance in Chemistry* **26**, 927-944.

94. Hu JP, Takahashi N and Yamada T (2000). Coptidis rhizoma inhibits growth and proteases of oral bacteria. *Oral Dis* **6**, 5: 297-302.

95. Huang MJ, Lee KS and Hurley SJ (2005). Nuclear magnetic resonance spectral analysis and molecular properties of berberine. *Int J Quantum Chem* **105**, 4:396-409.

96. Hunter CA (1993). Sequence-dependent DNA structure. The role of base stacking interactions. *J Mol Biol* **230**, 3: 1025-1054.

97. Hwang JM, Kuo HC, Tseng TH, Liu JY and Chu CY (2006). Berberine induces apoptosis through a mitochondria/caspases pathway in human hepatoma cells. *Arch Toxicol* **80**, 2: 62-73.

98. Iizuka N, Miyamoto K, Okita K, Tangoku A, Hayashi H, Yosino S, Abe T, Morioka T, Hazama S and Oka M (2000). Inhibitory effect of Coptidis Rhizoma and berberine on the proliferation of human esophageal cancer cell lines. *Cancer Lett* **148**, 1: 19-25.

99. Ikekawa T and Ikeda Y (1982). Antitumor activity of 13-methyl-berberrubine derivatives. *J Pharmacobiodyn* **5**, 7: 469-474.

100. Inbaraj JJ, Kukielczak BM, Bilski P, Sandvik SL and Chignell CF (2001). Photochemistry and photocytotoxicity of alkaloids from Goldenseal (Hydrastis canadensis L.) 1. Berberine. *Chem Res Toxicol* **14**, 11: 1529-1534.

101. Islam MM, Sinha R and Kumar GS (2007). RNA binding small molecules: studies on t-RNA binding by cytotoxic plant alkaloids berberine, palmatine and the comparison to ethidium. *Biophys Chem* **125**, 2-3: 508-520.

102. Iwasa K, Kamigauchi M, Ueki M and Taniguchi M (1996). Antibacterial activity and structure-activity relationships of berberine analogs. *Eur J Med Chem* **31**, 6: 469-478.

103. Jain A, Akanchha S and Rajeswari MR (2005). Stabilization of purine motif DNA triplex by a tetrapeptide from the binding domain of HMGBI protein. *Biochimie* **87**, 8: 781-790.

104. Jeener J (1971). Ampere International Summer School. *Basko Polje, Yugoslavia* **83**.

105. Jenkins TC and Lane AN (1997). AT selectivity and DNA minor groove binding: modelling, NMR and structural studies of the interactions of propamidine and pentamidine with d-(CGCGAATTCGCG)$_2$. *Biochim Biophys Acta* **1350**, 2: 189-204.

106. Jenkins TC, Lane AN, Neidle S and Brown DG (1993). NMR and molecular modeling studies of the interaction of berenil and pentamidine with d(CGCAAATTTGCG)$_2$. *Eur J Biochem* **213**, 3: 1175-1184.

107. Jeon YW, Jung JW, Kang M, Chung IK and Lee W (2002). NMR Studies on Antitumor Drug Candidates, Berberine and Berberrubine. *Bull Korean Chem Soc* **23**, 3: 391-394.

108. Kaneda Y, Tanaka T and Saw T (1990). Effects of berberine, a plant alkaloid, on the growth of anaerobic protozoa in axenic culture. *Tokai J Exp Clin Med* **15**, 6: 417-423.

109. Kaneda Y, Torii M, Tanaka T and Aikawa M (1991). In vitro effects of berberine sulphate on the growth and structure of Entamoeba histolytica, Giardia lamblia and Trichomonas vaginalis. *Ann Trop Med Parasitol* **85**, 4: 417-425.

110. Kearns DR, Patel DJ and Shulman RG (1971). High resolution nuclear magnetic resonance studies of hydrogen bonded protons of tRNA in water. *Nature* **229**, 5283: 338-339.

111. Kelland LR (2000). Flavopiridol, the first cyclin-dependent kinase inhibitor to enter the clinic: current status. *Expert Opin Investig Drugs* **9**, 12: 2903-2911.

112. Kettmann V, Kosfalova D, Jantova S, Cernakova M and Drimal J (2004). In vitro cytotoxicity of berberine against HeLa and L1210 cancer cell lines. *Pharmazie* **59**, 7: 548-551.

113. Khetrapal CL and Diehl P 1975 Nuclear magnetic resonance studies in lyotropic liquid crystals. *Springer.*

114. Kim SA, Kwon Y, Kim JH, Muller MT and Chung IK (1998). Induction of topoisomerase II-mediated DNA cleavage by a protoberberine alkaloid, berberrubine. *Biochemistry* **37**, 46: 16316-16324.

115. Kim SH, Lee SJ, Lee JH, Sun WS and Kim JH (2002). Antimicrobial activity of 9-O-acyl- and 9-O-alkylberberrubine derivatives. *Planta medica* **68**, 3: 277-281.

116. Kluza J, Baldeyrou B, Colson P, Rasoanaivo P, Mambu L, Frappier F and Bailly C (2003). Cytotoxicity and DNA binding properties of the plant alkaloid burasaine. *Eur J Pharm Sci* **20**, 4-5: 383-391.

117. Ko BS, Choi SB, Park SK, Jang JS, Kim YE and Park S (2005). Insulin sensitizing and insulinotropic action of berberine from Cortidis rhizoma. *Biol Pharm Bull* **28**, 8: 1431-1437.

118. Kohn W and Sham LJ (1965). Self-consistent equations including exchange and correlation effects. *Phys. Rev* **140**, 4A: A1133-A1138.

119. Kotovych G, Lown JW and Tong JP (1986). High-field 1H and 31P NMR studies on the binding of the anticancer agent mitoxantrone to d $[CpGpApTpCpG]_2$. *J Biomol Struct Dyn* **4**, 1: 111-125.

120. Krishnan P and Bastow KF (2000). The 9-position in berberine analogs is an important determinant of DNA topoisomerase II inhibition. *Anticancer Drug Des* **15**, 4: 255-264.

121. Kumar GS, Das S, Bhadra K and Maiti M (2003). Protonated forms of poly[d(G-C)] and poly(dG).poly(dC) and their interaction with berberine. *Bioorg Med Chem* **11**, 23: 4861-4870.

122. Kumar GS, Debnath D, Sen A and Maiti M (1993). Thermodynamics of the interaction of berberine with DNA. *Biochem Pharmacol* **46**, 9: 1665-1667.

123. Kunwar AC (1991). Spectroscopic Applications of Liquid Crystals. *Liquid crystals: applications and uses*: 225.

124. Kuo CL, Chou CC and Yung BY (1995). Berberine complexes with DNA in the berberine-induced apoptosis in human leukemic HL-60 cells. *Cancer Lett* **93**, 2: 193-200.

125. Kupka T, Pasterna G, Jaworska M, Karali A and Dais P (2000). GIAO NMR calculations for carbazole and its N-methyl and N-ethyl derivatives. Comparison of theoretical and experimental 13 C chemical shifts. *Magn. Reson. Chem* **38**: 149-155.

126. Labanowski JK and Andzelm JW (1991) Density functional methods in chemistry. *Springer-Verlag* New York, Inc. New York, NY, USA.

127. Lampert H, Mikenda W, Karpfen A and Kahlig H (1997). NMR shieldings in benzoyl and 2-hydroxybenzoyl compounds. Experimental versus GIAO calculated data. *J Phys Chem A* **101**, 50: 9610-9617.

128. Lane AN, Jenkins TC, Brown T and Neidle S (1991). Interaction of berenil with the EcoRI dodecamer d-$(CGCGAATTCGCG)_2$ in solution studied by NMR. *Biochemistry* **30**, 5: 1372-1385.

129. Langlois d'Estaintot B, Gallois B, Brown T and Hunter WN (1992). The molecular structure of a 4'-epiadriamycin complex with d(TGATCA) at 1.7A resolution: comparison with the structure of 4'-epiadriamycin d(TGTACA) and d(CGATCG) complexes. *Nucleic Acids Res* **20**, 14: 3561-3566.

130. Lau CW, Yao XQ, Chen ZY, Ko WH and Huang Y (2001). Cardiovascular actions of berberine. *Cardiovasc Drug Rev* **19**, 3: 234-244.

131. Lavery R and Sklenar H (1989). Defining the structure of irregular nucleic acids: conventions and principles. *J Biomol Struct Dyn* **6**, 4: 655.

132. Lavery R and Sklenar H (1996). CURVES 5.1 Helical analysis of irregular nucleic Acids. *Laboratory of Theoretical Biology. CNRS, Paris*.

133. Lavery R, Sklenar H, Zakrzewska K and Pullman B (1986). The flexibility of the nucleic acids:(II). The calculation of internal energy and applications to mononucleotide repeat DNA. *J Biomol Struct Dyn* **3**, 5: 989.

134. Lee C, Yang W and Parr RG (1988). Development of the Colle-Salvetti correlation-energy formula into a functional of the electron density. *Phys Rev B* **37**, 2: 785-789.

135. Lee YS, Kim WS, Kim KH, Yoon MJ, Cho HJ, Shen Y, Ye JM, Lee CH, Oh WK, Kim CT, Hohnen-Behrens C, Gosby A, Kraegen EW, James DE and Kim JB (2006). Berberine, a natural plant product, activates AMP-activated protein kinase with beneficial metabolic effects in diabetic and insulin-resistant states. *Diabetes* **55**, 8: 2256-2264.

136. Leonard GA, Brown T and Hunter WN (1992). Anthracycline binding to DNA. High-resolution structure of d(TGTACA) complexed with 4'-epiadriamycin. *Eur J Biochem* **204**, 1: 69-74.

137. Lerman LS (1961). Structural considerations in the interaction of DNA and acridines. *J Mol Biol* **3**: 18-30.

138. Letasiova S, Jantova S, Cipak L and Muckova M (2006). Berberine-antiproliferative activity in vitro and induction of apoptosis/necrosis of the U937 and B16 cells. *Cancer Lett* **239**, 2: 254-262.

139. Levitt M, Hirshberg M, Sharon R and Daggett V (1995). Potential energy function and parameters for simulations of the molecular dynamics of proteins and nucleic acids in solution. *Comput Phys Commun* **91**, 1-3: 215-231.

140. Li TK, Bathory E, LaVoie EJ, Srinivasan AR, Olson WK, Sauers RR, Liu LF and Pilch DS (2000). Human topoisomerase I poisoning by protoberberines: potential roles for both drug-DNA and drug-enzyme interactions. *Biochemistry* **39**, 24: 7107-7116.

141. Li WY and Lu ZH (1998). The Fluorescent Reaction between Berberine and DNA and the Fluorometry of DNA. *Microchem J* **60**, 1: 84-88.

142. Liu LF, Desai SD, Li TK, Mao Y, Sun M and Sim SP (2000). Mechanism of action of camptothecin. *Ann N Y Acad Sci* **922**: 1-10.

143. Long YH, Bai LP, Qin Y, Pang JY, Chen WH, Cai Z, Xu ZL and Jiang ZH (2006). Spacer length and attaching position-dependent binding of synthesized protoberberine dimers to double-stranded DNA. *Bioorg Med Chem* **14**, 13: 4670-4676.

144. Lown JW and Hanstock CC (1985). High field 1H-NMR analysis of the 1: 1 intercalation complex of the antitumor agent mitoxantrone and the DNA duplex [d (CpGpCpG)]. *J Biomol Struct Dyn* **2**, 6: 1097.

145. Lown JW, Hanstock CC, Bleackley RC, Imbach JL, Rayner B and Vasseur JJ (1984). Synthesis complete 1H assignments and conformations of the self-complementary hexadeoxyribonucleotide [d (CpGpApTpCpG)] 2 and its fragments by high field NMR. *Nucleic Acids Res* **12**, 5: 2519-2533.

146. Lyubchenko YL, Shlyakhtenko LS, Appella E and Harrington RE (1993). CA runs increase DNA flexibility in the complex of. lambda. Cro protein with the OR3 site. *Biochemistry* **32**, 15: 4121-4127.

147. Maiti M and Chatterjee A (1995). Production of singlet oxygen by sanguinarine and berberine. *Current science (Bangalore)* **68**, 7: 734-736.

148. Maiti M and Chaudhuri K (1981). Interaction of berberine chloride with naturally occurring deoxyribonucleic acids. *Indian J Biochem Biophys* **18**, 4: 245-250.

149. Maiti M and Kumar GS (2007). Molecular aspects on the interaction of protoberberine, benzophenanthridine, and aristolochia group of alkaloids with nucleic acid structures and biological perspectives. *Med Res Rev* **27**, 5: 649-695.

150. Majumdar A and Hosur RV (1992). Simulation of 2 D NMR spectra for determination of solution conformations of nucleic acids. *Prog Nucl Magn Reson. Spectrosc* **24**, 2: 109-158.

151. Makhey D, Gatto B, Yu C, Liu A, Liu LF and LaVoie EJ (1996). Coralyne and related compounds as mammalian topoisomerase I and topoisomerase II poisons. *Bioorg Med Chem* **4**, 6: 781-791.

152. Mantovani R (1998). A survey of 178 NF-Y binding CCAAT boxes. *Nucleic Acids Res* **26**, 5: 1135-1143.

153. Maple JR, Dinur U and Hagler AT (1988). Derivation of force fields for molecular mechanics and dynamics from ab initio energy surfaces. *Proc Nat Acad Sci U.S.A* **85**, 15: 5350-5354.

154. Maple JR, Thacher TS, Dinur U and Hagler AT (1990). Biosym force field research results in new techniques for the extraction of inter-and intramolecular forces. *Chem Design Automat News* **5**, 9: 5-10.

155. Marek R, Humpa O, Dostal J, Slavik J and Sklenar V (1999). $^{15}N$ NMR study of isoquinoline alkaloids. *Magn Reson Chem* **37**, 33: 195-202.

156. Marek R, Seckarova P, Hulova D, Marek J, Dostal J and Sklenar V (2003). Palmatine and berberine isolation artifacts. *J Nat Prod* **66**, 4: 481-486.

157. Marini JC, Levene SD, Crothers DM and Englund PT (1982). Bent helical structure in kinetoplast DNA. *Proc Nat Acad Sci U.S.A* **79**, 24: 7664-7668.

158. Marion D and Wüthrich K (1983). Application of phase sensitive two-dimensional correlated spectroscopy (COSY) for measurements of proton-proton spin-spin coupling constants in proteins. *Biochem Biophys Res Commun* **113**, 3: 967-974.

159. Mauvieux L, Leymarie V, Helias C, Perrusson N, Falkenrodt A, Lioure B, Lutz P and Lessard M (2002). High incidence of Hox11L2 expression in children with T-ALL. *Leukemia* **16**: 2417-2422.

160. Mazzini S, Bellucci MC, Dallavalle S, Fraternali F and Mondelli R (2004). Mode of binding of camptothecins to double helix oligonucleotides. *Org Biomol Chem* **2**, 4: 505-513.

161. Mazzini S, Bellucci MC and Mondelli R (2003). Mode of binding of the cytotoxic alkaloid berberine with the double helix oligonucleotide d-$(AAGAATTCTT)_2$. *Bioorg Med Chem* **11**, 4: 505-514.

162. Mazzini S, Mondelli R and Ragg E (1998). Structure and dynamics of intercalation complexes of anthracyclines with d $(CGATCG)_2$ and d $(CGTACG)_2$. 2D-$^{1}H$ and $^{31}P$ NMR investigations. *J Chem Soc Pak 2* **1998**, 9: 1983-1992.

163. Miura N, Yamamoto M, Ueki T, Kitani T, Fukuda K and Komatsu Y (1997). Inhibition of thymocyte apoptosis by berberine. *Biochem Pharmacol* **53**, 9: 1315-1322.

164. Mueller L (1979). Sensitivity enhanced detection of weak nuclei using heteronuclear multiple quantum coherence. *J Am Chem Soc* **101**, 16: 4481-4484.

165. Mujeeb A, Kerwin SM, Kenyon GL and James TL (1993). Solution structure of a conserved DNA sequence from the HIV-1 genome: restrained molecular dynamics simulation with distance and torsion angle restraints derived from two-dimensional NMR spectra. *Biochemistry* **32**, 49: 13419-13431.

166. Nandi R, Debnath D and Maiti M (1990). Interactions of berberine with poly(A) and tRNA. *Biochim Biophys Acta* **1049**, 3: 339-342.

167. Neidle S (2001). DNA minor-groove recognition by small molecules. *Natural product reports* **18**, 3: 291-309.

168. Ni YX (1988). Therapeutic effect of berberine on 60 patients with type II diabetes mellitus and experimental research. *Zhong Xi Yi Jie He Za Zhi* **8**, 12: 711-713, 707.

169. Noble RL (1990). The discovery of the vinca alkaloids--chemotherapeutic agents against cancer. *Biochem Cell Biol* **68**, 12: 1344-1351.

170. Nunn CM, Van Meervelt L, Zhang S, Moore MH and Kennard O (1991). DNA-drug interactions: the crystal structures of d (TGTACA) and d (TGATCA) complexed with daunomycin. *J Mol Biol* **222**, 2: 167-177.

171. Nussinov R (1985). Large helical conformational deviations from ideal B-DNA and prokaryotic regulatory sites. *J Theor Biol* **115**, 2: 179-189.

172. Ojha H, Murari BM, Anand S, Hassan MI, Ahmad F and Chaudhury NK (2009). Interaction of DNA Minor Groove Binder Hoechst 33258 with Bovine Serum Albumin. *Chem Pharm Bull* **57**, 5: 481-486.

173. Ott J and Eckstein F (1985). Phosphorus-31 NMR spectral analysis of the dodecamer d (CGCGAATTCGCG). *Biochemistry* **24**, 10: 2530-2535.

174. Ovadekova R, Jantova S, Letasiova S, Stepanek I and Labuda J (2006). Nanostructured electrochemical DNA biosensors for detection of the effect of berberine on DNA from cancer cells. *Anal Bioanal Chem* **386**, 7-8: 2055-2062.

175. Pal S, Kumar GS, Debnath D and Maiti M (1998). Interaction of the antitumour alkaloid coralyne with duplex deoxyribonucleic acid structures: spectroscopic and viscometric studies. *Indian J Biochem Biophys* **35**, 6: 321-332.

176. Pang JY, Qin Y, Chen WH, Luo GA and Jiang ZH (2005). Synthesis and DNA-binding affinities of monomodified berberines. *Bioorg Med Chem* **13**, 20: 5835-5840.

177. Panousis C and Phillips DR (1994). DNA sequence specificity of mitoxantrone. *Nucleic Acids Res* **22**, 8: 1342-1345.

178. Paquet F, Boudvillain M, Lancelot G and Leng M (1999). NMR solution structure of a DNA dodecamer containing a transplatin interstrand GN7-CN3 cross-link. *Nucleic Acids Res* **27**, 21: 4261.

179. Paquet F, Perez C, Leng M, Lancelot G and Malinge JM (1996). NMR solution structure of a DNA decamer containing an interstrand cross-link of the antitumor drug cis-diamminedichloroplatinum (II). *J Biomol Struct Dyn* **14**, 1: 67-77.

180. Pardi A, Martin FH and Tinoco Jr I (1981). Comparative study of ribonucleotides, deoxyribonucleotides, and hybrid oligonucleotide helixes by nuclear magnetic resonance. *Biochemistry* **20**, 14: 3986-3996.

181. Pardi A, Walker R, Rapaport H, Wider G and Wüthrich K (1983). Sequential assignments for the 1 H and 31 P atoms in the backbone of oligonucleotides by two-dimensional nuclear magnetic resonance. *J Am Chem Soc* **105**: 1652–1653.

182. Park H, Kim EH, Kang MR, Chung IK, Cheong C and Lee W (2004a). Spectroscopic Studies on Interaction of Protoberberines with the Deoxyoligonucleotide d (GCCGTCGTTTTACA)$_2$. *Bull Korean Chem Soc* **25**, 10: 1559-1563.

183. Park H, Kim EH, Sung YH, Kang M, Chung IK, Cheong C and Lee W (2004b). DNA binding mode of the isoquinoline alkaloid berberine with the deoxyoligonucleotide d (GCCGTCGTTTTACA)$_2$. *Bull Korean Chem Soc* **25**, 4: 539-544.

184. Parr RG and Yang W 1989 Density-functional theory of atoms and molecules. *Oxford University Press*, USA.

185. Patel DJ (1974). Peptide antibiotic-dinucleotide interactions. Nuclear magnetic resonance investigations of complex formation between actinomycin D and d-pGpC in aqueous solution. *Biochemistry* **13**, 11: 2388-2395.

186. Patel DJ (1977). d-CpCpGpG and d-GpGpCpC self-complementary duplexes: Nmr studies of the helix-coil transition. *Biopolymers* **16**, 8: 1635-1656.

187. Patel DJ (1979). Helix-coil transition of the dG-dC-dG-dC self-complementary duplex and complex formation with daunomycin in solution. *Biopolymers* **18**, 3: 553-569.

188. Patel DJ and Canuel LL (1976). Ethidium bromide-(dC-dG-dC-dG)$_2$ Complex in Solution: Intercalation and Sequence Specificity of Drug Binding at the Tetranucleotide Duplex Level. *Proc Nat Acad Sci U.S.A* **73**, 10: 3343-3347.

189. Patel DJ, Kozlowski SA, Marky LA, Broka C, Rice JA, Itakura K and Breslauer KJ (1982). Premelting and melting transitions in the d(CGCGAATTCGCG) self-complementary duplex in solution. *Biochemistry* **21**, 3: 428-436.

190. Petersheim M and Turner DH (1983). Proton magnetic resonance melting studies of CCGGp, CCGGAp, ACCGGp, CCGGUp, and ACCGGUp. *Biochemistry* **22**, 2: 269-277.

191. Philogene BJR, Arnason JT, Towers GHN, Abramowski Z, Campos F, Champagne D and McLachlan D (1984). Berberine: a naturally occurring phototoxic alkaloid. *J Chem Ecol* **10**, 1: 115-123.

192. Pilch DS, Yu C, Makhey D, LaVoie EJ, Srinivasan AR, Olson WK, Sauers RR, Breslauer KJ, Geacintov NE and Liu LF (1997). Minor groove-directed and intercalative ligand-DNA interactions in the poisoning of human DNA topoisomerase I by protoberberine analogs. *Biochemistry* **36**, 41: 12542-12553.

193. Preininger V 1986 Chemotaxonomy of papaveraceae and fumariaceae. The Alkaloids. 29. Brossi A, ed. Orlando: *Academic Press*.

194. Pruchnik FP, Banbula M, Ciunik Z, Chojnacki H, Skop B, Latocha M and Wilczok T (2002). Structure, properties and in vitro cytotoxic activity of hexakis(2-cyanoethyl)ditin(III). *J Inorg Biochem* **90**, 3-4: 149-154.

195. Pulay P and Hinton JF (1995). Encyclopedia of Nuclear Magnetic Resonance. *Willey, New York*: 4334.

196. Pullman A and Pullman B (1981). Molecular electrostatic potential of the nucleic acids. *Q Rev Biophys* **14**, 3: 289-380.

197. Qian Y, Fritzsch B, Shirasawa S, Chen CL, Choi Y and Ma Q (2001). Formation of brainstem (nor) adrenergic centers and first-order relay visceral sensory neurons is dependent on homeodomain protein Rnx/Tlx3. *Genes & Development* **15**, 19: 2533-2545.

198. Qin Y, Chen WH, Pang JY, Zhao ZZ, Liu L and Jiang ZH (2007a). DNA-binding affinities and sequence specificities of protoberberine alkaloids and their demethylated derivatives: a comparative study. *Chem Biodivers* **4**, 2: 145-153.

199. Qin Y, Pang JY, Chen WH, Cai Z and Jiang ZH (2006). Synthesis, DNA-binding affinities, and binding mode of berberine dimers. *Bioorg Med Chem* **14**, 1: 25-32.

200. Qin Y, Pang JY, Chen WH, Zhao ZZ, Liu L and Jiang ZH (2007b). Inhibition of DNA topoisomerase I by natural and synthetic mono- and dimeric protoberberine alkaloids. *Chem Biodivers* **4**, 3: 481-487.

201. Radha PK, Madan A, Nibedita R and Hosur RV (1995). Solution structure of the conserved segment of the Myb cognate DNA sequence by 2D NMR, spectral

simulation, restrained energy minimization, and distance geometry calculations. *Biochemistry* **34**, 17: 5913-5922.

202. Ragg E, Mondelli R, Battistini C, Garbesi A and Colonna FP (1988). $^{31}$P NMR study of daunorubicin-d (CGTACG) complex in solution. Evidence of the intercalation sites. *FEBS letters* **236**, 1: 231.

203. Rajagopal P, Gilbert DE, Van der Marel GA, Van boom JH and Feigon J (1988). Observation of Exchangeable Proton Resonances of DNA in Two-Dimensional NOE Spectra using a Presaturation Pulse: Application to d(CGCGAATTCGCG) and d(CGCGAm6ATTCGCG). *J Magn Reson* **78**: 526-537.

204. Rajeswari MR (1996). Tryptophan Intercalation In G, C Containing Polynucleotides: Z to B Conversion of Poly (d (G-5M C)) in Low Salt Induced By a Tetra Peptide. *J Biomol Struct Dyn* **14**, 1: 25-30.

205. Reid BR, Banks K, Flynn P and Nerdal W (1989). NMR distance measurements in DNA duplexes: sugars and bases have the same correlation times. *Biochemistry* **28**, 26: 10001-10007.

206. Ren J and Chaires JB (1999). Sequence and structural selectivity of nucleic acid binding ligands. *Biochemistry* **38**, 49: 16067-16075.

207. Roche CJ, Thomson JA and Crothers DM (1994). Site selectivity of daunomycin. *Biochemistry* **33**, 4: 926-935.

208. Rungsitiyakorn A, Wilairat P and Panijpan B (1981). On the pH dependence of binding of berberine to DNA. *J Pharm Pharmacol* **33**, 2: 125-127.

209. Rydzewski JM, Leupin W and Chazin W (1996). The width of the minor groove affects the binding of the bisquaternary heterocycle SN-6999 to duplex DNA. *Nucleic Acids Res* **24**, 7: 1287-1293.

210. Sack RB and Froehlich JL (1982). Berberine inhibits intestinal secretory response of Vibrio cholerae and Escherichia coli enterotoxins. *Infect Immun* **35**, 2: 471-475.

211. Saran A, Srivastava S, Coutinho E and Maiti M (1995). $^{1}$H NMR investigation of the interaction of berberine and sanguinarine with DNA. *Indian J Biochem Biophys* **32**, 2: 74-77.

212. Sauers RR (1995). An analysis of van der Waals attractive forces in DNA-minor groove binding. *Bioorg Med Chem Lett* **5**, 21: 2573-2576.

213. Schroeder SA, Roongta V, Fu JM, Jones CR and Gorenstein DG (1989). Sequence-dependent variations in the phosphorus-31 NMR spectra and backbone torsional angles of wild-type and mutant lac operator fragments. *Biochemistry* **28**, 21: 8292-8303.

214. Schumacher R, Buck F and Ruterjans H (1989). NMR study of the structural changes induced in the E. coli lac promoter by the specific binding of the CAP protein. *Nucleic Acids Res* **17**, 13: 5097-5105.

215. Searle MS, Hall JG, Denny WA and Wakelin LPG (1988). NMR studies of the interaction of the antibiotic nogalamycin with the hexadeoxyribonucleotide duplex d (5'-GCATGC)$_2$. *Biochemistry* **27**, 12: 4340-4349.

216. Shafer RH (1977). Spectroscopic studies of the interaction of daunomycin with transfer RNA. *Biochem Pharmacol* **26**, 18: 1729.

217. Singh MP, Joseph T, Kumar S, Bathini Y and Lown JW (1992). Synthesis and sequence-specific DNA binding of a topoisomerase inhibitory analog of Hoechst 33258 designed for altered base and sequence recognition. *Chem Res Toxicol* **5**, 5: 597-607.

218. Sinha R, Islam MM, Bhadra K, Kumar GS, Banerjee A and Maiti M (2006). The binding of DNA intercalating and non-intercalating compounds to A-form and protonated form of poly(rC).poly(rG): spectroscopic and viscometric study. *Bioorg Med Chem* **14**, 3: 800-814.

219. Sklenar V and Feigon J (1990). Formation of a stable triplex from a single DNA strand. *Nature* **345**, 6278: 836-838.

220. Slickers P, Hillebrand M, Kittler L, Löber G and Sühnel J (1998). Molecular modelling and footprinting studies of DNA minor groove binders: bisquaternary ammonium heterocyclic compounds. *Anti-Cancer Drug Des* **13**, 5: 463-488.

221. States DJ, Haberkorn RA and Ruben DJ (1982). A two-dimensional nuclear Overhauser experiment with pure absorption phase in four quadrants. *J. Magn. Reson.* **48**: 286-292.

222. Suh D and Chaires JB (1995). Criteria for the mode of binding of DNA binding agents Bioorg. *Med. Chem* **3**: 723-728.

223. Sundquist WI and Lippard SJ (1990). The coordination chemistry of platinum anticancer drugs and related compounds with DNA. *Coord Chem Rev* **100**: 293-322.

224. Tabernero L, Bella J and Aleman C (1996). Hydrogen bond geometry in DNA-minor groove binding drug complexes. *Nucleic Acids Res* **24**, 17: 3458-3466.

225. Teletchea S, Hartmann B and Kozelka J (2004). Discrimination between BI and BII conformational substates of B-DNA based on sugar-base interproton distances. *J Biomol Struct Dyn* **21**, 4: 489-494.

226. Tian X, Song Y, Dong H and Ye B (2008). Interaction of anticancer herbal drug berberine with DNA immobilized on the glassy carbon electrode. *Bioelectrochemistry* **73**, 1: 18-22.

227. Tonelli M, Ragg E, Bianucci AM, Lesiak K and James TL (1998). Nuclear magnetic resonance structure of d (GCATATGATAAG): a consensus sequence for promoters recognized by K RNA polymerase. *Biochemistry* **37**: 11745-11761.

228. Tran-Dinh S, Neumann JM, Huynh-Dinh T, Allard P, Lallemand JY and Igolen J (1982). DNA fragment conformations IV - Helix-coil transition and conformation of d-CCATGG in aqueous solution by $^{1}$H-NMR spectroscopy. *Nucleic Acids Res* **10**, 17: 5319-5332.

229. Tripathi AN, Chauhan L, Thankachan PP and Barthwal R (2007). Quantum chemical and nuclear magnetic resonance spectral studies on molecular properties and electronic structure of berberine and berberrubine. *Magn Reson Chem* **45**, 8: 647-655.

230. Ulyanov NB, Gorin AA, Zhurkin VB, Chen BC and Sarma RH (1992). Systematic study of nuclear Overhauser effects vis-à-vis local helical parameters, sugar puckers, and glycosidic torsions in B DNA: insensitivity of NOE to local transitions in B DNA oligonucleotides due to internal structural compensations. *Biochemistry* **31**: 3918-3930.

231. Ulyanov NB, Ivanov VI, Minyat EE, Khomyakova EB, Petrova MV, Lesiak K and James TL (1998). A Pseudosquare Knot Structure of DNA in Solution†. *Biochemistry* **37**, 37: 12715-12726.

232. Ulyanov NB, Mujeeb A, Du Z, Tonelli M, Parslow TG and James TL (2006). NMR structure of the full-length linear dimer of stem-loop-1 RNA in the HIV-1 dimer initiation site. *J Biol Chem* **281**, 23: 16168-16177.

233. Vlieghe D, Turkenburg JP and Van Meervelt L (1999). B-DNA at atomic resolution reveals extended hydration patterns. *Biol Crystallogr* **55**: 1495-1502.

234. Wall RK, Shelton AH, Bonaccorsi LC, Bejune SA, Dube D and McMillin DR (2001). H(2)D3: a cationic porphyrin designed to intercalate into B-form DNA (H(2)D3 = trans-di(N-methylpyridium-3-yl)porphyrin). *J Am Chem Soc* **123**, 46: 11480-11481.

235. Wang AH, Ughetto G, Quigley GJ and Rich A (1987). Interactions between an anthracycline antibiotic and DNA: molecular structure of daunomycin complexed to d(CpGpTpApCpG) at 1.2-A resolution. *Biochemistry* **26**, 4: 1152-1163.

236. Wang AHJ and Teng M 1990 Crystallographic and Modeling Methods in Molecular Design, edited by CE Bugg & SE Ealick. New York: *Springer-Verlag*.

237. Wang Z, Guo X, Liu Z, Cui M, Song F and Liu S (2008). Studies on alkaloids binding to GC-rich human survivin promoter DNA using positive and negative ion electrospray ionization mass spectrometry. *J Mass Spectrom* **43**, 3: 327-335.

238. Williams SD, Birch R, Einhorn LH, Irwin L, Greco FA and Loehrer PJ (1987). Treatment of disseminated germ-cell tumors with cisplatin, bleomycin, and either vinblastine or etoposide. *N Engl J Med* **316**, 23: 1435-1440.

239. Wilson WD and Jones RL (1982). Interaction of actinomycin D, ethidium quinacrine daunorubicin, and tetralysine with DNA: $^{31}$P NMR chemical shift and relaxation investigation. *Nucleic Acids Res* **10**, 4: 1399-1410.

240. Wright CW, Marshall SJ, Russell PF, Anderson MM, Phillipson JD, Kirby GC, Warhurst DC and Schiff PL (2000). In vitro antiplasmodial, antiamoebic, and cytotoxic activities of some monomeric isoquinoline alkaloids. *J Nat Prod* **63**, 12: 1638-1640.

241. Wu JF and Liu TP (1995). Effects of berberine on platelet aggregation and plasma levels of TXB2 and 6-keto-PGF1 alpha in rats with reversible middle cerebral artery occlusion. *Yao Xue Xue Bao* **30**, 2: 98-102.

242. Wüthrich K (1986). NMR of Proteins and Nucleic Acids, 1986. *NY John Willey & Sons*.

243. Yadav RC, Kumar GS, Bhadra K, Giri P, Sinha R, Pal S and Maiti M (2005). Berberine, a strong polyriboadenylic acid binding plant alkaloid: spectroscopic, viscometric, and thermodynamic study. *Bioorg Med Chem* **13**, 1: 165-174.

244. Yang IW, Chou CC and Yung BY (1996a). Dose-dependent effects of berberine on cell cycle pause and apoptosis in Balb/c 3T3 cells. *Naunyn Schmiedebergs Arch Pharmacol* **354**, 2: 102-108.

245. Yang Y, Huang L, Pon RT, Cheng SF, Chang DK and Lown JW (1996b). Solution Structure Studies of the Cobalt Complex of a Bleomycin Functional Model Bound to d $(CGCAATTGCG)_2$ by Two-Dimensional Nuclear Magnetic Resonance Methods and Restrained Molecular Dynamics Simulation. *Bioconjugate Chem* **7**, 6: 670-679.

246. Yin J, Hu R, Chen M, Tang J, Li F, Yang Y and Chen J (2002). Effects of berberine on glucose metabolism in vitro. *Metabolism* **51**, 11: 1439-1443.

247. Yoo KY, Hwang IK, Kim JD, Kang IJ, Park J, Yi JS, Kim JK, Bae YS and Won MH (2008). Antiinflammatory effect of the ethanol extract of Berberis koreana in a gerbil model of cerebral ischemia/reperfusion. *Phytother Res* **22**, 11: 1527-1532.

248. Zhang WJ, Ou TM, Lu YJ, Huang YY, Wu WB, Huang ZS, Zhou JL, Wong KY and Gu LQ (2007). 9-Substituted berberine derivatives as G-quadruplex stabilizing ligands in telomeric DNA. *Bioorg Med Chem* **15**, 16: 5493-5501.